Interface morphology in polylactic acid-sisal fibre composites

Prajer, Marek

Award date:
2011

Awarding institution:
University of Bath

Interface morphology in polylactic acid-sisal fibre composites

Marek Prajer

A thesis submitted for the degree of Doctor of Philosophy

University of Bath
Department of Architecture and Civil Engineering

June 2011

COPYRIGHT

“Dum spiro spero.”

To Michaela and to my family

Abstract

The thesis focuses on the investigation of natural fibre reinforced thermoplastic matrix composites with emphasis on the micromechanics of the fibre to matrix interface. Fully bio-based and biodegradable composites were manufactured from unidirectionally aligned sisal fibre bundles and a polylactic acid polymer matrix. Polylactic acid is a semicrystalline polyester formulated from renewable resources which has medium strength. The glass transition temperature is the highest of the commercially available bio-thermoplastics. Sisal fibres were chosen because of their low microfibril angle and their availability as long, straight fibre bundles.

The mechanical properties of sisal fibres were investigated in the untreated state and following caustic soda treatment, employed to modify the strength of fibres and to improve fibre to matrix adhesion. Fibres were soaked in aqueous caustic soda solution for 48 hours and their tensile strength was measured at different gauge lengths. Probability of failure was plotted versus the fibre strength and a statistical parameter (Weibull modulus) was estimated. The strength of untreated and caustic soda treated sisal fibres at a gauge length of 20 mm was 482 and 563 MPa respectively.

Composites with fibre volume fraction from 0.4 to 0.6 were compression moulded in a thin aluminium mould. Aluminium can quickly absorb/dissipate heat allowing the thermoplastic polymer matrix to flow/solidify which reduces processing times and prevents damage to the fibres and the matrix. Scanning electron (SEM) micrographs of the polished cross sections of composites revealed good fibre to matrix adhesion. Mechanical properties were measured as a function of fibre volume fraction and properties improved with increasing fibre content. Caustic soda treatment of fibres improved mechanical properties and the tensile strength and modulus increased from 164 MPa and 9.5 GPa respectively to 205 MPa and 12 GPa respectively at fibre volume fraction of V_f=0.5 Flexural strength and modulus increased from 279 MPa and 19.4 GPa respectively to 286 MPa and 22 GPa at a fibre volume fraction of V_f=0.6.

The glass transition temperature (T_g) of PLA and sisal-PLA composites were determined by dynamic mechanical thermal analysis (DMTA). The sisal fibres reinforcement

significantly improved the storage modulus of polylactic acid below and above the glass transition temperature. The glass transition temperatures decreased with increasing fibre volume fraction in composites reinforced with untreated sisal fibres due to interfacial friction. The damping at the caustic soda treated fibres-PLA interface was reduced probably due to the presence of transcrystalline morphology at the fibre to matrix interface.

The crystalline morphology of PLA at a single sisal fibre bundle to PLA matrix interface was investigated by the means of hot stage microscopy. Caustic soda treatment was advantageous in forming a well-defined transcrystalline layer at the fibre to thermoplastic matrix interface but it was necessary to cool the molten polymer to 120ºC in order to observe transcrystalline growth. More random nucleation and growth of spherulites occurred on the surface of untreated fibres. Hence it is proposed that caustic soda treatment will enhance surface adhesion of the PLA matrix to the sisal fibre bundles.

The influence of caustic soda treatment on the development of polymer matrix morphology at the bonded interface were assessed by a microbond pull-out shear test. Weibull analysis was used to characterise the interfacial shear strength. Caustic soda treatment improved the fibre to matrix adhesion but the Weibull moduli were similar suggesting that a brittle debond had occurred in both cases. The interfacial shear strength for untreated and caustic soda treated sisal fibres partially embedded in PLA matrix was 10.5 MPa and 15.3 MPa, respectively. The interfacial shear strength of single fibre composites correlated with the interlaminar shear strength of composites with a fibre volume fraction of 0.4 where values of 8.4 and 14.8 MPa respectively were measured.

Raman micro-spectroscopy was used to map the stress distribution along the sisal fibres partially embedded in the PLA matrix to estimate the compressive stress which builds up in the fibre during the solidification of the molten thermoplastic matrix. An axial residual compressive stress in the range 153-159 MPa was determined for unstrained fibres and also fibres strained at 1 and 1.5%.

Overall it has been demonstrated that high strength, high modulus sisal-PLA composites can be produced with effective stress transfer at well-bonded fibre to matrix interfaces.

Acknowledgement

I would like to acknowledge my supervisors for their support and inspiration and for giving me the freedom to define my subject of interest.

I would like to convey my sincere thanks to Hugh Perrott (Centre for Electron Optical Studies, University of Bath) for his helpful discussions and advice on using the scanning electron microscope.

Thanks to Dr. Matthew Jones (Department of Chemistry, University of Bath) for his help with gel permeation chromatography and NMR measurement of polylactic acid.

I would like to express my sincere thanks to Paul Redish (Department of Physics, University of Bath) for letting me work in his workshop.

I would like to thank Graham Mott (Department of Architecture and Civil Engineering, University of Bath) for his help with laboratory consumables.

I am very grateful to Neil Ball and Anthony Charles Scarratt from Struers Ltd UK for advice on the metallographic polishing method for polylactic acid reinforced with natural fibres.

My special thanks go to Steven Eichhorn, Kenny Kong and Andy Zach from the University of Manchester for letting me use their Raman micro-spectroscopy suite and for their kind advice on the spectroscopic analysis.

Finally I would like to acknowledge the BRE Trust for the financial support of my doctoral studies.

Contents

List of figures

List of tables

Symbols and abbreviations

Symbols

ΔH_m^c	enthalpy of fusion for 100 % crystalline material
T_m^0	equilibrium melting temperature
T_g^∞	glass transition temperature at infinite molecular weight
T_m^o	maximum melting temperature of an infinite polymer crystal
$\Delta\sigma$	interfacial free energy difference function for fibre/crystallite system
$\Delta\sigma'$	interfacial free energy difference function for melt heterogeneities/crystallite system
A	advantage of a polymer to crystallize at a fibre surface
A	cross section
A	number of skeletal atoms in the asymmetric unit of the polymer chain
a, b, c	principal crystallographic axes
b	width of the specimen
C	rate constant
C_p	heat capacity
c_p	specific heat capacity
d	fibre diameter
E	extraordinary (ray)
E''	loss modulus
E'	storage modulus
E	Young's modulus
E_c, E_f, E_m	Young's modulus of composite, fibre, matrix
E_I	crystal modulus
F	force
$f(x)$	probability density function
$F(x)$	probability of failure
F_m	maximum load
F_{max}	maximum pull out strength
G	strain energy release rate

G^L	free enthalpy of liquid phase
G^S	free enthalpy of solid phase
h	Planck's constant
h	specific enthalpy
h	thickness
I	intensity
k	geometry constant
k	slope of the tangent to the initial linear section of the load - deflection curve
K	constant
K	constant representing the excess free volume of the end-groups of polymer chains
K_g	kinetic constant for secondary nucleation
L	support span
L	fibre length
l_c	fibre critical length
L_0	gauge length
l_e	embedded length
l_m	length of the fibre embedded in the polymer matrix
m	median
M_n	number average molecular weight
M_p	peak molecular weight
M_v	viscosity average molar mass
M_w	weight average molecular weight
M_z	sedimentation average molar mass
M_{z+1}	sedimentation average molar mass
n	refractive index
O	ordinary (ray)
P	loading force
r_f	fibre radius
R	radial distance from the fibre axis
R	universal gas constant
r^*	critical radius of nucleus
S	cross sectional area of a molecule in a crystal lattice

S	stiffness
s	fibre aspect ratio
t	number of turns of the helix in the crystallographic repeat (in the chain direction)
t	time
$tan\ \delta$	loss factor
T	temperature
T_∞	temperature at which all the segmental mobility is frozen
T_c	crystallization temperature
T_g	glass transition temperature
T_m	melting temperature
T_{ref}	stress free temperature
u	number of the asymmetric units on the helix in the crystallographic repeat (in the polymer chain direction)
U^*	energy constant
V_c, V_f, V_m	composite, fibre, matrix volume fraction
W_a	work of adhesion
w_c	weight of composite
w_f	fibre weight fraction
W_{fa}	weight of the fibre in air
W_{fs}	weight of the fibre in the solvent
x	distance
X	random variable
α	refraction angle
α	thermal expansion coefficient
α, β, γ	principal crystallographic angles
α_{1f}	coefficient of thermal expansion in longitudinal direction
α_{2f}	coefficient of thermal expansion in transverse direction
β	incidence angle
β	parameter
β	shape parameter (Weibull modulus)
Γ	Gamma function
γ	interfacial tension
δ	constant

δ	phase angle
δ	scale parameter
ΔG^*	critical free enthalpy of nucleation
ΔG_m	molar Gibbs free energy
ΔG_v	free enthalpy change
ΔH	enthalpy change
Δh	specific enthalpy difference
ΔH_c	enthalpy of crystallization
ΔH_m	enthalpy of fusion
ΔT	temperature difference; degree of undercooling
$\Delta \upsilon$	frequency shift
ε	strain
ε_c, ε_f, ε_m	strain in the composite, fibre, matrix
θ	wetting angle
θ_c	critical angle of incidence for polarization
μ	mean
η_l	length correction factor
η_0	orientation correction factor
η_{RF}	stiffness index
ν	Poisson's ratio
ρ	density
ρ_b	bulk density of the fibre
ρ_m	matrix density
ρ_s	solvent density
σ	applied stress
σ^*	yield stress
σ^2	variance
σ_f	tensile stress in the fibre
σ_F	flexural strength
σ_T	tensile strength
σ_{th}	thermal residual stress in the fibre
τ	interfacial shear stress
τ_{IFSS}	interfacial shear strength
τ_{ILSS}	apparent interlaminar strength

υ_0	light frequency
υ_c	volume crystallinity at time *t*
$\upsilon_{c\infty}$	volume crystallinity
X_c	degree of crystallinity

Abbreviations

2D	two dimensional
3D	three dimensional
AFM	atomic force microscopy
bis-MPA	2,2-bis(methylol)propionic acid
BMC	bulk moulding compound
CCD	charge-coupled device
CF	carbon fibre
CL	ε – caprolactone
CLTE	coefficient of linear thermal expansion
CM	compression moulding
CTE	coefficient of thermal expansion
D-, L-	dextro, laevo
DMAP	4-dimethyl(aminopyridine)
DMF	dimethylformamide
DMTA	dynamic mechanical thermal analysis
DSC	differential scanning calorimetry
EX	extrusion
FEM, FEA	finite elements method, analysis
FIP	fibre identity period
FTIR	Fourier transform infrared spectroscopy
FW	filament winding
GF	glass fibre
HDT	heat deflection (distortion) temperature
I, II, III	regimes of crystallization
IFSS	interfacial shear strength
ILSS	interlaminar shear strength
IM	injection moulding

L – LA	L – lactic acid
LEFM	linear elastic fracture mechanics
MFI	melt flow index
MWD	molecular weight distribution
NFCs	natural fibre reinforced composites
NMR	nuclear magnetic resonance
PD	polydispersity index
RFI	resin film infusion
RH	relative humidity
RTM	resin transfer moulding
SEM	scanning electron microscopy
SFM	scanning force microscopy
SMC	sheet moulding compound
TC, TCL	transcrystallinity, transcrystalline layer
TGA	thermogravimetric analysis
THF	tetrahydrofurane
TOA	thermo-optical analysis
TVA	thermovolatile analysis
UD	unidirectional
UV-VIS	ultraviolet-visible spectroscopy

Indices:

a	amorphous; axial
c	composite; critical; crystalline
f	fibre
F	flexural
het	heterogeneous
hom	homogeneous
LV	liquid-vapour
m	matrix
max	maximum
Na-L	nucleating agent-liquid
Na-S	nucleating agent-solid
s	surface

SV	solid –vapour
t	transverse
T	tensile
th	thermal
v	volume

Glass fibres

AR	alkali resistant
C	acid resistant glass
E	alkali free alumino-borosilicate glass
S	high strength glass

Carbon fibres

HM	high modulus
HS	high strength
HT	high tenacity
IM	intermediate modulus
UHM	ultra-high modulus

Materials

ABS	acrylonitrile butadiene styrene copolymer
CA	cellulose acetate
CC-PS	crystal clear polystyrene
EP	epoxy resin
GFRPs	glass fibre reinforced polymers
GPPS	general purpose polystyrene
HD-PE	high density polyethylene
HI-PS	high impact polystyrene
i-PP	isotactic polypropylene
LD-PE	low density polyethylene
PA	polyamide

PAN	polyacrylonitrile
PBO	poly(*p*-phenylene benzo*bis*oxazole)
PBT	polybutylene terephthalate
PBZT	poly(*p*-phenylene benzo*bis*thiazole)
PC	polycarbonate
PCL	polycaprolactone
PDLA	poly-D-lactide
PDLLA	poly-DL-lactide
PE	polyethylene
PEEK	poly-ether-ether-ketone
PET	polyethylene terepthalate
PGA	polyglycolic acid; polyglicolide
PHB	polyhydroxybutyrate
PLA	poly-L-lactic acid
PLA, PLLA	polylactic acid, polylactide
PLA-*g*-MA	polylactic acid grafted with maleic anhydride
PLLA	poly-L-lactide
PMMA	polymethylmethacrylate
POM	polyoxymethylene
PP	polypropylene
PP-*g*-MA	maleic anhydride grafted polypropylene
PS	polystyrene
PTFE	polytetrafluorethylene
PUR	polyurethane
PVA	polyvinyl alcohol
PVC	polyvinylchloride
ROP	ring opening polymerization
UP	unsaturated polyester
UPE	unsaturated polyester
UPR	unsaturated polyester
XET	xyloglucan endotransglycosylase
XG	xyloglucan
XGO	xyloglucan oligosaccharides
α-*i*-PP	isotactic polypropylene with α crystalline morphology

α-PLLA	poly-L-lactide with α crystalline morphology
β-*i*-PP	isotactic polypropylene with β crystalline morphology
β-PLLA	poly-L-lactide with β crystalline morphology
γ-PLLA	poly-L-lactide with γ crystalline morphology

Chemical formulas

Al_2O_3	aluminium oxide
$Ca(OH)_2$	calcium hydroxide
SiC	silicon carbide
SiO_2	silicon oxide
NaOH	sodium hydroxide
HCN	hydrogen cyanide
Ni-Cr	nickel-chromium alloy
$Ca(OH)_2$	calcium carbonate
$Ca(SO)_4$	calcium sulphate
H_2O	water
CO_2	carbon dioxide
R-	alkyl group or hydrogen
R'-	alkyl group or hydrogen
-OH	hydroxyl group
M-	metal
X-	halogen
H_3O^+	oxonium ion
$Sn(Ph)_4$	tin tetraphenyl
Ph-	phenyl
$Sn(Br)_4$	tin (IV) bromide
$Sn(Oct)_2$	stannous octanoate; Tin 2-ethylhexanoate
$Zn(Ac)_2$	zinc acetate
Sb_2O_5	antimony oxide
$Al(OR)_3$	aluminium alkoxide
$Ti(OR)_4$	titanium alkoxide
R_3SnOR'	trialkyltin alkoxide
X_nMOR	halogen metal alkoxide

$CDCl_3$	deuterated chloroform
He-Ne	helium - neon (laser)
$(C_3H_4O_2)_n$	polylactic acid, polylactide
OsO_4	Osmium tetroxide

1 Introduction

This introductory chapter explains why natural fibres and biopolymers are challenging materials for composite fabrication. Furthermore it briefly describes the project, sets the objectives and outlines the chapters.

The thesis is submitted as a partial fulfilment of the requirements for the MPhil/PhD at the University of Bath. The research was carried out from February 2007 to February 2010 in the BRE Centre for Innovative Construction Materials (CICM) within the Faculty of Engineering and Design.
The Centre was established in July 2006 as a joint collaborative partnership between the University of Bath's Department of Architecture and Civil Engineering, Department of Mechanical Engineering and the Building Research Establishment Ltd (BRE), Watford. The Centre conducts leading research, development and consultancy in the field of innovative and sustainable construction materials.

The project was financially supported by BRE.
The thesis was supervised by:

Dr. Martin P. Ansell	Supervisor
Dr. Peter Walker	Co-supervisor
Dr. Ed Suttie, BRE	Co- supervisor

1.1 Background

Natural fibre reinforced polymers are documented from 1908, when sheets of phenol and melamine-formaldehyde resin were reinforced with paper and cotton (Bledzki and Gassan, 1999). Biocomposites are materials where both the matrix and the fibre reinforcement are derived from renewable resources. Such materials are intrinsically biodegradable because both matrix and reinforcement are plant derived. Cultivation, extraction and processing require limited energy compared to the production of synthetic fibres and resins. The low density and

highly crystalline cellulose content of natural fibres lead to their excellent specific properties, which enable them to compete with traditional glass fibres in structural applications. Natural fibres consist of long cells with relatively thick cell walls. Cellulose, which has a high theoretical strength (8-10 GPa) and modulus (130-250 GPa), is the main constituent responsible for natural fibre mechanical properties (Zimmermann *et al*., 2004). Obviously a polymer reinforced with cellulosic fibres could be used in structural applications because of their strength and low density. There are many indoor potential structural applications which can benefit from bio-based composite materials (desks, doors, and wall panels). The application of appropriate external coatings to bio-based composite materials could be a way to expand applications by replacing traditional materials in outdoor structural applications. Natural fibres are attractive because of their specific properties, low price, health advantages and recyclability. Thermoplastic matrices are increasingly used for industrially fabricated natural fibre composites. They offer several advantages in comparison with thermosets. Their processing is faster, requiring no curing times, they are less expensive, they have no toxic by-products and finally they are easy to recycle. However, there are some disadvantages which are related to thermoplastic composites processing: high viscosities and high melting temperatures of polymer matrices and the fact that wetting and impregnation of fibres may be difficult because of poor fibre to matrix adhesion. Composites with thermoplastic matrices are typically injection moulded. On the one hand injection moulding is fast, low cost and mass production operation; on the other hand it is impossible to use well aligned fibres and fibres longer than a few millimetres. Properties of fibre reinforced composites are improved when compression moulding is used instead of injection moulding. It is because long fibres can be used and their orientation can be controlled (Riedel and Nickel, 1999). Compression moulding uses thermoplastic pre-impregnated fibres and fabrics which are heated and pre-compacted under slight pressure and subsequently transferred to a pre-heated mould where they are compressed at higher pressure to get the desired shape. Processing temperature has an important influence on the mechanical properties of thermoplastic composites especially when matrix morphology development is desirable to improve the fibre to matrix adhesion. If the transcrystalline morphology has to be developed to improve the material properties, a tight control of thermal history is necessary. If the polymer matrix crystallizes slowly it slows down

the processing and injection moulding loses its main advantage over compression moulding (Ye *et al.*, 1995).

A naturally occurring material which is made of polymers reinforced with cellulosic fibres is wood. Generally speaking natural fibre composites may have superior mechanical properties compared to wood as they replace naturally occurring weak matrix (lignin) with engineering polymers. In contrast to wood it is possible to control the properties of natural fibre composites in different directions so they can adapt to the desired end-use application (Luo and Netravali, 2001). Furthermore wood (i.e. its main constituent cellulose) is not a thermoplastic material so it cannot be shaped by thermoforming or injection moulding (wood can be shaped by steam bending). An example of successful application of natural fibre composites in building industry are wood-fibre plastic composites (WPCs) which are currently replacing timber and synthetic polymers in non structural applications like decking, railings, fencing, window/door profiles, siding, shingles, flooring and wall frames. The WPCs are composed of wood flour/short wood fibres and thermoplastic matrix like polypropylene, polyethylene and polyvinylchloride. The market for WPCs in United States was estimated to be 350 millions of US $ (Hughes, 2004). Dimensional stability is usually mentioned as a disadvantage when natural fibre composites are compared to glass fibre composites. Glass fibres do not absorb water but when exposed to an atmosphere with high relative humidity they lose their strength due to leaching of soluble oxides (Ramirez *et al.*, 2008). The dimensional instability of natural fibre composites can be overcome by effective product design. Another usually mentioned disadvantage - water absorption - can be reduced by protective surface coating or fibre acetylation (Mwaikambo and Ansell, 1999) or a combination of both. A great advantage of natural fibre composites is the after use disposal: the material can be converted into heat energy by controlled burning or basically disposed of in a controlled landfill. It is concluded that modern science has enough means to engineer the properties of natural fibres and their polymer composites so suitable material with low environmental impact for structural applications can be developed.

1.2 Objectives

The thesis describes preparation of natural fibre composites from polylactic acid (PLA) and sisal fibres. The main objectives of the thesis were to:

- Prepare structural composites where both the matrix and the fibre are bio-sourced and biodegradable.
- Study the adhesion between the fibres and the matrix.
- Study the matrix morphology development at fibre to matrix interface.
- Study the influence of matrix morphology on fibre to matrix adhesion by modifying the crystalline structure of the PLA.
- Study the influence of caustic soda treatment on fibre to matrix adhesion, matrix morphology development and mechanical properties of composites.

The principal aim of the project was to design structural composite material where both the matrix and the fibres would be bio-sourced and biodegradable. It was decided to combine polylactic acid as a matrix with sisal fibres. Sisal fibres are nice and clean. The main reason for their choice was their low microfibril angle which is closely parallel to the cell axis. Some of the sisal fibres were caustic soda treated. Caustic soda changes the supramolecular structure of cellulose and is reported to improve the mechanical properties of natural fibres like hemp and sisal. (Mwaikambo and Ansell, 1999). The presence of a crystalline phase in semicrystalline thermoplastic usually improves its strengths and stiffness, chemical and heat resistance. It has been shown in the literature from the microbond test that the interfacial bond strength in several single fibre / thermoplastic composites can be raised up to several tens of % because of the presence of transcrystalline morphology (Zafeiropoulos *et al.*, 2001). In other words: strong fibre to matrix interface can be created intrinsically *in situ* without costly chemicals just by optimal cooling conditions during the processing.

There were some restrictions which had to be taken into account during the material processing. Natural fibres start to degrade at temperatures above 170°C. Polylactic acid (PLA) was chosen as a matrix because among the biodegradable thermoplastics it has the highest glass transition temperature T_g (which affects the end use temperature) and good mechanical

properties. The PLA melting temperature (T_m) is 170°C. Typical processing temperatures are usually 20-30°C higher to reduce the melt viscosity. Application of higher temperature to further reduce the melt viscosity and to wet the fibres does not help: temperatures higher than 230°C are not recommended as they cause PLA degradation and yellowing. Higher temperatures are also not good for the fibres which degrade and release water. Water at high processing temperatures can catalyse the chain scission of the polymer macromolecules. This results in strength reduction and void formation. In conclusion the processing of bio-based thermoplastics reinforced with natural fibres is demanding and challenging process which requires tight control of processing parameters.

1.3 Project description

To optimize the properties of biocomposite and to overcome some processing challenges the fibres were unidirectionally aligned prior to compression moulding and combined with thin polymer sheets. An aluminium mould was used to reduce the time the material needed to dwell at higher temperatures. Figure 1.1 shows schematically the project description, relationship between individual project levels and routes to producing the resulting composite. For example some of the fibres were caustic soda treated in order to improve their mechanical performance, promote the morphology development at fibre to matrix interface and produce stronger composites.

The hot stage microscopy was used to study the morphology development at fibre to matrix interface and to prepare micro-composites to test the strength of the fibre to matrix interface.

Through the hot stage one can check the influence of the fibre surface modification and thermal history on fibre to matrix adhesion. Such knowledge enables the microstructure of the composite to be engineered. As a first approximation one can expect stiffer and stronger interface with crystalline morphology around the fibres as a result of annealing at optimum crystallization temperatures (T_c) during melt solidification. The knowledge of thermal history-structure relationship is important for choosing the right processing cycle. Mechanical properties of resulting composites were evaluated with tensile, flexural and interlaminar shear strength test. The glass transition temperature as well as dynamic mechanical properties were evaluated by means of dynamic mechanical thermal analysis (DMTA). The glass transition

temperature and the melting temperature of the polymer matrix as well as the crystallinity development in single fibre micro-composites were studied by differential scanning calorimetry (DSC).

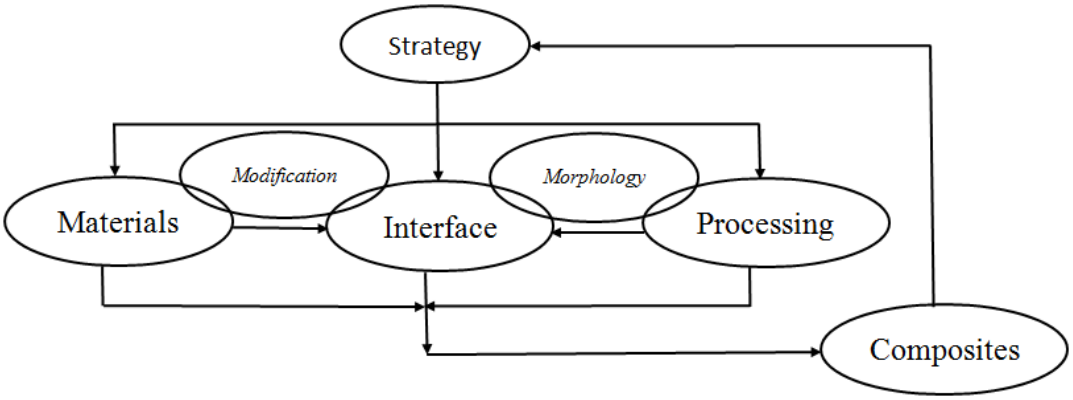

Phase	Materials	Interface	Processing	Composites
Variables	σ_T, E_T, T_g, T_m, E' E'', X_c	τ_{IFSS}, X_c Image analysis	ΔT, ΔP, Δt	σ_T, E_T, T_g, T_m, E' E'',X_c, τ_{ILSS}
Methods	Tensile test DMTA DSC	Hot stage SEM DSC Pull-out test	Compression moulding	Tensile test Flexural test ILSS test DMTA
Aims	Characterization	Adhesion Stress transfer optimization	Optimization	Characterization

Figure 1.1: Project description.

1.4 Layout of chapters

The thesis consists of eleven chapters. Chapter 1 is an introduction to the topic: it forms the background, states the aims and objectives and describes the project. Chapters 2 to 5 form the theoretical basis of the thesis and Chapters 6 to 8 deal with the experiments. Chapter 1 provides an introduction to the subject. The aim is to establish the background of the project,

set up the objectives and outline how to reach them. Chapter 2 focuses on natural fibres which are used as reinforcement in composite materials. The structure of natural fibres is described in detail in relation to their mechanical properties. Physico-mechanical properties of main vegetable fibres are reviewed. Specific fibre properties of natural fibres are compared to man-made fibres. Last section focuses on structural changes of cellulose due to the caustic soda treatment. Chapter 3 provides detailed description of polylactic acid (PLA). It starts with an introduction to thermoplastic polymers. It continues with PLA synthesis. Polylactic acid can be synthesized through a ring opening polymerization of lactide or by direct polycondensation of lactic acid. Development of crystalline morphology is discussed. Thermo-mechanical properties of polylactic acid are compared to conventional thermoplastics. Biodegradability, sustainability and end of use disposal are also discussed. The chapter finishes with the potential use of PLA in industrial applications. Chapter 4 treats composites with thermoplastic matrices. It covers the selection of the most appropriate bio-based matrix for natural fibre composites which are supposed to have structural qualities. The core of the chapter focuses on the review of the mechanical properties and processing technology of composites from thermoplastic matrices and natural fibres. Composites reinforced with long and short fibres are reviewed. The chapter finishes with recycling of natural fibre composites with thermoplastic matrices. Chapter 5 is devoted to composite interfaces. It is divided into three major sections. Firstly the theory of adhesion will be outlined followed by the most used strategies for adhesion optimization in thermoplastic composites reinforced with natural fibres. The second part of the chapter will be dedicated to polymer crystallization and the matrix morphology development in the presence of a fibre. The third section of the chapter is dedicated to the micromechanics and stress transfer at the interface. It starts with the law of mixture. Further the stress transfer in composites based on the shear lag theory will be explained. The models of single fibre fully embedded in a matrix and single fibre with an exposed end are presented. It follows with the fracture mechanics approach to measure the adhesion strength of the interface. The chapter concludes with the development of residual strains in a semicrystalline matrix and their influence on adhesion.

Experimental methods and their principles as well as materials are presented in Chapter 6. Matrix and fibres used in the composites manufacture are introduced followed by experimental methods to measure their physico-mechanical properties. Dynamic moduli and

the glass transition temperatures are measured with dynamic mechanical thermal analysis (DMTA). Transition temperatures and melting enthalpies are determined with differential scanning calorimetry (DSC). Hot stage microscopy which is used to follow the spherulitic growth at the fibre to matrix interface is introduced. Metallographic procedure to prepare samples for scanning electron microscopy (SEM) is discussed as well as the SEM fundamentals. The experimental procedure and statistical analysis to measure the strength of fibre to matrix adhesion is described. Finally methods to measure the mechanical properties of manufactured composites in tension and flexure will be outlined.

Several test samples were used in this study. The chapter 7 starts with hot pressing of polymer sheets, dog bones and bars for tensile and flexural test. It continues with the preparation of thin film samples for hot stage microscopy and partially embedded single fibre specimens for the microbond shear test. The chapter finishes with compression moulding of polymer composites reinforced with long fibre bundles. Processing of long fibre bundles composites made of natural fibres and its peculiarities are discussed.

Chapter 8 presents the experimental results. It starts with mechanical properties of sisal fibres and polylactic acid. It continues with the transcrystalline morphology development and results on fibre to matrix adhesion strength measurement. The mechanical and dynamic-mechanical properties of polylactic acid reinforced with sisal fibres are decribed.

Chapter 9 and 10 provide the discussion and the main conclusions. Chapter 11 gives some general suggestions on future work.

The appendices present data sheets for the materials used in the experimental work, the compression mould drawings, experimental results, detailed information on sisal fibres and hot stage microscopy images.

2 Structure and properties of natural fibres

This chapter focuses on the structure and properties of natural fibres which are used as reinforcement in composite materials. The structure of natural fibre is described in detail in relation to their mechanical properties. Physico-mechanical properties of the main vegetable fibres are reviewed and the specific fibre properties of natural fibres are compared to man-made fibres. The last section focuses on structural changes to cellulose following caustic soda treatment.

2.1 Introduction

In this chapter the structure and mechanical properties of natural fibres will be described and related to their performance in fibre reinforced composites. Understanding the structure–property relationships of fibres is a key issue for the design of composite materials and their industrial application. Natural fibres can be classified as wood fibres (softwoods and hardwoods), plant fibres (cotton, flax, hemp etc.), animal fibres (wool, silk etc.) and mineral fibres (inorganic whiskers). In this thesis the term "*natural fibre*" refers to plant fibres which exist as stem (or bast) fibres (e.g. jute), leaf fibres (e.g. sisal), seed fibres (e.g. cotton) and fruit fibres (e.g. palm). Plant fibres usually consist of multicellular arrays of elongated cells with high length to diameter ratio and a hollow central cavity. Each cell is called an *ultimate fibre* in engineering terminology or *tracheid* in botanical terminology. Tracheids are the cells which primary task is the water and nutrients distribution from plant roots into the whole plant (Toonen *et al*., 2007). They are long, strong and stiff and thus of technical interest and can be used as reinforcement in polymer composites. The cellular arrays which are used as fibres for polymer reinforcement or spun into yarns in textile applications are called *fibre bundles* (Vincent, 1982). Plant cells are surrounded by a rigid cell wall. During the plant growth, when the fibre is fully developed, intracellular organelles die and a hollow cavity called the lumen is formed. The main difference at cellular level between plant and animal species is that animal cells are not surrounded by a rigid cell wall. The cell wall consists of four layers, each layer is micro-structured and composed of cellulose, hemicelluloses and lignin at molecular level.

Cellulose polymer chains are organized in parallel arrays which are called *microfibrils* (Figure 2.1) Cellulose organized into microfibrils can be viewed as the "fibre" component of the cell wall whereas hemicelluloses and lignin can be viewed as the "matrix".

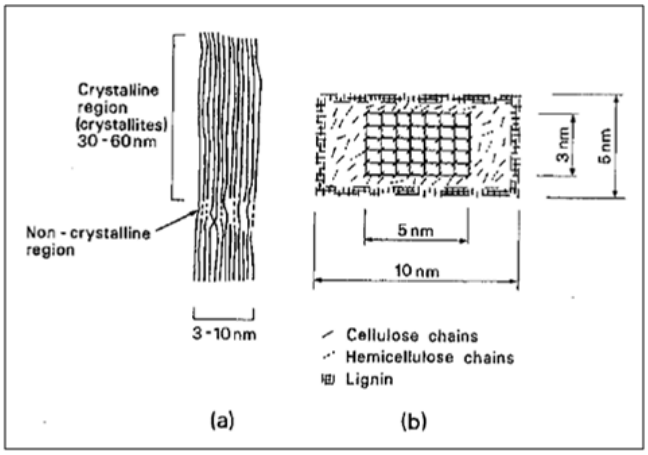

Figure 2.1: Proposed structure of a microfibril (Dinwoodie, 2001); (a) crystalline core in longitudinal section and (b) transverse section of core and surrounding matrix.

It is the scope of this chapter to find out where the strength and the stiffness of a plant fibre come from. It is not surprising that mechanical properties of natural fibres and their fibre bundles will be derived from the cell wall structure.

2.2 Chemical constituents of natural fibres

The principal chemical constituents of natural fibres are cellulose, hemicelluloses and lignin.

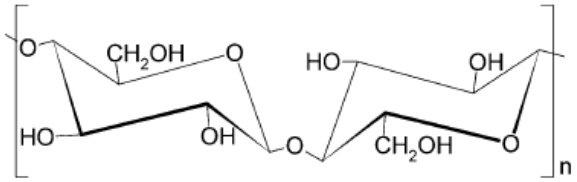

Figure 2.2: Cellulose structure(Sjöström, 1993).

These are the main chemical building blocks of the cell wall. Cellulose has an empirical formula $(C_6H_{10}O_5)_n$. It is a linear polysaccharide consisting of D-anhydro-glucopyranose units

joined together by β-1.4-glucosidic bonds (Figure 2.2). Each of the D-anhydro-glucopyranose units has one primary and two secondary hydroxyl groups which are responsible for inter and intra-molecular bonding in crystalline regions of a microfibril. The cellulose molecule is less flexible than polyethylene but much more flexible than Kevlar (poly(*p*-phenylene terephthalamide)). The flexibility comes from the rotation around the β-1.4-glucosidic bond between the two adjacent glucose rings (Carr, 1995). The cellulose molecule has a more or less rectangular cross section and a ribbon-like structure so in-plane bending is impossible but out-of plane bending is possible. In plane bending is only possible in association with twisting in the plane of the glucose ring (Figure 2.3).

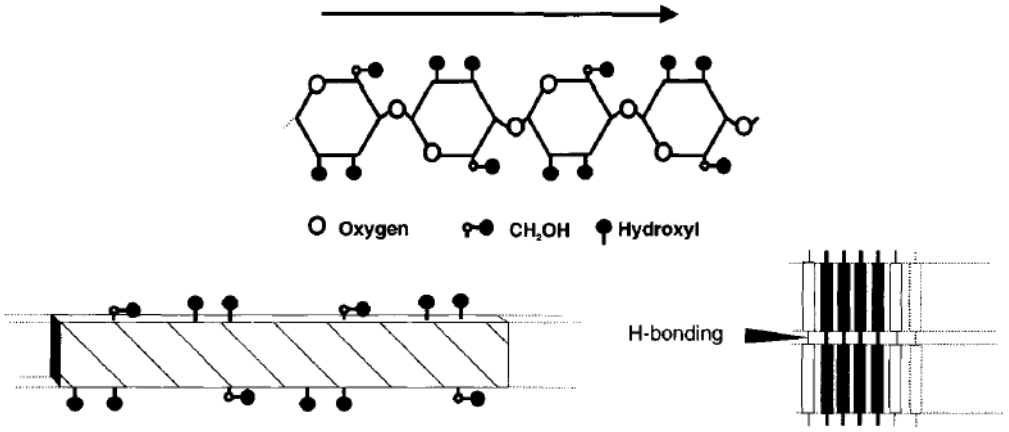

Figure 2.3: Ribbon-like structure of cellulose molecule (Carr, 1995).

Cellulose is a semicrystalline polymer and hydrogen bonds in the crystalline regions establish the crystalline morphology. Due to the extensive amount of hydrogen bonding in cellulose it is impossible to measure its melting temperature. When heated up cellulose does not behave thermoplastically. It does not melt and flow as the energy necessary for the destruction of intermolecular hydrogen bonds is high enough for cellulose thermal decomposition. In higher plants cellulose is found in the crystalline form of so called cellulose I (Figure 2.4). There have been several structural models proposed for cellulose I. According to Dinwoodie (1989) the mostly accepted one was proposed by Gardner and Blackwell (1974) who proposed a two chain model (one central plus four quarter chains), with monoclinic unit cell parameters of a=0.817 nm, b=0.786 nm, c=1.038 nm and γ=97° and parallel configuration of chains. In this

model the cellulose molecules are organized in parallel *ac* planes and the intermolecular hydrogen bonds in *cb* planes.

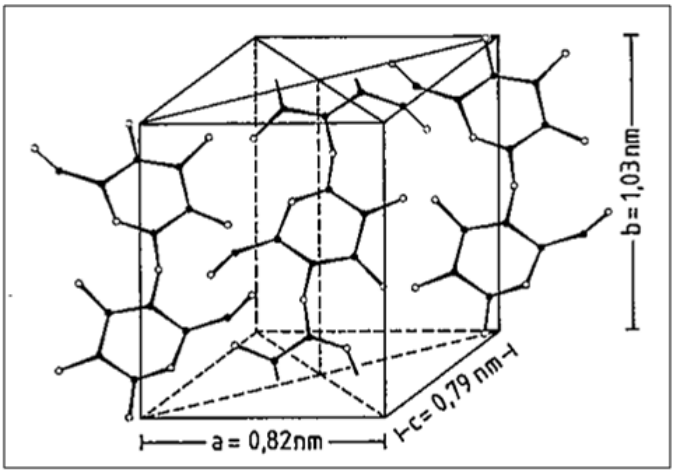

Figure 2.4: Monoclinic unit of cellulose (Fengel and Wegener, 1984).

Cellulose is a partially crystalline polymer with several crystal modifications. Figure 2.5 shows the transformation procedure among the cellulose polymorphisms.

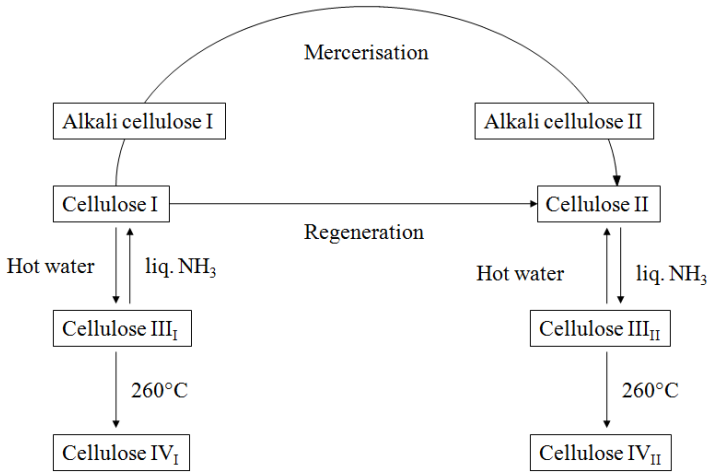

Figure 2.5: Crystal transformation map of a series of celluloses (Nishino, 2004).

Table 2.1 summarizes the elastic moduli of crystal cellulose polymorphisms.

Table 2.1: Crystal modulus E_I, cross sectional area S of a molecule in a crystal lattice, f-value and fibre identity period of cellulose polymorphs (Nishino *et al*., 1995).

Cellulose	E_I	**S	*f	FIP
	[GPa]	[Å^2]	[10^{-5} dyn]	[Å]
I	138.00	31.90	4.40	10.38
II	88.00	32.50	2.86	10.33
III_I	87.00	33.90	2.95	10.34
III_{II}	58.00	33.40	1.94	10.24
IV_I	75.00	32.70	2.45	10.37
Polyethylene	235.00	18.20	4.28	2.53

Note: *f = a force necessary to stretch a molecule by 1%; **S = cross section of a molecule in a polymer lattice; FIP = fibre identity period - the shortest distance along the chain axis for translational repetition of the chain structure (Allegra *et al*. 1989).

The elastic modulus of crystalline cellulose I in the direction parallel to the polymer chain axis was measured by X-ray diffraction and determined to be 138 GPa (Nishino *et al*., 1995; Table 2.1). The elastic modulus of cellulose I crystal is about two thirds of that of polyethylene. Their f-values are almost identical which means both PE and Cellulose I have the same extensibility and that the lower value of cellulose I E_I results from the large cross sectional area of one molecule in the crystal lattice. Nishino (2004) relates the low crystal modulus of cellulose II to the chain contraction in the crystal lattice and the decreased f-value and their effect on intramolecular hydrogen bonds. The chain contraction can be explained by the molecule rotation around the main chain ether linkage between the glucopyranose rings. Table 2.2 summarizes unit cell parameters of cellulose polymorphisms and their natural occurence. Hemicellulose is a mixture of low molecular weight (~200 units) branched and hydrophilic polysaccharides which are synthesized from glucose, mannose, galactose, xylose, arabinose, galacturonic acid and 4-O-methylglucuronic acid (Dinwoodie, 1989). Hemicelluloses (also called polyoses) are bonded to cellulose chains through non-covalent hydrogen bonds and enable their packing into microfibrils (Teeri *et al*, 2007). Lignin is a randomly branched polysaccharide consisting of a three-dimensional structure of cross-linked hydroxy- and methoxy- substituted phenylpropane units. Figure 2.6 displays the association of cellulose, lignin and hemicelluloses in the cell wall. Lignin is an amorphous thermoplastic with T_g ~108°C (Kadla and Kubo, 2004) and softening temperature of 120-150°C (Gosselink *et al*.,

2004). There are also complex organic compounds with no structural function present in natural fibres which are called extractives. They are usually toxic to micro-organisms and help to protect the plant fibres against the enzymes of biological predators.

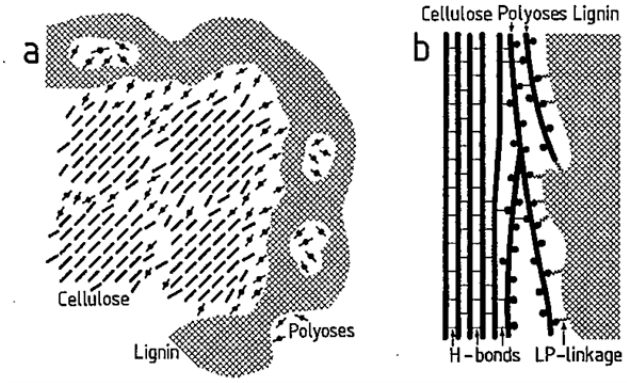

Figure 2.6: Association of cellulose, lignin and hemicelluloses in the cell wall; (a) transverse sction and (b) longitudinal section (Fengel and Wegener, 1984).

Table 2.1: Unit cell parameters[a] of cellulose (modified after Ganster and Fink, 2005).

Cellulose	Space group	Crystal system	a	b	c	α	β	γ
			[Å]	[Å]	[Å]	[°]	[°]	[°]
I_α	P1	Triclinic	6.74	5.93	10.36	117	113	81
I_β	$P2_1$	Monoclinic	7.85	8.14	10.34	90	90	96.6
II	$P2_1$	Monoclinic	8.01	9.04	10.36	90	90	117.1
III			10.25	7.78	10.34	90	90	122.4
IV			8.01	8.12	10.34	90	90	90

Note: [a]Parallel arrangement of chain packing is widely accepted for cellulose I, antiparallel packing for cellulose II. The I_α cell contains single chain with two glucose units whereas all the other cells contain two chains with two glucose units each.

2.3 Fibre structure

The cell wall of an ultimate fibre is multi-layered and the specific structure develops during plant growth (Figure 2.7).

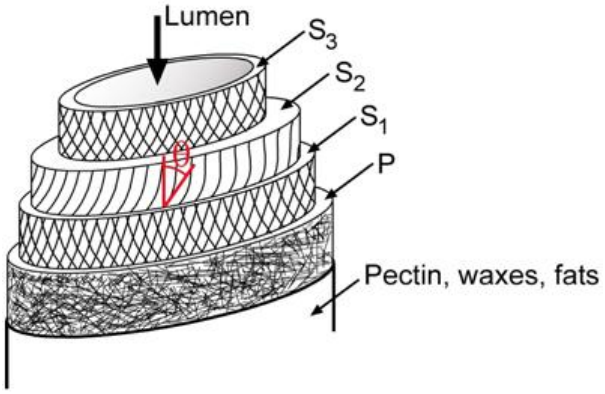

Figure 2.7: Cell wall structure (Aziz and Ansell, 2004).

The thin outer layer is called the primary wall as it is the first layer deposited during the cell development. The inner layer, secondary wall, is composed of three layers denoted as S1, S2 and S3. The S2 layer is the thickest and is built up mostly of cellulose. Microfibrils in the S layer are helically wound around the cell longitudinal axis: microfibrils in the S1 and S3 layer are disposed at a high microfibril angle to the cell axis (large microfibril angle), microfibrils in S2 layer are close parallel to the cell axis (smaller angle) (Dinwoodie, 2000).

Table 2.2: Chemical composition of selected plant fibres (Mwaikambo, 2006).

Plant fibre	Cellulose (%)	Hemicellulose (%)	Lignin (%)	Pectin (%)
Cotton[s]	82-96	2-6.4	0-5	<1-7
Flax[b]	60-81	14-20.6	2.2-5	1-4
Hemp[b]	70-92	18-22	3-5	1
Jute[b]	51-84	12-20	5-13	0.2
Kenaf[b]	44-87	22	15-19	2
Sisal[l]	43-78	10-24	4-12	0.8-2

[s]seed, [b]bast, [l]leaf fibres

As the S2 layer contains most of the cellulose microfibrils of the cell wall and these microfibrils are close parallel to the fibre longitudinal axis, the S2 layer determines

mechanical properties of the ultimate fibre (Bos *et al*., 2006; Fengel and Wegener, 1984). The chemical composition and structure of the cell wall vary among different plant fibres (Table 2.2).

2.4 Physical and mechanical properties of natural fibres

The importance of chemical composition and supramolecular structure of individual chemical constituents on physico-mechanical qualities of natural fibres is summarised in Table 2.3.

Table 2.3: Properties of natural fibres in correlation with their chemical composition (Sain an Panthapulakkal, 2004).

Strength	Thermal degradation	Moisture absorption
Crystalline cellulose	Hemicellulose	Hemicellulose
Non-crystalline cellulose	Cellulose	Non-crystalline cellulose
Hemicellulose + Lignin	Lignin	Lignin
Lignin	-	Crystalline cellulose
UV degradation	Biological degradation	
Lignin	Hemicellulose	
Hemicellulose	Non-crystalline cellulose	
Non-crystalline cellulose	Crystalline cellulose	
Crystalline cellulose	Lignin	
Note: Chemical constituents are listed according to the influence they have on a fibre quality, i.e. the most quality responsible chemical constituent is listed first in each column.		

Chemical constituents are listed according to the influence they have on a fibre quality, i.e. the most quality responsible chemical constituent is listed first in each column. For instance, amorphous cellulose and hemicelluloses are the most sensitive cell wall constituents to moisture absorption. Their moisture sensitivity comes from the lack of supramolecular structure. Lignin has a molecule which is three dimensionally cross-linked hence its higher moisture resistance compared to hemicelluloses. Crystalline cellulose is water resistant as a result of its supramolecular structure. In amorphous regions cellulose hydroxyl groups which are exposed at the edges of the molecule do not form inter- and intra-molecular bonds. Thus

when amorphous regions are attacked by water diffusion the hydroxyl groups can form hydrogen bonds with water molecules which can easily penetrate into the cell wall which swells. Higher ordered cellulose crystallites are also resistant to the attack of enzymes which may cause the biological degradation. Their intra and intermolecular hydrogen bonds as well as the cross-linked structure of lignin contribute to the thermal resistivity of natural fibres. The lignin molecule contains aromatic rings hence its susceptibility to absorb UV light. The formation of hydrogen bonds between cellulose chains of crystalline cellulose also explain its mechanical strength compared to other cell wall constituents. In other words the higher degree of crystalline order results in a higher elastic modulus and better chemical stability as the foreign molecules can penetrate easily into the structure.

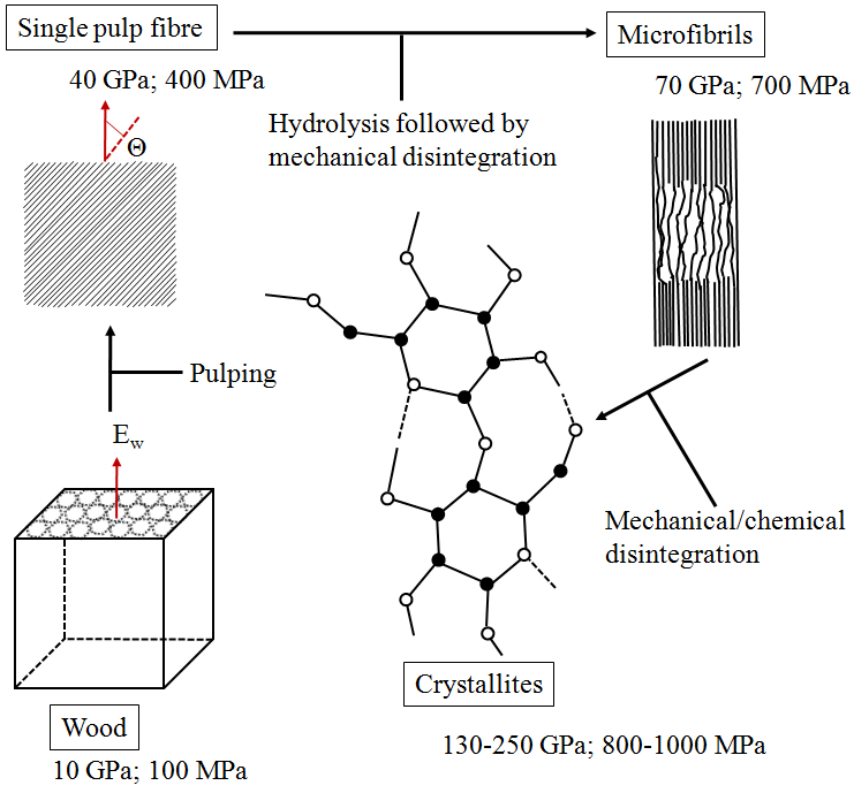

Figure 2.8: Reinforcing elements derived from wood with their elastic modulus and strength (modified after Zadorecki, 1989 and Zimmermann *et al*., 2004).

Theoretical models for the stiffness calculations of natural fibres usually use wood as a model material and are based on the determination of the cellulose I crystal modulus. Values of the cellulose I elastic modulus reported in the literature can vary considerably (Figure 2.8). Powell

(1994) identified the key structural components of wood at molecular and cellular level, estimated their strength and stiffness and calculated the overall stiffness of the wood using the rule of mixtures. The key structural element which is responsible for the strength and stiffness of wood cells (tracheids) is the microfibril. It is composed of long cellulose molecules embedded in a weaker and more flexible matrix of lignin and hemicelluloses. One cellulose molecule comprises 8-10 000 monomer units and is about 5 μm long. Because the crystalline regions in microfibrils are about 30-60 nm long, one cellulose molecule passes through several crystalline and amorphous regions. The microfibril can be treated as a composite where each of the constituents has its own function, modulus and volume fraction:

- Modulus of elasticity of crystalline cellulose, $E_c \approx 130\text{-}250$ GPa
- Modulus of elasticity of amorphous cellulose, $E_a \approx 50$GPa
- Modulus of elasticity of the matrix composed of lignin and hemicelluloses, $E_m \approx 1$GPa
- Volume fraction of crystalline regions of cellulose in a microfibril, $V_c \approx 0.4$
- Volume fraction of amorphous regions of cellulose in a microfibril, $V_a \approx 0.1$
- Volume fraction of the matrix composed of lignin and hemicelluloses, $V_m \approx 0.5$.

Applying the rule of mixture the longitudinal modulus of a microfibril can be estimated as E_{fib}=80 GPa. The modulus of the wood tracheid secondary cell wall (S2) with the microfibril angle of θ=10° to the longitudinal axis of the tracheid can be estimated as $E_{S2} \approx E_{fib}\cos^4\theta$=75 GPa. Neglecting other cell wall layers and knowing that the volume fraction of S2 layer in a cell wall is $V_{S2} \approx 0.8$ the axial modulus of a tracheid can be calculated as $E_{trach} \approx V_{fib}E_{S2}$=60 GPa. Taking into account that the cellular material of wood is about 25 % of wood volume (Powell, 1994), the longitudinal modulus of wood (i.e., along the axis of the tracheids) can be calculated as 15 GPa. Applying the same formulae and methodology to a sisal fibre and taking the average microfibril angle θ=16° (Table 2.4) results in values of $E_{S2} \approx 59$ GPa, $E_{trach} \approx 47$ GPa and the overall longitudinal modulus $E \approx 11.8$ GPa for a sisal fibre. Oksman *et al*. (2002) prepared composites of epoxy resin and sisal fibres and measured the composite E values of about 20 GPa for a fibre volume fraction of 46 % suggesting a fibre E value of ~40 GPa. Hence natural fibres exceed the E value for wood along the grain by a factor of over 2.5. The advantage is that they can be harvested annually or even several times per year depending on

the climate. The strength of natural fibres can vary due to the defects introduced during separation of mechanical fibres from the sisal leaves and due to growing conditions.

The shape of the cross section of synthetic fibres can vary considerably. Natural fibre bundles usually have non-circular cross sections. Figures 2.9 and 2.10 compare the cross sections of various synthetic fibres to the cross section of sisal fibre bundle.

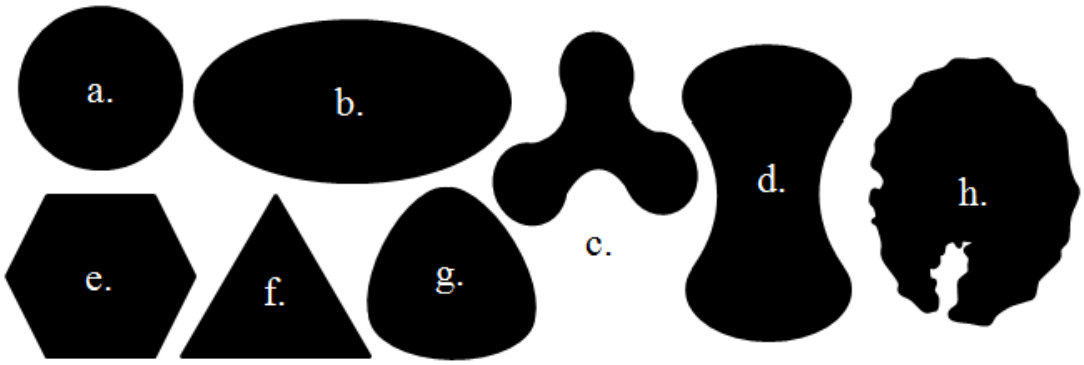

Figure 2.9: Fibres and their cross sections (after Chawla, 1998): a. Circular (glass, carbon, alumina, silicon carbide); b. Eliptical (alumina, mullite); c. Trilobal (carbon, rayon); d. Kidney bean (carbon); e. Hexagonal - sapphire (Al_2O_3) whiskers; f. Triangular (Silk, SiC whiskers); g. Rounded triangular - sapphire (Al_2O_3) single crystal fibre; h. Sisal fibre bundle (after Li and Mai, 2006). *Note*: the diameters are not to scale.

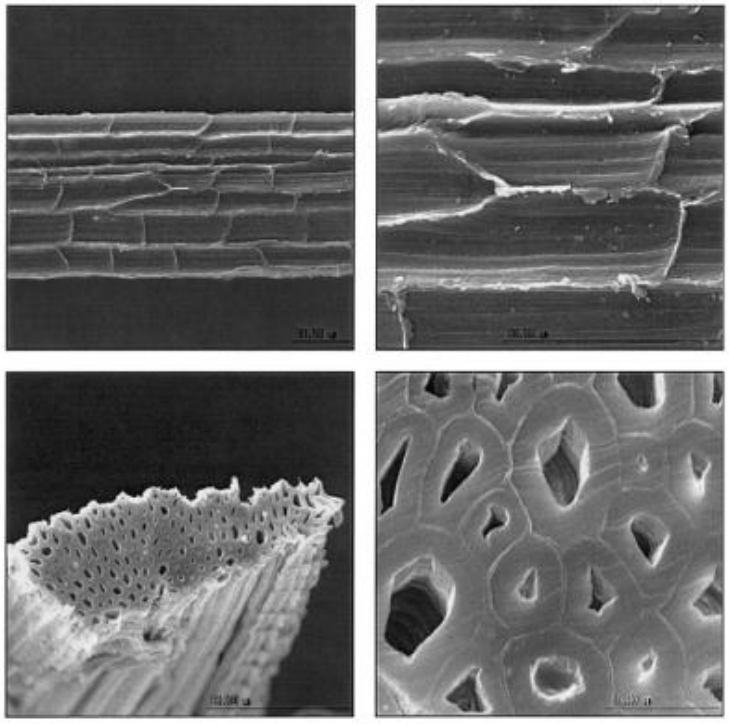

Figure 2.10: Longitudinal section and cross section of sisal fibre bundle (Oksman *et al.*, 2002).

Table 2.4: Physical and mechanical properties of selected plant and artificial fibres (Mwaikambo, 2006; [d]Bodros and Baley, 2008).

Plant fibre	Apparent density	Tensile strength	Young's modulus	Specific strength*	Specific modulus*	S_2 microfibril angle, θ
	[kg.m^{-3}]	[MPa]	[GPa]	[MPa]	[GPa])	[º]
Cotton[s]	1550	300-700	6-10	194-452	4-6.5	20-30
Flax[b]	1400-1500	500-900	50-70	345-620	34-48	5
Hemp[b]	1400-1500	310-750	30-60	210-510	20-41	6.2
Jute[b]	1300-1500	200-450	20-55	140-320	14-39	8.1
Kenaf[b]	1220-1400	295-1191	22-60	246-993	18-50	-
Sisal[l]	1300-1500	80-840	9-22	55-580	6-15	10-22
Nettle[b, d]	1530	954-2234	59-115	624-1460	39-75	-

Note: [s]seed, [b]bast, [l]leaf fibres; *ratio of the strength (modulus) and specific gravity ($\rho_{fibre}/\rho_{water}$)

Table 2.5: Properties of some important synthetic fibres (Chawla, 1998).

Material (fibres)	Tensile modulus	Tensile strength	Compressive strength	Density
	[GPa]	[GPa]	[GPa]	[g/cm^3]
Steel	200	2.8	-	7.8
Al-alloy	71	0.6	-	2.7
Ti-alloy	106	1.2	-	4.5
Alumina	350-380	1.7	6.9	3.9
Boron	415	3.5	5.9	2.5-2.6
SiC	200	2.8	3.1	2.8
S-glass	85	2.0-4.5	> 1.1	2.48
E-glass	69-72	2.0-4.5	-	2.54
C-glass	70	1.7-2.8	-	2.48
Carbon P 100 (pitch-based)	725	2.2	0.48	2.15
Carbon M60J (PAN based)	585	3.8	1.67	1.94
Kevlar 49	125	3.5	0.39-0.48	1.45
Kevlar 149[e]	185	3.4	0.32-0.46	1.47
PBZT[a]	325	4.1	0.26-0.41	1.58
PBO (Zylon®)[b]	360	5.7	0.2-0.4	1.58
Spectra® 1000 (PE)	172	3.0	0.17	1.0
Vectran®[c]	65	2.9	-	1.4
Technora®[d]	70	3.0	-	1.39
Nylon	6	1.0	0.1	1.14
Textile PET	12	1.2	0.09	1.39

Note: [a] poly(*p*-phenylene benzo*bis*thiazole); [b] poly(*p*-phenylene benzo*bis*oxazole); [c] liquid crystal polymer of aromatic polyester; [d] aramid fibre; [e] higher degree of crystallinity compared to Kevlar 49.

Tables 2.4 and 2.5 summarize the mechanical properties of selected natural and synthetic fibres. The strength and stiffness of natural fibres are low compared to the glass fibres but their specific properties are comparable or even higher due to the low density of natural fibres. The technical potential of natural fibres is clearly demonstrated especially when the strength-to-weight ratio is the criterion for materials selection. The main limiting factor for greater exploitation of natural fibres in composites industry is probably the reproducibility of their mechanical properties. The mechanical properties of plant fibres are also determined by plant variety, growth conditions, plant maturity at harvest and fibre extraction method. These factors are difficult to control. The manufacture of a product with consistent and repeatable quality is thus difficult. To overcome this disadvantage research on regenerated cellulose fibres as reinforcement for composite materials has been carried out by many researchers (Bax and Müssig, 2008).

2.5 Fibre modification

In this section the effect of aqueous sodium hydroxide solution on the structure and structural integrity of native cellulose will be discussed. Caustic soda treatment of cellulose is an important technical process which is used for the manufacture of regenerated cellulose. The process is called mercerization (1850) and is named after John Mercer (1791-1866) who first noticed the positive effect of aqueous sodium hydroxide solution on cotton properties including higher lustre, lower density, less crystallinity, improved dyeability and increased tensile strength. In 1889 Lowe found that the length contraction can be avoided if the fibres are stretched during mercerization. Typically 200g of NaOH are diluted in 1000g of water (0.17 wt%) and the solution is applied at 10-20°C for 30-180 seconds (Carr, 1995). Mercerization is a physical process. Cellulose swells in strong aqueous alkali solutions. The swollen polymer is called alkali or soda cellulose or Na-cellulose. Application of aqueous sodium hydroxide solution on cellulose results in conversion of crystalline structure from Cellulose I to Cellulose II (Mwaikambo and Ansell, 2002, 2006a and 2006b, Bismarck *et al*., 2001). Figure 2.11 shows SEM micrographs of alkali treated sisal fibre after application of

NaOH solutions of 2 and 5 wt% concentrations. As can be seen the surface of the treated sisal fibre is clean and smooth compared to the surface of the untreated sisal fibre.

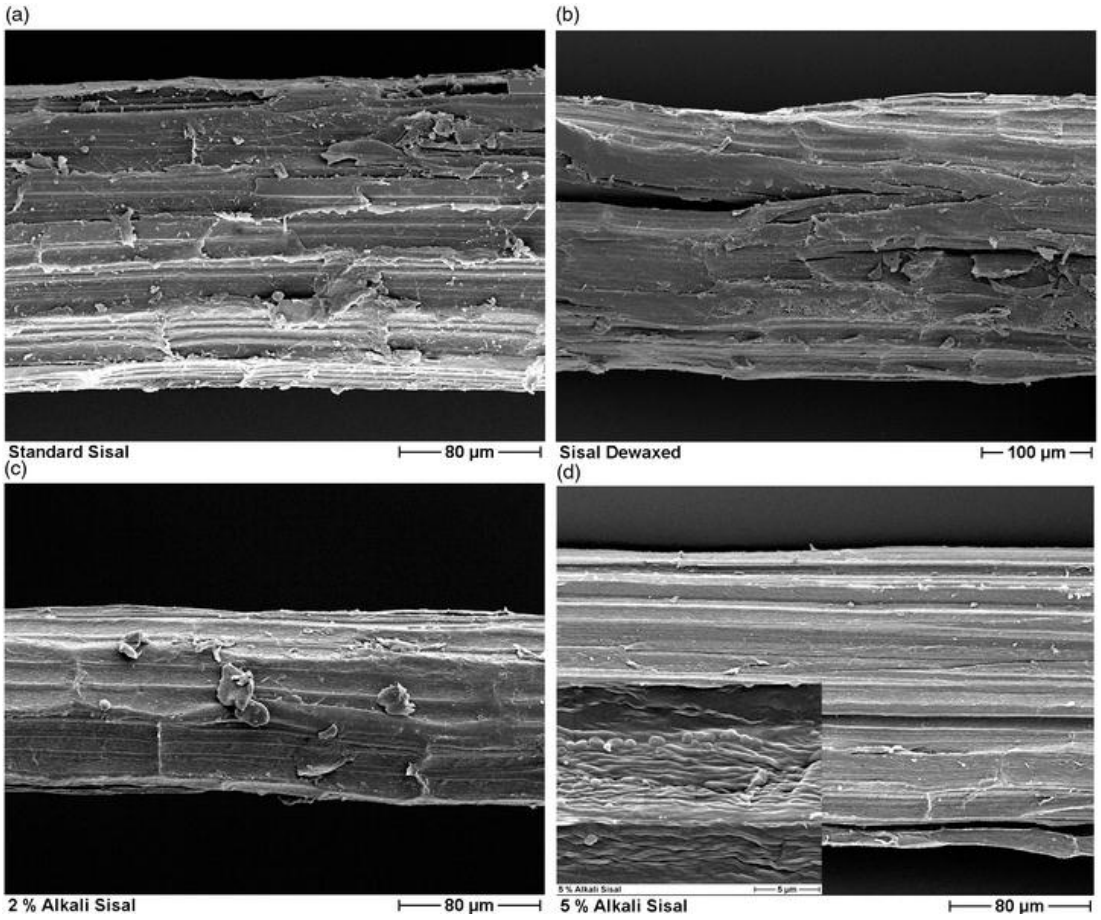

Figure 2.11: SEM micrographs of alkali treated sisal fibre surface morphology; a – untreated sisal fibre bundle; b –dewaxed surface of sisal fibre bundle; d – sisal fibre bundle treated with aqueous caustic soda solution (2 wt%); d - sisal fibre bundle treated with aqueous caustic soda solution (5 wt%) (Bismarck *et al*., 2001).

After soaking cellulosic fibre in aqueous NaOH solution of low concentration Krässig (1993) reported length shrinkage and increased cross-sectional area and the fibre became more circular. Kamide (1990) and his co-workers studied the mechanism of native (cellulose I) swelling in aqueous alkali solutions of different concentrations (7-12 wt%) at different temperatures (-5 to 30°C) with X-ray diffraction. Cellulose was allowed 60 minutes to swell. Dissolution occurred in 8-10 wt% concentrations with maximum dissolution at 4°C in NaOH solution of 8.5-9 wt%. The cellulose dissolution is higher at lower temperatures. They have

concluded that concentrations of 1-7 wt% lead to no structural changes in cellulose and that cellulose did not dissolve in NaOH solutions of lower concentrations. Only aqueous NaOH solutions of specific concentrations of 8-9 wt% lead to cellulose dissolution into solution. The dissolution starts at amorphous regions and the specific concentration causes widening of the cellulose I crystal lattice in the (002) plane. There was no dissolution in >11wt% but conversion of cellulose I to structurally stable Na-cellulose-I. Isogai and Atalla (1998) found that celluloses from higher plants which have a high degree of polymerization are only partially soluble in aqueous NaOH, only up to 37 %. They also came to the conclusion that hemicelluloses have no influence on cellulose dissolution but lignin reduces the cellulose solubility into aq. NaOH. Kamide *et al*. (1992) proved that the cellulose I dissolution into aqueous NaOH is controlled by the degree of break-down of O_3—H---- O_5' intramolecular hydrogen bonds.

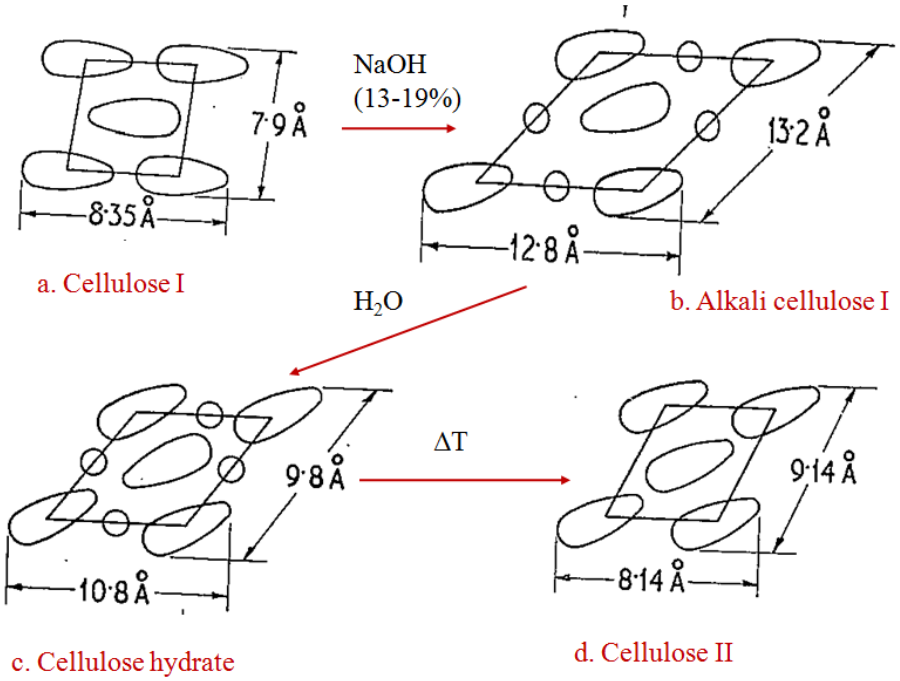

Figure 2.12: Diagram showing approximate arrangement of glucose units in cellulose I and II and alkali celluloses (modified after Trotman, 1964); (a) Cellulose I; (b) alkali-cellulose I; (c) replacement of NaOH by H_2O and cellulose-hydrate development; (d) cellulose II.

Trotman (1964) found that if the cellulose is treated with a solution of sodium hydroxide of 13-19 % concentration the space lattice changes and so called alkali-cellulose is formed. The

development of lattice changes are shown schematically in simplified manner in Figure 2.12. The lattice changes are irreversible. Roughly speaking, after the NaOH is removed by the diffusion of water molecules into the lattice and the cellulose is dried out, the lattice of cellulose I is distended and distorted and Cellulose II is created. Oval lines in Figure 2.12 represent glucose units in the space lattice. The little circles in steps (b) and (c) of Figure 2.12 represent NaOH and H_2O molecules respectively. Due to the action of alkali solution the inter and intra molecular hydrogen bonds which hold micro-fibrils together are interrupted (Figure 2.13).

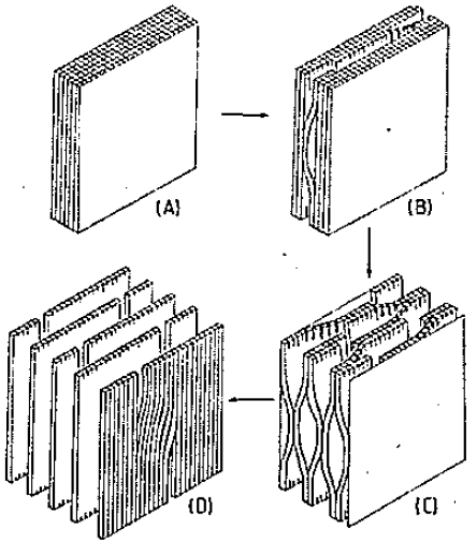

Figure 2.13: Proposed model of internal fibrillation of cellulose during swelling (Scallan, 1974).

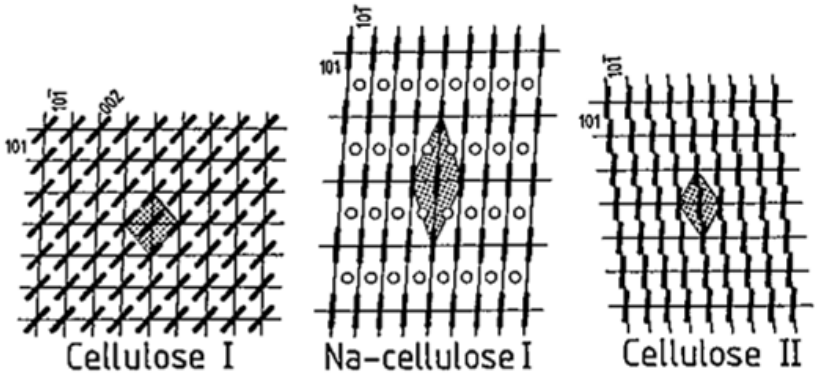

Figure 2.14: Changes of direction of molecular chains during the development of crystalline lattices of cellulose I, Na-cellulose and cellulose II. The dotted areas indicate the position of the space units (Fengel and Wegener, 1984).

On the molecular level the incorporation of alkali hydrate ions into the structure of cellulose I results in the dislocation of glucopyranose rings which lie in the 101 planes from their previous positions. Thus the hydroxyl groups pending on carbon atoms C(6) and C(2) project out of the plane into the wider space between the 101 planes (Krässig, 1993). Figure 2.14 shows the changes of direction of molecular chains during the development of cellulose II in cross section of the molecular chain at right angles to its longitudinal axis.

The cellulose II molecules are aligned approximately in the $10\bar{1}$ direction.

There are also dimensional changes of the space unit cell (Table 2.1 and Figure 2.14). Usually two parameters are reported to be responsible for the transformation of cellulose I into cellulose II: the concentration of sodium hydroxide solution and the temperature but the third parameter time should be also considered. The temperature is usually room temperature. Several concentrations of sodium hydroxide leading to cellulose lattice transformation are reported.

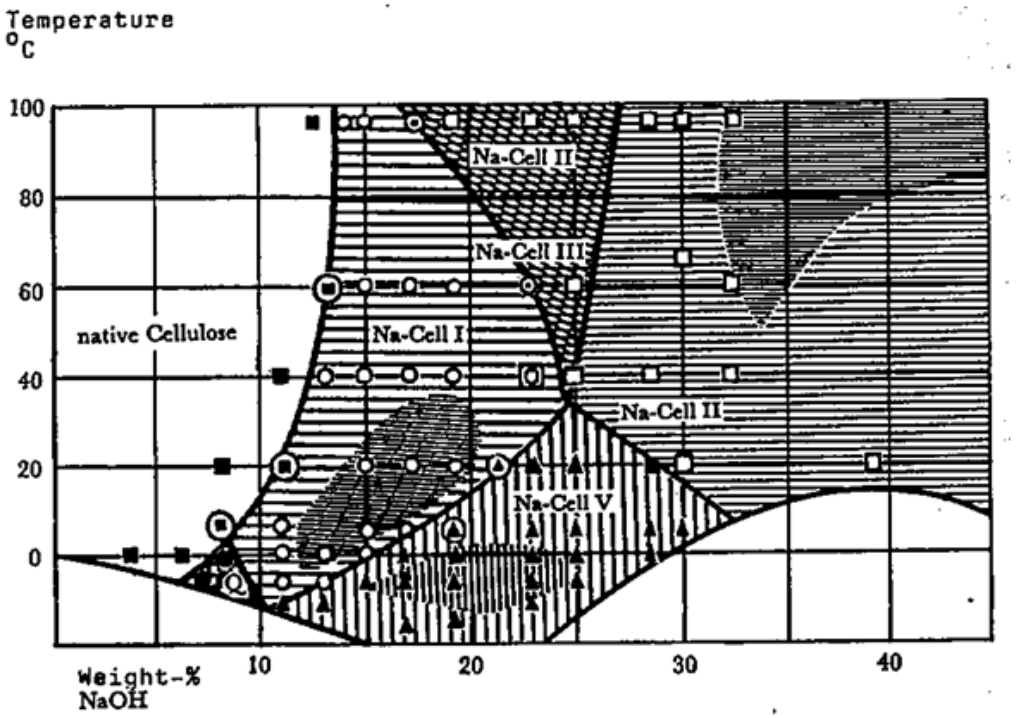

Figure 2.15: Phase diagram of formation of various alkali-celluloses as a function of temperature and aqueous NaOH concentration where the hatched areas are those of optimal formation of the alkali –cellulose in question (reprinted from Krässig, 1993).

Sobue *et al*. (1939) proposed a phase diagram for various types of alkali-cellulose formation as a function of temperature and NaOH concentrations (Figure 2.15). As mentioned before the lattice changes are irreversible and lowering the temperature or the dilution of the NaOH solution does not change the ultimate lattice transformation. Warwicker (1967) and Warwicker and Wright (1967) investigated the swelling of cotton and ramie cellulose in NaOH aqueous solutions and found that besides the lattice changes of cellulose I to cellulose II so called lateral disorder is introduced into the fibrils during the cellulose swelling. It means that sheets of cellulose chains which are held together by van der Waals forces can develop and in the extreme these sheets can be separated from the fibrils and found in the solution.

The ability of cellulose I to take up sodium hydroxide ions was originally thought to be a chemical reaction. Later it was found to be an absorption process based on Donan equilibrium theory and osmotic forces (Trotman, 1964). The uptake is based on complex formation between the alkali ions and cellulose hydroxyls. The key for cellulose swelling is the cellulose accessibility which depends on the morphology and supra-molecular structure and size of the crystallites (Krassig, 1993).

Fibrillation and lattice distortion which happens before the irreversible lattice change of cellulose crystallites results in accessibility of internal surfaces which enhances cellulose reactivity e.g. in etherification or acetylation. To conclude, caustic soda treatment is a physical treatment with no chemical reaction involved.

3 Polylactic acid

This chapter focuses on polylactic acid (PLA). It starts with an introduction to thermoplastic polymers and continues with PLA synthesis. Polylactic acid can be synthesized through a ring opening polymerization of lactide or by direct polycondenzation of lactic acid and development of crystalline morphology is discussed. Thermo-mechanical properties of polylactic acid are compared to conventional thermoplastics. Biodegradability, sustainability and end of use disposal are also discussed. The chapter finishes with the potential uses of PLA in industrial applications.

3.1 Introduction to thermoplastic biopolymers

There are three main groups of polymers: thermoplastics, thermosets and elastomers. Thermoplastics are polymers which flow upon heating as their long molecular chains are connected through weak van der Waals forces. They are formed from viscous liquids which solidify upon heating by cross linking, i.e. formation of tight three dimensional networks. Once they are cross-linked they cannot flow upon application of heat due to the covalent nature of the cross-links. Elastomers can be stretched to high extensions upon application of stress. The extension disappears if the stress is released. They deform elastically hence the name elastomers. Thermoplastic elastomers containing loosely associated cross-links can flow upon application of heat but most elastomers degrade by charring.

Molecules of some thermoplastic polymers with favourable conformation are able to pack into higher order structures depending upon their thermal history. They are called semicrystalline (or partially crystalline) as their crystalline content is much less than 90% by volume. The structure of semicrystalline polymers is more complex compared to amorphous polymers. They are neither completely crystalline nor amorphous. Semicrystalline polymers contain an amorphous phase which defines the glass transition temperature (T_g) of the polymer and crystalline phase which defines the melting temperature of the polymer (T_m). The concept of transition temperatures results from Figures 3.1 and 3.2 which show the variation of specific volume with temperature of a fully amorphous, fully crystalline and semicrystalline polymer.

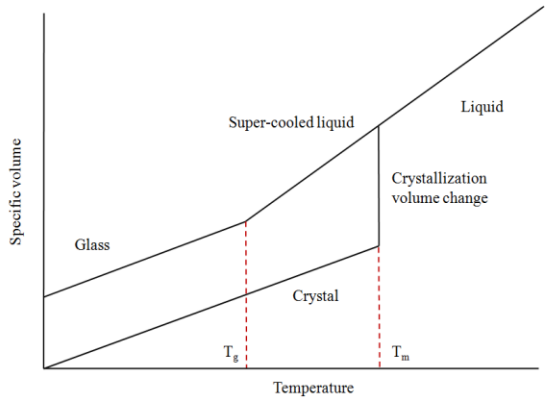

Figure 3.1: Specific volume versus temperature for 100 % crystalline and 100 % amorphous polymer (Brandrup *et al*., 2005)

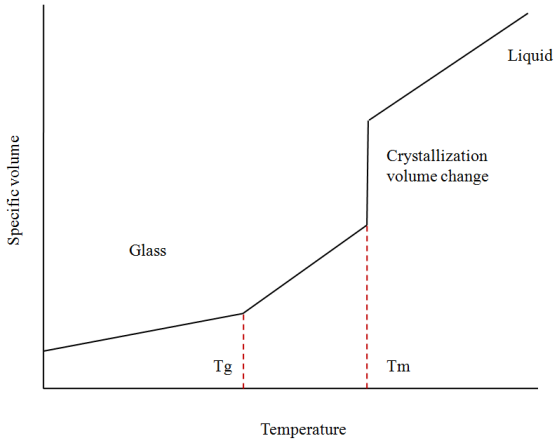

Figure 3.2: Specific volume versus temperature for semicrystalline polymer (Brandrup *et al*., 2005)

On heating to above T_g the polymer goes through a transition from brittle solid glass to an elastic rubber (amorphous polymers) or leather-like state (crystalline polymers) which is followed by a dramatic change in physical properties. The behaviour of polymer during the transition is described as viscoelastic. The elastic modulus decreases two to three orders of magnitude (Figure 3.3). Heat capacity, thermal expansion coefficient, refractive index, tensile strength and mechanical damping change at the glass transition temperature. Figure 3.1 and 3.2 shows a step increase in specific volume at the melting temperature and slope change at the glass transition temperature. Polymer chain segments at the glass transition temperature are given enough energy to move freely.

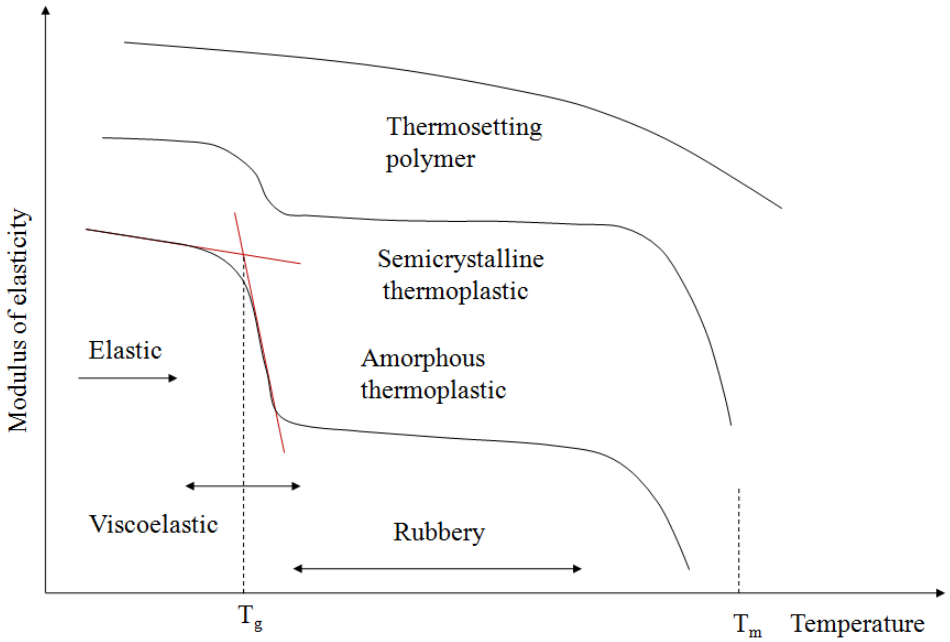

Figure 3.3: The change of elastic modulus with temperature for polymer classes (Aziz and Ansell, 2004).

Unlike metals, semicrystalline polymers do not have sharp melting temperature. Not all the polymer molecules have the same length, i.e. molecular weight. Thus not all of the molecules organized in crystallites can melt at the same time (at the same T_m). Some of the molecular chains fold regularly and rearrange into higher order structures called crystallites; e.g. spherulites which are the most common polymer crystal morphology. Molecular structure and the three dimensional conformation of polymer molecules influence the folding of polymer chains into crystallites.

In the last few decades biodegradable polymers from renewable resources were synthesised and marketed driven by increasing environmental awareness. The same physical rules which apply to conventional polymers apply to these materials. The difference lays in their origin (feedstock versus other natural resources) and their ability to disintegrate under controlled conditions (years versus decades of years). Polymers from renewable resources (bio-based polymers) include:

(a) Natural polymers (e.g. cellulose),

(b) Modified natural polymers (e.g. thermoplastic starch),

(c) Bio-based monomers polymerized using a conventional technology (e.g. polylactic acid),

(d) Polymers directly produced from genetically modified bacteria (e.g. polyhydroxybutyrate).

The following sections of this chapter discuss the synthesis, properties and morphology of polylactic acid (PLA) selected for this research because it is fully bio-based and biodegradable and suitable for the manufacture of structural composites reinforced with natural fibres.

3.2 Synthesis and chemical structure of PLA

Polylactic acid is a semicrystalline thermoplastic polyester formulated from renewable resources. It is synthesized from lactic acid through polymerization. Lactic acid was isolated in 1780 from sour milk by the Swedish chemist Scheele and produced commercially in 1881 by Charles E. Avery at Littleton, Massachusetts, USA. Lactic acid (2-hydroxypropionic acid) is the simplest hydroxyl acid with a chiral carbon atom in the molecule. Lactic acid molecules exist in the form of two stereoisomers, L- and D- lactic acid. Both molecules have a different effect on polarized light. The L-isomer rotates the plane of polarized light in a clockwise (*dextro*, +) direction and the D-isomer in an anticlockwise (*laevo*, -) direction. Both isomers can be produced by bacterial fermentation of carbohydrates. Lactic acid produced by bacterial fermentation is optically active. For example, L (+) - isomer can be produced by *Lactobacillus amylophilus* or *Lactobacillus bavaricus*. Synthetic lactic acid produced from petrochemical feedstock is an optically inactive racemic mixture consisting of 50% D- and 50% L-lactic acid (Figure 3.4). A racemic mixture is a mixture of equal amounts (1:1) of the two stereoisomers of an optically active substance. It shows no rotation of plane polarized light.

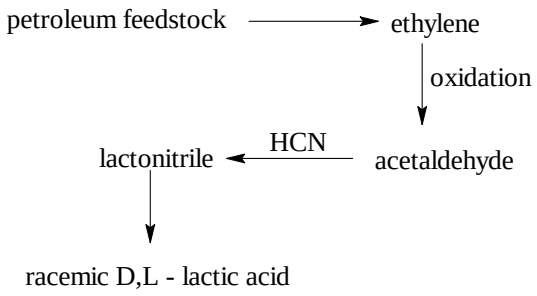

Figure 3.4: Synthetic production of lactic acid.

The biochemical route of lactic acid production (fermentation) starts with wet milling of corn to extract the starches from biomass. Starch is converted to sugar by enzymatic or acid hydrolysis and the sugar liquor is fermented by bacteria. L-lactic acid is produced from glucose via pyruvate (the carboxylate anion of pyruvic acid, $CH3COCOO^{-}$). The reaction is catalyzed by enzyme lactate dehydrogenase (Figure 3.5).

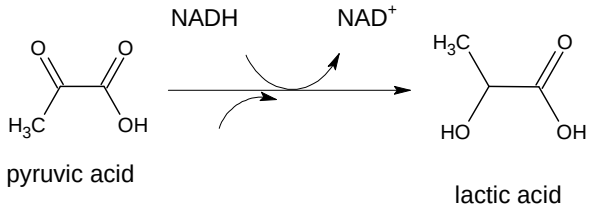

Figure 3.5: Production of lactic acid via bacterial fermentation; NADH is oxidizing form of Nicotinamide adenine dinucleotide; NAD^{+} is the reduced form – with accepted electrons.

Lactic acid is isolated from the fermentation broth, precipitated by $Ca(OH)_2$ and treated with sulphuric acid to obtain free acid. This is then purified by a membrane separation processes. In order to achieve thermostable lactic acid, purification is followed by esterification, distillation, subsequent hydrolysis of the ester and recovery of the alcohol by evaporation (Södergård and Stolt, 2002).

In 1932 Carothers carried out direct polycondensation of polylactic acid. Because of its sensitivity to humidity, the product was a low molecular weight polymer. In 1954 DuPont improved lactide purification and patented higher molecular weight polylactic acid. In 1970s medical resorbable sutures based on a copolymer of lactic and glycolic acid were introduced. In 1980/90 the chemical companies DuPont, Coors and Brewing (Chronopol) ran research on bulk applications of PLA (Södergård and Stolt, 2002). Bulk processing of polylactic acid started in 1994 with Cargill's semi-scale production in Minnesota. In January 2000 a joint venture between Cargill and Dow was formed to commerciallize PLA. In spring 2005 Dow pulled out of the project.

Polylactic acid can be prepared by direct polycondensation of lactic acid or through ring opening polymerization of its intermediate cyclic dimer – lactide (Figure 3.6). Direct polymerization leads to poly (lactic acid) ≈ PLA. Indirect polymerization via lactide leads to

poly (lactide) ≈ PLLA (Södergård and Stolt, 2002). In literature such a strict distinction is not common and both products are referred to as PLA.

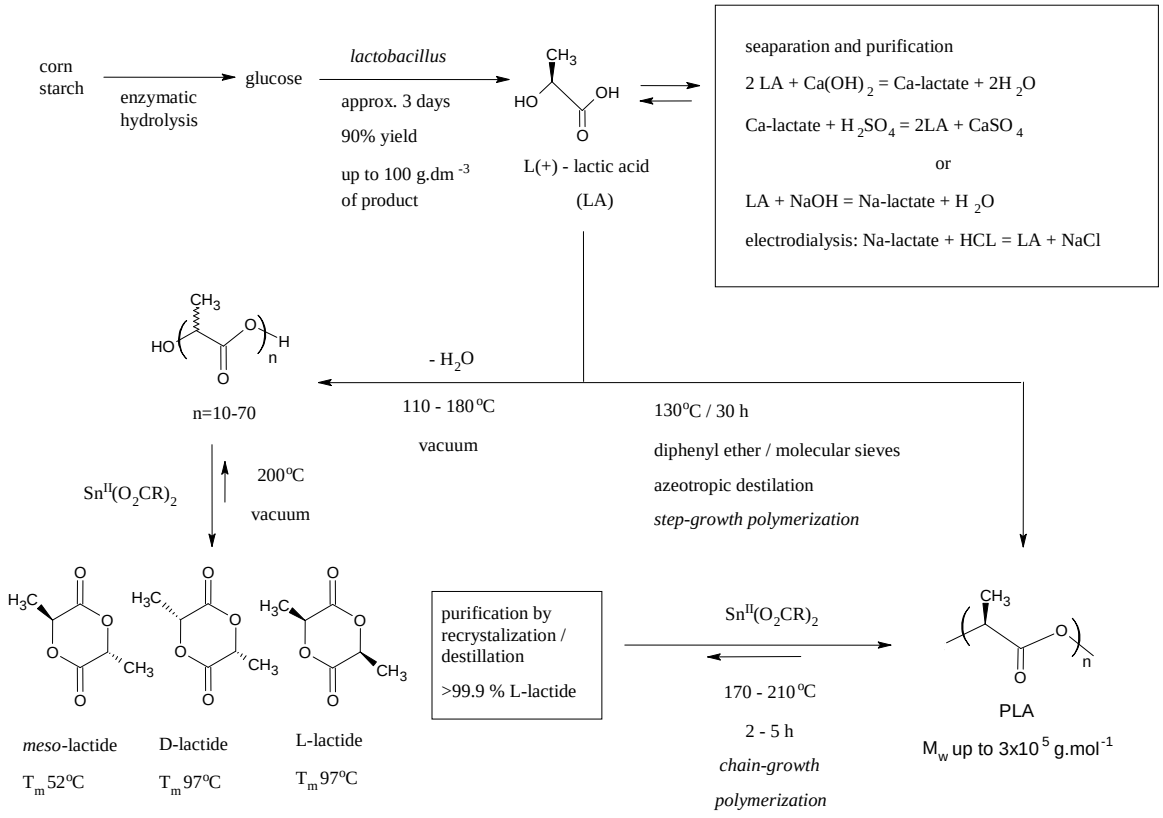

Figure 3.6: PLA synthesis (modified by Mecking, 2004).

PLA synthesis starts with an aqueous solution of lactic acid. Polycondensation is a step growth reaction. Due to its equilibrium nature and difficulties with removing condensation water in later stage of polymerization, direct condensation can produce only low to medium molecular weight polymers. To overcome this problem and to produce high molecular weight polymer, Mitsui Toatsu uses continuous azeotropic distillation of high boiling point solvent (diphenyl ether) (Chiellini *et al*., 2002). Water is removed from the reaction solution in two steps: (1) distillation at reduced pressure at 130°C is carried out for 2-3 hours. Subsequently, catalyst and solvent are added. A tube packed with molecular sieves is attached to the reaction vessel. The refluxing solvent is returned to the reactor through the molecular sieves (3 Å) for an additional 30-40 hours at 130°C (Ajioka *et al*., 1995) resulting in high molecular weight

polymer (M_w > 300,000) containing residual catalyst, which can cause degradation during further processing (Garlotta, 2001).

The Cargill Dow process starts with a continuous condensation reaction of aqueous solution of lactic acid resulting in low molecular weight PLA linear oligomers (pre-polymers). Increasing the temperature and lowering the pressure sets conditions for controlled depolymerisation of oligomers, producing a mixture of lactide stereoisomers. Tin catalyst is used to enhance the rate and selectivity of intramolecular cyclization reactions. Molten lactide mixture is purified by vacuum distillation. Finally, high molecular weight polymer is produced by ring opening polymerization in the melt. Both cyclization and polymerization of lactide is catalyzed by tin (II) bis-2-ethylhexanoic acid. This catalyst system has been chosen because of its solubility in molten lactide, high catalytic activity and low rate of racemisation of polymer resulting in 90% conversion and >1% of racemisation. A coordination-insertion mechanism was proposed to describe kinetics and nature of lactide ring opening and insertion of two lactic acid molecules to the growing end of the polymer chain. The catalyst type and concentration, temperature and residence time are the key parameters which control the ratio and sequencing of D- and L-lactic acid units in the polymer. The ratio and sequence of stereoisomers in PLA polymer influence crystallization kinetics and the degree of crystallinity. Typical reaction conditions are 180-210°C, 100-1000 ppm catalyst concentration, 2-5 hours duration and 95% conversion. Initiators (1-octanol) are used to control the molecular weight and to accelerate the reaction (Drumright *et al.*, 2000). Figure 3.7 – 3.9 show the mechanism of ring opening polymerization of lactide catalysed through Lewis-acid catalysts or metal alkoxides.

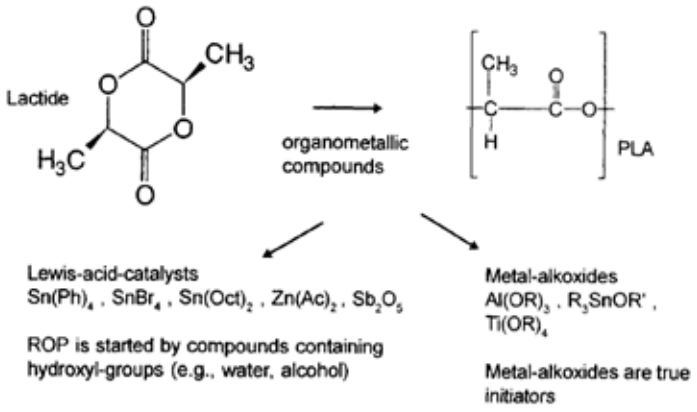

Figure 3.7: Ring opening polymerization and synthesis of polylactide (Jacobsen *et al*., 1999).

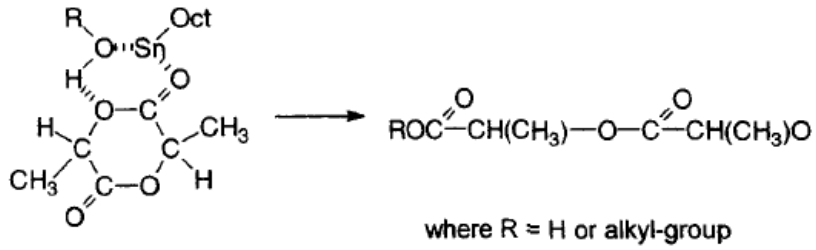

Figure 3.8: Ring opening polymerization through Lewis acid catalyst (Jacobsen *et al*., 1999).

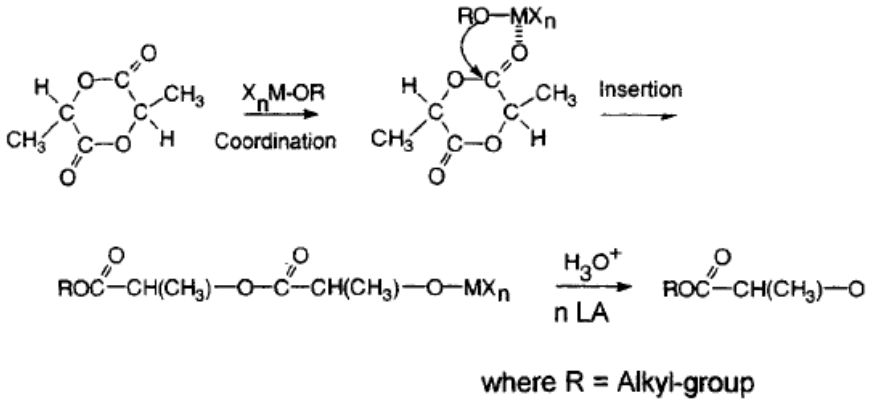

Figure 3.9: Ring opening polymerization through metal alkoxides (Jacobsen *et al*., 1999).

3.3 Morphology

PLA is a semicrystalline thermoplastic polymer with a melting temperature of 170°C. The morphology of PLA crystals is influenced by monomer composition of the polymer chains (L and D isomers) and their thermal history. General crystallization behaviour of PLA was studied by Kalb and Pennings (1980), Miyata and Masuko (1998), Kolstad (1996) and Urbanovici *et al*. (1996). PLA is a slowly crystallizing polymer compared to polypropylene. There are three regimes of crystallization (I, II and III). The difference between individual regimes is in the deposit mechanism of molecular nuclei on the growing lamella (Monasse and Haudin, 1985). The regimes are also connected with the degree of supercooling ΔT. Regime I occurs at small ΔT, regime II at increasing supercooling and regime III at high ΔT > 20°C

(Wool, 1995). Clearly most semicrystalline thermoplastics are processed at conditions of regime III which result in spherulitic morphology. Mazzullo *et al*. (1992) reported a transition temperature from regime II to III of 140°C for PLA of M_v = 700 000 g/mol. Vasanthakumari and Pennings (1983) reported a regime I to II transition temperature for PLA (M_v 150 000 g/mol) of 163°C.

Table 3.1: Regimes of crystallization of PLA.

Regime of melt crystallization	III	II	I
Transition temperature [°C]		140	163
Polymer morphology	α	β	hexagonal lamellar stacking

Spherulitic morphology is observed at crystallization temperatures below 163°C. Crystallization of PLA at temperatures above 163°C results in hexagonal lamellar stacking crystalline morphology (Table 3.1).

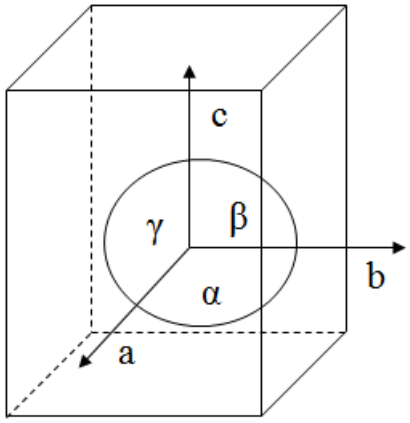

Figure 3.10: Orthorhombic ($a \neq b \neq c$; $\alpha = \beta = \gamma = 90°$) unit cell with outlined crystallographic axes and angles.

A polymer crystal in a three dimensional space is built up by a continuously repeating unit cell. The unit cell is specified by six *lattice constants* - the lengths of cell edges *a*, *b* and *c* and interaxial angles *α*, *β* and *γ*. Figure 3.10 shows a cell of the orthorhombic system with crystallographic axes and angles. Table 3.2 summarizes crystal systems and their lattice constants.

Table 3.2: Crystal systems and Bravais space lattices (Tadokoro, 1979).

Crystal system	Axial length	Interaxial angle	Symbol of space lattice
Triclinic	$a \neq b \neq c$	$\alpha \neq \beta \neq \gamma$ *	P
Monoclinic	$a \neq b \neq c$	$\alpha = \gamma = 90° \neq \beta$	P, A(C)
Orthorhombic	$a \neq b \neq c$	$\alpha = \beta = \gamma = 90°$	P, A(B, C), F, I
Tetragonal	$a = b \neq c$	$\alpha = \beta = \gamma = 90°$	P, I
Rhombohedral (Trigonal)	$a = b = c$	$\alpha = \beta = \gamma < 120°$ ($\neq 90°$)	R
Hexagonal	$a = b \neq c$	$\alpha = \beta = 90°, \gamma = 120°$	P
Cubic	$a = b = c$	$\alpha = \beta = \gamma = 90°$	P, F, I

Note: *The angle between the *a* and *b* axes is denoted α.

Table 3.3: Unit cell parameters reported for non-blended PLLA and stereocomplex crystals (modified after Tsuji, 2005).

		Crystal system	Chain orientation	Number of helices per unit cell	[h]Helical conformation	a	b	c	α	β	γ
						[nm]	[nm]	[nm]	[°]	[°]	[°]
[a]	PLLA α-form	Pseudo-orthorhombic	-	2	10_3	1.07	0.645	2.78	90	90	90
[b]	PLLA α-form	Pseudo-orthorhombic	-	2	10_3	1.07	0.6126	2.894	90	90	90
[c]	PLLA α-form	Pseudo-orthorhombic	-	2	10_3	1.06	0.61	2.88	90	90	90
[d]	PLLA α-form	Orthorhombic	-	2	10_3	1.05	0.61	2.88	90	90	90
[c]	PLLA β-form	Orthorhombic	-	6	31	1.031	1.821	0.90	90	90	90
[e]	PLLA β-form	Trigonal	Random	3		1.052	1.052	0.88	90	90	120
[f]	PLLA γ-form	Orthorhombic	Up-down Antiparallel	2	31	0.995	0.625	0.88	90	90	90
[g]	Stereocomplex	Triclinic	Parallel	2	31	0.916	0.916	0.87	109.2	109.2	109.8

[a] De Santis and Kovacs, 1968; [b]Marega *et al*., 1992; [c] Hoogsten *et al*., 1990; [d] Kobayashi *et al*., 1995; [e] Puigalli *et al*., 2000; [f] Cartier *et al*., 2000; [g] Okihara *et al*., 1991.

Note: [h]left handed helical conformation; up-rise; 3_1 helix means three repeated units per 360° turn of the helix.

Table 3.4: Details of the crystal structures of various common polymers (shortened from Young and Lovell, 1991).

Polymer	Crystal system	Space group[a]	Molecular helix[b]	Unit cell axes			Unit cell angles			Chain repeat units per unit cell	ρ_c[d]
				a	b	c	α	β	γ		
			A*u/t	[Å]	[Å]	[Å]	[°]	[°]	[°]		[g.cm^{-3}]
Polyethylene I	Orthorhombic	Pnam	1*2/1	7.418	4.946	2.546*[c]	90	90	90	4	0.9972
Polyethylene II	Monoclinic	C2/m	1*2/1	8.09	2.53*	4.79	90	108	90	4	0.998
Polypropylene (iso)	Monoclinic	$P2_1/c$	2*3/1	6.66	20.78	6.495*	90	99.6	90	12	0.946
Polystyrene (iso)	Trigonal	$R\bar{3}\bar{c}$	2*3/1	21.9	21.9	6.65*	90	90	120	18	1.127
Polypropylene (syndio)	Orthorhombic	$C222_1$	4*2/1	14.50	5.60	7.40*	90	90	90	8	0.930
Polyoxymethylene I	Trigonal	$P3_1$ or $P3_2$	2*9/5	4.471	4.471	17.39*	90	90	120	9	1.491
Polyoxymethylene II	Orthorhombic	$P2_1P2_12_1$	2*2/1	4.767	7.660	3.563*	90	90	90	4	1.533
Poly(ethylene terephthalate)	Triclinic	$P\bar{1}\bar{}$	12*1/1	4.56	5.96	10.75*	99	118	112	1	1.457
Nylon 6, α	Monoclinic	$P2_1$	7*2/1	9.56	17.24*	8.01	90	67.5	90	8	1.235
Nylon 6.6, α	Triclinic	$P\bar{1}\bar{}$	14*1/1	4.9	5.4	17.2*	49	77	64	1	1.24

Note: [a] as a result of packing and the symmetry of polymer segments in the unit cell; [b] A = number of skeletal atoms in the asymmetric unit of the chain, u = number of these units on the helix in the crystallographic repeat (in the chain direction), t = number of turns of the helix in the crystallographic repeat (in the chain direction); [c] asterix indicates the chain axis; [d] determined from the crystal structure.

Table 3.3 summarizes crystal systems with unit cell parameters of polylactic acid which are reported in literature. PLA mostly crystallizes in orthorhombic or pseudo-orthorhombic crystal systems. Table 3.4 gives examples of crystalline morphologies of conventional thermoplastics derived from feedstock with their unit cell parameters. Polypropylene which is often mentioned as a PLA competitor in polymer composites also crystallizes in the monoclinic system (*i*-PP). One of the objectives of this thesis is to examine the crystallization and morphology of PLA in natural fibre composites. The match between the lattices of the crystalline morphology of cellulose and the matrix is usually given among the factors which are thought to be responsible for transcrystalline morphology development. Figure 3.11 displays graphically the difference between α and β crystalline morphologies of polylactic acid.

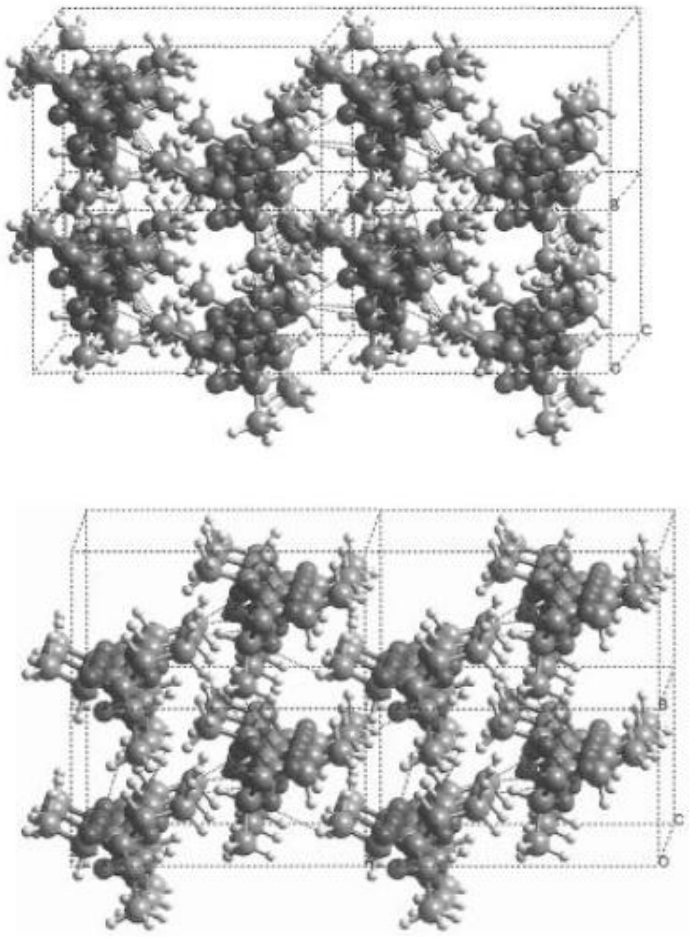

Figure 3.11: Structure of α-PLLA (top) and of β-PLLA (bottom) (Brizzolara *et al*., 1996).

3.4 Physical and mechanical properties of PLA

Commercially available PLA ranges from amorphous glassy grades with T_g~55-65°C to semi-crystalline and highly crystalline grades with T_m~160-180°C and melting enthalpy of 40-50 J/g (Dorgan *et al*., 2000; Pyda *et al*., 2004; Table 3.5).

Table 3.5: Physical, mechanical and thermal properties of commercially available PLA (modified after Wolf, 2005).

Company	NatureWorks®	Biomer®	Hycail[d]
Product	PLA	L9000	HM 1011
Physical properties			
Melt flow rate (g/10 min)	-	3-6	2-4
Density (g/cm^3)	1.25	1.25	1.24
Haze	2.2	-	-
Yellowness index	20 - 60	-	-
Mechanical properties			
Tensile strength at yield (MPa)	53	70	62
Elongation at yield (%)	10;100[a]	2.4	3-5
Flexural Modulus (MPa)	350 - 450	3600	-
Thermal properties			
Heat deflection temperature (°C)	40 – 45; 135[b]	-	-
Vicat softening point(°C)	-	56[c]	-
Glass transition temperature T_g (°C)	55 - 65	-	60-63
Melting point T_m (°C)	120 - 170	-	150-175

Note: [a]Oriented and unoriented respectively; [b]Amorphous and crystalline respectively; [c]Close to T_g; [d]www.hycail.fi\chemicals\Datasheet HM1011.pdf

PLA mechanical properties are compared to those of general purpose polystyrene (e.g. high modulus and strength and lack of toughness) and polyethyleneterepthalate (PET), e.g. oil resistance and barrier properties. Compared to PET (T_m~254°C) PLA has a lower melting point. Compared to polystyrene, PLA has a low melt strength, which implies certain restriction on its application. PLA's Charpy impact strength is low and it is comparable to that of non-plasticized polyvinylchloride (PVC, Wolf *et al*., 2005). PLA's toughness is usually compared to that of polypropylene. PLA has a $T_g \approx$ 50-60°C and PP has a $T_g \approx$ -20°C (Table 3.6) Thus at

the room temperature PLA is a brittle solid as room temperature lies below its glass transition temperature. Polypropylene is "leathery" at room temperature as its T_g lies below room temperature. For this reason unmodified PLA does not have the same toughness as unmodified polypropylene. The degree of crystallinity determines thermo mechanical properties and the polymer melting point. Introduction of *meso*-lactide units into the polymer chain results in melting point depression from 180°C to 120°C (Lunt, 1997; Wolf *et al*., 2005). A lower melting point enables lower processing temperatures which reduce hydrolysis, oxidative degradation and lactide reformation.

The crystalline phase in PLA improves its strength, stiffness and chemical and thermal resistance. The crystalline state is preferred for applications at temperatures of 40-50°C or higher (Perego *et al*., 1996). Crystallinity in the PLA can be developed during injection moulding (adding nucleating agents to the polymer melt) or it can be induced by stress applied at 10°C above the glass transition temperature (bi-axially oriented films; Drumright *et al*., 2000). As it is an aliphatic polyester, the PLA melt viscosity is not very shear sensitive. PLA has poor melt strength as a result of the low degree of molecular chain entanglement (PLA is a linear polymer). Melt strength or melt tension are processing terms for low shear viscosity which is an important technological parameter in blow moulding and foam processing (Maier and Calafut, 1998). Branching with a low concentration of peroxides or multifunctional monomers during polymerization can improve melt strength but it reduces melt viscosity at high shear rates. Transition temperatures (T_g and T_m) are not influenced by the chain architecture. Rate of crystallization is affected and the branched PLA crystallizes more quickly (Dorgan *et al*. 2000).

Table 3.6: Tensile and thermal properties of some thermoplastic polymers (selected from Brandrup *et al*., 2005).

Property	Unit	PP	LD-PE	HD-PE	HI-PS	ABS
Mechanical						
Density	[g/cm^3]	0.93	0.921	0.941-0.967	1.04	1.04
Tensile strength	[MPa]	35.5	10.3	19-30	24	40
Tensile modulus	[GPa]	1380	165.5	800-1400	1650	2140
Flexural modulus	[GPa]	1690	-	700-1700	1910	2580
Notched Izod at room temperature	[J/m]	37	42.7 (at -50°C)	27-160	112	72
Thermal						
Deflection temperature at 1.82 MPa	[°C]	55	-	-	74	103
Deflection temperature at 0.45 MPa	[°C]	101	41	65-95	87	107
Vicat softening point	[°C]	154	91	120-130	101	111
Linear coefficient of thermal expansion	[mm/mm/°C]	90 x 10^{-6}	250 x 10^{-6}	100-200 x 10^{-6}	0.9 x 10^{-6}	6.7 x 10^{-6}
Glass transition temperature	[°C]	-20	-35	Not measurable	93-105	110
Melting temperature	[°C]	164	-	130-137	-	-

Another way to overcome PLA's low melt strength is copolymerization of lactic acid with glycolic acid and hydroxyhexanoic acid (Ajioka *et al*., 1998). Copolymers can be prepared by either direct polycondensation of hydroxyacids and ring opening polymerization of cyclic monomers. A copolymer of L-lactic acid and 6-hydroxyhexanoic acid (direct condensation), and a copolymer of L-lactide and ε-caprolactone (ring opening polymerization) were synthesized. Both copolymers were amorphous with T_g~24°C and T_g~34°C respectively and no melting point. Block copolymer of L-lactic acid and ε-caprolactone prepared by sequential method had a melting point of 127°C. First, L-lactic acid was converted to polylactic acid through direct condensation and then ε-caprolactone was polymerized through ring opening polymerization. Compared to neat PLA, the tensile strength of copolymers decreased and the elongation increased significantly.

The physical, chemical and mechanical properties of polylactic acid were reviewed by Garlotta (2001) and Södergård and Stolt (2002). Crystallization and crystallization kinetics, solubility, solution and melt rheology and the results of NMR, UV-VIS and FTIR spectroscopy are briefly discussed.

3.5 Biodegradation and environmental impact

Polylactic acid is a thermoplastic polyester formulated from renewable resources. Compared to traditional thermoplastics polylactic acid is biodegradable polymer. Albertsson and Karlsson (1994) define biodegradability as "*an event which takes place through the action of enzymes and/or chemical decomposition associated with living organisms (bacteria, fungi, etc.) and their secretion products"*. Biodegradability is thought to be a solution to waste-disposal problems. After its lifetime PLA products can be controllably disintegrated through the action of bacteria without any harm to the environment. Biodegradation of PLA occurs in two steps. Firstly, hydrolysis of polyester bonds causes chain scission and leads to low molecular weight oligomers. High humidity and temperatures of 55-70°C accelerates PLA degradation. Macromolecules with Mn~40,000 are digested by soil bacteria and converted into carbon dioxide and water (Lunt, 1997). PLA is stable under ambient conditions and will not degrade

in typical garden compost (Wolf et al., 2005). Hydrolysis retardant additives can further stabilize PLA.

Sustainability seems to be the key term when we are trying to underline the low environmental impact of newly developed green materials. The Brundtland Report (Azapagic *et al*., 2003) defines the sustainable development as a development which "*meets the needs of the present without compromising the ability of future generations to meet their own needs*".

Looking at the key qualities of a "*sustainable material*" (Table 3.7) the sustainability of PLA can be debated. Natural does not mean sustainable. For instance cotton cultivation requires deforestation of large areas as it grows only in certain climates with enormous use of fertilizers and pesticides and huge levels of irrigation - 1 kg of cotton fibre requires 40,000 litres of water which a human being consumes in a lifetime (Blackburn, 2007).

Table 3.7: Key qualities of idealized sustainable material (Blackburn, 2007).

Ideal sustainable material:
Provides an equivalent function to the product it replaces.
Performs as well as or better than the existing product.
Is available at a competitive or lower price.
Has a minimum environmental footprint for all the processes involved.
Is manufactured from renewable resources.
Uses only ingredients that are safe to both humans and the environment.
Has no negative impact on food supply or water.

Life cycle assessment (LCA) is an environmental management system which enables quantification and assessment of environmental performance of a product, process or an activity from "cradle to grave" (Azapagic *et al*., 2003). It is a systematic set of procedures which quantifies the use of input/output materials, energies and emissions and waste associated with the product (goods/services) development and functioning throughout its life-cycle. The LCA methodology is standardized through the ISO 14040 series which defines four stages of LCA:

1. *Goal and scope definition* of the LCA study.
2. *Inventory analysis*. In this stage the studied system is described quantitatively through:
   - Definition of the system boundaries

- Flow diagrams of the system
- Data collection
- Allocation of environmental burdens
- Calculation and reporting of the results

3. *Impact assessment*. In this stage qualitative and quantitative methods are used to characterize the impact of the system to the environment. The following environmental impacts are assessed:
   - Resources depletion
   - Global warming
   - Ozone depletion
   - Acidification
   - Eutrophication
   - Photochemical smog
   - Human toxicity
   - Aquatic toxicity
4. *Interpretation*. In this stage the major environmental burdens are identified and measures are proposed to reduce their environmental impact.

In conclusion LCA can be used in order to identify and quantify the processes which contribute most to the overall environmental impact in the life-cycle of a product. It can be also used to compare products. Such comparison is based on the environmental impact of the product, like fossil energy use or production of greenhouse gases during its life-time.

Table 3.8 summarizes cradle-to-factory gate energy use and CO_2 production of PLA and compares it to other polymers. All the production steps from corn growing, dextrose production, conversion to lactic acid, further conversion of lactic acid to lactide and its ring opening polymerization into polylactide were analyzed (referred to as PLA-year 1). The next generation technology which is referred to as PLA-year 5 makes the environmental impact even lower. The changes include the use of electricity from wind power and the use of dextrose from organic waste. It can be concluded that PLA is semi-synthetic material derived from natural resources which will definitely become more sustainable, with improvements in production efficiency, resulting in lower costs and new applications.

Table 3.8: Cradle-to-factory gate energy use and CO_2 production of PLA and polymers (Rudnik, 2008).

Polymer	Process energy-fossil sources	Feedstock energy-fossil sources	Total fossil energy	Fossil CO_2 from process energy	CO_2 absorption at plant growth	Net CO_2 *
	[GJ/10^3kg plastic]	[GJ/10^3kg plastic]	[GJ/10^3kg plastic]	[kg/ 10^3kg plastic]	[kg/ 10^3 kg plastic]	[kg/ 10^3 kg plastic]
PLA - Year 1	54	0	54	3450	-2190	1260
PLA - Target year 5	7	0	7	520	-2280	-1760
HDPE	31	49	80	1700	0	1700
PET (bottle grade)	38	39	77	4300	0	4300
PA 6	81	39	120	5500	0	5500

*Equals the sum of "Fossil CO_2 from process energy" and "CO_2 absorption at plant growth".

3.6 Technical applications for PLA

PLA can be processed by sheet extrusion, film blowing, thermoforming, film forming, fibre spinning and injection moulding. Controlling molecular weight, ratio of stereoisomers , degree of crystallinity and branching enables production of different PLA grades. PLA grades with > 1% of D-isomer are designed for injection moulding of heat resistant articles (higher degree of crystallinity). PLA grades with 4-8 % of D-isomer are designed for thermoforming/extrusion (Drumright et al., 2000). Table 3.9 summarizes the possible substitution potential for PLA.

Table 3.9: Technical substitution potential for PLA according to interviews with experts from Cargill Dow, Hycail and Biomer (Wolf *et al*, 2005).

Polymer	Cargill Dow	Hycail	Biomer
PVC	-	+	-
PE-HD	+	-	-
PE-LD	+	-	-
PP	+	+	-
CC-PS	-	+	++
PMMA	-/+	+	-
PA	+	+	-
PET	+	+	-
PBT	-	+	-
PC	-	-	-
POM	-	-	-
PUR	-/+	-	-
HIPS	-	+	-
ABS	-	+	+

CC-PS: crystal clear polystyrene; HI-PS: high impact polystyrene;
++ full substitution, + partial substitution, - no substitution

The data are based upon a survey carried out between representatives of PLA producers in 2003 (Cargill Dow, Hycail and Biomer). PLA could partially replace PMMA, PA and PET. There is also possibility for replacing PP. No possibility was seen for substituting PC, POM and non-polymeric materials (wood, leather).

The potential for PLA fibre reinforced composites in building applications is difficult to assess. Adequate performance after 20 year life time and the price competitiveness seem to be the most limiting factors. PLA fibre has potential in the furniture sector (home furnishing) (Wolf et al., 2005). PLA is still more expensive when compared to the traditional thermoplastics. Its price will strongly depend on large scale applications and technology improvements. During the period of 2000-7 the cost of PLA dropped about 40-45% as can be seen from Table 3.10. The mass production and technology of conventional polymers such as polypropylene or polyethylene have been continuously developed and improved over at least fifty years whereas PLA is still a relatively new material.

Table 3.10: Cost comparison of traditional and biodegradable polymers (Blackburn, 2007).

Traditional/Biodegradable	Polymer	Average cost ($/kg in 2007)
Traditional polymers	PP	0.73
	HDPE	0.82
	PET	1.15
Biodegradable polymers	PLA	1.50-2.42
		3.30-6.60 (in 2000)
	PHAs	8.80-13.90

This chapter has demonstrated that the mechanical properties of PLA are as good as or even better than those of traditional thermoplastics. Another way to reduce the cost is to replace part of the polymer with a filler. Assuming the price of sisal fibres is 0.27-0.32 $/lb (Sain and Panthapulakkal, 2004) and the price of PLA is 1.50-2.42 ($/kg) and applying a simple rule of mixtures, neglecting cost of mixing the fibres with the matrix and assuming V_f=0.5, the price for sisal reinforced PLA is about 1 $/kg. This is the average price of a general purpose thermoplastic. As a first approximation it seems to be convenient to reinforce PLA with natural fibres as a cheap filler. In reality natural fibre can perform much better as an reinforcement rather than as a cheap filler. Price per unit strength or stiffness shows that natural fibres can compete with glass fibres in certain applications and that their composites can posess structural qualities.

4 Natural fibre composites with thermoplastic matrices

The chapter starts with an introduction to composites with thermoplastic matrices. It continues with the selection of the most appropriate bio-based matrix for natural fibre composites with structural qualities. The core of the chapter focuses on the review of the mechanical properties and processing technology of composites from thermoplastic matrices and natural fibres. Composites reinforced with long and short fibres are reviewed. The chapter finishes with recycling of natural fibre composites with thermoplastic matrices.

4.1 Introduction of natural fibre composites

Natural fibres are often compared to glass fibres. They offer environmental and cost advantage over glass fibres because of their low carbon footprint and price (Figure 4.1 and 4.2). Glass fibre used for composites manufacture has cost of 1.3 - 2 $/kg whilst, for example, flax fibre has costs of 0.22 – 1.10 $/kg (Joshi *et al*., 2004).

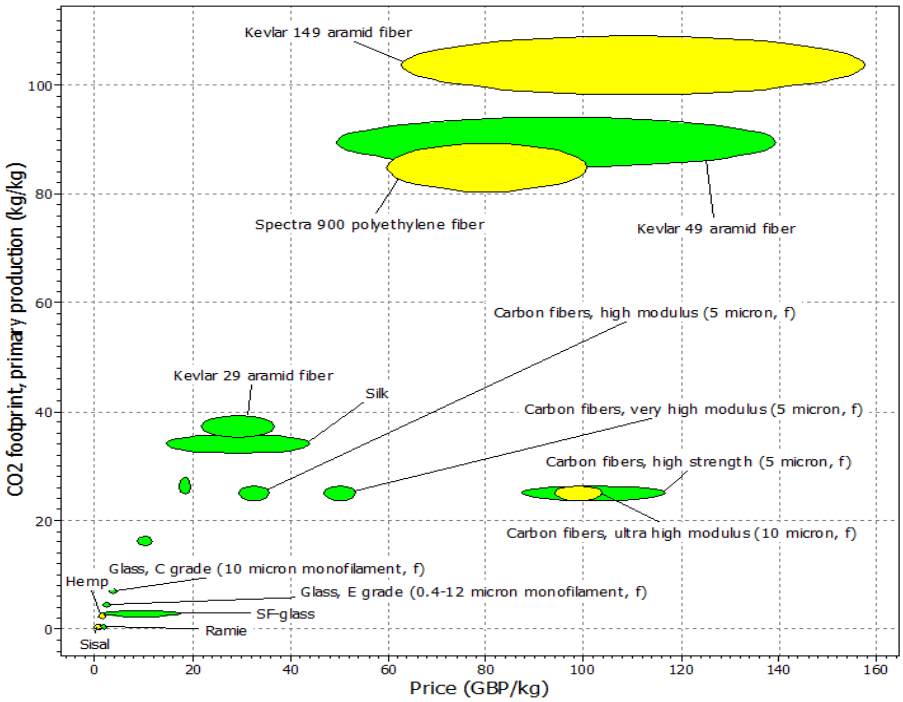

Figure 4.1: Carbon footprint versus price for synthetic and natural fibres (Ansell, 2010).

Natural fibres have lower density compared to glass fibres. For example the density of flax or hemp is about 1400-1500 kg.m^{-3} meanwhile the density of E-glass which is used in composites formulations is about 2500 kg.m^{-3} (Table 2.4 and 2.5).

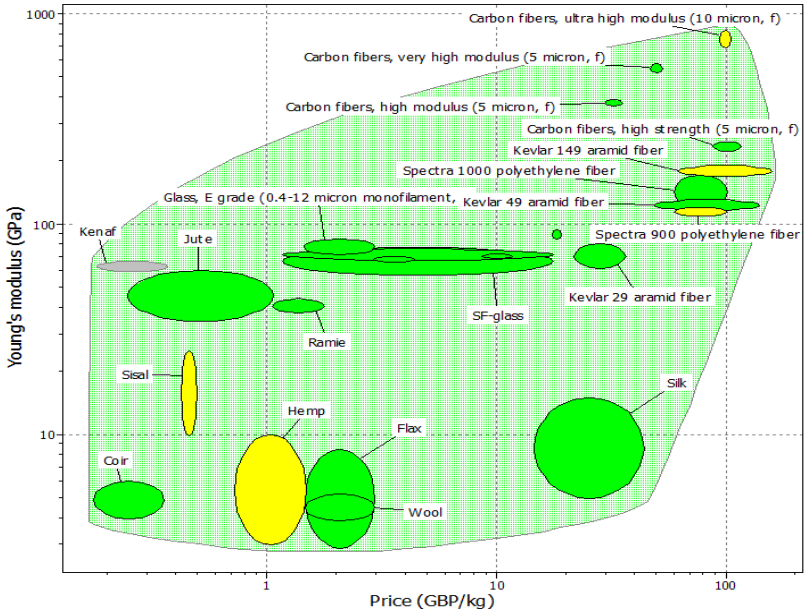

Figure 4.2: Young's modulus of synthetic and natural fibres in relation for the price/kg of the fibre (Ansell, 2010).

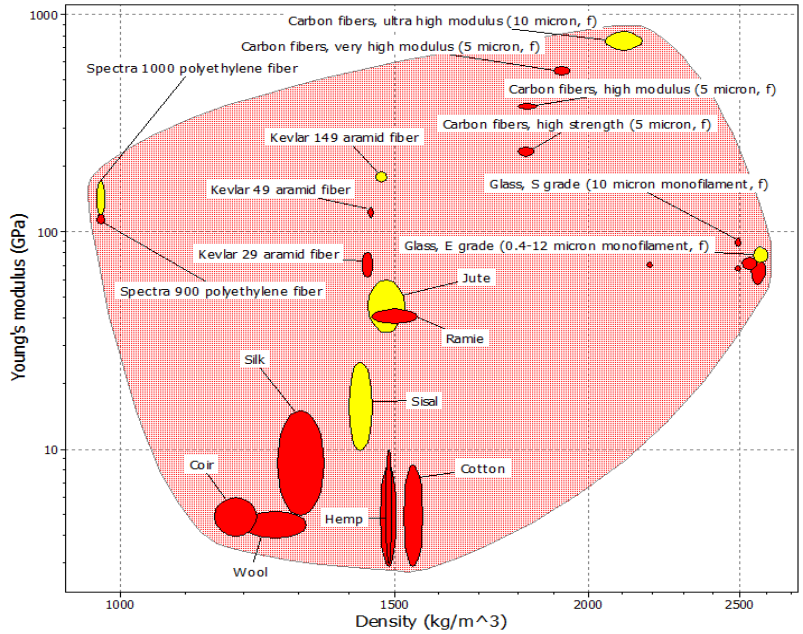

Figure 4.3: Specific Young's modulus versus density of synthetic and natural fibres (Ansell, 2010).

By dividing the Young's modulus of natural fibres by their density one can obtain their specific modulus. Figure 4.3 compares specific Young's moduli of selected natural and synthetic fibres.

The natural fibres are mostly less stiff per unit weight than the synthetic fibres. However the price and CO_2 footprint data is very advantageous. Specific modulus of hemp is about 20-41 GPa, 34-48 GPa is the specific modulus of flax and 28-29 GPa is the specific modulus of E-glass. It can be concluded that specific mechanical properties of natural fibres are comparable to glass fibres if one takes into account the lower bound of the presented intervals of specific moduli and its variability. Therefore natural fibre reinforced polymer composites (NFCs) could replace glass fibre reinforced polymer composites (GFRPs) in low-cost and low-weight applications where the variability of their mechanical properties is not essential (Eichhorn and Young, 2004). Table 4.1 summarizes the often claimed advantages of ligno-cellulosic natural fibres when compared to conventional glass fibres.

Table 4.1: Comparison of natural and glass fibres (Wambua *et al*., 2003).

	Natural fibres	Glass fibres
Density	low	approximately twice of natural fibres
Cost	low	low (but higher than natural fibres)
Renewability	yes	no
Recyclability	yes	no
Energy consumption	low	high
CO_2 neutral	yes	no
Abrasion to machines	no*	yes
Health risk when inhaled	no	yes
Disposal	biodegradable	not biodegradable

*except where SiO_2 content is high

One can expect that thermoplastic polymer matrices derived from petroleum feedstock will be steadily replaced by bio-based and biodegradable resins, like polyhydroxyesters (PLA) or polyhydroxyalkanoates (PHB). Consider a composite comprising a polylactic acid matrix and natural fibre reinforcement, e.g., sisal, flax or hemp. Assuming the composite is composed of aligned long fibre bundles with fibre volume fraction of V_f=0.7, taking values of fibre and matrix strength and modulus from Table 2.4 and Table 3.5 and applying the rule of mixture (Section 5.4.1) the calculated average tensile strength and modulus are about 400 MPa and 30

GPa respectively for flax and hemp composites (Table 4.2). As can be seen from Table 4.3 theoretical strength of natural fibre composites is comparable to that of aluminium alloys.

Table 4.2: Theoretical mechanical properties of polylactic acid reinforced with unidirectional natural fibres calculated from the rule of mixtures.

Material ($V_f = 0.7$)	Average density	Tensile strength	Specific tensile strength	Tensile modulus	Specific tensile modulus
-	[$g.cm^{-3}$]	[MPa]	[$MPa.cm^{-3}.g^{-1}$]	[GPa]	[$GPa.cm^{-3}.g^{-1}$]
PLA/sisal	1.4	74 - 606	54 - 440	7.4-16.5	5 - 12
PLA/flax	1.4	368 - 648	260 - 459	36 - 50	26 - 36
PLA/hemp	1.4	235 - 543	166 - 384	22 - 43	16 - 31

Table 4.3: Strength properties of 35 vol. % glass reinforced polypropylene compared with various traditional engineering materials (Jones, 1994).

Material	Average density	Tensile strength	Specific tensile strength	Normalized specific tensile strength
	[$g.cm^{-3}$]	[MPa]	[$MPa.cm^{-3}.g^{-1}$]	[-]
Glass/PP $[0]_8$ laminate	1.48	720	486	1.00
Glass/PP $[0/90]_S$ laminate	1.48	360	243	0.50
Stainless steel	7.8	286-500	36-64	0.07-0.13
Mild steel	7.8	220	28	0.06
Copper alloys	8.3	60-960	7-116	0.01-0.24
Aluminium alloys	2.8	100-627	36-224	0.07-0.46
Aluminium	2.6	40	15	0.03
Magnesium alloys	1.8	80-110	44-61	0.09-0.13

Price always limits newly developed and newly marketed materials. Bio-based thermoplastics cannot compete with traditional polymers like polypropylene which are supported with decades of technology, research and development meanwhile the bio-based polymers are at the beginning of their era.

4.2 Selection of biopolymer matrices for natural fibre composites

Van de Velde and Kiekens (2002) reviewed properties of several thermoplastic biopolymers and co-polymers to find out the most suitable matrix for all biobased composites. Density and thermal properties are limiting criteria for a suitable polymer matrix. Low polymer density is important for making a lightweight product and the glass transition temperature (T_g) is important for predicting the polymer behaviour at ambient conditions. Melting temperature (T_m) of semicrystalline polymers is related to energy consumption in composites production. High melting temperatures increase the processing temperature and the cost of the processing. Table 4.4 summarizes ranges of glass transition temperature and melting temperature of selected semicrystalline biopolymers together with their density and tensile properties.

Table 4.4: Thermo-mechanical properties of some thermoplastic biopolymers (Van de Velde and Kiekens, 2002).

Polymer	Density	Tensile strength	Tensile modulus	Elongation to break	T_g	T_m
	[g/cm^3]	[MPa]	[GPa]	[%]	[°C]	[°C]
PLA	1.21 - 1.25	21 - 60	0.35 - 3.5	2.5 - 6	45 - 60	150 - 162
PGA	1.5 - 1.707	60 - 99.7	6 - 7	1.5 - 20	35 - 45	220 - 233
PCL	1.11 - 1.146	20.7 - 42	0.21 - 0.44	300 - 1000	-60 to -65	58 - 65
PHB	1.18 - 1.262	40	3.5 - 4	5 - 8	5 - 15	168 - 182

The mechanical strength of biopolymers is not considered as a limiting property, as the strength of unidirectionally reinforced composites is primarily determined by the fibres. PLA is probably the best choice as a matrix of all bio-based composites due to its low density, acceptable mechanical properties, high T_g and relatively low melting temperature (T_m-T_g for PLA is only ~ 100°C). Among the conventional thermoplastics, polypropylene is considered to be the best choice of a matrix for natural fibre composites (Velde and Kiekens, 2001). Apart from its low density and good thermo-mechanical properties, the recyclability and low cost of PLA and its wide use as a substitute for polypropylene should be also considered in its favour.

4.3 Unidirectional composites

Unidirectional fibre composites have high mechanical strength in the longitudinal direction. In this section, research on unidirectional composites reinforced with spun yarns of natural fibres is reviewed. Strength and modulus either in tension or flexure, fibre volume fraction and manufacturing methods of the composites discussed in this section are summarised in Table 4.5. Composites with thermoplastic matrices prepared by compression moulding are reviewed in the Table 4.6. For comparative purposes composites prepared by compression moulding of a jute and flax yarn with a thermosetting matrix are also mentioned (Roe and Ansell, 1985; Goutianos *et al*., 2006). Natural fibres are usually spun into long and continuous yarns to allow continuous manufacture of composites. It shall be pointed out that the additional energy consumption in spinning and weaving makes such reinforcements less attractive for environmentally friendly applications.

Table 4.5: Processing methods and mechanical properties of unidirectional composites reinforced with plant fibre yarn.

Composite (Matrix/fibre)	V_f	w_f	σ_T	E_T	σ_F	E_F	Method	Reference
	[%]	[%]	[MPa]	[GPa]	[MPa]	[GPa]		
PP/flax	-	50-75	251-321	27-29	-	-	CM	Madsen and Lilholt, 2003
PET/hemp	48	-	280	28	-	-	CM	Madsen *et al*., 2008
Vinyl ester/flax	37	-	198	17	-	-	FW	Goutianos *et al*., 2006
PP/jute	49	-	107	6	91	8.8	CM	Khondker *et al.*, 2005
UPE/jute	32		170	20	-	-	CM	Roe and Ansell, 1985
PLA/jute[a]	22.5	-	-	-	110	7-8	CM	Khondker *et al.*, 2006

Note: [a]microbraided yarn;CM = compression moulding; FW = filament winding; PP = polypropylene; PET = polyethylene terepthalate; UPE = unsaturated polyester.

Khondker *et al*. (2006) investigated the fabrication of unidirectional thermoplastic composites using jute yarn. Jute fibres formed the straight central part of the yarn around which was

braided the PLA fibre. PLA was meant to melt and penetrate the fibres during processing and form the matrix of the composite. Micro-braided yarn was wound onto a metallic frame in two layers (Figure 4.4), inserted in a preheated mould and compressed.

Figure 4.4: Consolidation set-up for compression moulding: (a) unidirectional arrangement of fibres in a tension rig, (b) moulding die and (c) consolidation by compression moulding (Khondker *et al*., 2006).

A three-point bending test was performed to analyze the effect of moulding temperature and pressure on the mechanical properties of composites. Samples moulded at 175°C at 2.7 MPa for 10 min. with 22.5 vol. % of jute fibres had a flexural strength of 110 MPa and flexural modulus of 7-8 GPa. Composites were reported to fail in compression as a result of poor interfacial adhesion and fibre impregnation. Scanning electron micrographs showed no micro-voids between the fibre and the matrix and a properly melted and distributed PLA matrix.

Madsen and Lilholt (2003) studied mechanical properties of unidirectional polypropylene composites reinforced with flax yarn. Composites with 50–75 wt% of flax fibres were compression moulded. Flax yarn was wound onto a metal frame and laid up with polypropylene films (0.025 mm of thickness), vacuum heated (190°C/15 min.) and press consolidated (2.2 MPa for 1 min). The composites axial strength and stiffness were 251–321 MPa and 27–29 GPa, respectively. Madsen *et al*. (2007 and 2008) prepared unidirectional composites reinforced with two types of hemp yarn The fibre volume fraction of the composites varied from 0.3 to 0.5. Thermoplastic matrices were polyethylene terepthalate (PET), polyethylene (PE) and polypropylene (PP) in the form of filament yarn. Hemp yarn and thermoplastic yarn were concurrently wound on a metal frame, heated under vacuum (200°C, 15min., 10 mbar) and press consolidated (2.6 MPa/30°C/min.). The effect of processing temperature (180, 200 and 220°C) and conditioning humidity (35, 65 and 85% relative

humidity, RH) on composites properties was investigated. Composites reinforced with yarn of lower linear density, produced under the same conditions showed higher stiffness (20.1 GPa vs. 17.3 GPa) and ultimate stress (221 MPa vs. 205 MPa). With increasing processing temperature the strength decreased and the stiffness slightly increased, for example from 244 to 170 MPa and from 19.4 to 22.5 GPa respectively. PET composites with fibre volume fraction of 0.48 resulted in Young's modulus of 28 GPa and ultimate stress of 280 MPa. These composites were processed at 200°C and conditioned at 65%RH. Ansell and Roe (1985) reported stiffness of 20 GPa and ultimate stress of 170 MPa for aligned jute yarn/unsaturated polyester composites with fibre volume fraction of 0.32.

Goutianos *et al*. (2006) manufactured unidirectional composites produced by filament winding of low twist yarn (47 turns/m) with 37 vol.% reinforcement and reported a tensile modulus of 24GPa and tensile strength of 248MPa. Khondker *et al*. (2005) prepared unidirectional PP/jute yarn (207 tex) composites (V_f=0.49) by compression moulding. Jute yarn was wound onto a metal frame in four layers. Between the two jute layers two stripes of PP foil were inserted. This assembly was compressed at 160°C and pressure of 2 MPa for 15 min. Flexural strength and modulus of the composites improved by 190 and 460 %, compared to neat polypropylene. Flexural modulus and strength were reported to improve about 10 and 20% respectively, when the jute yarn was coated with polyvinyl alcohol/polypropylene (PVA/PP).

4.4 Laminar composites:

Laminar composites consist of two-dimensional fabrics with a preferred high strength in one direction. Sheets are usually preimpregnated with matrix resin. The main advantage of laminar composites is their fast processing. In this section, research on natural fibre reinforced laminar composites is reviewed. Mechanical properties of the composites reviewed are presented in Table 4.6. As can be seen from the Table 4.6 composites based on thermoplastic matrix made of polylactic acid are compared to composites with thermosetting matrix and two geometries of the reinforcement with and without yarn crimp.

Katayama *et al*. (2006) prepared polylactic acid composites reinforced with jute plain weave fabric (430 g/m^2). A PLA matrix (melting temperature T_m = 140°C) was used and a jute non-

woven fabric sheet was manufactured into a composite by melt-blown process. In this process, melted resin is blown from the nozzles with hot air and non woven sheet is formed on the conveyer. Composites were made by vacuum (0.1 MPa) compression moulding of lay-ups of jute fabrics between four PLA sheets and composites contained 48 vol% of jute fibres. It took 5 min. for the resin to impregnate the fibre bundles at 3 MPa. SEM pictures of composite cross-sections showed no voids inside the jute yarn. Composites with 53 vol.% of jute fibres moulded under these ideal conditions reached a bending strength of 115 MPa and a flexural modulus of 6 GPa. These values were reported to be comparable to polypropylene reinforced with 20 wt. % of long glass fibres.

Table 4.6: Mechanical properties of compression moulded laminar composites.

Composite (Matrix/fibre)	Fabric	V_f	σ_T	E_T	σ_F	E_F	Reference
	Weave/g.m^{-2}	[%]	[MPa]	[GPa]	[MPa]	[GPa]	
Vinyl ester/flax	Plain/600	41	74	10	-	-	Goutianos *et al*. (2006)
Vinyl ester/flax	Roving[a]	31	248	24	-	-	Goutianos *et al*. (2006)
PLA/jute	Plain/430	53	-	-	115	6	Katayama *et al*. (2006)

Note: properties tested in warp direction; [a] knitted together in weft direction.

Although this chapter is on thermoplastic matrix composites reinforced with natural fibres it is worth mentioning the work of Goutianos *et al*. (2006) who developed flax fibre based fabrics (biaxial plain weaves, unidirectional fabrics and non-crimp fabrics) for composite structural applications. Firstly long flax fibre bundles were converted into pre-yarns with low twist (29 turns/m) and linear density of 524 and 609 tex. Unidirectional (UD) composites were manufactured via pultrusion. Interlaminar shear strength (ILSS) was determined to evaluate the adhesion of thermosetting resin to the fibres. Composites made from unsaturated polyester (UPE) resin and flax fibres with fibre volume fraction of 30% possessed an ILSS of 22 MPa compared with 30 MPa for epoxy composites. These values were reported to indicate reasonable adhesion between fibre and matrix and typical values for glass fibre reinforced polyesters and epoxies are 35 and 50 MPa respectively). Alkali treatment of natural fibres

improved the ILSS of polyester based composites by 10%. There are composites processing techniques where fabrics are used preferentially to fibres, as they enable easier handling. Secondly the flax yarns with low twist were converted into warp knitted uniaxial fabrics. In the knitting process, each warp thread (14 tex polyester PET yarn) is knitted forming interlaced loops. At the same time straight inlays of the flax yarn in the weft direction were introduced. The fabrics produced were crimp free in both directions. Flax yarns were oriented in uni-axial direction. Woven fabrics with plain weave structure and threads of different linear densities in the warp and weft direction were also manufactured and RTM was used to produce composite laminates. Vinyl ester was used as a matrix. Unidirectional warp knitted composites (V_f=0.3) had a longitudinal flexural modulus of 17 GPa and strength of 198 MPa. The composites were reinforced with fabric of 185 g/m^2 areal density. The weft yarn was made from long flax fibres and had linear density of 210 tex and twist of 223 turns/m. The weft density was 100 threads/m (flax thread) and the warp density was 50 threads/cm (PET thread). Composites reinforced with plain weave fabric (600g/m^2) had a tensile modulus and strength of 10 GPa and 74 MPa, respectively.

4.5 Short fibre composites:

Discontinuous fibres are cheap and faster and easier to fabricate into complicated shapes. Short natural fibres are usually mixed with a thermoplastic matrix via extrusion and then injection moulded into complicated shapes. Other common practice is compression moulding of mats made of short randomly oriented fibres and thermoplastic sheets of polymer matrix.

Inoue and co-workers (2007) developed bio-based plastics for housing of electronic products consisting of PLA and short kenaf fibres. The composites reinforced with fibres of 3 mm length were prepared by twin screw extrusion at 184°C. The best properties were obtained for composites containing 20 wt% of kenaf fibres. The flexural modulus increased from 4.5 GPa to 7.6 GPa. The flexural strength decreased from 132 MPa to 93 MPa. By adding a flexibilizer based on a copolymer of polylactic acid and aliphatic polyester the impact strength of composites was improved. The properties of the composites were comparable to glass fibre reinforced ABS.

Oksman and co-workers (2003) studied polylactic acid reinforced with flax fibres. Composites with 30 and 40 wt% fibre were manufactured by twin screw extrusion (temperatures profile: 180-200°C) followed by compression moulding (50°C/70 MPa). Samples with 30 wt% of flax fibres were reported to have a tensile modulus of 8.3 GPa and tensile strength of 53 MPa. SEM micrographs of fractured surfaces indicated poor fibre matrix adhesion ("clean" fibre surface) and separation of fibre bundles into single fibres during extrusion.

Injection moulded PLA composites reinforced with 10-40 wt% of flax and regenerated cellulose fibres were prepared by Bax and Müssig (2008). Composites reinforced with 30 wt% of regenerated cellulose fibres exhibited a Charpy impact strength of 72 kJ/m^2 and tensile strength of 58 MPa and Young's modulus of 4.9 GPa. Composites reinforced with 30 wt% of flax fibres had a Charpy impact strength of 11 kJ/m^2, tensile strength of 54 MPa and modulus of 6.31 GPa. Multilayer webs made from PLA fibre (0.67 tex) and rayon fibre (0.18 tex) or flax fibre were manufactured using a carding machine. Webs were compressed at 170°C and 18 MPa for 5 min. The resulting composite plates were shredded to prepare pellets suitable for injection moulding. Before injection moulding, shredded pellets were mixed with the original PLA pellets (T_g 60-65°C, T_m 160-170°C).

Plackett (2003) developed polylactic acid composites reinforced with jute mats using a film stacking technique. Composites contained about 40 wt% of jute fibres. PLA pellets were converted into 1.2 mm thick films using a single screw extruder (temperatures at barrel zones were set to 160,180,190°C and the die to 190°C). Jute fibre mats were laid up with several PLA films, pre-compressed for 15 seconds at the pressure of 3.3 MPa and heated under a vacuum for 3–10 min. at temperatures of 180–220°C. After the heating stage the assemblies were transferred to the press and consolidated at 3.3 MPa/60°C for 1 min. Composites with 40 wt% of jute fibre manufactured at 210-220°C exhibited a tensile strength of approximately 100 MPa and a tensile stiffness of 9.5 GPa. Limited PLA degradation was reported during the heating stage under the vacuum.

Bodros *et al*. (2007) studied tensile properties of flax fibre reinforced thermoplastic bio-polymers. PLA composites with 30 % flax fibre volume fraction had higher tensile strength and modulus than polypropylene composites (100 MPa and 9.5 GPa). PLA/flax composites exhibited higher specific strength than unsaturated polyester/flax fibre composites. They conclude that it is possible to substitute polyester glass fibre laminates with PLA/flax fibre

composites in structural applications when the structures are subjected to tensile stresses. Mechanical properties of polylactic acid reinforced with short natural fibres and prepared either by injection or compression moulding which were discussed in this section are summarized in Table 4.7.

Table 4.7: Processing methods and mechanical properties of PLA reinforced with short natural fibres.

Composite (Matrix/fibre)	V_f	w_f	σ_T	E_T	σ_F	E_F	Method[a]	Reference
	[%]	[%]	[MPa]	[GPa]	[MPa]	[GPa]		
PLA/kenaf	20	-	-	-	93	7.6	E/IM	Inoue *et al*., 2007
PLA/jute	-	40	100	9.5	-	-	CM	Plackett, 2003
PLA/jute	30	-	100	9.5	-	-	CM	Bodros *et al*., 2007
PLA/flax	-	30	54	6.3	-	-	CM/IM	Bax and Müssig, 2008
PLA/flax	-	30	53	8.3	-	-	E/CM	Oksman *et al*. (2003)

Note: [a] NaOH treated; E = extrusion; CM = compression moulding; IM = injection moulding

4.6 Unidirectional composites processed by wet impregnation

Pre-impregnation of reinforcement by partially cured resin (thermosets) is a popular manufacturing method within aerospace industry. It enables the manufacturer to cut the desired shape from the prepreg, lay it over the mould and apply heat and pressure. The time for manufacturing the desired part is significantly reduced and workers are not exposed to un-reacted resin (Tucker, 2004). High melt viscosity makes impregnation with thermoplastics difficult. Common impregnation techniques are solution casting, melt impregnation, film stacking, filament coating, comingling and powder pre-impregnation. For example Nishino *et al*. (2003) impregnated kenaf sheets with PLA solution in 1,4-dioxane to manufacture composites through wet impregnation process. Kenaf sheets were dried at 120°C and than immersed in a dioxane solution (10 wt%) under vacuum. After impregnation the sheets were dried at room temperature for 24 hours and then dried under vacuum until they reached a constant weight. Cast PLA film had a low Young's modulus (1.3 GPa) and tensile strength (21

MPa). PLA reinforced with 70 vol.% of kenaf fibres had a Young's modulus of 6.4 GPa and tensile strength of 60 MPa. Composites with higher fibre content exhibited lower properties due to insufficient impregnation of fibres. PLA composites reinforced with silane treated kenaf fibres showed superior tensile properties to untreated composites (Nishino *et al*., 2006). Using X-ray diffraction, it was found, that stress applied to the composites was effectively transferred to the fibres thorough the matrix.

Ochi (2006) developed high strength material composed of unidirectional Manila hemp long fibre bundles and starch-based emulsion type thermoplastic resin. Optical micrograph of transverse section of such composite reveals good fibre to matrix adhesion and high fibre volume fraction (Figure 4.5).

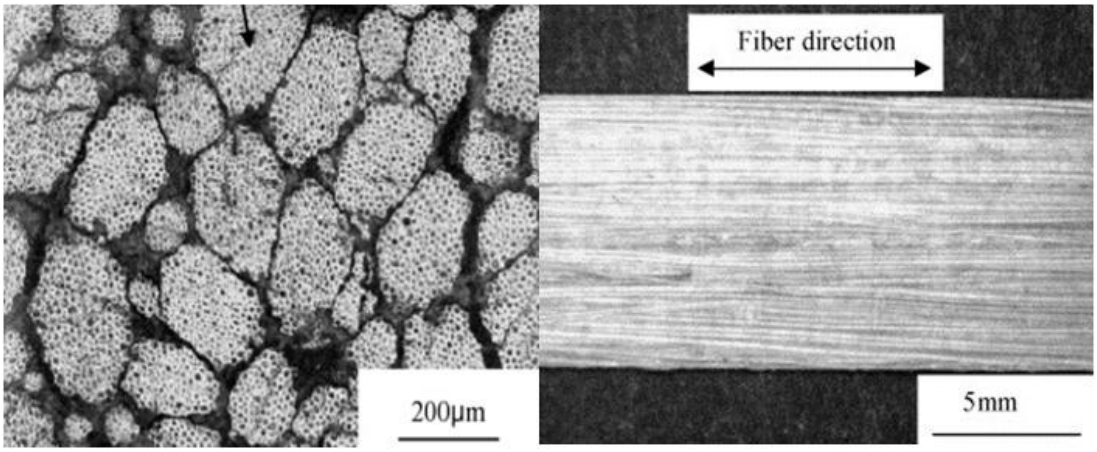

Figure 4.5: Optical micrograph of transverse section of biodegradable composites with V_f=0.7 of kenaf fibres (left) and photograph of such composite (right) prepared by Ochi (2006).

Fine particles of the resin in aqueous solution were placed on the surface of the fibres and dried at 105°C / 120 min. Consequently, the composites were placed in a mould preheated at 130°C for 5 min. After consolidation they were hot pressed at 130°C / 10 MPa for 10 min. The tensile and flexural strength were 365 and 223 MPa, respectively with a fibre volume fraction of 70 %. Composites were fabricated by compression moulding of preforms of fibres coated with emulsion type biodegradable resin based on starch.

Takagi and co-workers (cited in Goda and Cao, 2007) developed composites reinforced with 75 wt% of Manila hemp fibres. Composites were fabricated by compression moulding of preforms of fibres coated with emulsion type biodegradable resin based on starch. The pre-

forming technique was similar to the one used by Gomes et al. (2007). The technique is described in detail further in this section. Axial tensile strength and modulus of 307 MPa and 35 GPa were reported.

Gomes *et al*. (2007) compression moulded biodegradable composites reinforced with 70 vol.% of curaua fibres. Hydrophilic resin based on a blend of corn starch and polycaprolactone (PCL) was used as a matrix (T_g: -60°C and T_m: 60°C). The resin was supplied as water emulsion of 5 μm polymer particles. Composites were prepared by so called direct method, pre-forming method and prepreg sheet method to control the fibre alignment and fibre volume fraction in manufactured composites. Table 4.8 summarizes the processing parameters of individual methods.

Table 4.8: Summary of processing parameters and mechanical properties of starch based composites reinforced with curaua fibres (Gomes *et al*., 2007).

Processing parameters	Compression moulding method		
	Direct	Pre-forming	Pre-preg
Alignment control	No	Yes	Yes
Resin distribution	Non-distributed	Distributed	Distributed
Pre-drying (°C/MPa/h)	No	30/0/24	120/ P→0/ - *
Compression moulding (°C/MPa/h)	150/ P→0/1	150/6.54/1	150/3.27/1
Cooling pressure (MPa)	3.27	13.1	16.9
Composite properties			
Fibre vol. fraction V_f (%)	69.3	67	69.9
Tensile modulus E (GPa)	13	29	36

Note: P→0: "slight" pressure; *: not listed.

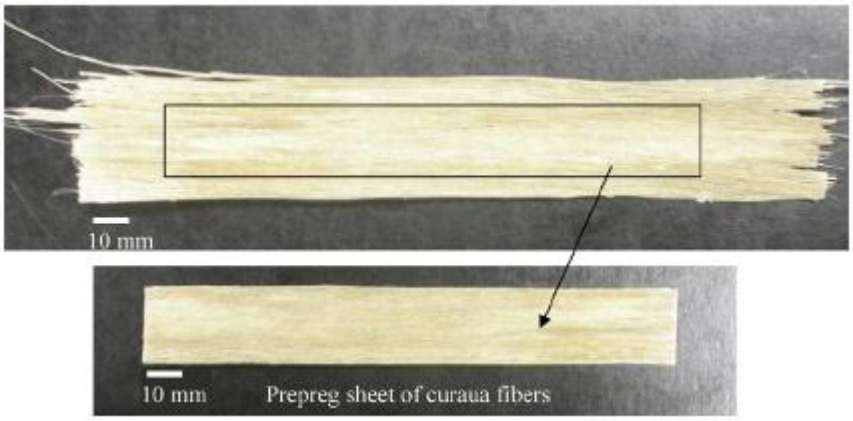

Figure 4.6: Prepreg sheet of curaua fibres and thermoplastic starch based matrix (Gomes *et al*., 2007).

In the *direct method* fibres were placed into a metal mould, resin was poured onto fibres, and fibres were lightly pressed at 150°C for 1 hour. Composites were cooled down at a pressure of 3.27 MPa to room temperature. In the *pre-forming method* in order to control fibre alignment, fibres were wound and stretched around a metallic plate. Resin emulsion was painted onto the fibres by brush. Preforms were dried at 30°C for 24 hours. Composites were prepared by compression of two pre-forms at 150°C at 6.54 MPa for 1 hour. Composites were cooled down at 13.1 MPa to room temperature. In the *prepreg sheet method* (Figure 4.6) the fibres were wound and stretched around a metallic plate. Resin emulsion was painted onto the fibres by brush. Preforms were dried at 120°C under minimum pressure. Composites of five sheets were compression moulded at 150°C at 3.27 MPa for 1 hour. Composites were cooled down at a pressure of 16.9 MPa to room temperature. Composites manufactured by the prepreg sheet method had a tensile strength and modulus of 327 MPa and 36 GPa. Composites made from alkali treated curaua fibres (10 wt% solution/2 h) achieved tensile strength and modulus of 334 MPa and 32 GPa respectively. The fracture strain of alkali treated fibres increased about 50 %. Evaluating the toughness of the material by the area under the stress–strain diagram, it was concluded that treating curaua fibres with10 wt% NaOH solution improved the toughness and conserved the strength of the composites.

Mechanical properties of composites based on starch thermoplastic matrices which were discussed in this section are summarized in Table 4.9 together with their fibre volume fractions.

Table 4.9: Mechanical properties of unidirectional composites with starch based thermoplastic matrix.

Composite (Matrix/fibre)	V_f	σ_T	E_T	Method	Reference
	(%)	MPa	GPa		
Thermoplastic starch/hemp	75	307	35	CM	Goda and Cao, 2007
Thermoplastic starch/hemp	70	365	30	CM	Ochi, 2006
Thermoplastic starch/curaua	70	327	36	CM	Gomes *et al.*, 2007

Note: CM = compression moulding.

Ochi (2008) prepared unidirectional biodegradable composites reinforced with kenaf fibres using emulsion-type PLA as a matrix (PL-1000, Miyoshi Oil & Fat Co). PLA was supplied as a suspension of particles of 5 μm diameter. These particles were suspended in an aqueous solution with PLA content of 40 wt%. Composites were compression moulded at 160°C at 10 MPa for 10min. The composites had V_f=0.7 and tensile and flexural strengths were 223 and 254 MPa respectively. Tensile and flexural moduli were about 23 GPa. Tensile and flexural strength were increasing linearly up to kenaf fibre volume fraction content of 50 %.

All cellulose composites with high fibre volume fraction were prepared by Soykeabkaew *et al*. (2008) by partial surface dissolution of aligned ramie fibres using lithium chloride/N,N-dimethylacetamide. Suction in the solvent for 2 hours resulted in composites with high fibre volume fraction (V_f=0.84) and excellent tensile strength of 460 MPa and modulus of 28 GPa respectively. Strong interfacial adhesion was also demonstrated with transverse tensile strengths in the range of 22–40 MPa depending on the suction time.

4.7 Recycling

Bourmaud and Baley (2007) investigated the influence of recycling on mechanical properties of injection moulded polypropylene reinforced with 30wt% of hemp and sisal short fibres (1.5mm). The melt temperature was 180°C and the mould temperature was 50°C. It was found that the fibre length decreased significantly during reprocessing. PP-*g*-MA improved fibre-matrix adhesion, but the effect disappeared after seven injection cycles. Due to the nucleating ability of natural fibres, polypropylene in composites showed a higher degree of crystallinity. After seven injection moulding cycles the modulus and tensile strength of PP/hemp composites decreased, by 10 and 17% respectively, while modulus and tensile strength of PP/sisal composites remained unchanged. Tensile modulus was reported to be 3.5 GPa and 3.8 GPa for sisal and hemp reinforced PP composites. The work has demonstrated the potential of the recyclability of polypropylene reinforced with natural fibres. Mechanical properties of recycled samples decreased slightly. Thus for example composites reinforced with unidirectional long fibre bundles could be shredded after their use life and converted into low cost products.

As already pointed out at the beginning of this chapter natural fibre reinforced polymer composites (NFCs) could replace glass fibre reinforced polymer composites (GFRPs) in low-cost and low-weight applications where the variability of their mechanical properties is not so critical.

As expected the literature review on natural fibre reinforced polymer composites with thermoplastic matrices shows that the best mechanical properties are obtained in systems where long fibres or fibre bundles without twist are used and where the matrix can be easily distributed among the fibres prior to the moulding. The highest mechanical properties so far reported belong to all cellulose composites. The technique of partial dissolution of the surface of natural fibres and its conversion into cellulose acetate enables manufacture of composites with high fibre volume fractions.

5 Interfaces in micro-composites

This chapter focuses on composite interfaces and it is divided into three major sections. Firstly the theory of adhesion is outlined followed by an assessment of the strategies used for optimization of adhesion in thermoplastic composites reinforced with natural fibres. The second part of the chapter is dedicated to polymer crystallization and matrix morphology development in the presence of a fibre. The third section of the chapter is dedicated to the micromechanics of stress transfer at the fibre to matrix interface based on shear lag theory. Micromechanics models for a single fibre fully embedded in a matrix and a single fibre with an exposed end are presented. The fracture mechanics approach for the measurement of the adhesive strength of the interface is explained. The chapter concludes with a discussion of the development of residual strains in a semicrystalline matrix and their influence on adhesion.

5.1 Theory of adhesion

By combining fibres with a polymer matrix to create a composite, fibre to matrix interfaces are created. The polymer matrix is applied as a liquid, i.e. a thermoplastic melt during the processing of a composite. The polymer melt "wets" the fibre and wetting is the prerequisite for adhesion. In turn, the adhesion of a matrix to a fibre is a prerequisite for stress transfer.
The level of adhesion can be predicted from the knowledge of surface energies of the individual phases. From the force equilibrium (Figure 5.1) between the solid, liquid and vapour phases the following equation results (Packham, 2003):

$$\frac{\gamma_{SV} - \gamma_{SL}}{\gamma_{LV}} = \frac{A}{A_0}\cos\theta = r\cos\theta \tag{5.1}$$

Where γ is an interfacial tension between *solid –vapour*, *liquid-vapour* and *liquid-vapour* phases, θ is the contact angle between the phases and r is the roughness factor (Wenzel, 1949). The roughness factor applies if the solid-liquid interface is not perfectly flat and is defined as the ratio between the 'true' surface area A and the nominal area A_0. If $\theta=0$ the liquid

completely wets the solid surface, i.e. the fibre. The surface energies are also associated with the failure at the interface through the work of adhesion which is defined as the work necessary to separate two surfaces which meet at the interface (Cherry, 1981):

$$W_a = \gamma_{SL} - \gamma_{SV} + \gamma_{LV} \cos\theta \tag{5.2}$$

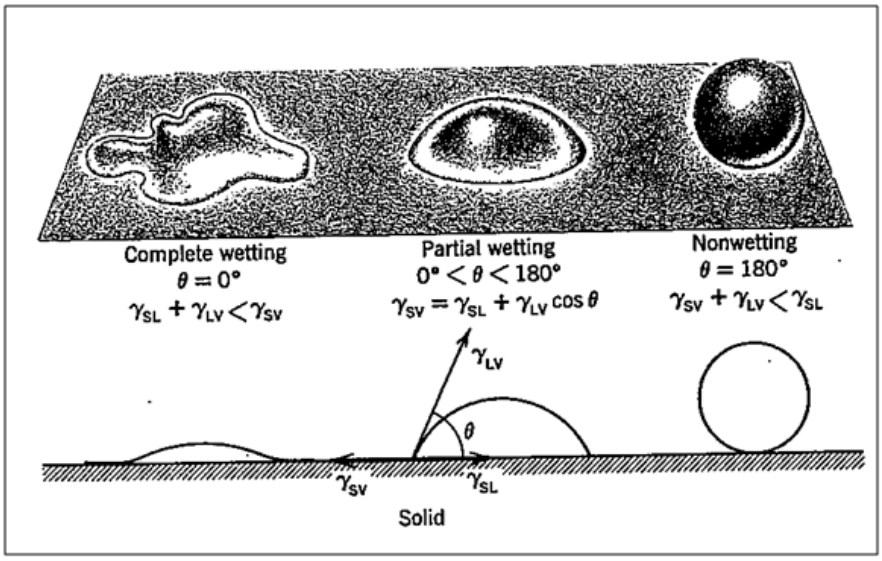

Figure 5.1: Wetting of a solid substrate by a liquid (Harris and Bunsell, 1977).

The contact angle can be measured at the liquid to solid interface and W_a calculated. There is a relationship between work of adhesion W_a and the interfacial shear strength (Nardin and Schultz, 1993):

$$\tau_{IFSS} = \delta \sqrt{\frac{E_m}{E_f}} W_a \tag{5.3}$$

where δ is a constant and, E_m and E_f are the matrix and fibre modulus respectively.

5.2 Optimization of adhesion

The chemistry of adhesion modification in natural fibre composites to promote interfacial bonding and improved stress transfer between fibre and matrix is mainly focused on the hydroxyl groups exposed on the surface of cellulosic fibres. Improvement in fibre to matrix adhesion is usually achieved through covalent linkages between fibre and matrix or through hydrophobization of the cellulose surface. Cellulose is a linear polysaccharide consisting of D-anhydro-glucopyranose units joined together by β-1.4-glucosidic bonds. Each unit has two secondary hydroxyl groups (in position 2 and 3) and one primary hydroxyl group (in position 6) which can enter chemical reactions. The hydroxyl group in position 6 is sterically hindered. These factors influence the reactivity and accessibility of cellulose hydroxyl groups (Sjöström, 1993). Widespread techniques for promoting better adhesion include caustic soda treatment, acetylation and silylation (Mohanty *et al*., 2001). However these techniques are usually related to natural fibre composites with thermosetting matrices. Mwaikambo and Ansell (1999) studied the effect of various concentrations of NaOH solutions on the surface topography of cellulosic fibres. SEM micrographs and X-ray diffraction showed that alkalisation changed surface topography and increased the order of cellulose crystallites packing. Towo *et al*. (2005) analysed interfacial adhesion between sisal fibres and polyester resin droplets by a micro-bond shear test and the interfacial shear strength increased significantly (55%) after alkali treatment of the sisal fibres (0.06 mol% NaOH). Gandidni and Belgacem (2005) adopted several approaches to modifying the surface structure of cellulosic fibres to improve fibre to matrix adhesion such as:

(i) Grafting with oligomeric molecules bearing functional groups capable of reacting with cellulose hydroxyl groups. Selected molecules had either other functional group capable of reacting with polymer matrix or long terminal chains which could cover the fibre surface like an umbrella (Figure 5.2).

(ii) Grafting with polymerisable molecules. Molecules bore two functional groups: one capable of reacting with the cellulose surface and the second capable of forming covalent bonds with the polymer matrix.

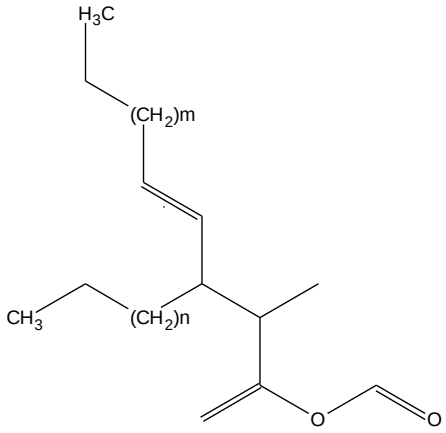

Figure 5.2: Proposed molecular umbrella for physical shielding of cellulose surface (Gandini and Belgacem, 2005).

Teeri *et al*. (2007) reviewed cellulose interactions with other biopolymers in plant tissue in the context of natural fibre biocomposites, their processing and fibre to matrix adhesion. According to their work mimicking plant cell wall "bio-compatibilizers" would be a way to overcome poor interfacial adhesion between cellulose and hydrophobic artificial polymer.

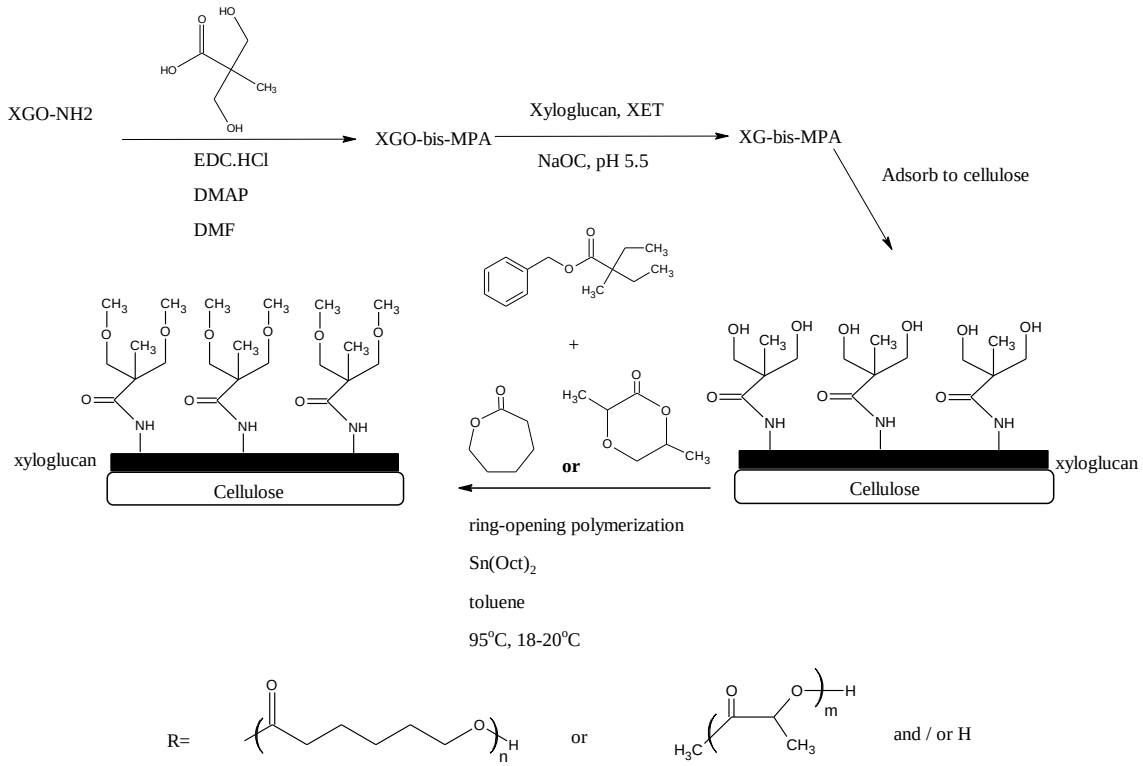

Figure 5.3: Modification reaction of cellulose with XG-bis-MA and subsequent ring opening polymerization of CL or L-LA (Lönnberg *et al.*, 2006)

Cellulose microfibrils deposited in the plant cell wall are coated with polysaccharides. These polysaccharides bind cellulose to other cell wall polymers and proteins. Chemically modified xyloglucan adsorbed at cellulose surfaces and bearing functional groups which act as initiators of polymerization reactions can result in cellulosic fibres coated with polymer. This approach was adopted by Lönnberg *et al*. (2006) who grafted PLA onto a cellulose substrate activated with 2,2-bis(methylol)propionic acid (bis-MPA) (Figure 5.3).

Maleic anhydride grafted polymers are usually used as a compatibilizer between cellulosic fibres and thermoplastic matrices. For example the interfacial bonding between natural fibres and polypropylene matrices is usually improved with polypropylene grafted maleic anhydride (PP-*g*-MA; Mohanty, 2001). Polylactic acid grafted maleic anhydride (PLA-*g*-MA; Figure 5.4) was examined as a compatibilizer between jute fibres and PLA (Plackett, 2003 and Plackett, 2004). Jute fibres were combined with PLA films and compression moulded at 200°C for 5 min. Some of the fibres were previously treated with a solution of PLA-*g*-MA in chloroform. Composites containing PLA-*g*-MA had a tensile strength of 60 MPa. Composites with no PLA-*g*-MA had a tensile strength of 100 MPa. The reduction in tensile strength was explained by the low molecular weight of PLA-*g*-MA. The matrix of treated composites contained about 25 wt% of maleated polylactic acid.

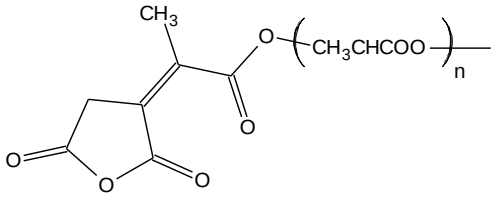

Figure 5.4: Structure of maleic anhydride grafted PLA.

Huda *et al*. (2007) investigated the influence of alkali treatment and silane treatment on thermo-mechanical properties of polylactic acid reinforced with 40 wt% of kenaf fibres. Composites were prepared by compression moulding of short kenaf fibres (18-24 mm) and PLA films with thickness of 1 mm. Three layers of kenaf fibres were placed between four PLA films, compressed at 190°C / 4.8 MPa for 12 min. and then compacted at a pressure of 11.7 MPa for 5 min. followed by cooling under pressure. The flexural modulus for alkali and silane treated fibres increased from 5.6 GPa to 8.3 and 9.5 GPa respectively. The flexural

strength of PLA decreased with the addition of kenaf fibres. Composites reinforced with treated fibres exhibited higher flexural strengths in comparison with untreated fibres In order to improve fibre matrix adhesion in PLA / kenaf fibre composites Nishino (2003) treated kenaf fibres with silane coupling agent Ajioka *et al*. (1998) copolymerized PLA with cellulose derivatives in order to improve the melt tension of PLA and prepare material for foam production and blow moulding. Obviously copolymers of PLA and cellulose could improve the adhesion between cellulosic fibres and the PLA matrix. Juntaro *et al*. (2007) grafted the surface of sisal fibres with bacterial cellulose simply by cultivating bacteria in the presence of sisal fibres. Modified fibres were used for fabrication of unidirectional composites with fibre weight fraction of 0.34. The tensile strength of composites with grafted sisal fibres was 114 MPa and the modulus was 11.2 GPa. Compared to composites reinforced with unmodified sisal fibres the tensile strength increased by 44%. Composites were also tested in a direction transverse to the fibre axis to measure the quality of the fibre to matrix bond. Composites showed off-axis (90°) tensile strength and modulus of 17 MPa and 3.1 GPa respectively. Compared to composites with unmodified fibres the composites with modified fibres had transverse tensile strength higher by a factor of 66%. Applying simple linear regression one can predict that composites with double the fibre content (V_f=0.68) would have a tensile strength of 228 MPa and modulus of 22.4 GPa. The same procedure was also applied to hemp fibres but with no improvement. Hemp fibres are finer fibres compared to sisal ones. In the case of hemp fibres the nanocellulose fibrils produced by bacteria created a dense network over several fibre bundles holding them together and preventing the polymer melt from wetting the fibre surface. Fibre bundles which were not impregnated by the polymer led to the premature failure of the composite under applied stress.

5.3 Matrix morphology development

In this section the development of crystalline morphology in semicrystalline polymers in the presence of reinforcing fibres will be discussed. Polymer crystallization and spherulitic morphology will be briefly outlined and transcrystallinity will be defined. Mechanisms for transcrystalline layer development will be proposed and the development of transcrystallinity in thermoplastic composites and its influence on adhesion strength and mechanical properties of composites will be reviewed.

5.3.1 Spherulitic morphology

The amount of crystalline content depends on thermal history of the semicrystalline polymer. The spherulite is the most common supramolecular structure found in thermoplastic polymers crystallized from their melts.

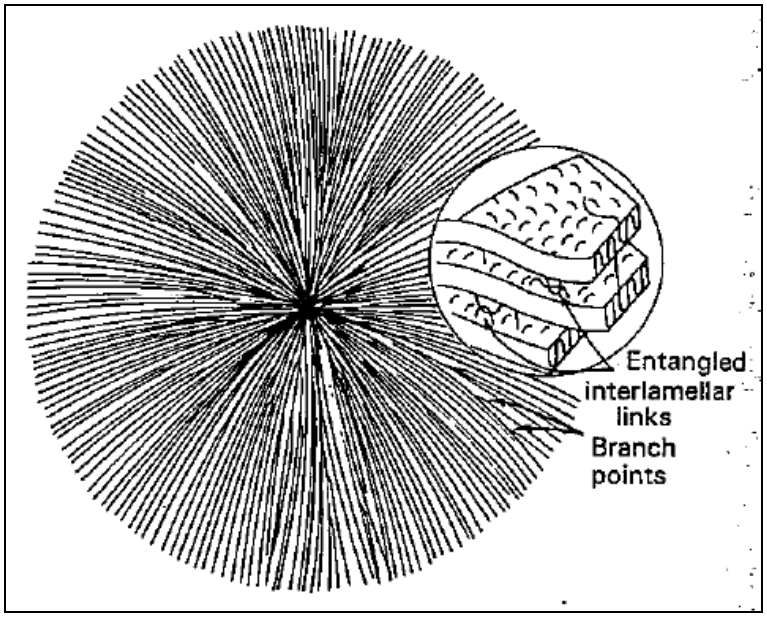

Figure 5.5: Schematic illustration of spherulite morphology (Lin and Argon, 1994).

They are aggregates of small lamellar crystals growing outwards from a central nucleus (Figure 5.5 and 5.6). The size of a spherulite depends on the degree of under-cooling. Generally speaking fast cooling rates from the melt lead to finer structure whereas slow cooling rates result in larger spherulites. When the spherulite is growing new crystallites are added to the aggregate uniformly at the growing front. There are two main types of spherulites – banded and non-banded. Banding can be usually be found in spherulites which are crystallized at a high rate of undercooling (Gedde, 1999).

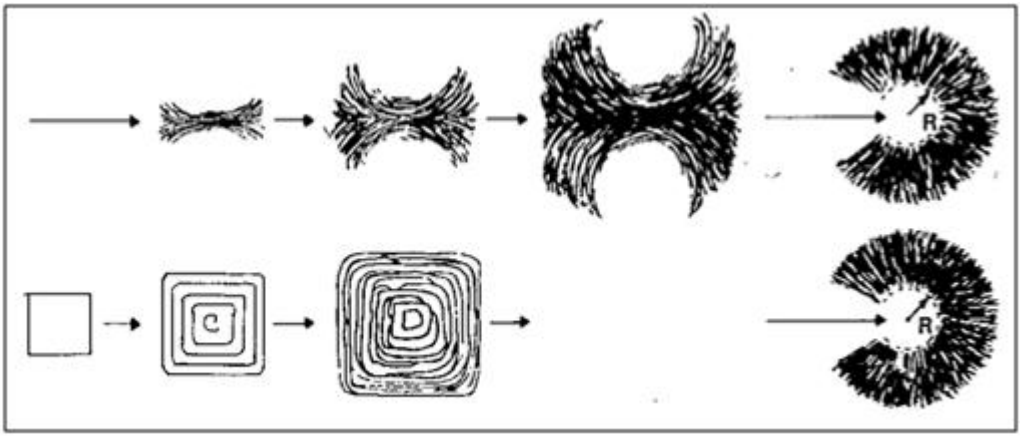

Figure 5.6: Schematic representation of successive stages in the development of a spherulite: a– edge on view; b- plan view (Lin and Argon, 1994).

When bulk material is crystallizing the spherulites grow until they fill the space and touch. Their boundaries are non-spherical after impingement and under polarized light they show a Maltese cross pattern.

5.3.2 Theory of crystallization

Detailed description of polymer crystallization can be found in monographs by Bassett (1981), Gedde (1999) and Schultz (2001) and will be discussed in this section.

Suppose a little spherical region of a new phase α develops within the parental phase β. The overall free enthalpy associated with the phase change is:

$$\Delta G = \Delta G_v + \Delta G_s$$
$$\Delta G = \frac{4}{3}\pi r^3 \Delta G_v + 4\pi r^2 \gamma_{SL} \qquad (5.4)$$

Where ΔG_v first term represents the energy associated with the creation of a spherical nucleus of the radius r and ΔG_s the other term represents the energy associated with the phase boundary creation. The results of the equation (5.4) at a temperature $T < T_m$ are shown graphically in Figure 5.7 with both terms plotted separately as a function of a radius r.

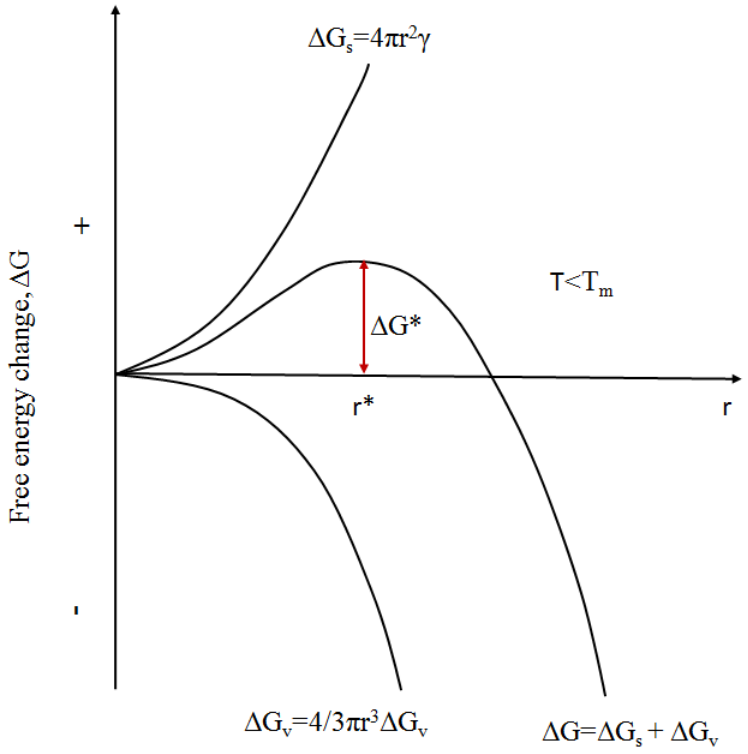

Figure 5.7: Energy barrier for homogeneous nucleation (Schultz, 2001).

It can be seen that first term of equation (5.4) is always negative reducing the energy barrier for nucleation and the second term is always positive. As the nucleus is small it has big surface to volume ratio and thus the energy associated with the creation of new surface is high. At small values of *r* the surface term dominates and the ΔG is positive. At large *r* the volume term dominates as it is proportional to r^3 and ΔG is negative. If the nucleus is to grow its creation must be associated with a decrease in free enthalpy. It is seen from figure (5.7) results that ΔG passes through a maximum (ΔG^*) which represents the energy barrier for nucleation:

$$\left(\frac{d\Delta G}{dr}\right)_{r=r^*} = 0$$

$$\Delta G^* = \frac{16\pi\gamma_{SL}^3}{3\Delta G_v^2} \qquad (5.5)$$

$$r^* = \frac{2\gamma_{SL}}{\Delta G_v}$$

Once the nucleus reaches the critical size denoted by critical radius r^* it has the same chance of shrinking or growing. Nuclei with $r < r^*$ are unstable and re-dissolve because ($d\Delta G/dr$) > 0. Nuclei with $r > r^*$ are stable and grow because ($d\Delta G/dr$) < 0.

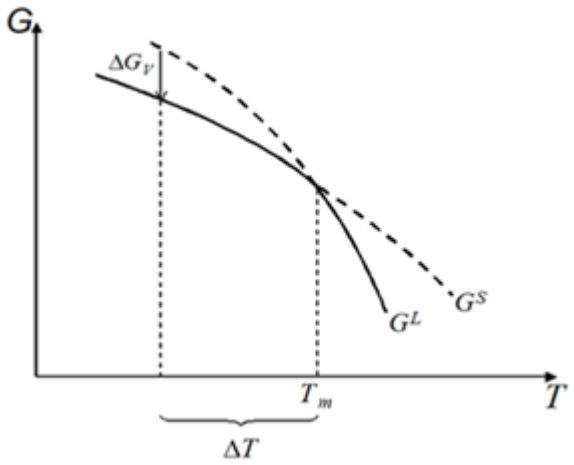

Figure 5.8: The effect of under-cooling on nucleation; free enthalpy of a solid phase (G^S) and a liquid phase (G^L) as a function of temperature (Burke, 1965).

The temperature dependence of nucleation lies in the first term ΔG_v of equation (5.4):

$$\Delta G_v = const(T_E - T)$$
$$\Delta G_v = \Delta H_v - T\Delta S_v = \Delta H_v - T\frac{\Delta H_v}{T_E} = \frac{\Delta H_v}{T_E}(T_E - T) = \frac{\Delta H_v}{T_E}\Delta T \qquad (5.6)$$

Figure 5.8 shows the free enthalpy of the solid and liquid phases as a function of temperature. It can be assumed that over small temperature intervals both relationships are almost linear and thus put the difference in free energy ($\Delta G_v = G^S - G^L$) is proportional to the degree of under-cooling ($\Delta T = T_E - T$).

Heterogeneous nucleation is more likely to occur than homogeneous nucleation. It can start at higher temperatures compared to homogeneous nucleation as the potential energy barrier is lower. If a nucleus develops at a solid surface then fewer crystallisable molecules are necessary for growth than for a nucleus with the same critical size which develops by homogeneous nucleation. The liquid has to wet the surface at $\theta < 180°$ (Figure 5.9) for heterogeneous nucleation to be active.

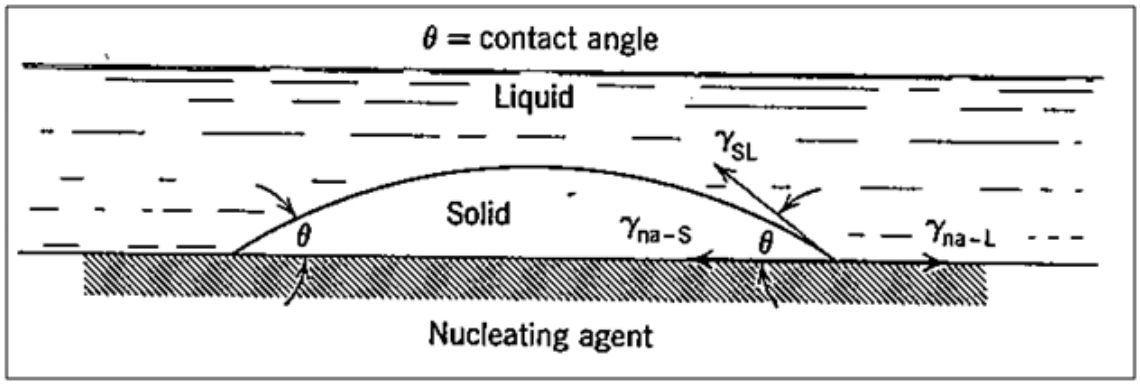

Figure 5.9: Heterogeneous nucleation and the wetting angle between the polymer melt and the solid surface (Harris and Bunsell, 1977).

Figure 5.9 shows the formation of a crystal nucleus on a solid surface in a polymer melt. From the force equilibrium γ_{SL} can be expressed as a function of the contact angle θ:

$$\gamma_{SL} = \gamma_{Na-S} + \gamma_{Na-L}\cos\theta \qquad (5.7)$$

Where γ is an interfacial tension between the pairs of phases: *solid nucleus–liquid (SL)*, *nucleating agent-solid nucleus (Na-S)* and *nucleating agent-liquid (Na-L).*

Equation (5.7) can be combined with Equation (5.5) and the critical free enthalpy for heterogeneous nucleation can be then expressed as a function of the critical free enthalpy for the homogeneous nucleation and contact angle θ:

$$\Delta G^{*} = \frac{16\pi\gamma_{SL}^{3}}{3\Delta G_{v}^{2}}\left[\frac{(2+\cos\theta)(1-\cos^{2}\theta)}{4}\right] \qquad (5.8)$$

$$\Delta G_{het}^{*} = \Delta G_{\mathrm{hom}}^{*} \cdot f(\theta)$$

If $\theta = 0$ then $\cos\theta = 1$ and the nucleation barrier disappears. If $\theta = 180°$ then $\cos\theta = -1$ and the liquid (melt) does not wet the solid surface (nucleating agent) such that heterogeneous nucleation is inactive and the nucleation can be realized only through the homogeneous mechanism.

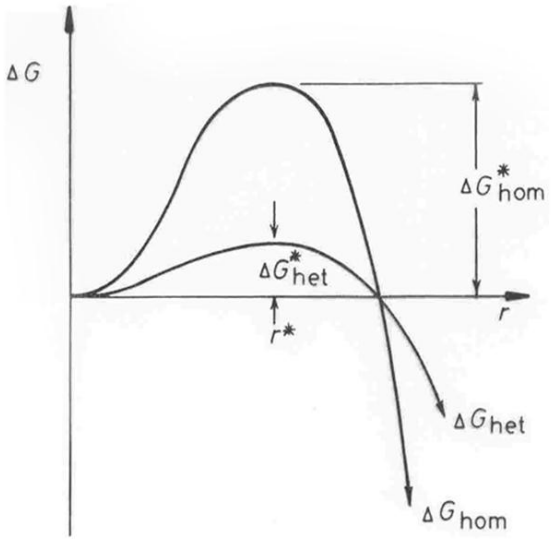

Figure 5.10: Energetical barrier for the heterogeneous nucleation (Bassett, 1981).

With reference to Figure 5.10 and from Equation 5.8 it is seen that $\Delta G_{het}^{*} < \Delta G_{\mathrm{hom}}^{*}$ at a fixed temperature $T<T_m$. Heterogeneous nucleation begins at higher temperatures than for homogeneous nucleation and reducing the degree of under-cooling.

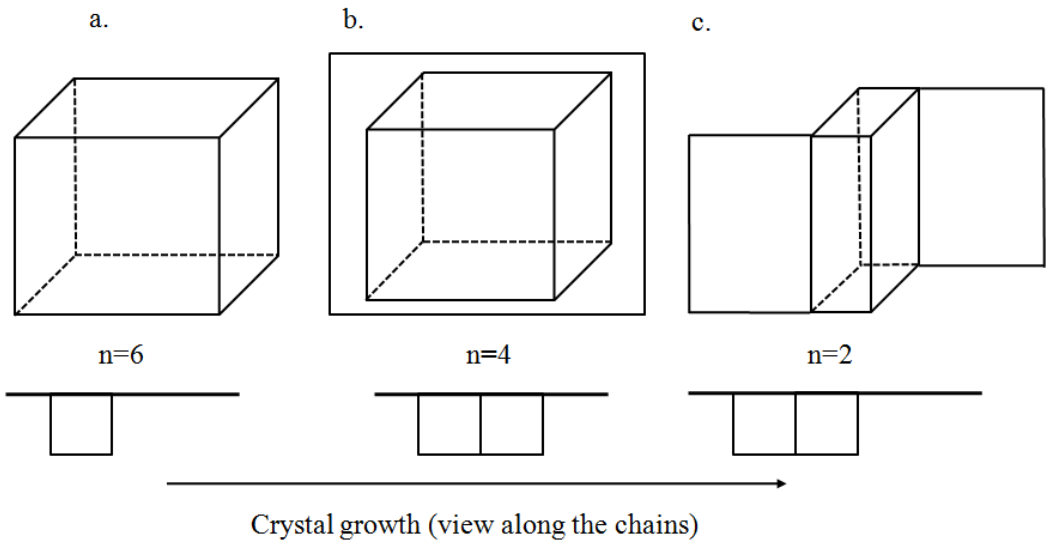

Figure 5.11: Main types of nucleation; n is the net number of newly formed surfaces (Gedde, 1999).

Once a nucleus is formed (primary nucleation – involves creation of six new surfaces) and the energetical barrier is broken the nucleus grows and becomes a crystal. Crystal growth occurs through a series of secondary (formation of four new surfaces) and tertiary nucleation (formation of two new surfaces) events (Figure 5.11; Gedde, 1999). Crystallization depends on nucleation and on diffusion of crystallisable molecules. The overall crystallization rate (ω_c) can be described by the following equation:

$$\omega_c = C \exp\left(-\frac{U^*}{R(T_c - T_\infty)}\right) \exp\left(-\frac{K_g}{T_c(T_m^0 - T_c)}\right) \qquad (5.9)$$

Where C is a rate constant, U^* is an energy constant, R is the gas constant, T_c is the crystallization temperature, T_∞ is a temperature at which all the segmental mobility is frozen, K_g is a kinetic constant for the secondary nucleation and T_m^0 is the equilibrium melting temperature.

The constant C depends on segmental mobility of crystallisable polymer chains. The first exponential term is the temperature dependence of the transport of the crystallizing polymer

molecule segments. The second exponential term expresses the temperature dependence of the nucleation rate.

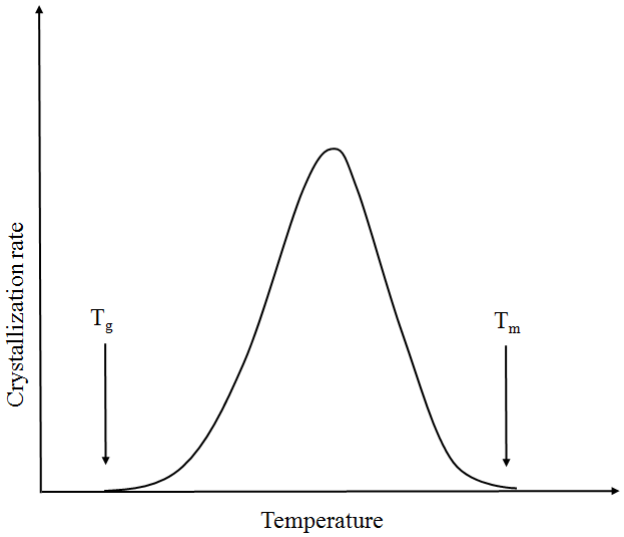

Figure 5.12: Crystallization rate as a function of temperature (Gedde, 1999).

The curve in Figure 5.12 shows the overall crystallization rate as a function of a temperature T_c and in fact as a function of the degree of under-cooling.
The overall crystallization can be also described by the Avrami equation:

$$1-\frac{\upsilon_c}{\upsilon_{c\infty}}=\exp\left(-Kt^n\right) \qquad (5.10)$$

Where υ_c is the volume crystallinity at time t, $\upsilon_{c\infty}$ is the final volume crystallinity and K and n are constants.

5.3.3 Transcrystallinity

Studying transcrystallinity of thermoplastic polymers containing fibre reinforcement is of technological importance when the polymer or polymer composite is melted and cooled down to achieve the desired shape during processing. Studies of transcrystallinity are usually made by means of differential scanning calorimetry (DSC), polarized light hot stage microscopy and X ray diffraction. They are usually completed with adhesion tests because the presence of a new morphology influences the stress transfer at the fibre to matrix interface. Transcrystallinity was first reported by Jenckel *et al*. in 1952. It still remains a controversial issue as the mechanism of transcrystallinity development is not fully understood. Thus it is difficult to say exactly whether and under which circumstances the transcrystalline morphology will develop and whether it will or will not improve the mechanical properties of a material. Crystallites can grow at large continuous surfaces like fibres in fibrous composites and they usually start growing simultaneously. Because of the high density of nuclei at the fibre surface at the same time the neighbouring crystallites touch and the only direction they can grow is the normal direction to the longitudinal fibre axis. They are laterally restricted and create a columnar structure with longitudinal axis parallel to the longitudinal axis of the fibre. Such a structure is called the *transcrystalline layer* or *transcrystallinity* (Billon *et al*., 1994). This is quite vague definition because the only requirements for calling the structure "transcrystalline" are "lateral restriction" and "columnar growth". Ishida and Bussi (1991) approached the problem more rigorously and defined the "advantage of a polymer to crystallize at a fibre surface (transcrystalline layer) rather than in a bulk (heterogeneous nucleation in the matrix)" as a ratio of free energies of the system:

$$A = \Delta\sigma' / \Delta\sigma \tag{5.11}$$

Where $\Delta\sigma$ is an interfacial free energy difference function for fibre/crystallite system and $\Delta\sigma'$ is an interfacial free energy difference function for melt heterogeneities/crystallite system. Table 5.1 summarizes expected values of A and describes situations which lead to surface-induced or bulk nucleation. Factors affecting heterogeneous nucleation also affect

transcrystalline growth at the fibre surface. The factors which reduce the energy barrier necessary for nucleation include temperature gradients, match of the polymer and a fibre crystal lattices, chemical composition (functional groups), crystalline morphology, surface energy, polymer molecular weight, residual stresses, fibre and matrix moduli and shear stresses (Huson and McGill, 1984).

Table 5.1: Values of a parameter *A* as a qualitative measure of transcrystalline growth (Ishida and Bousi, 1991).

$A \approx 0$ ($\Delta\sigma >> \Delta\sigma'$)	Inactive substrate. The polymer melt is unaffected by the presence of the fibre and there is no nucleation at the fibre/matrix surface.
$0 < A < 1$	Moderately active substrate. Spherulitic surface morphology is observed. Transcrystallinity becomes more probable as *A* approaches 1.
$A \geq 1$	Very active substrate. Nucleation is heavily favoured at the fibre surface. Transcrystallinity is observed.

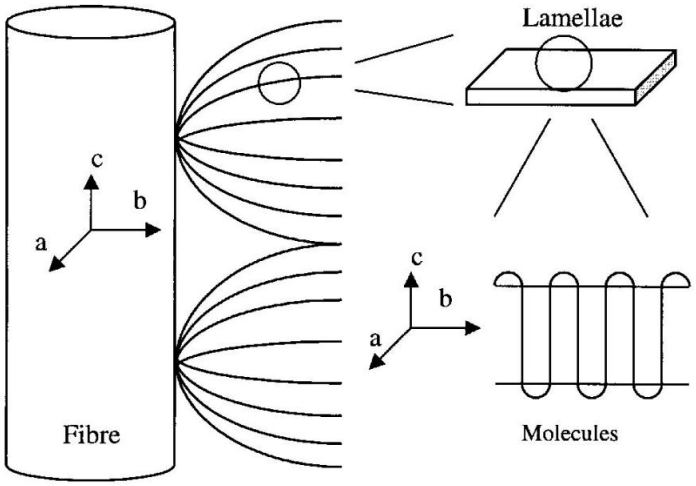

Figure 5.13: Highly oriented spherullites growing from fibre surface (Chen and Hsiao, 1992).

The elastic moduli of highly oriented fibres like polyethylene (PE) ≈ 235 GPa and isotactic polypropylene (*i*-PP) ≈ 34 GPa give a broad indication of how transcrystallinity influences the mechanical properties of polymer-fibre composites (Nakamae and Nishino, 1991). These values are order of magnitude higher than those of bulk polymers. Highly crystalline fibres spun from PLA melt were reported to have a tensile strength of 550-805 MPa (Grijpma *et al*., 1994). Compared to the tensile strength of commercially available polylactic acid which has a tensile strength of 70 MPa one may expect that the reinforcing fibres and the presence of a phase which is crystalline and oriented will improve the mechanical properties of the

composite. The structure of the transcrystalline layer depends on the lamellar arrangement (Figure 5.13). The orientation of polymer chains in transcrystalline layer must have an impact on fibre to matrix adhesion. Suppose that the *b*-*c* plane of a lamella in a crystallite contains the chain folds and that the c-axis is identical with the polymer chain axis. Klein *et al*., (1996) proposed six simple geometrical models of polymer lamellae orientation in a transcrystalline layer in relation to the fibre axis. Two of them have the chain axes (c-axis) parallel to the fibre axis, four of them perpendicular. Generally speaking the more the *b*-*c* plane inclines to the fibre axis and the axis of the polymer chains are parallel to the fibre surface the higher is the possibility of creation of non-covalent bonds among the polymer molecules and active sites on a fibre surface (Figure 5.14).

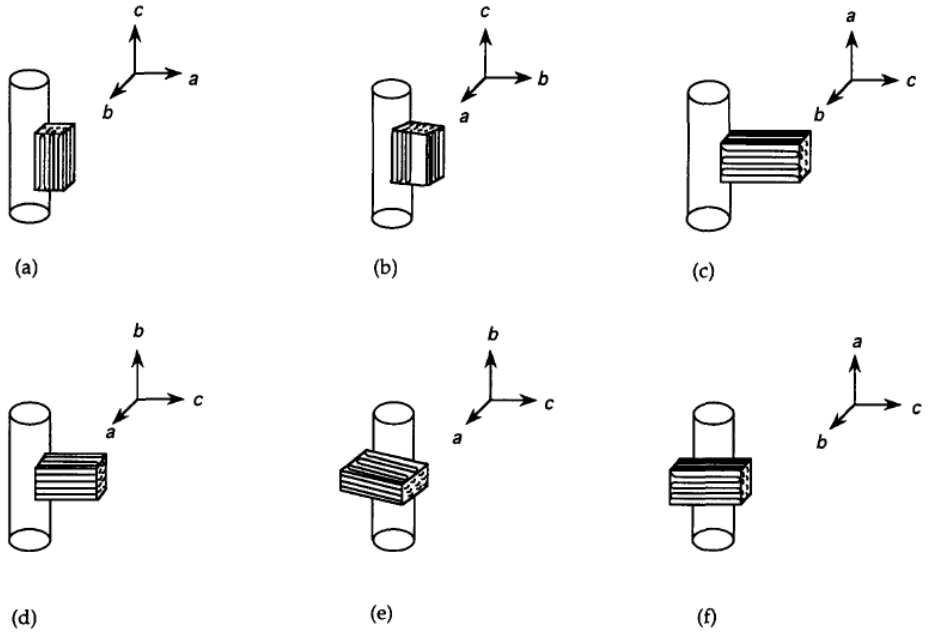

Figure 5.14: Possible allocations of polymer chains in transcrystalline layer (Klein *et al*., 1996).

Moreover the strong covalent bonds of the polymer chain backbone are oriented along the fibre axis and add more strength in the composite when loaded in tension.

The knowledge of lamellae orientation in the transcrystalline layer (TCL) seems to be crucial for the explanation of the fibre to matrix adhesion, stress transfer at the interface and mechanical properties of resulting macro-composites. Amitay-Sadovsky *et al*. (2001) performed nano-shear and indentation measurements on *α*-*i*-PP reinforced with high modulus carbon fibres using scanning force microscopy (SFM). It was supposed that mechanical

measurements at the nano-level would reveal the differences in the structure of the *α*-*i*-PP transcrystalline layer. It was found that the morphology of the TCL changes with the distance from the fibre surface. The shear modulus anisotropy ratio changed from 2.3 to 0.5 as a function of the distance from the fibre surface. These changes were attributed to the morphological changes in the structure of TCL. Progressive lamellar twist up to a constant configuration or a lamellar sheafing with/or without twisting (Figure 5.15) might be possible morphologies which account for changes in mechanical properties previously described.

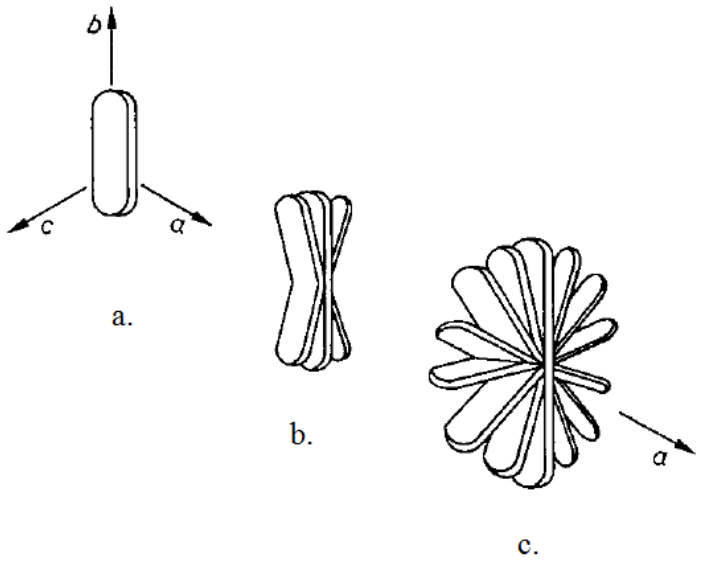

Figure 5.15: Development of a lamella (a) into a sheaf (b) and then into a cartwheel (c), where the "axle" is the crystallographic a-axis. Out of plane sheaving beyond (c) then leads to a spherulite (Blundell *et al*., 1989).

Klein *et al*., 1996 studied the structure of TCL in polyamide 66 reinforced with carbon and aramid fibres by AFM and X-ray diffraction. As a consequence of the crystal growth (from fibre to matrix direction) it was found that the *c*-axes of the crystallites were perpendicular to the fibre axis. Ninomiya *et al*. (2007) prepared PLLA films isothermally transcrystallized at 122°C on Teflon (PTFE) sheet. X-ray diffraction showed that the *b*-axis of PLLA crystals in TCL was parallel to the lamellae growth direction (Figure 5.16).

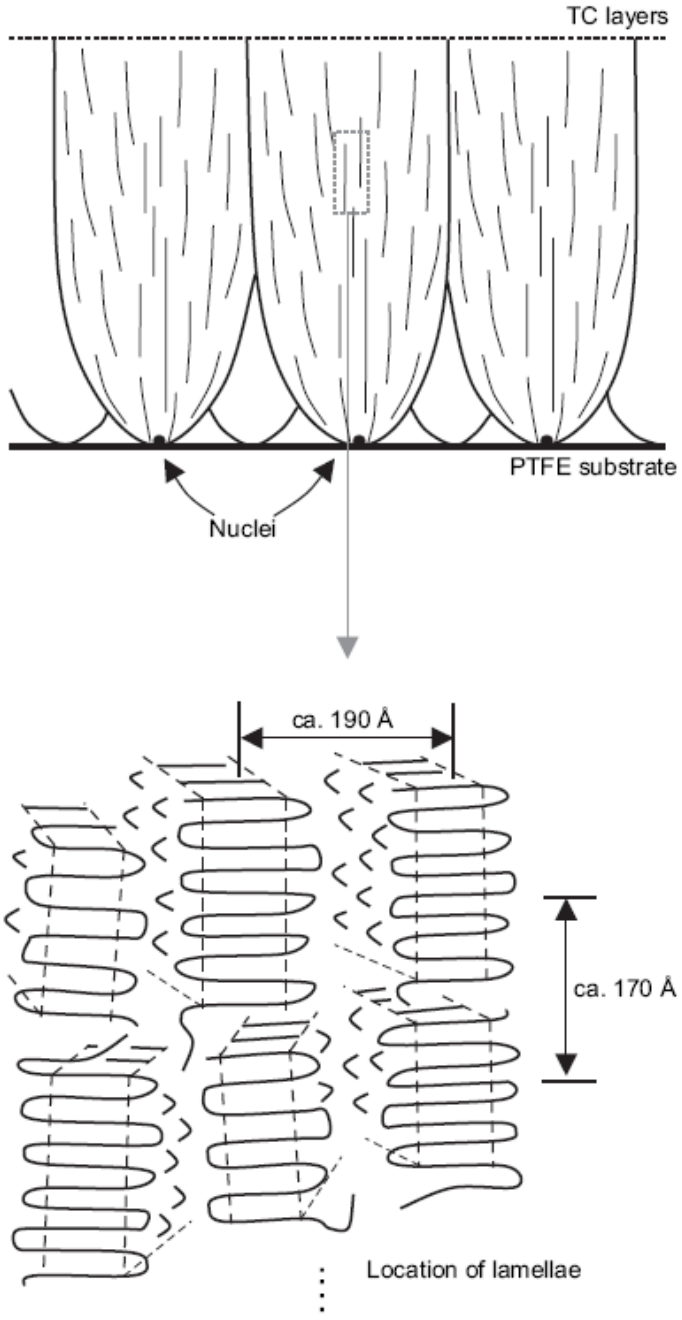

Figure 5.16: Structure of PLLA transcrystalline layer grown from PTFE substrate (Ninomiya *et al*., 2007).

Two transcrystalline morphologies can develop in isotactic polypropylene (*i*-PP): α-transcrystallinity which has monoclinic structure and edge-on lamellae relative to the sample

thickness and *β*-transcrystallinity which has hexagonal structure and flat-on lamellae (Figure 5.17; Lustiger *et al*., 1995).

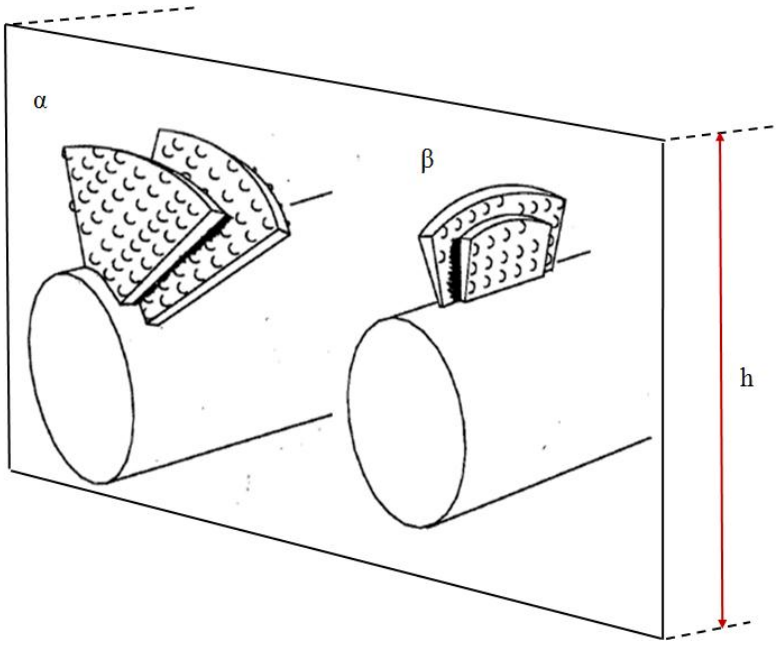

Figure 5.17: Lamellae orientation in α and β transcrystalline layers developed in isotactic polypropylene; h = sample thickness (modified after Lustiger *et al*, 1995).

Crazes in *β* morphology, revealed by SEM after tensile testing of polymer films with induced transcrystallinity, were distributed more uniformly compared to α morphology. It was concluded that polymer films with induced β transcrystallinity were tougher due to the tendency of β transcrystallinity for uniform intralamellar deformation in conjunction with crazing.

Nuriel *et al*. (1999) studied the influence of transcrystallinity on mechanical properties of Nylon 66 reinforced with Kevlar 29 aramid fibres. The prepared micro-composites had a fibre volume fraction of 0.675. It was found that the thinner the TCL the higher were both the flexural strength and stiffness of the composites. It was assumed that TCL could have a positive effect on the composite's mechanical properties only if the *c*-axis (identical with the polymer chain axis) of the polymer crystallites in the TCL is parallel to the fibre axis. This can be achieved in composites with high fibre volume fractions. Lamellar sheafing was the revealed as the morphology of the transcrystalline layer.

Stern *et al*. (1997) studied polyethylene based single polymer composites and revealed significantly oriented crystalline structure in the transcrystalline layer. The *a* axis of TCL crystallites made an angle of 39° to the fibre axis and the *b*-axis was directed radially outwards from the fibre surface.

The morphology of transcrystalline structures is highly oriented and anisotropic. Their mechanical properties depend on the lamellae orientation with respect to the applied stress and are also anisotropic. It has been already mentioned that the presence of a new morphology influences the adhesion and stress transfer at the fibre to matrix interface. Zafeiropoulos and Baillie (2001) studied the development of transcrystallinity in a polypropylene/dew retted flax fibre system. It was concluded from the fibre fragmentation test that the presence of transcrystallinity improved fibre to matrix adhesion. The interfacial shear strength (IFSS) without transcrystalline growth was 12.75 MPa. Single fibre composites with a transcrystalline phase isothermally crystallized at 140 and 145°C had an IFSS of 23.05 MPa. The ability of the fibre to induce the TCL was attributed to the micro-roughness of the fibre surface. It was also suggested that the crystallinity of the fibre does not significantly influence TCL formation. Garkhail, Peijs *et al*. (2009) reported reduced IFSS in the presence of transcrystallinity in their study of polypropylene TCL at the flax fibre surface. Transcrystallinity induced samples were crystallized at 130°C and the IFSS determined by a pull-out test was 7.8 MPa whereas TC free samples had an IFSS of 9.8 MPa. Compression moulded short fibre macro-composites followed the same pattern and samples with induced transcrystallinity had lower tensile strength and modulus. The differences in the results of Zafeiropoulos and Baillie (2001) and Garkhail, Peijs *et al*. (2009) may be explained by the different micromechanical tests used. Gassan *et al*. (2001) studied isothermal and non-isothermal development of TCL at the polypropylene/jute fibre interface. The jute fibres were untreated, caustic soda treated (26 wt%/20°C/20 min.) and grafted with maleic anhydride polypropylene. In the case of isothermal crystallization in the range 130 to 140°C cooling rate had no influence on growth rate and maximum TCL thickness. The fibre treatments had no significant influence on TCL growth. In the case of non-isothermal crystallization slower cooling rates led to faster TCL growth. Theoretically (Wagner, 1996) transcrystallinity should strongly affect interfacial adhesion due to thermal residual stresses coming from the specimen preparation and the anisotropy of the TCL layer. Gati and Wagner (1997) studied the adhesion of

polycaprolactone (PCL) to Kevlar fibres with the microdroplet test. They applied a micromechanical (IFSS) and fracture mechanics approach (energy release rate) to study the level of adhesion. They found no improvement or deterioration in the interfacial adhesion in the presence of transcrystallinity. According to Thomason and van Rooyen (1992a and 1992b) transcrystallinity is a result of stress-induced nucleation. The stresses built up during the cooling come from the difference in thermal expansion coefficients between the fibre and the polymer melt. Competition between surface and bulk nucleation seems to be crucial in the early stages of TCL formation. A faster nucleation rate at the fibre surface (compared to the bulky polymer matrix) is a necessary condition for the creation of a visible transcrystalline layer. The thickness of the TCL is limited by the bulk crystallinity. The fibre/TCL and TCL/bulk matrix boundary can be distinguished (Pompe and Mäder, 2000). Guigon *et al*. (1989) found that in polyamide reinforced with glass fibres the flexural failure occurs preferentially at the TCL/bulk matrix boundary. Keith and Padden (1963) explained the strength at the interface with diffusion of polymer defects towards the interface as a result of competition between matrix nucleation and surface induced nucleation. If matrix nucleation dominates, the defects like atactic, entangled and branched molecules or chain ends move towards the fibre and weaken the interface. If surface nucleation is favoured the transcrystalline front pushes defects towards the matrix. Consequently these defects are pushed away from the matrix because of the matrix crystallization and spherulite formation. The defects accumulate at the TCL/matrix boundary making it weaker.

5.4 Micromechanics of the interface

Mechanical properties of fibre reinforced polymer composites result from fibre length distribution, fibre orientation distribution and interfacial shear strength. To maximize the mechanical properties of natural fibre reinforced composites the fibres and composites should fulfil the following criteria formulated by Aziz and Ansell (2004): the microfibril angle of the fibres shall be small and their cellulose content shall be high; fibre surface shall be treated to improve the fibre to matrix adhesion; fibres should oriented parallel to the direction of applied load.

5.4.1 Rule of mixtures

The mechanical properties of composites can be theoretically estimated from the properties of their constituents (Hull and Clyne, 1996). To reinforce the polymer matrix the fibre should be stronger and stiffer than the matrix and the matrix should not break before the fibre:

$$\sigma_f > \sigma_m ; E_f > E_m$$

$$\varepsilon_m > \varepsilon_f$$

Assuming that both fibre and matrix deform elastically the "rule of mixtures" estimates the properties of a unidirectional composite:

$$\begin{aligned} \sigma_c &= \eta_l \eta_0 \sigma_f V_f + \sigma_m^* \left(1 - V_f\right) \\ E_c &= \eta_l \eta_0 E_f V_f + E_m \left(1 - V_f\right) \end{aligned} \tag{5.12}$$

Where η_l is the length correction factor (Cox, 1952), η_0 is the orientation efficiency factor (Krechnel, 1964). E, σ, ε and V are the modulus, strength, elongation and volume fraction. The subscripts c, f and m denote composite, fibre and matrix and the superscript * has the meaning of yield stress.

The minimum fibre length at which the fibre is able to bear the load transferred from the matrix is defined as:

$$l_c = \frac{\sigma_f}{\tau} \cdot \frac{d}{4} \tag{5.13}$$

Where l_c is the critical fibre length, d is the fibre diameter, σ_f is the fibre tensile stress and τ is the shear strength of the interface. The critical length depends on the adhesion quality between the fibre and the matrix. Critical length of natural fibres is long compared to glass fibres which in turn have critical length long compared to carbon fibres.

5.4.2 Stress transfer and adhesion measurement

The adhesion strength can be measured directly with a short beam shear test (ILSS), transverse tensile test, single fibre pull out test, microdroplet test or embedded single fibre test (fragmentation test) (Figure 5.18). Raman spectroscopy (Young, 1994) has been used to determine the strain distribution along crystalline aramid fibres through the stretching of strain sensitive bond which is manifested by a frequency shift in the Raman spectrum. The adhesion strength is then calculated through mathematical models of stress transfer and the strain profile in the fibre.

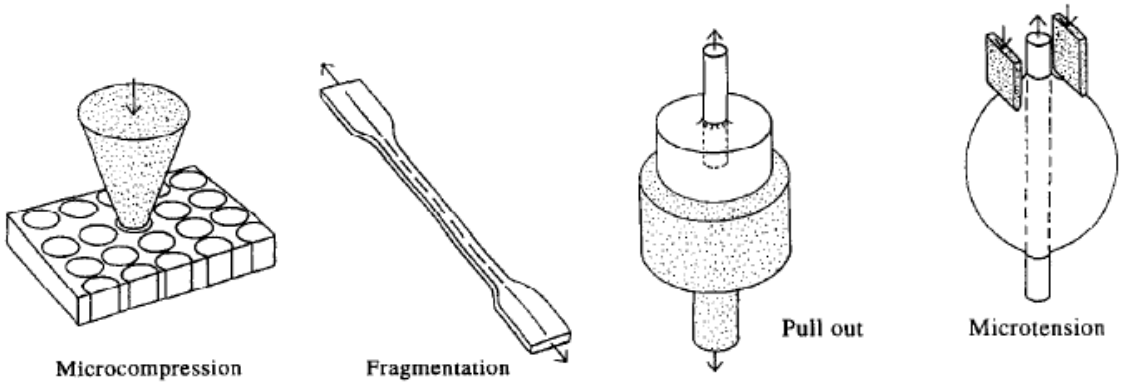

Figure 5.18: Test for interfacial shear strength measurement (Piggott, 1997).

X-ray diffraction (Feldman *et al*., 2006) can be also used for the study of stress transfer. For example it measures the lattice strain of cellulose crystalline regions in the fibre in a polymer composite which is globally strained. The difference between the global fibre strain and the local lattice strain is a measure of the stress transfer and fibre to matrix adhesion quality (Nishino *et al*., 2006).

Table 5.1 lists values of interfacial shear strength measured by various experimental techniques. Slivka *et al*. (1997) studied the adhesion of PLA to AS4 carbon fibre with fragmentation test and microbond test. The interfacial shear strength was 22 MPa for a fragmentation test and 33.9 MPa for a microbond test. Samples were quenched cooled from the melting temperature to the room temperature. Czigány *et al.* (2007) focused on adhesion of sisal fibres to polypropylene, thermoplastic starch and lactide-glycolide copolymer. Interfacial shear strengths resulting from microdroplet test were 4.6, 3.2 and 14.3 MPa respectively.

Nishino *et al*. (2006) applied transverse stress to kenaf fibre reinforced PLA and measured the stress transfer efficiency by X- ray diffraction. Effective stress transfer from matrix to fibre resulted from good interfacial adhesion. Silane treated fibres were found to be even more efficient in transferring load.

Table 5.1: Interfacial adhesion measured by various experimental techniques (Jones, 2005).

Fibre	Matrix	Treatment	IFSS (MPa)				ILSS (MPa)
			τ^a	τ^b	τ^c	$\tau_{max}{}^d$	
Aramid	Epoxy	None	-	8	-	-	55
E-glass	Epoxy	Silane	79	-	56	-	-
E-glass	Polyester	Silane	28	-	23	-	-
E-glass	Vinyl ester	Silane	18	-	-	-	51
AR[e]_glass	Vinyl ester	Silane	14.5-16	-	-	-	41-51
AR_glass	Vinyl ester	None	14.5	-	-	-	38
Carbon HS[f]	Epoxy	None	12	28	28	124	24-70
Carbon HS	Epoxy	-	37-44	65	-	151	80-100

Note: [a] fragmentation test; [b] pull-out test; [c] microindentation test - debonding strength; [d] pull-out test - τ_{max} determined from an extrapolation of maximum pull-out force/embedded length; [e] alkaline resistant; [f] high strength; IFFS – interfacial shear strength; ILSS – interlaminar shear strength.

5.4.3 Stress transfer

For a fibre fully embedded in a polymer matrix, Cox (1952) developed a theoretical model (shear lag theory) of fibre to matrix stress transfer. He assumed that both fibre and the matrix behave in a linear elastic manner, there is a perfect adhesion between the fibre and the matrix, the fibre is a cylinder with a circular cross section, both fibre and the matrix are isotropic solids, dynamic effects are neglected, the fibre axial stress vanishes at the fibre ends, there is no interaction between the broken fibre segments, the matrix tensile strain is equal to the applied strain at some radial distance R from the fibre axis (Lacroix, 1992). Axial fibre stress and shear stress along an embedded fibre under longitudinal loading according to the Cox theory of stress transfer are illustrated in the Figure 5.19.

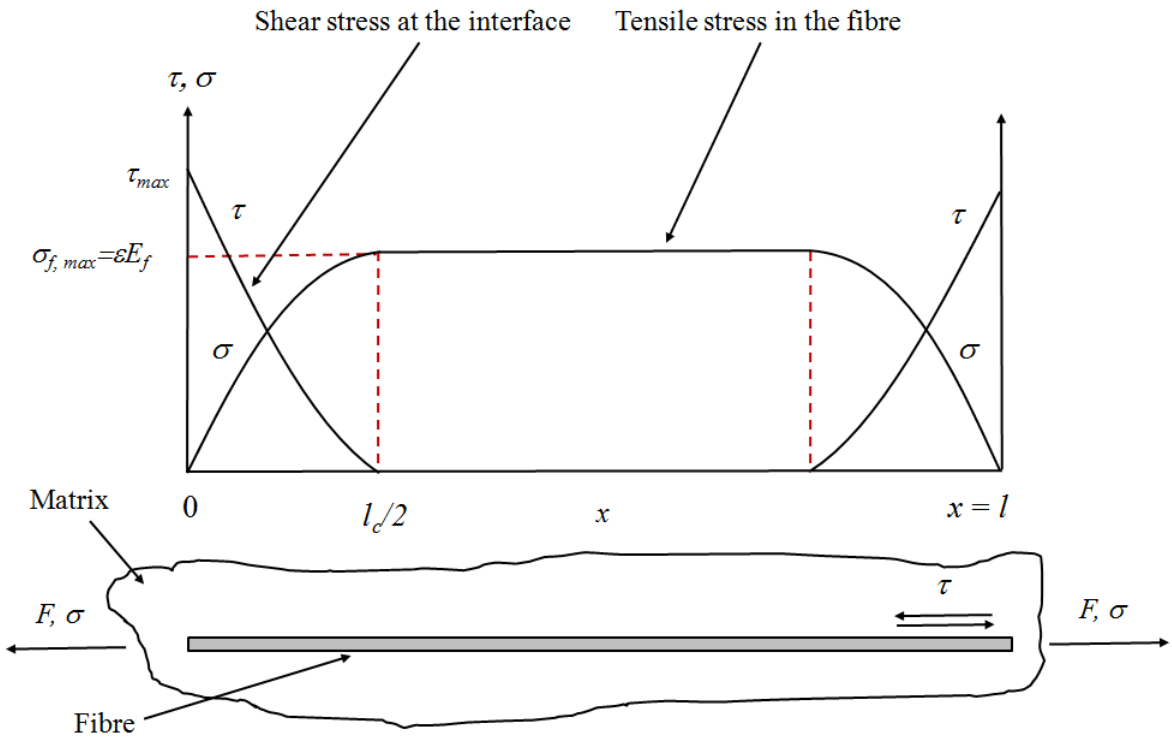

Figure 5.19: Axial fibre stress and shear stress along an embedded fibre under longitudinal loading according to the Cox theory of stress transfer (Hull and Clyne, 1996).

Assuming the above considerations we obtain the following distribution of the axial fibre stress and shear stress at the fibre surface.

$$\sigma_f(x) = \varepsilon_f E_f \left[1 - \frac{\cosh(2nx/d)}{\cosh(ns)}\right] \tag{5.14}$$

$$\tau(x) = \frac{n}{2} E_f \varepsilon \frac{\sinh(2nx/d)}{\cosh(ns)} \tag{5.15}$$

Where n is a non-dimensional part of the argument and s is the fibre aspect ratio $s=L/r$.

$$n^2 = \frac{E_m}{E_f(1+\nu_m)\ln\left(\frac{R}{r}\right)}$$

Maximum axial fibre tensile stress occurs at the centre of the fibre length and can be described by the following equation:

$$\sigma_{f,\max}\left(x = l_c/2\right) = E_f \varepsilon\left[1 - \sec h(ns)\right] \tag{5.16}$$

The maximum shear strength occurs at the fibre ends.

$$\tau_{\max}\left(x = 0, l\right) = \frac{1}{2} nE_f \varepsilon \tanh(ns) \tag{5.17}$$

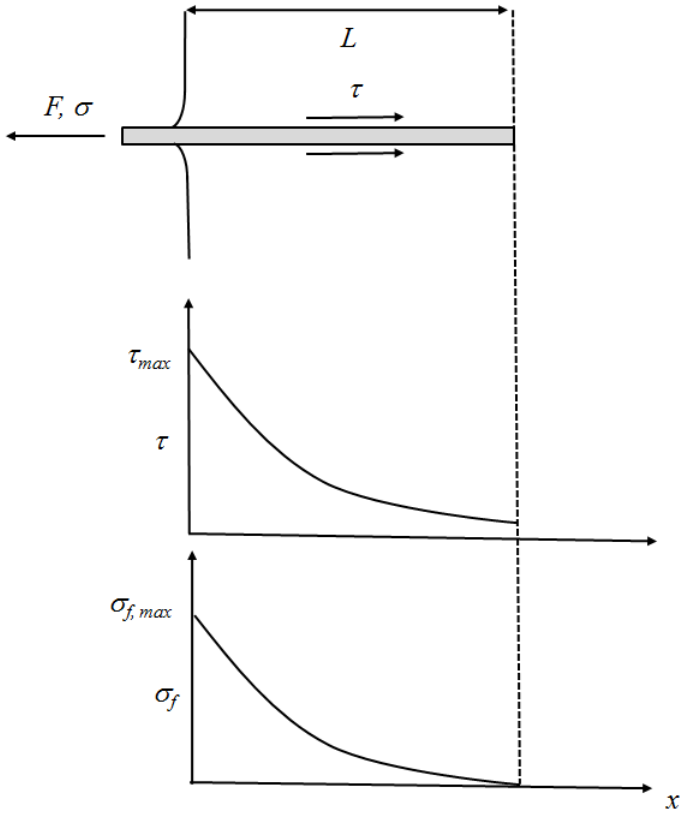

Figure 5.20: Axial fibre stress and shear stress along an embedded fibre under longitudinal loading according to the Cox theory of stress transfer in a pull out test specimen (Piggott, 1992).

Figure 5.20 shows a scheme of a pull out test specimen with one fibre end embedded in a polymer matrix and the other one exposed. The shear stress and fibre tensile stress distributions for a pull out test geometry of a purely elastic matrix and fibre are also included.

Assuming the considerations of the Cox model and the new boundaries the following equations for fibre strain, tensile stress distribution and the shear stress distribution apply.

The fibre strain in the pull out test specimen,

$$\varepsilon_f = \varepsilon_0 \frac{\sinh\left[n(L-x)/r\right]}{\sinh\left[ns\right]} \tag{5.18}$$

The shear stress at the fibre surface can be estimated to be,

$$\tau = E_f \frac{r}{2} \frac{d\varepsilon_f}{dx} \tag{5.19}$$

$$\tau = \frac{n}{2} E_f \varepsilon_0 \frac{\cosh\left[n(L-x/r)\right]}{\sinh\left[ns\right]} \tag{5.20}$$

And the tensile strength in the fibre:

$$\sigma_f = \sigma_{f,\max} \frac{\sinh\left(n(L-x)/r\right)}{\sinh\left(ns\right)} \tag{5.21}$$

Where $\sigma_{f,\max}$ is the stress in the fibre at the point where the fibre enters the polymer matrix (x=0; Figure 5.20).

In a typical pull out test experiment (Figure 5.21) a partially embedded fibre is pulled out from the fixed matrix. A maximum force to pull out the fibre is recorded as a function of the embedded length and interfacial shear strength is calculated as:

$$\tau_{ISS} = \frac{F_{\max}}{2\pi r_f l_e} \tag{5.22}$$

Where r_f is the fibre effective radius and l_e is the embedded fibre length. Physically this is the average interfacial shear strength at the time of failure (Nairn, 2001).

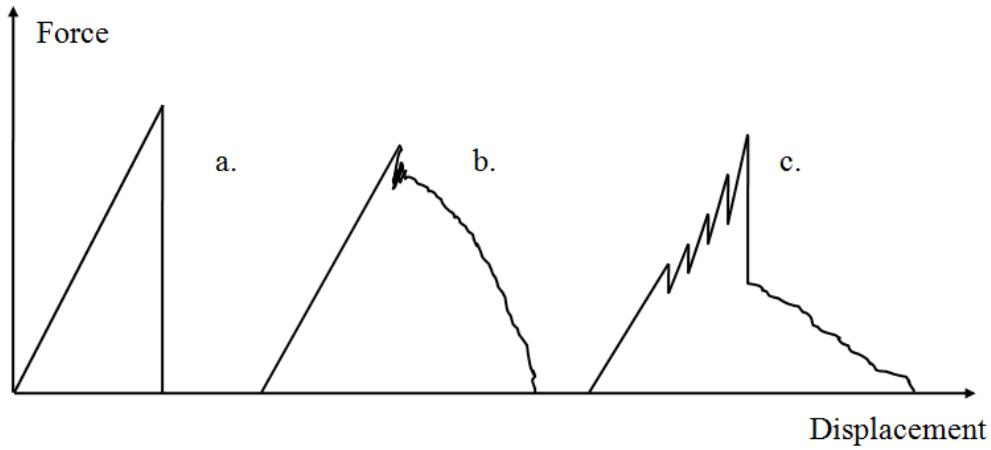

Figure 5.21: Force-displacement curves for the single fibre pull out test (Bannister *et al*., 1997): a. Strongly bonded interface; b. weakly bonded interface; c. frictional de-bond.

Failure at the interface can be also characterized by means of linear fracture mechanics. In such approach the failure at the interface is modelled as an infinitesimal interfacial debonding crack which starts from some initial imperfection at the free surface of the matrix and propagates along the fibre to matrix interface (Nairn, 2001). Instead of interfacial shear strength the energy release rate G_{II} is determined. Finite elements analysis based on shear lag theory performed by Singletary *et al*. (1997) and Beckert and Lauke (1996) showed that equation 5.22 can be used to model the strain energy release rate in a pull out test specimen because the main contribution to G_{II} at short crack lengths is the free fibre for which Outwater and Murphy (1970) derived the following analytical formula:

$$G_{II} = \frac{P^2}{4E_f \pi^2 r_f^3} \tag{5.23}$$

If thermal residual stresses are included an extra term is added to equation 5.22 (Beckert and Lauke, 1997):

$$G_{II} = \frac{P^2}{4E_f \pi^2 r_f^3} + \frac{(\alpha_f - \alpha_m)\Delta T \cdot P}{2\pi r_f} \tag{5.24}$$

where G_{II} is the energy release rate, P is a constant loading force, r_f is a fibre effective radius, E_f is a fibre elastic modulus, ΔT is the temperature difference and α is the thermal expansion coefficient. The thermal residual stresses can develop in polymer fibre composites during processing due to the different coefficients of thermal expansion (CTEs) of its constituents. In a moulding operation the thermoplastic matrix is heated up above its glass transition temperature (T_g, amorphous polymers) or melting temperature (T_m, semicrystalline polymers) to fill a mould and later cooled down to room temperature to solidify. Both fibre and the matrix shrink and change their dimensions during the cooling down stage. The volumetric shrinkage of the thermoplastic matrix is significantly higher compared to the fibres. As a result both the matrix and the fibre are strained and thermal residual stresses develop. Assuming perfect fibre to matrix bonding, residual compressive stress builds up in the fibre and the fibre is stressed along its longitudinal axis as well as radially towards the centre of its cross section. Consequently a residual tensile stress develops in the matrix around the embedded fibre and the matrix is stressed longitudinally and radially along the fibre (Figure 5.22). In the case of semicrystalline thermoplastics the development of matrix morphology also contributes to the development of thermal stresses because the matrix shrinkage and Young's modulus depend on the degree of crystallinity (Nairn and Zoller, 1985b). Thermal residual stresses can be estimated using the following equation (Zhou *et al*., 1999):

$$\sigma_{th}^{a} = \left(\alpha_m - \alpha_f\right)\left(T - T_{ref}\right)\frac{E_f}{1+\left(\frac{V_f}{V_m}\right)\left(\frac{E_f}{E_m}\right)} \tag{5.25}$$

Where E is the Young's modulus, σ_{th} is the thermal residual stress in the fibre, V is the volume fraction, subscripts f and m refer to fibre and matrix, α is the coefficient of thermal expansion, T is the test temperature (i.e. room temperature) and T_{ref} is the stress free temperature and superscript a means axial.

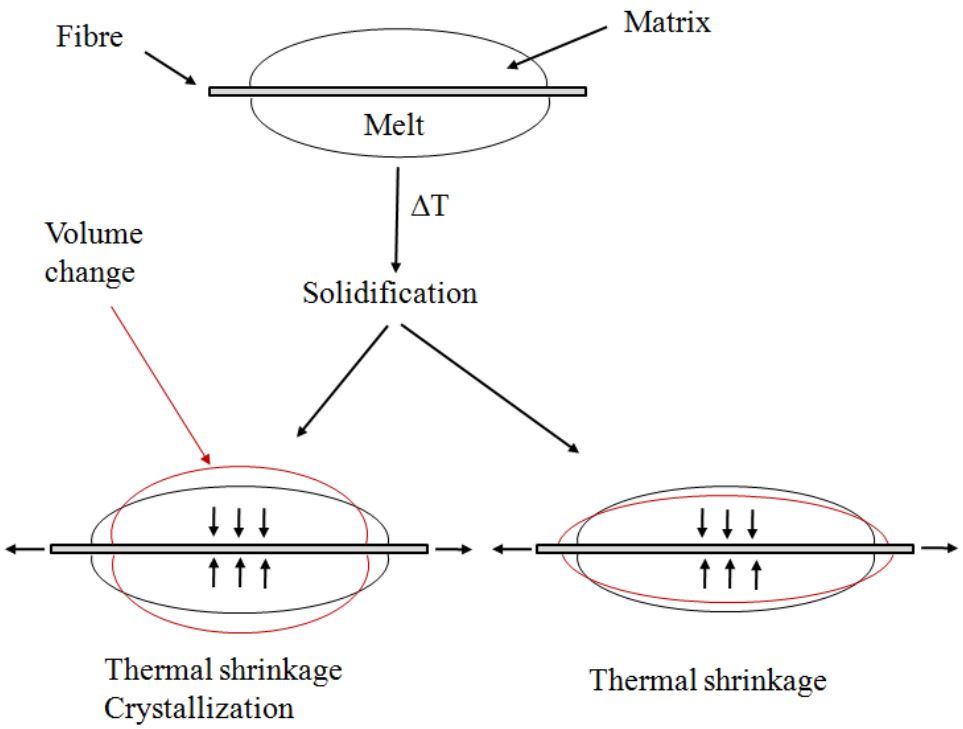

Figure 5.22: Development of thermal stresses in a single fibre composite with a semicrystalline thermoplastic matrix.

The stress-free temperature is not well defined. Usually the glass transition temperature (T_g) and the peak crystallization temperature (T_c; DSC) are taken for amorphous and semicrystalline thermoplastics (Nairn and Zoller, 1985a). In a semicrystalline thermoplastic polymer the stress free temperature (T_c) will depend on cooling rates. As one can expect fast cooling rates generate lower stress free temperature and larger degree of under-cooling ΔT.

Assuming a fibre embedded in an indefinite matrix the radial thermal stress at the fibre surface can be calculated (Di Landro and Pegoraro, 1996) to be:

$$\sigma_{th}^{r} = -\frac{\varepsilon_1 \left(\nu_m - \nu_{af}\right)}{\left(1+\nu_m\right)/E_m + \left(1-\nu_{tf} - 2\nu_{af}^2\right)/E_{tf}} \tag{5.26}$$

Where ε_1 is the specimen strain, ν is the Poisson's ratio, E is the elastic modulus, and subscripts a, t, f, m refer to axial, transverse, fibre and matrix.

Typical thermal residual stresses in unidirectional epoxy composites ($V_f \approx 0.65$) reinforced with glass, Kevlar or carbon fibres are 30-36 MPa (Harris, 1999). Wagner and Nairn (1997) theoretically modelled thermal residual stresses in polypropylene reinforced with high modulus graphite fibres (E =750 GPa) in the presence of transcrystallinity. In a typical single fibre embedded micro-composite with a $V_f \approx 3x10^{-6}$ and no developed morphology they estimated the fibre axial compressive stress to be 11 GPa and the matrix axial stress to be 0.03 MPa. The high axial compressive stress induced in the fibre during the cooling of thermoplastic matrix was mainly due to the high modulus of the fibre

The presence of transcrystalline morphology, either α or β, made the axial compressive stress in the fibre also 11 GPa. Macro-composites with $V_f \approx 0.5$ and the same degree of under-cooling of ΔT=-130°C experienced an axial compressive stress of about 80-90 MPa with and without transcrystalline morphology. The transcrystalline layer increased the radial stresses at the fibre surface in the single fibre embedded micro-composites.

The structure and properties of fibre to matrix interface play an important role in mechanical properties of composites. This chapter reviewed aspects which can influence the structure and properties of the interface. It discussed the adhesion, adhesion modification and also the development of crystalline morphology at fibre to matrix interface.

A theoretical analysis of stress transfer at fibre to matrix interface was also given. This analysis is an important guide to what can be expected to happen in a real composite material.

6 Experimental methods

In this chapter the experimental methods, their principles and a description of the test instrumentation are presented. Matrix and fibres used in the manufacture of composites are introduced followed by experimental methods to measure their physico-mechanical properties. Dynamic mechanical properties and the glass transition temperature are measured using Dynamic Mechanical Thermal Analysis (DMTA). Transition temperatures and melting enthalpies are determined with differential scanning calorimetry (DSC). Hot stage microscopy is used to follow spherulitic growth at the fibre to matrix interface. Metallographic procedure to prepare samples for scanning electron microscope (SEM) will be discussed as well as the the fundamentals of scanning electron microscopy. The experimental procedure for measuring the strength of fibre to matrix adhesion and statistical analysis are described. Finally methods to measure the mechanical properties of manufactured composites in tension and flexure are outlined.

6.1 Materials

Polylactic acid (PLLA, Biomer 9000, M_w = 180,000 g/mol, melt flow index of 5g/10 min. at 2.16 kg/190°C, density of 1.27 g/cm^3) was purchased from Biomer GmbH, Krailing, Germany. Sisal fibre bundles (A*gave sisalana*) were sourced in Tanzania. Caustic soda was obtained from Sigma Aldrich, UK. Mould release agent used in composites manufacture was PAT-607/PCM and was purchased from E. P. Wurtz GmbH, Germany. Metallographic consumables were purchased from Struers Ltd., UK.

For the manufacture of composites and most of the experimental work it was necessary to convert polylactic acid granules into polymer sheets. Polylactic acid granules were oven dried overnight at 50°C and compression moulded in foils of 0.3 – 0.4 mm thickness placing 5g of PLA between two steel plates (200 x 200 mm). Compression moulding was carried out in two stages. Firstly the PLA was consolidated at 190°C and low pressure for 10 minutes. Secondly the PLA was compressed at 190°C and 0.1 MPa for 10 minutes. After being released from the hot press the sheets were left to cool down at room temperature for 24 h. Moulded sheets were

stored in polyethylene sealed bags at room temperature and 50% relative humidity. The shape of the sheets was adjusted to fit in the compression mould for manufacture of composites or their shape was adjusted according to the requirements of the experimental methods used.

Sisal fibre bundles could not be used as received and prior to processing, the fibres were washed for 2 hours in hot water at 90°C to remove all the dust particles and impurities. Fibres were dried using paper tissues at room temperature for 12 hours and then placed in a circulating air oven at 80°C overnight. Dried fibres were stored in sealed PE bags at room temperature with a calcium chloride dehumidifier. Figure 6.1 shows sisal fibres without any surface treatment after the cleansing process.

Figure 6.1: Untreated sisal fibre bundles (left) and caustic soda treated (right) sisal fibres (6 wt%).

One half of the cleaned sisal fibre bundles was treated with caustic soda (Figure 6.1). Fibres were immersed in 0.06 M NaOH solution for 48 hours, then rinsed with an excess of distilled water and neutralised with dilute acetic acid (1 wt% solution). Fibres were dried as already described in the previous paragraph.

6.2 Density measurement

The Archimedes principle (buoyancy method) was used to determine the bulk density of sisal fibres. The principle states that a body immersed in a fluid apparently loses weight by an amount equal to the weight of the fluid it displaces. This method allows determination of the

density of solids of irregular shapes. Sisal fibres of known weight which was recorded as W_{fa} were immersed in a solvent of lower density than was the expected density of the fibre. The weight of fibres submerged in the solvent was recorded as W_{fs}. All the measurements were taken at the temperature of 21°C. The bulk (apparent) density was calculated using the following equation:

$$\rho_b = \frac{\rho_s W_{fa}}{W_{fa} - W_{fs}} \tag{6.1}$$

where ρ_b is the bulk density of the fibre in kg.m^3, ρ_s is the solvent density in kg/m^3, W_{fa} is the weight of the fibre in air in kg and W_{fs} is the weight of the fibre in the solvent in kg.

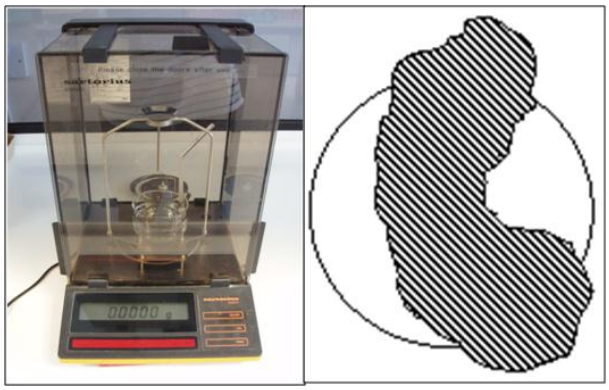

Figure 6.2: Experimental set up for the density measurement (left) and determination of the effective diameter (right).

Figure 6.2 shows the Archimedes principle set up for the density measurement and also visualises how the irregular shape of the fibre cross section can be converted into an effective circular cross section which enables straightforward calculation of the effective fibre diameter. Fibres were stored at 22°C and 50% relative humidity before testing in a polyethylene bag containing a few granules of calcium chloride. Benzene was used for the determination of sisal fibre bundle density because it is a non-polar solvent so it cannot form hydrogen bonds with cellulose hydroxyl groups exposed on the surface of natural fibres. The Archimedes principle was also used for the bulk density determination of polylactic acid. Samples of polylactic acid with dimensions of 15 x 15 x 2 mm^3 were cut from compression moulded sheets. Polylactic

acid is soluble in benzene, thus the benzene was replaced by ethanol. The density of ethanol and benzene was determined by pyknometry, i.e. the weight of precisely known volume of a liquid was measured.

Once knowing the fibre density and the length of the fibre, the apparent cross sectional area and hence the effective diameter of a fibre can be calculated as:

$$A = \frac{m_f}{\rho l_f} \tag{6.2}$$

where A is the apparent cross sectional area, l_f is the length of the fibre and ρ is the bulk density of the fibre.

6.3 Differential Scanning Calorimetry

Differential Scanning Calorimetry (DSC) was used to determine the glass transition temperature, melting temperature, crystallization kinetics, degree of crystallinity and the heat of fusion of PLA. It was also employed to determine the influence of physical aging and thermal history on glass transition and melting temperatures and the crystallinity of thermoplastic polymers. The main advantage of DSC is that it works with small sample sizes (5–20 mg). DSC measures the difference in heat capacity changes between a polymer sample and a reference sample. Polymer dimensions are temperature dependent and it is impossible to keep their volume constant while changing the temperature in order to measure their heat capacity directly at constant volume. However, it is possible to measure their heat capacity at constant pressure:

$$C_p = \left(\frac{\partial Q}{\partial T}\right)_p = \left(\frac{\partial H}{\partial T}\right)_p \tag{6.3}$$

Heat capacity indicates how much heat is needed to increase the temperature of a material by 1°C. For practical purposes there is specific heat capacity defined as “the heat necessary to

increase the temperature of one mol of a material by 1°C" and it is measured in J/(K.mol) or J/(K.kg). A DSC can be designed as a heat flux DSC or a power compensation DSC. Figure 6.3 shows the experimental instrumentation of power compensation DSC.

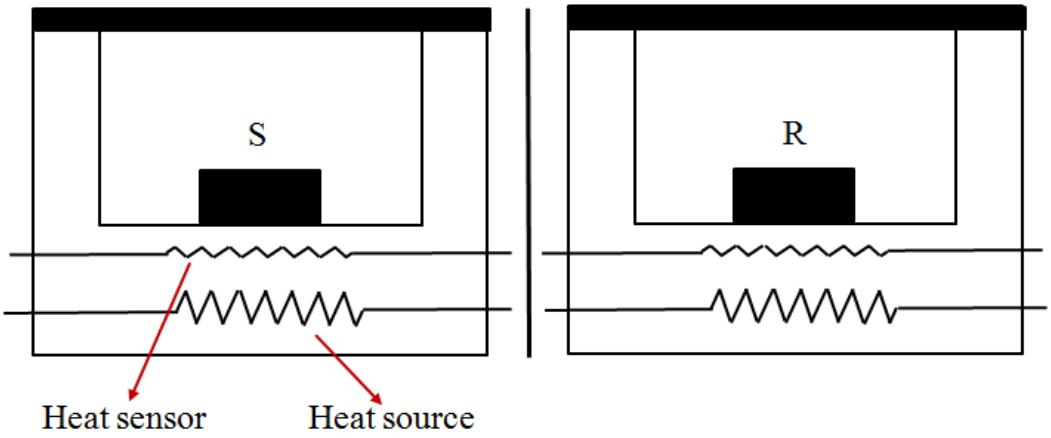

Figure 6.3: Schematic representation of power compensation DSC Perkin Elmer; S = sample, R = reference (Wunderlich, 2005).

In a power compensated DSC both the sample and the reference are kept at the same temperature. The sample and the reference are placed in separate cells and their energy supplies are independent. Both the sample and the reference are subjected to the same controlled temperature programme. A transition in a polymer sample is accompanied by heat release (exothermic process) or heat consumption (endothermic process). As a consequence the energy input to keep the constant temperature in the sample cell varies. The energy input for a reference cell is constant as the reference does not undergo any thermal transition. The difference in energy supplies (heat flow) between the sample and the reference is recorded and plotted against the programme temperature. Endothermic transitions are plotted as positive deviations from the DSC baseline whilst exothermic transitions are plotted as negative deviations from the DSC baseline. The DSC baseline basically represents the dependence of the reference heat capacity on temperature. Figure 6.4 shows an idealized DSC trace of a semicrystalline polymer (e.g. PP, PET) with highlighted transitions including the initial glass transition, an exotherm associated with crystallization and an endotherm associated with the melting of the crystalline component of the polymer. The first deviation from the baseline corresponds to the glass transition temperature (T_g). The glass transition temperature is a

second order transition which means that it is accompanied only by heat capacity changes and no enthalpy changes (dH/dT shows a step change meanwhile d^2H/d^2T goes to infinity).

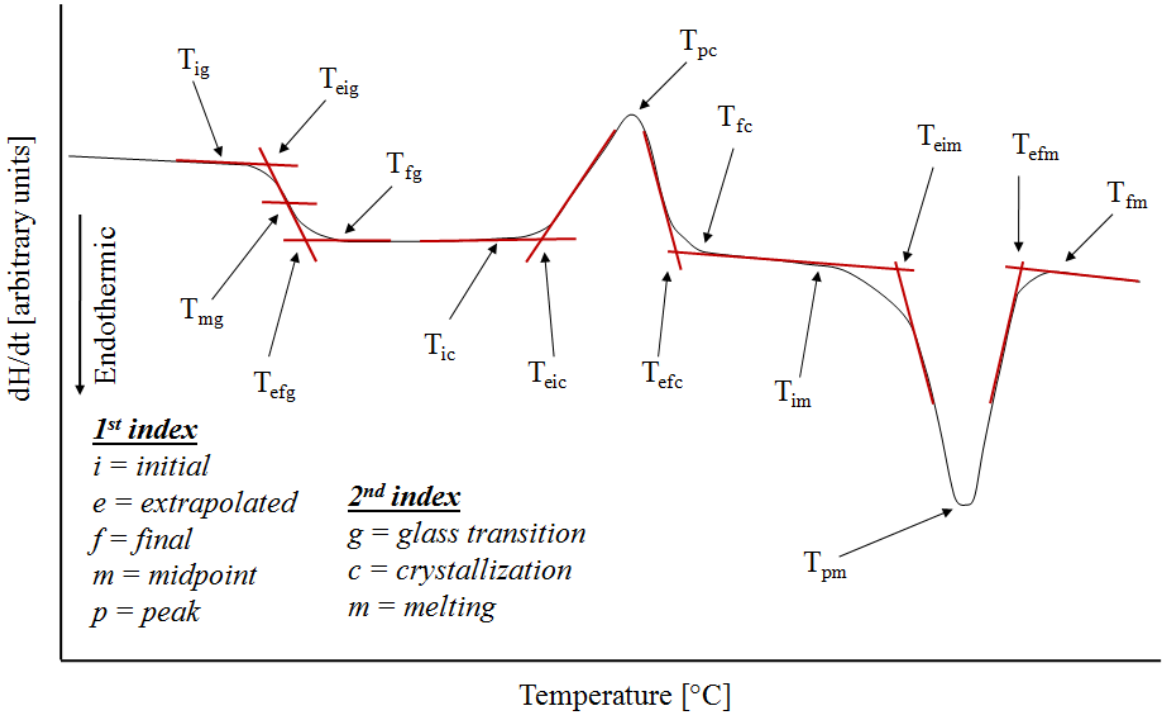

Figure 6.4: Typical DSC curve for a semicrystalline thermoplastic polymer (BS EN ISO 11357-1).

The way to determine the glass transition temperature is described in Figure 6.5. The mid-point glass transition temperature T_{mg} is defined by drawing three tangents to the z-shaped transition. The tangents intersect at points of T_{eig} and T_{efg}. T_g is calculated to be the mean of T_{eig} and T_{efg}.

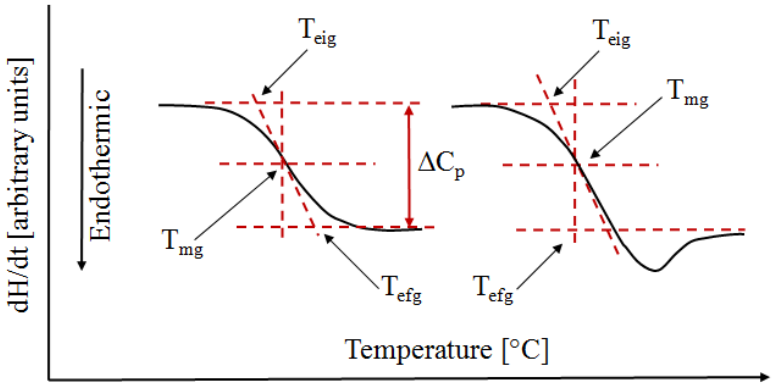

Figure 6.5: Determination of the glass transition temperature (BS EN ISO 11357-2).

The second thermal event in the DSC trace depicted in Figure 6.4 is the cold crystallization exotherm. When a quenched semicrystalline polymer is heated up, cold crystallization occurs at T_{pc}, the peak crystallization temperature, which is above T_g and below T_m. The crystallisation exotherm is shown in Figure 6.6.

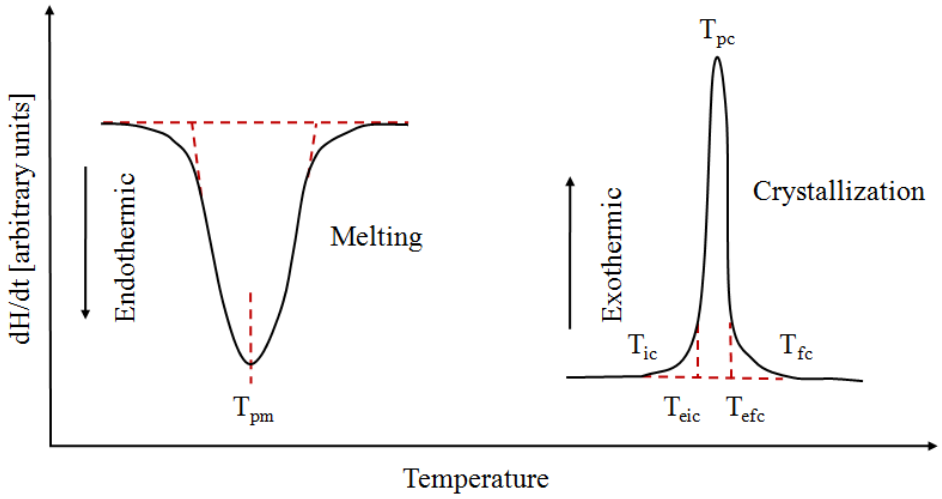

Figure 6.6: Determination of characteristic temperatures (melting and cold crystallization) (BS EN ISO 11357-3).

The last thermal event in Figure 6.4 is the melting endotherm (detail in Figure 6.7) with a peak melting temperature of T_{pm}. The area under the melting and crystallization peak of a DSC curve is related to the enthalpy change of such a thermal event and is known as the peak area method.

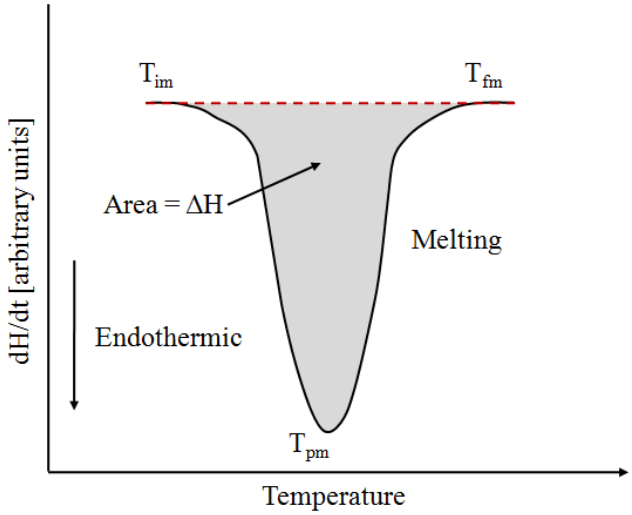

Figure 6.7: Determination of the enthalpy of a transition (BS EN ISO 11357-3).

When a molten semicrystalline polymer is cooled down, crystallization starts at a higher temperature which is closer to the melting point. This crystallization is called high temperature crystallization. Figure 6.7 shows the procedure for determining the heat of fusion *ΔH* for a semicrystalline polymer from the melting peak area. Determining the heat of fusion is important for calculating the degree of crystallinity (χ_c) of a semicrystalline polymer. The degree of crystallinity can be evaluated according to the following equation:

$$\chi_c(\%) = 100 \cdot (\Delta H_m - \Delta H_c) / \Delta H_m^c \qquad (6.4)$$

where ΔH_m^c is the enthalpy of fusion of purely crystalline polymer, ΔH_m is the enthalpy of fusion of the tested sample and ΔH_c is the enthalpy of the cold crystallization of tested sample. The enthalpy of fusion of purely crystalline polylactic acid is 93.1 J/g (Jamshidi *et al*., 1988).
There is a correlation between the glass transition temperature and the melting temperature of semicrystalline polymers. As already pointed out the T_g is manifested as a step change in heat capacity in a typical DSC plot and is well pronounced in amorphous samples. The degree of crystallinity influences the glass transition temperature and a higher degree of crystallinity broadens the transition region. DSC curves of polymers with a high degree of crystallinity usually show glass transition as a minor event which is sometimes difficult to detect (Chartoff *et al*., 1994). The higher the degree of crystallinity of the sample the less pronounced is T_g and other techniques such as DMTA are more suitable for T_g determination as it links glass transition with mechanical properties.

6.4 Dynamic mechanical thermal analysis

Dynamic mechanical thermal analysis (DMTA) is a dynamic method based on non-resonant forced vibrations applied to a sample (Figure 6.8 and 6.9). A sample is heated up at a constant rate of heating (ºC/min) and an oscillating sinusoidal stress at a constant frequency is applied to the sample and the resulting strain is measured. DMTA can be instrumented in tension, shear or flexure (single cantilever, dual cantilever or three point bending) modes. Each of the fixtures is suitable for certain samples (tension for fibres and films, compression for foams)

depending on the stiffness of the sample. For example flexural arrangements are preferred for stiff materials (metals, composites) as less force is required to obtain measurable deformation. Figure 6.10 describes the stress response of a viscoelastic material to an applied strain.

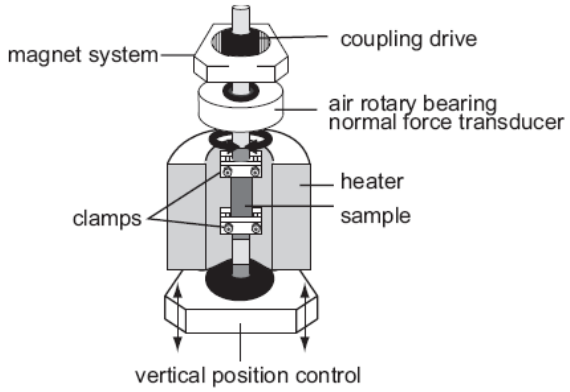

Figure 6.8: Section through a DMTA apparatus with a tensile test fixture (Ehrenstein *et al*., 2004).

Figure 6.9: Triton Tritec DMA 2000 dynamic mechanical analyzer.

The oscillating sinusoidal strain in a polymer sample can be described by the following equation (Figure 6.10):

$$\varepsilon = \varepsilon_o \sin(\omega t) \tag{6.5}$$

In a viscoelastic material such as a thermoplastic, the stress leads the strain by the phase angle δ:

$$\sigma = \sigma_0 \sin(\omega t + \delta) = (\sigma_0 \cos\delta)\sin\omega t + (\sigma_0 \sin\delta)\cos\omega t \tag{6.6}$$

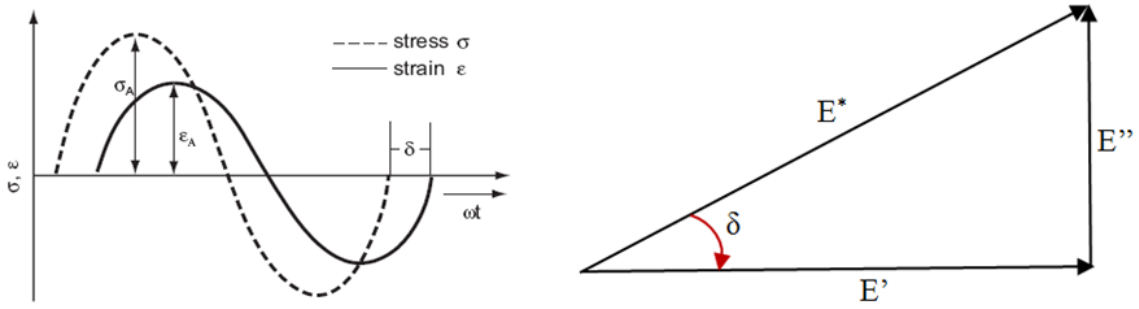

Figure 6.10: Stress response of a viscoelastic material to the applied strain (left) and dynamic moduli in complex notation (Ehrenstein *et al*., 2004).

Equation 6.6 defines the dynamic moduli. It can be clearly seen that $\sigma_0 \cos\delta$ is the stress component which is in phase with the strain. This component is analogous to a spring and we define the storage modulus (E') as

$$E' = \frac{\sigma_0}{\varepsilon_0}\cos\delta \tag{6.7}$$

It is also evident that the stress component $\sigma_0 \sin\delta$ is exactly 90° (or π/2) out of phase with the strain. This component is analogous to a dashpot and we define the loss modulus (E'') as

$$E'' = \frac{\sigma_0}{\varepsilon_0} \sin \delta \tag{6.8}$$

Using the moduli definitions the equation (6.6) can be rewritten as

$$\sigma = \varepsilon_0 E' \sin \omega t + \varepsilon_0 E'' \cos \omega t \tag{6.9}$$

The phase lag δ can be expressed as a ratio of the loss modulus to the storage modulus:

$$\tan \delta = E''/E' \tag{6.10}$$

Both the stress and the strain and consequently both dynamic moduli can be also expressed in a complex notation as

$$\begin{aligned} \varepsilon &= \varepsilon_0 \exp i\omega t \\ \sigma &= \sigma_0 \exp i(\omega t + \delta) \end{aligned} \tag{6.11}$$

The overall complex modulus then becomes

$$\begin{aligned} E^* &= \frac{\sigma_0}{\varepsilon_0} \exp i\delta = \frac{\sigma_0}{\varepsilon_0}(\cos \delta + i \sin \delta) \\ E^* &= E' + iE'' \end{aligned} \tag{6.12}$$

The right part of the Figure 6.10 shows graphically the relationship between the storage modulus, loss modulus and phase angle in the complex notation.

Dynamic moduli E' and E'' are frequency dependent material properties. As pointed out before the storage modulus E' describes the ability of a material to store energy (spring analogue – ideal elastic behaviour) and the loss modulus E'' gives information about the material's ability to dissipate energy by flow (dashpot analogue – ideal viscous behaviour). Tan δ describes the damping of a viscoelastic material. DMTA equipment usually enables material testing at wide range of temperatures and frequencies. DMTA is most often used to

identify the glass transition temperature of polymers or polymer composites. DMTA is a more sensitive method for identifying T_g compared to DSC.

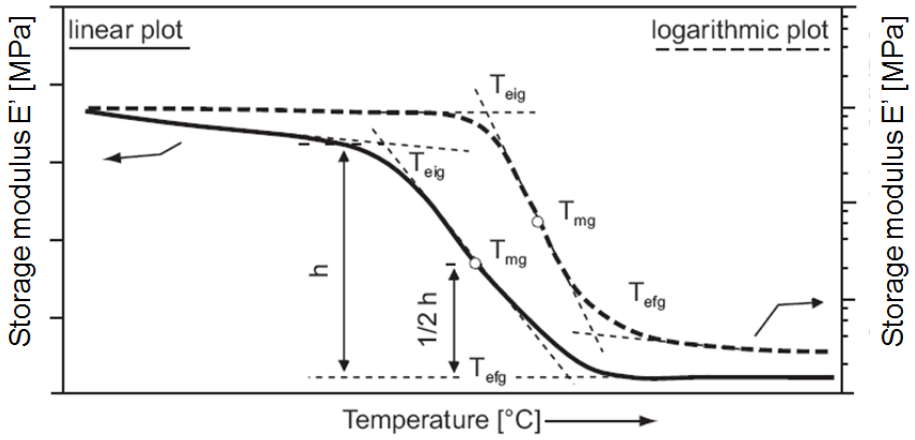

Figure 6.11: Determination of glass transition temperature from DMTA plot (Ehrenstein *et al*., 2004).

At the glass transition temperature (T_g) some of the polymer chain segments in the amorphous phase gain enough energy to move freely and the polymer goes through a transition from a frozen glass to leather-like state (semicrystalline polymer) or rubbery state (amorphous polymer). The damping (tan δ) goes through a maximum just above T_g and the storage modulus (E') decreases by a factor of 10^2-10^3 (Figure 6.11). A typical output from a DMTA experiment is a plot of storage modulus (E'), loss modulus (E'') and tan δ as a function of temperature (Figures 6.11 and 6.12).

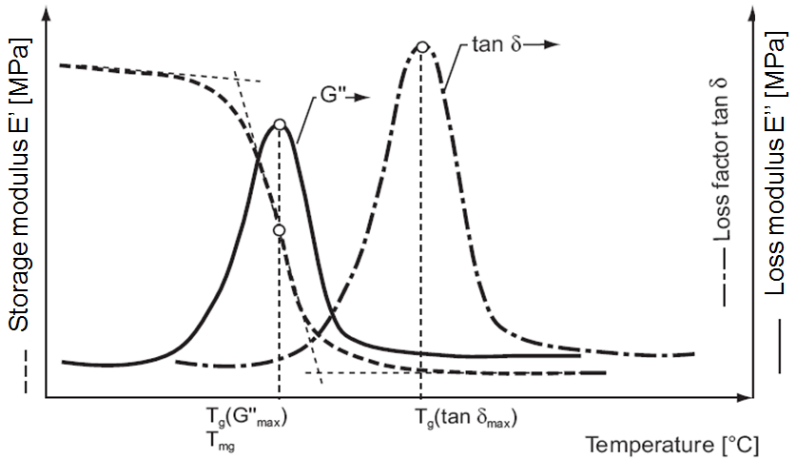

Figure 6.12: Glass transition temperature determination from the peaks of a DMTA experiment in dynamic shear (Ehrenstein *et al*., 2004).

Figure 6.11 shows how T_g is determined from a plot of the storage modulus versus temperature. The terminology and the methodology is exactly the same as used for T_g determination from DSC trace described in Figure 6.5. Glass transition temperature can also be determined simply as the peak temperature for E'' or tan δ (Figure 6.12). Ehrenstein *et al*. (2004) states that $T_g(\tan \delta_{max})$ is always > $T_g(E''_{max})$ and always > $T_g(E')$. Also, $T_g(E''_{max}) \approx T_{mg}$ (DMTA) = T_{mg} (DSC), where T_{mg} means the "midpoint T_g".

Ferrillo and Achorn (1996) found that the T_g measured by DSC and DMTA for commercially available polymers agree within ± 4°C. Chemical structure, polymer chain symmetry, side groups, molecular weight, plasticizer, cross-linking, copolymer and crystallinity are some of the factors affecting the glass transition temperature. Apart from the T_g determination it is possible to abstract more information about the material behaviour from the DMTA experiment. For example, the tan δ magnitude and broadening provides information about the sample fracture energy and adhesion between the polymer and the filler (in case of composites) and structural changes (homopolymers, copolymers and blends).

As pointed out before dynamic moduli as well as the T_g are frequency dependent. Typical DMTA apparatus (e.g. Triton Tritec DMA, Figure 6.13) can generate wide range of frequencies (0 to 300 Hz) in the temperature range of -150 to 400°C. A typical DMTA experiment is performed at a fixed frequency of 1 Hz, with a fixed strain amplitude and controlled heating rate of 2°C/min. to avoid a non-equilibrium response (Chartoff *et al*., 1994).

6.5 Hot stage microscopy (Polarized light thermomicroscopy)

Hot stage microscopy, also called thermomicroscopy (TM) or thermo-optical analysis (TOA), enables visual observation of structural changes in a polymer sample as it is heated up at a controlled heating rate. Polarized light is transmitted through the sample in a typical hot stage microscopy experiment. The sample is placed between a glass slide and a cover slip and heated on a block containing a Ni-Cr heating element and fitted with a sapphire or quartz window which makes it possible to observe the sample visually in a transmitted light. Sample is viewed under crossed polars. As a result the only light which passes through the sample is the polarized light which was rotated by the crystalline structure in the polymer. Figure 6.13

shows the experimental set up with Mettler Toledo hot stage and temperature controller, Leica optical microscope and a displayed digital image captured with Studio Capture® software.

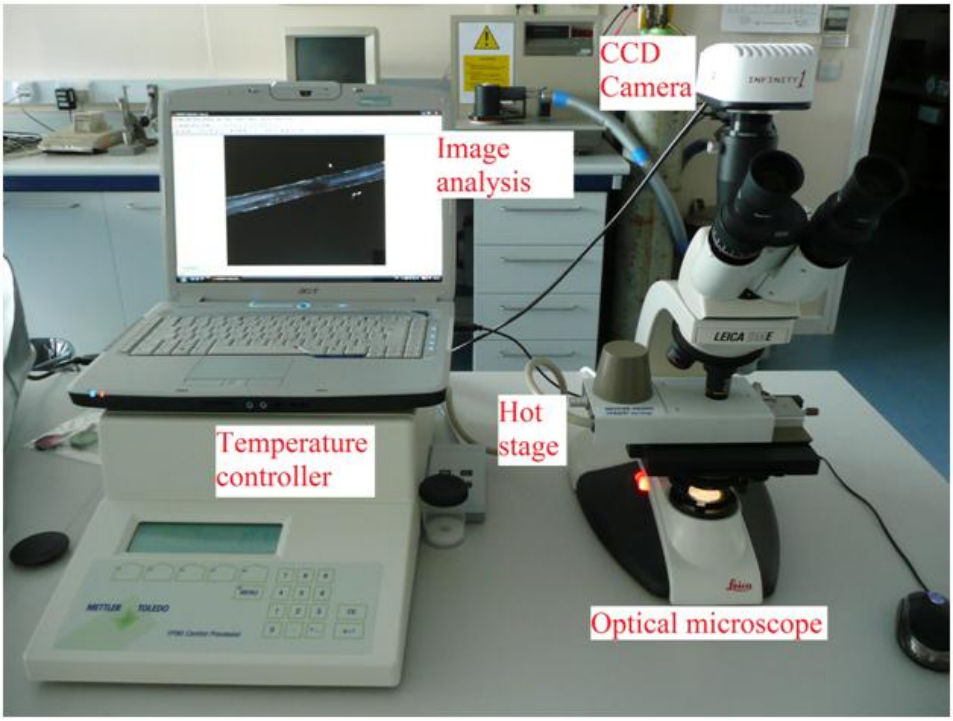

Figure 6.13: Hot stage microscopy set up. From left to right: PC, FP 82 control unit and the hot stage inserted into the Leica DME transmission optical microscope.

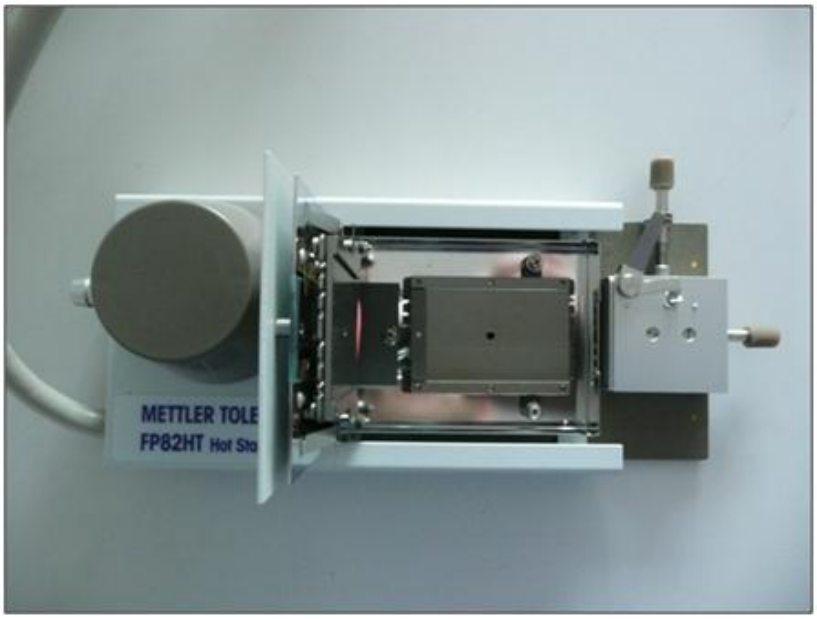

Figure 6.14: Hot stage (Metler Toledo FP82).

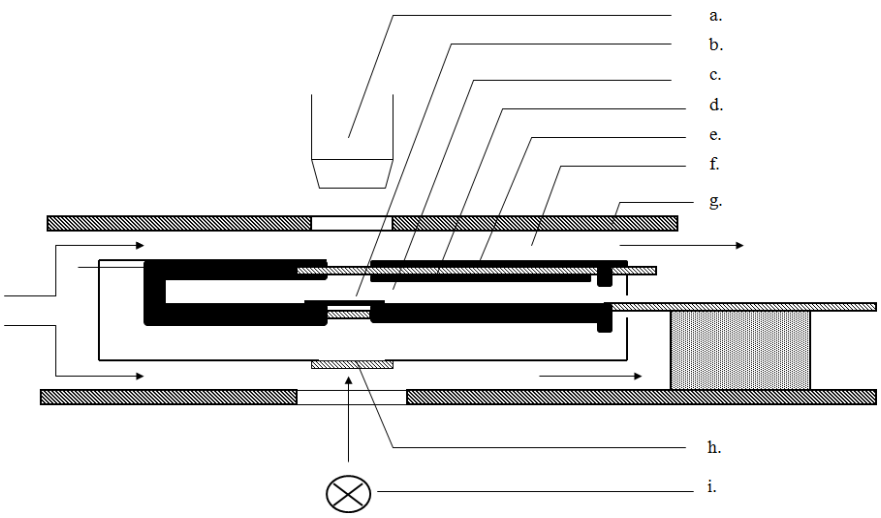

Figure 6.15: a. Section through hot stage microscope: a. Microscope objective; b. microscope slide with sample; c. flat furnace with Pt 100; d. heat protection filter; e. inner casing, warm; f. Cooling air; g. outer casing, cold; h. protective glass; i. light source of microscope

The open hot stage is seen in Figure 6.14 and a diagrammatic section through the hot stage is illustrated in Figure 6.15.

Hot state microscopy allows phase changes to be observed and melting temperature, crystallization temperature, heat distortion temperature and onset flow temperature can be measured (Scheirs, 2000). It is also possible to directly observe thermal events like degradation, bubbles and void formation, colour changes, shrinkage and stress cracking. The crystallization temperature (T_c) can be determined using a polymer foil sample. The melted polymer is cooled down gradually until crystals begin to appear. The melting temperature (T_m) can also be determined by slowly heating a polymer foil sample with crystalline morphology at a controlled rate. The melting temperature is defined as a temperature at which the last crystal disappears.

Table 6.1 summarizes melting temperatures of some common thermoplastic polymers which were determined by hot stage microscopy. Comparing the hot stage melting temperature with a DSC melting temperature, the hot stage melting point should be close to the T_{efm} (extrapolated final melting temperature) or T_{fm} (final melting temperature). Thus hot stage microscopy will give higher values of T_m because in the DSC T_m is typically the peak temperature T_{pm}. Figure 6.16 explains the principle of light polarization and the creation of a typical spherulitic pattern of a polymer crystallite.

Table 6.1: The optical melting points of some common polymers (Hemsley, 1984).

Polymer	Melting temperature (°C)
Polyethylene high density	135
Polyethylene low density	118
Polypropylene	168
Nylon 6	220
Nylon 11	185
Nylon 6:6	260
Polyacetal	180
Poly(4-methyl-1-pentene)	245
Poly(ethylene terepthalate)	270
Poly(tetrafluoroethylene)	330

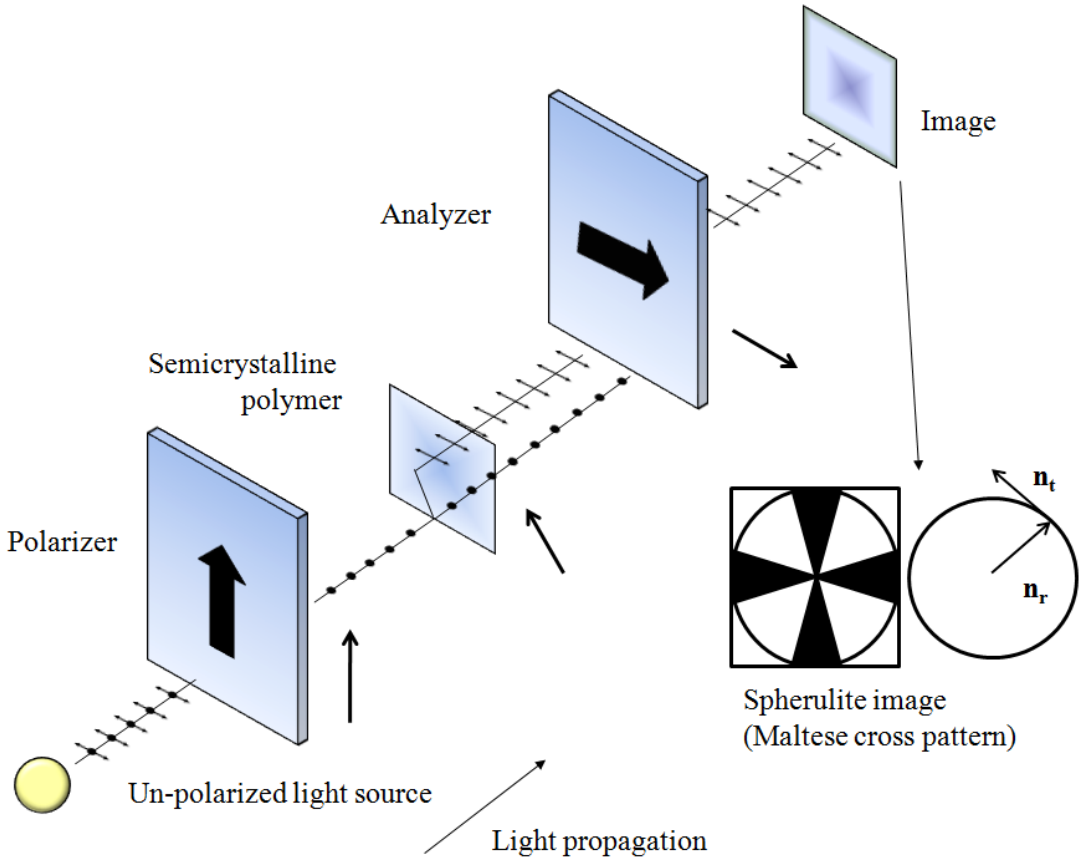

Figure 6.16: Polarized light passing through a birefrigent polymer crystal and development of typical Maltese cross pattern; n_r = radial refractive index, n_t = tangential refractive index.

When light passes through the boundary of two continua with different refractive indices it can be reflected or refracted. The condition of refraction at the boundary is described by the Snell's law

$$\frac{\sin\alpha}{\sin\beta} = \frac{n_1}{n_2} \qquad (6.13)$$

Where α and β are the refraction and incidence angles and n_1 and n_2 are the refractive indices of the two continua. At a certain incidence angle no light is reflected but all is refracted. This angle follows the Brewster's law $\tan\theta_c = n_1 / n_2$, where θ_c is the critical angle of incidence for polarization (polarization angle), n_1 and n_2 are refractive indices of media below/above reflecting plane. A beam of ordinary light consists of light waves vibrating in all directions transverse to the direction of beam propagation. Light which is forced to vibrate in a single plane is called polarized light. When a ray of polarized light passes through an anisotropic crystal other way than along an optical axis, it is reorganized into two rays which vibrate at fixed planes mutually perpendicular. Both rays follow different paths through the crystal. One of the rays (O-ray = ordinary ray) obeys Snell's law and travels through the crystal in all directions with the same velocity. The other one (E-ray = extraordinary ray) travels with a direction dependent velocity and thus does not obey Snell's law. A crystal with such quality is called *birefringent* (i.e. double refracting). The difference between the refractive indices of the two rays is called the *birefringence* of the crystal. When polarized light passes through a birefringent polymer spherulite a typical Maltese cross pattern can be observed (Figure 6.16).

6.6 Scanning electron microscopy (SEM)

SEM micrographs of composites and their cross-sections, single fibre composites and composite fractured specimens were taken using a scanning electron microscope Model JEOL 6310. Figure 6.17 describes a conventional scanning electron microscope. The SEM is used to study the topography of a specimen. Instead of light it uses electrons which are focused into a beam when passing through a system of magnetic lenses. The electron beam scans

systematically the specimen surface. The electrons in the beam (primary electrons) hit the surface and generate the secondary electrons which create the image.

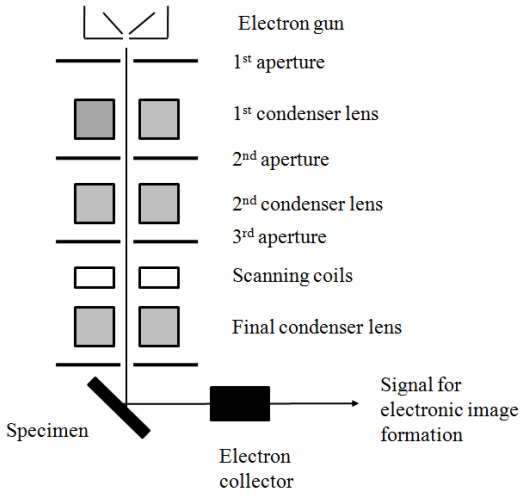

Figure 6.17: Schematic description of conventional Scanning electron microscopy (Gedde, 1999).

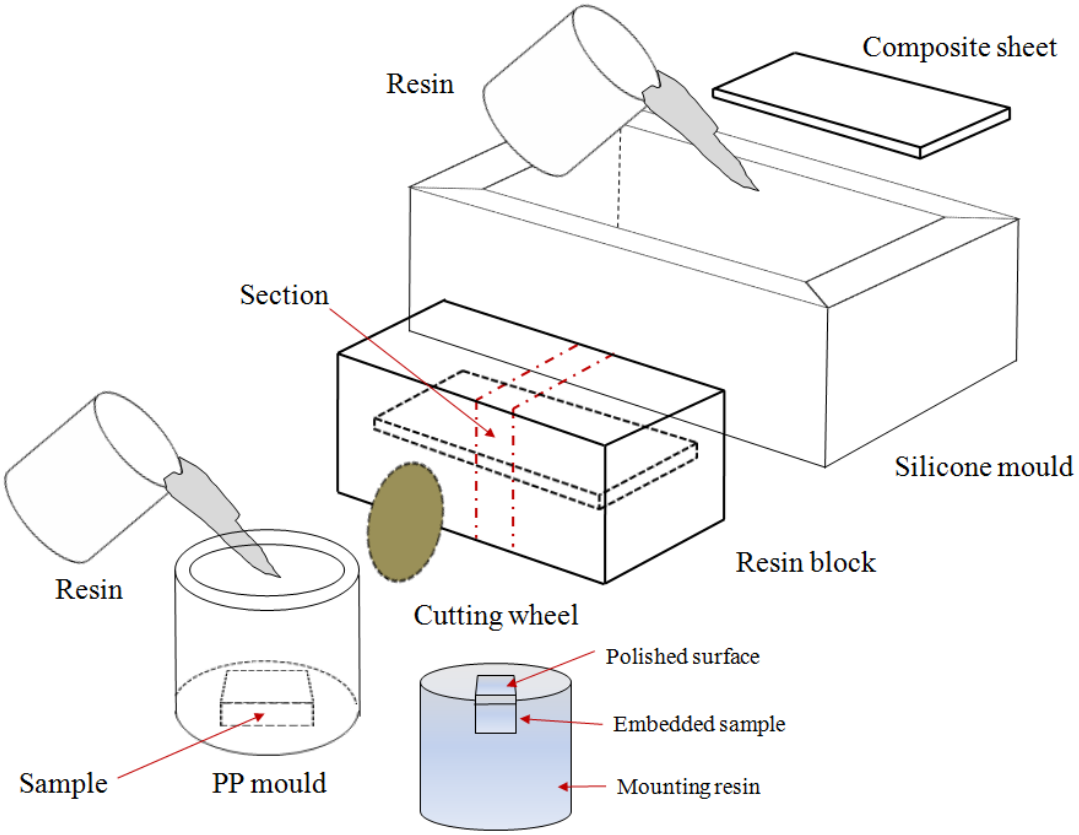

Figure 6.18: Metallographic sample preparation.

Prior to SEM evaluation the samples must be coated with gold by means of plasma sputtering. Cross sections of compression moulded fibre composites were embedded in an epoxy resin and polished prior to SEM inspection and gold coating. Figure 6.18 shows schematically the whole metallographic operation in detail. Sections of composites reinforced with 40 and 60 vol.% of fibres were prepared to inspect the fibre impregnation, fibre to matrix adhesion and to see whether the polymer melt flowed properly among the aligned fibres. The whole composite beam was mounted in a square silicone rubber (Dow Corning Silastic S) mould (110 x 20 x 20 mm) with an epoxy resin (EC 141 / W 241) system and sectioned. A 100 ml quantity of the epoxy resin EC 141 was mixed with 50 ml of the hardener W241. Sections were placed into plastic multi-clips (polypropylene) and mounted into plastic cups (polypropylene) with 35 mm diameter and 25 mm height. The mould was wiped with a mould release agent (Struers). The epoxy resin (Struers Specifix 40) was mixed with a hardener in a weight ratio of 1:2 and the mixture was poured into the round plastic mould containing the specimen (Figure 6.18). Specimens were released after 48 hours of curing at room temperature and ground and polished. A series of coarse to fine abrasive papers was used for the polishing operation. The grinding and polishing procedure is described in Table 6.2 and Figure 6.19 shows the specimens after the surface grinding and polishing.

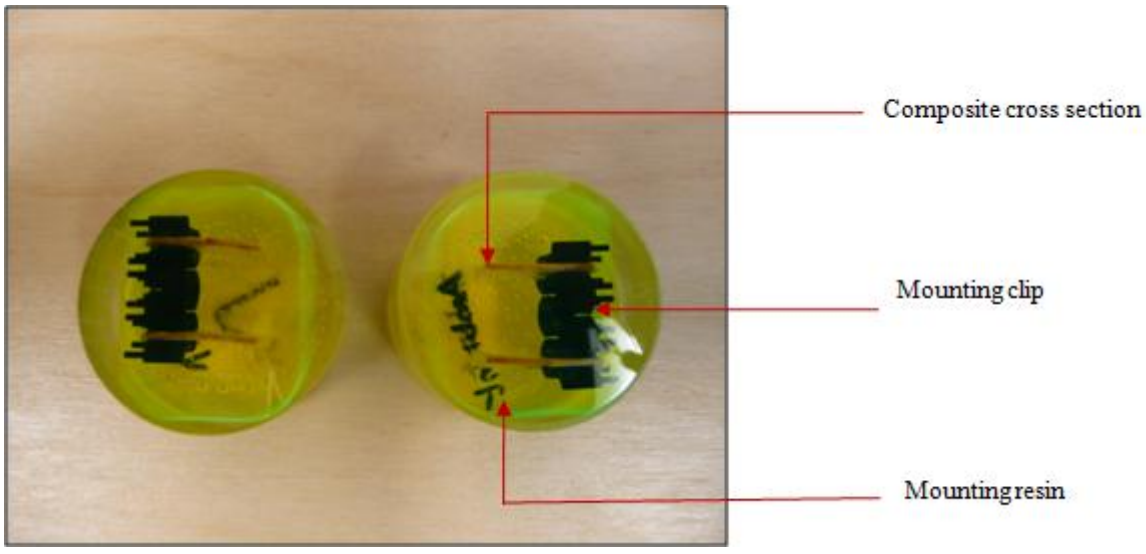

Figure 6.19: Composites cross sections embedded in epoxy resin after the surface was ground and polished.

Table 6.2: Metallographic preparation of the cross section of composites.

Description/Step	1	2	3	4	5
Paper/cloth	SiC	SiC	SiC	SiC	MD - Chem
Paper grade	# 500	# 1200	# 2400	# 4000	-
Speed [rpm]	300	300	300	300	150
Abrasive	-	-	-	-	OP-U, 0.04 μm
Lubricant	water	water	water	water	-
Holder force [N]	10/60	10/61	10/62	10/63	15/90
Holder direction	»	»	»	»	»
Holder speed	150	150	150	150	150
Time [min.]	0.5	0.5	0.5	0.5	5.00
Pause between steps	No	No	No	No	No

6.7 Microbond shear test

The microbond shear test is used to measure the strength of the fibre to matrix adhesion. The test can be instrumented as a droplet test, pull-out test or fragmentation test. In this work the pull-out test was used because it was necessary to use thin specimens where the development of transcrystallinity could be observed in the optical microscope prior to the pull-out test. In addition, making a symmetrical thermoplastic droplet around a natural fibre is very demanding. The microdroplet test was originally designed for glass fibre embedded in epoxy resin. Compared to melted thermoplastics, uncured epoxies have low viscosity and they form symmetrical, smooth droplets on fibres. Polylactic acid is difficult to process at the high temperatures required to reduce its viscosity and both PLA and natural fibres cannot withstand prolonged periods at higher temperatures. Another possibility to reduce the viscosity of thermoplastic polymers at room temperature is the use of an appropriate solvent. In case of PLA the solvent would be chlorophorm or 1,3-dioxolane. The disadvantage of such approach is that some of the solvent can stay trapped in the polymer. The solvent must be evaporated above RT under vacuum and crystallization can occur during evaporation so the droplet method has been rejected. A fragmentation test was also rejected due to the fact that not all the tested fibres fail in pure tension. Some fibres have split ends after failure and it is difficult to measure the length of the fragments under the optical microscope. To conclude, the pull-out

test was found to be the best method for measuring adhesion at the fibre to matrix interface. Sample preparation is described in detail in Section 7.3.

6.8 Tensile test – sisal fibres

Untreated and caustic soda treated sisal fibres were tested in tension to measure their tensile strength. Fibres were tested in tension at different gauge lengths (10, 15, 20, 25 and 30 mm). Twenty specimens of each set were tested. Mean strengths obtained at different gauge lengths were plotted against the gauge lengths and fitted with a straight line to extrapolate the tensile strength at the zero gauge length. The length of fibres was measured prior to testing (85 mm). Fibres were weighted and glued onto a supporting paper card with cyanoacrylate adhesive (Figure 6.20). Paper cards with fibres were gripped in the jaws of an Instron 3369 tensile test machine with a 100 N load cell and loaded in tension till failure at cross-head speed of 1mm/min.

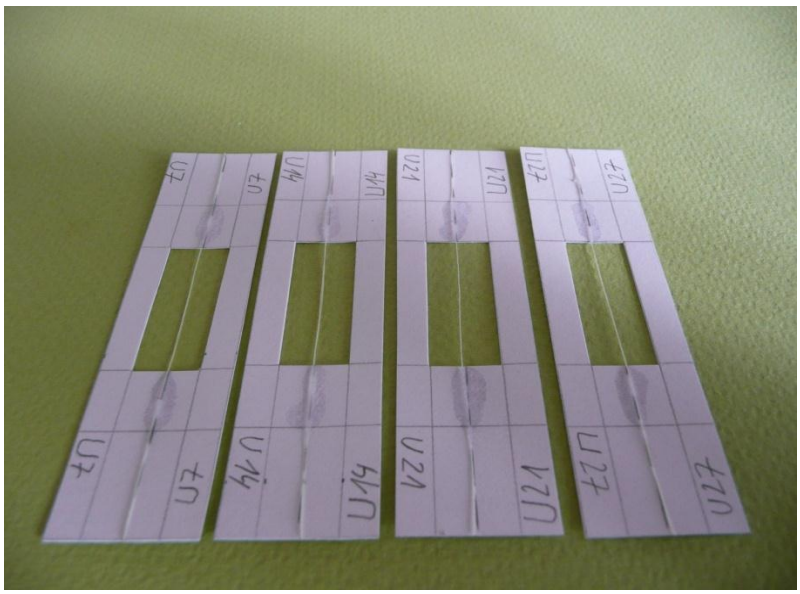

Figure 6.20: Sisal fibre bundles glued onto a supporting paper card prior to tensile test.

Weibull analysis was used to treat the data obtained from the tensile test. The Weibull modulus, mean strength and variability were calculated as described in detail in the following section.

6.9 Statistical analysis

The Weibull distribution is a continuous probability distribution which typically describes the distribution of largely scattered data. It is used in engineering applications to describe for example tensile failure of ceramic fibres, fatigue failure of composites and strength of unidirectional composites. The probability density function of a random variable X is defined as:

$$p(x) = \frac{\beta}{\delta}\left(\frac{x}{\delta}\right)^{\beta-1} \exp\left[-\left(\frac{x}{\delta}\right)\right] \tag{6.14}$$

for $x > 0$, $\delta > 0$ and $\beta > 0$ (Montgomery *et al.*, 2007; Figure 6.21). The δ parameter is called a scale parameter; the β parameter is called a shape parameter or Weibull modulus. Integrating the Equation 6.14 we obtain the cumulative density function (CDF; Figure 6.22):

$$P_f(x) = 1 - \exp\left[-\left(\frac{x}{\delta}\right)\right]^{\beta} \tag{6.15}$$

where x is a variable (for example tensile strength σ or interfacial shear strength τ) and $P_f(x)$ is a probability of failure (for example the strength of a fibre or an interface). The mean μ, variance s and the median m of two parameter Weibull distribution are defined as follows:

$$\mu = \delta\Gamma\left(1+\frac{1}{\beta}\right) \tag{6.16}$$

$$s^2 = \delta^2\Gamma\left(1+\frac{2}{\beta}\right) - \delta^2\left[\Gamma\left(1+\frac{1}{\beta}\right)\right]^2 \tag{6.17}$$

$$m = \alpha \cdot \left(\left(-\ln(2)\right)^{\frac{1}{\beta}}\right) \tag{6.18}$$

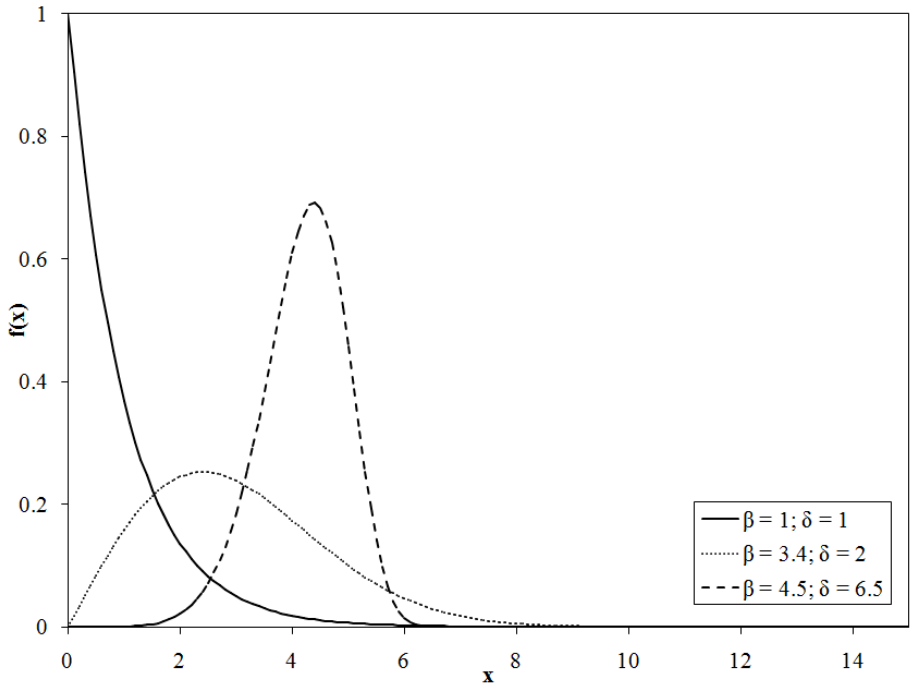

Figure 6.21: Examples of Weibull distribution function of random variables with different parameters β and δ (Montgomery *et al*., 2007).

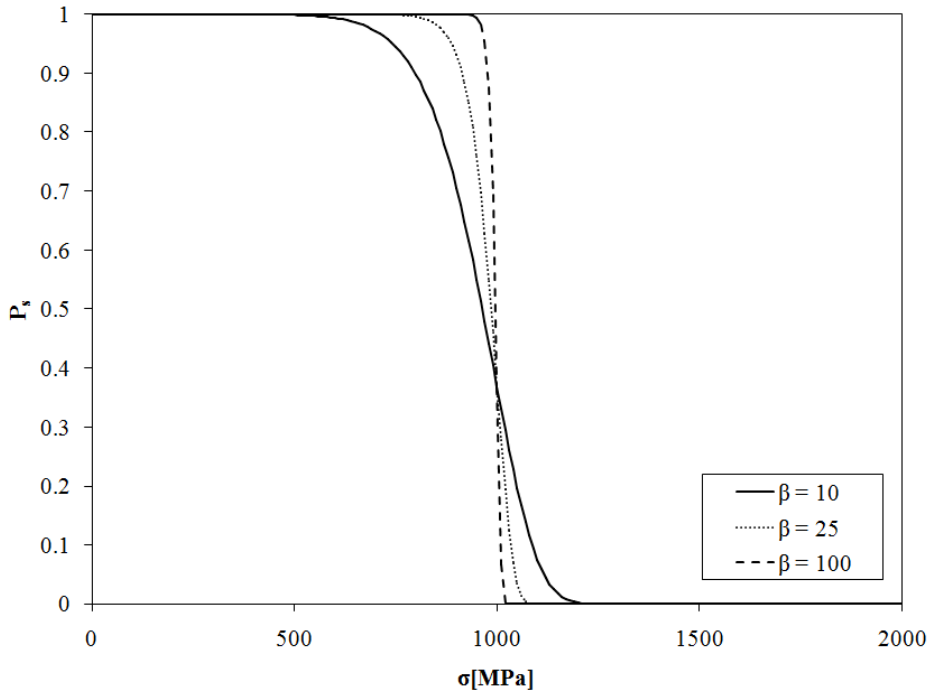

Figure 6.22: Weibull cumulative density function. The picture shows the scatter of data for three different Weibull moduli (β = 10, 25 and 100; δ = σ_0 = 1 GPa). (Le Bourhis, 2008).

The shape parameter β (Weibull modulus) can be determined graphically by linear regression. The first step consists in taking natural logarithms of both sides of Equation 6.15. After some algebraic manipulation Equation 6.15 becomes the equation of a straight line:

$$\ln\left[-\ln\left(1-P_f(x)\right)\right] = \beta \ln x - \beta \ln \delta \tag{6.16}$$

Suppose the variable x is the experimentally determined tensile strength of a fibre σ. The values of strength are further ordered in an ascending way:

$\sigma_1 < \sigma_2 < \ldots < \sigma_n < \sigma_{N-1} < \sigma_N$

Where n is the *n-th* value of a variable σ and N is the total number of specimens tested.
A probability of failure is assigned to each σ_n :

$P_{f,1} < P_{f,2} < \ldots < P_{f,n} < P_{f,N-1} < P_{f,N}$ where $0 < P_f < 1$.

The probability of failure $P_{f,n}$ of each σ_n is unknown and it has to be estimated. The most common estimation functions of the probability of failure are:

$$P_{f,a} = \frac{n-0.5}{N} \tag{6.17}$$

$$P_{f,d} = \frac{n-3/8}{N+0.25} \tag{6.18}$$

$$P_{f,b} = \frac{n}{N+1} \tag{6.19}$$

$$P_{f,c} = \frac{n-0.3}{N+0.4} \tag{6.20}$$

Generally speaking the estimators of the probability of failure usually have the following form (Le Bourhis, 2008):

$$P_{f,e} = \frac{n-a}{N+b} \tag{6.21}$$

Where, as already stated, *n* is the *n-th* value of a variable σ and *N* is the total number of specimens tested. After combining Equation 6.16 with one of Equations 6.17 – 6.20 and plotting the probability of failure versus the strength, the Weibull modulus can be estimated as the slope of the plotted straight line. The characteristic strength can be estimated from the y-intercept of the straight line.

Another method to estimate the parameters of the Weibull distribution is the maximum likelihood method (Cohen, 1965; Pham, 2006; Khalili and Kromp, 1991). In this method the two parameters of the distribution – Weibull modulus (β) and the characteristic strength (σ) - are sought to find out the Weibull distribution which describes the experimental data most closely (Equation 6.15). The probability that a Weibull distribution with the two parameters describes the experimental data is maximised if all σ_n occur simultaneously. The likelihood function is defined as a product of all failure probabilities:

(6.22)

$$L \equiv f_N = \prod_n \left[\frac{\beta}{\delta} \left(\frac{\sigma_n}{\delta} \right)^{\beta-1} \exp\left[-\left(\frac{\sigma_n}{\delta} \right) \right] \right] \tag{6.23}$$

To find the maximum of Equation 6.23 the partial derivatives of *L* with respect to the parameters β and δ must be equal to zero. Taking natural logarithms of Equation 6.23 and setting the derivatives with respect to β and δ equal to zero we obtain a set of algebraic equations (6.24 and 6.25). The Weibull modulus β is found by solving Equation 6.24 with an iterative technique. The characteristic strength δ is calculated from Equation 6.25 once β is known. The Weibull modulus is the measure of the variability of the data.

$$\frac{N}{\beta}+\sum_{n=1}^{N}\ln\sigma_n-\frac{N\sum_{n=1}^{N}\sigma_n^{\beta}\ln\sigma_n}{\sum_{n=1}^{N}\sigma_n^{\beta}}=0 \tag{6.24}$$

and

$$\delta=\left[\frac{1}{N}\sum_{n=1}^{N}\sigma_n^{\beta}\right]^{-\frac{1}{\beta}} \tag{6.25}$$

The smaller the β is, the larger is the variability. Table 6.3 summarizes the Weibull moduli of some artificial fibres.

Table 6.3: Weibull moduli of strength distributions of some artificial fibres (Chawla, 1998).

Fibre	Glass	Carbon	Boron	Aramid	Ceramic*
Weibull modulus	10-12	5-6	3-6	10-12	3-6

* For example SiC, Al_2O_3 and Al_2O_3+SiO_2.

The Cramer von Misés test can be performed to decide whether a set of experimental data follows the Weibull distribution (Murthy *et al*., 2004). It is a non-parametric goodness of fit test which seeks the maximum distance between the hypothetical cumulative distribution function (CDF) and the estimated distribution function (EDF). This is calculated as:

$$W^2=W_N^2=\sum_{n=1}^{N}\left[F(x_n)-\frac{n-0.5}{N}\right]^2+\frac{1}{12N} \tag{6.26}$$

Where $F(x_n)$ is calculated from Equation (6.15). If the calculated value of $W_N^2 > w_\alpha$ the EDF is rejected at a level of significance α. The percentiles w_α of the distribution W_N^2 are tabulated and can be found in Stephens (1974). To decide whether k independent samples come from different populations the Kruskal – Wallis test can be used (Siegel and Castellan, 1988; Sprent, 1993).

6.10 Tensile test – neat resin and composites

A tensile test was used to produce a stress-strain diagram from which the ultimate tensile strength and modulus of PLA could be determined. The tensile modulus was taken as the tangent to the initial linear portion of the stress–strain curve. The procedure consisted of gripping a tensile test specimen at a specified grip separation in the jaws of a mechanical testing machine. A load was applied at a constant rate of 2 mm/min. An extensometer was attached to the central part of the test specimen to measure the specimen extension. Elastic modulus in tension was calculated from the linear portion of the stress-strain plot. Dog bone specimens were used for tensile testing of the PLA.

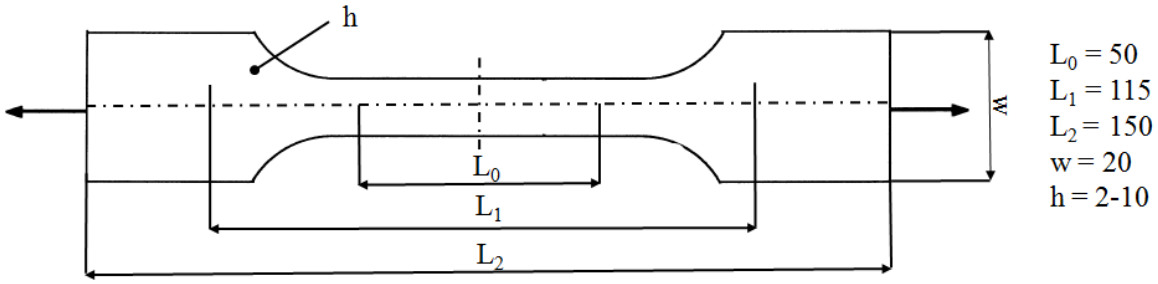

Figure 6.23: Dimensions and shape of a test specimen for plastics tensile testing in mm; L_0 = gauge length; L_1 = initial distance between grips; L_2 = overall length; h = thickness and w = width.

Table 6.4: Polishing of neat resin tensile test specimens.

Process	Pad	Liquid	Time [min.]
Grinding	SiC paper 400 #	Water	2
Grinding	SiC paper 600 #	Water	2
Grinding	SiC paper 1200 #	Water	2
Grinding	SiC paper 2400 #	Water	2
Polishing	Buehler Microcloth®	0.02 microns colloidal silica suspension	5
Cleaning	-	Distilled water	-

The PLA dog bone specimens were compression moulded (Figure 6.23). Due to shrinkage, especially in the central part of the dog bone, it was necessary to adjust the shape of the specimens. By grinding and polishing the faces of the specimens to make them parallel on a Buehler Motopol 12 polishing machine according to the schedule in Table 6.4.

Compression moulded composites of polylactic acid (PLA) reinforced with untreated and caustic soda treated sisal fibres (fibres immersed into 6 wt% solution of NaOH for 48 hours) were tested as received. Test specimens were compression moulded using a specially design aluminium mould. The dimensions of test specimens were 100 x 15 x 1 mm. The reason for using smaller test specimens (ASTM and EN standards require the length of 250 mm) was the area of the hot press (200 x 200 mm). It was necessary to ensure that all polymer phase melted at the same time and that the mould maintained the required temperature. Compression moulding is discussed in detail in Section 7.4. Figure 6.24 shows the shape and dimensions of tensile test specimens which were end tabbed with aluminium plates of 35 x 15 x 1.5 mm to avoid the test machine grips damaging the specimen.

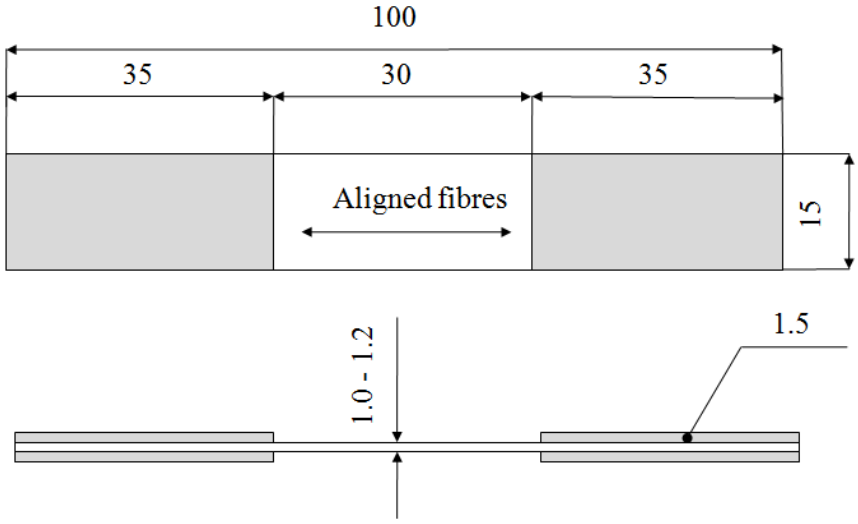

Figure 6.24: Dimensions of tensile test specimens in mm. Aluminium end tabs. (modified after Gomes *et al*., 2007).

The inner face of the end tab was abraded with a Silicon Carbide paper (400 #), washed with acetone and etched with acidic ferric sulphate to promote better adhesion between the end tab and the composite specimen. End tabs were attached with epoxy adhesive (Hysol 9461) on both sides of the composite ends. Cold cure adhesive was chosen because of the low glass transition temperature of the polymer. The gauge length of the composite specimens was set to 30 mm.

Tensile strength was calculated according to the equation (6.27) and the Young's modulus was calculated from the slope of the initial part of the load–deflection curve.

$$\sigma_T = \frac{F_m}{A} \tag{6.27}$$

Where σ_T is the tensile strength in MPa, F is the load in N and A is the cross section in mm^2.

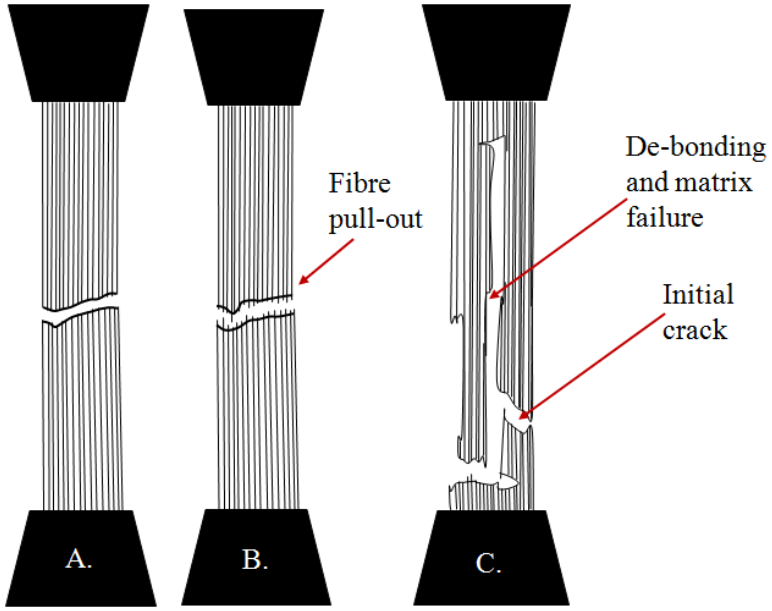

Figure 6.25: Longitudinal tensile failure modes; A. Brittle; B. brittle with fibre pull-out; C. irregular (Chamis, 1974).

Unidirectional composites subjected to tensile load can fail in a (Figure 6.25):

- brittle mode
- brittle mode with fibre pull out
- brittle mode with fibre pull out combined with interlaminar matrix shear or constituent debonding (matrix breaks away from the fibres)

6.11 Flexural test

A three point bend test consists of deflecting a flat rectangular bar of tested material with a rectangular cross section. The bar is supported at two lines as a beam and deflected at a constant rate with a centrally applied load. Figure 6.26 shows the shear force and the bending moment diagram for the three point bending test.

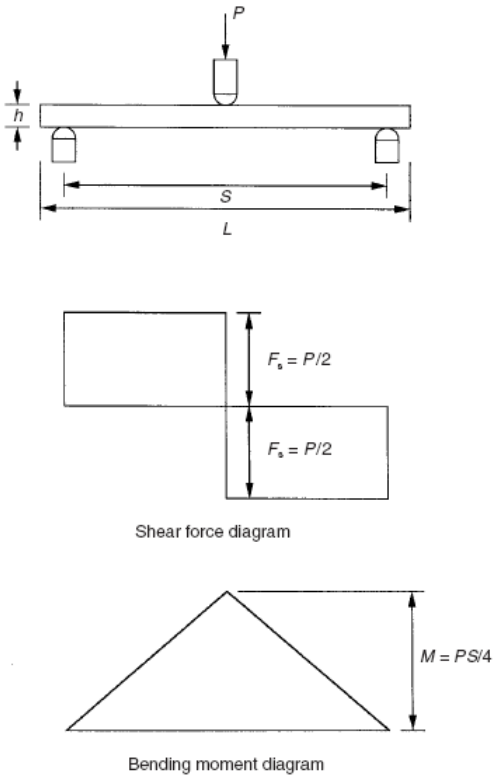

Figure 6.26: Three-point bending test; shear force and bending moment diagram; P = load, F = force, S = span and L = specimen length (Hodgkinson, 2000).

If the properties of a unidirectional composite are uniform through its thickness the distribution of normal stress is linear from a maximum in compression at the inner surface to equal maximum in tension at the outer surface. The normal stress passes through zero at the mid plane (so called neutral axis). The distribution of the shear stress is parabolic and reaches the maximum at the neutral axis and zero at specimen surfaces. The bending moment diagram increases linearly from zero at the ends to the maximum at the centrally loaded point. The shear force which produces the interlaminar shear stress at the mid plane is uniform along the

beam length. The method prescribes the use of large span to thickness ratio (L/h = 16) to promote the flexural failure which is accompanied with fibre breakage rather than matrix shear. Figure 6.27 shows failure modes in three point bending test.

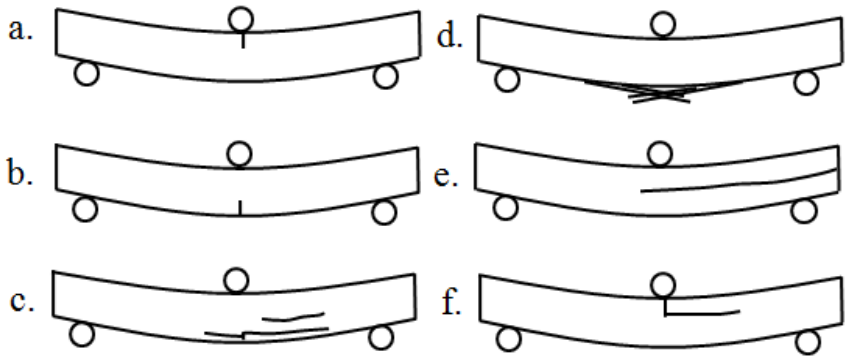

Figure 6.27: Failure modes in three-point bending test (Hodgkinson, 2000); a. Compression fracture of outer surface; b. Tensile fracture of outer surface; c. Tensile fracture with interlaminar shear; d. Tensile fracture of fibres; e. Tensile fracture with interlaminar shear; f. Compression fracture with interlaminar shear.

Flexural strength in the three-point bending test is calculated as the flexural stress sustained by the specimen at maximum load:

$$\sigma_F = \frac{3F_m L}{2bh^2} \tag{6.28}$$

where σ_F is the flexural strength in MPa, F_m is the maximum load in N, L is the span in mm, b is the width of the specimen in mm and h is the thickness of the specimen in mm. The flexural modulus is calculated as the tangent slope of the initial linear portion of the load–deflection curve:

$$E_F = \frac{L^3 m}{4bh^3} \tag{6.29}$$

Where E_F is the flexural modulus in MPa, L is the support span in mm, b is the sample width in mm, h is the sample thickness in mm and m is the slope of the tangent to the initial linear section of the load - deflection curve.

6.12 Interlaminar shear test (ILSS)

The test is also called the short beam shear test. It is widely used to measure the interlaminar shear strength as an estimate of the quality of the adhesion between the fibres and the matrix in laminar composites. The interlaminar shear strength can be calculated using the equation (6.30).

$$\tau_{ILSS} = \frac{3F_{\max}}{4bh} \tag{6.30}$$

Where τ_{ILSS} is the apparent interlaminar shear strength, F_{max} maximum load in N, b is the width of the specimen and h is the thickness of the specimen. The width, thickness and the length of the specimen shall satisfy the following relations: b/h = 5 and l/h = 10. The span (L) to thickness ratio shall be adjusted to L = 5h.

Acceptable and unacceptable interlaminar shear failure modes are summarized in the Figure 6.28.

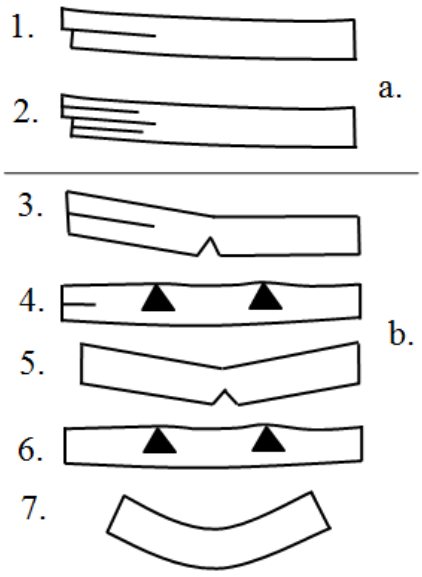

Figure 6.28: Short beam shear test: a. acceptable failure modes, b. unacceptable failure modes. 1. Single shear, 2. Multiple shear, 3. Shear and failure, 4. Shear and compression, 5. Tension, 6. Compression and 7. Plastic shear (BS EN ISO 14130).

6.13 Raman spectroscopy

Raman spectroscopy can be used to observe the behaviour of materials when they are subjected to deformation. It has been found that frequencies of bands in Raman spectra of some materials change under applied stress (σ) or strain (ε) (Young, 1994). The change which can be expressed as $d\Delta\upsilon/d\sigma$ or $d\Delta\upsilon/d\varepsilon$ results from the deformation of individual bonds in the molecular structure of the material (Young, 1996). Raman deformation experiments started with polydiacetylene single crystals (Galiotis *et al*., 1984 and Robinson *et al*., 1987). Since then several fibres and fibre/polymer matrix systems have been studied. For example Huang and Young (1996) studied carbon fibres embedded in epoxy or polymethylmethacrylate. Andrews *et al*. (1993) and Bannister *et al*. (1995) studied the behaviour of aramid fibres in epoxy resin. Polyethylene fibres were pulled-out from the epoxy resin (Li and Grubb, 1994) and the axial stress distribution along the fibre was determined. Micromechanics of regenerated cellulose fibres as well as natural cellulosic fibres was extensively studied by Eichhorn and Young (2004), Eichhorn *et al*. (2003) and Kong and Eichhorn (2005). It is also possible to use Raman spectroscopy to explore the interaction and stress distribution between broken and unbroken fibres during the fracture of composite materials (Wagner *et al*., 1996) as well as the effect of residual thermal stresses which arise during the composites preparation because of the difference in the coefficient of linear thermal expansion (CLTE) between the fibre and the matrix (Grubb and Li, 1994).

When a photon of incident light with energy $E = h\upsilon_0$ hits a sample absorption can happen (which is the basis of the infrared spectroscopy), emission can happen (which is the basis of fluorescence spectroscopy) and scattering can happen (which is the basis of Raman spectroscopy). The light can be scattered elastically, i.e. the frequency of scattered light remains unchanged (Rayleigh scattering), or inelastically (frequency difference between the incident and scattered light). Figure 6.29 illustrates energy transitions where υ_0 is the frequency of the incident light, $\upsilon = 0$ is the ground state and $\upsilon = 1$ is the excited vibrational state. The frequency difference between the incident and scattered light results from the transitions between the energy levels in molecules after interaction with the incident monochromatic light.

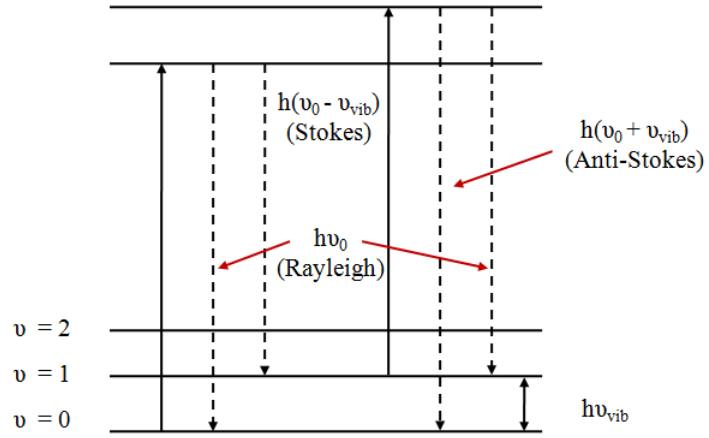

Figure 6.29: Energy transitions for elastic (Rayleigh) and inelastic (Stokes) light scattering (Campbell *et al.*, 2000).

The energy transitions come from the stretching and bending vibrations of the interatomic bonds in a molecule. Frequencies of these vibrations are characteristic of functional groups in molecules. At room temperature the interatomic bonds vibrate in the so called ground state. In order to excite them to higher energy levels they must absorb energy. This can be achieved by their interaction with light radiation. In case of Stokes scattering the photon of incident light transfers energy to the polymer sample and transition from the ground (0) state to the excited (1) state occurs. In case of Anti-Stokes scattering energy is transferred from the polymer sample to the photon and a transition from the excited (1) to the ground (0) state is induced. Equations 6.31-33 express the energies of scattered light:

$$E_{Stokes} = h(\upsilon_0 - \upsilon_{vib}) \tag{6.31}$$

$$E_{Anti-Stokes} = h(\upsilon_0 + \upsilon_{vib}) \tag{6.32}$$

$$E_{Rayleigh} = h\upsilon_0 \tag{6.33}$$

Stokes scattering is associated with a decrease in energy and a shift to shorter wavelength (or higher wavenumber). Anti-Stokes scattering has the opposite properties – increased energy, and a shift to longer wavelength (or smaller wavenumber).

If a molecule is able to scatter the light and produce a Raman signal it has to be polarizable, i.e. the interatomic bonds must deform when subjected to a periodic electric field like light. The intensity of Raman scattering is expressed by the following formula (Bloor *et al*., 1976):

$$I_{if} = N_i \frac{64\pi^2}{3c^2}\left(\upsilon_0 - \upsilon_{if}\right)^4 P_{if}^2 \qquad (6.34)$$

Where N_i is the population of molecules in the initial level, subscripts *i* and *f* have the meaning of the initial and final vibrational levels, υ_0 is a frequency of the incident radiation which causes the excitation, *c* is the velocity of light and *h* is the Planck constant. P_{if} is the electric moment associated with the transition from level *i* to *f* and can be expressed as:

$$P_{if} = \alpha_{if} E \qquad (6.35)$$

Where α_{if} is the polarizability tensor and *E* is the electric field vector. Hence polarizability is a molecule property which describes the ability of a molecule to scatter the incident radiation. In other words it represents the ease with which the electron cloud around the molecule is distorted by the interaction with an external electric field. The polarizability tensor can be expressed as:

$$\alpha_{if} = \frac{1}{h}\sum_e \left[\frac{\mu_{ef}\mu_{ie}}{\upsilon_{ei} - \upsilon_0 + i\delta_e} + \frac{\mu_{ie}\mu_{ef}}{\upsilon_{ef} + \upsilon_0 + i\delta_e} \right] \qquad (6.36)$$

Where μ_{ab} is the transition electric dipole moment for transition from level *a* to level *b* and δ_e is the damping constant of the excited level *e*.

A typical Raman spectrometer contains an excitation source (laser), sample illumination system, light collection optics, wavelength selector (filter) and detector (CCD). Figure 6.30 shows the components of a Raman spectrometer.

Monochromatic light is emitted from a laser and passes through the sample. Mirror M_1 reflects the light after passing through the sample to intensify the signal. Raman scattering is observed perpendicular to the direction of the incident light and is focused by a lens to an entry slit (1). Mirror M_2 doubles the intensity of the scattered light because of the low intensity of Raman

scattering. The light is separated into its spectral components by a grating and focused onto a photoelectric detector after passing through the exit slit (2).

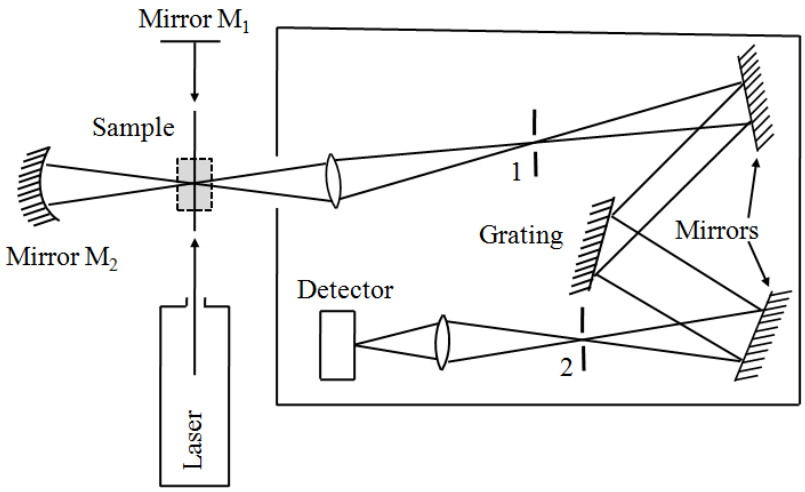

Figure 6.30: Components of a Raman spectrometer (Hesse *et al*., 2008).

To obtain high quality Raman spectra the spectrometers contain a series of optical filters to filter out the Rayleigh scattering because only about 0.001% incident light produces Raman signal with frequencies $\upsilon_0 \pm \upsilon_m$.

As already pointed out Raman spectroscopy can be used to study the deformation of polymer composites and to map the stresses which built up in the sample at the fibre to matrix interface. The procedure for stress transfer determination in single fibre polymer composites with Raman micro-spectroscopy involves:

1. Identification of the stress dependent frequency

2. Drawing a calibration curve which plots the position of the stress-dependent frequency as a function of stress (applied to the fibre). In other words the position of the stress dependent frequency in relation to its initial position in the spectrum of an un-stressed fibre usually plotted as a difference – frequency shift versus stress (strain) applied to the fibre (see Figure 6.31). The slope of the plot is,

$$\frac{d(\Delta\upsilon)}{d\varepsilon} \approx E \tag{6.37}$$

3. Measurement of the spectrum of a fibre embedded in a matrix

4. Conversion of the frequency into local stresses

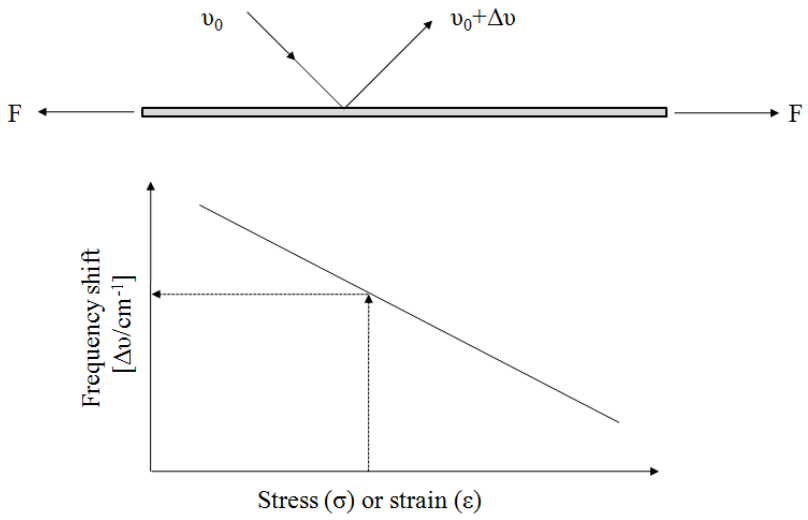

Figure 6.31: Calibration of the Raman peak position as a function of fibre stress (strain).

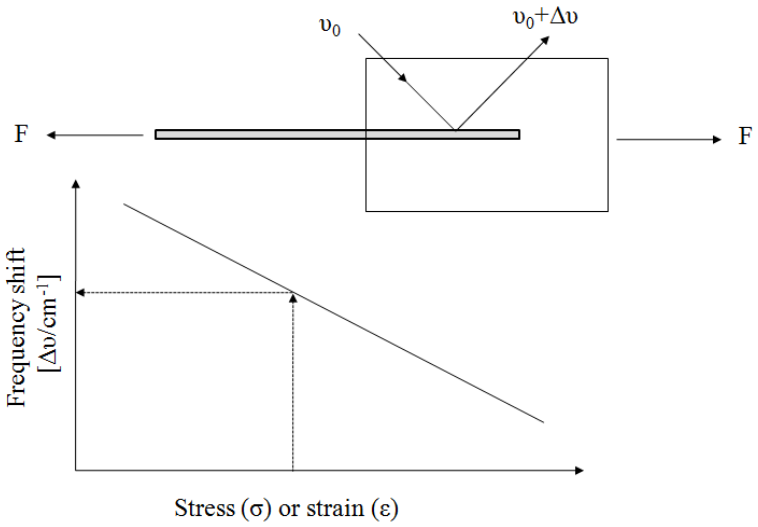

Figure 6.32: Stress (strain) mapping along the fibre length embedded in a polymer matrix.

In other words an applied stress (strain) applied to the polymer fibre stretches the bonds in the fibre molecules. A chemical bond which must be selected which is most susceptible to the stress (strain) deformation and its frequency identified in the Raman spectrum under no applied stress. By applying the stress to the fibre the bonds are distorted and their electron clouds are shifted from their ground energy positions. Consequently the dipole moments of the

bonds change. Such a strained (stressed) bond (or dipole moment) when inserted in a periodic electric field (e.g. laser light) will vibrate with a different frequency. This frequency will be different from the bond frequency in an unstrained (unstressed) molecule. The frequency position in the Raman spectra is shifted (usually to higher frequencies). In a typical experiment one has to map the frequency along the fibre embedded in a matrix (Figure 6.32) with a constant step (e.g. 10 μm). The fibre is strained (stressed) under a global stress. Through the calibration curve (Figure 6.31) it is possible to convert the measured frequencies (frequency shifts) into stresses. As a result a stress profile of local stresses along the fibre embedded in a matrix at a constant global stress applied to the fibre is obtained. The profile can be fitted with a curve and micromechanical models allow the calculation of the interfacial shear stress at the fibre to matrix interface. The interfacial shear stress distribution is usually calculated through the equilibrium of forces which act upon a fibre element *dx* (Bannister *et al.*, 1995):

$$\tau = E_f \frac{r_f}{2} \frac{d\varepsilon_f}{dx} \tag{6.38}$$

Figure 6.33 shows typical experimental set up consisting of the straining rig and Raman spectrometer with an attached microscope.

The stress-dependent frequencies (also called Raman bands) for regenerated cellulose are 895 cm^{-1} and 1095 cm^{-1} (Attala and Nagel, 1974). The first one is attributed to C-O stretching within the cellulose ring. The second one is attributed to C-C-C and C-H-O mixed mode vibrations. In natural cellulose no peak at 895 cm^{-1} was found (Eichhorn, Sirichaisit and Young, 2001) so the peak at 1095 cm^{-1} is used to follow the stress dependent frequency shift.

Raman spectra of polylactic acid show characteristic lines at 923 and 520 cm^{-1} which are assigned to C=O stretching and CCO bending (Kister *et al.*, 1995).

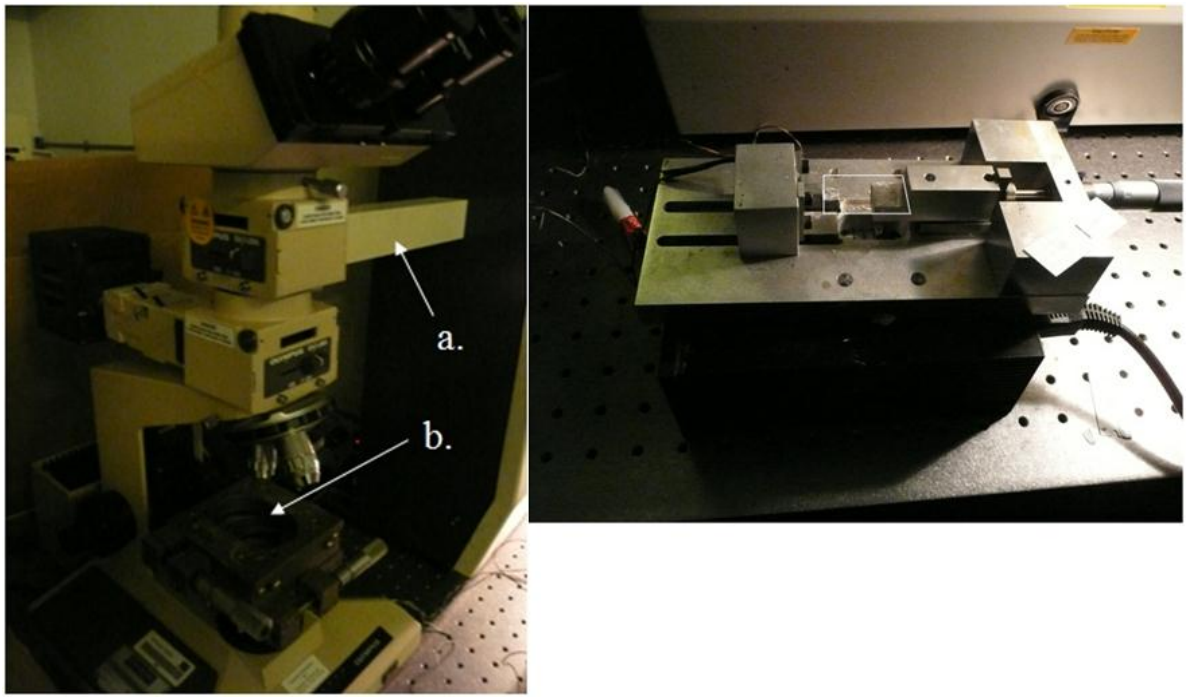

Figure 6.33: Raman spectrometer (a) with attached microscope and position of the straining rig (b) (left); straining rig - white rectangle in the middle of the strain rig represents the position of the sample, e.g. fibre mounted on a paper card.

How accurate is Raman spectroscopy in the determination of interfacial shear stress? Galiotis (1991) calculated the final cumulative error in the determination of IFSS for the Kevlar-49 and HM-carbon fibres embedded in a epoxy matrix to be 16 and 25 % respectively.

7 Specimen preparation

Several test samples were used in this study. The chapter starts with hot pressing of polymer sheets, dog bones and bars for tensile and flexural test. It continues with the preparation of thin film samples for hot stage microscopy and partially embedded single fibre specimens for the microbond shear test. The chapter finishes with compression moulding of polymer composites reinforced with long fibre bundles. Processing of long fibre bundles composites made of natural fibres and its peculiarities are discussed.

7.1 Hot pressing

Polylactic acid (PLA) granules were used as purchased, oven dried overnight at 50°C and compression moulded in sheets of about 0.4 mm thickness using a picture frame mould. The picture frame mould was a compression mould consisting of a bottom steel plate (200 x 200 x 5 mm) and a similarly sized centre plate with a hole in the centre (diameter of 150 mm). The top part of the mould was a circular plate with a diameter of 150 mm. Compression moulding was carried out in two stages. In the first stage PLA was consolidated at 190°C at no pressure applied for 10 min. In the second stage PLA was compressed at 190°C/ 0.1 MPa / 10 min. Sheets were cooled down at room temperature for 24 h. Moulded sheets were stored in polyethylene sealed bags at room temperature and 50% relative humidity. Such PLA sheets were used for different sample preparation. They were combined with sisal fibre bundles and compression moulded into composites. They were also used for the preparation of thin film samples for hot stage microscopy and partially embedded single fibre specimens for the microbond shear test. Some of the sheets were also used for the determination of the glass transition temperature, melting temperature and degree of crystallinity through differential scanning calorimetry (DSC). In order to determine mechanical properties of PLA tensile test samples (dog-bones) were compression moulded. Figure 7.1 shows the mould filling with solid polymer pellets. The mould was filled with 10 % excess of granules to make the polymer melt flow under pressure. As a result the individual molten pellets were compacted and took the shape of the mould. The central part of the mould was a steel plate with a central hole in a

dog bone shape. It was placed on a steel sheet and filled with an excess of polymer granules. The mould was covered with another steel sheet, wrapped in an aluminium foil and transferred into the hot press. The mould was kept at 190°C with no pressure applied for 10 min. After this preheating stage the mould was compressed at 190°C at 0.1 MPa for 10 min. When the mould was released from the hot press it was cooled down at room temperature for 24 h. Due to the polymer shrinkage mainly in the central narrow part the tensile test samples were ground and polished to make their surface flat and their cross-section rectangular (Table 7.1).

Figure 7.1: Compression mould for PLA dog bone samples for tensile testing. Open mould (left) and the mould filled in with PLA granules.

PLA samples for three-point bend test were also compression moulded using a picture frame mould. The mould consisted of a bottom and top steel plate (200 x 200 x 5 mm). The inner plate had a central cavity with diameter of 150 mm and thickness of 5 mm. Compression moulding was carried out in a similar way as described previously. Rectangular bars for flexural test were cut from the moulded article using a hand saw. The bars were also ground and polished to have a rectangular cross section using a Buehler Motopol 12 polishing machine. Detailed procedure is described in Table 7.1.

Table 7.1: Grinding and polishing procedure for PLA tensile/flexural test specimens.

Process	Pad	Liquid	Time [min.]
Grinding	SiC paper 400 #	Water	2
Grinding	SiC paper 600 #	Water	2
Grinding	SiC paper 1200 #	Water	2
Grinding	SiC paper 2400 #	Water	2
Polishing	Buehler Microcloth®	0.02 μm colloidal silica suspension	5
Cleaning	-	Distilled water	-

7.2 Thin film samples

Thin film samples were prepared for hot stage microscopy. The samples were prepared by sandwiching single sisal fibre between two films of the polymer matrix of a thickness of approximately 100 µm on a separate hot plate (Figure 7.2). Such samples were later transferred into the hot stage.

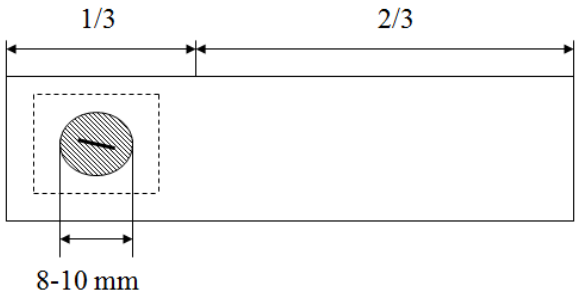

Figure 7.2: Polymer single fibre composite sample on a glass slide. Dotted area represents the glass cover slip.

All PLA samples were first heated at 180°C and kept at this temperature for 10 minutes to erase the previous crystalline morphology. Isothermal crystallization was then studied at different thermal conditions with different crystallization temperatures (T_c~120-140°C) and different cooling rates (2-9°C/min.) applied. Crystallization was observed on untreated and caustic soda treated sisal fibres.

7.3 Pull out samples

Figure 7.3 and 7.4 schematically describes the sample preparation. A square of 10 x 10 mm was cut from the compression moulded sheet and stored in a dehumidified environment. A glass slide (76 x 26 x 1 mm) was wrapped in an aluminium foil (thickness = 0.04 mm).

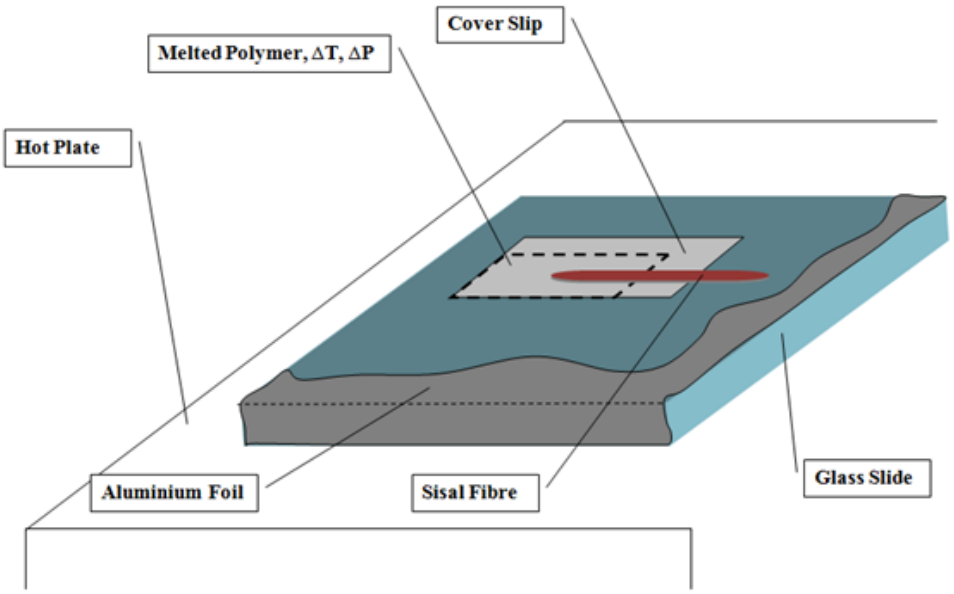

Figure 7.3: Fibre embedding and pull out test sample preparation.

Mould release agent (Wurth PAT-607/PCM) was applied on the top surface of the foil. A PLA square was placed on top of the glass slide. The glass slide was placed on a hot plate heated up to 190°C and a sisal fibre bundle was dipped (using tweezers) in the edge of the molten PLA square. The melted polymer was covered with a glass cover slip (22 x 22 x 0.15 mm) and slightly pressed with tweezers. After this, the sample was removed from the hot plate and air quenched. After 20 min. the foil was peeled off. The fibre embedded in the plastic adhered to the cover slip.

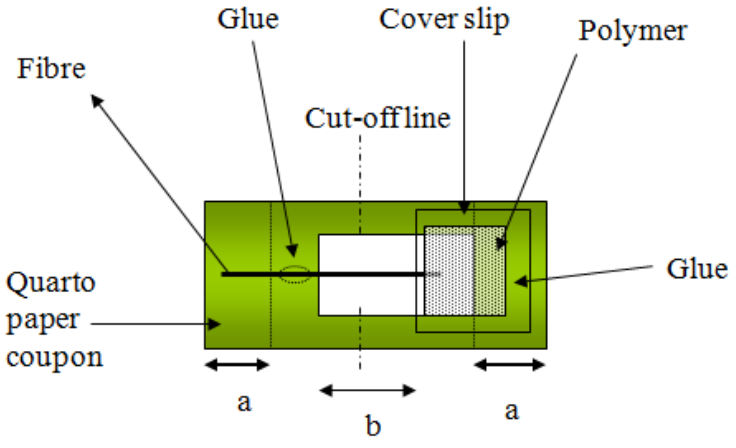

Figure 7.4: Mount card with a pull out test sample. (a) Gripping area. (b) Gauge length.

The cover slip was glued to a paper mount card (65 x 24 x 0.22 mm; gauge length of 10 mm) as described at Figure 7.4. The embedded fibre length and fibre diameter were measured with an optical microscope (Leica DME, magnification 100x, transmitted light) equipped with a digital camera (Lumenera Infinity 1) and Studio Measure software (Metler Toledo). The microscope lens (scale bar) was calibrated using calibrated stage micrometer. Figure 7.5 shows pull out test samples prepared for testing.

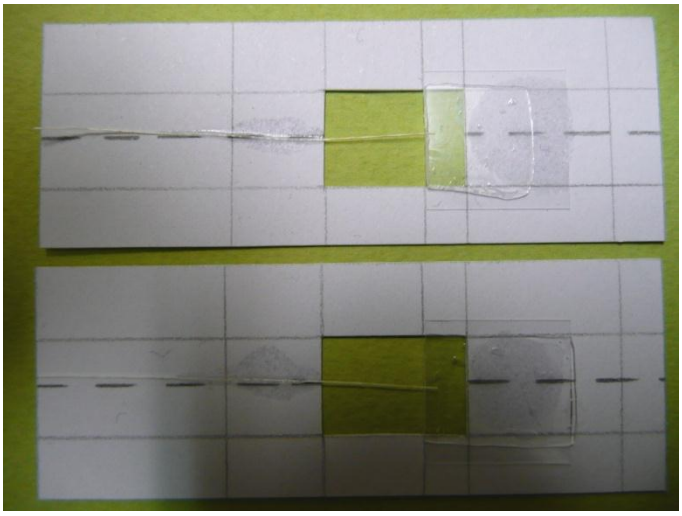

Figure 7.5: Sisal fibre embedded in a block of PLA and glued onto a supporting paper card.

7.4 Composite samples for mechanical testing

Combining PLA with cellulosic fibres into a good quality composite with reasonable structural properties was complicated and challenging process. Firstly the factors which influenced the processing of PLA composites will be discussed in this section. Secondly the manufacture of polylactic acid reinforced with long sisal fibre bundles unidirectionally aligned will be described.

Thermoplastic composites can be produced by injection moulding, extrusion (pultrusion) and compression moulding. The mostly used process is the injection moulding. According to Ehrenstein (2006) thermoplastic polymers are usually reinforced with short fibres (0.2 mm), long fibres (~ 25 mm) and continuous fibres. In this place it is very important to define the term of long fibre and explain the difference in terminology. Figure 7.6 explains why the

injection moulders (Oksman *et al.*, 2001) talk about long fibres and they mean fibres of lengths of few millimetres. It is because the properties of the composite reinforced with short glass fibres reach their maximum at the length of about 25 mm. It is possible to manufacture a continuous glass fibre and use this fibre in the pultrusion process. In case of cellulosic natural fibres it is impossible. The only way to make a continuous cellulosic fibre is the process of cellulose regeneration. But the strength of such fibre (like lyocell) is poor compared to the original natural cellulosics.

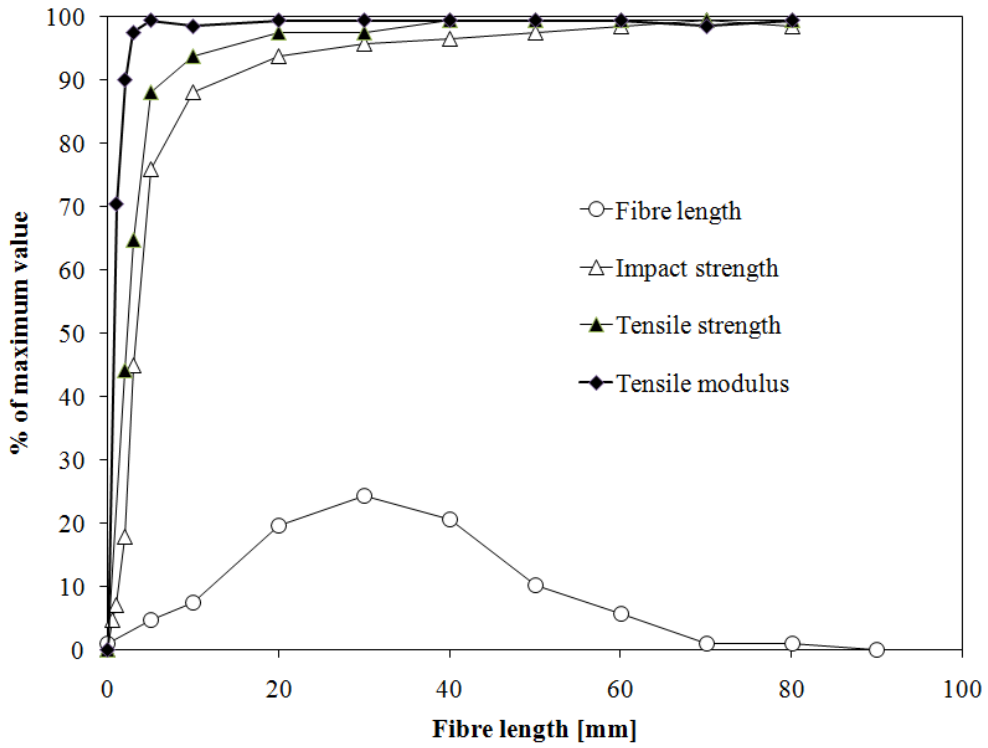

Figure 7.6: Influence of the glass fibre length on selected mechanical properties of injection moulded thermoplastic composites (Ehrenstein, 2006).

Natural fibres can be spun into yarns. The fibre bundles are cut to smaller portions and twisted into continuous yarns in the spinning process. To make it clear in the experimental section of this thesis when composites reinforced with long fibres or long fibre bundles are discussed the following definition applies: composites reinforced with well aligned and untwisted fibres which lay in the axis of the predominant load and which are of the same length as the composite structure is (e.g. tensile test specimen). Clearly continuous natural fibres can't be

produced without damaging their structure. Long natural fibres which can be used for the manufacture of unidirectional composites without being spun into yarns are for example hemp, flax and sisal.

The most striking difference between thermosetting and thermoplastic matrices in terms of processing is their viscosity and its dependence on temperature. Most thermoplastics are brittle solids at room temperature. To reduce their viscosity they need to be heated up. Thermosets exist as liquids at room temperature and solidify by cross-linking at increased temperature. Hence thermosets will wet natural fibres easily compared to thermoplastics. Table 7.2 summarizes viscosities of some common polymer matrices. Riedel and Nickel (1999) stated that the viscosity of thermoplastics should be reduced to 100 mPa.s in order to wet natural fibres as thermosets do.

Table 7.2: Viscosity of some common thermosetting liquids and thermoplastic polymer melts at their processing temperatures (Ehrenstein, 2006).

Matrix	Processing temperature	Viscosity at processing temperature
Unsaturated polyester (UPR) (low curing temperature)	10-40°C	10^2-10^3 mPa.s
Unsaturated polyester (UPR) (high curing temperature)	≈ 140°C	≈1000 mPa.s
Epoxy (EP)	e.g. 130°C	10^2-10^3 mPa.s
Polypropylene (PP)	200-270°C	10^3 Pa.s
Polyetheretherketone (PEEK)	≈ 350-400°C	10^3-10^4 Pa.s

Figure 7.7 shows the temperature dependence of PLA viscosity measured by cone plate viscometer (Bodros *et al.*, 2007). The melting temperature of PLA is about 170 °C. Processing temperatures for semicrystalline thermoplastics are usually about T_m + 30°C. It is apparent that at these temperatures it is not possible to reduce the viscosity to achieve the value stated by Riedel and Nickel. Viscosity depends on molecular weight. The lower the molecular weight the lower the viscosity and higher flowability but the lower the consequent mechanical properties of the product. Viscosity of thermoplastic polymer can be reduced if a solution of a polymer in a solvent is used. This approach has its limitations: long dissolution times for long

polymer molecules – a usually days or weeks - and only low concentration solutions can be prepared (~ 5wt%). Solvent can remain trapped in a polymer matrix and then cause voids during the processing or "environmental stress cracking" during the life of the structure.

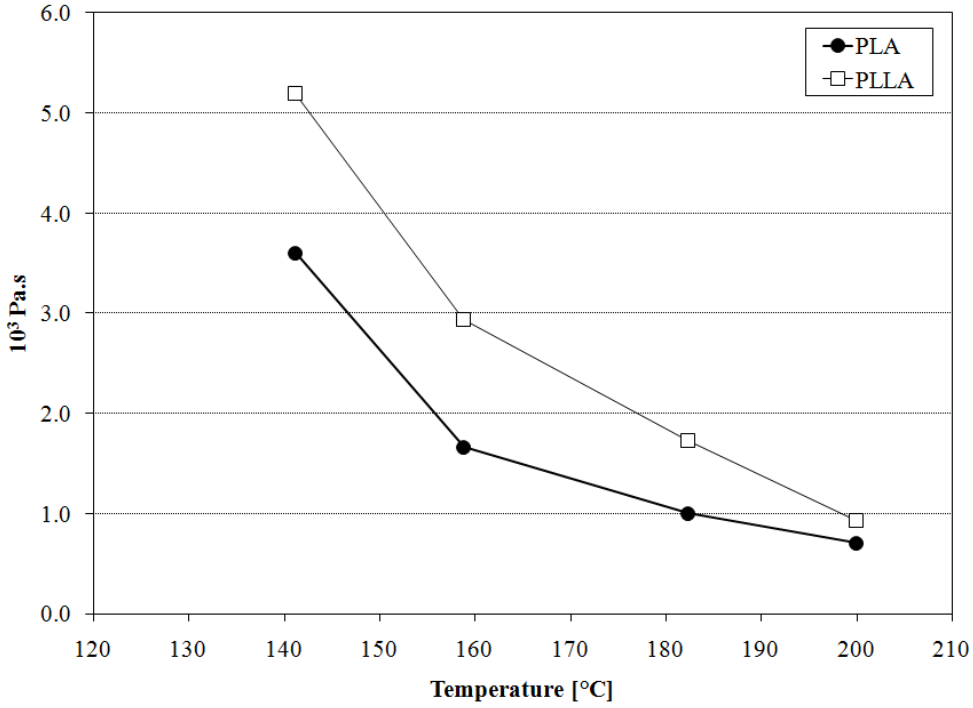

Figure 7.7: Viscosity of PLA melt versus temperature (Bodros *et al.*, 2007).

Table 7.3: Implications of the choice of reinforcement format for fibrous composites (Bader, 2001).

Reinforcement format	$V_{f,\,max.}$	Orientation efficiency factor, η_0	*Stiffness index, η_{RF}	Manufacturing process
UD tow	0.80	1.00	0.80	Filament winding, pultrusion, hot pressing
UD prepreg	0.65	1.00	0.65	Autoclave, RFI
Multi-axial prepreg	0.60	0.31	0.19	Autoclave, RFI
2D non-crimp fabric	0.55	0.30	0.11	RFI, RTM
Woven 2D fabric[a, b]	0.50	0.27	0.14	RTM, wet lay-up
Orthogonal 3D fabric	0.40	0.30	0.12	RTM
Random planar	0.30	0.30	0.09	SMC, RTM, wet lay-up
Random 3D short fibre	0.20	0.12	0.02	BMC, IM (thermoplastic)

Note: *product of the orientation efficiency factor and the maximum fibre volume fraction.

Another way to overcome the high viscosity of the thermoplastic is the fabrication of hybrid fabrics or yarns. Khondker *et al.* (2006) used hybrid yarn made of commingled polypropylene and jute fibres. This way the polymer is placed close to the fibres as much as possible without viscosity change. The aim of further hot pressing is to melt the matrix and make the assembly compact. There is no necessity of the flow and viscosity reduction as the matrix is already there. Table 7.3 shows how the fibre orientation and fibre volume fraction control mechanical properties of composites. The best mechanical properties are attributed to the matrices reinforced with well aligned long fibre bundles. Figure 7.8 shows the detail of a plain weave fabric made of untreated hemp fibres. The figure shows clearly that the fibre bundles have to be twisted while they are spun into the yarn. Thus not all of the fibres lay in the axis of the yarn. Also the microfibrils in the cell wall are influenced by the twisting and don't lay in the axis of the yarn. Fibre bundles are closely packed into the yarn hence it is difficult for the viscous polymer melt to penetrate the yarn and wet properly individual fibre bundles. Composite reinforced with a yarn may fail by pulling out centrally placed fibre bundles from the yarn. Fibre fracture volume is limited in composites reinforced with fabrics (Figure 7.8). High fibre volume fractions are possible with satin with low fibre twist.

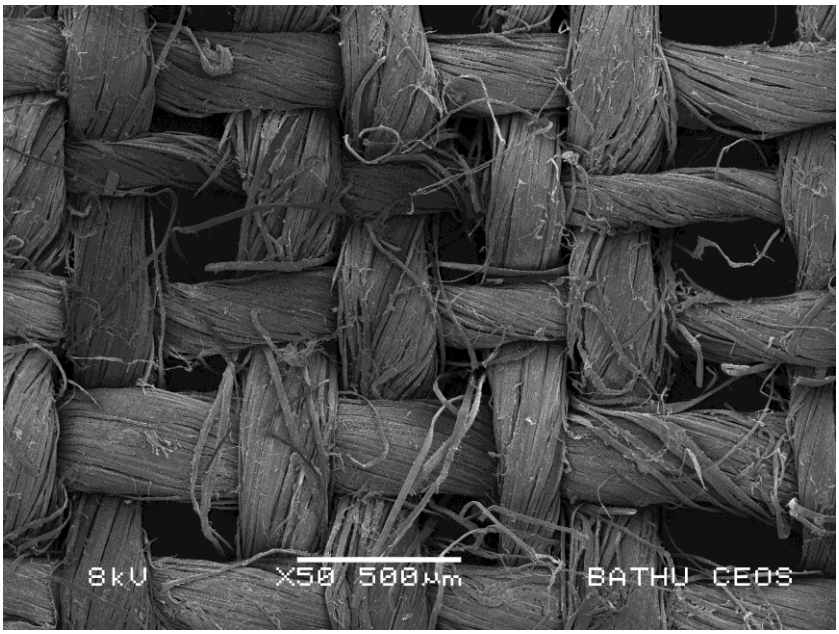

Figure 7.8: Hemp plain weave fabric.

Understanding the polymer thermal decomposition is vital to find out the optimal processing conditions. The influence of water and alkali on cellulose and polylactic acid is discussed due to the fact that alkali treated fibres are combined with PLA and due to the fact that water can develop as thermal degradation product and both can catalyse further degradation. Jamshidi *et al.* (1988) found PLA to decompose thermally at temperatures above 190°C. McNeill and Leiper (1985a and 1985b) studied the thermal decomposition of polylactic acid with thermogravimetric analysis (TGA), and DSC at the heating rate 10°C/min. PLA was found to decompose in a single stage between 250-450°C. The DSC thermograph showed large endothermal peak at 365°C and the TGA maximum volatilisation at 372°C. Thermovolatile analysis (TVA) identified PLA oligomers to be the most abundant (> 50 wt%) degradation products. Other degradation products were lactide monomers and volatiles like acetaldehyde, carbon dioxide, carbon monoxide and ketene. Water evolution during PLA degradation remained uncertain. The main reactions which take place within the thermal decomposition of polylactic acid were summarized by Rudnik (2008):

- Hydrolysis by water traces at which lactic acid works as a catalyst.
- Depolymerization catalysed by polymerization catalyst residua.
- Oxidative decomposition of the polymer chain into lower molecular weight oligomers.
- Intermolecular transesterification leading to oligomeric esters formation.
- Intramolecular transesterification cyclic oligomers formation.

Kopinke *et al.* (1996) identified the intramolecular transesterification (at the maximum decomposition temperature of 360°C) to be the main reaction pathway of PLA degradation resulting in formation of cyclic oligomers. Polymer chain scission leads to the formation of acetaldehyde, methylketene and carbon oxides.

Even though the caustic soda treated fibres were washed thoroughly and neutralized with acetic acid alkali catalyzed hydrolysis of polylactic acid and cellulose was considered as a potential degradation process which could take place during the composites manufacture.

Polylactic acid is a semicrystalline polyester. Generally speaking polyesters can be hydrolyzed in alkaline media. PLA contains crystalline and amorphous regions. PLA crystalline α-form is

composed of 10_3 helices and β-form of 3_1 helices (Table 3.4). The difference in crystalline structure is responsible for alkaline hydrolysis: amorphous regions are more susceptible to alkaline hydrolysis compared to crystalline regions and 3_1 helices are more susceptible to alkaline hydrolysis than 10_3 helices (Serizawa *et al.*, 2003).

Velde and Kiekens (2002) studied the thermal degradation of alkali treated flax fibres. They have found that the alkali treatment of cellulosic fibres increases the amount of amorphous regions in cellulose and shortens the lengths of cellulose crystallites. It worsens the thermal stability and makes the onset temperature of degradation decrease (TGA).

Alkaline oxidation of cellulose as a degradation event has to be considered due to compression moulding of treated fibres at higher temperatures in oxidizing atmosphere. There are two pathways of alkaline oxidation of cellulose: β-elimination at the reducing end of the molecule and the alkaline hydrolysis of glycosidic bonds (Golova and Nosova, 1973). Both mechanisms take place at temperatures >150°C. The β-elimination takes place also at lower temperatures.

It has to be pointed out that the reviewed thermal degradation of PLA and cellulose were conducted under the protecting atmosphere (helium or nitrogen). One can expect that under the oxygen atmosphere the decomposition reactions will run faster and even at lower temperatures.

There are two pathways of water evolution during the thermal degradation of cellulose: physical loss of water at temperatures < 220°C and chemical loss of water at temperatures 220-550°C. Scheirs *et al.* (2001) found that moisture desorbed at 105°C under controlled heating and it represented 9 % of the overall water evolved. Chemical elimination of water had the maximum at 300°C and represented the remaining 91% of developed water. It has been found that within temperatures 25-400°C cellulose paper evolved 6.1 % water and craft paper 14.3% water. It can be roughly concluded from the extensive review of Scheirs *et al.* (2001) that chemically bound water does not develop at temperatures below 200°C. Water loss below 200°C can be attributed to desorption of physically bound water. According to Tang and Bacon (1964) in temperatures 25–150°C physical desorption occurs and between the temperatures 150-240°C chemical decomposition takes place. The chemical reaction is the transformation of hydroxyl groups into keto groups. Julien *et al.* (1991) found that the dehydration reactions of cellulose take place at temperatures of 210-325°C. Chemical dehydration of cellulose usually starts with the anhydrocellulose development especially at

low temperatures and slow heating rates. Most of the hydrolyzed water developed during the thermal degradation comes from the intramolecular elimination of –hydroxyl group on C3 atom resulting in ketone group or from unsaturation within the pyranose ring (C2-C3 atoms) (Scheirs *et al.*, 2001).

Chemical processes which could result in voids formation and composites of poor quality were summarized in previous paragraphs. It is well known that thermodynamics and kinetics are driving forces of chemical reactions.

Thus if the processing time is reduced to minimum (kinetics) it shall be possible to keep the pressing stage even at high temperature (thermodynamics) without damaging the fibres.

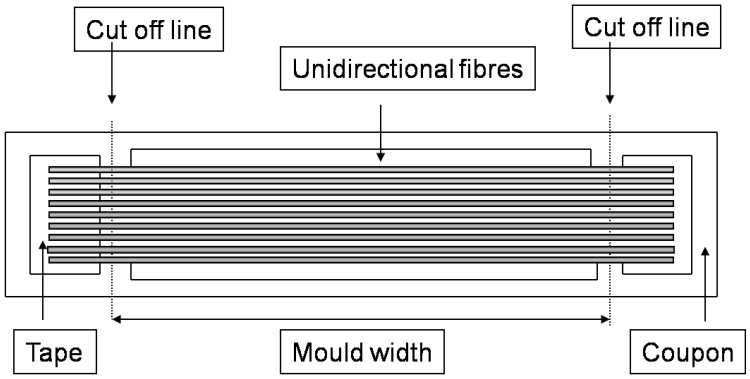

Figure 7.9: Fibre preforms: Aligned and unidirectional sisal fibres were attached to the quarto paper with selotape.

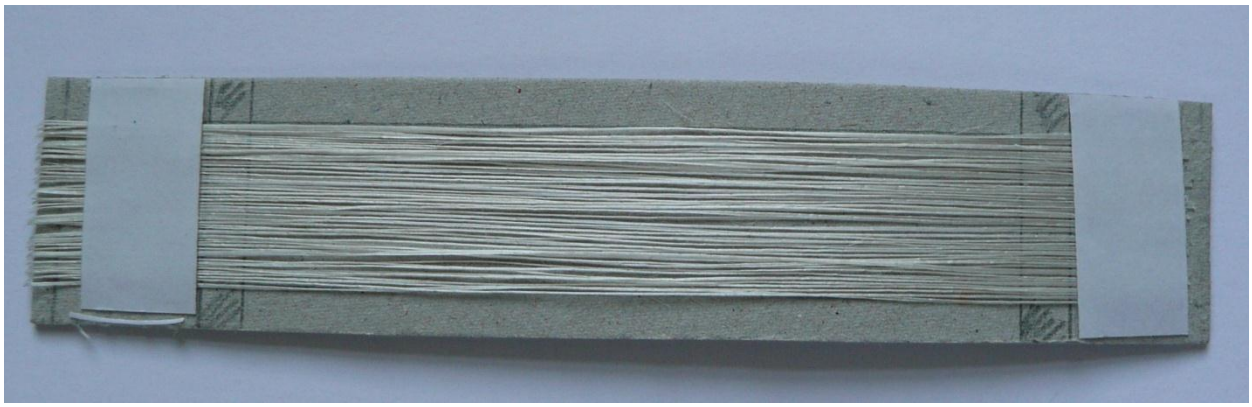

Figure 7.10: A fibre preform - aligned untreated sisal fibres glued onto a paper card (170 x 25 x 2 mm).

During the processing of natural fibre composites it was necessary to overcome few limiting factors: High matrix viscosity, matrix degradation at temperatures above 230°C and the fact

that at temperatures in excess of 150ºC, most natural fibres are unable to withstand prolonged periods at such temperatures without significant deformation or degradation.
To reduce the adverse effect of high temperatures the following measures were taken:

- Sisal fibre bundles were aligned prior to compression moulding so it was easier for the polymer melt to flow among the fibres and wet them properly. Aligned fibres were glued to a supporting paper card with selotape (Figure 7.9 and 7.10).
- Preforms of aligned fibres were combined with polymer sheets.
- The mould was made of aluminium, so it was possible to heat it up and cool it down quickly.

Thus both the polymer and the fibres could stay in the mould for a shorter period of time and the possibility of their degradation was reduced.

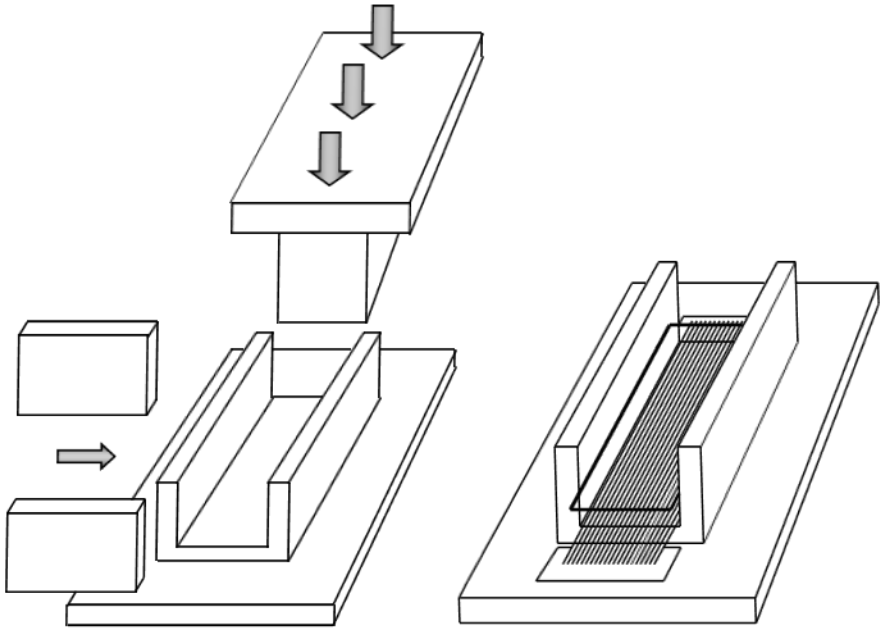

Figure 7.11: An opened compression mould.

Figures 7.11 - 7.18 describe the manufacturing process. The fibre preforms were combined with PLA foils in an open mould and the whole assembly was heated up above the PLA glass transition temperature (T_g) and slightly compressed at 80°C for 10 min. The supporting paper

was cut off and the mould was closed (Figure 7.11 and 7.12). The closed mould with fibres and polymer foils was transferred into the hot press. Firstly it was kept at a temperature of 190°C under no pressure for 5 min. After this preheating stage the mould was compressed at 200°C at 0.1 MPa for 3.5 min. (Figures 7.16-7.19).

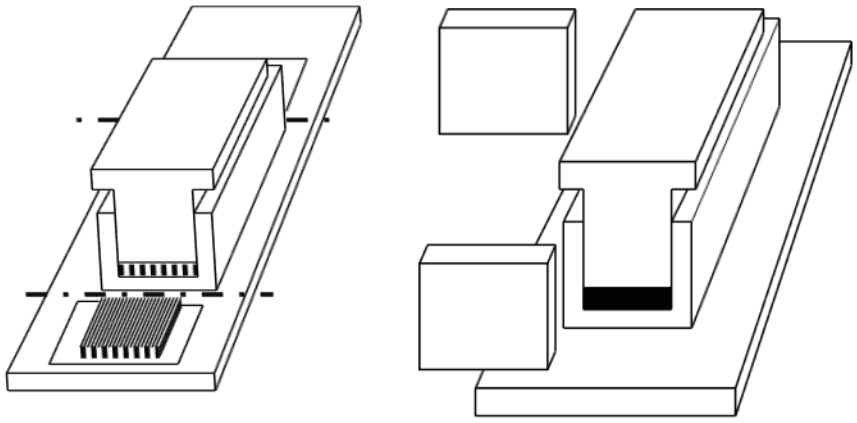

Figure 7.12: Combining polymer sheets with fibre preforms.

When the mould was released from the hot press it was left to cool down at room temperature for two hours in a cold press at a pressure of 3 MPa. Figure 7.19 shows the final composite sheet. Transformation of fibre weight fraction to fibre volume fraction was calculated by the following expression assuming no voids (i.e. $V_m + V_f = V_c$):

$$V_f = \frac{\left(V_c - \frac{w_c - w_f}{\rho_m}\right)}{V_c} \cdot 100 \qquad (7.1)$$

Where V_c is the volume of the composite in m^3, w_c is the weight of the composite in kg, ρ_m is the matrix density in $kg.m^{-3}$, V_f is the fibre volume fraction and w_f is the fibre weight fraction.

Figure 7.13 displays six preforms of aligned fibres. Ends of the fibres were glued to the supporting cardboard paper using double-sided sticky tape. Individual preforms were cut prior to mould filling.

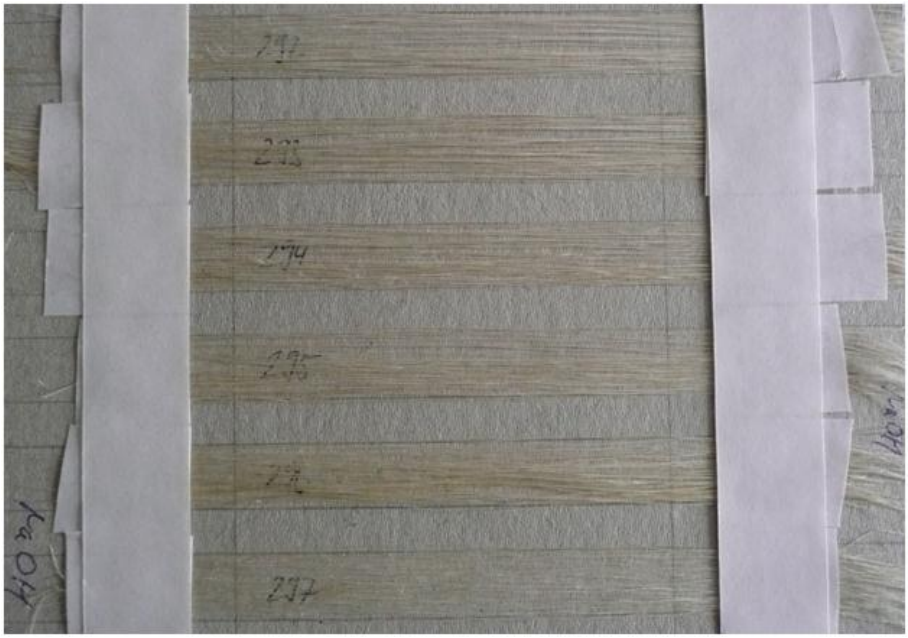

Figure 7.13: Fibre preforms - aligned untreated sisal fibres glued onto a supporting paper card.

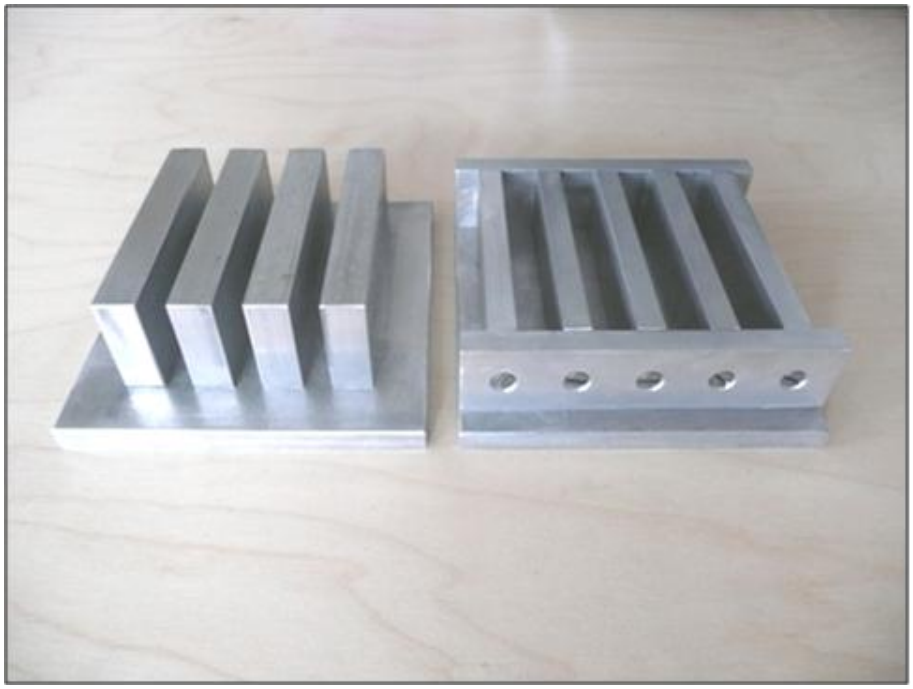

Figure 7.14: Opened compression mould.

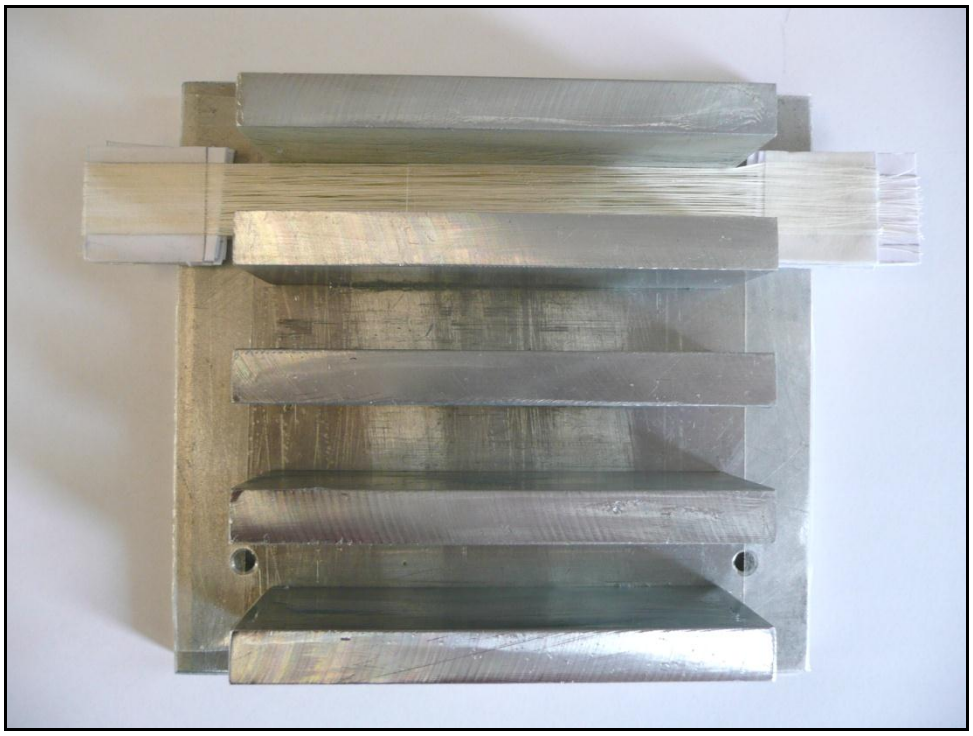

Figure 7.15: Arranging fibre preforms into a mould slot. Preforms are combined with polymer foils.

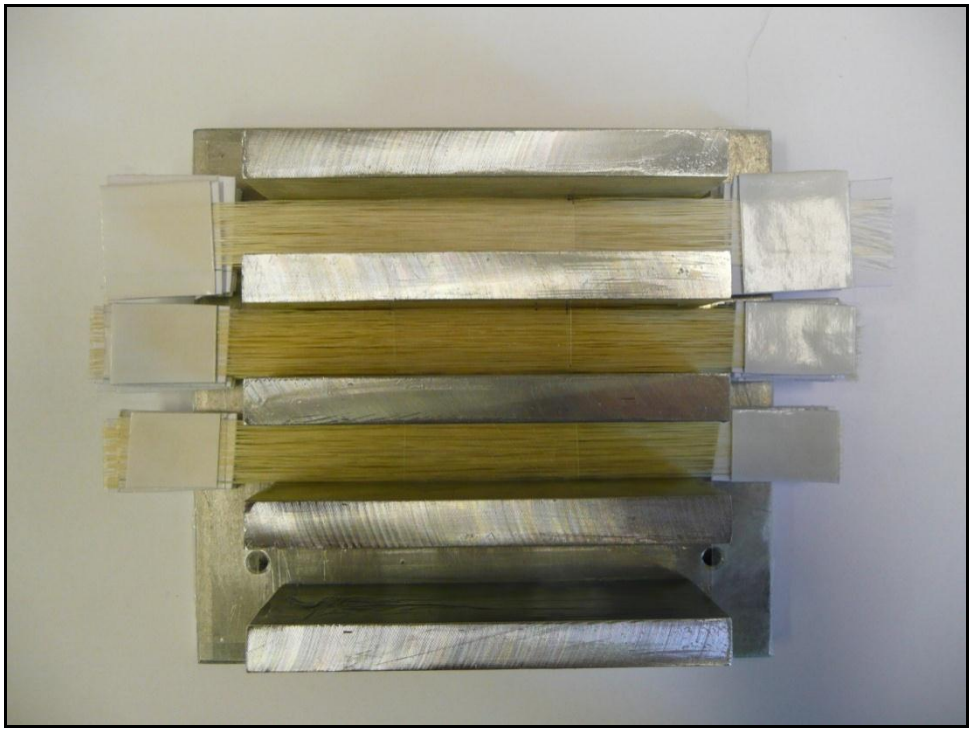

Figure 7.16: Filling in the mould with multi-layer preforms.

Figure 7.17: Closed mould prepared for hot pressing.

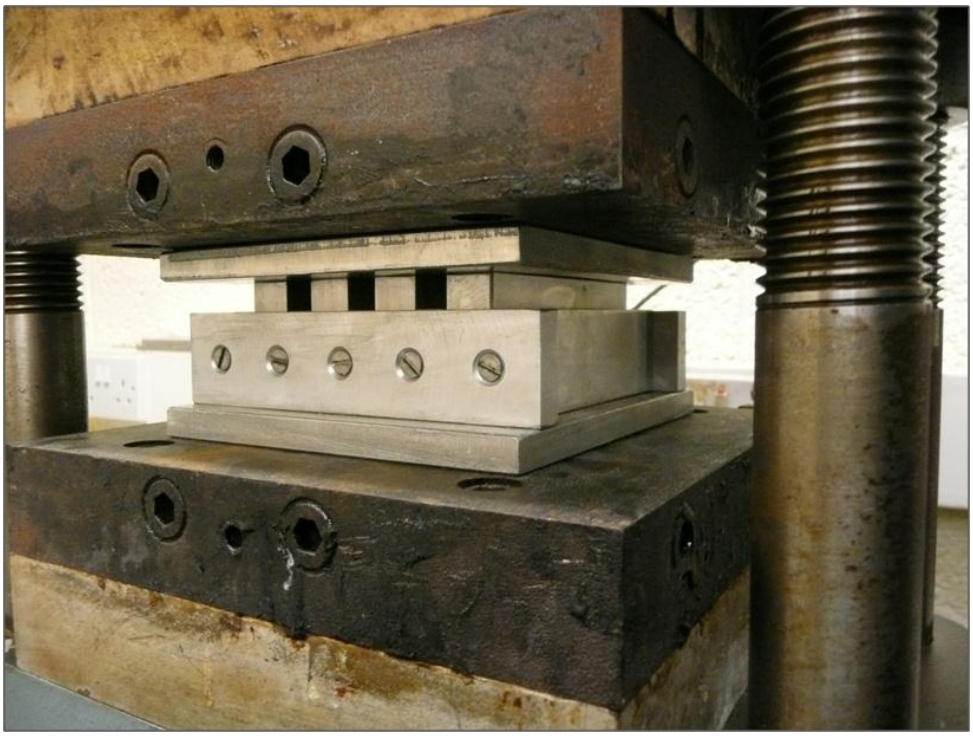

Figure 7.18: Mould transferred into a hot press.

Figures 7.15 and 7.16 show how the fibre preforms were combined with the polymer sheets and how they were supported outside the mould using the cardboard ends and the selotape.

Figure 7.19: PLA / sisal fibre unidirectional composite (100 x 15 x 1 mm).

It was crucial to keep the fibres aligned and well in place before the mould was partially closed and heated up at a certain temperature T above the glass transition temperature T_g and below the cold crystallization temperature - T_c (=104°C) > T > T_g (= 0-60°C). Above the glass transition temperature the amorphous phase of the semicrystalline polymer softens. The assembly of fibre preforms and the polymer sheets was heated at 80°C for 10 minutes. This temperature lays above the T_g and well below the cold crystallization temperature at which the semicrystalline phase crystallizes during heating up the solid polymer from room to T_m. It was found to be essential to stretch the fibres over the central part of the mould when laying them up. It was also essential to make the polymer sheets as thin as possible and matching the mould dimensions as much as possible to prevent the movement of the fibres together with the polymer melt. Otherwise regions with low fibre volume fraction and high matrix content would be created and lead to premature failure of composite structures. Ideally the polymer melt shall flow only in the long axis of the mould. If during the compression moulding the fibres were deviated from the mould axis significantly but remained unidirectional the resulting composites maintained approximately 80% of their mechanical strength.

First experiments to produce composites of well aligned natural fibres and thermoplastic matrix used jute fabrics. The structure of the fabric was plain weave (210 and 300 g/m^2), twill weave (860 g/m^2), unidirectionally aligned stitched yarn and plaited yarn. The composites

were moulded in a large steel mould with uneven temperature profile. The quality of resulting composites was poor.

Attempts were also made with stitching the aligned fibre bundles to prepare fibre preforms resembling the carbon fibre preform (Figures 7.20-7.22). Such preforms could be easily preimpregnated with powdered matrix and easy to handle and lay-up.

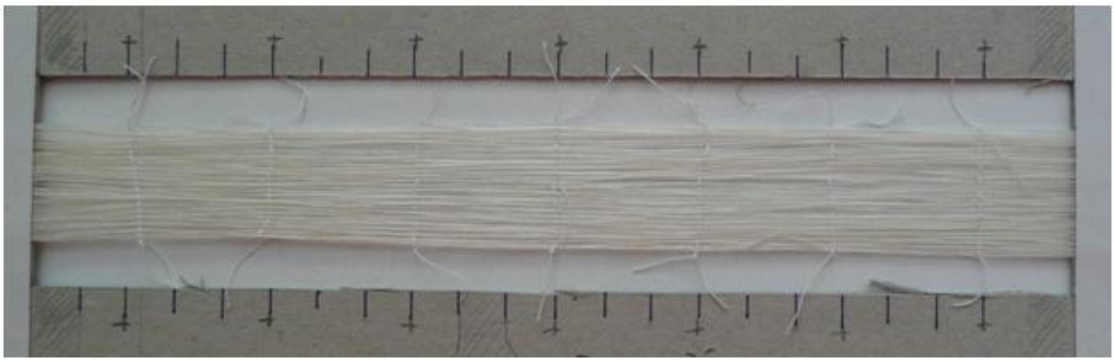

Figure 7.20: Stitched fibre bundle preform. Long sisal fibre bundles stitched with a cotton thread.

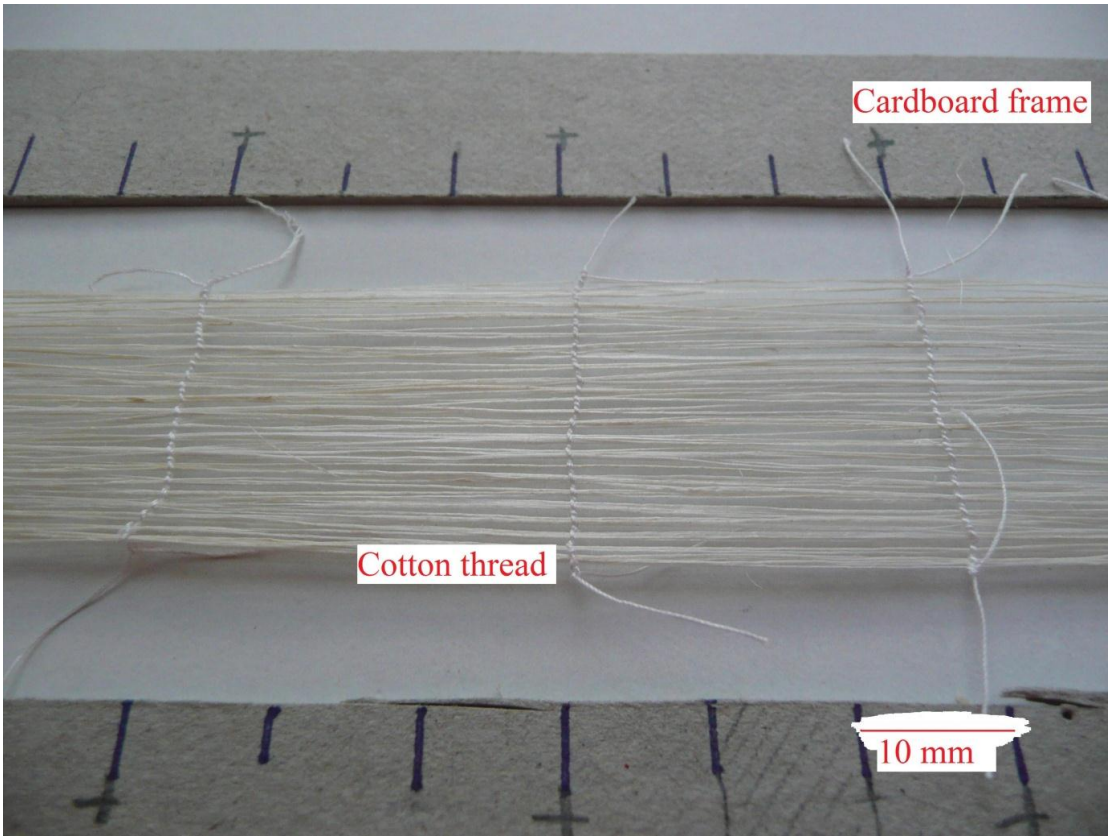

Figure 7.21: Detail of a stitched fibre bundle preform.

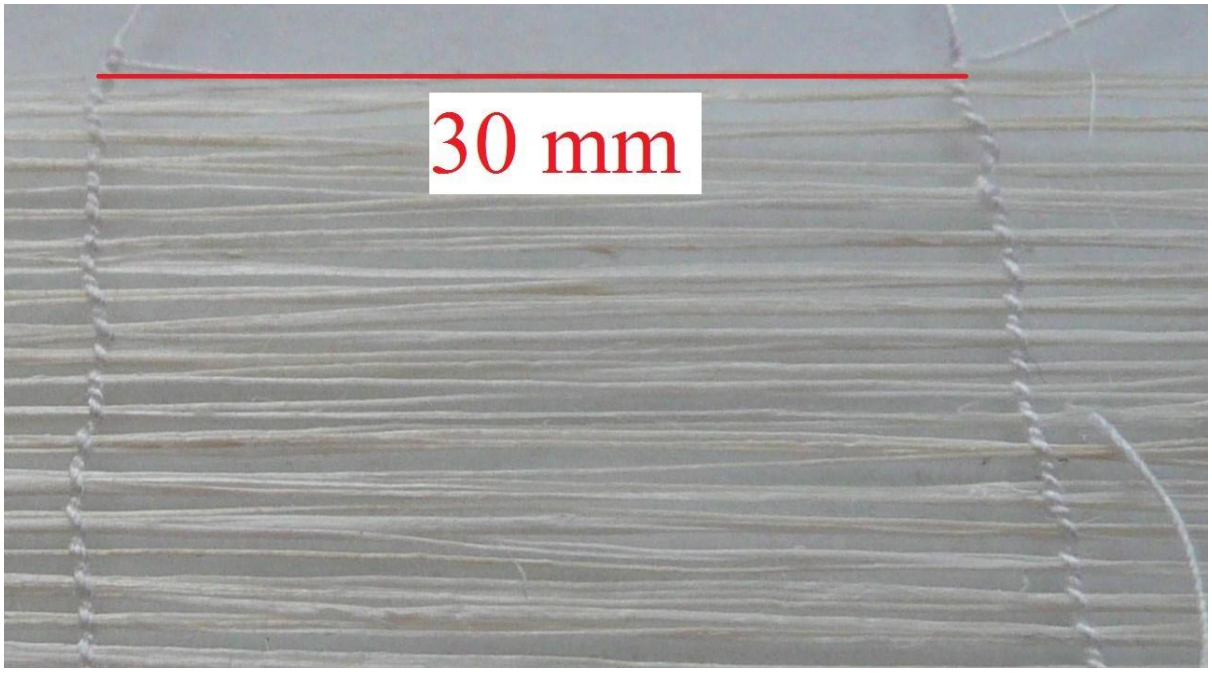

Figure 7.22: Detail of stitching.

Stitched preforms were not supported by the cardboard at their ends during the lay-up and mould filling. The stitched preforms were not stretched. As a result applied pressure during the moulding stage displaced the fibres between neighbouring transverse stitches from their positions. The fibres were moved laterally. It was also difficult for the viscous polymer melt to flow into the stitches (cotton thread around the sisal fibre) and wet the sisal fibres. It looks like the main advantage of glass and carbon fibres over the natural cellulosic fibres is that they are hard enough to resist the flow of the melt and that it is possible to make them infinitely long for continuous processing.

8 Results

This chapter summarizes experimental results. The first section presents experimental results for the physico-mechanical properties of polylactic acid and sisal fibres which were used as the matrix and fibre components for composites fabrication. Secondly the results of crystalline morphology development using hot stage microscopy and differential scanning calorimetry are presented. Further are presented the results of the microbond shear test for the evaluation of fibre to matrix adhesion: results of adhesion of PLA to untreated and caustic soda treated fibres with and without developed matrix morphology are presented. The next section focuses on the dynamic-mechanical properties of composites. Further the stress-strain relationship for sisal fibres evaluated by Raman micro-spectroscopy is presented. The chapter closes by reporting the mechanical properties of multiple fibre composites.

8.1 Fibre and matrix characterization

This section presents basic physico-mechanical characteristics of the polymer matrix and fibres used in this research for composites fabrication. The section starts with the characterization of polylactic acid. Nuclear Magnetic Resonance (NMR) was used to characterize the microstructure of the polylactic acid used in this study. Size exclusion chromatography (SEC) was used to determine the molecular weights of the polylactic acid as well as the polydispersity index. Glass transition temperature (T_g) and the melting temperature (T_m) were determined using differential scanning calorimetry (DSC). Strength and modulus were determined from the tensile and three point bending test. Melt flow index was measured to provide basic information on the polymer melt behaviour. Untreated and caustic soda treated sisal fibres were tested in tension to determine their strength, modulus and strain at break.

8.1.1 Polylactic acid

Size exclusion chromatography (SEC) was used to determine the molecular weight of polylactic acid. ^{1}H-Nuclear magnetic resonance (NMR) was used to determine the structure of the polymer matrix used in this thesis. Principal mechanical properties of the PLA were tested in three-point bending and tension. Transition temperatures were determined with differential scanning calorimetry (DSC). The melt flow index was measured at 190°C with a weight of 2.16 kg.

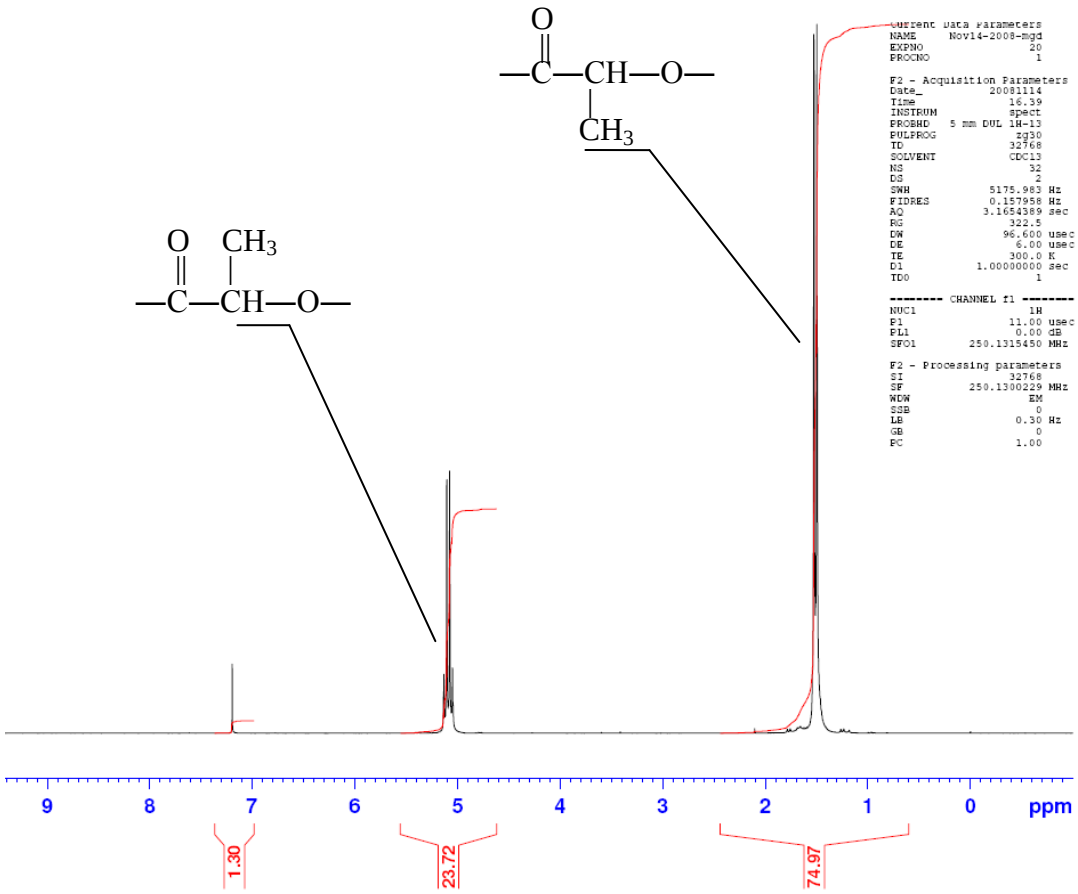

Figure 8.1: ^{1}H-NMR spectrum of poly(L-lactide).

^{1}H and NMR spectra were recorded on a Bruker Avance spectrometer operating at 250 MHz and referenced to residual solvent peaks. The ^{1}H NMR spectral data of PLA are given in Figure 8.1 Two peaks are observed at chemical shifts of 1.5 ppm and 5.1 ppm. The signal at

7.2 ppm belongs to the solvent. A total of 32 scans were acquired each with 32 000 data points at a spectral width of 5 kHz corresponding to an acquisition time of 3.2 s. A pulse delay of 1 s was used between the transients. A spectrum of the solution of polylactic acid dissolved in deutero-chlorophorm $CDCl_3$ (1 % solution) was recorded at a temperature of 300 K. It was confirmed that the thermoplastic polyester used in this work was poly(L-lactide). As discussed in Chapter 3 the structure and the ratio of D- and L-lactide monomers have a profound effect on thermal and mechanical properties of polylactic acid.

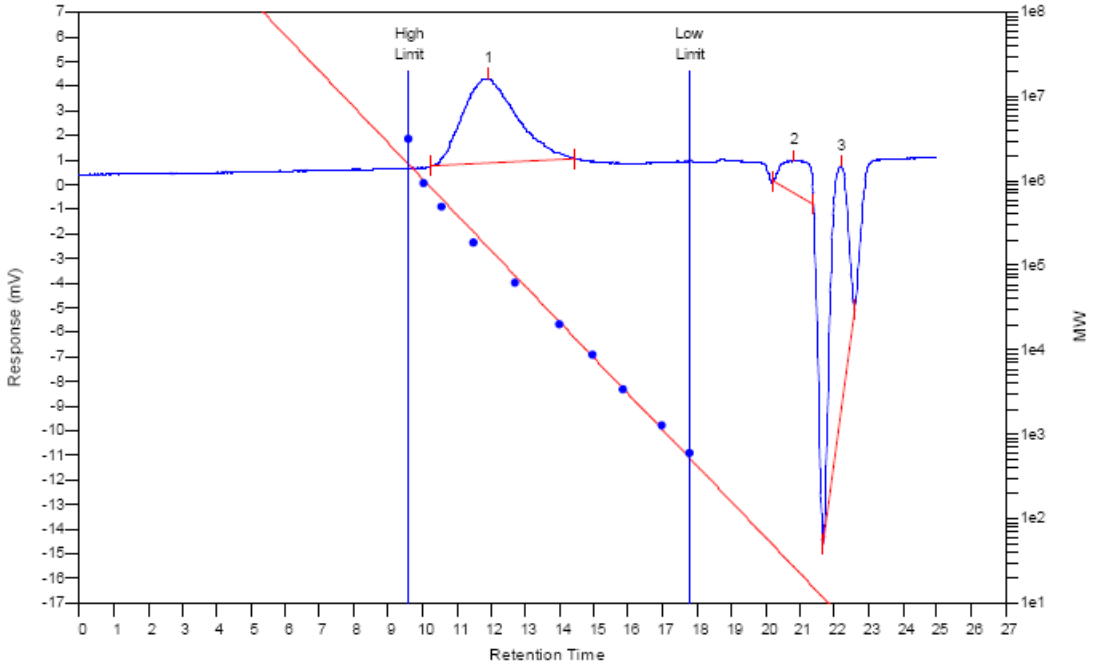

Figure 8.2: Size exclusion chromatogram of PLA.

Table 8.1: Molecular weight of polylactic acid determined by size exclusion chromatography.

Molecular weight averages							
Peak No.	M_p	M_n	M_w	M_z	M_{z+1}	M_v	PDI
1	176642	105869	178846	258771	332625	167585	1.68931
2	18	23	25	27	30	25	1.08696
3	8	7	7	7	8	7	1

Note: M_p = peak molecular weight; M_n = number average molar mass; M_w = weight average molar mass; M_{z+1} and M_z = sedimentation average molar masses; M_v = viscosity average molar mass; PDI = polydispersity index.

Size exclusion chromatography (SEC) was used to determine molecular weights (M_n and M_w) of the received polylactic acid. Sample was dissolved in chlorophorm at a concentration of 0.10 mg/ml and the SEC analysis was performed on a Polymer Laboratories PL-GPC 50 integrated system using a PLgel 5 μm MIXED-D 300 x 7.5 mm column. Separation according to molecular size was performed at 35°C using THF solvent as an eluent at flow rate of 1 ml/min. The polydispersity index (PDI) was determined from M_w/M_n, where M_n is the number average molecular weight and M_w the weight average molecular weight. The polymer was referenced to 10 narrow molecular weight polystyrene standard with a range of M_w 615–568 kDa. Table 8.1 summarizes the molecular weights of polylactic acid used in this work as determined by size exclusion chromatography. Figure 8.2 shows the chromatogram of PLA.

Table 8.2: Measured physico-mechanical properties of polylactic acid.

Tensile strength	[MPa]	62.8 ± 4.9
Tensile modulus	[GPa]	2.7 ± 0.4
Elongation at break	[%]	2.9 ± 0.5
Flexural strength	[MPa]	114 ± 16
Flexural modulus	[GPa]	3.6 ± 0.5
T_g (DSC-midpoint)	[°C]	56*
T_m (DSC)	[°C]	169
Melt flow index (2.16 kg/190°C)	[g/10min.]	5
Molecular weight (M_w) (SEC)	[g/mol]	178,846

Note: SEC = size exclusion chromatography; DSC = differential scanning calorimetry; *as received pellet.

Table 8.2 summarizes the principal physico-mechanical properties of polylactic acid. Figure 8.3 shows the surface of a specimen broken in three-point bending test. A yielding pattern can be observed running from the compression to tension side of the tested specimen.

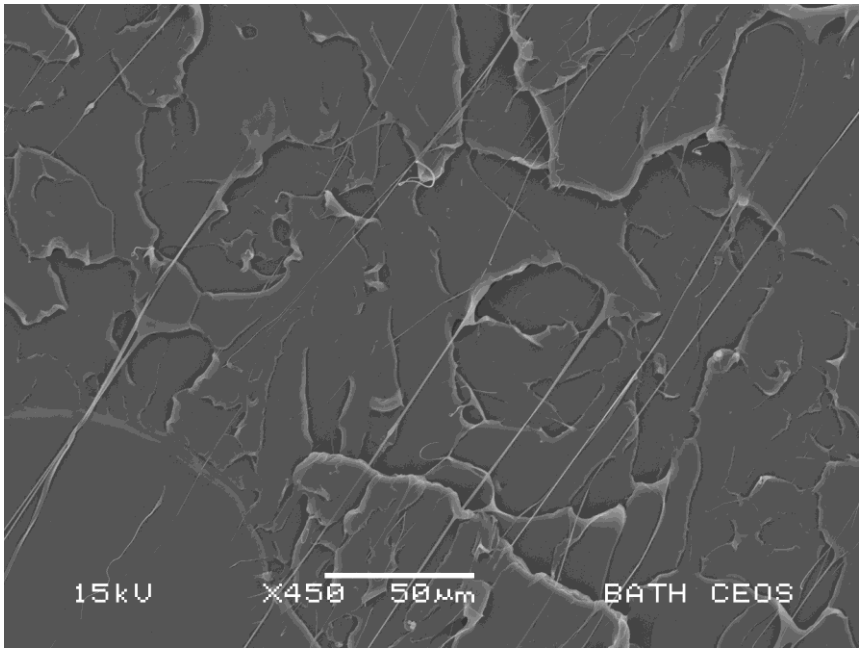

Figure 8.3: Surface of PLA specimen broken in three-point bending.

8.2 Characterization of sisal fibres

This section presents the tensile properties of as-received sisal fibres and sisal fibres treated with caustic soda and hydrogen peroxide aqueous solutions. The reason for evaluating the influence of hydrogen peroxide on the mechanical properties of sisal fibres was the application of Raman spectroscopy for measuring the tensile modulus of the fibres and interfacial shear strength. Cellulose fibres require the application of hydrogen peroxide to suppress the fluorescence for better Raman spectra resolution. Fibres were soaked in an aqueous solution of caustic soda at room temperature for 48 hours. Table 8.3 shows the transformation of caustic soda weight concentration (wt%) into molar concentration (mol/dm^3). Fibres were soaked in an aqueous solution of hydrogen peroxide (3 wt%) at room temperature for 10 minutes. Untreated sisal fibres and sisal fibres treated with a caustic soda aqueous solution of 6 wt% were tested at gauge lengths of 10, 15, 20, 25 and 30 mm. Sisal fibres treated with caustic soda aqueous solutions of 0.16 and 2 wt% were tested in tension at a gauge length of 25 mm. Untreated and caustic soda treated (6 wt%) sisal fibres which were treated with hydrogen peroxide (3 wt%) were tested in tension at a gauge length of 25 mm.

Table 8.3: Transformation of mass to molar concentration of caustic soda aqueous solutions used for sisal fibres treatment.

Mass concentration	Molar concentration
c [wt%]	c [mol/dm^3]
0.16	0.04
2	0.51
6*	1.6

*i.e., 6 g of NaOH dissolved in 94 g of H_2O.

Sample preparation and the test procedure are described in detail in Section 6.8. Twenty fibres were tested at each gauge length using the Instron 3369 tensile test machine with 10 kg (100 N) load cell at cross-head speed of 1 mm/min. Tensile strength, strain at break and Young's modulus were calculated for sisal fibres tested at all gauge lengths and treatments. Tensile strength and strain at break of sisal fibres were modelled with a two parameter Weibull analysis. The procedure to find Weibull distribution parameters is described in Section 6.9. The tensile modulus was determined to follow a normal distribution. The cross-sectional area of sisal fibres which is necessary for the calculation of tensile stress was determined from the density method described in Section 6.2. The density of benzene was determined with pycnometry. The apparent density of untreated sisal fibres was determined to be 1.115 g/cm^3. The density of caustic soda treated sisal fibres (6 wt%) was determined to be 1.4382 g/cm^3. Figure 8.4 displays the topography of an untreated sisal fibre bundle surface. The surface is generally irregular in shape. Figure 8.5 shows SEM micrograph of a typical cross-section of various sisal fibre bundles.

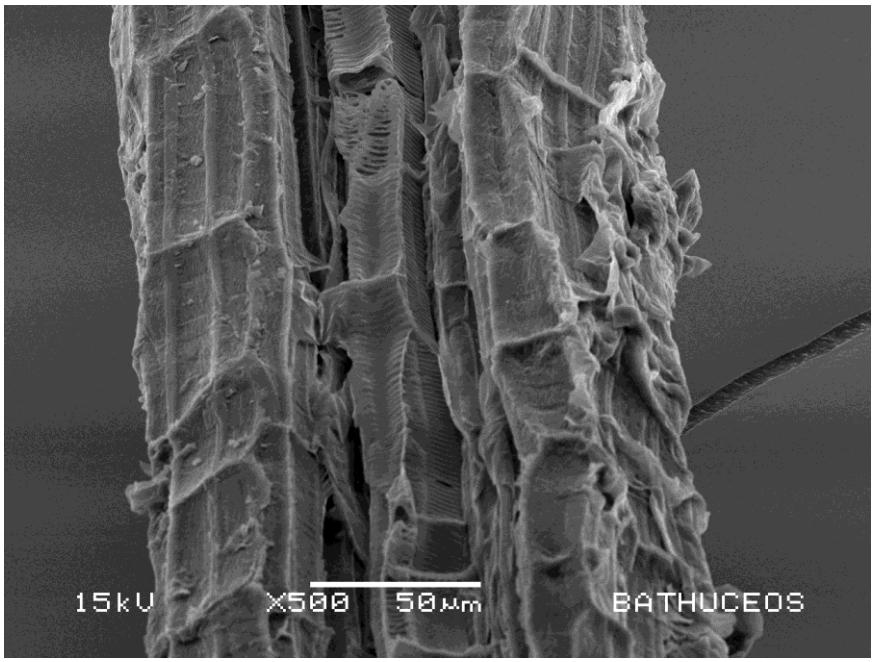

Figure 8.4: SEM micrograph of untreated sisal fibre bundle.

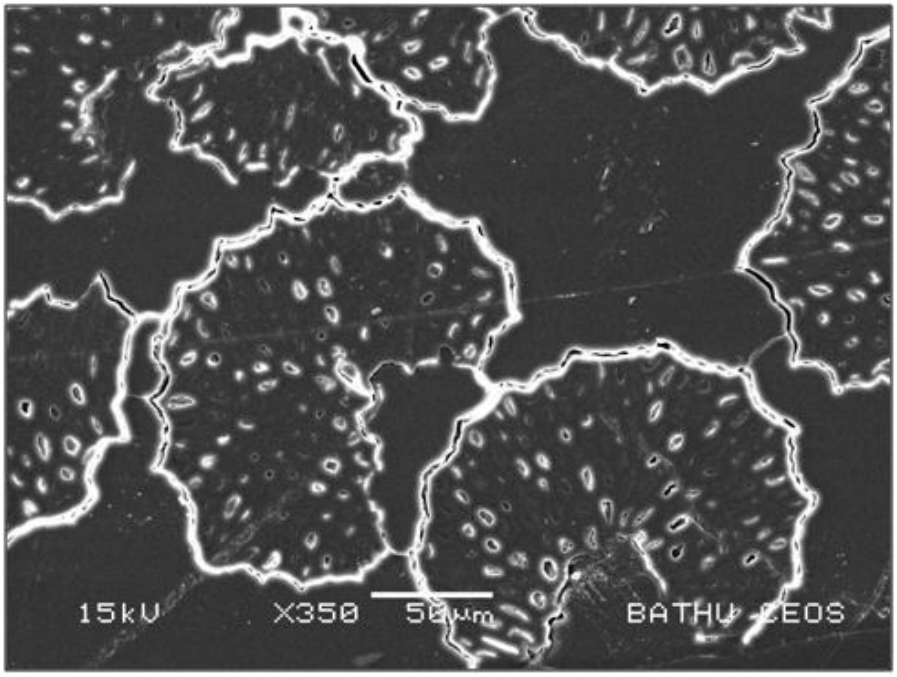

Figure 8.5: SEM micrograph of cross sections of sisal fibre bundles.

Figure 8.6 is an optical micrograph of untreated sisal fibre. Tensile fracture of untreated sisal fibres is shown in Figure 8.7 (brittle fracture) and Figure 8.8 (splitting of the fibre at break).

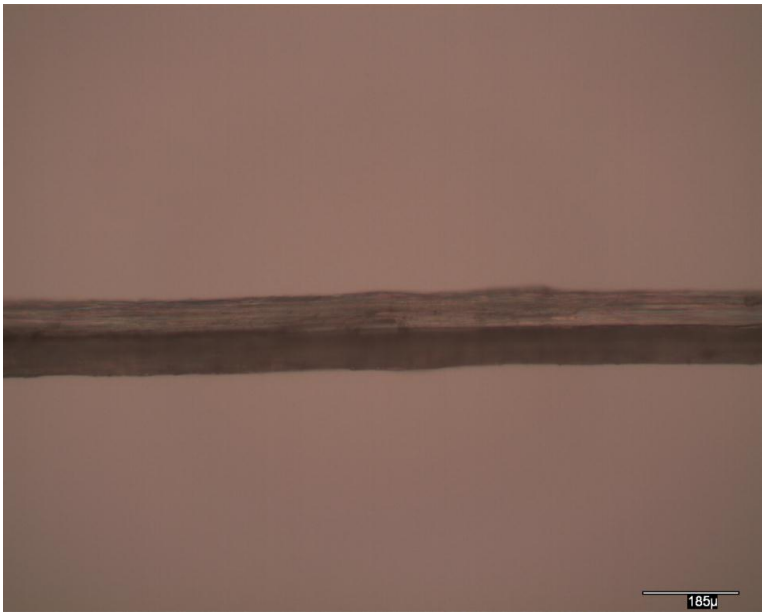

Figure 8.6: Optical micrograph of untreated sisal fibre bundle (crossed polars).

Figure 8.7: Brittle fracture of untreated sisal fibre bundle. Optical micrograph (crossed-polars).

Figure 8.9 presents stress-strain curve for untreated and caustic soda treated (6 wt%) sisal fibres at a gauge length of 20 mm and probability of failure $P_f = 0.625$.

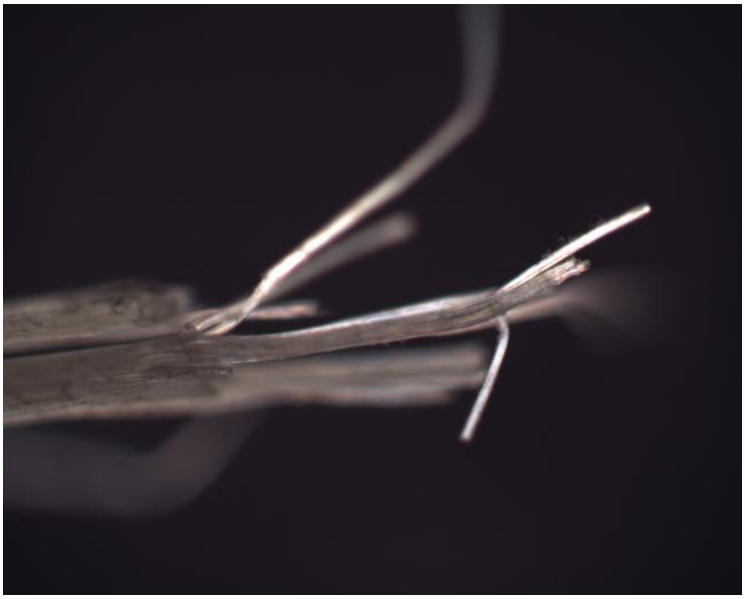

Figure 8.8: Tensile test fracture of untreated sisal fibre bundle. Optical micrograph (crossed polars).

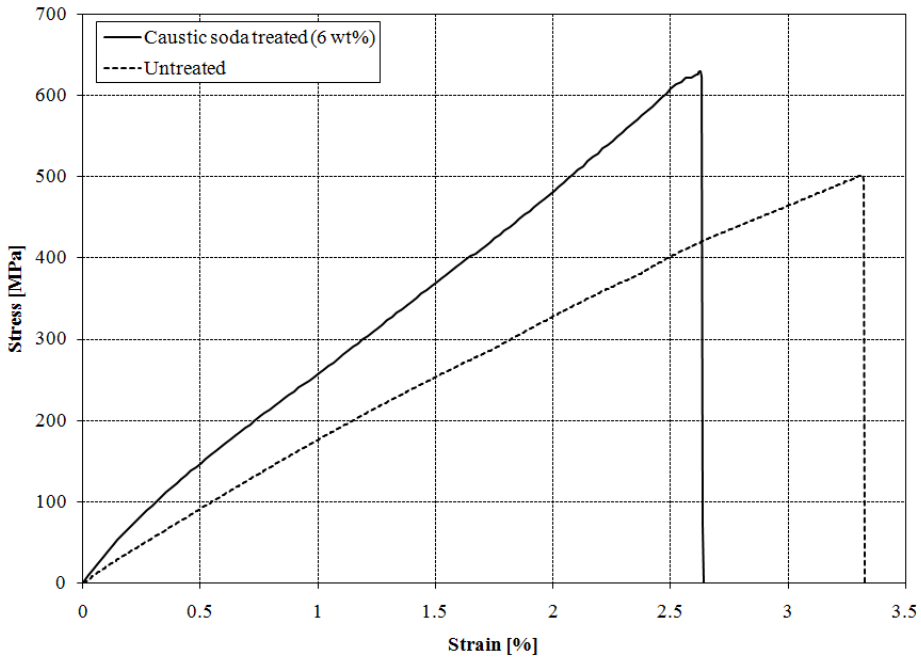

Figure 8.9: Stress-strain curve of sisal fibres tested in tension at a gauge length of 20 mm. Fibres with $P_f = 0.625$ are displayed.

Figures 8.10–12 show the variation of fibre strength, strain at failure and modulus with fibre diameter for untreated and caustic soda treated (6 wt%) sisal fibres. Plotted values were obtained at all gauge lengths.

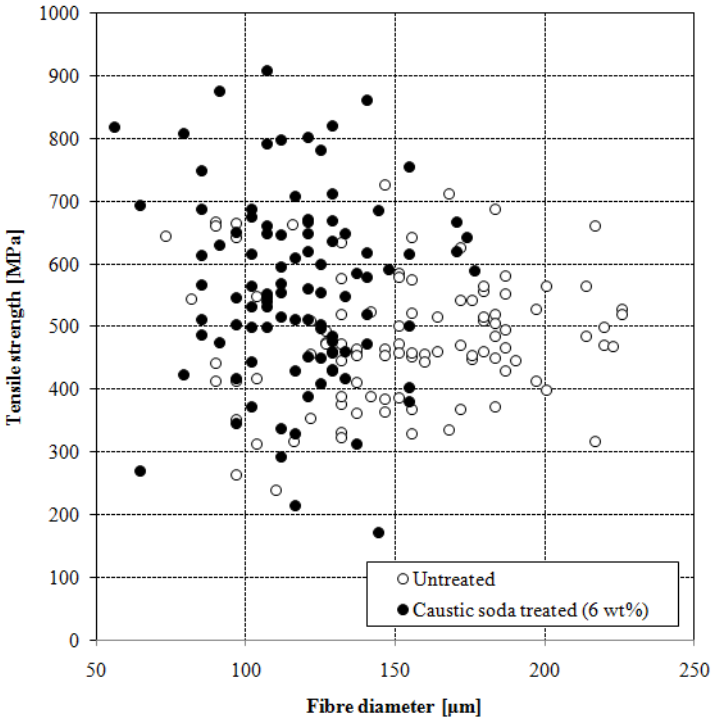

Figure 8.10: Fibre strength versus fibre diameter for untreated and caustic soda treated (6 wt%) sisal fibres. Gauge length varies from 10 to 30 mm.

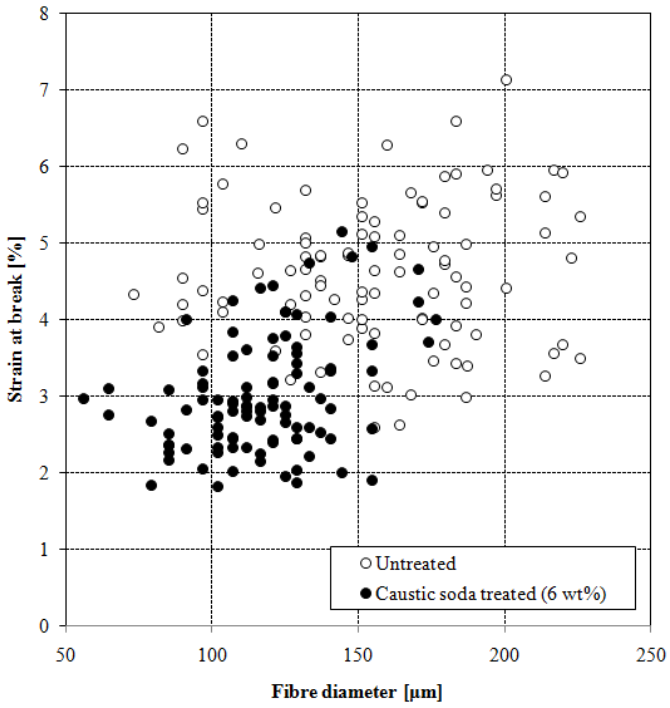

Figure 8.11: Fibre strain at failure versus fibre diameter for untreated and caustic soda treated (6 wt%) sisal fibres. Gauge length varies from 10 to 30 mm.

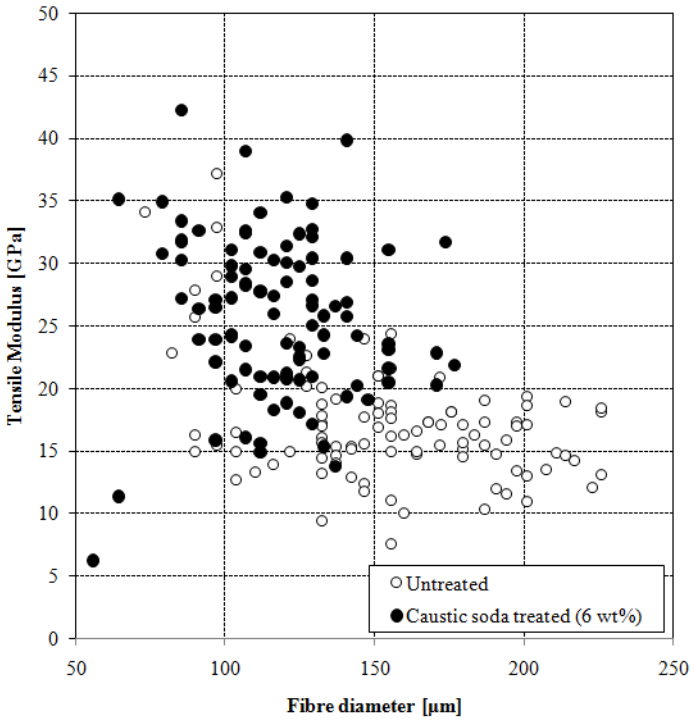

Figure 8.12: Fibre tensile modulus versus fibre diameter for untreated and caustic soda treated (6 wt%) sisal fibres. Gauge length varies from 10 to 30 mm.

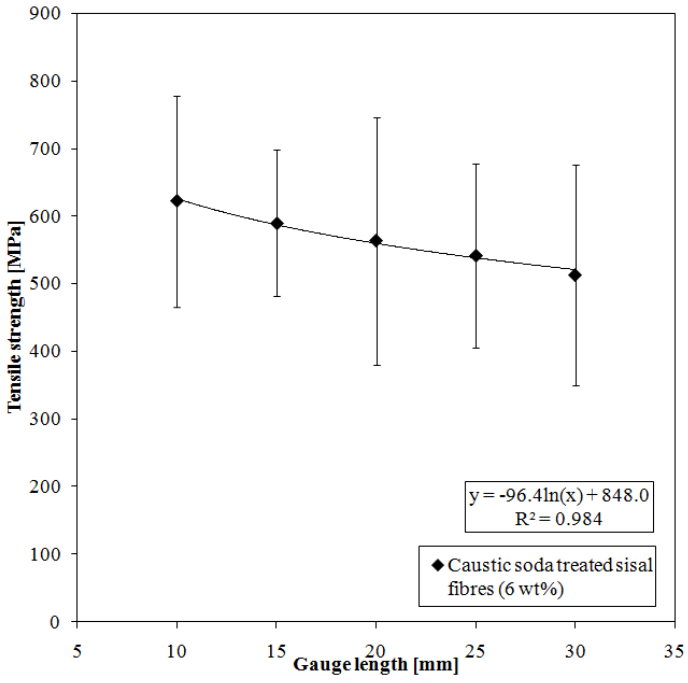

Figure 8.13: Mean tensile strength of caustic soda treated sisal fibres (6 wt%) as a function of gauge length.

Figure 8.13 shows the mean tensile strength and standard deviation of caustic soda treated sisal fibres (6 wt%) plotted as a function of gauge length. The data were fitted with a logarithmic trend line. Figure 8.14 shows the mean tensile strength and standard deviation of untreated sisal fibres plotted as a function of gauge length. The data were also fitted with a logarithmic trend line. As can be seen from both figures the tensile strength of untreated and caustic soda (6 wt%) treated sisal fibres decreases with an increasing gauge length. Caustic soda treated sisal fibres (6 wt%) show higher tensile strength values at all tested gauge lengths. The logarithmic trend line represented a better fit than a linear trend line.

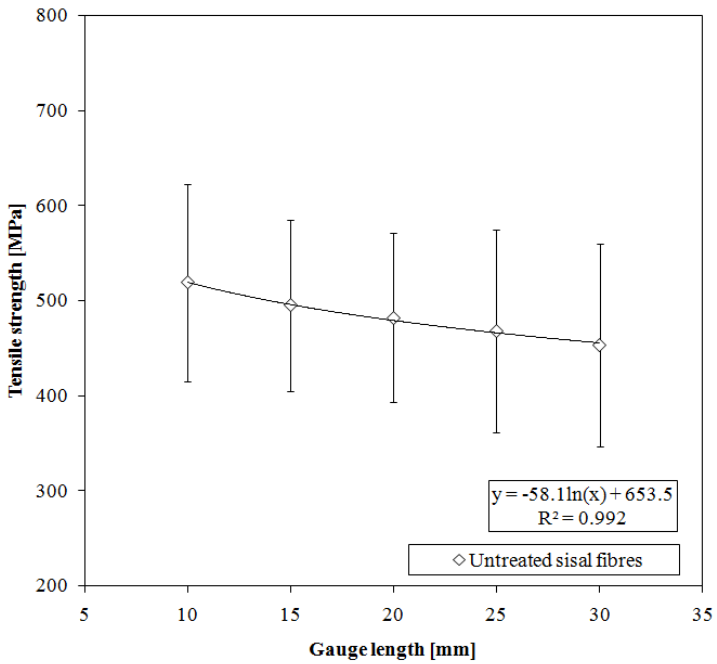

Figure 8.14: Mean tensile strength of untreated sisal fibres plotted as a function of gauge length.

Figures 8.15–24 show Weibull plots and probability of failure plots for the strength of untreated and caustic soda (6 wt%) treated sisal fibres.

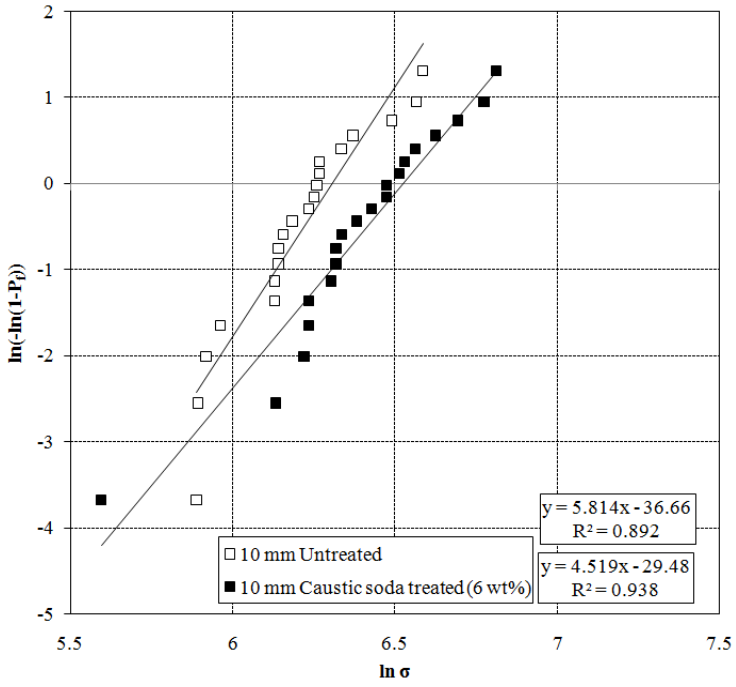

Figure 8.15: Weibull plot for strength of untreated and caustic soda treated (6 wt%) sisal fibres at 10 mm length.

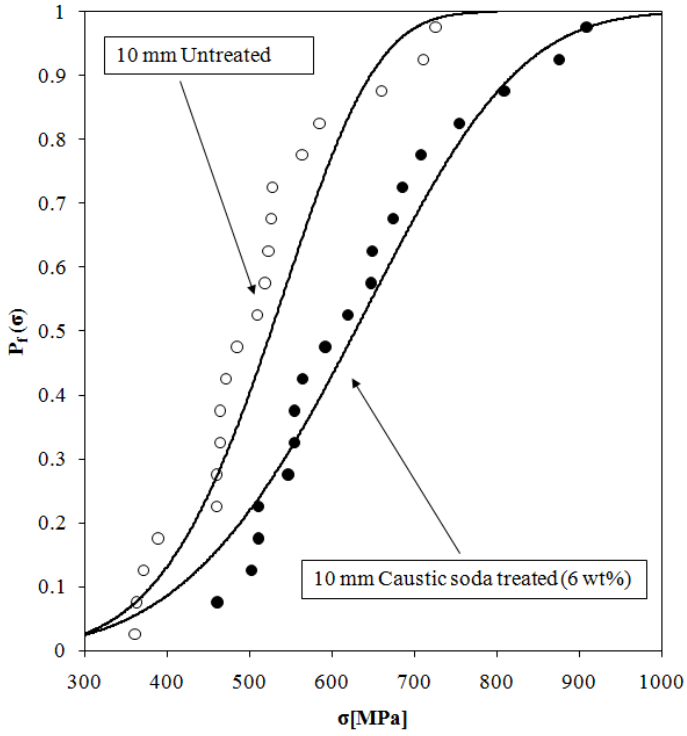

Figure 8.16: Probability of failure ($P_f = 1-P_s$) versus strength for untreated and caustic soda treated (6 wt%) sisal fibres at gauge length of 10 mm.

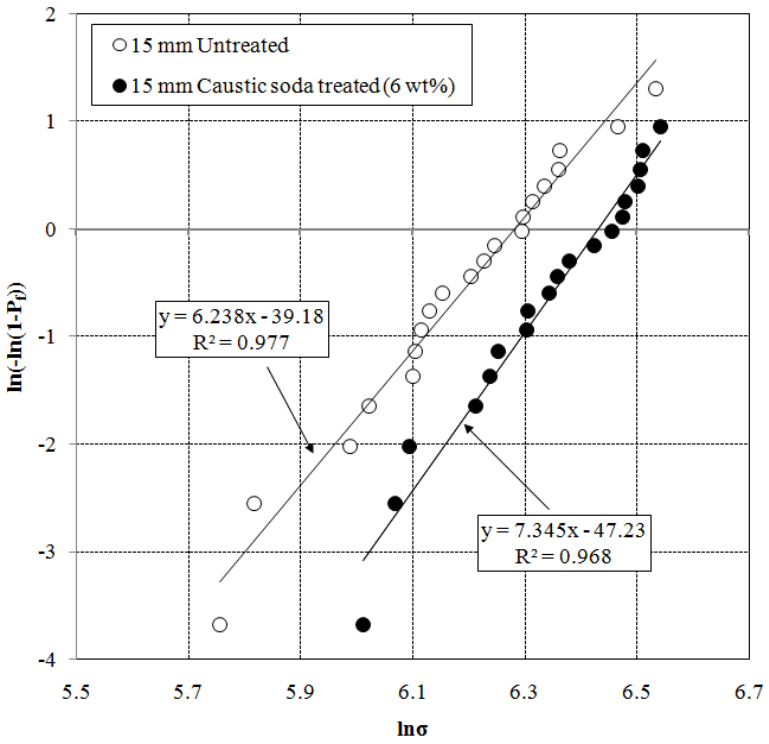

Figure 8.17: Weibull plot for strength of untreated and caustic soda treated (6 wt%) sisal fibres at 15 mm length.

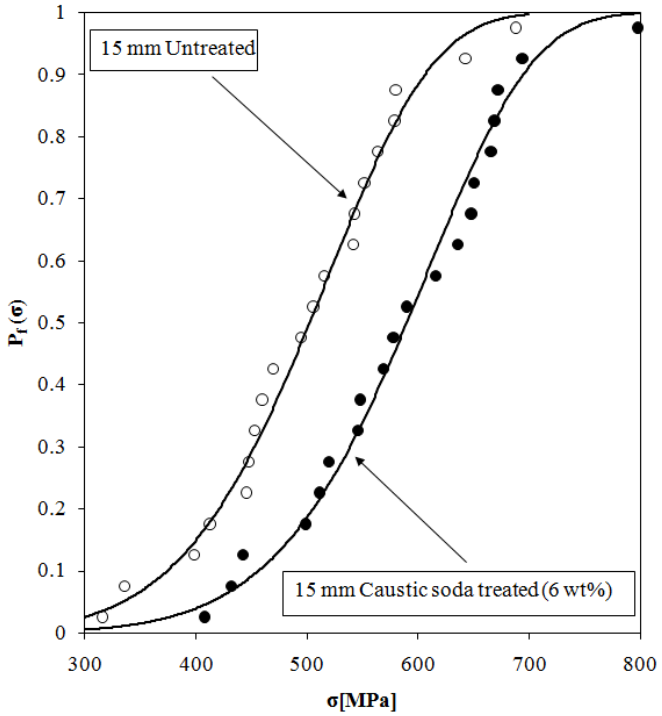

Figure 8.18: Probability of failure (P_f = 1-P_s) versus strength for untreated and caustic soda treated (6 wt%) sisal fibres at gauge length of 15 mm.

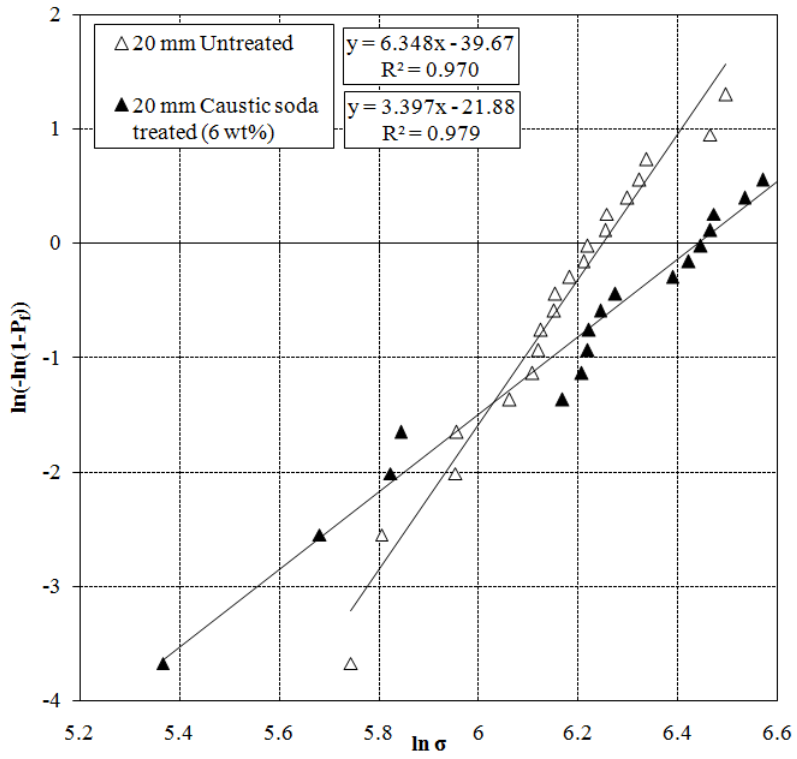

Figure 8.19: Weibull plot for strength of untreated and caustic soda treated (6 wt%) sisal fibres at 20 mm length.

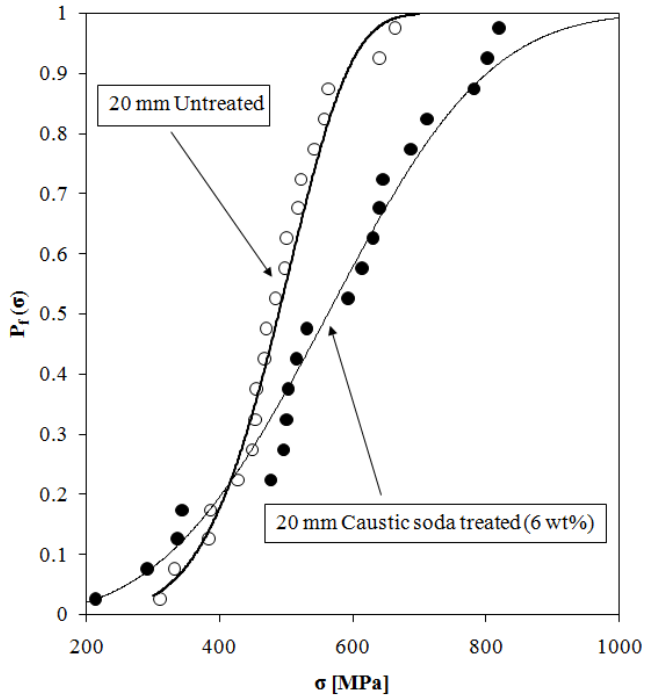

Figure 8.20: Probability of failure ($P_f = 1-P_s$) versus strength plots for untreated and caustic soda treated (6 wt%) sisal fibres at a gauge length of 20 mm.

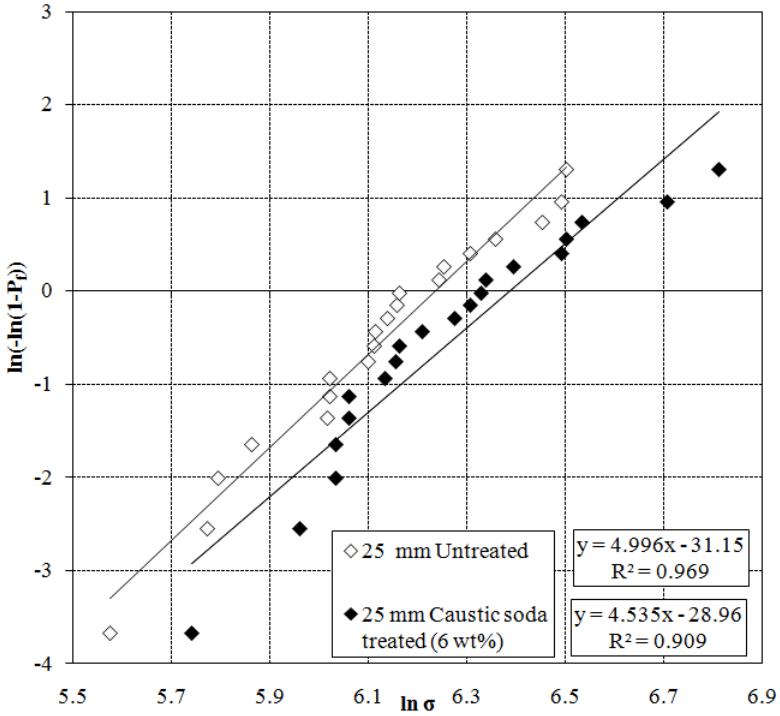

Figure 8.21: Weibull plot for strength of untreated and caustic soda treated (6 wt%) sisal fibres at 25 mm length.

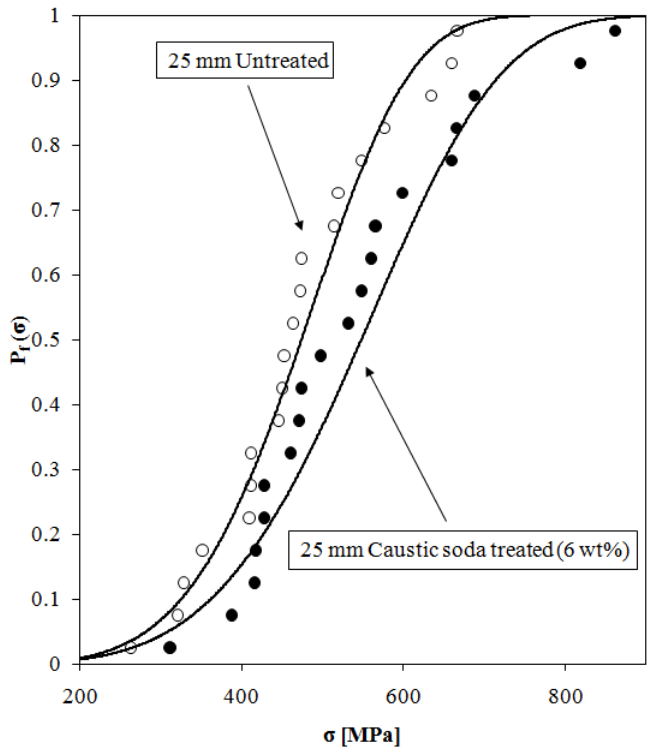

Figure 8.22: Probability of failure ($P_f = 1-P_s$) versus strength for untreated and caustic soda treated (6 wt%) sisal fibres at gauge length of 25 mm.

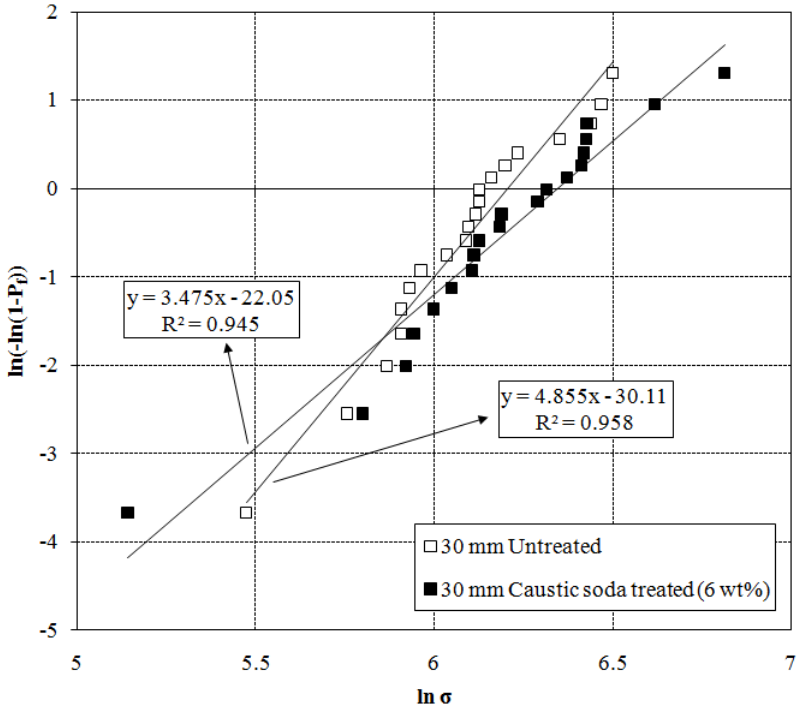

Figure 8.23: Weibull plot for strength of untreated and caustic soda treated (6 wt%) sisal fibres at 30 mm length.

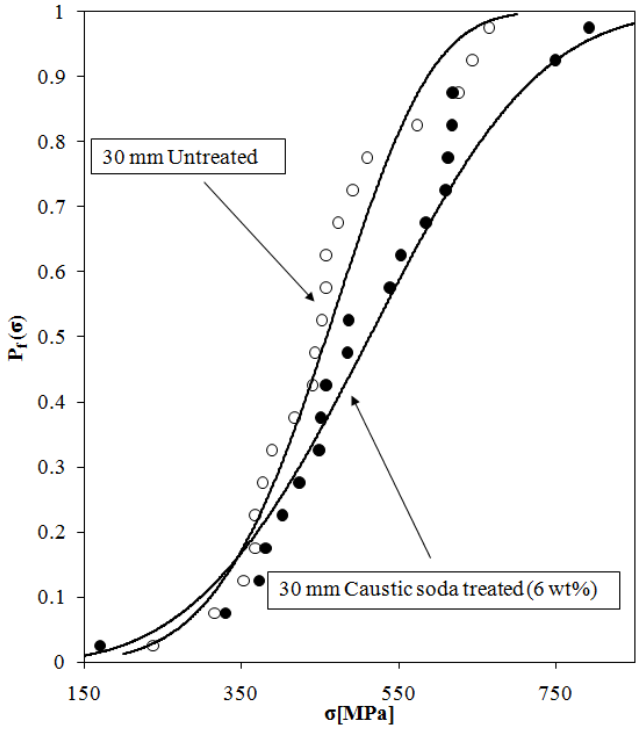

Figure 8.24: Probability of failure (P_f = 1-P_s) versus strength plots for untreated and caustic soda treated (6 wt%) sisal fibres at a gauge length of 30 mm.

Figure 8.25 presents Weibull plots for strength of hydrogen peroxide treated sisal fibres. Figure 8.26 shows Weibull plots for strength of sisal fibres treated with 0.16 and 2 wt% caustic soda aqueous solutions.

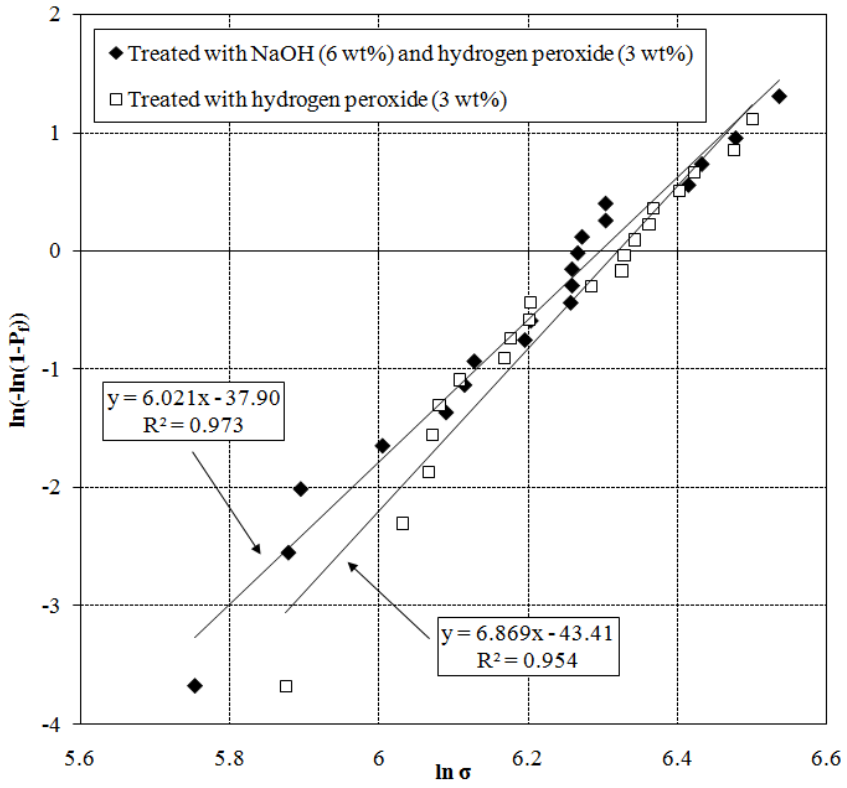

Figure 8.25: Weibull plot for strength of hydrogen peroxide treated sisal fibres at 25 mm gauge length.

Weibull parameters for the fibre strength and strain at break were estimated from Weibull plots at each gauge length with the linear regression fit. The procedure applied is described in detail in Section 6.9. The Weibull modulus was estimated from the slope of the linear trend line. The characteristic strength (or strain) was calculated from the y-intercept.

Weibull modulus and characteristic parameters were used for the calculation of the mean strength or strain as well as the median and standard deviation. The probability of failure was estimated with the expression (n-0.5)/N for the strength data and n/(N+1) for the strain data where *N* is the number of tested samples and *n* is the *ith*-rank of stress (or strain) value in the data set (Le Bourhis, 2008). Different probability estimators were used for stress and strain at break because they were giving better linear fit. Probability of failure estimated as P_f = (n-0.5)/N was reported by Bergman (1984) to give a less biased estimation of Weibull modulus.

Another method to estimate Weibull parameters is the maximum likelihood method (Cohen, 1965) which is known to give overestimated values of Weibull modulus (Bergman, 1985). The Cramer von Misés test (Murthy *et al*., 2004) was performed to decide whether the data followed the Weibull distribution. The Weibull distribution was successfully used to describe the strength distribution of several natural fibres (Virk *et al*. 2009 and 2010; Zafeiropoulos and Baillie, 2007; Towo and Ansell, 2005).

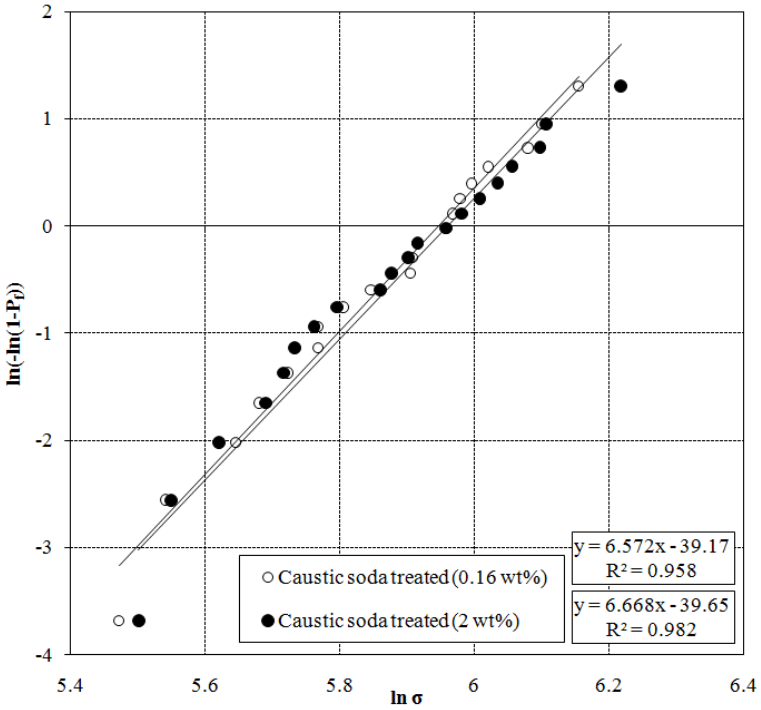

Figure 8.26: Weibull plot for strength of caustic soda treated (0.16 and 2 wt%) sisal fibres at 25 mm gauge length.

Figure 8.27-29 present Weibull plots for strains at break of untreated and caustic soda treated (6 wt%) sisal fibres. Figure 8.30 includes Weibull plots for strains at break of hydrogen peroxide treated sisal fibres. Figure 8.31 shows Weibull plots for strain of caustic soda treated (0.16 and 2 wt%) sisal fibres.

Tables 8.4–6 display the strength, strain at break and Young's moduli of all treated and untreated sisal fibres tested. Where the Weibull distribution was applicable the mean, median and standard deviation as well as the coefficient of variation were calculated using the formulae described in Section 6.9. The Young's modulus was estimated as the slope of the

initial linear portion of the stress-strain curve. Higher values of Young's moduli were determined at larger gauge lengths.

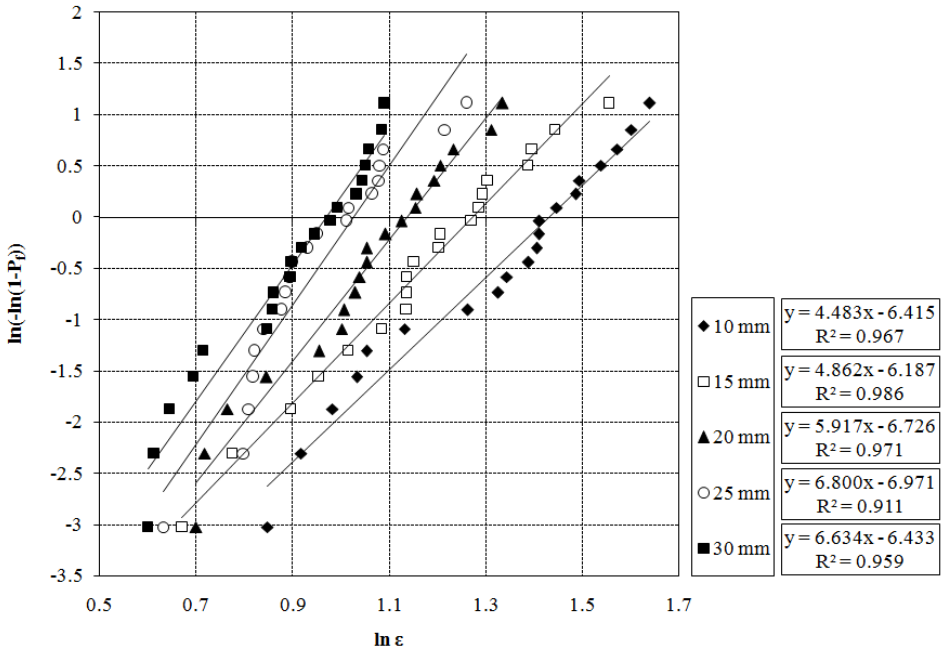

Figure 8.27: Weibull plots of strains at failure for caustic soda (6 wt%) treated sisal fibres at different gauge lengths.

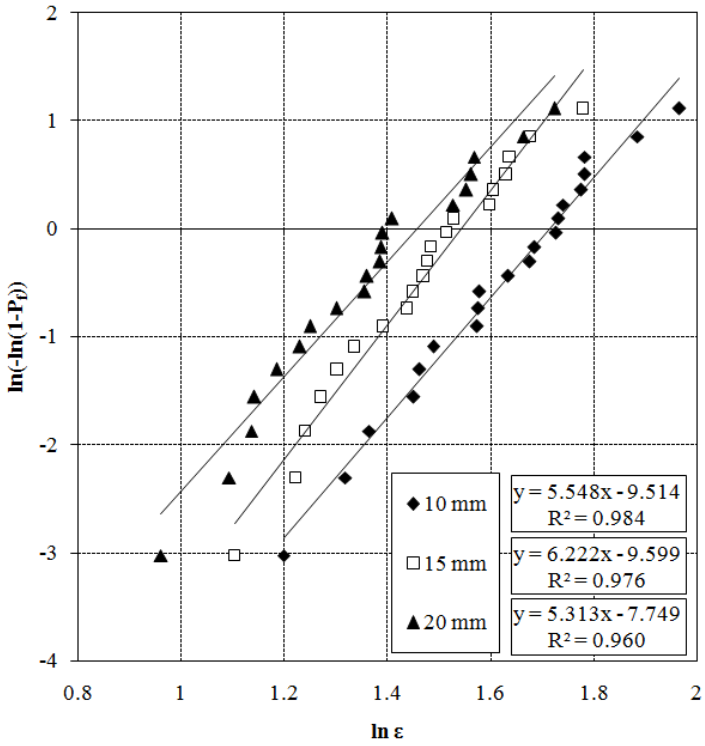

Figure 8.28: Weibull plots of strain at failure for untreated sisal fibres at 10, 15 and 20 mm gauge lengths.

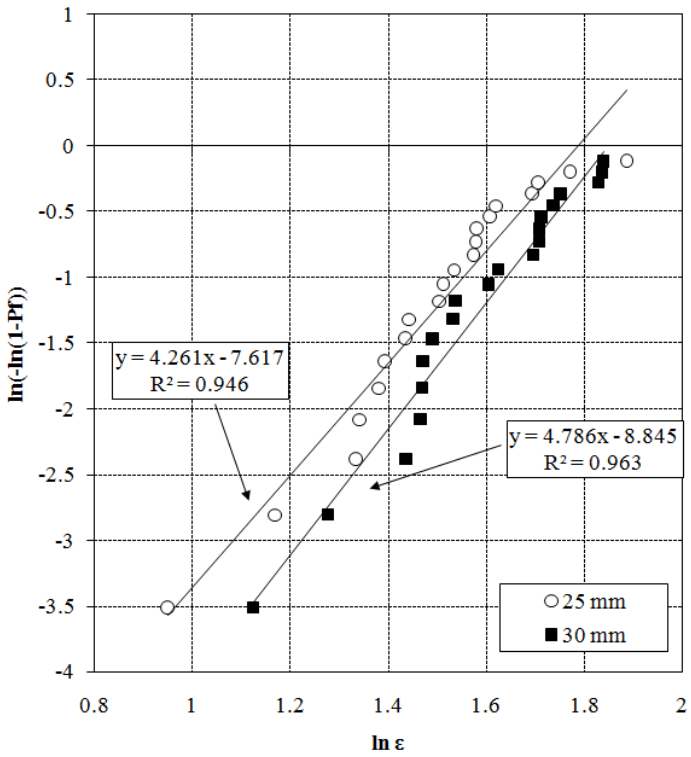

Figure 8.29: Weibull plots of strain at failure for untreated sisal fibres at 25 and 30 mm gauge lengths.

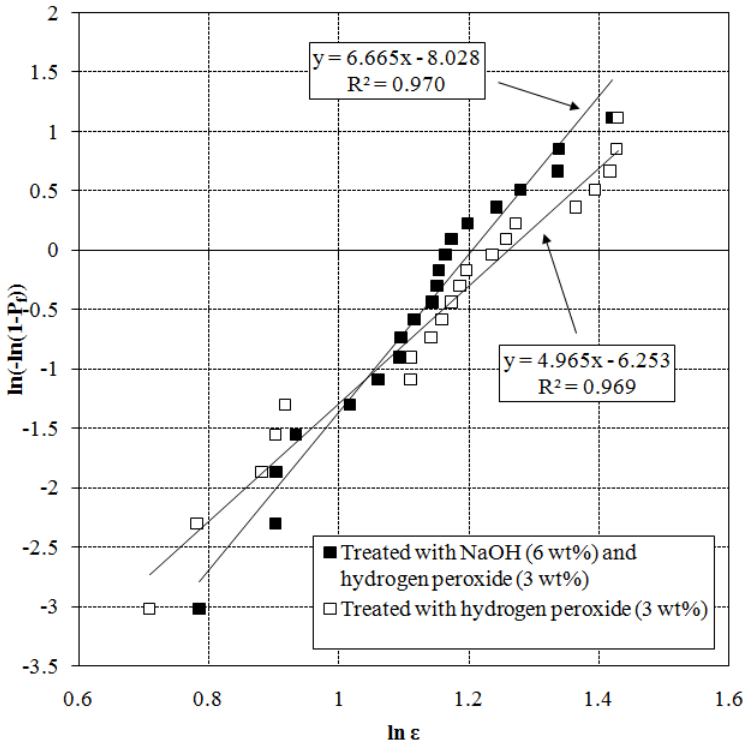

Figure 8.30: Weibull plots of strains at failure of hydrogen peroxide treated sisal fibres.

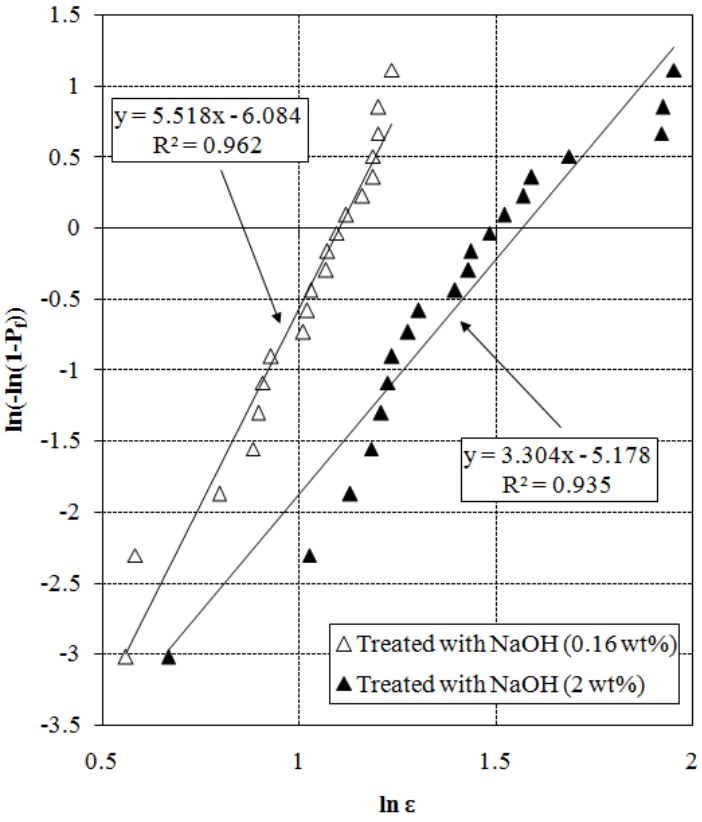

Figure 8.31: Weibull plots of strains at failure for sisal fibres treated with 0.16 and 2 wt% caustic soda solutions.

It is possible that at a constant strain rate and longer gauge length the elastic fibre has more time to relax and to accommodate to the applied stress. Caustic soda treated (6 wt%) sisal fibres strained less at all gauge lengths tested compared to untreated sisal fibres. As can be seen from the Table 8.6 the characteristic strength which is assigned to the probability of failure $P_f = 0.63$ is higher than the median strength which is assigned to $P_f = 0.5$ probability of failure. It can be seen that the strength of untreated and caustic soda treated (6 wt%) sisal fibres decreases with the increasing gauge length. Caustic soda treated sisal fibres (6 wt%) showed higher tensile strength values at all tested gauge lengths. The influence of caustic soda on natural fibres is discussed in Chapter 2. It shall be pointed out that a typical natural fibre like sisal has a multi-walled microstructure. It has been composed of several concentric layers with same chemical composition but different microstructure. The strength of the solution and the time of action are key factors to decide how deeply the fibre will be attacked and which structural layers will be affected.

Table 8.4: Tensile modulus of treated and untreated sisal fibres at different gauge lengths.

		Tensile Modulus [GPa]					
Gauge length [mm]	Fibre treatment	Mean	Median	Maximum	Minimum	Standard deviation	CoV[a]
10	Untreated	14.89	14.95	23.98	11.09	2.87	0.19
15	Untreated	16.21	16.78	20.99	10.30	2.68	0.17
20	Untreated	17.58	18.90	22.80	10.08	3.19	0.18
25	Untreated	18.50	15.82	37.14	7.57	7.57	0.41
30	Untreated	18.89	17.04	34.08	13.27	5.35	0.28
10	NaOH treated (6 wt%)[b]	22.46	20.67	34.90	11.33	5.85	0.26
15	NaOH treated (6 wt%)	24.45	24.08	35.08	14.84	5.26	0.22
20	NaOH treated (6 wt%)	27.45	28.08	35.22	15.61	6.15	0.22
25	NaOH treated (6 wt%)	26.54	25.39	39.79	18.79	4.72	0.18
30	NaOH treated (6 wt%)	29.33	30.29	42.19	21.15	5.29	0.18
25	Untreated/H_2O_2 treated (3 wt%)[c]	27.20	27.21	34.91	18.70	4.63	0.17
25	NaOH treated (6 wt%)/H_2O_2 treated (3 wt%)	21.64	20.53	32.01	11.91	5.52	0.26
25	NaOH treated (0.16 wt%)	17.63	17.70	21.86	13.83	1.89	0.11
25	NaOH treated (2 wt%)	15.13	15.63	20.74	9.56	2.73	0.18

Note: [a]Coefficient of variation; [b]Fibres were treated with caustic soda aqueous solution for 48 hours; [c]Fibres were treated with hydrogen peroxide aqueous solution for 10 minutes; The concentration of the solution is listed in the brackets.

Table 8.5: Strain at break of untreated and treated sisal fibres at different gauge lengths.

		Strain at break [%]								
Gauge length [mm]	Fibre treatment	N	Weibull modulus	Char. strain	Mean	Median	Max.	Min.	Standard deviation	CoV[a]
10	Untreated	20	5.55	5.56	5.14	5.20	7.14	3.13	1.07	0.21
15	Untreated	20	6.22	4.68	4.35	4.41	5.35	3.46	0.82	0.19
20	Untreated	20	5.31	4.30	3.96	4.01	5.61	2.65	0.86	0.22
25	Untreated	20	4.26	5.98	5.44	5.49	6.60	2.59	1.44	0.26
30	Untreated	20	4.79	6.35	5.82	5.88	6.30	3.08	1.39	0.24
10	NaOH treated (6 wt%)[b]	20	4.48	4.18	3.81	3.85	5.15	2.33	0.96	0.25
15	NaOH treated (6 wt%)	20	4.86	3.57	3.27	3.31	4.74	1.96	0.77	0.24
20	NaOH treated (6 wt%)	20	5.92	3.12	2.89	2.93	3.80	2.01	0.57	0.20
25	NaOH treated (6 wt%)	20	6.80	2.79	2.61	2.64	3.52	1.88	0.45	0.17
30	NaOH treated (6 wt%)	20	6.63	2.64	2.46	2.50	2.97	1.82	0.43	0.17
25	Untreated/H_2O_2 treated (3 wt%)[c]	20	4.97	3.52	3.23	3.27	4.18	2.03	0.74	0.23
25	NaOH treated (6 wt%)/H_2O_2 treated (3 wt%)	20	6.67	3.33	3.11	3.15	4.14	2.19	0.55	0.18
25	NaOH treated (0.16 wt%)	20	5.52	3.01	2.78	2.82	3.44	1.75	0.58	0.21
25	NaOH treated (2 wt%)	20	3.30	4.79	4.30	4.29	7.05	1.95	1.43	0.33

Note: [a]Coefficient of variation; [b]Fibres were treated with caustic soda aqueous solution for 48 hours; [c]Fibres were treated with hydrogen peroxide aqueous solution for 10 minutes. The concentration of the solution is listed in the brackets.

Table 8.6: Tensile strength of untreated and treated sisal fibres at different gauge lengths.

			Tensile strength [MPa]							
Gauge length [mm]	Fibre treatment	N[a]	Weibull modulus	Char. strength	Mean	Median	Max.	Min.	Standard deviation	CoV[b]
10	Untreated	20	5.81	548	508	515	726	361	101	0.20
15	Untreated	20	6.24	534	496	504	688	316	93	0.19
20	Untreated	20	6.35	518	482	489	663	312	89	0.18
25	Untreated	20	5.00	510	468	474	667	264	107	0.23
30	Untreated	20	4.86	494	453	458	665	238	107	0.24
10	NaOH treated (6 wt%)[c]	20	4.52	681	622	628	909	269	156	0.25
15	NaOH treated (6 wt%)	20	6.35	634	590	598	798	408	109	0.18
20	NaOH treated (6 wt%)	20	3.40	627	563	563	821	214	183	0.33
25	NaOH treated (6 wt%)	20	4.54	594	542	548	862	312	136	0.25
30	NaOH treated (6 wt%)	20	3.48	570	513	513	792	171	163	0.32
25	Untreated/H_2O_2 treated (3 wt%)[d]	20	6.87	555	519	526	689	315	89	0.17
25	NaOH treated (6 wt%)/H_2O_2 treated (3wt%)	20	6.02	542	503	510	665	356	97	0.19
25	NaOH treated (0.16 wt%)	20	6.68	382	356	362	471	238	63	0.18
25	NaOH treated (2 wt%)	20	6.24	387	360	365	502	245	67	0.19

Note: [a]Minimum tested samples; [b]Coefficient of variation; [c]Fibres were treated with caustic soda aqueous solution for 48 hours; [d]Fibres were treated with hydrogen peroxide aqueous solution for 10 minutes. The concentration of the solution is listed in the brackets.

Table 8.7: Diameter of untreated and caustic soda treated (6 wt%) sisal fibres.

Fibre treatment	Gauge length	Fibre diameter	Standard deviation	CoV[b]
	[mm]	[μm]	[μm]	
Untreated	10	169	26	0.15
Untreated	15	182	25	0.14
Untreated	20	168	41	0.24
Untreated	25	125	26	0.21
Untreated	30	132	28	0.21
NaOH treated (6 wt%)[a]	10	117	25	0.21
NaOH treated (6 wt%)	15	123	28	0.23
NaOH treated (6 wt%)	20	117	21	0.18
NaOH treated (6 wt%)	25	114	21	0.18
NaOH treated (6 wt%)	30	117	23	0.20

Note: [c]Fibres were treated with caustic soda aqueous solution for 48 hours; The concentration of the solution is listed in the brackets; [b] Coefficient of variation.

Table 8.7 summarizes the average fibre diameters of untreated and caustic soda treated (6 wt%) sisal fibres tested at 10–30 mm gauge lengths. The density method was used to determine the cross-sectional area of sisal fibres. The diameter was calculated assuming a circular cross-section of the fibre.

Conclusions:

- The density method was used to determine the cross-sectional area of untreated and treated sisal fibres. The diameter was calculated assuming a circular cross-section of the fibre.
- Tensile properties of untreated and caustic soda treated (6 wt%) sisal fibres were evaluated at gauge lengths of 10, 15, 20, 25 and 30 mm.
- Tensile strength and strain at break were analysed using the Weibull method. Parameters for the Weibull distribution were found via the least squares method.
- Tensile strength was found to decrease with increasing gauge length. The tensile strength of untreated sisal fibres was 508 ± 101 MPa at the gauge length of 10 mm and

453 ± 107 MPa at the gauge length of 30 mm. The tensile strength of caustic soda treated (6 wt%) sisal fibres was 622 ± 156 MPa at the gauge length of 10 mm and 513 ± 163 MPa at the gauge length of 30 mm.

- The strength of caustic soda treated (6 wt%) sisal fibres was higher at all tested gauge lengths compared to untreated sisal fibres.
- Tensile properties of untreated and caustic soda treated (6 wt%) sisal fibres which were also subjected to hydrogen peroxide treatment (3 wt%) were evaluated at the gauge length of 25 mm.
- Hydrogen peroxide deteriorated the strength of untreated sisal fibres but improved the strength of caustic soda treated (6 wt%) sisal fibres. The tensile strength of untreated sisal fibres decreased from 519 ± 89 to 468 ± 107 MPa after they were treated with hydrogen peroxide meanwhile the tensile strength of caustic soda (6 wt%) treated sisal fibres increased from 503 ± 97 to 542 ± 136 MPa after the same treatment.
- Tensile properties of caustic soda treated (0.16 and 2 wt%) sisal fibres were evaluated at the gauge length of 25 mm.
- Fibres treated with aqueous caustic soda solutions of low concentrations (0.16 and 2 wt%) had the tensile strength of 356 ± 63 and 360 ± 67 MPa respectively. These values were lower compared to the tensile strength of untreated sisal fibres tested at the same gauge length (468 ± 107 MPa).
- Caustic soda treated (6 wt%) sisal fibres strained less at break compared to untreated sisal fibres.
- The strain at break of caustic soda treated (6 wt%) sisal fibres decreased with increasing gauge length from 3.81 ± 0.96 % at the gauge length of 10 mm to 2.46 ± 0.43 % at the gauge length of 30 mm.
- Untreated sisal fibres strained from 3.96 ± 0.86 to 5.82 ± 1.39 % at break at tested gauge lengths. There was no clear relationship between the gauge length and strain at break of untreated sisal fibres. In the range of 10 to 20 mm gauge lengths the strain at break decreased from 5.14 ± 1.07 to 3.96 ± 0.86 %. In the range of 25 to 30 mm gauge lengths the strain at break increased from 5.44 ± 1.44 to 5.82 ± 1.39 %.

- Hydrogen peroxide increased the strain at break of caustic soda treated (6 wt%) sisal fibres from 2.61 ± 0.45 to 3.11 ± 0.55 %.
- Sisal fibres treated with hydrogen peroxide strained less (3.23 ± 0.74 %) compared to the untreated ones (5.44 ± 1.44 %).
- The strain at break of caustic soda treated (0.16; 2 and 6 wt%) sisal fibres was 2.78 ± 0.58, 4.30 ± 1.43 and 2.61 ± 0.45 % at the gauge length of 25 mm.
- Young's modulus was found to increase with increasing gauge length. It has increased from 14.89 ± 2.87 to 18.89 ± 5.35 GPa and from 22.46 ± 5.85 to 29.33 ± 5.29 for untreated and caustic soda (6 wt%) treated sisal fibres respectively. The higher values of Young's moduli measured at longer gauge lengths could be explained by the card mount contribution to the overall stiffness of the specimen. So the Young's moduli obtained from the longer specimens are more representative. Ideally the strain in the fibre shall be determined by a non-contacting laser sensor (Reder *et al*., 2003).
- The highest Young's modulus of 29.33 ± 5.29 GPa was measured at the gauge length of 30 mm of caustic soda treated (6 wt%) sisal fibres.
- Hydrogen peroxide improved the modulus of untreated sisal fibres which increased from 18.5 ± 7.57 to 27.2 ± 4.63 GPa. The modulus of caustic soda (6 wt%) treated sisal fibres decreased from 26.54 ± 4.72 to 21.64 ± 5.52 GPa after the fibres were treated with hydrogen peroxide.
- The moduli of sisal fibres treated with different caustic soda solutions (0.16; 2 and 6 wt%) were 17.63 ± 1.89, 15.13 ± 2.73 and 26.54 ± 4.72 GPa respectively).

8.3 Hot stage microscopy

This chapter characterizes the sisal fibre-polylactic acid interface and the results of hot stage microscopy and microbond shear tests are presented. The development of crystalline morphology at fibre to matrix interface was studied under isothermal and non-isothermal conditions using hot stage microscopy. Cooling rates, crystallization temperatures and times were varied to develop and characterize the crystalline morphology at the interface. Fibres were modified with aqueous caustic soda solutions of various concentrations in order to enhance the development of crystallinity. A microbond shear test was used to characterize the shear strength of the interface as a function of fibre surface treatment and the crystalline morphology of the PLA.

The development of transcrystalline (TC) growth of PLA on sisal fibre bundles was studied using hot stage microscopy of single sisal fibre-PLA model composites. TC growth is expected to have a beneficial effect on interfacial adhesion (see Section 5.3.3).

8.3.1 Transcrystalline growth

Untreated and caustic soda treated sisal fibre bundles were used. In a typical experiment the single fibre-polymer composite was heated up to 180°C which is above the melting temperature of PLA and held for 10 min. at this elevated temperature to neutralise the influence of previous thermal history on crystalline phase formation in the matrix. The model composites were then cooled down at specific cooling rates to the required temperature of crystallization temperature (T_c). After reaching this temperature the composites were isothermally crystallized for at least 20 minutes. In the case of transcrystallinity development the thickness of the transcrystalline layer (TCL) was measured at two-minute intervals. The development of the TCL at fibre to matrix interface was studied at cooling rates of 2 and 5°C/min. for untreated and 6 wt% NaOH treated fibres. The samples were isothermally crystallized at temperatures of 120, 125, 130, 135 and 140°C. Samples could not be isothermally crystallized at temperatures below 120°C as they usually started to crystallize spontaneously as the temperature of 120°C was reached during the cooling down stage.

The concentration of 6 wt% NaOH was chosen as it was reported to improve interfacial bonding between sisal fibres and the polymer matrix (Mwaikambo and Ansell, 2006a). The influence of different concentrations of caustic soda treatment on PLA crystallization at the fibre to matrix interface was studied at the crystallization temperature of 120°C where the growth of TCLs was optimum. Treated fibres were soaked in an aqueous caustic soda solution with a concentration of 0.16, 2, 4, 6 and 8 wt%. The PLA matrix was melted and then cooled down at a rate of 5°C/min. to 120°C and isothermally crystallized. More detailed isothermal experiments were carried out at the crystallization temperature of 120°C with cooling rates of 2, 3, 4, 5, 6, 7 and 9 C°/min. for 6 wt% caustic soda treated fibres. Untreated and caustic soda (6 wt%) treated sisal fibres were also air quenched after melting at 180°C for ten minutes. Figure 8.32 shows schematically the temperature profiles of isothermal crystallization of PLA/single sisal fibre composite performed in a hot stage microscope at cooling rates of 2, 5 and 7 C°/min with a crystallization temperature of 120°C.

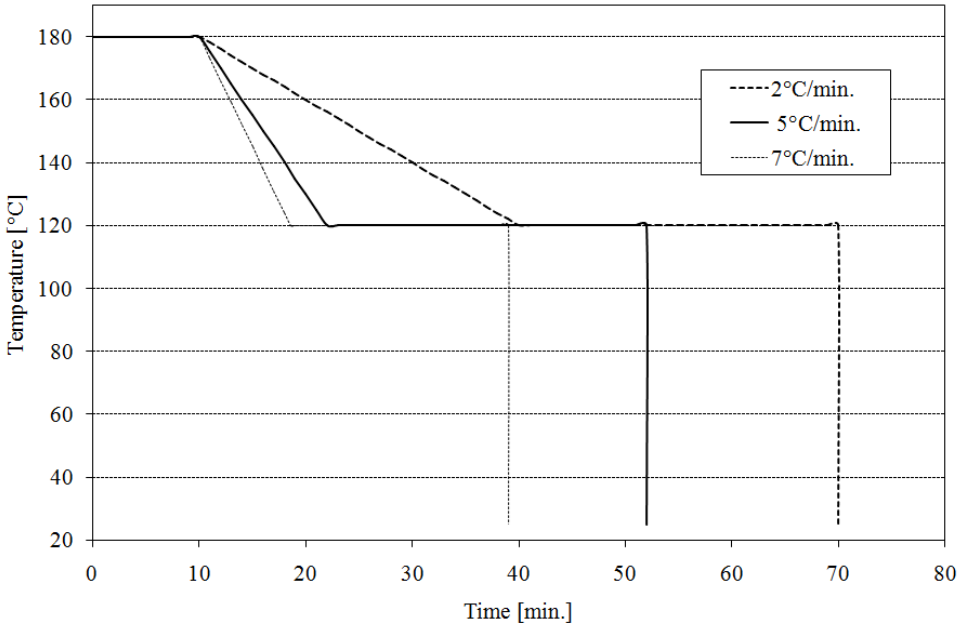

Figure 8.32: Temperature profile of isothermal crystallization of PLA/single sisal fibre composite performed in a hot stage microscope.

Sisal fibre bundles rather than ultimate fibres were used in the experiments because compression moulded macro-composites are composed of sisal fibre bundles and the aim was

to see whether it is possible to form transcrystallinity in a real composites during the processing or post-processing after application of special thermal cycle.

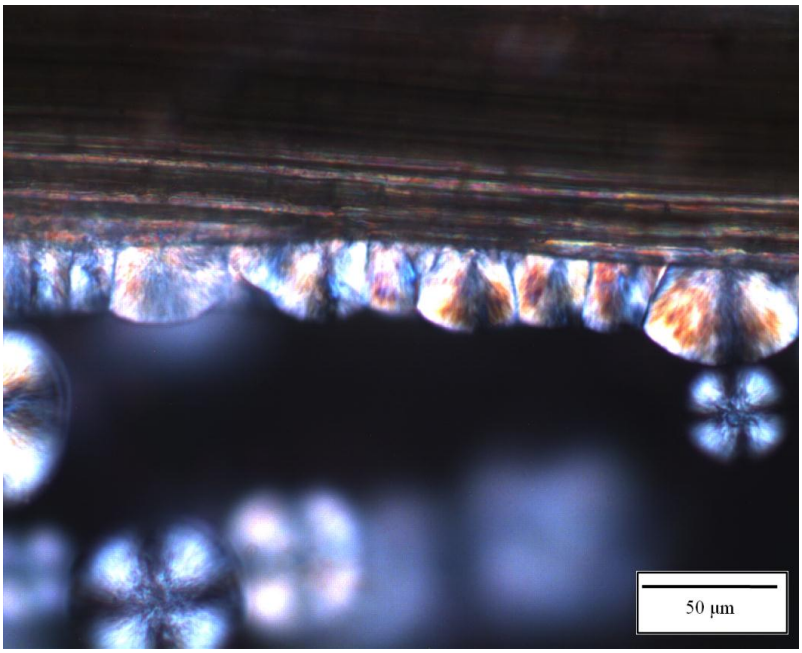

Figure 8.33: Early stage of transcrystallinity development (Isothermal crystallization at 120°C) at the surface of sisal fibre treated with 6 wt% NaOH for 48 h at room temperature.

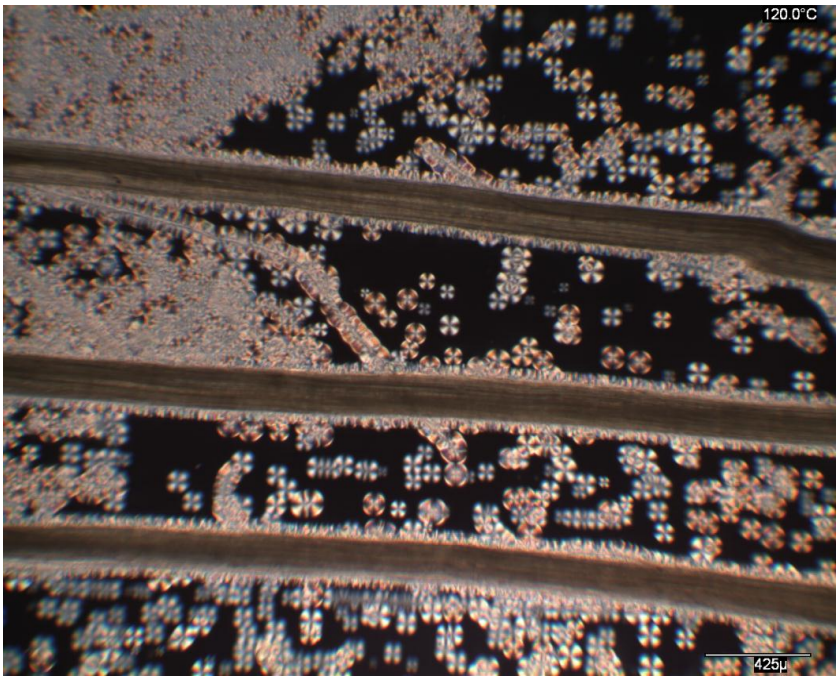

Figure 8.34: Transcrystallinity development in a sample with three caustic soda treated sisal fibres. Cooling rate 5°C/min. Isothermal crystallization at 120°C after 20 minutes.

Figure 8.33 displays the early stage of nucleation at the surface of sisal fibre treated with 6wt% NaOH. Figure 8.34 shows a micro-composite with three embedded fibres. Detailed observation of Figure 8.34 shows a single ultimate fibres branching from the surface of the upper sisal fibre bundle on the left hand side.

8.3.2 Isothermal spherulitic growth

Ultimate fibres promote fast development of crystallinity. It was found that untreated sisal fibres did not promote the formation of a TCL. In some cases not only they did not support TC formation they also did not support the development of individual spherulites. The spherulitic morphology without TCL development but with individual separated crystals was called "spherulitic growth" for practical reasons. In this case the fibres acted as a nucleation site but the density of nuclei was uneven leading to individual spherulites which did not form laterally restricted columnar growth. Figure 8.35 is representative of uneven growth for crystal growth at 125°C and 8.36 is typical of even TC growth at 120°C following treatment with 6 wt% NaOH in both cases.

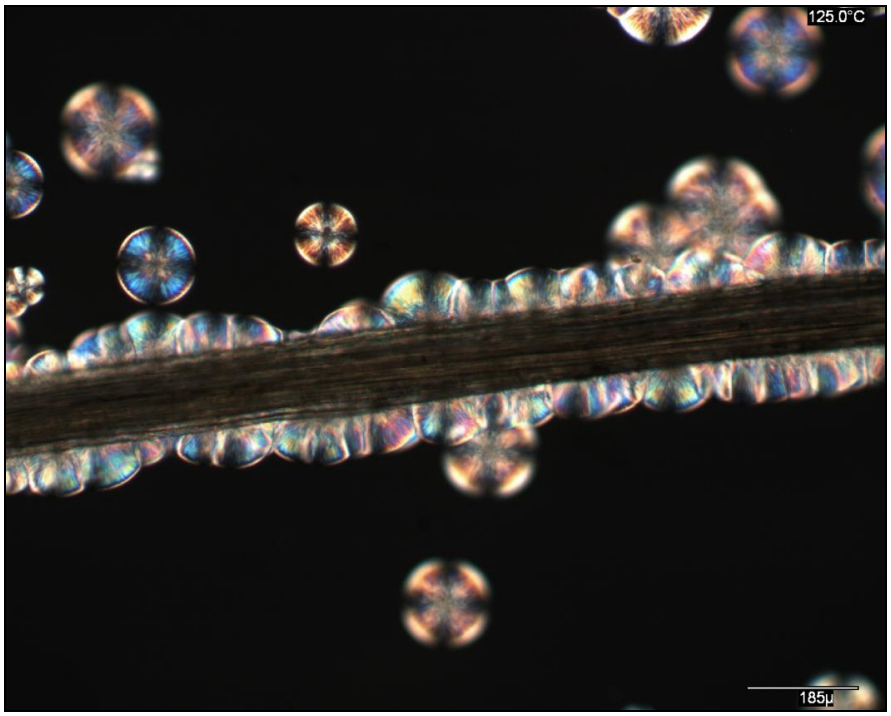

Figure 8.35: Sisal treated with 6 wt% NaOH for 48 h at room temperature. Isothermal spherulitic growth at 125°C after 30 minutes. Cooling rate from 180°C to 125°C: 5°C/min.

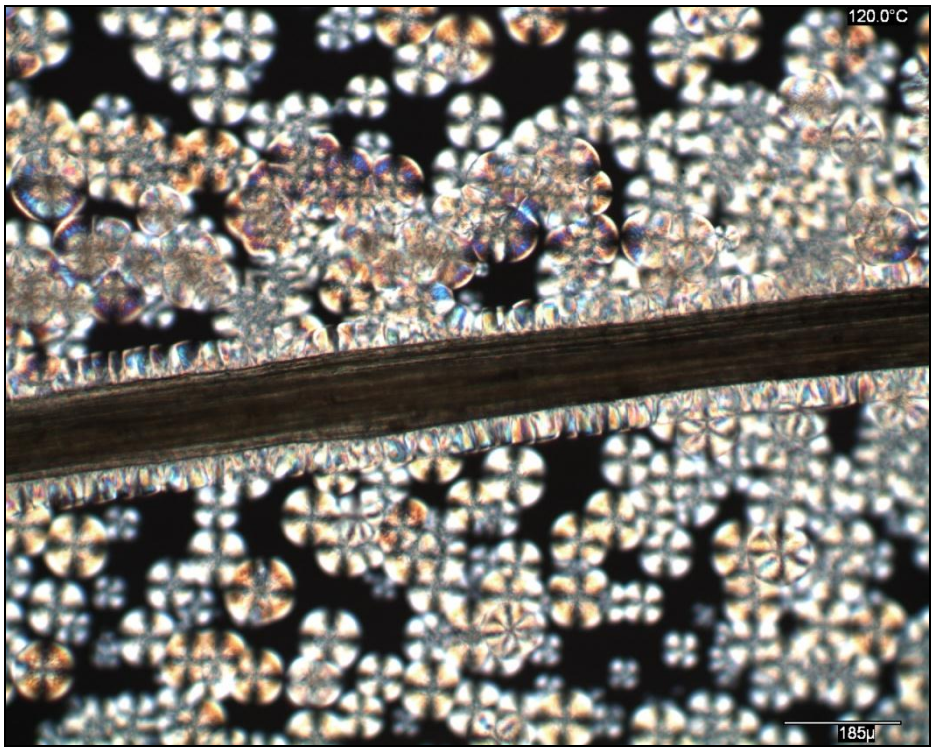

Figure 8.36: Sisal treated with 6 wt% NaOH for 48 h at room temperature. Transcrystalline growth at 120°C after 20 minutes. Cooling rate from 180°C to 120°C: 5°C/min.

If the isothermal annealing lasts for long periods of time isothermal spherulitic growth develops to the extent that crystals became so large that they touch neighbouring crystals and start to form columnar structures typical of transcrystalline growth (Figure 8.37). Such development of transcrystallinity has no practical application for composites processing because fibres are close together and long periods of thermal processing are not possible. It is instructive to image spherulitic growth unconstrained by the presence of natural fibres. Figure 8.38 shows spherulites of PLA isothermally crystallized at 120°C for 60 minutes after being cooled down at a rate of 9°C/min. to 120°C. Figure 8.39 shows spherulites of polylactic acid which were crystallized after 60 minutes of isothermal growth at 120°C after cooling at a rate of 5°C/min. The cooling rate has a clear effect on the rate of crystal growth often distinguished by the appearance of concentric banding in polymer crystals at high cooling rates. However, PLA spherulites did not show banding caused by concentric light extinctions (Strobl, 2007) which has been observed in polyethylene spherulites which were crystallized at high degrees of super-cooling (Gedde, 1999).

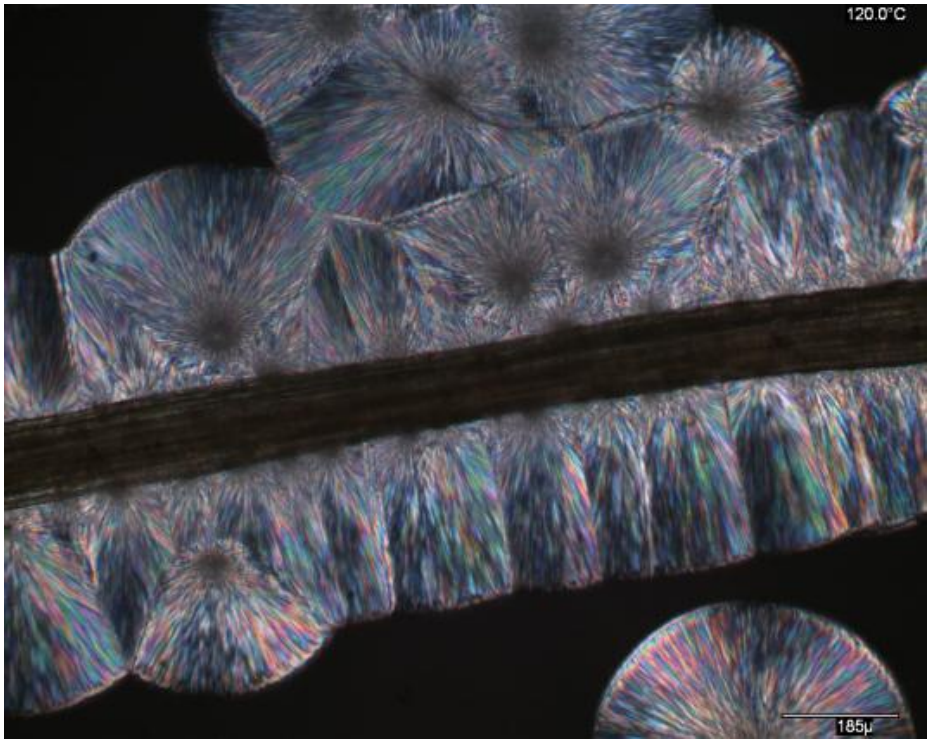

Figure 8.37: Columnar growth after 60 minutes of isothermal crystallization at 120°C (6 wt% caustic soda treated sisal fibre; 9°C/min. cooling rate).

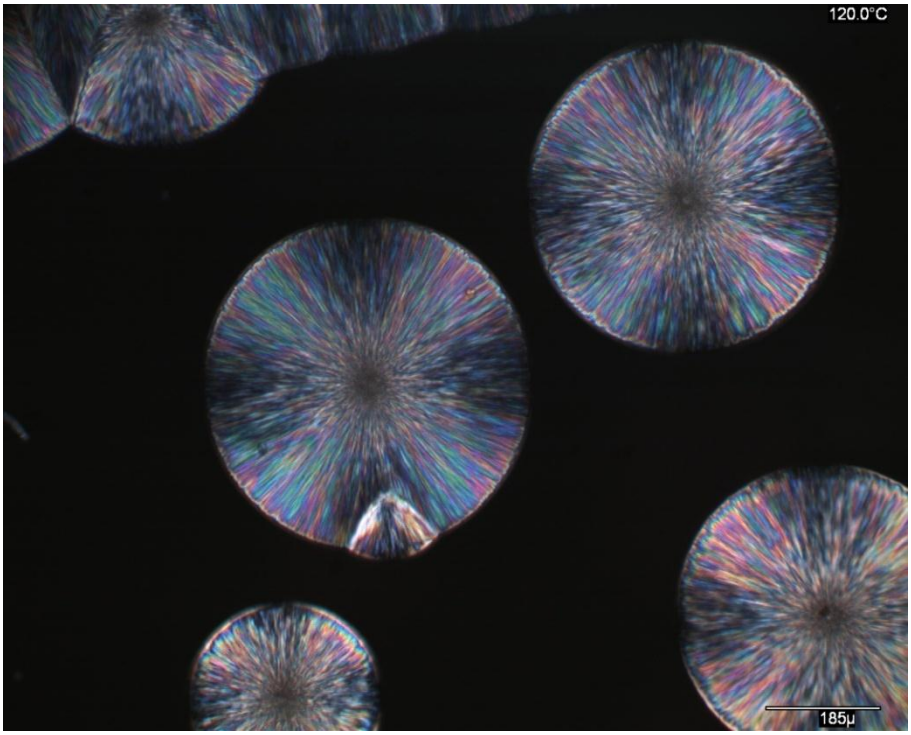

Figure 8.38: PLA crystallites isothermally crystallized at 120°C after 60 minutes. PLA was melted at 180°C for 10 minutes and then cooled down with a rate of 9°C/min. to 120°C.

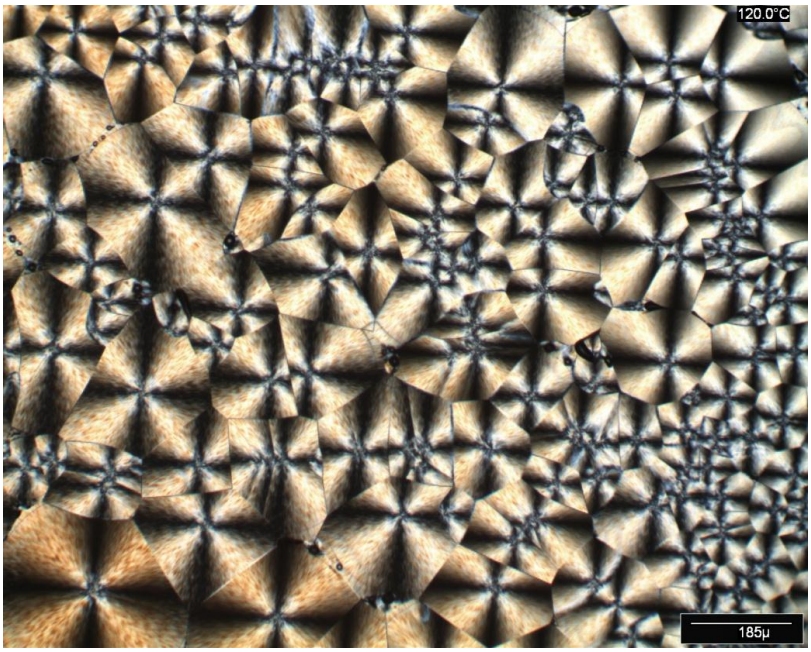

Figure 8.39: PLA crystallites after 60 minutes of isothermal growth at 120°C. PLA melt was cooled to the isothermal temperature with a cooling rate of 5°C per minute.

8.3.3 SEM imaging of the transcrystalline layer

Images from the hot stage microscope are necessarily two dimensional so there is considerable interest in producing 3-D images of the TCL on the surface of sisal fibres in order to evaluate the physical integrity of the layer. A sisal fibre, treated with 6 wt% NaOH for 48 hours, was drawn through a PLA melt between a glass slide and a cover slip. The fibre, coated with a thin layer of PLA, was placed on top of a molten PLA film on a glass slide and slightly pressed in with tweezers. The sample on the glass slide was then put in the hot stage microscope and heated to 180°C and cooled down to 120°C at a cooling rate of 5°C/min. Transcrystalline growth was controlled through the transmitted light microscope. Following removal of the specimen from the light microscope the sample was gold coated (Edwards sputter coater S150B for 4 minutes). SEM images were taken with an accelerating voltage of 20 kV.

Figure 8.40 shows a diagram of the sisal fibre mounted on a glass slide and covered with a layer of PLA together with SEM images of the TC PLA film attached to the fibre. Where the fibre emerges from the PLA (Figure 8.40a) the TC growth can be clearly seen with good wetting of the fibre surface. Figure 8.40b is imaged above the central portion of the fibre and the TC growth is also discernable on either side of the sisal fibre bundle.

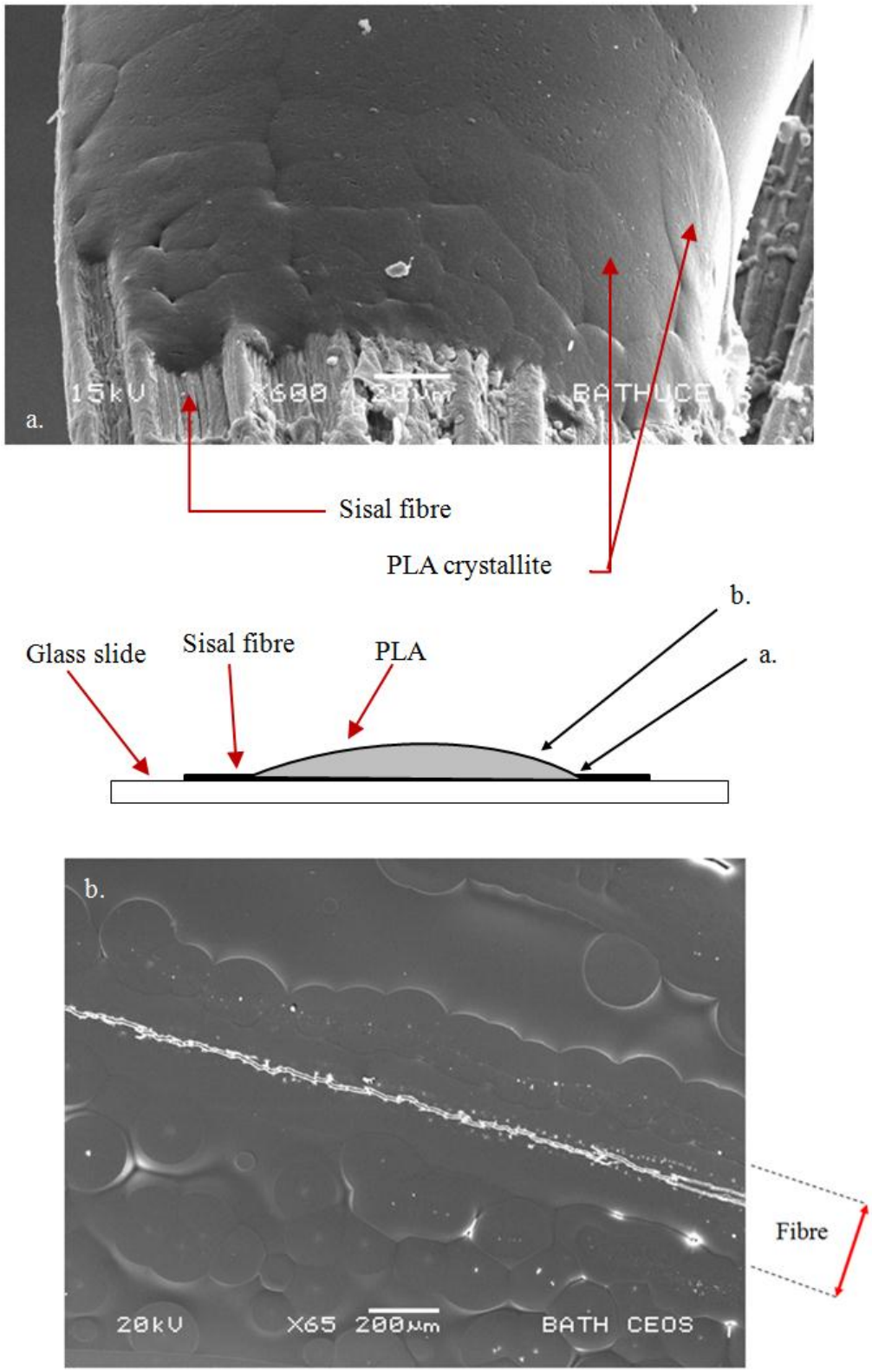

Figure 8.40: SEM images of sisal treated with 6 wt% NaOH for 48h. Isothermal transcrystalline growth at 120°C after 40 minutes. Cooling rate from 180°C to 120°C at 5°C/min. (a). TCL at edge of PLA film, (b) TCL imaged above central portion of fibre bundle. Diagram indicates position of (a) and (b).

8.3.4 The thickness of the transcrystalline layer as a function of annealing time

The effect of (a) cooling rate and (b) the concentration of caustic soda used for fibre treatment on the thickness of the transcrystalline layer has been evaluated in the hot stage microscope (see Appendix A). Figure 8.41 shows the thickness of the transcrystalline layer plotted against the annealing time for isothermal crystallization at 120°C for 6 wt% NaOH treated sisal fibres at different cooling rates.

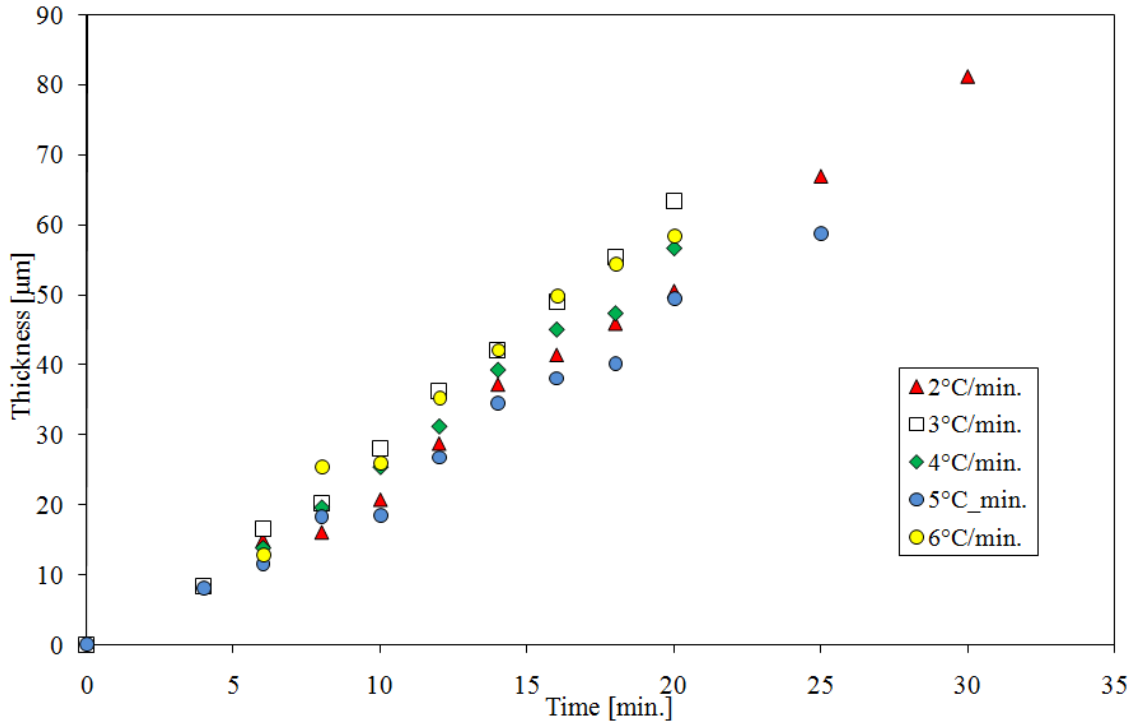

Figure 8.41: Sisal treated with 6 wt% NaOH for 48h. Isothermal transcrystalline growth at 120°C. Cooling rate from 180°C to 120°C at 2, 3, 4, 5 and 6°C/min.

It was found that at cooling rates from 2 to 6°C/min. TC growth was observed and at cooling rates of 7 and 9°C/min. the TCL did not develop. The TCL was also absent in samples which were air quenched and annealed at 120°C for 30 minutes. Figure 8.41 demonstrates that cooling rate has no significant effect on TCL development. It was also found that the concentration of NaOH in the range of 0.16 to 6 wt% has no significant effect on the rate of TC growth (Figure 8.42). The main conclusion is that is important to modify fibres with NaOH to promote growth of the TCL and low concentrations are as effective as high concentrations. However the literature (Mwaikambo and Ansell, 2006a) indicates that higher

concentrations of NaOH optimise the performance of fibres in their role as a composite reinforcement.

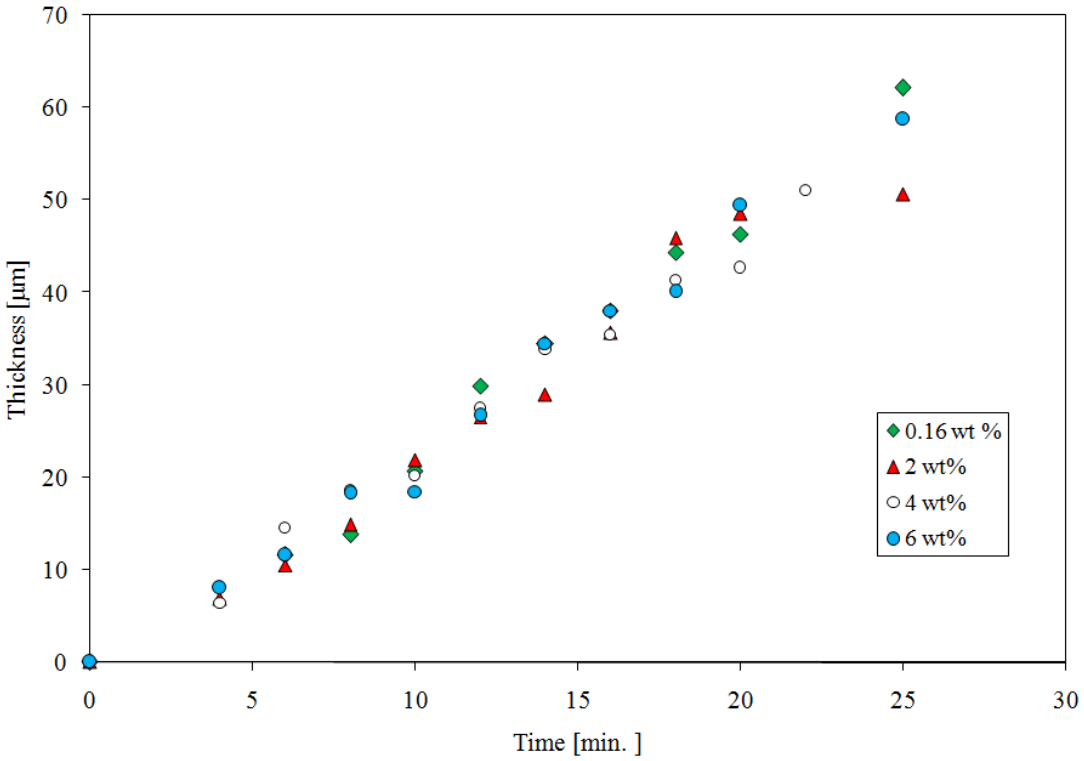

Figure 8.42: Sisal treated with 0.16; 2, 4 and 6 wt% NaOH for 48h. Isothermal transcrystalline growth at 120°C. Cooling rate from 180°C to 120°C: 5°C/min.

The effect of fibre treatment with concentrations of NaOH higher than 6 wt% on TC growth was also explored. It was found that fibre treatment with 8wt% NaOH enabled TCL development after isothermal crystallization at 130°C following cooling from 180°C at rates of 5 and 7°C/min. It can be concluded that the 8wt% NaOH concentration enabled the isothermal development of TCL at higher crystallization temperature compared to tests reported in Figures 8.41 and 8.42 and also after faster cooling rates, e.g. 7°C/min.

Table 8.8 summarizes the conditions under which TC growth or spherulitic growth (SG) occurred following the treatment of fibres with 6 wt% NaOH and growth rate of the TCL is included. Table 8.9 summarises experiments involving untreated fibre where TC growth was not observed. The effect of the concentration of NaOH used to treat the sisal fibres on TC growth is summarised in Table 8.10.

Table 8.8: Development of crystalline morphology at PLA/sisal fibre interface; isothermal crystallization; sisal fibres treated with caustic soda 6 wt% solution.

Cooling rate	[°C/min]	2	2	2	2	2	3	4	5	5	5	5	5	6	7	9
Crystallization temperature	[°C]	120	125	130	135	140	120	120	120	125	130	135	140	120	120	120
Matrix morphology	[-]	TCL	SG	SG	SG	SG	TCL	TCL	TCL	SG	SG	SG	SG	TCL	SG	SG
$h(TCL)_{20min.}$ *	[μm]	51	** -	-	-	-	63	57	50	-	-	-	-	58	-	-
Growth rate	[μm/min.]	2.6	-	-	-	-	3	2.7	2.3	-	-	-	-	3	-	-
See Appendix A, Figure		A6	A7	A8	A9	A10	A24	A33	A3	A2	A1	A4	A5	A30	A29	A23

Note: TCL = transcrystalline layer; SG = spherulitic growth; * thickness of transcrystalline layer after 20 min. of isothermal crystallization; ** not determined.

Table 8.9: Development of crystalline morphology at PLA/sisal fibre interface; isothermal crystallization; untreated sisal fibres.

Cooling rate	[°C/min]	2	2	2	2	2	5	5	5	5	5
Crystallization temperature	[°C]	120	125	130	135	140	120	125	130	135	140
Matrix morphology	[-]	SG	SG	SG	SG	SG	SG	SG	SG	SG	SG
See Appendix A, Figure		A17	A18	A19	A20	A21	A11	A12	A13	A14	A15

Note: SG = spherulitic growth.

Table 8.10: Development of crystalline morphology at PLA/sisal fibre interface; isothermal crystallization; caustic soda treated sisal fibres.

Fibre treatment	[NaOH wt%]	0.16	2	4	6	8	8	8
Cooling rate	[°C/min]	5	5	5	5	5	5	7
Crystallization temperature	[°C]	120	120	120	120	120	130	130
$h(TCL)_{20min.}$ *	[µm]	46	49	43	50	55	48	43
Growth rate	[µm/min.]	2.4	2.2	2.3	2.3	2.7	2.3	2.2
Matrix morphology	[-]	TCL	TCL	TCL	TCL	TCL	TCL	TCL
See Appendix A, Figure		A22	A16	A25	A3	A28	A27	A26

Note: TCL = transcrystalline layer; *thickness of transcrystalline layer after 20 min. of isothermal crystallization.

8.3.5 Non-isothermal crystallization of PLA

Non-isothermal crystallization of PLA in the presence of caustic soda treated (6 wt% / 48 hours) sisal fibre was also studied and the cooling profile for the PLA model composites is depicted in Figure 8.43 including cooling rates of 2 and 5°C/min.

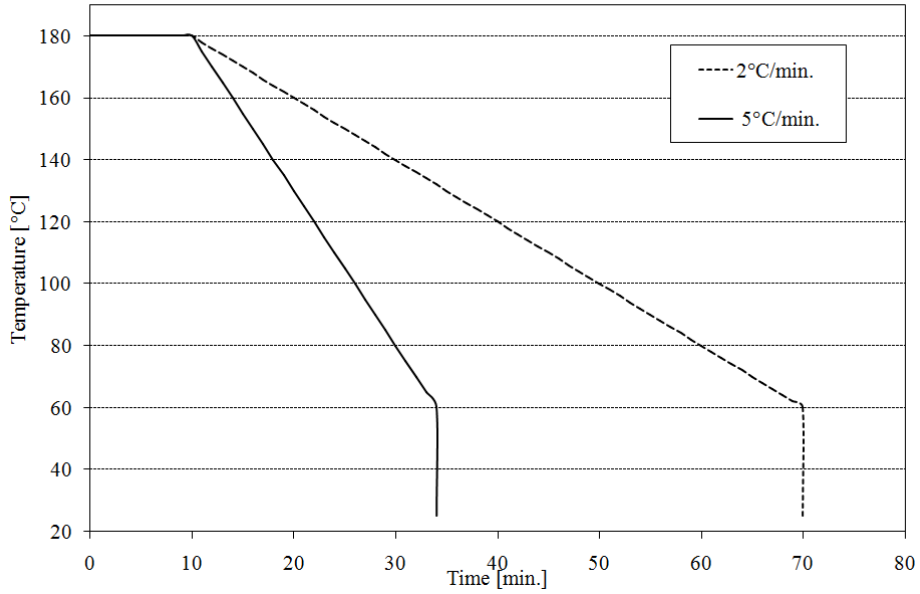

Figure 8.43: Temperature profile of non-isothermal crystallization of PLA/single sisal fibre composite performed in a hot stage microscope.

The samples were heated at 180°C for ten minutes to erase their previous thermal history and cooled down with a predefined cooling rate of 2 and 5°C/min. Results of non-isothermal crystallization are summarized in Table 8.11.

Table 8.11: Development of crystalline morphology at PLA/sisal fibre interface; non- isothermal crystallization; sisal fibres treated with aqueous caustic soda solution of 6 wt% concentration.

Fibre treatment	[NaOH wt%]	6	6
Cooling rate	[°C/min]	2	5
Temperature interval of crystallization	[°C]	120-100	120-80
Matrix morphology	[-]	TCL	TCL
See Appendix A, Figure		A32	A31

At both cooling rates TCLs are formed but very fine crystals are formed. Figure 8.44 shows transcrystallinity development at a temperature of 80°C following cooling at 5°C/min. The thickness of the TCL was determined to be 8 μm at 100°C during the cooling cycle. The same thickness was measured at 80°C so no further growth had occurred. At a cooling rate of 2°C/min the thickness of the transcrystalline layer during the cooling cycle was 12 μm at 100°C.

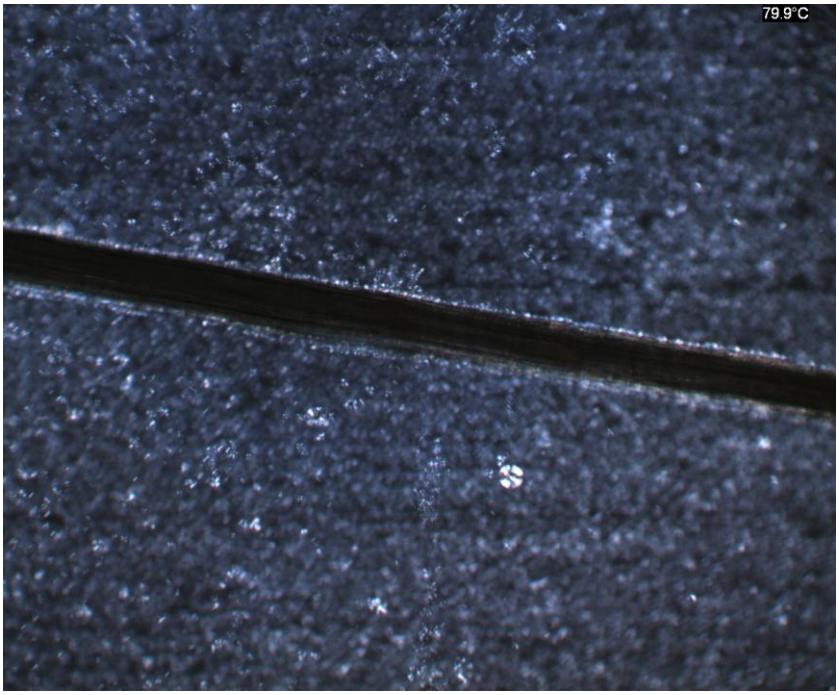

Figure 8.44: Non-isothermal trans-crystallization of polylactic acid.

Non-isothermal crystallization was studied because it can be expected to occur during the compression moulding of macro-composites in a hot press. A further experiment was conducted to investigate the effect of slow cooling in the hot stage overnight. The sample was melted at 180°C for 10 min. and then the hot stage was switched off. The aim was to simulate compression moulding of macro-composites in a hot press and see whether transcrystallinity could develop during processing of sisal fibre reinforced PLA. Figure 8.45 shows a caustic soda treated sisal fibre (6 wt% NaOH for 48 hours) embedded in PLA following slow cooling overnight.

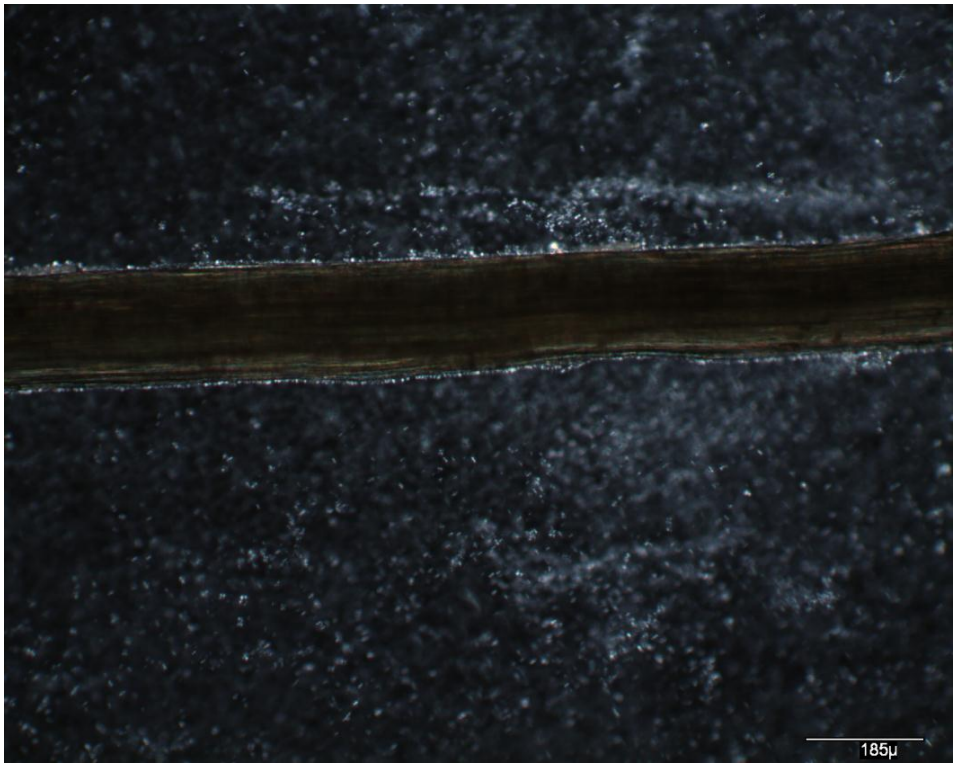

Figure 8.45: Caustic soda treated sisal fibre (6 wt%) embedded in PLA matrix. The polymer was melted at 180°C. After 10 min. the heat source of the hot stage was turned off and the sample was kept inside; TCL thickness ≈ 5 µm.

Very fine crystal morphology results from slow cooling overnight.

8.3.6 Discussion

Zafeiropoulos studied the development of TCL in flax/polypropylene system and suggested that surface micro-roughness plays an important role in TCL formation. Chen and Hsiao (1992) suggested that the transcrystallinity development could result from the thermal conductivity mismatch between the fibre and the matrix. In that case the lower temperature of fibre surface would lead to supercooling at the fibre to matrix interface and higher nucleation rate which causes transcrystallinity development. Figure 8.46 shows microcrystalline cellulose dispersed in PLA matrix close to the sisal fibre treated with 6 wt% caustic soda solution.

Figure 8.46: Microcrystalline cellulose washed out from the caustic soda treated sisal fibre.

Such type of sample was discarded in a typical hot stage microscopy experiment and only samples with "clean" matrix were used. It is a speculation but it could be possible that the TCL formation at fibre to matrix interface in the system of PLA-caustic soda treated sisal fibres is due to the presence of nano-cellulose whiskers at the interface. These whiskers or sheets could be released from the fibre surface and washed out to the polymer matrix because of the melt flow at the fibre to matrix interface during the preparation of single fibre composites. It is well known that caustic soda treatment is used in the formation of cellulose nano-whiskers (Wang and Sain, 2007). Further it could be speculated that there is a matrix

region close to the fibre surface where the cellulose whiskers are mixed with the polymer at almost molecular level. In fact they could act as a compatibilizer in polymer blends. The phenomena definitely require more investigation and further research. The existence of such cellulose nano-whiskers and mixing region would support the theory of TCL formation proposed by Billon *et al.* (1994) which is discussed in Chapter 5.

Conclusions:

- The non-isothermal and isothermal development of PLA crystalline morphology at the fibre to matrix interface was studied with hot stage microscopy of a single fibre-model composite. Untreated and caustic soda treated (0.16 to 8 wt% NaOH) sisal fibres were used. Transcrystalline growth was observed at several cooling rates and crystallization temperatures.
- Caustic soda treatment promoted the development of transcrystalline morphology at PLA/sisal fibre interface whereas untreated fibres promoted single spherulitic growth. Untreated fibres at 120 to 140°C did not exhibit transcrystalline growth but individual spherulitic growth occurred.
- It was found that annealing is necessary to create the TCL around the caustic soda treated fibres under isothermal experiments because PLA is a slowly crystallizing thermoplastic polyester. Continuous TCL usually started to appear after 2 to 4 min. of isothermal annealing.
- Caustic soda treatment of sisal fibres promoted the creation of a TCL at the fibre to matrix interface.
- Non isothermal crystallization at cooling rates of 2, 5 and 7°C/min resulted in transcrystallinity around caustic soda treated fibres (6 wt% NaOH treated fibres for 48 hours).
- The influence of concentration of caustic soda solution on transcrystalline growth rate was studied under special thermal conditions (cooling rate of 5°C/min. and isothermal temperature of 120°C). Overall it can be concluded that caustic soda treatment is advantageous in forming well-defined TCLs at the fibre to thermoplastic matrix interface which should improve stress transfer in the composite.

- The influence of cooling rate on transcrystalline growth rate was studied at isothermal temperature of 120°C for 6 wt% caustic soda treated fibres. It can be concluded that caustic soda treatment provides higher density of nuclei and that the density increases with lower temperatures.
- The transcrystalline morphology was imaged in the SEM and the TCL was found to be coherent with the fibre surface.

8.4 Differential scanning calorimetry

Differential Scanning Calorimetry (DSC) was performed on PLA compression moulded films and single fibre reinforced composites with different thermal histories. The single fibre composites contained a sisal fibre which had been caustic soda treated. Prior to embedding, the fibre was soaked in an aqueous caustic soda solution of 6 wt% concentration for 48 hours. The DSC thermal analysis was performed on a DSC 2920 Differential Scanning Calorimeter (TA Instruments). Samples of 5 mg in weight were sealed in an aluminium pan and heated from 20°C to 300°C at a scanning rate of 10°C/min scanning. A nitrogen flow of 25 ml/min was maintained throughout the test. The glass-transition temperature (T_g), cold crystallization temperature (T_c), melting temperature (T_m), enthalpy of crystallization (ΔH_c) and enthalpy of fusion (ΔH_m) were determined from DSC first scans as described in section 6.3. The enthalpy of crystallization (ΔH_c) and enthalpy of fusion (ΔH_m) were calculated by integrating the area between the baseline and the transition peak. The degree of crystallinity (χ_c) of the PLA films was evaluated according to Eqn 6.4 from Section 6.3. The samples were subjected to the following thermal treatments before evaluation in the DSC:

- PLA was melted at 190°C in an aluminium mould for 10 min. After mould release it was air quenched to room temperature (Figure 8.47).
- PLA was compression moulded between two Teflon® sheets to enhance the sample crystallinity. PLA was melted at 190°C for 10 min. and subsequently cooled down at 5°C/min. to 115°C. After reaching 115°C it was kept at this temperature for 40 min. (Figures 8.48 and 8.49).
- PLA was melted at 190°C for 10 min. and subsequently cooled down at a cooling rate of 7°C/min. to room temperature (Figure 8.50).

- PLA was melted at 190°C for 10 min. and subsequently cooled down at the cooling rate of 2°C/min. to room temperature (Figure 8.51).
- Caustic soda treated sisal fibre-polylactic acid composite was processed at 190°C for 10 min. and subsequently cooled down at 5°C/min. to 115°C. After reaching the temperature of 115°C it was kept at this temperature for 30 min. (Figure 8.52).

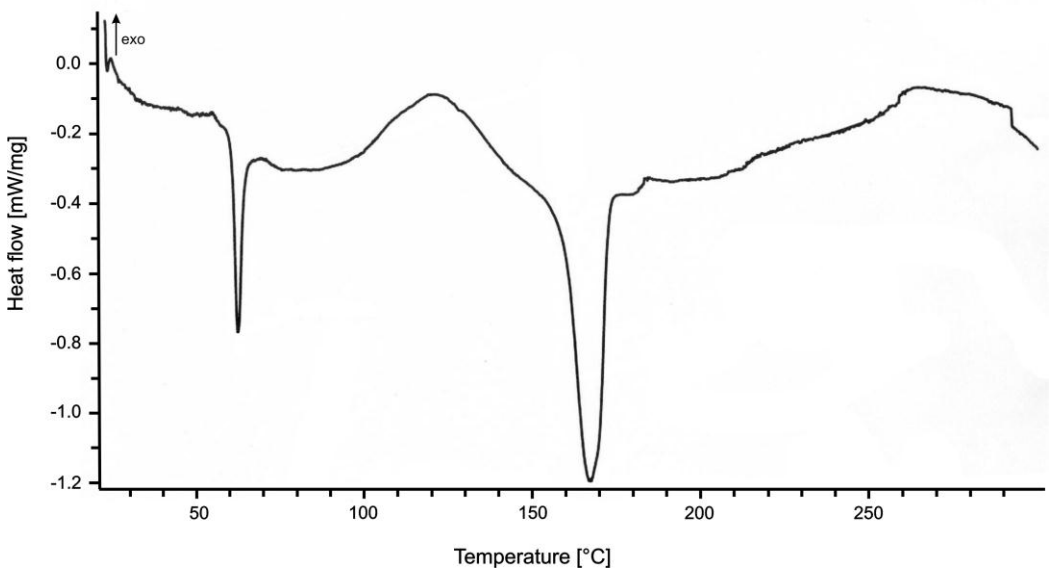

Figure 8.47: DSC thermogram of air quenched polylactic acid.

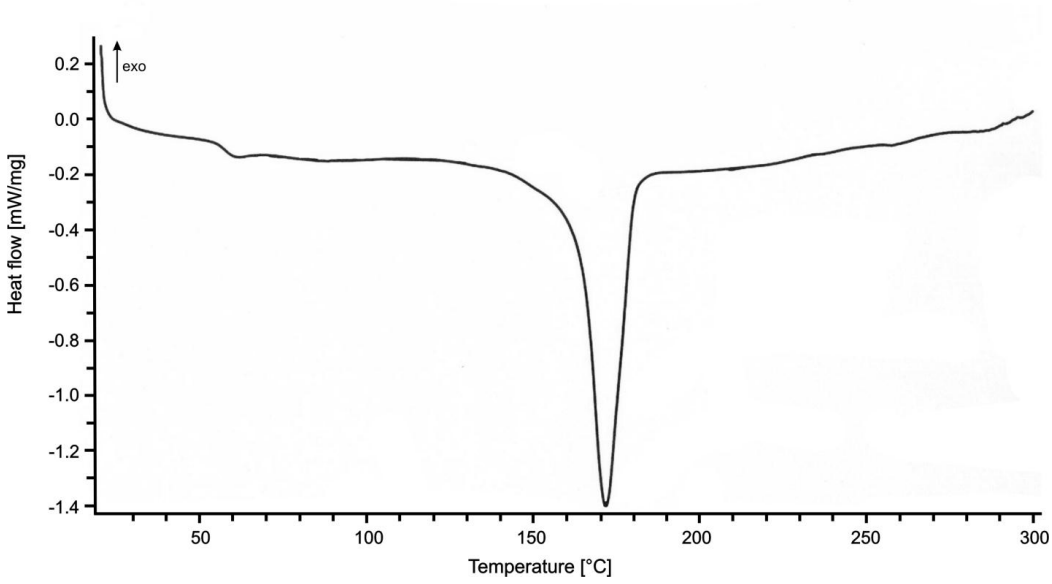

Figure 8.48: DSC thermogram of polylactic acid compression moulded between Teflon® sheets. PLA was melted at 190°C for 10 min. and subsequently cooled down at 5°C/min. to 115°C. After reaching 115°C it was kept at this temperature for 40 min.

Compared to the hot stage microscopy, which makes possible the visual observation of the crystalline morphology development, the DSC enables detection of the glass transition temperature (T_g) and calculation of the amount of crystalline portion in the sample. Figure 8.47 shows the DSC curve for air quenched polylactic acid. Generally speaking fast cooling rates can suppress crystallinity development in a slowly crystallizing semicrystalline polymer and such a polymer is almost amorphous. This results in secondary crystallization during the DSC scan and the development of a broad crystallization peak. Polymer degradation can be observed at temperatures above 200°C. Polylactic acid compression moulded between two Teflon® sheets was annealed at 115°C for 40 minutes. The DSC thermogram of such sample shows no peak attributed to secondary crystallization (T_c~104°C) (Figure 8.48) which means that the crystallinity in the scanned sample is fully developed and it does not re-crystallize during the DSC thermal treatment. High amounts of crystalline phase in semicrystalline polymers mean that the glass transition is less pronounced (Scheirs, 2000). Figure 8.48 also illustrates that it is difficult to detect the glass transition temperature (T_g) in a polymer sample with high degree of crystallinity by differential scanning calorimetry. The DSC curves presented in Figures 8.48 and 8.50 show unusual changes in the shapes of the glass transition region which may result from sub-T_g annealing as pointed out by Menczel and Prime (2009) and Scheirs (2000). Before the DSC analysis the PLA sheets were compression moulded and stored for a few weeks in sealed polyethylene bags at room temperature. Because the T_g of polylactic acid lies in the interval of 50-60°C based on its molecular weight, storing the processed polymer sheets at room temperature could be considered as a sub-T_g annealing. According to Scheirs (2000) the appearance of the second endothermic peak is due to the melting of imperfect crystals formed during annealing. The second melting peak appears as a clear "shoulder" ($T_{m\beta}$=171.6°C) in Figure 8.51 and a less pronounced "shoulder" ($T_{m\beta}$=177.5°C) in Figure 8.52. Temperatures of both secondary peaks are listed in Table 8.12. Zafeiropoulos et al. (2001) speculated that such a shoulder could be a result of transcrystalline melting. This could be the case for the DSC thermogram in Figure 8.52 which belongs to the caustic soda treated fibre embedded in a PLA matrix. As previously mentioned this sample was cooled down from a melt to the temperature of 115°C at the rate of 5°C/min. and annealed at this temperature for 30 min. Hot stage microscopy proved the development of transcrystallinity in samples with such a thermal history. Table 8.12 summarizes the transition

temperatures and transition enthalpies (see Section 6.3) deduced from DSC scans. The highest T_m was achieved in samples of PLA compression moulded in Teflon® and in the single fibre composite containing an embedded caustic soda treated sisal fibre. In both samples a higher degree of crystallinity and crystalline order can be expected. Ohtani et al. (2003) observed the melting temperature to increase with annealing time at higher temperatures.

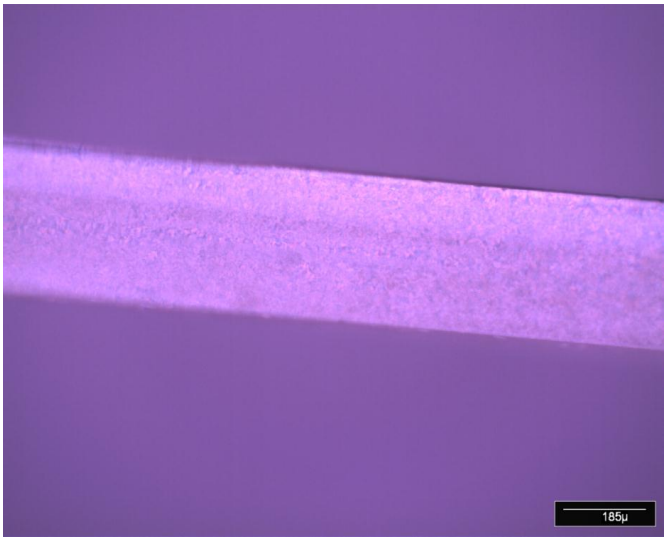

Figure 8.49: Cross section through a PLA foil compression moulded between Teflon® sheets (the thickness of PLA foil was 330 µm; the microtomed section was approximately 50 µm thick). Scale bar = 185 µm.

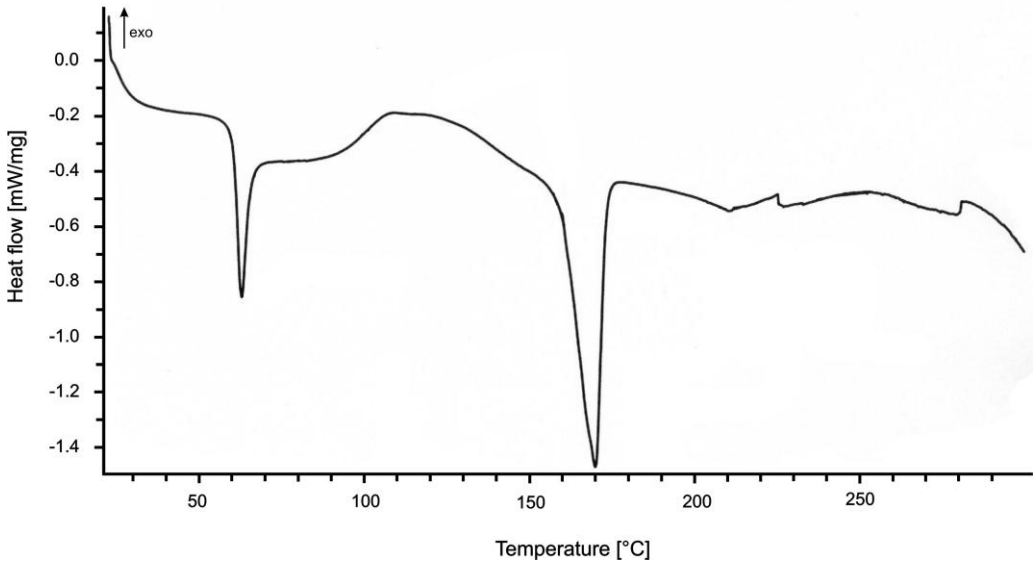

Figure 8.50: DSC thermogram of polylactic acid melted at 190°C for 10 min. and subsequently cooled down at a cooling rate of 7°C/min. to room temperature.

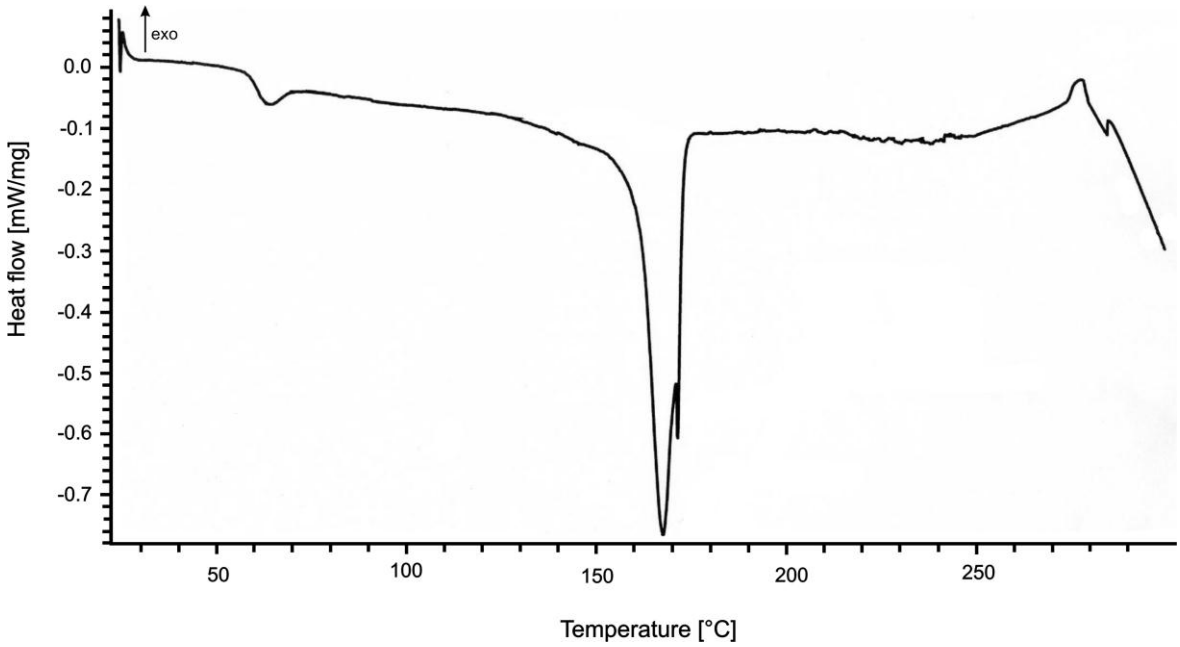

Figure 8.51: DSC thermogram of polylactic acid melted at 190°C for 10 min. and subsequently cooled down at a cooling rate of 2°C/min. to room temperature.

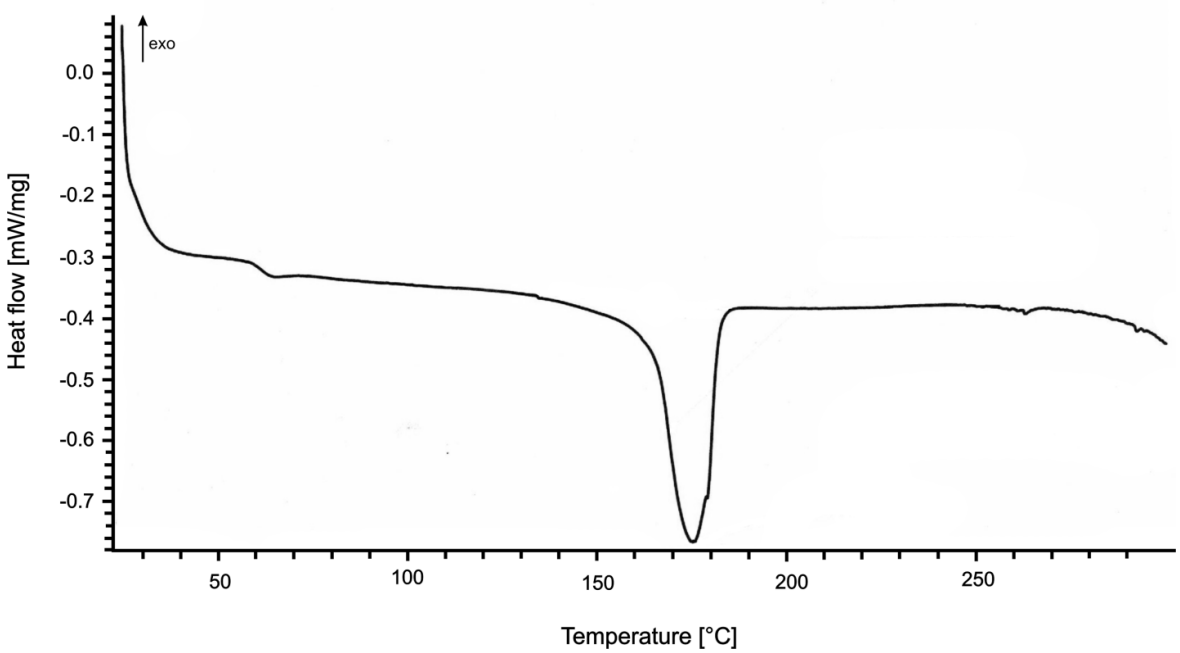

Figure 8.52: Caustic soda treated sisal fibre-polylactic acid composite processed at 190°C for 10 min. and subsequently cooled down at 5°C/min. to 115°C. After reaching 115°C it was kept at this temperature for 30 min.

Table 8.12: Thermal transition temperatures and enthalpies of thermo-compressed PLA sheets and composites.

Sample description		Thermal history			DSC results**								
Sample	Crystallization	Cooling rate	Annealing temperature/time	End temperature	T_{eig}	T_{mg}	T_c	T_{eim}	T_m	$T_{m\beta}$***	ΔH_c	ΔH_m	χ_c
		[°C/min.]	[°C/min.]	[°C]	[°C]	[°C]	[°C]	[°C]	[°C]	[°C]	[J/g]	[J/g]	[%]
Air quenched PLA	Non-isothermal	-	-	25	60	61	120	157	167.4	-	29.47	46.48	0.18
PLA compression moulded in Teflon®	Isothermal	5	115/40	-	53.8	59.4	-	164.1	172	-	-	61.91	0.66
PLA sheet	Non-isothermal	7	-	25	60	61	110	155	170.1	-	23.60	42.34	0.20
PLA sheet	Non-isothermal	2	-	25	58.8	61.3	-	161.4	167.7	171.6	-	56.09	0.60
Single fibre composite *	Isothermal	5	115/30	-	55	57.5	-	162.8	173.6	177.5	-	46.61	0.50

Note: *caustic soda treated sisal fibre (aqueous solution of 6 wt% concentration for 48 hours); **thermal transition temperatures and enthalpies are defined in Section 6.3; ***second melting peak.

Conclusions:

- The DSC showed that annealing time, cooling rates and surface morphology have an effect on the thermal behaviour of polylactic acid and sisal fibre-polylactic acid composites.
- Samples which were slowly crystallized or annealed had a higher degree of crystallinity and higher melting temperature. The DSC thermograms of such samples did not show the exothermic peak of cold crystallization.
- Samples which were air quenched or non-isothermally crystallized at high cooling rates cold crystallized during the DSC scan. Such samples had a low degree of crystallinity.

8.5 Pull-out microbond shear test

This section presents results of the pull-out test which was used to measure the adhesion strength between the untreated and caustic soda treated sisal fibres and polylactic acid. The test was also performed on single sisal fibres partially embedded in a polylactide matrix with developed crystalline morphology. Interfacial shear strength, strain energy release rate, critical length, toughness and thermal residual stresses are discussed.

Adhesion strength between sisal fibres and polylactic acid was determined using a single fibre pull-out test. Figure 8.53 shows a typical pull-out test specimen. The specimen supported on a paper card and clamped in a testing machine prior to the test is seen in Figure 8.54. Specimen preparation and test conditions are described in Chapter 6.

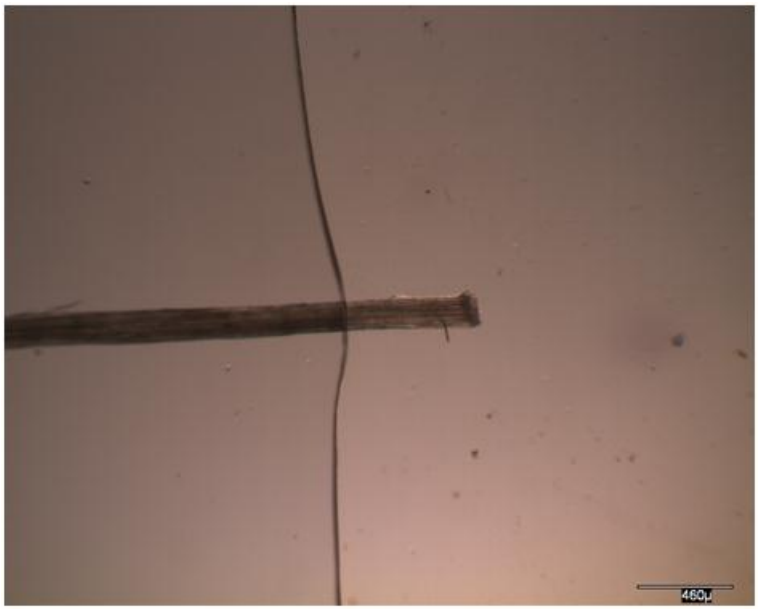

Figure 8.53: Optical photograph with cross-polars of a pull-out test specimen. Caustic soda treated sisal fibre (6 wt%) partially embedded in a PLA matrix (matrix situated in the right part of the photograph).

Figure 8.54: Pull-out test specimen clamped in Instron 3369 jaws prior to testing.

The surface area of embedded fibre was calculated from the fibre diameter and the embedded length which were both determined with optical microscopy.

Table 8.13: Interfacial shear strength at sisal fibre/PLA interface.

Fibre	Treatment	Matrix	N^c [-]	IFSS [MPa]
Sisal	untreated	PLA	34	10.5 ± 3.72
Sisal	[a]NaOH treated	PLA	26	15.3 ± 5.96
Sisal	[b]NaOH treated/TCL	PLA	15	12.8 ± 4.96

Note: [a] fibres were treated with a 6 wt% solution of caustic soda for 48 h; [b] transcrystallinity developed at 104° C for 2 minutes; [c] number of samples with an adhesion failure.

Table 8.13 also includes the interfacial shear strength of caustic soda treated (6 wt%) sisal fibres embedded in a polymer matrix with developed crystalline morphology. Figure 8.55 displays the history of thermal treatment which led to the development of crystalline morphology. Due to the anisotropy, non uniform cross section and surface roughness of the fibres a Weibull distribution of interfacial shear strength was expected (Figure 8.56-58). Parameters of the distribution (Weibull modulus and characteristic strength) were calculated from the linear regression via Weibull plots (Figure 8.56-58).

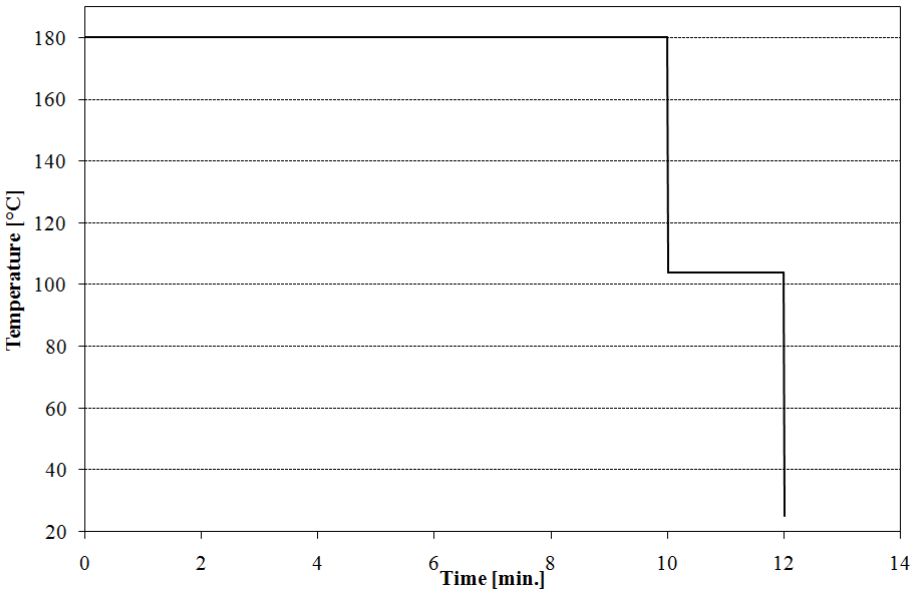

Figure 8.55: Temperature profile of isothermal crystallization of PLA/single sisal fibre pull-out test specimen performed in a hot stage microscope.

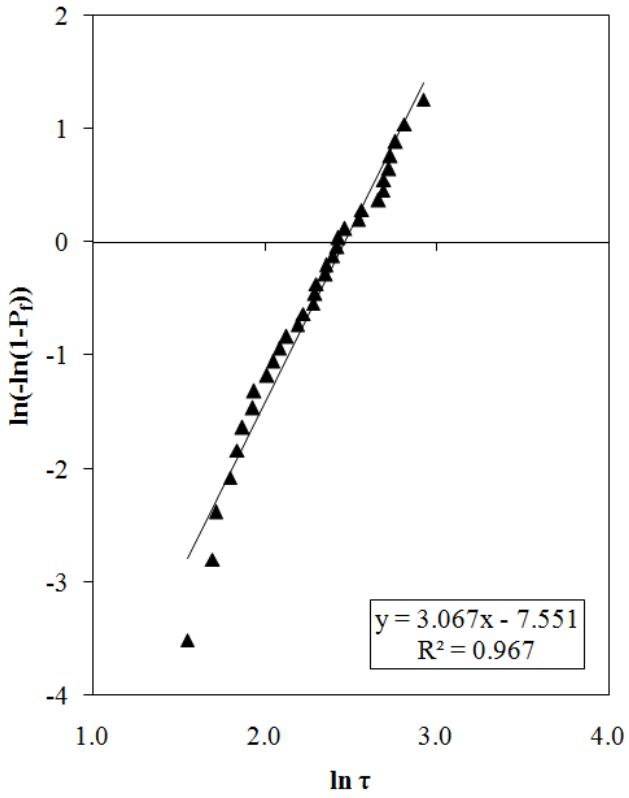

Figure 8.56: Sisal fibres without surface treatment. IFSS plotted as a Weibull distribution.

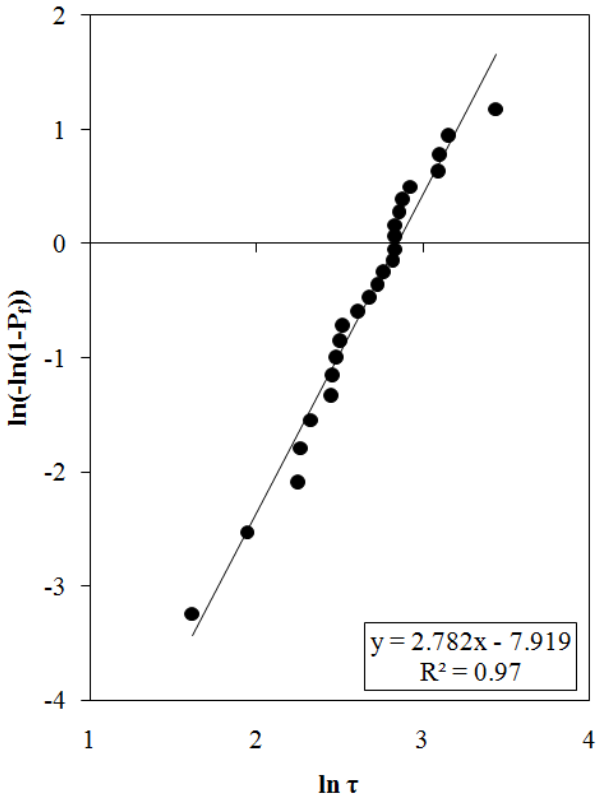

Figure 8.57: Caustic soda treated sisal fibres. IFSS plotted as a Weibull distribution.

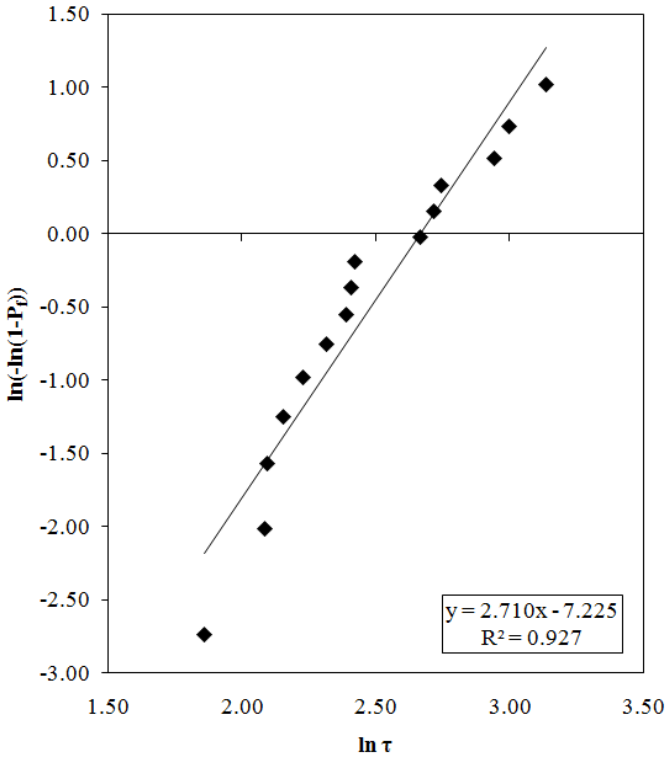

Figure 8.58: Caustic soda treated (6 wt%) sisal fibres. PLA crystalline morphology around the embedded fibre. IFSS plotted as a Weibull distribution.

Weibull parameters which were used to calculate the mean interfacial shear strength and its variation come from the approximation of the cumulative density function with an estimation function *n/(N+1)* where *N* represents the number of samples in the population and *n* has the meaning of the *nth*-rank. The n/(N + 1) estimator gave the best fit of the linear regression of $ln(-(ln-P_f)$ versus $ln\ \tau$. Weibull parameters of the distribution based on other estimators are summarized in the Table 8.14. Weibull parameters estimated with the maximum likelihood method (Cohen, 1965) were also calculated and are included in the Table 8.15.

Table 8.14: Weibull parameters of IFSS calculated with linear regression. Different estimators were used to estimate the probability of failure.

Fibre/matrix	Fibre treatment		n/(N+1)	(n-0.5)/N	(n-0.5)/ (N+0.25)	(n-0.3)/ (N+0.4)
Sisal/PLA	untreated	β	3.067	3.344	3.218	3.262
		δ	11.73	11.66	11.69	11.68
Sisal/PLA	[a]NaOH treated	β	2.783	3.132	2.970	3.026
		δ	17.22	17.04	17.12	17.09
Sisal/PLA	NaOH treated/TCL[b]	β	2.711	3.130	2.935	3.002
		δ	14.37	14.22	14.28	14.26

Note: [a] fibres were treated with a 6 wt% aqueous solution of caustic soda for 48 h; [b] transcrystallinity developed at 104 °C for 2 minutes; [c] number of samples with an adhesion failure;

Table 8.15: Weibull parameters of IFSS calculated with the maximum likelihood method.

Fibre	Treatment	Matrix	N[c]	Weibull modulus β	Characteristic strength δ
			[-]	[-]	[MPa]
Sisal	untreated	PLA	34	3.151	11.734
Sisal	[a]NaOH treated	PLA	26	2.894	17.093
Sisal	NaOH treated/TCL[b]	PLA	15	2.865	14.306

Note: [a] fibres were treated with a 6 wt% aqueous solution of caustic soda for 48 h; [b] transcrystallinity developed at 104 °C for 2 minutes.

It is well known that the maximum likelihood method gives overestimated parameters of Weibull distribution (Bergman, 1985). Figures 8.59-61 show plots of maximum load (F_{max}) reached during the pull-out test versus embedded length (l_e). Each point represents an

individual test. Successful pull out tests with failure at the interface and samples with fibre failure in tension are distinguished.

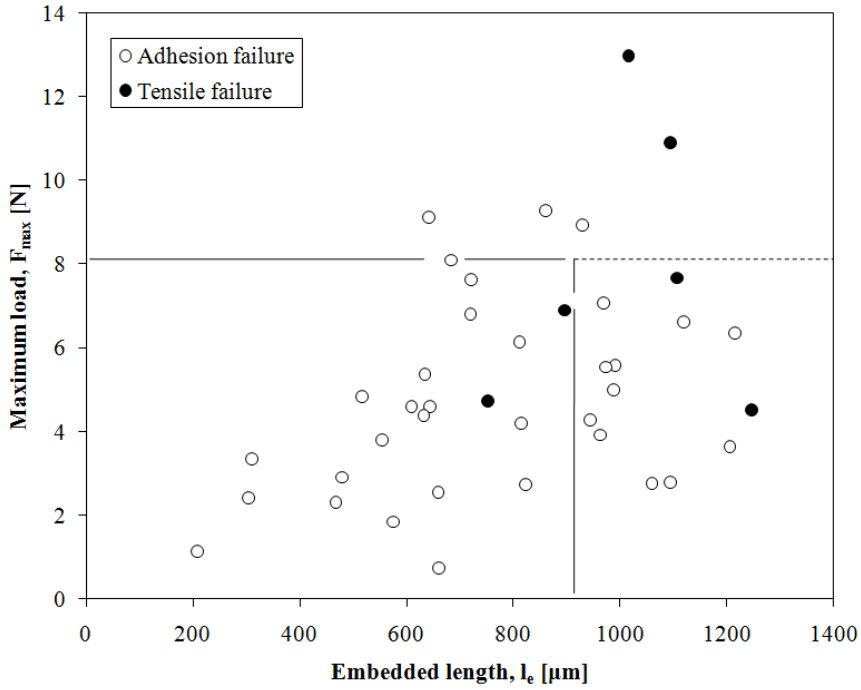

Figure 8.59: Untreated sisal fibres. Plot of maximum load (F_{max}) versus embedded length (l_e). Each point represents an individual test: ○ successful pull out test; ● fibre failure in tension (to emphasise different scales the solid box displays the range of values for Figure 8. 60; the dotted box displays the range of values for figure 8. 61).

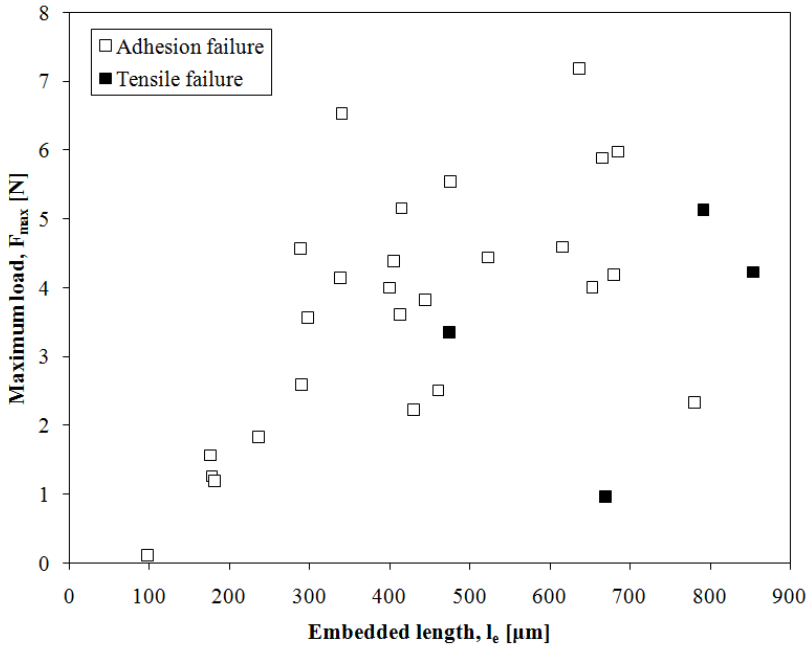

Figure 8.60: Caustic soda treated sisal fibres. Plot of maximum load (F_{max}) versus embedded length (l_e). Each point represents an individual test: □ successful pull out test; ■ fibre failure in tension.

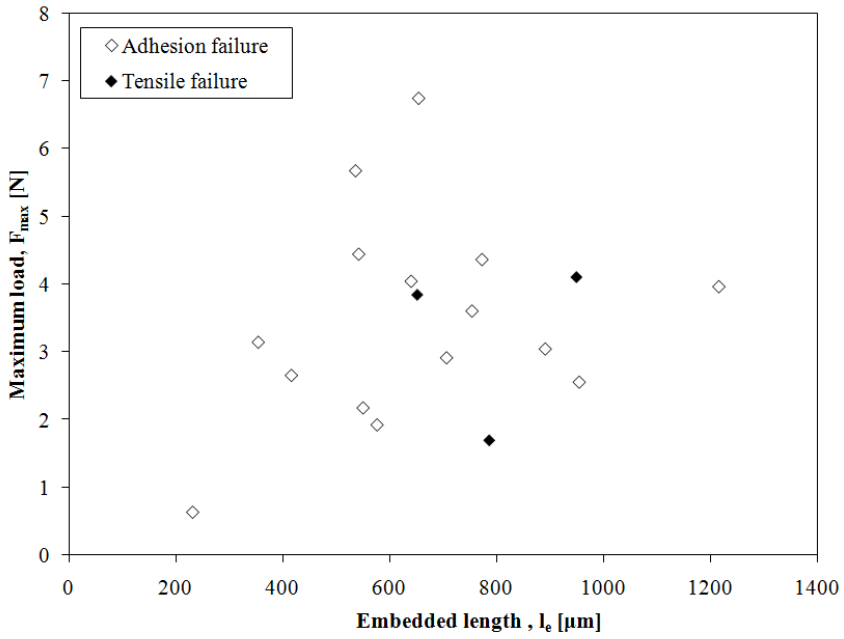

Figure 8.61: Caustic soda treated (6 wt%) sisal fibres. Transcrystalline morphology at the interface. Plot of maximum load (F_{max}) versus embedded length (l_e). Each point represents an individual test: ◊ successful pull out test; ♦ fibre failure in tension.

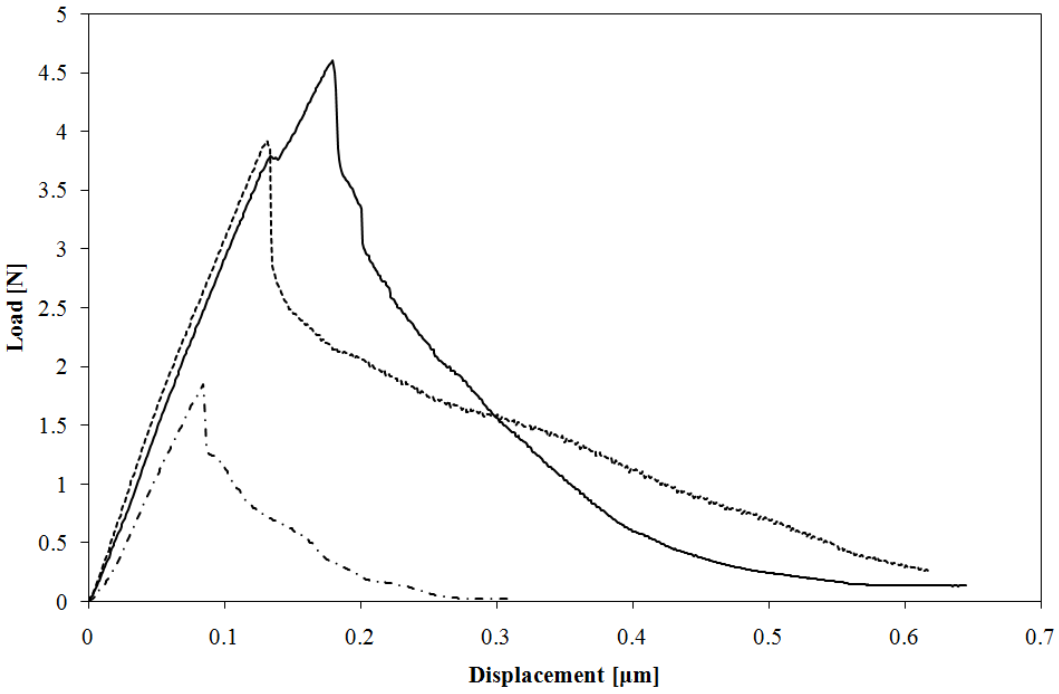

Figure 8.62: Typical load - displacement curves obtained from successful single fibre pull out tests of untreated sisal fibres.

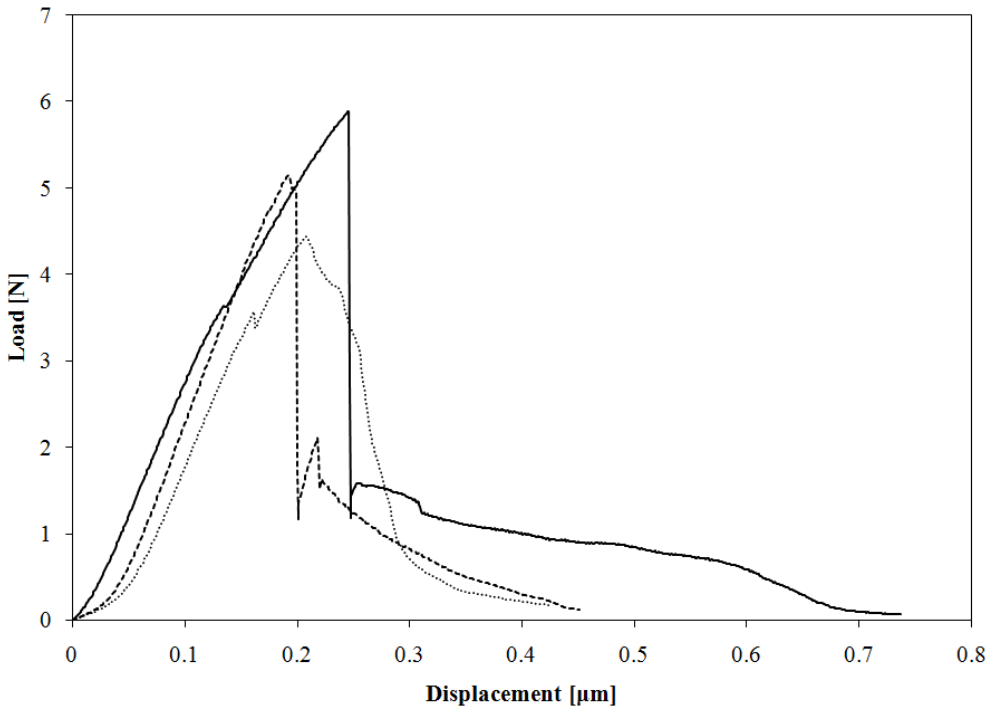

Figure 8.63: Typical load - displacement curves obtained from successful single fibre pull out tests of caustic soda (6 wt%) treated sisal fibres.

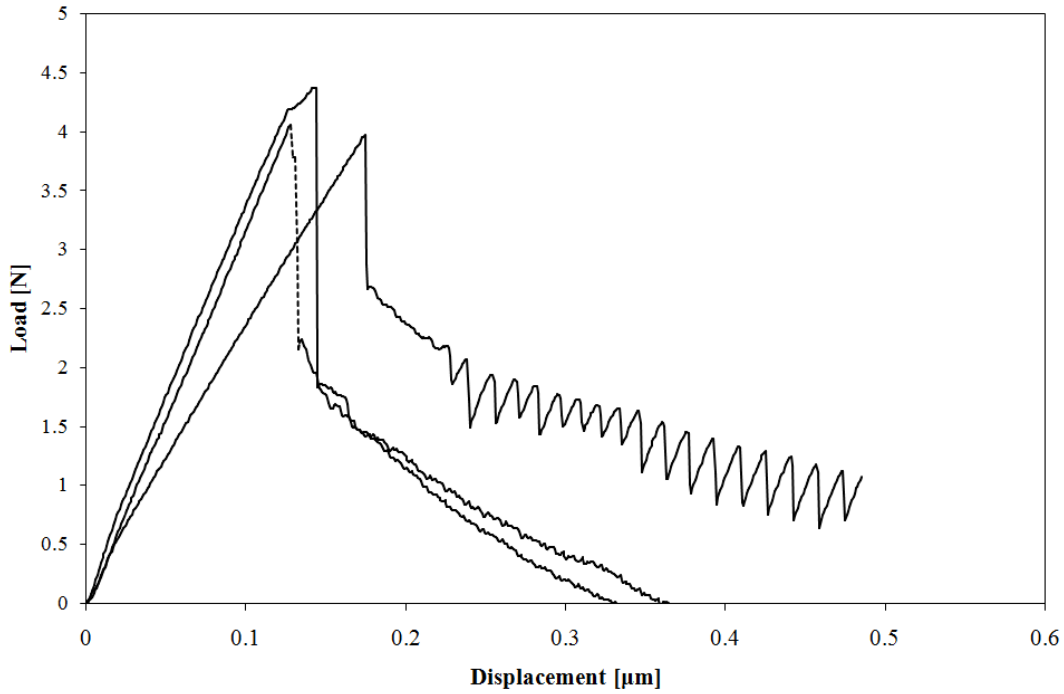

Figure 8.64: Typical load - displacement curves obtained from successful single fibre pull out tests of caustic soda (6 wt%) treated sisal fibres with PLA crystalline morphology around the embedded part of the fibre.

Figure 8.62 shows typical microbond pull out curves for untreated sisal fibres embedded in polylactic acid. Figures 8.63 and 8.64 show typical microbond pull out curves for caustic soda treated (6 wt%) sisal fibres embedded in a PLA matrix with and without crystalline morphology developed after thermal treatment. The maximum debonding forces in each figure are not directly comparable because of the different embedded lengths of the fibres in the matrix. The shape of the curve is similar to those reported by Bannister et al (1995).

At least 30 specimens were tested for untreated and caustic soda treated (6 wt%) sisal fibres and 85 % of pull out tests were successful (interface failure). At least 18 samples of caustic soda treated (6 wt%) sisal fibres embedded in a polylactic acid with crystalline morphology developed were tested and 80 % of the pull out tests were successful (interface failure). The interfacial shear strength for untreated and treated sisal fibres partially embedded in PLA matrix was 10.5 ± 3.72 MPa and 15.3 ± 5.96 MPa, respectively.

Thus caustic soda treatment improved the fibre to matrix adhesion. The interfacial shear strength for treated sisal fibres partially embedded in PLA matrix with transcrystallinity was 12.8 ± 4.96 MPa. The reason for lower IFSS strength compared to caustic soda treated fibres without TCL might be due to the lamellae orientation in the transcrystalline layer. Supposing that non covalent bonds between hydroxyl cellulose groups and polyester PLA groups are responsible for the strength at the interface we can say that the lamellae orientation probably does not favour the creation of non-covalent bonds at the interface. Due to the polylactide chain packing in the lamella the polyester functional groups might be moved apart from the hydroxyl groups of cellulose exposed at the fibre surface so the functional groups are too distant to form a non-covalent bond.

Caustic soda treatment (6 wt%) makes the stress transfer between the polylactic acid and sisal fibre more efficient. Assuming the diameter of an average fibre to be 200 μm and taking the IFSS values for untreated and caustic soda treated sisal fibres from the Table 8.13 and taking the values for fibre strength from Table 8.6 (for example at 20 mm gauge length: untreated sisal ~ 482 MPa and caustic soda treated (6 wt%) ~ 563 MPa) we can calculate the critical fibre length from the Equation 5.13: 4.6 mm for untreated sisal fibres and 3.7 mm for caustic soda (6 wt%) treated sisal fibres.

From the knowledge of the fibre critical length the work of fracture can be calculated (Kelly and Tyson, 1965):

$$\gamma_f = \frac{\sigma_f l_c V_f}{24} \qquad (8.1)$$

Where γ_f is the work of fracture, l_c is the fibre critical length, σ_f is the fibre tensile strength and V_f is the fibre volume fraction. Assuming a composite with a fibre volume fraction 0.6 we get γ_f = 55.5 kJ/m^2 for a composite reinforced with untreated sisal fibres and γ_f = 52.1 kJ/m^2 for a composite reinforced with caustic soda treated sisal fibres. Thus better adhesion results in shorter critical length and reduced toughness. Figure 8.65 shows an SEM micrograph of an untreated sisal fibre embedded in a block of polylactic acid before the pull-out test. Figure 8.66 shows a hole in a matrix block after successful pull-out test.

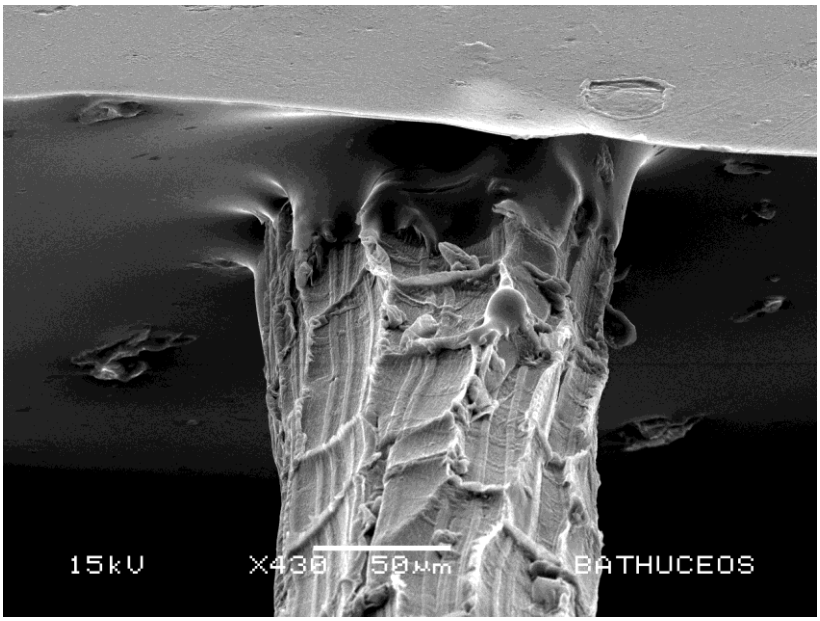

Figure 8.65: Untreated sisal fibre partially embedded in a block of PLA sheet. Single fibre pull out test specimen.

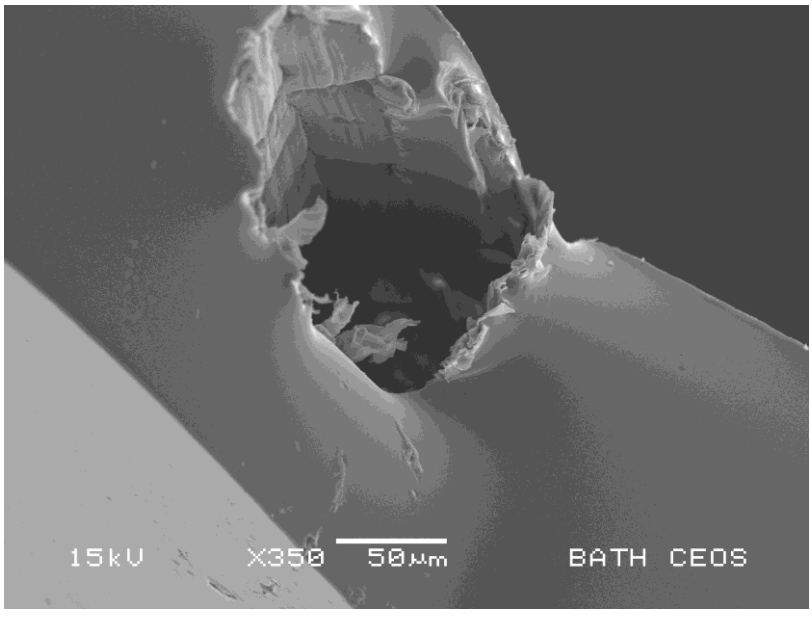

Figure 8.66: A hole in a PLA block after pulling out an untreated sisal fibre.

The axial thermal residual stress in the untreated sisal fibre was estimated to 159 MPa and 241 MPa for 6 wt% caustic soda treated sisal fibres (Equation 5.25). Table 8.16 summarizes constants which were put in equation 5.25. Fibre volume fraction used was: $V_f \approx 3.10^{-6}$ This value was calculated for a single fibre polymer composite by Wagner and Nairn (1997). It seems that the axial thermal residual stress which develops in a fibre during composite processing depends "only" on the modulus of the fibre. When it comes to the semicrystalline matrix there are no data on CLTE as a function of temperature and % of crystallinity. The only member in Equation 5.25 which could deal with the effect of transcrystallinity development is the matrix modulus E_m. But there were no data available on modulus of PLA transcrystalline layer. It could be assumed that the modulus of the transcrystalline layer is no different to the bulk modulus of PLA.

Radial thermal residual stress was estimated from the Equation 5.26. The constants which were put into the Equation 5.26 are summarized in the Table 8.17. Radial thermal residual stress at the fibre surface was calculated as 66.7 MPa. The same value of the radial thermal residual stress was calculated for both untreated and caustic soda (6 wt%) treated sisal fibres due to the constants available for the calculation - because of the scarcity of data in the literature and probably difficulties with measurement of such properties. The value of the radial thermal residual stress is only an estimate: the fibre transverse Poisson's ratio comes from jute fibres (Cichocki and Thomason, 2002).

Table 8.16: Input data for the calculation of axial thermal residual stress in the fibre according to the Equation 5.25 (Zhou et al., 1999) and Energy release rate from Equations 5.23 and 5.24 (Beckert and Lauke, 1997).

Physical property	Sisal fibe (Untreated)	Sisal fibre (Treated[c])	PLA
Young's modulus E (GPa)[a]	17.21	26.05	2.7
CLTE α (10^{-6}.°C^{-1})[b]	15-30	15-30	126-145
Test temperature T (°C)	-	-	22
Stress-free temperature T_{ref} (°C)	-	-	104
Temperature of the melt (°C)	-	-	180

Note: [a]Moduli were taken as an average over all gauge lengths tested (Section 8.2); [b]Data taken from Materials Database CS EDU Pack (2010); [c]Caustic soda aqueous solution (6 wt%).

Table 8.17: Input data for the calculation of radial thermal residual stress at the fibre surface according to the equation (5.26; Di Landro and Pegoraro, 1996).

Physical property		Reference
ε_1 (%)	$\varepsilon_f < \varepsilon_{PLA}$ (2.9 < 5.14)[a]	-
v_m	0.38-0.4	CES EduPack (2010)
v_{af}	0.359 - 0.374	CES EduPack (2010)
v_{tf}	0.01[b]	Cichocki and Thomason (2002)
E_m (GPa)	2.7	-
E_{tf} (GPa)	1.424	Ntenga *et al*. (2008)

Note: υ = Poisson's ratio; E = tensile modulus; subscripts a, f, m and t means axial, fibre, matrix and transverse; [a] strain at break of sisal fibres was put into equation 5.26; [b]jute fibre.

Both the transverse modulus of the fibre E_{tf} and the fibre transverse Poisson's ratio υ_{tf} are literature values calculated from sisal/epoxy laminated composites. The Equation 5.25 was probably originally developed for the single fibre composite (single fibre fully embedded in a polymer matrix). It may not be sensible to put in the equation the strain measured during the pull out test. So the strain of sisal fibre was put in the Equation 5.25 to calculate the radial thermal residual stress because of $\varepsilon_f < \varepsilon_{PLA}$ (2.9 < 5.14).

Table 8.18: Pull-out test. Energy release rate results from Equations 5.23 and 5.24.

Fibre	Matrix	N	Fibre diameter	Load	Strain energy release rate	
					G_{II}	$G_{II} = f(\alpha)$
		[-]	[μm]	[N]	[J/m^2]	[J/m^2]
Untreated sisal	PLA	34	103.7 ± 33.5	4.75 ± 2.27	29.85 ± 8.93	92.53 ± 14.39
Treated sisal[a]	PLA	26	99.7 ± 23.2	3.72 ± 1.77	13.76 ± 6.77	65.1 ± 16.08

Note: [a] fibres were treated with a 6 wt% solution of caustic soda for 48 h; N = number of samples.

Table 8.18 summarizes energy release rates calculated from the pull-out test of untreated and caustic soda treated (6 wt%) sisal fibres calculated from (Equations 5.23 and 5.24). The G_{II} values are quite low suggesting that the interfacial binding energy is not high, perhaps confirmed by the electron micrographs showing pull-out with smooth surfaces (Figure 8.66). Chandra and Ghonem (2001) reported similar G_{II} values on a completely

different fibre-matrix system. The system consisted of titanium based matrices reinforced with silicon carbide fibres.

Figure 8.67 illustrates typical pull-out test curve. The force at which the debonding of the interface starts represents the load to be put into Equations 5.23 and 5.24 to calculate the energy release rate. Unfortunately not all the pull-out curves showed such significant "hump". For example in a pull-out test of caustic soda treated (6 wt%) sisal fibre with transcrystalline morphology of matrix where 20 samples were tested, only at two curves it was possible to distinguish the debonding of the interface. Thus an average maximum force of all samples was put into the equations to calculate the energy release rate. This could be a reason for the huge scatter of the data. Checking the input data for the Equations 5.23 and 5.24 for caustic soda treated sisal fibres and caustic soda treated sisal fibres with crystalline morphology at the interface one can realize that the input data are almost identical in both cases. Equation 5.24 would require the data on CLTE of PLA with transcrystallinity developed and such data were unavailable. Thus the Equation 5.24 does not make difference between the pull-out test system with and without transcrystalline morphology. For the presented reasons it was decided not to calculate the energy release rate for the pull-out test samples with transcrystallinity.

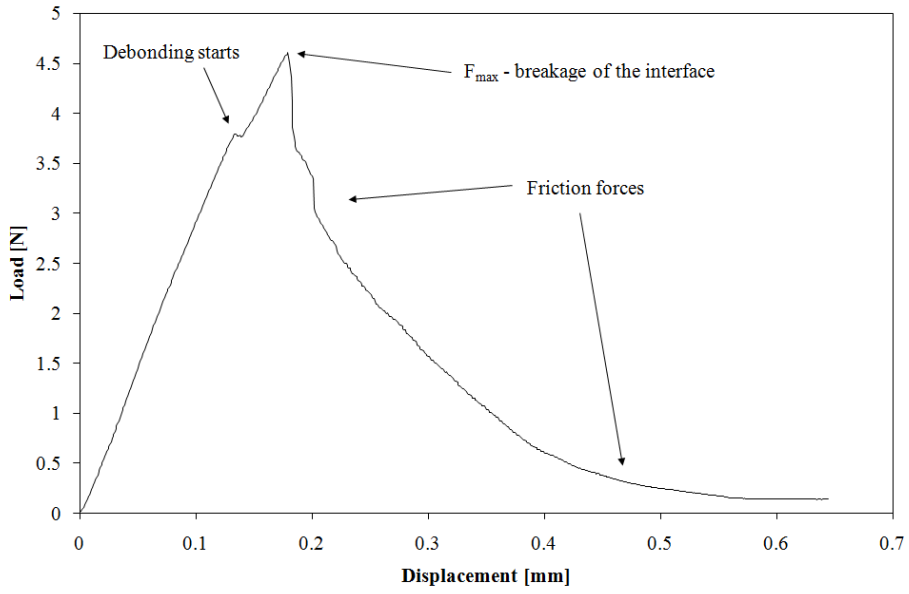

Figure 8.67: Untreated sisal fibre embedded in PLA. Pull-out test curve. Embedded length l_m = 383 μm.

Conclusions:

- Caustic soda treatment (6 wt%) improved the adhesion between the sisal fibres and the PLA matrix. The interfacial shear strength for untreated and treated sisal fibres partially embedded in PLA matrix was 10.5 ± 3.7 MPa and 15.3 ± 6 MPa, respectively.
- The interfacial shear strength for caustic soda treated (6 wt%) sisal fibres partially embedded in PLA matrix with transcrystallinity was 12.8 ± 5 MPa.
- The reason for lower interfacial shear strength in the presence of crystalline morphology might be due to the lamellae orientation in transcrystalline layer. Supposing that non-covalent bonds between hydroxyl cellulose groups and polyester functional groups in polylactide are responsible for the strength at the interface it is possible that the lamellae orientation in the transcrystalline layer probably does not favour the creation of non-covalent bonds at the interface. Due to the polylactide chain packing in the lamella the polyester functional groups might be moved apart from the hydroxyl groups of cellulose exposed at the fibre surface so the functional groups are too distant to form a non-covalent bond.

8.6 Dynamic Mechanical Thermal Analysis

Samples for Dynamic Mechanical Thermal Analysis (DMTA) were cut from compression moulded flat sheets of polylactic acid (PLA) and sheets of PLA reinforced with unidirectional sisal fibre bundles. The samples had the dimensions of 20 x 5 x 1.2 mm. Untreated sisal fibre-polylactic acid composites with fibre volume fractions of 0.4 and 0.6 were tested. Caustic soda treated sisal fibre-polylactic acid composites with fibre volume fraction of 0.6 were also tested. The fibres were treated with aqueous caustic soda solution of 6 wt% concentration for 48 hours. The PLA samples were cut from compression moulded and air quenched sheet. The storage modulus (E’), loss modulus(E’’) and loss tangent (tan δ) were measured as a function of temperature in the range of 25–120°C using a Triton Tritec 2000 DMTA analyzer equipped with a single-cantilever bending fixture (span of 16 mm) at a frequency of 1 Hz and a constant rate of heating of 2°C/min. the glass transition temperature was determined from the maximum of the loss modulus (E’’) and loss factor (tan δ) peaks and from the curve of storage modulus (E’) as a function of

temperature using a tangent construction. A heating rate of 2°/min. was used to avoid artificial damping peaks (Thomason, 1993). A single cantilever fixture was used because flexure modes are more sensitive to changes at the fibre to matrix interface (Dong and Gauvin, 1993). Testing mode also influences the measured glass transition temperature. In a single cantilever fixture the area of specimen under the clamps is lower compared to, for example, a dual cantilever fixture which results in less difference between the sample temperature and that determined by the instrument (Atkinson and Jones, 1996). Figure 8.68 shows the storage modulus of untreated sisal fibre-polylactic acid composites as a function of temperature and fibre volume fraction. It can be observed that the storage modulus at the glass transition region increases with the fibre volume fraction. Figure 8.68 also shows the construction for the determination of onset glass transition temperature (T_g) using a tangent construction. Cold crystallization is responsible for the E' increase above the T_g in the temperature range of 90-100°C (Menard, 1999 and Nielsen and Landel, 1994). The damping in a composite is a function of its constituents, namely fibre, matrix and their interface.

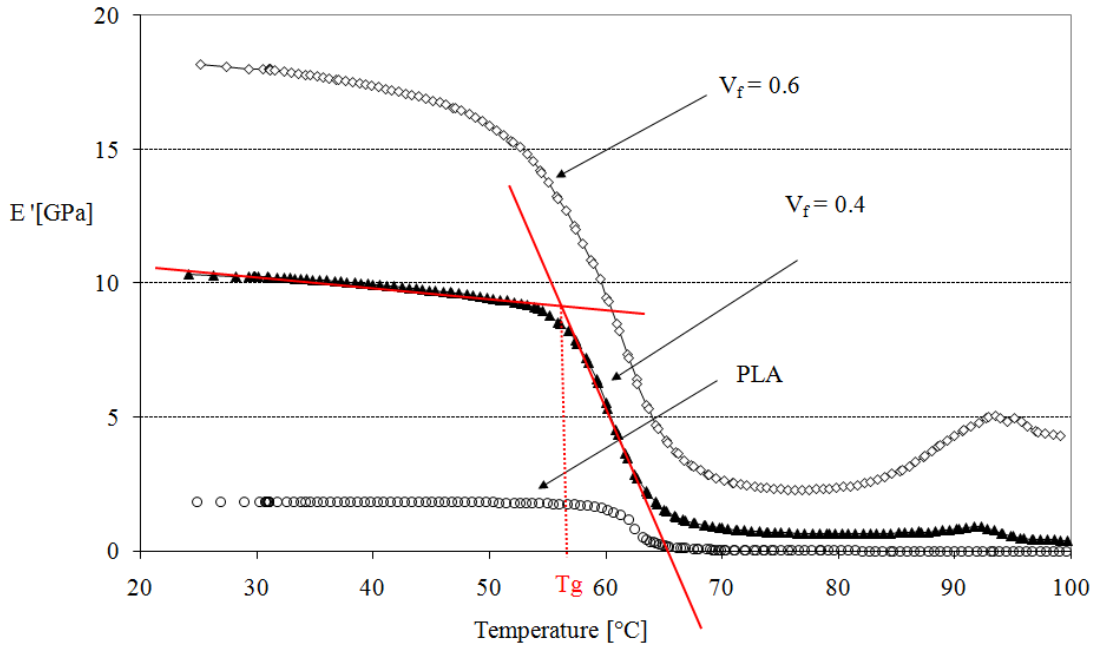

Figure 8.68: Storage modulus of untreated sisal fibre-polylactic acid composites as a function of temperature.

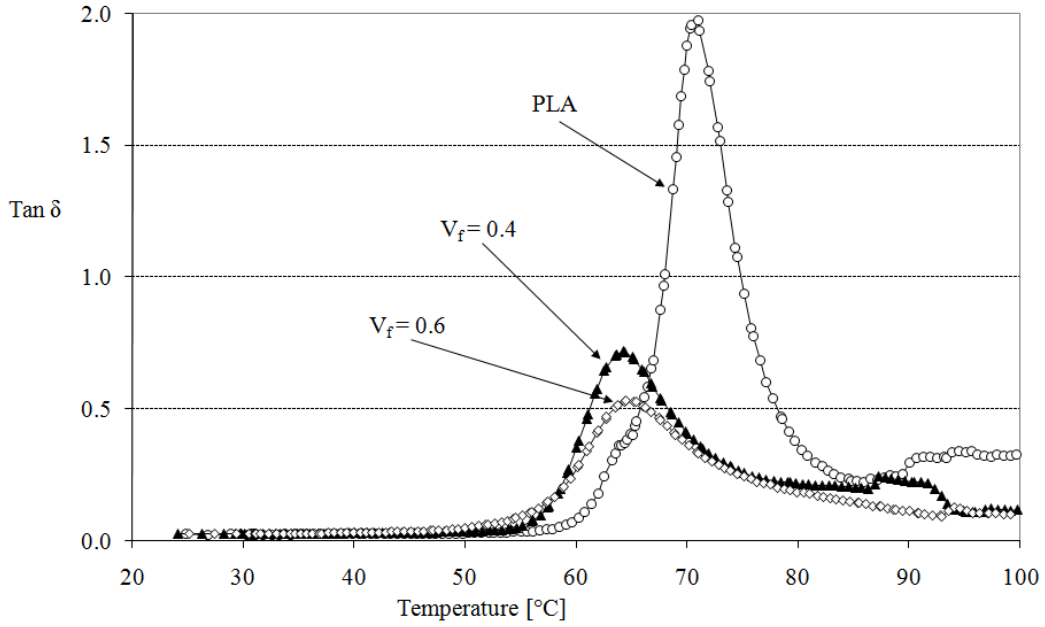

Figure 8.69: Tan δ of untreated sisal fibre-polylactic acid composites as a function of temperature.

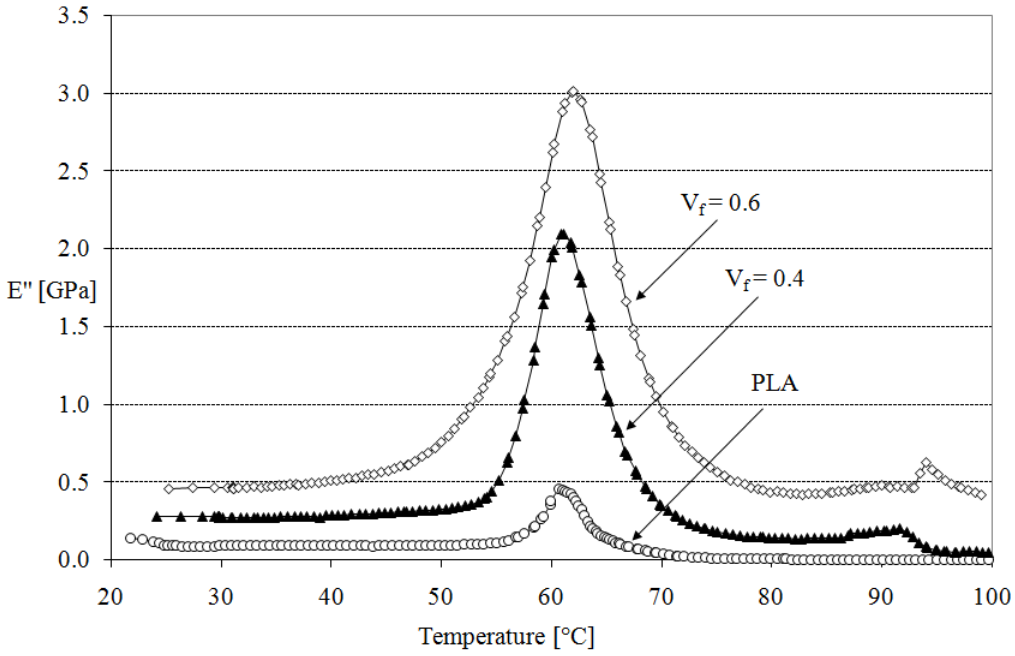

Figure 8.70: Loss modulus of untreated sisal fibre-polylactic acid composites as a function of temperature.

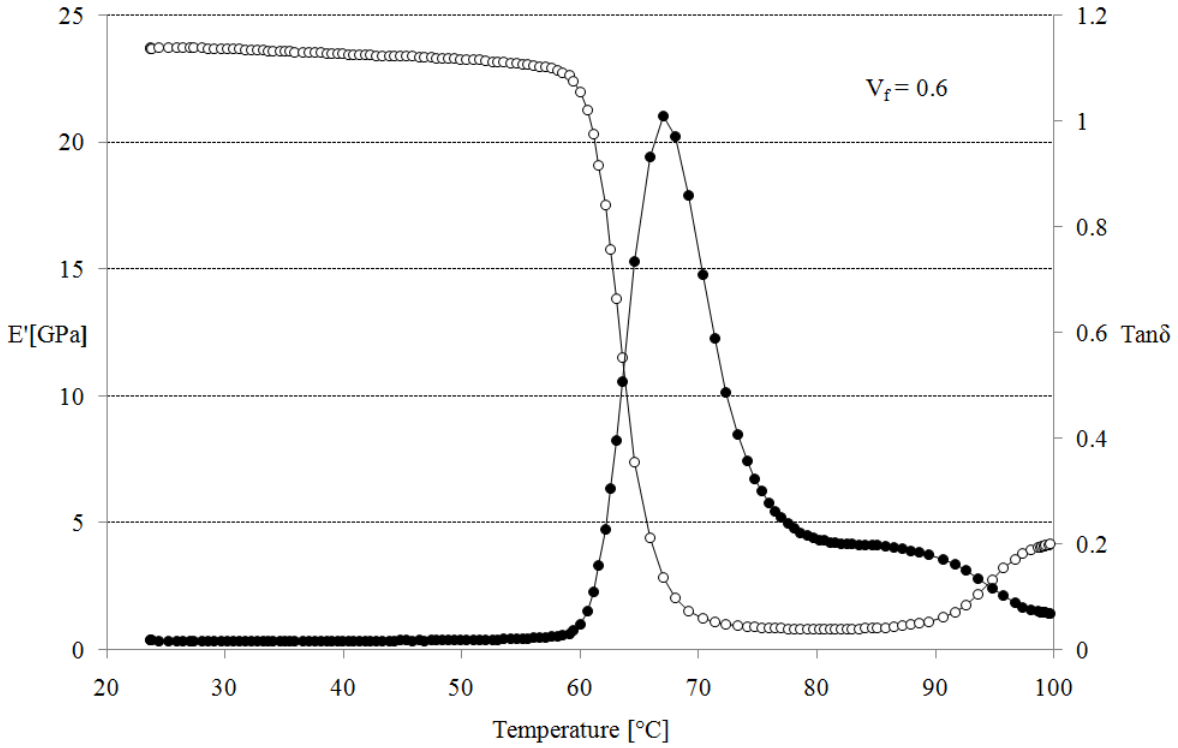

Figure 8.71: Storage modulus and tan δ of caustic soda treated sisal fibre-polylactic acid composites as a function of temperature (V_f = 0.6; treatment = aqueous 6 wt% solution / 48 hours).

Zorowski and Murayama (1971) and Murayama and Lawton (1973) were probably the first to characterize fibre to matrix adhesion using dynamic mechanical measurements and related the energy dissipation (tan δ) to poor fibre to matrix adhesion. Thus composites with good fibre to matrix adhesion tend to dissipate less energy compared to the ones with poor interfacial adhesion (Edie *et al.*, 1993). The damping peak of the composites reinforced with untreated sisal fibres is lower compared to the neat polylactic acid and its maximum is shifted to lower temperatures (Figure 8.69). Figure 8.70 shows the variation of the loss modulus with temperature for polylactic acid and composites reinforced with untreated sisal fibres with the fibre volume fraction of 0.4 and 0.6. Loss modulus as well as tan δ are sensitive to the molecular motions at fibre to matrix interface and thus reflect the quality of the adhesion. Figure 8.70 shows that the maximum of the loss modulus peak decreases with the fibre volume fraction. Composites with higher fibre volume fractions have larger interfacial area and thus more energy is lost at the interface. Figure 8.71 shows the storage modulus and tan δ of caustic soda treated sisal fibre-polylactic acid composites as a function of temperature. The fibre volume fraction of the composites was 0.6.

Table 8.19: Determination of glass transition temperature of PLA.

Experimental method*	Glass transition temperature (T_g)**	
		[°C]
DMTA	T_g (E")$_{max}$	60.7
	T_g (tan δ)$_{max}$	69.4
	T_{mg}	60
	T_{eig}	58.4
	T_{efg}	63.9
DSC	T_{mg}	61
	T_{eig}	60
	T_{eif}	-

Note: *Procedures of T_g determination are explained in sections 6.3 and 6.4; ** subscripts: g = glass, m = midpoint, e = extrapolated, i = initial, f = final.

Tables 8.19 and 8.20 compare glass transition temperatures and degree of crystallinity χ (%) as determined from DSC and DMTA. The procedure of T_g determination is explained in sections 6.3 and 6.4 of this thesis. The extrapolated initial glass transition temperature (T_{eig}) is highlighted because it is widely used for T_g determination. It is often called the "tangent method". As can be seen from Table 8.19 it is always important to mention the procedure for the determination of T_g.

Table 8.20: Degree of crystallinity in PLA.

Experimental method	Degree of crystallinity (χ)
	[%]
DMTA[a]	15.9
DSC	17.7[b]
	8.5[c]

Note: [a]according to Khanna (1989); [b] air quenched compression moulded sample allowed to cool down at room temperature; [c] quenched in iced water after compression moulding.

Table 8.21: Storage modulus as a function of temperature. PLA reinforced with sisal fibres.

Matrix	Fibre	Fibre treatment	V_f	E' (25°C)	E' (40°C)	E' (60°C)
				[GPa]	[GPa]	[GPa]
PLA	-	-	-	1.9	1.8	1.5
PLA	sisal	-	0.4	10.3	10	5.5
PLA	sisal	-	0.6	18.2	17.4	9.5
PLA	sisal	caustic soda*	0.6	23.7	23.5	22

Note: * fibres treated with aqueous caustic soda solution of 6 wt% concentration for 48 hours.

Table 8.21 demonstrates the decrease of storage modulus with increasing temperature in the temperature range of 25 to 60°C. The positive effect of fibre volume fraction as well as caustic soda treatment on the storage modulus depression within the glass transition is obvious. Table 8.22 summarizes the glass transition temperatures of untreated and caustic soda treated sisal fibre-polylactic acid composites. Comparing the T_{eig} of composites with untreated sisal fibres with the T_{eig} of neat PLA it can be concluded that the addition of fibres to the matrix leads to the depression of the glass transition temperature. In the case of composites with caustic soda treated sisal fibres the glass transition temperature is slightly higher than that of polylactic acid.

Table 8.22: Glass transition temperature determined from DMTA scans. PLA reinforced with sisal fibres.

Glass transition temperature*	PLA	PLA/sisal	PLA-sisal	PLA/treated sisal***
[°C]		(V_f = 0.4)	(V_f = 0.6)	(V_f = 0.6)
T_g $(E'')_{max}$	60.7	60.9	62	63.7
T_g $(\tan\delta)_{max}$	69.4	64.3	64.5	67.0
T_{mg}	60	60.4	60	63.9
T_{eig}	58.4	56.1	53.5	60.0
T_{efg}	63.9	64.8	66.3	65.8
$(T_{ef}-T_{ei})_g$	5.5	8.7	12.8	5.8

Note: *Procedures of T_g determination are explained in section 6.4; ** subscripts: g = glass, m = midpoint, e = extrapolated onset, i = initial, f = final; *** fibres treated with aqueous caustic soda solution of 6 wt% concentration for 48 hours.

The reason could be the improved adhesion between caustic soda treated fibres and the polymer matrix or the development of crystalline morphology at the fibre to matrix interface during compression moulding. The last row of the table 8.22 compares the width

of the glass transition region given as the difference of extrapolated onset temperatures. The glass transition of caustic soda treated sisal fibre-polylactic acid composites is narrower compared to the composites with untreated sisal fibres.

Dong and Gauvin (1993) observed that the damping of epoxy/glass fibre composites decreased with the fibre volume fraction. It was explained by the difference in coefficients of linear thermal expansion (CLTEs) between the fibres and the matrix. The CLTE of the matrix is higher than the CLTE of the fibres. During processing at elevated temperatures the matrix expansion is restrained by the fibres and so is the molecular motion at the interface.

Comparing the tan δ of untreated and caustic soda treated sisal fibre-PLA composites (Figures 8.69 and 8.71) it can be seen that the damping at the caustic soda treated fibres-PLA interface is reduced. It could be caused by the presence of transcrystallinity which has a specifically organized morphological structure which possibly restrains the motion of polymer chains at the interface.

The modulus depends on the degree of crystallinity and the morphology of the crystals. The damping in semicrystalline polymers is complex because the temperature of $(\tan \delta)_{max}$ shifts with crystallinity in some polymers and not in others (Nielsen and Landel, 1994).

Conclusions:

- Sisal fibre reinforcement in a polylactic acid matrix significantly improved the storage modulus of polylactic acid below and above the glass transition temperature.
- It is inferred from DMTA experiment that cold crystallization raises the Tg of PLA.
- The glass transition temperatures (T_{eig}) decreased with increasing fibre volume fraction in composites reinforced with untreated sisal fibres.
- The glass transition temperature (T_{eig}) of composites reinforced with 60 % of caustic soda treated sisal fibres was higher compared to polylactic acid and composites reinforced with untreated sisal fibres.
- The damping at the caustic soda treated fibres-PLA interface was reduced probably due to the presence of transcrystalline morphology at fibre to matrix interface.
- Addition of fibres into the PLA matrix increases the damping at the fibre to matrix interface.

- The damping peak of the composites reinforced with untreated sisal fibres is lower compared to the neat polylactic acid and its maximum is shifted to lower temperatures.
- Comparing the tan δ of untreated and caustic soda treated sisal fibre-PLA composites it is observed that the damping at the caustic soda treated fibres-PLA interface is reduced. The damping reduction could be explained by the development of transcrystallinity or by thermal stresses built up during processing.

8.7 The stress-strain relationship for sisal fibres evaluated by Raman micro-spectroscopy

Caustic soda treated (6 wt%) and untreated sisal fibres were soaked in a hydrogen peroxide aqueous solution of 3 wt% concentration prior to examination by Raman spectroscopy in order to suppress the effect of fluorescence in the fibre. Fibres were mounted to supporting paper card-frames with a cyanoacrylate adhesive. The gauge length of the mount tabs was 10 mm (See Section 6.8). The mount tabs with fibres were glued to the aluminium blocks of the strain rig which was placed on the stage of an Olympus BH-2 microscope. The straining rig was fitted with a micrometer to strain the fibres in incremental steps. Prior to fibre straining the lateral part of the paper mount cards were burnt with a soldering iron. Raman spectra were collected with a Renishaw 1000 Raman imaging microscope during the fibre deformation in air. A He-Ne laser (633 nm; 25 mW) was used. When focused on the fibre surface the spot size was about 2 μm in diameter and with a power of about 1 mW. The peak position of the strain sensitive 1095 cm^{-1} Raman band was used to map the strain/stress profiles at several levels of strain applied to the fibre. The deformation rig was equipped with a micrometer for increasing the strain and with a high precision load cell to measure the load on the fibre. It took about 120 s to collect a spectrum at individual strain/stress levels. The back-scattered light was collected with the 50x objective lens of the Olympus microscope. The excited Raman radiation was then filtered using a holographic notch filter. The resultant radiation was converted to a spectrum with a diffraction grating. A highly sensitive Peltier cooled CCD detector recorded all the spectra. The spectra were collected on a computer with Renishaw software. The spectra were curve fitted with a Lorentzian-Gaussian distribution function to determine the peak position based on a mathematical algorithm (Marquardt, 1963). The stress in the fibre was calculated from the known load exerted on the fibre and the average cross-sectional area computed from the fibre length, weight and density (Equation 6.2). Figure 8.72 shows the Raman spectrum for an untreated sisal fibre with no strain applied to the fibre with a peak at 1095 cm^{-1}. The peak is seen to shift to the left under the application of a strain of 3.8%. A similar shift can be observed in Figure 8.73 which represents 1095 cm^{-1} Raman band peaks for strained (3%) and unstrained sisal fibre treated with caustic soda (6 wt%).

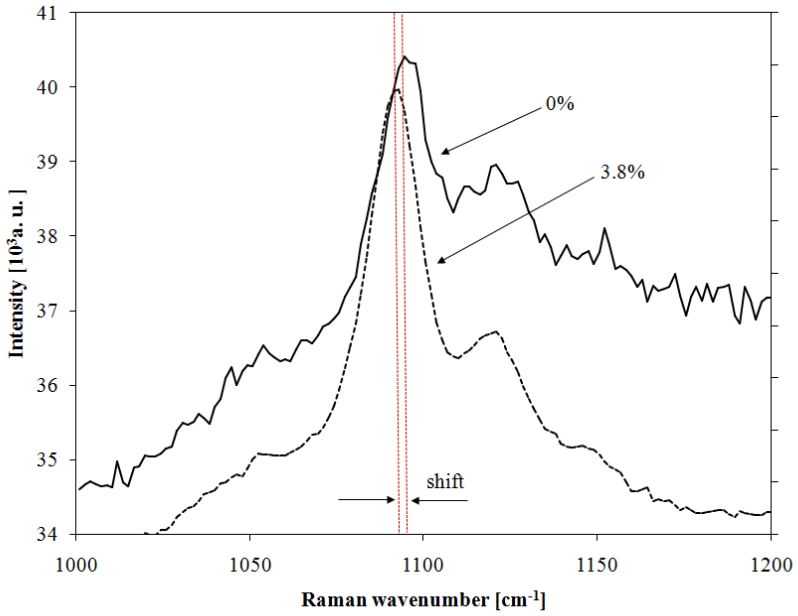

Figure 8.72: Shift in the 1095cm^{-1} peak of the Raman spectrum for untreated sisal fibres following the application of 3.8% strain. Red dotted lines indicate the strain induced shift.

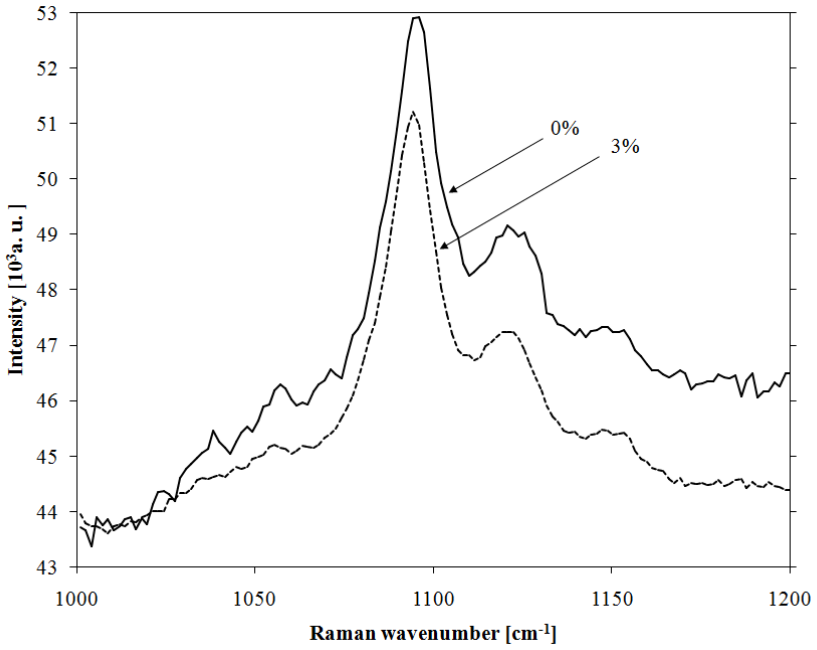

Figure 8.73: Shift in the 1095cm^{-1} peak of the Raman spectrum for caustic soda treated (6 wt%) sisal fibres.

In Figure 8.74 a typical Raman frequency shift is plotted as a function of applied strain for the 1095 cm^{-1} band of the untreated sisal fibre spectrum and a linear relationship is obtained.

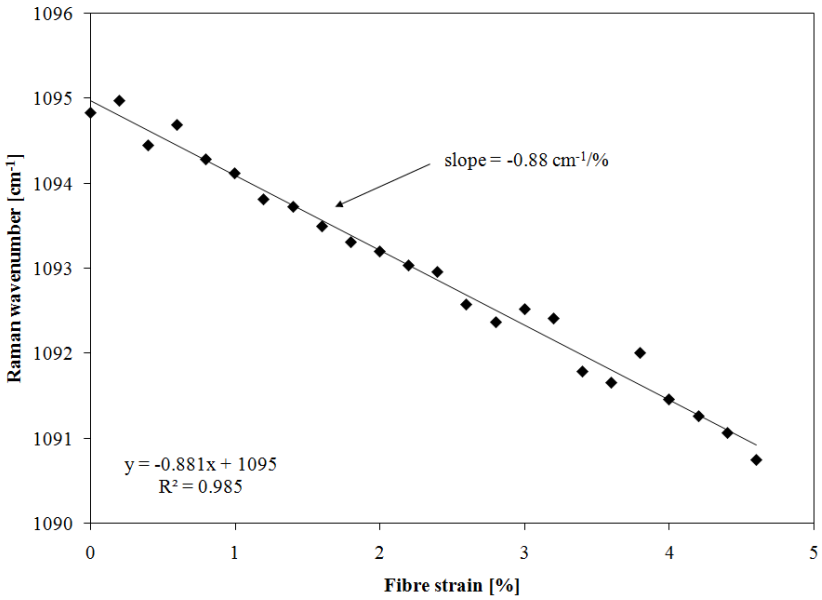

Figure 8.74: Shift in the peak position of the 1095cm^{-1} Raman band as a function of fibre strain for an untreated sisal fibre.

Figure 8.75-78 display the Raman band shift Δv as a function of tensile strain/stress for untreated and caustic soda (6 wt%) treated sisal fibres. The 1095 cm^{-1} peak was found to shift linearly with applied strain/stress towards lower wave numbers for both untreated and caustic soda treated sisal fibres.

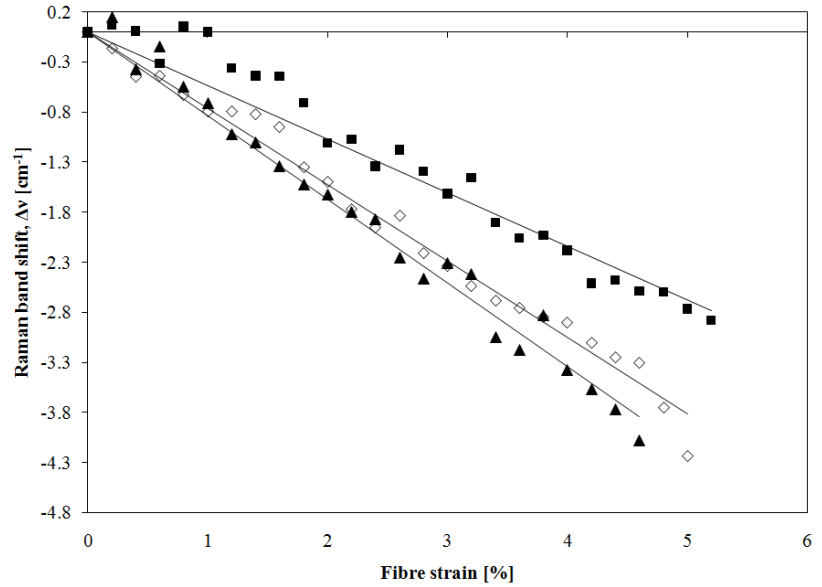

Figure 8.75: Incremental shift in the peak position of the 1095cm^{-1} Raman band as a function of fibre strain for three untreated sisal fibres as a function of the fibre strain.

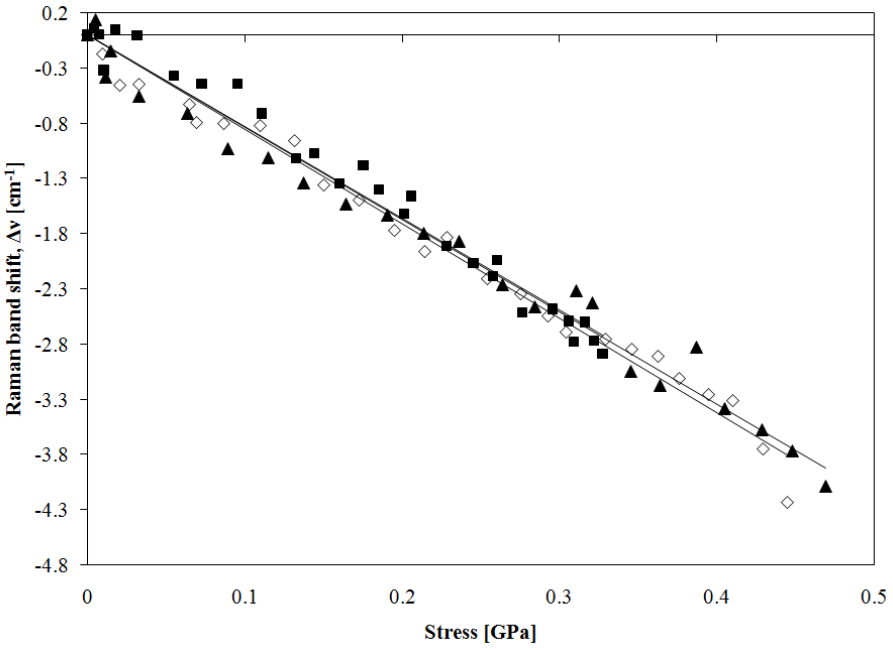

Figure 8.76: Shift in the peak position of the 1095cm^{-1} Raman band for untreated fibres as a function of fibre stress.

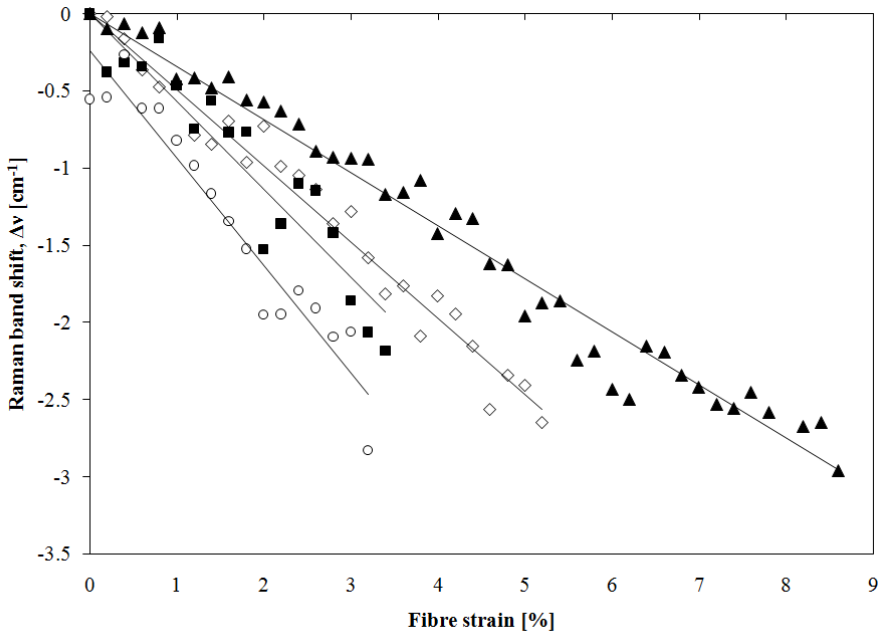

Figure 8.77: Shift in the peak position of the 1095cm^{-1} Raman band for four caustic soda treated (6 wt%) sisal fibres as a function of the fibre strain.

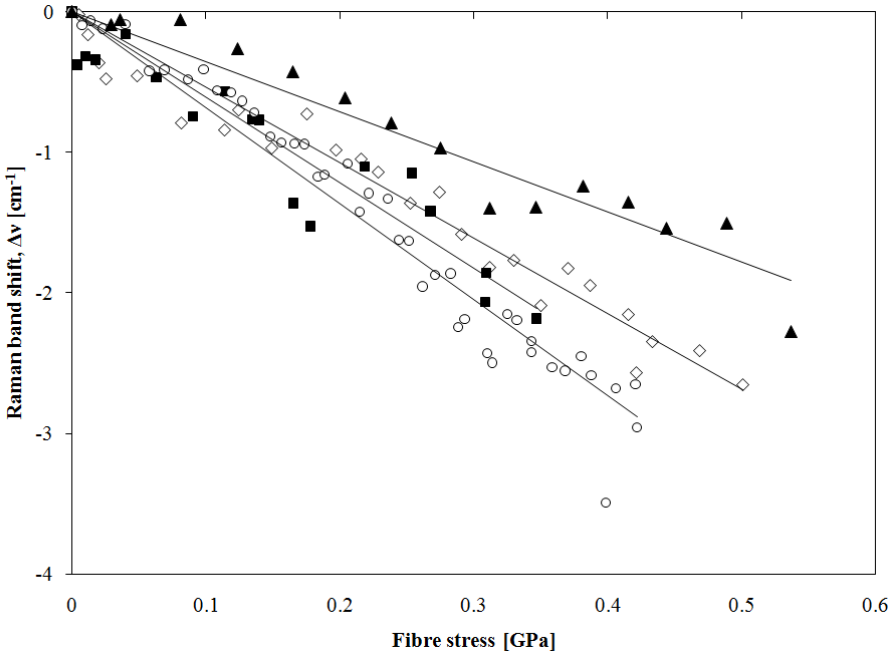

Figure 8.78: Shift in the peak position of the 1095cm^{-1} Raman band for caustic soda treated (6 wt%) sisal fibres as a function of the fibre stress.

The strain sensitivities of the Raman bands as well as the stress sensitivities are summarized in Table 8.23.

Table 8.23: Stress and strain sensitivity and fibre modulus of untreated and caustic soda treated (6 wt%) sisal fibres.

Fibre	d(Δν)/dε	d(Δν)/dσ	E
-	[cm^{-1}/%]	[cm^{-1}/GPa]	[GPa]
Untreated	-0.71±0.16	-8.40±0.14	6.4-10
Treated	-0.52±0.15	-5.46±1.40	5.0-9.5

The values represent the means of three sets of measurements for the untreated and four for caustic soda treated sisal fibres. The sensitivity of the Raman band shift to strain was found to be proportional to the fibre modulus *E*. The Young's modulus can be calculated from the stress and strain sensitivity of Raman wave number according to the following relationship (Eichhorn and Young, 2001):

$$E = \frac{d\sigma}{d(\Delta\nu)} \times \frac{d(\Delta\nu)}{d\varepsilon} = \frac{d\sigma}{d\varepsilon} \qquad (8.2)$$

The results of the evaluation of the elastic properties of sisal fibres with Raman spectroscopy are summarized in Table 8.23. The large difference in the Young's modulus determination is probably due to the variability of properties of natural fibres. In a tensile test the fibre is continuously strained with a rate of 1mm/min but in a Raman spectroscopy experiment cellulosic fibres are strained step by step and each straining increment requires about 150 seconds including 30 seconds for focusing and 120 seconds for spectrum collection (Eichhorn et *al*., 2001). If the fibre is, for example, strained with 30 increments of 0.2 μm before it breaks it takes about one and half hour to break the fibre. The fibre is strained very slowly and stepwise it may stress relax. The elastic moduli of untreated sisal fibres range from 6.4 to 10 GPa. For caustic soda treated sisal fibres the modulus of elasticity ranges from 5 to 9.5 GPa with one fibre having a modulus of 19.5 GPa. Measured moduli are in agreement with the values reported in literature which are 9-22 GPa (Mwaikambo, 2006). Sisal fibres are less strain sensitive compared to artificial fibres such as carbon fibres or aramid fibres. The Raman band shift in tension for carbon fibres is reported to be -24.2 cm^{-1}/% for the 2660 cm^{-1} Raman band (Huang and Young, 1996) and for aramid fibres it is 4.6 – 4.9 cm^{-1}/% (Bennett and Young, 1997) for the 1610 cm^{-1} Raman band. The Raman band shift in tension for hemp, flax and wood were reported to be -1.29, -1.22 and -1.14 cm^{-1}/% for the 1095 cm^{-1} Raman band (Eichhorn and Young, 2001). The strain sensitivity of untreated sisal fibres is similar to that of cellulose acetate. Cellulose acetate has a strain sensitivity of -0.88 cm^{-1}/% (Eichhorn and Young, 2001).

Stress was also mapped along the untreated sisal fibre partially embedded in the polylactic acid matrix. The fibre was subjected to an external strain of 0, 1 and 1.5% and the Raman band shift was recorded as a function of position along the fibre. The frequency shift was converted into the local stress along the embedded fibre (Figure 8.79 and 8.80). The measured axial stress in the fibre was the residual compressive stress due to the matrix shrinkage. The average fibre axial compressive stress was 153.4±17.1, 155±17.3 and 159±10 MPa at fibre external strain of 0, 1 and 1.5%. Grubb and Li (1994) used Raman spectroscopy to calculate the axial compressive residual stress in high modulus polyethylene fibres embedded in epoxy resin. The residual compressive stress was found to be 0.3 GPa. Figure 8.81 and 8.82 show theoretically calculated strain and shear stress distribution along the untreated and caustic soda (6 wt%) treated sisal fibre partially embedded in PLA matrix (see Equation 5.18 and 5.20).

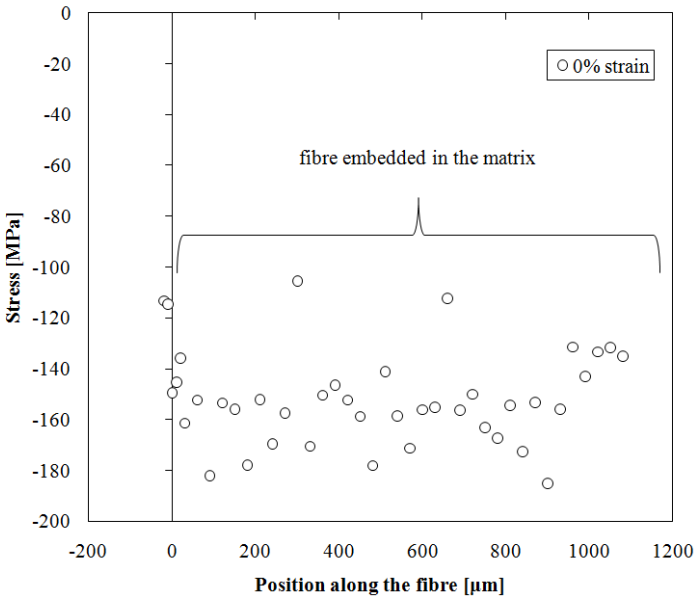

Figure 8.79: Axial stress in an untreated sisal fibre partially embedded in a polylactic acid as a function of position along the embedded fibre at an external strain of 0 %.

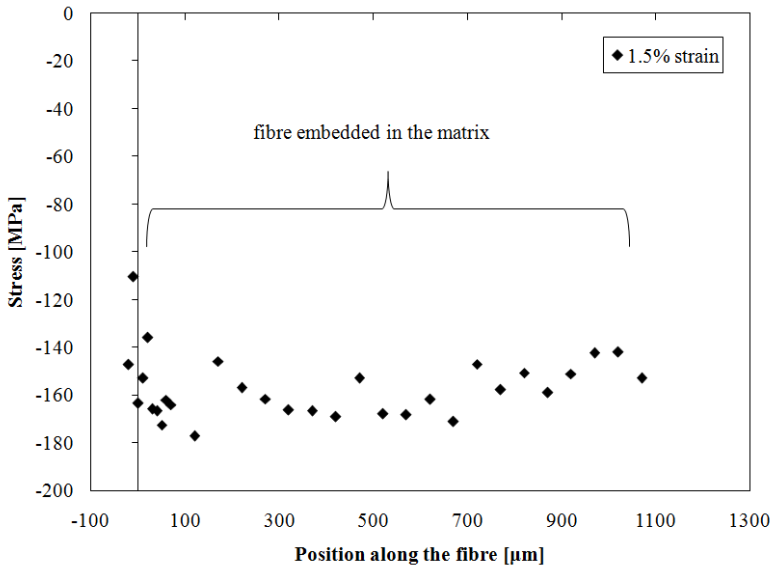

Figure 8.80: Axial stress in an untreated sisal fibre partially embedded in a polylactic acid as a function of position along the embedded fibre at an external strain of 1.5 %.

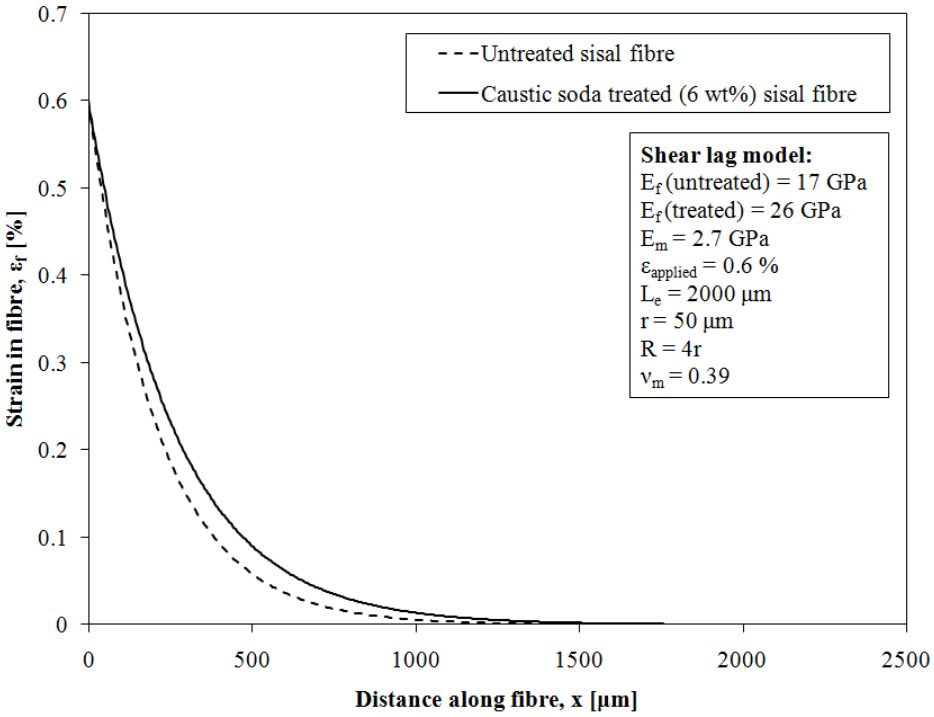

Figure 8.81: Theoretically calculated strain distribution along the sisal fibres partially embedded in PLA matrix. Fibre moduli taken from the Table 8.4 as an average over all gauge lengths tested.

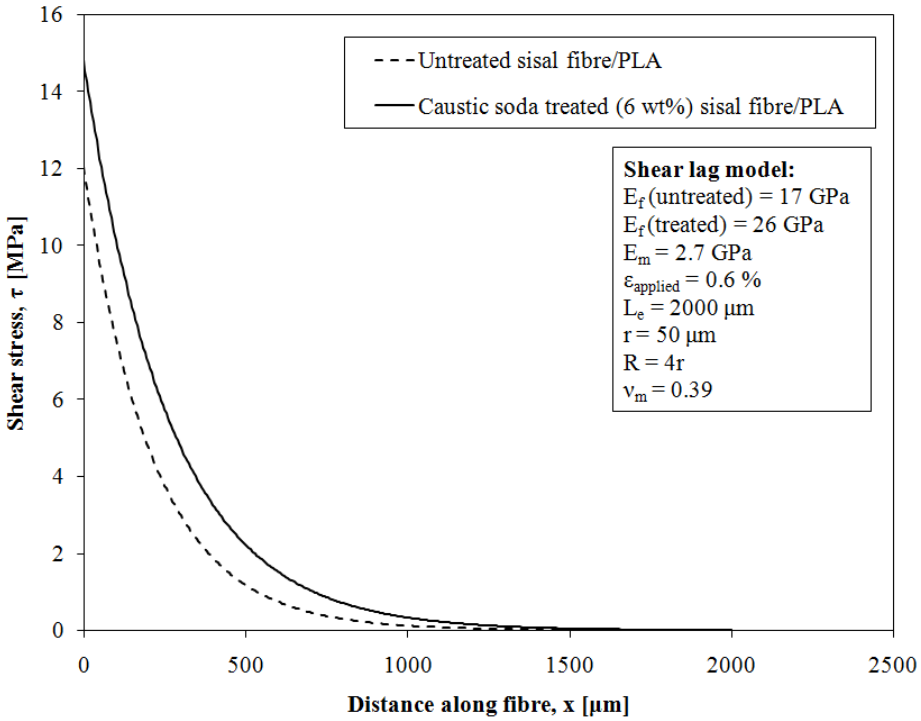

Figure 8.82: Theoretically calculated shear stress distribution along the sisal fibres partially embedded in PLA matrix. Fibre moduli taken from the Table 8.4 as an average over all gauge lengths tested.

Conclusions:

- The Young's modulus of sisal fibres determined from Raman spectroscopy lies within the values reported in the literature.
- Large scatter in the Young's modulus values determined from Raman spectroscopy could be explained by the variability in properties of natural fibres as well as the small sample size.
- The Young's modulus of sisal fibres determined by a tensile test (see Section 8.2) gave higher values compared to those obtained through Raman spectroscopy. Raman micro-spectroscopy is employed at considerably lower strain rates compared to conventional tensile fibre tests. Thus the fibres may have time to accommodate to the applied strain/stress resulting in a reduced Young's modulus.
- Sisal fibres are less strain sensitive compared to artificial fibres, for example, carbon fibres or aramid fibres.
- Caustic soda treated (6 wt%) sisal fibres were found to be less strain sensitive compared to untreated sisal fibres.
- The residual axial compressive stress in untreated sisal fibres determined from Raman spectroscopy (153-159 MPa) is in agreement with the theoretically calculated value (159 MPa).

8.8 Mechanical properties of composites

This Section summarizes mechanical properties of compression moulded composites of polylactic acid reinforced with untreated and caustic soda treated sisal fibres. Composites were tested in three point bending, short beam shear and tension.

Composites sheets for mechanical testing were manufactured by compression moulding. The details of the manufacturing process are discussed in Section 7.4.

Sections of compression moulded composites were taken and microscopically inspected (Figure 8.83-85). Prior to SEM evaluation the samples were coated with gold by means of plasma sputtering apparatus (Edwards Sputter coater model S 150 B). An accelerating voltage of 10 kV was used to limit the loss of surface detail in the micrographs resulting from excessive depth of penetration of the electron beam within the polymeric samples.

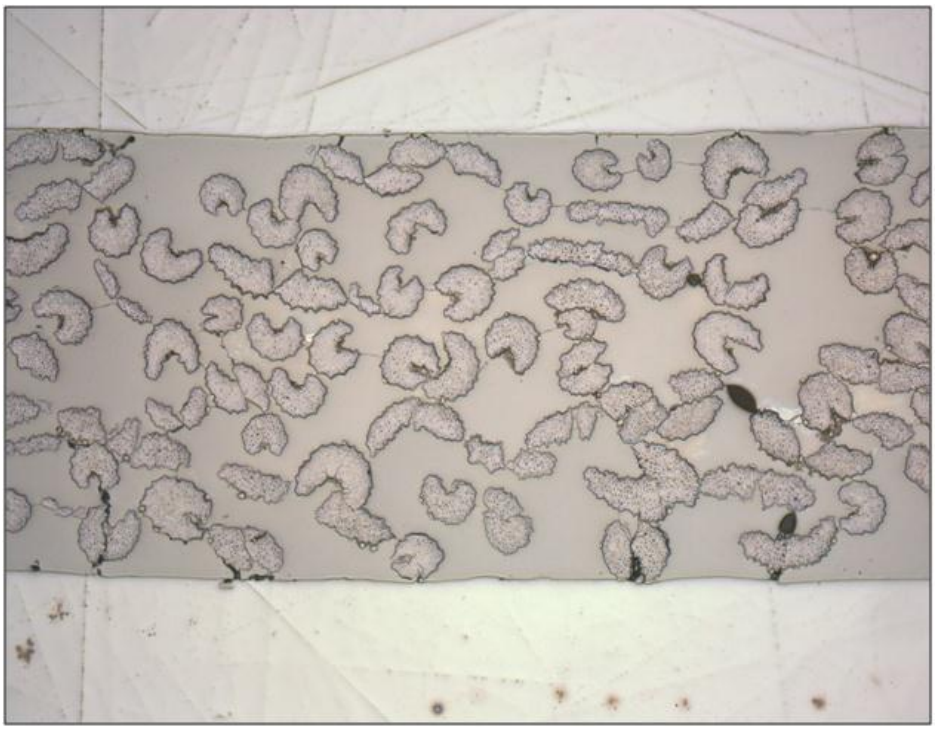

Figure 8.83: Reflected light micrograph of a cross section through a specimen of PLA reinforced with V_f = 0.4 of untreated sisal fibres at 50x magnification.

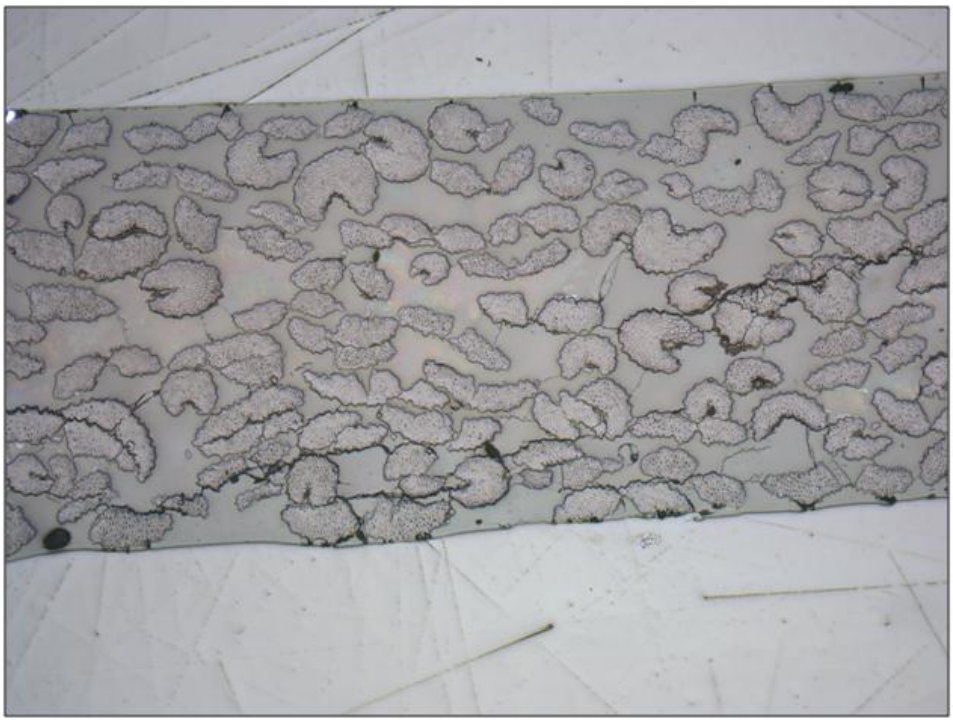

Figure 8.84: Reflected light micrograph of a cross section through a specimen of PLA reinforced with V_f = 0.6 of untreated sisal fibres at 50x magnification.

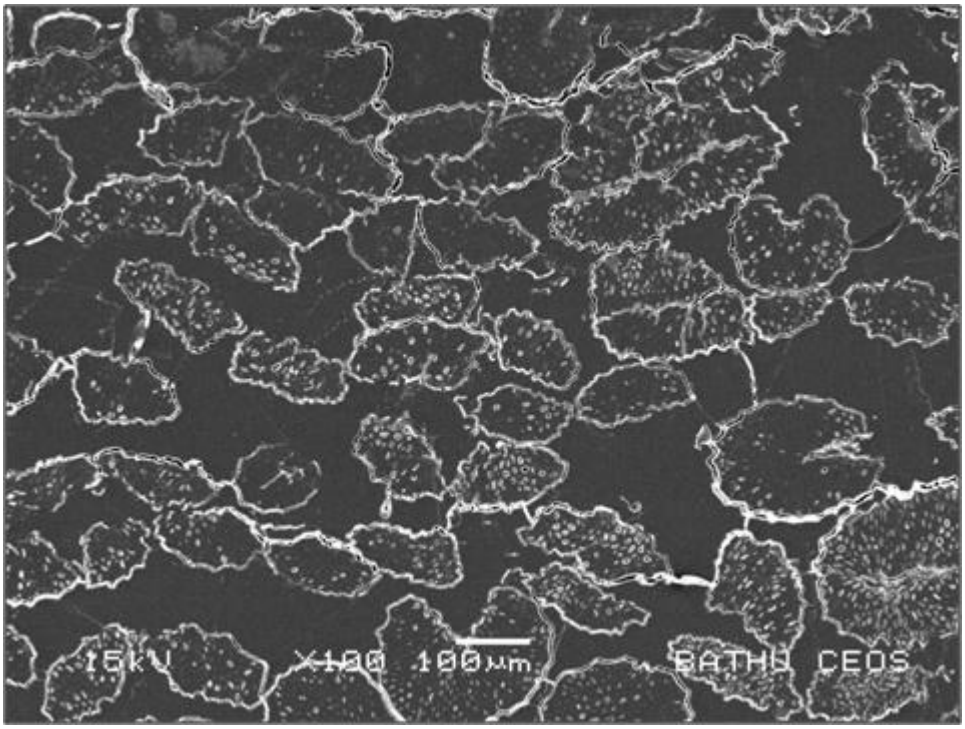

Figure 8.85: SEM micrograph of a section through a specimen of PLA reinforced with V_f = 0.6 of untreated sisal fibres.

The Instron 3369 testing machine was used to carry out mechanical tests of composites reinforced with untreated and caustic soda treated (6 wt%) sisal fibres.

The flexural test was performed at a cross head speed of 2 mm/min. The span of supporting members was adjusted to provide a span to thickness ratio of L/h = 16. Average width and thickness of the specimens were measured using a vernier calliper and recorded. Six specimens of composites reinforced with untreated and caustic soda treated sisal fibres were tested at fibre volume fractions of 0.4 and 0.6. Flexural strength was calculated as the flexural stress sustained by the specimen at maximum load according to Equation 6.28. Flexural modulus was calculated as the tangent slope of the initial linear portion of the load–deflection curve following the (Equation 6.29).

The Instron 3369 testing machine in three-point bending fixture was used to carry out the short beam shear test at cross head speed of 1 mm/min. The width (b), thickness (h) and the length (l) of the specimen satisfied the following relations: b/h = 5 and l/h = 10. The span (L) to thickness ratio was L/h = 5. The interlaminar shear strength was calculated according to the Equation 6.30. Eight specimens of composites reinforced with untreated and caustic soda treated sisal fibres were tested with a fibre volume fraction of 0.4.

The Instron 3369 testing machine was used to carry out the tensile test with a cross-head speed of 1 mm/min. Six specimens of composites reinforced with untreated and caustic soda treated sisal fibres were tested with a fibre volume fraction of 0.5. Tensile specimens were end tabbed with aluminium plates (see Section 6.10 and Figure 8.86).

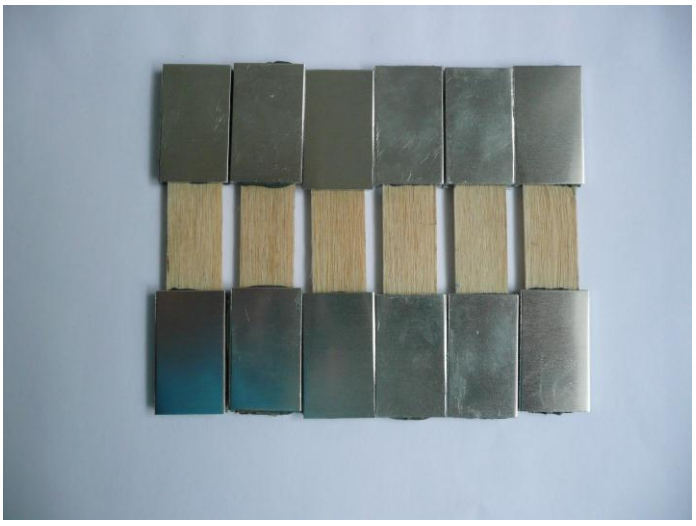

Figure 8.86: Tensile test specimens.

Figure 8.87 and and 8.88 show examples of fractured composites. Figure 8.87 shows compression and tension side of composites following failure in three-point bending.

Figure 8.87: Three point bending test. Samples after fracture: compression (left) and tension (right) side of a PLA reinforced with untreated sisal fibres.

Figure 8.88: Failed tensile test specimen.

Figure 8.88 shows a typical failure of composites tested in tension. Mechanical properties of composites tested in three point bending, tension and short beam shear test are summarized in Tables 8.24 and 8.25. Table 8.26 includes flexural properties of some softwood species.

Table 8.24: Mechanical properties of composites reinforced with untreated sisal fibres.

Matrix/fibre system	PLA/UN		
V_f	0.4	0.5	0.6
Flexural strength [MPa]	236 ± 36	-	279 ± 43
Flexural modulus [GPa]	9.8 ± 0.95	-	19.4 ± 1.36
Tensile strength [MPa]	-	164 ± 22	-
Tensile modulus [GPa]	-	9.5 ± 1.47	-
ILSS [MPa]	8.4 ± 1.2	-	-
Note: UN = untreated sisal fibres.			

Table 8.25: Mechanical properties of composites reinforced with caustic soda treated sisal fibres.

Matrix/fibre system	PLA/CS		
V_f	0.4	0.5	0.6
Flexural strength [MPa]	240 ± 10	-	286 ± 18
Flexural modulus [GPa]	11.1 ± 0.69	-	22 ± 1.18
Tensile strength [MPa]	-	205 ± 17	-
Tensile modulus [GPa]	-	12 ± 1.39	-
ILSS [MPa]	14.8 ± 2.6	-	-
Note: CS = caustic soda treated (6 wt%) sisal fibres.			

Table 8.26: Mechanical properties of selected softwood species (Forest Product Laboratory, 1999).

Material	Flexural strength	Flexural modulus
	[MPa]	[GPa]
Fir, Douglas	85	13.4
Pine, longleaf	100	13.7
Spruce, Sitka	70	10.8
Note: span to thickness ratio of 14:1.		

Conclusions:

- Mechanical properties improve as fibre volume fraction increases.
- Flexural strength of composites reinforced with untreated sisal fibres with 0.4 and 0.6 fibre volume fraction was 236 ± 36 MPa and 279 ± 43 MPa.
- Flexural strength of composites reinforced with caustic soda (6 wt%) treated sisal fibres with 0.4 and 0.6 fibre volume fraction was 240 ± 10 MPa and 286 ± 18 MPa.

- Flexural modulus of composites reinforced with untreated and caustic soda treated sisal fibres with a fibre volume fraction of 0.4 was 9.8 ± 0.95 and 11.1 ± 0.69 GPa respectively.
- Flexural modulus of composites reinforced with untreated and caustic soda treated sisal fibres with a fibre volume fraction of 0.6 was 19.4 ± 1.36 and 22 ± 1.18 GPa respectively.
- The interlaminar shear strength of laminar composites reinforced with a fibre volume fraction 0.4 of untreated sisal fibres was 8.4 ± 1.2 MPa and 14.8 ± 2.6 MPa of caustic soda treated (6 wt%) sisal fibres.
- Tensile strength of composites reinforced with untreated and caustic soda treated sisal fibres with a fibre volume fraction of 0.5 was 164 ± 22 and 205 ± 17 MPa respectively.
- Tensile modulus of composites reinforced with untreated and caustic soda treated sisal fibres with a fibre volume fraction of 0.5 was 9.5 ± 1.47 and 12 ± 1.39 GPa respectively.
- Table 8.27 summarizes experimentally determined and theoretically calculated elastic moduli of PLA/sisal fibre composites showing good correlation between the theory and the experiment.

Table 8.27: Experimentally determined and theoretically calculated elastic moduli of PLA/ sisal fibre composites.

Flexure						
Matrix/Fibre	V_f	[b]E_f	V_m	[c]E_m	E_c (calculated[d])	E_c (experimental)
	[-]	[GPa]	[-]	[GPa]	[GPa]	[GPa]
PLA/untreated sisal	0.4	17.6	0.6	2.7	8.7	9.8
PLA/treated sisal*	0.4	27.5	0.6	2.7	12.6	11.1
PLA/untreated sisal	0.6	17.6	0.4	2.7	11.6	19.4
PLA/treated sisal*	0.6	27.5	0.4	2.7	17.6	22
Tension						
PLA/untreated sisal	0.5	17.6	0.5	2.7	10.2	9.5
PLA/treated sisal*	0.5	27.5	0.5	2.7	15.1	12

Note: [a] fibres treated with aqueous caustic soda solution (6 wt%) for 48 hours; [b] data taken from Table 8.4; [c] data taken from Table 8.2; [d] values calculated from the rule of mixtures assuming $n_l = 1$ and $n_0 = 1$; $E_c = V_f E_f + V_m E_m$ (Equation 5.12); subscripts m, f and c have the meaning of matrix, fibre and composite.

9 General discussion

This chapter summarises and discusses the main findings of the thesis. Experimental results are related to the findings of the literature review. Firstly the development of unidirectional composites made of natural fibres and their mechanical properties is discussed. Secondly, interfacial adhesion and experimental techniques used to measure the interfacial shear strength are considered. Finally the development of transcrystalline morphology at the fibre to matrix interface is discussed.

The aim of this thesis was to produce fully bio-based and biodegradable composites with properties suitable for structural applications. Composites were made of sisal fibres and polylactic acid. The following bullet points summarize the properties of polylactic acid and sisal fibres measured during the programme of research and the reasons for choosing the polylactide matrix and sisal fibres for composites fabrication. Some of the sisal fibres were caustic soda treated in order to promote better fibre to matrix adhesion and obtain composites with improved mechanical properties.

9.1 Mechanical properties of sisal fibres and polylactic acid

In this section mechanical properties of sisal fibres and polylactic acid are summarized and the reasons for combining them in a composite material are explained and discussed.

- *The tensile strength of PLA was 63±5MPa and the Young's modulus was 2.7±0.4 GPa. The glass transition temperature T_g was 56°C and the melting temperature T_m of the crystalline portion was 169°C. The PLA had high molecular weight of 180 kDa.*
- *The density of untreated and caustic soda treated sisal fibres was determined using Archimedes' principle as 1.115 g/cm^3 and 1.438 g/cm^3 respectively.*
- *The strength, Young's modulus and strain at failure of sisal fibres at different gauge lengths was characterised using Weibull analysis.*
- *The tensile strength, Young's modulus and strain at failure of sisal fibres tested in tension at the gauge length of 10 mm was 508±101 MPa, 17.6±3.2 GPa and*

5.14±1.07% for untreated fibers and 681±156 MPa, 27.5±6.2 GPa and 3.81±0.96 % for caustic soda treated sisal fibres.

- *The fibre modulus calculated from the Raman band shift of fibres with a gauge length of 10 mm was 6.4-10 and 5-9.5 GPa for untreated and caustic soda treated sisal fibres, respectively.*

PLA is probably the best choice for a matrix of all bio-based polymers due to its low density, acceptable mechanical properties, high glass transition temperature and relatively low melting temperature. Other bio-based polymers which could be used in the manufacture of natural fibre composites are polycaprolactone and polyhydroxybutyrate. Polycaprolactone (PCL) has a tensile strength of 21-42 MPa and Young's modulus of 0.21-0.44 GPa, glass transition temperature T_g of -60 to -65°C and a melting temperature T_m of 58-65°C. Polyhydroxybutyrate (PHB) has a tensile strength of 40 MPa, Young's modulus of 3.5-4 GPa, a glass transition temperature T_g of 5-15°C and a melting temperature T_m of 168-182°C (van de Velde (2001) and Kiekens (2002)). Both PCL and PHB are disadvantaged compared to PLA due to their low T_g (PHB) and T_m (PCL). PLA has superior mechanical properties compared to widely used polypropylene which has a tensile modulus of 36 MPa, Young's modulus of 1.4 GPa, glass transition temperature T_g of -20°C and a melting temperature T_m of 164°C (Brandrup *et al*., 2005).

Sisal is a nice and clean natural fibre extracted from the leaves of the *Agave sisalana* plant with high cellulose content of 43-78% and a low microfibril angle (10-22°), high tensile strength 80-840 MPa and Young's modulus 9-22 GPa. The specific tensile strength of sisal fibres is 55-580 MPa and specific Young's modulus 6-15 GPa (Mwaikambo, 2006; see Table 2.4). Compared to E-glass fibre, with a tensile modulus of 69-72 GPa and density of 2.54 g/cm^3 which has a specific modulus of 27.6 GPa (Chawla, 1998), the properties of sisal fibre are not quite as good. Untreated sisal fibres used in this thesis had specific Young's modulus of 16 GPa. Caustic soda treated (6 wt%) sisal fibres used in this thesis had a specific Young's modulus of 19 GPa.

The fibre modulus calculated from the strain/stress induced Raman band shift of fibres with the gauge length of 10 mm was 6.4-10 GPa and 5-9.5 GPa for untreated and caustic soda treated sisal fibres, respectively. The values reported are still within the range of the literature values but lower compared to the Young's moduli obtained from the tensile tests. The difference could be explained by the different straining rates of Raman micro-

spectroscopy and the conventional tensile test and stress relaxation is likely to occur in the Raman experiment.

Aqueous sodium hydroxide converts crystalline Cellulose I to Cellulose II. The action of an alkali solution interrupts the inter- and intra-molecular hydrogen bonds which hold micro-fibrils together. On the molecular level the incorporation of alkali hydrate ions into the structure of cellulose I results in the dislocation of glucopyranose rings which lay in the 101 planes from their previous positions. Thus the hydroxyl groups pending on carbon atoms C(6) and C(2) project out of the plane into the wider space between the 101 planes (Krässig, 1993).

9.2 Composites

Combining sisal fibres with a PLA matrix to manufacture composites with good mechanical properties was a challenging process. The melting temperature of PLA is about 170°C and processing temperatures for semicrystalline thermoplastics are usually about T_m + 30°C. Riedel and Nickel (1999) stated that the viscosity of thermoplastics should be reduced to 100 mPa.s, which is equivalent to an infusion/RTM resin, in order to wet natural fibres as easily as thermosetting matrices do. Such a low viscosity is not achievable by simply increasing the melt temperature because damage to the molecular structure of the polymer will result in the loss of mechanical properties. It is not recommended to process PLA at temperatures above 230°C. Sisal fibre bundles were unidirectionally aligned to maximize their properties in a resulting composite system as recommended by Bader (2001). PLA/sisal fibre composites were manufactured by compression moulding. The influence of water and alkali on cellulose and polylactic acid at high temperatures was analyzed and discussed due to the fact that alkali treated fibres are combined with PLA and due to the fact that water can develop as thermal degradation product and both can catalyse further degradation. Measures were taken to reduce the moulding times in order to avoid the matrix and fibre degradation during the processing. Aligned fibre preforms were combined with polymer sheets in order to facilitate the polymer melt flow in between the fibres and good fibre to matrix adhesion. A thin walled aluminium mould was designed to be heated up/cooled down quickly. Thus both the polymer and the fibres remained in the mould for a shorter period of time and the possibility of degradation was reduced.

- *The composites were compression moulded from unidirectional and well-aligned fibre preforms combined with thin PLA sheets. The composites were moulded in an aluminium thin walled mould.*

The following paragraph summarizes the main conclusions relating to the mechanical and dynamic mechanical properties of the composites prepared in this research programme.

- *Mechanical properties improve as the fibre volume fraction increases.*
- *Flexural strengths of composites reinforced with untreated sisal fibres with fibre volume fractions of 0.4 and 0.6 were 236 ± 36 MPa and 279 ± 43 MPa respectively.*
- *Flexural strengths of composites reinforced with caustic soda (6 wt%) treated sisal fibres with fibre volume fraction s of 0.4 and 0.6 were 240 ± 10 MPa and 286 ± 18 MPa respectively.*
- *Tensile strength of composites reinforced with untreated and caustic soda treated sisal fibres with 0.5 fibre volume fraction was 164 ± 22 and 205 ± 17 MPa respectively.*
- *Tensile modulus of composites reinforced with untreated and caustic soda treated sisal fibres with 0.5 fibre volume fraction was 9.5 ± 1.47 and 12 ± 1.39 GPa respectively.*
- *DMTA shows that T_g decreases with V_f. and composite properties are temperature sensitive above 50°C. The glass transition temperature of PLA was 58.4°C and it further decreased to 53.5°C if the composites were reinforced with a fibre volume fraction of 0.6 for untreated sisal fibres.*
- *In the case of composites reinforced with a fibre volume fraction of 0.6 of caustic soda treated (6 wt%) sisal fibres the glass transition temperature was 60°C.*
- *The interlaminar shear strength of laminar composites reinforced with a fibre volume fraction of untreated sisal fibres equal to 0.4 was 8.4±1.2 MPa and 14.8 ± 2.6 MPa for untreated and caustic soda treated (6 wt%) sisal fibres respectively.*

Composites prepared in this research programme possessed mechanical properties which were superior to the mechanical properties of some wood species, for example higher than the flexural strength (85 MPa) and flexural modulus (13.4 GPa) of Douglas fir.

A review of the literature shows that natural fibre composites with thermoplastic matrices have the best mechanical properties if they use unidirectional aligned fibre systems and are compression moulded (Table 9.1). Madsen and Lilholt (2003) prepared unidirectional composites made of polypropylene and hemp fibres with a fibre weight fraction of 0.5-0.75 which resulted in an axial tensile strength of 251-321 MPa and axial tensile modulus of 27-29 GPa .These values are much greater compared to injection moulded PLA/short flax fibre composites prepared by Oksman and her co-workers (2003). Their composites with 0.3 fibre weight fraction were reported to have a tensile in-plane modulus of 8.3 GPa and tensile strength of 53 MPa. Composites with randomly oriented flax fibres fabricated by Bodros *et al*. (2007) had a tensile strength and modulus of 100 MPa and 9.5 GPa respectively at 0.3 fibre weight fraction. Ochi (2006) developed high strength material composed of unidirectional hemp long fibre bundles and starch-based emulsion type thermoplastic resin. Composites had tensile and flexural strengths of 365 and 223 MPa, respectively at a fibre volume fraction of 0.7. Gomes *et al*. (2007) studied compression moulded biodegradable composites reinforced with 70 vol. % of curaua fibres with a hydrophilic resin based on a blend of corn starch and polycaprolactone (PCL) used as a matrix (T_g: -60°C and T_m: 60°C). Composites had a tensile strength and modulus of 327 MPa and 36 GPa. Composites made from alkali treated curaua fibres (10 wt% solution / 2 h) achieved tensile strength and modulus of 334 MPa and 32 GPa respectively. Ochi (2008) prepared unidirectional biodegradable composites reinforced with kenaf fibres (70 vol. %) using emulsion-type PLA as a matrix. The tensile and flexural strengths were 223 and 254 MPa respectively. Tensile and flexural moduli were about 23 GPa. All cellulose composites with high fibre volume fraction were prepared by Soykeabkaew et al. (2008) by partial surface dissolution of aligned ramie fibres using lithium chloride/N,N-dimethylacetamide. Composites with high fibre volume fraction (V_f=0.84) had an excellent tensile strength of 460 MPa and modulus of 28 GPa.

Interlaminar shear strength was found to be 8.4 MPa and 14.8 MPa for untreated and caustic soda treated sisal fibres. This value is lower compared to values obtained by Goutianos *et al* (2006) for composites made from unsaturated polyester (UP) resin and flax fibres with fibre volume fraction of 0.3 which possessed an ILSS of 22 MPa and which increased to 30 MPa with an epoxy matrix. The ILSS of PLA/sisal fibre composites obtained from the short beam shear test is in good relation to the IFSS results obtained from the microbond shear test discussed further in this section.

Table 9.1: Natural fibre composites with thermoplastic matrices.

Fibre/matrix	Processing method	[d]η_0	[e]w_f	[f]V_f	Tensile strength	Flexural strength	Tensile modulus	Flexural modulus	Reference
	[-]	[-]	[-]	[-]	[MPa]	[MPa]	[GPa]	[GPa]	
Flax/PLA	[b]IM	0.12	0.3	-	53	-	8.3	-	Oksman *et al.*, 2003
Flax/PLA	[c]CM	0.3	0.3	-	100		9.5	-	Bodros *et al.*, 2007
Hemp/PP	CM	1	0.5-0.75	-	251-321	-	27-29	-	Madsen and Lilholt, 2003
Hemp/starch based thermoplasic	CM	1	-	0.7	365	223	-	-	Ochi, 2006
Curaua/starch based thermoplastic	CM	1	-	0.7	327	-	36	-	Gomes *et al.*, 2007
Curaua[a]/starch based thermoplastic	CM	1	-	0.7	334	-	32	-	Gomes *et al.*, 2008
Kenaf/PLA	CM	1	-	0.7	223	254	23	23	Ochi, 2008
Ramie/cellulose thermoplastic polyester	CM	1	-	0.84	460	-	28	-	Soykeabkaew *et al.*, 2008

Note: [a]caustic soda treated fibre, [b]injection moulding; [c]compression moulding; [d]orientation efficiency factor (Bader, 2001); [e]fibre weight fraction, [f]fibre volume fraction

Dynamic mechanical thermal analysis results demonstrate that by adding fibres into the PLA matrix the storage modulus (E') at room temperature considerably increases with increasing fibre volume fraction. The glass transition temperature decreases with increasing amount of untreated sisal fibres embedded in the PLA matrix but was found to slightly increase when caustic soda treated sisal fibres were used at 0.6 fibre volume fraction. High fibre volume fractions result in large areas of fibre to matrix interface and increased damping at the interface during sinusoidal oscillation explains the decrease in glass transition temperature. The slightly higher T_g of composites with caustic soda treated sisal fibres points to improved fibre to matrix adhesion.

The tensile test specimens in this thesis were smaller than those prescribed by the standardized test. The reason for the production of shorter tensile test specimen was the area of the hot press which was 20 x 20 cm. In order to ensure an even temperature profile and heat distribution the mould was design to fit the press. In fact Gomes *et al*. (2007), Ochi (2006) and Soykeabkaew *et al*. (2008) all used non-standard tensile test specimens:

- 100 x 15 x 1-1.5 mm (length x width x thickness); gauge length of 50 mm (Gomes *et al*., 2007)
- 200 x 10 x 1 mm; gauge length of 70 mm (Ochi, 2006)
- 3 mm wide specimens tested at gauge length of 10 mm (Soykaebkaew *et al*., 2008)

9.3 Interfacial morphology

As already mention PLA is a semicrystalline thermoplastic polyester thus it can crystallize at the fibre to matrix interface. The development of crystalline morphology of PLA was observed at sisal fibre to matrix interface under different thermal conditions. The primary reason for understanding the development of crystalline morphology at sisal fibre/PLA interface was the possibility of tailoring and optimising the properties of composites during compression moulding. The idea was to control the adhesion strength and composite toughness by simple promotion/suppression of matrix crystalline morphology at the fibre to matrix interface. The following conclusions can be drawn:

- *PLA is a slowly crystallizing polymer.*
- *Isothermal crystallization was studied.*
- *Fibre treatment has significant effect on transcrystallinity development.*

- *Transcrystallinity was observed for NaOH treated fibres.*
- *Cooling rate influences the initiation and growth rate of transcrystalline layers.*
- *Transcrystalline growth was linear.*

Polylactic acid is a slowly crystallizing polymer. If crystallinity/transcrystallinity is to be developed during processing on an industrial scale a nucleating agent must be added into the polymer melt or the fibre surface must be engineered. The question is how this will affect fibre to matrix adhesion or even the fibre strength.

The adhesive strength of untreated and caustic soda (6 wt%) treated sisal fibres was determined using a microbond shear test. Single fibres were partially embedded in a PLA matrix and slowly pulled out. Caustic soda treated sisal fibres with crystalline morphology developed at the fibre to matrix interface were also tested for adhesive strength. The following observations were made:

- *Caustic soda treatment increased the interfacial shear strength (IFSS) measured in the single fibre shear test.*
- *The Weibull modulus (m) values for the single fibre shear tests are similar for untreated and treated fibres. The values of m are low because debonding is essentially brittle.*
- *Lower IFSS in the presence of TCL could be explained by the lamellae orientation which affects non-covalent bonding at the interface.*
- *The interfacial shear strength was modelled with Weibull analysis. Caustic soda treatment (6 wt%) improved the adhesion between the sisal fibres and the PLA matrix. The interfacial shear strength for untreated and treated sisal fibres partially embedded in PLA matrix was 10.5 ± 3.72 MPa and 15.3 ± 5.96 MPa, respectively.*
- *The interfacial shear strength for caustic soda treated (6 wt%) sisal fibres partially embedded in PLA matrix with transcrystallinity was 12.8 ± 4.96 MPa.*

The reason for lower interfacial shear strength in the presence of crystalline morphology might be due to the lamellae orientation in the transcrystalline layer. Supposing that non-covalent bonds between hydroxyl cellulose groups and polyester functional groups in polylactide are responsible for the strength at the interface it might be possible that the

lamellae orientation in the transcrystalline layer does not favour the creation of non-covalent bonds at the interface. Due to the polylactide chain packing in the lamella the polyester functional groups might be moved apart from the hydroxyl groups of cellulose exposed at the fibre surface so the functional groups are too distant to form a non-covalent bond.

From the tensile strength of fibres measured at gauge length of 10 mm and the interfacial shear strength the fibre critical length was predicted to be 4.6 mm and 3.7 mm for untreated and caustic soda treated sisal fibres respectively. Work of fracture was also predicted to be 55.5 kJ/m^2 for untreated sisal fibres and and 52.1 kJ/m^2 for caustic soda treated sisal fibres using the Kelly and Tyson (1965) equation because better adhesion results in lower toughness.

Mechanical properties of PLA-sisal composites are good and interfacial shear strength is improved by caustic soda treatment of fibres. The challenge now is to upscale into the manufacture of construction-scale components. On the one hand it would be really interesting to produce preforms of natural fibres which could be pre-impregnated and compression moulded or vacuum bagged/autoclaved in the same way as carbon fibres are. On the other hand prepreging is probably neither economically nor environmentally feasible. Natural fibre composites have already been widely used in automotive applications and are increasingly used in the building industry. A future challenge is to create lightweight aircraft structures or marine structures with natural fibre composites.

In conclusion, there are difficulties in manufacturing high fibre volume fraction NFCs with bio-thermoplastic matrices, but high quality, totally sustainable composites can be produced (i.e. at an optimised balance of economic, environmental, social and governance factors). The thermal processing route controls microstructure and preforms could be developed for hot pressing of components.

10 Conclusions

This chapter summarizes the conclusions of experimental results following the structure of Chapter 8. Each paragraph starts with a short introduction which outlines the test procedure followed by a list of the conclusions which resulted from experimental work. The chapter is structured as follows: characterization of the fibres and the matrix; transcrystallinity development, hot stage microscopy and differential scanning calorimetry; microbond shear test and fibre to matrix adhesion; mechanical and dynamic mechanical properties of the composites.

PLA – the polymer matrix

Polylactic acid (PLLA, Biomer 9000, M_w = 180,000 g/mol, melt flow index of 5g/10 min at 2.16 kg/190°C, density of 1.27 g/cm^3) was used in this thesis as the polymer matrix. The tensile strength and modulus of PLA were 62.8±4.9 MPa and 2.7±0.4 GPa respectively. Nuclear Magnetic Resonance (NMR) confirmed that the polylactic acid used in this thesis was poly(L-lactide). The glass transition temperature T_g was found to be 56°C and the melting temperature T_m was 169°C.

Sisal fibres

Sisal fibre bundles (A*gave sisalana*) were sourced in Tanzania. Some of the fibres were caustic soda treated in order to enhance their mechanical properties, improve fibre to matrix adhesion and manufacture composites with improved mechanical properties. Some of the fibres were also treated with hydrogen peroxide for Raman micro-spectroscopy testing. Untreated and caustic soda treated sisal fibres were tested in tension to measure their tensile strength, strain at break and Young's modulus. Fibres were tested in tension at different gauge lengths (10, 15, 20, 25 and 30 mm). Twenty specimens of each set were tested. Mean strengths obtained at different gauge lengths were plotted against the gauge lengths and fitted with a logarithmic function to extrapolate the tensile strength at the zero gauge length. Tensile strength and strain at break were analysed using Weibull statistics. The parameters of the Weibull distribution were deduced using Weibull plots and least squares method. Young's moduli followed normal distribution.

- *The density of untreated sisal fibre bundles was 1.115 g/cm^3 (Archimedes Principle).*
- *The density of caustic soda treated (6 wt%) sisal fibre bundles was 1.438 g/cm^3 (Archimedes Principle).*
- *Tensile strength was found to decrease with increasing gauge length.*
- *The strength of caustic soda treated (6 wt%) sisal fibres was higher at all tested gauge lengths compared to untreated sisal fibres.*
- *Hydrogen peroxide improved slightly the strength of untreated sisal fibres but deteriorated significantly the strength of caustic soda treated (6 wt%) sisal fibres.*
- *Fibres treated with 0.16 and 2 wt% of caustic soda solution showed lower values of tensile strength compared to untreated sisal fibres.*
- *Caustic soda treated (6 wt%) sisal fibres strained less at break compared to untreated sisal fibres.*
- *The strain at break of caustic soda treated (6 wt%) sisal fibres decreased with increasing gauge length.*
- *Untreated sisal fibres strained at 2 – 6 % break at different gauge lengths. There was no clear relationship between the gauge length and strain at break of untreated sisal fibres. In the range of 10 to 20 mm gauge lengths the strain at break decreased with increased gauge length.*
- *Hydrogen peroxide increased the strain at break of caustic soda treated (6 wt%) sisal fibres.*
- *The strain at break increased with increasing concentration of aqueous caustic soda solution.*
- *Young's modulus was found to increase with increasing gauge length.*
- *The highest Young's modulus was measured at the gauge length of 30 mm for caustic soda treated (6 wt%) sisal fibres.*
- *Hydrogen peroxide treatment improved the modulus of untreated sisal fibres but lowered the modulus of caustic soda (6 wt%) treated sisal fibres.*

Micro-mechanics of deformation of sisal fibres assessed by Raman micro-spectroscopy

Untreated and caustic soda treated sisal fibres were treated with hydrogen peroxide aqueous solution (3 wt%; 10 min.) to suppress fluorescence. Fibres were glued with an adhesive to supporting paper cards with 10 mm gauge length and strained. The stress/strain-dependent frequency (also called the Raman band) in natural cellulose is 1095 cm^{-1}. It is attributed to C-C-C and C-H-O mix mode vibrations. This peak was used to follow the stress/strain dependent frequency shift which was later used to calculate the fibre modulus. It was concluded that:

- *Sisal fibres are less strain sensitive compared to artificial fibres like, for example, carbon fibres or aramid fibres.*
- *Caustic soda treated (6 wt%) sisal fibres were found to be less strain sensitive compared to untreated sisal fibres.*
- *The Young's modulus of sisal fibres determined from Raman spectroscopy lies within the values reported in the literature.*
- *The large scatter in the Young's modulus values determined from Raman spectroscopy could be explained by the variability in properties of natural fibres as well as the small sample size.*
- *The Young's modulus of sisal fibres determined from tensile tests gave higher values compared to those obtained through Raman spectroscopy. Raman micro-spectroscopy is employed at considerably lower strain rates compared to conventional tensile testing of fibres so fibres have time to relax and to accommodate the applied strain/stress.*
- *The residual axial compressive stress in untreated sisal fibres determined from Raman spectroscopy (153-159 MPa) is in agreement with the theoretically calculated value (159 MPa).*

Hot stage microscopy and transcrystallinity development at the sisal fibre/PLA interface

Hot stage microscopy was used to follow the spherulitic growth of polylactic acid at the surface of sisal fibres. A length of sisal fibre was sandwiched between two pieces of PLA sheet, slightly heated and placed between the glass slide and the cover slip and pressed with tweezers. The glass slide with the sample was inserted into the hot stage and subjected to thermal treatment. The development of crystalline morphology was studied on fibres which were untreated or treated with different caustic soda aqueous concentrations. Samples were heated at 180°C for ten minutes to erase previous thermal history and cooled down at different cooling rates to a selected temperature which was held constant for at least twenty minutes. The polymer was allowed to crystallize isothermally and the development of crystalline morphology was observed using crossed-polars. It was concluded that:

- *The non-isothermal and isothermal development of PLA crystalline morphology at the fibre to matrix interface was studied by hot stage microscopy of single fibre-polylactic acid composites. Some of the fibres were treated with caustic soda solutions of different concentrations (0.16-8 wt%). Various cooling rates and crystallization temperatures were applied to promote transcrystalline growth at the interface.*
- *Caustic soda treatment promoted the development of transcrystalline morphology at PLA/sisal fibre interface whereas untreated fibres promoted single spherulitic growth. Untreated fibres at 120 to 140°C did not exhibit transcrystalline growth but individual spherullitic growth occurred.*
- *It was found that annealing is necessary to create the transcrystalline layer (TCL) around the caustic soda treated fibres in isothermal experiments. PLA is a slowly crystallizing thermoplastic polyester. A continuous TCL usually started to appear after 2 to 4 min. of isothermal annealing.*
- *Caustic soda treated fibres promoted the creation of a TCL at the fibre to matrix interface possibly due to the formation of cellulose II at the fibre bundle surface and the removal of pectins.*

- *Transcrystalline growth at 105 - 120°C was fine and fast for both untreated and treated fibres used in the study but it was not always possible to prepare an isothermal experiment as the matrix usually started to crystallize once it reached a temperature of 120°C. So the transcrystalline growth at temperatures below 120°C was studied only if the crystals had not started to appear before the crystallization temperature was achieved.*
- *Non isothermal crystallization at 2, 5 and 7°C also resulted in transcrystallinity around caustic soda treated fibres (6 wt%/48 hours).*
- *The influence of strength of caustic soda solution on transcrystalline growth rate was studied under special thermal conditions (cooling rate of 5°C/min and isothermal temperature of 120°C).*
- *The influence of cooling rate on transcrystalline growth rate was studied at isothermal temperature of 120°C for 6 wt% caustic soda treated fibres.*
- *Overall it can be concluded that caustic soda treatment is advantageous in forming well-defined TCLs at the fibre to thermoplastic matrix interface which should improve stress transfer in the composite.*
- *It can be concluded that caustic soda treatment provides higher density of nuclei and that the density increases as the temperature is reduced.*
- *Some of the samples were also crystallized in the hot stage without the cover glass. The aim was to inspect the transcrystalline morphology with electron microscopy without etching and staining the polymer matrix to enhance the resolution of crystalline regions*

Differential scanning calorimetry

Differential scanning calorimetry (DSC) was performed on PLA compression moulded films and single fibre reinforced composites with different thermal histories. The single fibre composites contained sisal fibre which was caustic soda treated (6 wt%). Samples of 5 mg were sealed in an aluminium pan and heated from 20 to 300°C at a 10°C/min scanning rate. A nitrogen flow (25 ml/min) was maintained throughout the test. Glass-transition temperature (T_g), cold crystallization temperature (T_c), melting temperature (T_m), enthalpy of crystallization (ΔH_c) and enthalpy of fusion (ΔH_m) were determined from DSC

first scans. The degree of crystallinity (χ_c) of the PLA films was also determined. It was concluded that:

- *The DSC showed that annealing time, cooling rates and surface morphology have an effect on the thermal behaviour of polylactic acid and sisal fibre-polylactic acid composites.*
- *Samples which were slowly crystallized or annealed possessed a higher degree of crystallinity and a higher melting temperature. The DSC thermograms of such samples did not show the exothermic peak associated with cold crystallization.*
- *Samples which were air quenched or non-isothermally crystallized at high cooling rate showed cold crystallization during the DSC scan. Such samples had a low degree of crystallinity.*

Microbond shear test

Adhesion strength between sisal fibres and polylactic acid was determined with a microbond shear test. Interfacial shear strength (IFSS) was obtained from the pull-out test of untreated and caustic soda treated (6 wt%) sisal fibres partially embedded in polylactic acid. The interfacial shear strength of caustic soda treated (6 wt%) sisal fibres embedded in a polymer matrix with developed crystalline morphology was also determined. Due to the anisotropy, non uniform cross-section and surface roughness of the fibres, a Weibull distribution of interfacial shear strength was expected. Parameters of the distribution (Weibull modulus and characteristic strength) were calculated by linear regression via Weibull plots. It was concluded that:

- *Caustic soda treatment (6 wt%) improved the adhesion between the sisal fibres and the PLA matrix. The interfacial shear strength for untreated and treated sisal fibres partially embedded in PLA matrix was 10.5 ± 3.72 MPa and 15.3 ± 5.96 MPa, respectively.*
- *The interfacial shear strength for caustic soda treated (6 wt%) sisal fibres partially embedded in PLA matrix with transcrystallinity was 12.8 ± 4.96 MPa.*
- *The reason for the lower interfacial shear strength obtained in the presence of transccrystalline morphology at PLA/caustic soda treated (6 wt%) sisal fibre*

interface might be due to the orientation of lamellae in the transcrystalline layer. Supposing that non-covalent bonds between hydroxyl cellulose groups and polyester functional groups in polylactide are responsible for the strength at the interface it might be possible that the orientation of lamellae in transcrystalline layer probably does not favour the creation of non-covalent bonds at the interface. Due to the polylactide chain packing in the lamella the polyester functional groups might be moved apart from the hydroxyl groups of cellulose exposed at the fibre surface so the functional groups are too distant to form a non-covalent bond.

Dynamic mechanical thermal analysis

Samples for dynamic mechanical thermal analysis (DMTA) were cut from compression moulded flat sheets of polylactic acid (PLA) and sheets of PLA reinforced with unidirectional sisal fibre bundles. Untreated sisal fibre-polylactic acid composites with fibre volume fractions of 0.4 and 0.6 were tested. The storage modulus (E'), loss (E'') modulus and loss factor (tan δ) were measured as a function of temperature in the range 25–120°C in a single-cantilever bending fixture with a span of 16 mm at a frequency of 1 Hz and a constant rate of heating of 2°C/min. It was concluded that:

- *Sisal fibres added into the polylactic acid significantly improved the storage modulus of polylactic acid below and above the glass transition temperature.*
- *Cold crystallization was observed during the DMTA experiment.*
- *The glass transition temperature (T_{eig}) decreased with increasing fibre volume fraction in composites reinforced with untreated sisal fibres.*
- *The glass transition temperature (T_{eig}) of composites reinforced with 60 % of caustic soda treated sisal fibres was higher compared to polylactic acid and composites reinforced with untreated sisal fibres.*
- *Damping at the caustic soda treated fibres-PLA interface was reduced probably due to the presence of transcrystalline morphology at the fibre to matrix interface.*
- *Addition of fibres into the PLA matrix increases damping at the fibre to matrix interface.*

- *The damping peak of the composites reinforced with untreated sisal fibres is lower compared to the neat polylactic acid and its maximum is shifted to lower temperatures.*
- *Comparing the tan δ of untreated and caustic soda treated sisal fibre-PLA composites it can been seen that the damping at the caustic soda treated fibres-PLA interface is reduced. The damping reduction could be explained by transcrystallinity development or by thermal stresses built up during the processing.*

Mechanical properties of composites

Compression moulded sheets of composites reinforced with untreated and caustic soda treated sisal fibres were tested in tension and flexure to determine their mechanical properties. Interlaminar shear strength was determined from a short beam shear test in three point bending with a span to thickness ratio L=5h. Eight specimens of composites with a fibre volume fraction of 0.4 were tested. Composites with both untreated and caustic soda treated (6 wt%) sisal fibres were prepared.

- *The interlaminar shear strength of laminar composites reinforced with a fibre volume fraction of untreated sisal fibres of 0.4 was 8.4±1.2 MPa and for caustic soda treated (6 wt%) sisal fibres it was 14.8 ± 2.6 MPa.*

Composites with 0.4 and 0.6 fibre volume fraction were tested in three point bending with the geometry preserving the span to thickness ratio (L/h = 16). Six specimens were tested for each fibre volume fraction and fibre treatment.

- *The mechanical properties improved as the fibre volume fraction was increased.*
- *The flexural strength of composites reinforced with untreated sisal fibres with 0.4 and 0.6 fibre volume fraction was 236 ± 36 MPa and 279 ± 43 MPa respectively.*
- *The flexural strength of composites reinforced with caustic soda (6 wt%) treated sisal fibres with 0.4 and 0.6 fibre volume fraction was 240 ± 10 MPa and 286 ± 18 MPa respectively.*

Six specimens of composites with fibre volume fraction of 0.6 were tested in tension. Composites reinforced with untreated and caustic soda treated sisal fibres were tested. The dimensions of test specimens were 100 x 15 x 1 mm and their ends were tabbed with aluminium sheets. The Young's modulus was calculated from the slope of the initial part of the load–deflection curve. It was concluded that:

- *Tensile strength of composites reinforced with untreated and caustic soda treated sisal fibres with 0.5 fibre volume fraction was 164 ± 22 and 205 ± 17 MPa respectively.*
- *Tensile modulus of composites reinforced with untreated and caustic soda treated sisal fibres with 0.5 fibre volume fraction was 9.5 ± 1.47 and 12 ± 1.39 GPa respectively.*

11 Future work

This chapter suggests future work in relation to producing good quality composites reinforced with long natural fibre bundles. Firstly it summarizes the demands on manufacturing process and propose further steps which shall apply. Secondly possible future work on microstructure and its relation to ultimate physico-mechanical properties is reviewed. Thirdly tests to assess long term behaviour and environmental stability of natural fibre composites are proposed.

The author manufactured composites, looked deeply into their microstructure and morphology and the way the structure is connected with the processing conditions and ultimate mechanical properties. Having good quality fibres and good quality matrix does not automatically mean a good quality composite. Their qualities should not worsen during their combination and transformation into composites. Thus proper manufacturing method is important to get the best of the fibres. Future work shall also focus on the three levels and the way they influence each other: manufacturing, micromechanics of composites and matrix morphology at fibre to matrix interphase.

Future work should focus on making quality composites with the best properties as possible. Well aligned fibres at high fibre volume fractions give the best mechanical properties. The challenge is to upscale the processing and to make it cost effective, repeatable, reliable and fast. Only if the conditions apply can cellulosic fibres compete with the glass fibres and can make it through to industry applications. Fibres have to be aligned to get the best mechanical properties. Fibre preforms if any have to be easy to handle, easy to produce and process. Key point seems to be the way to keep fibres aligned and in place. Once it is possible to make unidirectional laminates it shall be possible to make cross-ply laminates to eliminate the poor mechanical properties of natural fibres in the transverse direction. The thermoplastic matrix could be replaced with an epoxy resin. It is impossible to make fully bio-based biodegradable and recyclable composites with thermosetting matrices but there are other advantages. Low matrix viscosity will make the fibre volume fractions higher compared to thermoplastic-matrix composites. If fibre preforms are used the flow of low viscosity epoxy should not displace the fibres from their intended positions. Sisal fibres are clean and due to their roughness easy to handle when aligning the fibres at laboratory. On the other hand quality hemp or flax fibres are much

stronger and taking into account the previous composites strength results which obey the law of mixture they could result in stronger and tougher composites which will almost have the mechanical properties of the individual fibres at high fibre volume fractions (600-800 MPa). If compression moulding is found to be the most appropriate manufacturing process then the mould design shall improve. Finite element analysis shall be applied to improve the heat transfer, minimize the temperature gradients and reduce the residence time of the composite in the mould. The mould shall be made of aluminium. It will be interesting to reduce the thickness of the mould walls to the minimum so they withstand the pressure on the one side and uptake/release the heat quickly on the other side. Processing conditions such as temperature, pressure and time shall be optimized e.g. with two-level factorial analysis.

It might be also possible to make composites combining natural fibres with high temperature melting thermoplastics (like polyamide) providing the compression moulding time at high temperatures is reduced to the minimum. The polymer shall have enough heat to melt, flow and wet the fibres on the one hand. On the other hand the kinetics of cellulose thermal decomposition shall be still slow or even inactive to spoil the compression moulding. May be at the beginning the protective atmosphere of nitrogen/helium or a vacuum shall apply. The mould could be filled and enclosed into a vacuum bag which withstands temperatures >200°C and hot pressed.

There are some detailed test suggestions:

- It will be interesting to find out the maximum fibre volume fraction of sisal fibres in PLA matrix which corresponds to the maximum mechanical properties. Scaled-up prototypes shall be compression moulded and tested for their mechanical properties. Four point bending and tensile testing using standardized specimens (250 x 25 x 4 mm) shall apply.
- Long term mechanical properties of composites shall be determined.
- PLA is still an expensive polymer. Sandwich beam prototypes shall be manufactured and tested in four-point flexure. PLA reinforced with sisal could be attached to balsa wood through solvent etched (chloroform) surface and applied slight pressure.
- Fracture toughness shall be tested in tension with centrally notched specimens.

- Raman spectroscopy shall be used to test the adhesion strength of PLA to un/treated sisal fibres. As the Raman spectroscopy requires transparent matrix the influence of developed crystalline morphology on fibre to matrix adhesion shall be evaluated with X-ray diffraction.
- X-ray diffraction to study the structure of transcrystalline layer at fibre to matrix interface especially in early stages of development.
- It has to be decided what is responsible for the transcrystallinity development: whether fibre surface or nano-cellulose whiskers dissolved in the matrix in the close proximity of the fibre surface. Possible experimental design: caustic soda treated fibres (concentrated solutions to make a strong signal) could be partially embedded in PLA meanwhile laying on a glass slide. Fibres shall be pulled out from the polymer sheet. The resulting polymer sheet shall be dissolved in chloroform and the composition and molecular weight distribution of the solution shall be determined in size exclusion chromatography (SEC) and nuclear magnetic resonance (NMR). Matrix from pull-out tests inspected using X-ray diffraction.
- Composites sheets shall be shredded into a powder and re-compression moulded into low cost composites and tested for the mechanical properties of recycled material.
- Water uptake and its influence on mechanical properties shall be tested.
- Three-point bent samples shall be compression moulded and tested up-side down with centrally applied load. The process of compression moulding-mechanical testing shall be repeated several times.
- It would be interesting to develop etching procedure to make the PLA crystalline structure visible in transmission electron microscopy (TEM). . The melt crystallized films would be exposed to an atmosphere saturated with allylamine and later on exposed to OsO_4 vapours. Fourier spectroscopy (FTIR) could determine the mechanism of the chemical reaction between the etchant and the crystallites in PLA.
- Half fringe photoelasticity could be used to study the stress fields in the matrix which develop in a single fibre composite which is strained.
- Loop test with sisal fibres to assess the strength from kink bands. Weibull analysis shall be applied and the strength determined correlated with the ultimate tensile strength.

- DMTA is a versatile experimental method which makes possible to obtain lots of information about the material behaviour with small samples sizes: fatigue, creep, frequency scans, time-temperature superposition, the influence of humidity and temperature on dynamic mechanical properties.
- Develop the transcrystallinity in polymer foils and determine the mechanical properties of TCL. Test the foils in tensile test and DMTA.
- Measure the transverse modulus of natural fibres.
- Measure the axial and transverse CLTE of natural fibres because this information is very useful and there is a gap in the literature.

All the tests shall apply to natural fibres with/without surface treatment and developed crystalline morphology in the matrix if applicable.

It would also be a challenge to upscale natural fibre composites into the manufacture of construction-scale components and to make them usable in the automotive or aircraft industries. As can be seen from the extensive literature review in Chapter 4 of this thesis best mechanical properties are usually attributed to composites with aligned unidirectional fibres. It would be very convenient to come up with unidirectionally aligned fibre preforms. To date the only available technology comes from the textiles industry. Natural fibres are usually spun into yarns and further woven into fabrics which can be impregnated and compression moulded into large boards. Nevertheless such approach has difficulties for example with yarn impregnation and fibre to matrix adhesion. Compared to glass or carbon fibres making preforms of natural fibre bundles is difficult. The length of natural fibre bundles is limited so it is impossible to use them in continuous processes because they are not rigid enough to be held in place in the preform during processing.
Low cost, low density and high specific mechanical properties are usually mentioned as factors which make natural fibres comparable to glass fibres in technical applications.
It is proposed that natural fibre composites could become structural materials usable in automotive and perhaps aircraft industry according to the following points:

- Unidirectionally aligned preforms of natural fibres could be prepared by partial dissolution of their surface and conversion of cellulose into thermoplastic cellulose acetate. The procedure was described for example by Soykeabkaew *et al*. (2008).

Resulting thin sheet all-cellulose composite would act as a fibre preform which would be further combined with aluminium sheets into laminar composites. Fibres in each ply could be oriented at 0°, 45° and 90° with respect to the longitudinal axis of the composite.

- Such preforms could also diminish the variability in properties of natural fibres to an acceptable limit. The variability in mechanical properties of such preforms is expected to be lower compared to individual fibre bundles.
- Aluminium is expected to provide the laminar composite with dimensional stability, strength and stiffness, paint-ability and surface corrosion resistance.
- The dimensions of natural fibre laminates are limited by the ultimate length of natural fibre bundles. This would be overcome by overlapping finger joints created before the partial surface dissolution of the fibres (See Section 4.6).
- The laminates could be shaped with CNC manufacturing methods and their thickness determined according to the needs of the structural element.
- It would be also interesting to prepare such preforms by partial surface dissolution of natural fibre yarns woven into fabrics with low crimp. The yarn shall be made of spun natural fibres with low twist.

In conclusion, it is a big challenge to introduce natural fibre composites into real structural applications.

12 References

Ajioka, M, Enomoto, K, Suzuki, K and Yamaguchi, A (1995), "The basic properties of poly (lactic acid) produced by the direct condensation polymerization of lactic acid", Journal of Polymers and the Environment, **3**, 4, 225-234.

Ajioka, M, Suizu, H, Higuchi, C and Kashima, T (1998), "Aliphatic polyesters and their copolymers synthesized through direct condensation polymerization", Polymer Degradation and Stability, **59**, 1-3, 137-143.

Albertsson, A-C and Karlsson (1994), "Chemistry and biochemistry of polymer degradation", in Griffin, GJL (1994), "Chemistry and Technology of biodegradable polymers", Blackie Publishing, Glasgow, UK, pp. 7-17.

Allegra, G, Corradini, P, Elias, H-G, Geil, PH, Keith, HD and Wunderlich, B (1989), "Definitions of terms relating to crystalline polymers", Pure and Applied Chemistry, **61**, 769-785.

Amitay-Sadovsky, E, Cohen, SR and Wagner, HD (2001), "Nanoscale shear and indentation measurement in transcrystalline alpha-isotactic polypropylene", Macromolecules, **34**, 5, 1252-1257.

Andrews, MC, Day, RJ, Hu, X and Young, RJ (1993), "Deformation micromechanics in high-modulus fibres and composites", Composites Science and Technology, **48**, 255-261.

Ansell, MP (2010), "Natural fibre composites and their role in engineering", Institute for the Sustainable Energy and the Environment (I-SEE) Seminar, 23rd of March 2010, University of Bath, UK.

Atkinson, KE and Jones, C (1996), "A study of the interphase region in carbon fibre/epoxy composites using dynamic mechanical thermal analysis", Journal of Adhesion, **56**, 247-260.

Attala and Nagel (1974), “Cellulose: its regeneration in the native lattice”, Science, **185**, 4150, 522-523.

Azapagic, A, Emsley, A and Hamerton, I (2003), “Polymers: the environment and sustainable development”, John Wiley & Sons, Chichester, UK, pp. 1-15, 126-149.

Aziz, SH and Ansell, MP (2004), “Optimizing the properties of green composites”, in Baillie C. (ed.), “Green composites: polymer composites and the environment”, Woodhead Publishing, Cambridge, UK, pp. 154-180.

Bader, MG (2001), “Polymer composites in 2000: structure, performance, cost and compromise”, Journal of Microscopy, **201**, 2, 110-121.

Bannister, DJ, Andrews, MC, Cervenka, AJ and Young, RJ (1995), “Analysis of the single-fibre pull-out test by means of Raman spectroscopy: Part II. Micromechanics of deformation for an aramid/epoxy system”, Composites Science and Technology, **53**, 411-421.

Bassett, DC (1981), “Principles of polymer morphology”, Cambridge University Press, Cambridge, UK.

Bax, B and Müssig, J (2008), “Impact and tensile properties of PLA/Cordenka and PLA/flax composites”, Composites Science and Technology, **68**, 7-8, 1601-1607.

Beckert, W and Lauke, B (1996), “Finite element calculation of energy release rate for single fibre pull-out test”, Computational Materials Science, **5**, 1-11.

Beckert, W and Lauke, B (1997), “Critical discussion of the single-fibre pull-out test: Does it measure adhesion?”, Composites Science and Technology, **57**, 1689-1706.

Bennett, JA and Young, RJ (1997), “Micromechanical aspects of fibre/crack interactions in an aramid/epoxy composite”, Composites Science and Technology, **57**, 8, 945-956.

Bergman, B (1984), “On the estimation of the Weibull modulus”, Journal of Materials Science Letters, **3**, 689-692.

Billon, N, Magnet, C, Haudin, JM and Lefebvre, D (1994), “Transcrystallinity effects in thin polymer films. Experimental and theoretical approach”, Colloid and Polymer Science, **272**, 633-654.

Bismarck, A, Mohanty, AK, Aranberri-Askargorta, I, Czapla, S, Misra, M, Hinrichsen, G and Springera, J (2001), “Surface characterization of natural fibers; surface properties and the water up-take behavior of modified sisal and coir fibres”, Green Chemistry, **3**, 100–107.

Blackburn, RS (2007), "A sustainable future for nonwovens", presented at Nonwovens network, 10th Anniversary Seminar "Global Perspectives", 21st of June 2007, Bradford, UK.

Bledzki AK, Gassan, J (1999), “Composites reinforced with cellulose based fibres”, Progress in Polymer Science, **24**, 2, 221-274.

Bloor, D, Preston, FH, Ando, DJ and Batchelder, DN (1991), “Resonant Raman scattering from diacetylene polymers”, in Ivin, KJ (ed.) (1976), “Structural studies of macromolecules by spectroscopic methods”, John Wiley & Sons, London, UK, pp. 93-109.

Blundell, DJ, Crick, RA, Fife, B, Peacock, J, Keller, A and Waddon, A (1989), “Spherulitic morphology of the matrix of thermoplastic PEEK/carbon fibre aromatic polymer composites”, Journal of Materials Science, **24**, 2057-2064.

Bodros, E and Baley, Ch (2008), “Study of the tensile properties of stinging nettle fibres (Urtica dioica)”, Materials Letters, **62**, 14, 2143-2145.

Bodros, E, Pillin, I, Montrelay, N and Baley, Ch (2007), “Could biopolymers reinforced by randomly scattered flax fibre be used in structural applications?”, Composites Science and Technology, **67**, 462-470.

Bos, HL, Mussig, and van den Oever, MJA (2006), "Mechanical properties of short-flax-fibre reinforced compounds", Composites: Part A, **37**, 1591-1604.

Bourmaud, A and Baley, C (2007), "Investigations on the recycling of hemp and sisal fibre reinforced polypropylene composites", Polymer Degradation and Stability, **92**, 1034-1045.

Brandrup, J (ed.), Immergut, EH (ed.), Grulke, EA (ed.), Abe, A (ed.) and Bloch (ed.), DR (ed.) (2005), "Polymer Handbook", 4th edition, John Wiley & Sons, pp. VI/194-VI/196, V/162-V/167.

Brizzolara, D, Cantow, H-J, Diederichs, K, Keller, E and Domb, AJ (1996), Mechanism of the stereocomplex formation between enantiomeric poly(lactides)s", Macromolecules, **29**, 191-197.

Burke, J (1965), "The kinetics of phase transformation in metals, Pergamon, Oxford, UK, pp. 98-151.

Campbell, D, Pethrick, RA and White, JR (2000), "Polymer characterization-physical techniques", Second edition, Stanley Thornes Publishers, Cheltenham, UK, pp. 67-107.

Carr, CM (ed.) (1995), "Chemistry of the textiles industry", Blackie Academic & Professional, Glasgow, UK, pp. 6-9, 275.

Cartier, L, Okihara, T, Ikada, Y, Tsuji, H, Puiggali, J and Lotz, B (2000), "Epitaxial crystallization and crystalline polymorphism of polylactides", Polymer, **41**, 8909-8919.

Chandra, N and Ghonem, H (2001), "Interfacial mechanics of push-out tests: theory and experiments", Composites: Part A, **32**, 575–584.

Chamis, CC (1974), "Micromechanics strength theories", in Broutman, LJ (ed.) (1974), "Composite Materials, Volume 5, Fracture and Fatigue", Academic Press, New York and London, pp. 108-110.

Chartoff, RP, Weissman, PT and Sircar, A (1994), "The application of dynamic mechanical methods to T_g determination in polymers: an overview", in Seyler, RJ (ed.), "Assignment of the glass transition", ASTM STP 1249, American Society for Testing and Materials, Philadelphia, USA, pp. 88-107.

Chawla, KK (1998), "Fibrous materials", Cambridge University Press, Cambridge, UK, pp. 28, 30, 204 and 264.

Chen, EJH and Hsiao, BS (1992), "The effects of transcrystalline interphase in advanced polymer composites", Polymer Engineering Science, **32**, 280-286.

Cherry, BW (1981), "Polymer surfaces", Cambridge University Press", London, pp. 18-33.

Chiellini, E, Chiellini, F and Cinelli, P (2002), "Polymers from renewable resources", in Door, GS (ed.) (2002), "Degradable polymers: principles and applications", 2nd edition, Kluwer Academic Publishers, Dordrecht, The Netherlands, p. 208.

Cichocki, FR and Thomason, JL (2002), "Thermoelastic anisotropy of a natural fiber", Composites Science and Technology, **62**, 5, 669-678.

Cohen, AC (1965) "Maximum likelihood estimation in the Weibull distribution based on complete and on censored samples", Technometrics, **7**, 4, 579-588.

Cox, HL (1952), "The elasticity and strength of paper and other fibrous materials", British Journal of Applied Physics, **3**, 72-79.

Czigány, T, Morlin, B and Mezey, Z (2007), "Interfacial adhesion in fully and partially biodegradable polymer composites examined with microdroplet test and acoustic emission", Composite Interfaces, **14**, 7-9, 869-878.

De Santis, P and Kovacs, A (1968), "Molecular conformation of poly (S-lactic acid)", Biopolymers, **6**, 3, 299 – 309.

Di Landro, L and Pegoraro, M (1996), "Evaluation of residual stresses and adhesion in polymer composites", Composites Part A, **27A**, 847-853.

Dinwoodie, JM (2000), "Timber: its nature and behaviour", Second edition, E & FN Spon, London, UK, pp. 23-26.

Dong, S and Gauvin, R (1993), "Application of dynamic mechanical analysis for the study of the interfacial region in carbon fibre/epoxy composite materials", Polymer Composites, **14**, 5, 414-420.

Dorgan, JR, Lehermeier, H and Mang, M (2000), "Thermal and rheological properties of commercial-grade poly(lactic acid)s", Journal of Polymers and the Environment, **8**, 1, 1-9.

Drumright, RE, Gruber, PR and Henton, DE (2000), "Polylactic acid technology", Advanced Materials, **12**, 23, 1841-1846.

Edie, DD, Kennedy, JM, Cano, RJ and Ross, RA (1993), "Evaluating surface treatment effects on interfacial bond strength using dynamic mechanical analysis", in Stinchcomb, WW and Ashbaugh, NE (1993), "Composite materials: fatigue and fracture", Volume 4, ASTM STP 156, Philadelphia, USA, pp. 419-429.

Ehrenstein, GW (2006), "Faserverbund–Kunststoffe: Werkstoffe, Verarbeitung, Eigenschaften", Hanser, Munchen, Germany, pp.120-125, 165-168.

Ehrenstein, GW, Riedel, G and Trawiel, P (2004), "Thermal analysis of plastics: theory and practice", Hanser Gardner Publications, New York, USA, pp. 236-256.

Eichhorn, SJ and Young, RJ (2001), "The Young's modulus of a microcrystalline cellulose", Cellulose, **8**, 197-207.

Eichhorn, SJ and Young, RJ (2004), "Composite micromechanics of hemp fibres and epoxy resin microdroplets", Composites Science and Technology, **64**, 767-772.

Eichhorn, SJ, Sirichaisit, J and Young, RJ (2001), "Deformation mechanisms in cellulose fibre, paper and wood", Journal of Materials Science, **36**, 3129-3135.

Eichhorn, SJ, Young, RJ, Davies, RJ and Riekel, C (2003), "Characterization of the microstructure and deformation of high modulus cellulose fibres", Polymer, **44**, 5901-5908.

Feldman, AY, Wachtel, E, Zafeiropoulos, NE, Schneider, K, Stamm, M, Davies, RJ, Weinberg, A and Marom, G (2006), "In situ synchrotron microbeam analysis of the stiffness of transcrystallinity in aramid fibre reinforced nylon 66 composites", Composites Science and Technology, **66**, 2009-2015.

Fengel, D and Wegener, G (1984), "Wood: chemistry, ultrastructure, reactions", Walter de Gruyter, Berlin, New York, pp. 13-16.

Ferrillo, RG and Achorn, PJ (1996), "Comparison of thermal techniques for glass transition assignment. II. commercial polymers", Presented in part at the 24th North American Thermal Materials Analysis Society (NATAS) Conference, San Francisco, CA, USA, 10-13th of September, 1995.

Forest Product Laboratory, (1999), "Wood handbook-wood as an engineering material", General Technical Report FPL–GTR–113, U.S. Department of Agriculture, Forest Service, Forest Products Laboratory, Madison, Wisconsin.

Galiotis, C (1991), "Interfacial studies on model composites by laser Raman spectroscopy", Composites Science and Technology", **42**, 125-150.

Galiotis, C, Young, RJ, Yeung, PHJ and Batchelder, DN (1984), "The study of model polydiacetylene/epoxy composites. Part I: The axial strain in the fibre", Journal of Materials Science, **19**, 3640-3648.

Gandini, A and Belgacem, MN (2005), "Modified cellulose fibres as reinforcing fillers for macromolecular matrices", Macromolecular Symposia, **221**, 1, 257–270.

Ganster, J and Fink, H-P (2005), “Physical constants of cellulose” in Brandrup, J (ed.), Immergut, EH (ed.), Grulke, EA (ed.), Abe, A (ed.) and Bloch, DR (ed.) (2005), “Polymer Handbook”, 4th edition, John Wiley & Sons, New York, pp. V/135-V/136.

Garkhail, S, Wieland, B, George, J, Soykeabkaew, N and Peijs, T (2009), "Transcrystallization in PP/flax composites and its effect on interfacial and mechanical properties", Journal of Materials Science, **44**, 510-519.

Gardner, KH and Blackwell, J (1974), “The structure of native cellulose”, Biopolymers, **13**, 10, 1975-2001.

Garlotta, D (2001), “A literature review of poly(lactic acid)”, Journal of Polymer and the Environment, **9** (2), 63-84.

Gassan, J, Mildner, I and Bledzki, A (2001), “Transcrystallization of polypropylene on different modified jute fibres”, Composite Interfaces, **8**, 6, 443-452.

Gati, A and Wagner, HD (1997), “Stress transfer efficiency in semicrystalline-based composites comprising transcrystalline interlayers”, Macromolecules, **30**, 3933-3935.

Gedde, UW (1999), “Polymer physics”, Kluwer Academic Publishers, London,UK, pp. 152, 170-171 and 245.

Goda, K and Cao, Y (2007), “Research and development of fully green composites reinforced with natural fibers”, Journal of Solid Mechanics and Materials Engineering, **1**, 9, 1073-1084.

Golova, OP and Nosova, NI (1973), “Degradation of cellulose by alkaline oxidation”, Russian Chemical Reviews, **42**, 4, 327-338.

Gomes, A, Matsuo, T, Goda, K and and Ohgi, J (2007), “Development and effect of alkali treatment on tensile properties of curaua fiber green composites”, Composites: Part A, **38**, 1811-1820.

Gosselink, RJA, Snijder, MHB, Kranenbarg, A, Keijsers, ERP, de Jong, E and Stigsson, LL (2004), "Characterisation and application of NovaFiber lignin", Industrial Crops and Products, **20**, 191–203.

Goutianos, S, Peijs, T, Nystrom, B and Skrifvars, M (2006), "Development of flax fibre based textile reinforcements for composite applications", Applied Composites Materials, **13**, 199-215.

Grijpma, DW, Penning, JP and Pennings, AJ (1994), "Chain entanglement, mechanical properties and drawability of poly(lactide)", Colloid and Polymer Science, **272**, 1068-1081.

Grubb, DT and Li, Z-F (1994), "Single-fibre polymer composites. Part II: Residual stresses and their effects in high-modulus polyethylene fibre composites", Journal of Materials Science, **29**, 203-212.

Guigon, M, Laporte, P and Echalier, B (1989) in Anales des Composites: Association pour les Matériaux Composites (Ed.), Edition Pluralis, Paris, France, p. 91.

Harris, B (1999), "Engineering composite materials", Institute of Materials, Minerals and Mining, London, UK, Second edition, p. 80.

Harris, B and Bunsell, AR (1977), "Structure and properties of engineering materials", Prentice Hall Press, London, UK, pp. 54, 98-109.

Hemsley, DA (1984), "The light microscopy of synthetic polymers", Oxford University Press, Oxford, UK, pp. 50-53.

Hesse, M, Meier, H and Zeeh, B (2008), "Spectroscopic methods in organic chemistry", Second edition, Georg Thieme Verlag, Stuttgart, New York, p. 72.

Hodgkinson, JM (2000), "Mechanical testing of advanced fibre composites", Woodhead Publishing, Cambridge, UK, pp. 124-142.

Hoogsteen, W, Postema, AR, Pennings, AJ, ten Brinke, G and Zugenmaier, P (1990), "Crystal structure, conformation and morphology of solution-spun poly(L-lactide) fibres", Macromolecules, **23**, 634-642.

Huang, Y and Young, RJ (1996), "Interfacial micromechanics in thermoplastic and thermosetting matrix carbon fibre composites", Composites Part A, **27A**, 973-980.

Huda, MS, Drzal, LT and Mohanty, AK (2006), "Chopped glass and recycled newspaper as reinforcement fibers in injection molded poly (lactic acid) (PLA) composites: a comparative study", Composites Science and Technology, **66**, 1813-1824.

Hughes, M (2004), "Applications", in Baillie, C (ed.) (2004), "Green composites: Polymer composites and the environment", Woodhead Publishing, Cambridge, UK, pp. 233-251.

Hull, D and Clyne, TW (1996), "An introduction to composite materials", Cambridge University Press, Cambridge, UK, p. 92.

Huson, MG and McGill, WJ (1984), "Transcrystallinity in polypropylene", Journal of Polymer Science: Polymer Chemistry, **22**, 11, 3571-3580.

Inoue, K, Serizawa, S, Yamashiro, M and Iji, M (2007), "Highly functional bioplastics (PLA compounds) used for electronic products", IEEE Polytronic 2007, 6th International Conference on Polymers and Adhesives in Microelectronics and Photonics,. Tokyo, Japan, 16-18th of January 2007.

Ishida, H and Bussi, P (1991), "Surface induced crystallization in ultrahigh-modulus polyethylene fibre-reinforced polyethylene composites", Macromolecules, **24**, 12, 3569-3577.

Isogai, A and Atalla, RH (1998), "Dissoluton of cellulose in aqueous NaOH solutions", Cellulose, **5**, 309-319.

Jacobsen, S, Degeé, PH, Fritz, HG, Dubois, PH and Jérōme, R (1999), "Polylactide (PLA) – a new way of production", Polymer Engineering and Science, **39**, 7, 1311-1319.

Jamshidi, K, Hyon, S-H and Ikada, Y (1988), "Thermal characterization of polylactides", Polymer, **29**, 2229-2234.

Jenckel, E, Teege, E and Hinrichs, W (1952), "Transkristallisation in Hochmolekularen Stoffen", Kolloid-Zeitschrift, **129**, 19-24.

Jones, FR (ed.) (1994), "Handbook of polymer fibre composites", Longman Scientific & Technical, Harlow, UK, p. 82.

Jones, FR (2005), "Fibre-matrix adhesion – assessment techniques", in Packham, DE (ed.) (2005), "Handbook of adhesion", Wiley & Sons, Chichester, UK, pp. 173-176.

Joshi, SV, Drzal, LT, Mohanty, AK and Aroa, S (2004), "Are natural fiber composites environmentally superior to glass reinforced composites?", Composites: Part A, **35**, 371-376.

Julien S, Chornet, E, Tiwari, PK and Overend RP (1991), "Vacuum pyrolysis of cellulose: Fourier transform infrared characterization of solid residues, product distribution and correlations", Journal of Analytical and Applied Pyrolysis, **19**, 81-104.

Juntaro, J, Pommet, M, Mantalaris, A, Shaffer, M and Bismarck, A (2007), "Nanocellulose enhanced interfaces in truly green unidirectional fibre reinforced composites", Composite Interfaces, **14**, 7-9, 753-762.

Kadla, JF and Kubo, S (2004), "Lignin-based polymer blends: analysis of intermolecular interactions in lignin–synthetic polymer blends", Composites: Part A **35**, 395–400.

Kaisersberger, E (1985), "Determination of viscoelastic properties with TMA, DMTA and DSC", Thermochimica Acta, **93**, 291-293.

Kalb, B and Pennings, AJ (1980), "General crystallization behaviour of poly(L-lactic acid)", Polymer, **21**, 6, 607-612.

Kamide, K, Okajima, K and Kowsaka, K (1992), "Dissolution of natural cellulose into aqueous alkali solution: role of super-molecular structure of cellulose", Polymer Journal, **24**, 1, 71-86.

Kamide, K, Yasuda, K, Matsui, T, Okajima, K and Yamashiki, T (1990), "Structural change in alkali-soluble cellulose solid during its dissolution into aqueous alkaline solution", Cellulose Chemistry and Technology, **24**, 23-31.

Katayama, T, Kanaka, K, Murakami, T and Uno, K (2006), "Compression moulding of jute fabric reinforced thermoplastic composites based on PLA non-woven fabric", WIT Transactions on The Built Environment, **85**, 159-167.

Keith , HD and Padden, FJ (1963), "A phenomenological theory of spherulitic crystallization", Journal of Applied Physics, **34**, 2409-2422.

Kelly, A and Tyson, WR (1965), "Tensile properties of fibre-reinforced metals-copper/tungsten and copper/molybdenum", Journal of the Mechanics and Physics of Solids, **13**, 329-350.

Khalili, A and Kromp, K (1991), "Statistical properties of Weibull estimators", Journal of Materials Science, **26**, 6741-6752.

Khanna, YP (1989), "Estimation of polymer crystallinity by dynamic mechanical techniques", Journal of Applied Polymer Science, **37**, 9, 2719-2726.

Khondker, OA, Ishiaku, US, Nakai, A and Hamada, H (2005), "Fabrication of unidirectional jute/PP composites using jute yarns by film stacking method", Journal of Polymers and the Environment, **13**, 2, 115-126.

Khondker, OA, Ishiaku, US, Nakai, A and Hamada, H (2006), "A novel processing technique for thermoplastic manufacturing of unidirectional composites reinforced with jute yarns", Composites: Part A, **37**, 2274-2284.

Kister, G, Cassanas, G, Vert, M, Pauvert, B and Térol, A (1995), "Vibrational analysis of poly(L-lactic acid)", Journal of Raman Spectroscopy, **26**, 307-311.

Klein, N, Marom, G and Wachtel, E (1996), "Microstructure of nylon 66 transcrystalline layers in carbon and aramid fibre reinforced composites", Polymer, **37**, 24, 5493-5498.

Kobayashi, j, Asahi, T, Ichiki, M, Oikawa, A, Suzuki, H, Watanabe, T, Fukada, E and Shikinami, Y (1995), "Structural and optical properties of poly lactic acids", Journal of Applied Physics, **77**, 7, 2957-2973.

Kolstad, JJ (1996), "Crystallization kinetics of poly(L-lactide-co-meso-lactide)", Journal of Applied Polymer Science, **62**, 1079-1091.

Kong, K and Eichhorn, SJ (2005), "Crystalline and amorphous deformation of process-controlled cellulose-II fibres", Polymer, **46**, 6380-6390.

Kopinke, F-D, Remmler, M, Mackenzie, K, Möder, M and Wachsen, O (1996), "Thermal decomposition of biodegradable polyesters – II. Poly(lactic acid)", Polymer Degradation and Stability, **53**, 329-342.

Krässig, HA (1993), "Cellulose: structure, accessibility and reactivity", Gordon and Breach Science Publishers, Yverdon, Switzerland, pp. 258-277, 306-7.

Krechnel, H (1964), "Fibre reinforcement", Akademisk Forlag, Copenhagen, Denmark.

Lacroix, T, Tilmans, B, Keunings, R, Desaeger, M and Verpoest, I (1992), "Modelling of critical fibre length and interfacial debonding in the fragmentation testing of polymer composites", Composites Science and Technology, **43**, 379-387.

Le Bourhis, E (2008), "Glass: Mechanics and Technology", Wiley-VCH Verlag GmbH & Co KGaA, Weinheim, Germany, p. 157.

Li, Y, Mai, YW and Ye, L (2000), "Sisal fibre and its composites: a review of recent developments", Composites Science and Technology, **60**, 2037-2055.

Li, Z-F and Grubb, DT (1994), "Single-fibre polymer composites. Part I: Interfacial shear strength and stress distribution in the pull-out test", Journal of Materials Science, **29**, 189-202.

Lin, L and Argon, AS (1994), "Review. Structure and plastic deformation of polyethylene", Journal of Materials Science, **29**, 294-323.

Lönnberg, H, Zhou Q, Brumer, H, Teeri, TT, Malström, E and Hult, A (2006), "Grafting of cellulose fibers with poly(ε-caprolactone) and poly(L-lactic acid) via ring-opening polymerization", Biomacromolecules, **7**, 2178-2185.

Lowe, H (1889), British patent No. 20, 314; ibid. (December 22, 1890) 4, 452.

Lunt, J (1998), "Large-scale production, properties and commercial applications of polylactic acid polymers", Polymer Degradation and Stability, **59**, 145-152.

Luo, S and Netravali, AN (2001), "Characterization of henequen fibres and the henequen fibre/poly(hydroxybutyrate-co-hydroxyvalerate) interface", Journal of Adhesion Science and Technology, **15**, 4, 423-437.

Lustiger, A, Marzinsky, CN, Mueller, RR and Wagner, HD (1995), "Morphology and damage mechanisms of the transcrystalline interphase in polypropylene", Journal of Adhesion, **53**, 1-14.

Madsen B, Hoffmeyer, P and Lilholt, H (2008), "Hemp yarn reinforced composites – II. Tensile properties", Composites Part A: Applied Science and Manufacturing, **38**, 10, 2204-2215.

Madsen B, Hoffmeyer, P, Thomsen, AB and Lilholt, H (2007), "Hemp yarn reinforced composites – I. Yarn characteristics", Composites: Part A, **38**, 10, 2194-2203.

Madsen, B and Lilholt, H (2003), "Physical and mechanical properties of unidirectional plant fibre composites - an evaluation of the influence of porosity", Composites Science and Technology, **63**, 1265-1272.

Maier, C and Calafut, T (1998), "Polypropylene - The definitive user's guide and databook", William Andrew Publishing/Plastics Design Library, Norwich, NY, USA, pp. 69-70.

Marega, C, Marigo, A, Di Noto, V, Zannetti, R, Martorana, A and Paganetto, G (1992), "Structure and crystallization kinetics of poly(L-lactic acid)", Die Makromolekutare Chemie, **193**, 7, 1599-1606.

Marquardt, DW (1963), "An algorithm for least-squares estimation of nonlinear parameters", Journal of the Society for Industrial and Applied Mathematics, **11**, 431-441.

Mazzullo, S, Paganetto, G and Celli, A (1992), "Regime III crystallization in poly-(l-lactic) acid", Progress in Colloid and Polymer Science, **87**, 32-34.

McNeill, IC and Leiper, HA (1985a), "Degradation studies of some polyesters and polycarbonates-1. Polylactide: general features of the degradation under programmed heating conditions", Polymer Degradation and Stability, **11**, 267-285.

McNeill, IC and Leiper, HA (1985b), "Degradation studies of some polyesters and polycarbonates–2. Polylactide: Degradation under isothermal conditions, thermal degradation mechanism and photolysis of the polymer", Polymer Degradation and Stability, **11**, 309-326.

Mecking, S (2004), "Nature or petrochemistry? - Biologically degradable materials", Angewandte Makromolekulare Chemie, **43**, 1078-1085.

Menard, KP (1999), "Dynamic mechanical analysis: a practical introduction", CRC Press, London, UK, pp. 75, 100-109.

Menczel, JD and Prime RB (2009), "Thermal analysis of polymers: fundamentals and applications", Wiley & Sons, New Jersey, USA, p.69.

Mercer, J (1850), British patent No. 13, 296.

Miyata, T and Masuko, T (1998), "Crystallization behaviour of poly(L-lactide)", Polymer, **39**, 22, 5515-5521.

Mohanty, AK, Misra, M and Drzal, LT (2001), "Surface modification of natural fibres and performance of the resulting biocomposites: an overview", Composites Interfaces, **8**, 313-343.

Monasse, B and Haudin, JM (1985), "Growth transition and morphology change in polypropylene", Colloid and Polymer Science, **263**, 822-831.

Montgomery, DC, Runger GC and Hubele, NF (2007), "Engineering statistics", 4th edition. Wiley & Sons, pp.79-81.

Murayama, T and Lawton, EL (1973), "Dynamic loss energy measurement of tire cord adhesion to rubber", Journal of Applied Polymer Science, **17**, 669-677.

Murthy, DNP, Xie, M and Jiang, R (2004), "Weibull models", John Wiley & Sons, New Jersey, USA, p 92.

Mwaikambo, LY (2006), "Review of the history, properties and application of plant fibres", African Journal of Science and Technology, **7**, 2, 120-133.

Mwaikambo, LY, Ansell,MP (1999), "The effect of chemical treatment on the properties of hemp, sisal, jute and kapok for composite reinforcement", Die Angewandte Makromolekulare Chemie, **272**, 108-116.

Mwaikambo, LY and Ansell, MP (2002), "Chemical modification of hemp, sisal, jute, and kapok fibers by alkalization", Journal of Applied Polymer Science, **84**, 2222–2234.

Mwaikambo, LY and Ansell, MP (2006a), "Mechanical properties of alkali treated plant fibres and their potential as reinforcement materials II. Sisal fibres", Journal of Materials Science, **41**, 2497–2508.

Mwaikambo, LY and Ansell, MP (2006b) "Mechanical properties of alkali treated plant fibres and their potential as reinforcement materials. I. hemp fibres", **41**, 2483–2496.

Nairn, JA (2004), "Fracture mechanics of the microbond and pull-out tests", in Moore, DR (2004), "The application of fracture mechanics to polymers, adhesives and composites", Elsevier, Amsterdam, pp. 213-218.

Nairn, JA and Zoller, P (1985a), "Matrix solidification and the resulting residual thermal stresses in composites", Journal of Materials Science, **20**, 355-367.

Nairn, JA and Zoller, P (1985b), " The development of residual thermal stresses in amorphous and semicrystalline thermoplastic matrix composites", in Proceedings of Symposium on toughened composites, Houston, Texas, USA, 13-15th of March 1985, ASTM STP 937, pp. 328-341.

Nakamae, K and Nishino, T (1991), "Crystal moduli of high polymers and their temperature dependence", Integration of Fundamental Polymer Science and Technology, **5**, 121-130.

Nardin, M and Schultz, J (1993), "Relationship between fibre matrix adhesion and the interfacial shear strength in polymer based composites", Composite Interfaces, **1**, 2, 177-192.

Nielsen, LE and Landel, RF (1994), "Mechanical properties of polymers and composites", Second edition, Marcel Dekker, New York, Basel, Hong Kong, pp. 50-53, 157-159, 175-181, 491-492.

Ninomiya, N, Kato, K and Fujimori, A (2007), "Transcrystalline structures of poly(L-lactide)", Polymer, **48**, 4874-4882.

Nishino, T (2004), “Natural fibre source”, in Baillie C. (ed.), “Green Composites: polymer composites and the environment”, Woodhead Publishing, Cambridge, UK, pp. 54-55.

Nishino, T, Hirao, K, Kotera, M (2006), “X–ray diffraction studies on stress transfer of kenaf reinforced poly (L – lactic acid) composite”, Composites: Part A, **37**, 2269-2273.

Nishino, T, Hirao, K, Kotera, M, Nakamae, K, Inagaki, H (2003), “Kenaf reinforced biodegradable composite”, Composite Science and Technology, **63**, 1281-1286.

Nishino, T, Takano, K and Nakamae K (1995), “Elastic modulus of the crystalline regions of cellulose polymorphs”, Journal of Polymer Science, Part B: Polymer Physics, **33**, 11, 1647-1651.

Ntenga, R, Béakou, A, Atangana Atéba, J and Ayina Ohandja, L (2008), “Estimation of the elastic anisotropy of sisal fibres by an inverse method”, Journal of Material Science, **43**, 6206–6213.

Nuriel, H, Klein, N and Marom, G (1999), “The effect of the transcrystalline layer on the mechanical properties of composite materials in the fibre direction”, Composites Science and Technology, **59**, 11, 1685-1690.

Ochi, S (2006), “Development of high strength biodegradable composites using Manila hemp fiber and starch-based biodegradable resin”, Composites: Part A, **37**, 1879-1883.

Ochi, S (2008), “Mechanical properties of kenaf fibers and kenaf/PLA composites”, Mechanics of Materials, **40**, 446-452.

Ohtani, Y, Okumura, K and Kawaguchi, A (2003), “Crystallization behaviour of amorphous poly(L-lactide)”, Journal of Macromolecular Science, Part B: Physics, **42**, 3, 875-888.

Okihara, T, Tsuji, M, Kawaguchi, A and Katayama, K (1991), “Crystal structure of stereocomplex of poly(L-lactide) and poly(D-lactide)”, Journal of Macromolecular Science, Part B: Physics, **30**, 1-2, 119-140.

Oksman, K, Skrifvars, M and Selin, JF (2003) "Natural fibres as reinforcement in polylactic acid (PLA) composites", Composites Science and Technology, **63**, 1317-1324.

Oksman, K, Wallström, L, Berglund, LA and Dias Toledo Filho, R (2002), "Morphology and mechanical properties of sisal-epoxy unidirectional composites", Journal of Applied Polymer Science, **84**, 2358-2365.

Outwater, JO and Murphy, MC (1970), "Fracture energy of unidirectional laminates", Modern Plastics, **47**, 160-169.

Packham, DE (2003), "Surface energy, surface topography and adhesion", International Journal of Adhesion & Adhesives, **23**, 437-448.

Perego, G, Cella, GD and Bastioli, C (1996), "Effect of molecular weight and crystallinity on poly(lactic acid) mechanical properties", Journal of Applied Polymer Science, **59**, 37-43.

Pham, H (ed.), (2006), "Springer handbook of engineering statistics, Springer-Verlag, London, UK, pp. 63-78.

Piggott, MR (1992) "Interface properties and their influence on fibre reinforced polymers", in Vigo, T (ed.) and Kinzig, B (ed.), (1992), "Composite applications: the role of the matrix, fibre and interface", Wiley Blackwell, pp. 230-234, 242-243.

Piggott, MR (1997), "Why interface testing by single-fibre methods can be misleading", Composites Science and Technology, **57**, 965-974.

Plackett, D (2004), "Maleated polylactide as an interfacial compatibilizer in biocomposites, Journal of Polymers and the Environment, **12**, 3, 131-138.

Plackett, D, Andersen, TL, Pedersen, WB and Nielsen, L (2003), "Biodegradable composites based on L-polylactide and jute fibres", Composites Science and Technology, **63**, 1287-1296.

Pompe, G and Mäder, E (2000), "Experimental detection of transcrystalline interphase in glass-fibre/polypropylene composites", Composites Science and Technology, **60**, 2159-2167.

Powell, PC (1994), "Engineering with fibre-polymer laminates", Chapman & Hall, Glasgow, UK, first edition, pp. 173-174.

Puiggali, J, Ikada, Y, Tsuji, H, Cartier, L, Okihara, T and Lotz, B (2000), "The frustrated structure of poly(L-lactide)", Polymer, **41**, 8921-8930.

Pyda, M, Bopp, RC and Wunderlich, B (2004), "Heat capacity of poly(lactic acid)", J. Chem. Thermodynamics, **36**, 731-742.

Ramirez FA, Carlsson, LA and Acha, BA (2008), "Evaluation of water degradation of vinylester and epoxy matrix composites by single fiber and composite tests", Journal of Materials Science, **43**, 5230–5242.

Rankilor, PR (2000), "Textiles in civil engineering. Part 1 – geotextiles", in Horrocks,AR (ed.) and Anand, SC (ed.) (2000), "Handbook of technical textiles", Woodhead Publishing in association with The Textile Institute, Abington, Cambridge, UK, p. 384.

Reder, C, Loidl, D, Puchegger, S, Gitschthaler, D, Peterlik, H, Kromp, K, Khatibi, G, Betzwar-Kotas, A, Zimprich, P and Weiss, B (2003), "Non-contacting strain measurements of ceramic and carbon single fibres by using the laser-speckle method", Composites Part A, **34**, 1029–1033.

Riedel, U and Nickel, J (1999), "Nature fibre-reinforced biopolymers as construction materials-new discoveries", Die Angewandte Makromolekulare Chemie, **272**, 34-40.

Robinson, IM, Young, RJ, Galiotis, C and Batchelder, DN (1987), "The study of model polydiacetylene/epoxy composites. Part II: Effect of resin shrinkage", Journal of Materials Science, **22**, 3642-3646.

Roe, PJ and Ansell, MP (1985), "Jute-reinforced polyester composites", Journal of Materials Science, **20**, 11, 4015-20.

Rudnik, E (2008), "Compostable Polymer Materials", Elsevier Science, Oxford and Amsterdam, pp. 40, 73-82.

Sain, M and Panthapulakkal, S (2004), "Green fibre thermoplastic composites", in Baillie C. (ed.) (2004), "Green composites: polymer composites and the environment", Woodhead Publishing, Cambridge, UK, pp. 181-206.

Scallan, AM (1974), "The structure of the cell wall of wood: a consequence of anisotropic inter- microfibrillar bonding",Wood Science and Technology, **6**, 266-271.

Scheirs, J (2000), "Compositional and failure analysis of polymers: a practical approach", John Wiley & Sons, Chichester, UK, pp. 108-138.

Scheirs, J, Camino, G and Tumiatti, W (2001), "Overview of water evolution during the thermal degradation of cellulose", European Polymer Journal, **37**, 933-942.

Schultz, JM (2001), "Polymer crystallization: the development of crystalline order in thermoplastic polymers", Oxford University Press, Oxford, New York, pp. 90-91, 140-148.

Serizawa, T, Arikawa, Y, Hamada, K, Yamashita, H, Fujiwara, T Kimura, Y and Akashi, M (2003), "Alkaline hydrolysis of enantiomeric poly(lactide)s stereocomplex deposited on solid substrates", Macromolecules, **36**, 1762-1765.

Siegel, S and Castellan Jr., NJ (1988), "Nonparametric statistics for the behavioural sciences", Second edition, McGraw-Hill, London, UK, pp. 206-216.

Singletary, J, Baines, RW, Beckett, W and Friedrich K (1997), "Examination of fundamental assumptions of analytical modelling of fibre pull-out test", Mechanics of Composite Materials and Structures, **4**, 2, 95-112.

Sjöström, E (1993), “Wood chemistry: fundamentals and applications”, Second edition, Academic Press, London, UK, pp. 204-205.

Slivka, MA, Chu, CC and Adisaputro, IA (1997), “Fibre-matrix interface studies on bioabsorbable composite materials for internal fixation of bone fractures. I. Raw material evaluation and measurement of fibre-matrix interfacial adhesion”, Journal of Biomedical Materials Research Part A, **36** ,4, 469–477.

Sobue, H, Kiessig, H and Hess, K (1939), “The cellulose-sodium hydroxide-water system as a function of the temperature”, Journal of Physical Chemistry, **B 43**, 309-328.

Södergård, A and Stolt, M (2002), “Properties of lactic acid based polymers and their correlation with composition”, Progress in Polymer Science, **27**, 1123-63.

Soykeabkaew, N, Arimoto, N, Nishino, T and Peijs, T (2008) “All-cellulose composites by surface selective dissolution of aligned ligno-cellulosic fibres”, Composites Science and Technology, **68**, 2201-2207.

Sprent, P (1993), “Applied nonparametric statistical methods”, Second edition, Chapman & Hall, London, UK, pp. 102-130.

Stephens, MA (1974), “ EDF statistics for goodness-of-fit and some comparisons”, Journal of the American Statistical Association, **69**, 730-737.

Stern, T, Marom, G and Wachtel, E (1997), “Origin, morphology and crystallography of transcrystallinity in polyethylene-based single-polymer composites”, Composites Part A, **28**, 437-444.

Strobl, G (2007), “The physics of polymers: concepts for understanding their structures and behaviour”, Springer-Verlag, Berlin, Heidelberg, Germany, p. 171.

Tadokoro, H (1979), “Structure of crystalline polymers", John Wiley & Sons, Chichester, UK, pp. 19-35.

Tang, MM and Bacon, R (1964), "Carbonization of cellulose fibres-I. Low temperature pyrolysis", Carbon, **2**, 211-220.

Teeri, TT, Brumer, H, Daniel, G and Gatenholm, P (2007), "Biomimetic engineering of cellulose-based materials", Trends in Biotechnology, **25**, 7, 299-306.

Thomason, JL (1993), "Investigation of composite interphase using dynamic mechanical analysis: artifacts and reality", Polymer Composites, **11**, 2, 105-113.

Thomason, JL and van Rooyen, AA (1992a), "Transcrystallized interphase in thermoplastic composites. Part I: Influence of fibre type and crystallization temperature", Journal of Materials Science, **27**, 889-896.

Thomason, JL and van Rooyen, AA (1992b), "Transcrystallized interphase in thermoplastic composites. Part II: Influence of interfacial stress, cooling rate, fibre properties and polymer molecular weight", Journal of Materials Science, **27**, 897-907.

Toonen, M, Ebskamp, M and Kohler, R (2007), "Improvement of fibre and composites for new markets", in Ranalli, P (2007), "Improvement of crop plants for industrial end uses", pp. 155-180.

Towo, AN, Ansell, MP, Pastor, M-L, Packham, DE (2005), "Weibull analysis of microbond shear strength at sisal fibre-polyester resin interfaces", Composite Interfaces, **12**, 1-2, 77-93.

Trotman, ER (1964), "Dyeing and chemical technology of textile fibres", Griffin, London, UK, pp. 54-61.

Tsuji, H (2005), "Polylactides", in Steinbüchel, A and Marchessault, RH (2005), "Biopolymers for medical and pharmaceutical applications", Volume 1, Wiley – VCH, Veinheim, Germany, p. 183-231.

Tucker, N (2004), “Clean production”, in Baillie C. (ed.) (2004), “Green Composites: polymer composites and the environment”, Woodhead Publishing, Cambridge, UK, pp. 218-219.

Urbanovici, E, Schneider, HA, Brizzolara, D and Cantow, HJ (1996), “Isothermal melt crystallization kinetics of poly(L-lactic acid)”, Journal of Thermal Analysis, **47**, 931-939.

Van de Velde, K and Kiekens, P (2001), “Thermoplastic polymers: overview of several properties and their consequences in flax fibre reinforced composites”, Polymer Testing, **20**, 885-893.

Van de Velde, K and Kiekens, P (2002), “Biopolymers: overview of several properties and consequences on their applications”, Polymer Testing, **21**, 433-442.

Van de Velde, K and Kiekens, P (2002), Thermal degradation of flax: the determination of kinetic parameters with thermogravimetric analysis”, Journal of Applied Polymer Science, **83**, 12, 2634-2643.

Vasanthakumari, R and Pennings, AJ (1983), “Crystallization kinetics of poly(L-lactic) cid”, Polymer, **24**, 2, 175-178.

Vincent, JFV (1982), “The mechanical design of grass”, Journal of Materials Science, **17**, 856-860.

Virk, AS, Hall, W and Summerscales, J (2009), “Tensile properties of jute fibres”, Materials Science and Technoogy, **25**, 10, 1289-1295.

Virk, AS, Hall, W and Summerscales, J (2010), “Failure strain as the key design criterion for fracture of natural fibre composites”, Composites Science and Technology **70**, 995–999.

Wagner (1996), “Thermal residual stress in composites with anisotropic interphases”, Physical Review B: Condensed Matter and Materials Physics, **53**, 5055-5058.

Wagner, HD and Nairn, JA (1997), "Residual thermal stresses in three concentric transversely isotropic cylinders: application to thermoplastic-matrix composites containing a transcrystalline interphase", Composites Science and Technology, **57**, 1289-1302.

Wagner, HD, Amer, MS and Schadler, LS (1996), "Fibre interactions in two-dimensional composites by micro-Raman spectroscopy", Journal of Materials Science, **31**, 1165-1173.

Wambua, P, Ivens, J and Verpoest, I (2003), "Natural fibres: Can they replace glass in fibre reinforced plastics?", Composites Science and Technology, **63**, 9, 1259-1264.

Wang, B and Sain, M (2007), "Dispersion of soybean stock-based nanofiber in a plastic matrix", Polymer International, **56**, 538-546.

Warwicker, JO (1967), "Effect of chemical reagents on the fine structure of cellulose. Part IV. Action of caustic soda on the fine structure of cotton and ramie", Journal of Polymer Science: Part A, **5**, 2579-2593.

Warwicker, JO and Wright, AC (1967), "Function of sheets of cellulose chains in swelling reactions on cellulose", Journal of Applied Polymer Science, **11**, 659-671.

Wenzel, RN (1949), "Surface roughness and contact angle", Journal of Physical and Colloid Chemistry, **53**, 1466-1467.

Wolf, O, Crank, M, Patel, M, Marscheider-Weidemann, F, Schleich, J, Hüsing, B and Angerer, G (2005), "Techno-economic feasibility of large-scale production of bio-based polymers in Europe", Technical Report EUR 22103 EN.

Wool, RP (1995), "Polymer interfaces: Structure and strength", Hanser/Gardner, New York, pp. 21-29.

Wunderlich, B (2005), "Thermal analysis of polymeric materials", Springer-Verlag Berlin Heidelberg, pp. 329-355, 412-419.

Ye, L, Scheuring, T and Friedrich, K (1995), "Matrix morphology and fibre pull-out strength of T700/PPS and T700/PET thermoplastic composites", Journal of Materials Science, **30**, 4761 4769.

Young, RJ (1994), "Raman spectroscopy and mechanical properties" in Spells, SJ (ed.) (1994), "Characterization of solid polymers: new techniques and developments", Chapman & Hall, London, pp. 225-275.

Young, RJ (1996), "Deformation studies of polymers using Raman spectroscopy", in Fawcett, AH (1996), "Polymer spectroscopy", John Wiley & Sons, Chicester, UK, pp. 202-230.

Young,RJ and Lovell, PA (1991), "Introduction to polymers, "Second edition, Chapman & Hall, London, pp. 248-252.

Zadorecki, P (1989), "Future prospects for wood cellulose as reinforcement in organic polymer composites", Polymer Composites, **10**, 2, 69-77.

Zafeiropoulos, NE and Baillie, CA (2007), "A study of the effect of surface treatments on the tensile strength of flax fibres: Part II. Application of Weibull statistics", Composites Part A, **38**, 629-638.

Zafeiropoulos, NE, Baillie, CA and Matthews, FL (2001), "A study of transcrystallinity and its effect on the interface in flax fibre reinforced composite materials", Composites, Part A: Applied Science and Manufacturing, **32**, 525-543.

Zimmermann, T, Pöhler, E and Geiger, T (2004), "Cellulose fibrils for polymer reinforcement", Advanced Engineering Materials, **6**, 9, 754-761.

Zhou, X-F, Nairn, JA and Wagner, HD (1999), "Fibre-matrix adhesion from the single composite test: nucleation of interfacial debonding", Composites: Part A, **30**, 1387-1400.

Zorowski, CF and Murayama, T (1971), “Bonding characterization in reinforced composites, Proceedings of the International Conference on Mechanical Behaviour of Materials, Kyoto, Japan, 1971.

Technical standards:

BS EN ISO 178: 2003: Plastics - Determination of flexural properties.

BS EN ISO 527-1: 1996: Plastics - Determination of tensile properties - Part1:General principles.

BS EN ISO 527-2: 1996: Plastics - Determination of tensile properties - Part 2: Test conditions for moulding and extrusion plastics.

BS EN ISO 527-5: 1997: Plastics - Determination of tensile properties – Part 5: Test conditions for unidirectional fibre-reinforced plastic composites.

BS EN ISO 11357-1: 1997: Plastics - Differential scanning calorimetry (DSC) - Part 1: General principles.

BS EN ISO 11357-2: 1999: Plastics - Differential scanning calorimetry (DSC) - Part 2: Determination of glass transition temperature.

BS EN ISO 11357-3: 1999: Plastics - Differential scanning calorimetry (DSC) - Part 3: Determination of temperature and enthalpy of melting and crystallization.

BS EN ISO 14125:1998: Fibre-reinforced plastic composites. Determination of flexural properties.

BS EN ISO 14040:2006: Environmental management - Life cycle assessment - Principles and framework.

BS EN ISO 14130: 1997: Fibre-reinforced plastic composites. Determination of apparent interlaminar shear strength by short-beam method.

Personal bibliography

Presentations:

Ansell, MP and Prajer, M, "Overview of natural fibre composites (NFCs) research at BRE CICM", BRE Trust Materials Conference '08, 12th of December 2008, Garston, Watford, UK.

Prajer, M and Ansell, MP, "Interfacial micromechanics in PLA/sisal fibre composites", 11th International Conference on Non-conventional Materials and Technologies (NOCMAT 11), 6-9th of September 2009, Bath, UK.

Prajer, M and Ansell, MP, "Thermo-mechanical evaluation of sisal-PLA composites", 17th International Conference on Composite Materials (ICCM 17), 27th-31st of July 2009, Edinburgh, UK.

Prajer, M and Ansell, MP, "Effect of transcrystallinity on microbond shear strength at sisal fibre–polylactic acid interface", Natural Fibres '09, Institute of Materials, Minerals and Mining, 14-16th of December 2009, London, UK.

Prajer, M and Ansell, MP (2011), "Observation of transcrystalline growth of PLA crystals on sisal fibre bundles using hot stage microscopy and the effect of crystal structure on interfacial shear strength", 4th International Conference on Sustainable Materials, Polymers and Composites, 6-7th of July 2011, Birmingham, UK. Also submitted for publication in Composites Part A.

Appendix A: Development of crystalline morphology in PLA/sisal single fibre composites

Table A1: List of figures describing the development of crystalline morphology in PLA/sisal single fibre composites.

Figure No.	Fibre treatment	Cooling rate	Isothermal temperature	Polymer morphology
[-]	[wt% $(NaOH)_{aq.}$/48 hours]	[°C/min.]	[°C]	[-]
A1	treated (6 wt%)	5	130	Spherulitic
A2	treated (6 wt%)	5	125	Spherulitic
A3	treated (6 wt%)	5	120	Transcrystalline
A4	treated (6 wt%)	5	135	Spherulitic
A5	treated (6 wt%)	5	140	Spherulitic
A6	treated (6 wt%)	2	120	Transcrystalline
A7	treated (6 wt%)	2	125	Spherulitic
A8	treated (6 wt%)	2	130	Spherulitic
A9	treated (6 wt%)	2	135	Spherulitic
A10	treated (6 wt%)	2	140	Spherulitic
A11	untreated	5	120	Transcrystalline
A12	untreated	5	125	Spherulitic
A13	untreated	5	130	Spherulitic
A14	untreated	5	135	Spherulitic
A15	untreated	5	140	Spherulitic
A16	treated (2 wt%)	5	120	Transcrystalline
A17	untreated	2	120	Spherulitic
A18	untreated	2	125	Spherulitic
A19	untreated	2	130	Spherulitic
A20	untreated	2	135	Spherulitic
A21	untreated	2	140	Spherulitic
A22	treated (0.16 wt%)	5	120	Transcrystalline
A23	treated (6 wt%)	9	120	Spherulitic
A24	treated (6 wt%)	3	120	Transcrystalline
A25	treated (4 wt%)	5	120	Transcrystalline
A26	treated (8 wt%)	7	130	Transcrystalline
A27	treated (8 wt%)	5	130	Transcrystalline
A28	treated (8 wt%)	5	120	Transcrystalline
A29	treated (6 wt%)	7	120	Transcrystalline
A30	treated (6 wt%)	6	120	Transcrystalline
A31	treated (6 wt%)	5	non-isothermal	Transcrystalline
A32	treated (6 wt%)	2	non-isothermal	Transcrystalline
A33	treated (6 wt%)	4	120	Transcrystalline

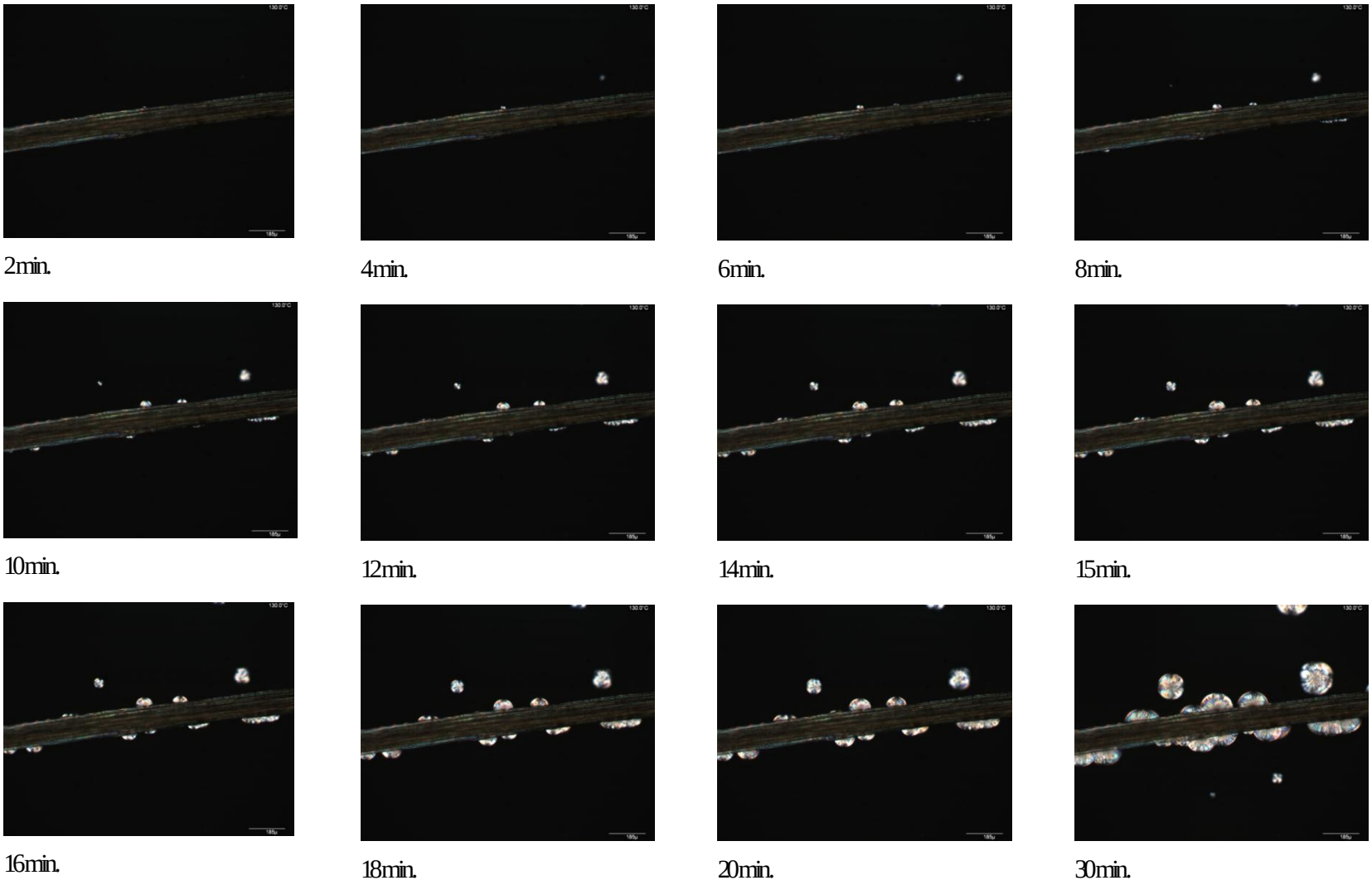

Figure A1: Isothermal spherullitic growth. Caustic soda treated sisal fibre (6 wt%). Cooling rate 5°C/min. Isothermal temperature 130°C

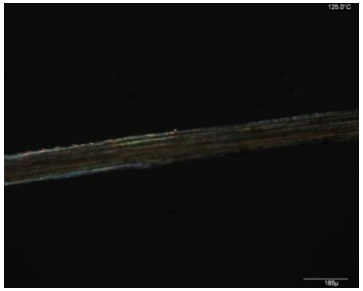

2min.

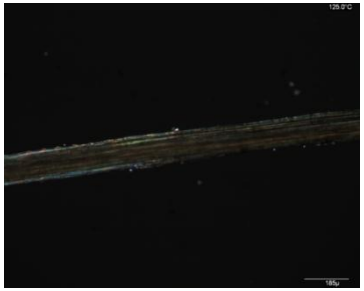

4min.

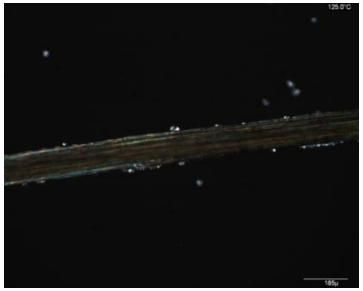

6min.

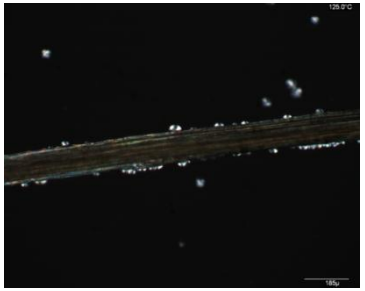

8min.

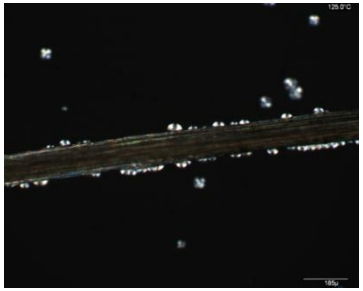

10min.

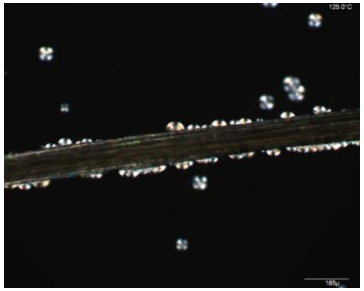

12min.

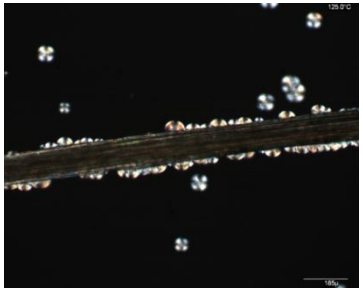

14min.

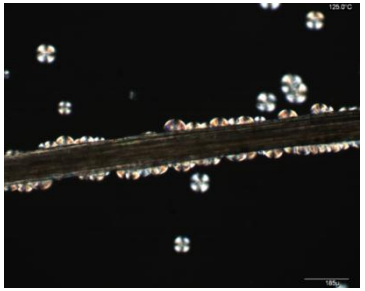

16min.

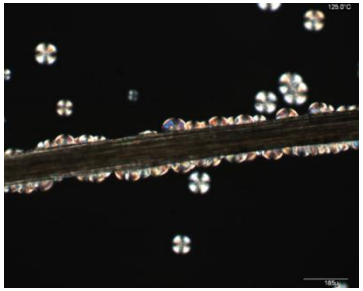

18min.

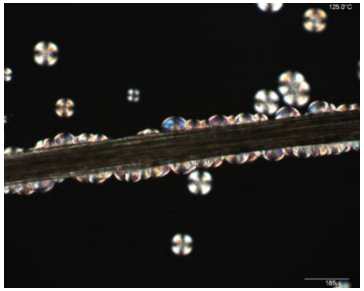

20min.

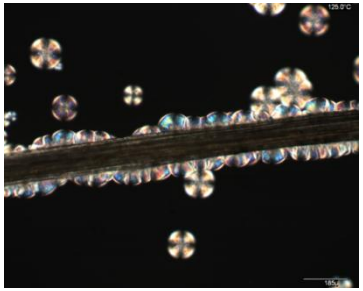

25min.

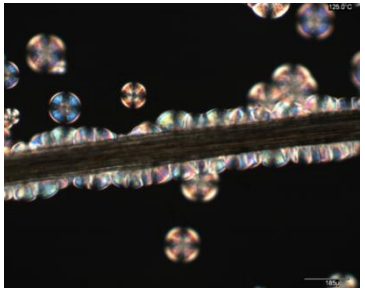

30min.

Figure A2: Isothermal spherullitic growth. Caustic soda treated sisal fibre (6wt%). Cooling rate 5°C/min. Isothermal temperature 125°C.

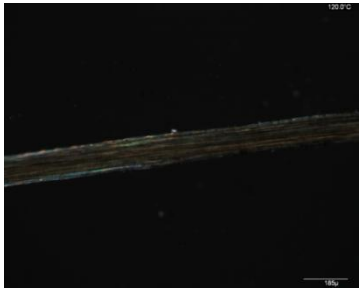

2min.

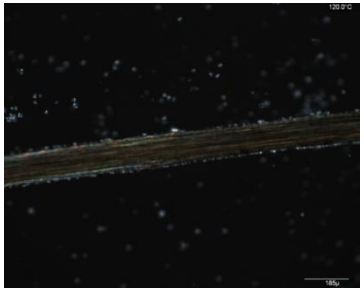

4min.

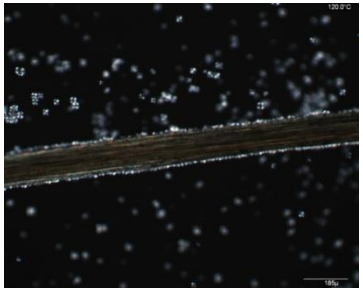

6min.

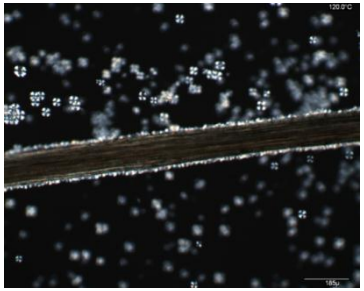

8min.

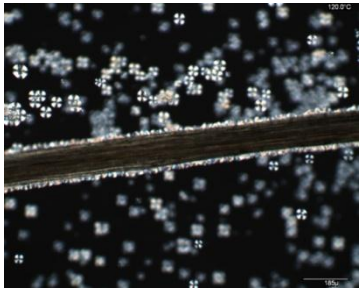

10min.

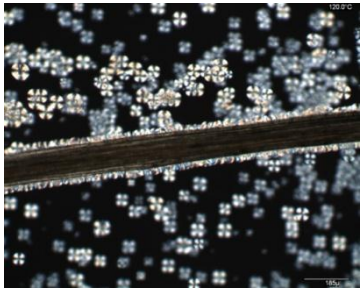

12min.

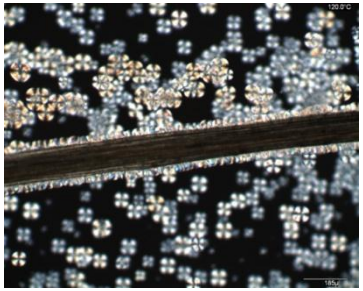

14min.

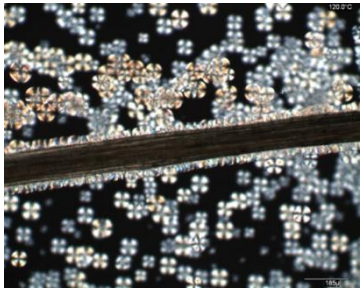

15min.

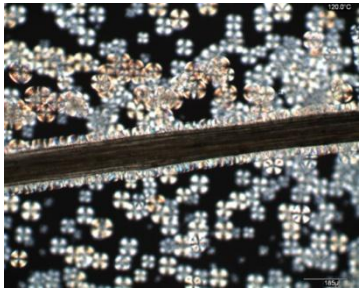

16min.

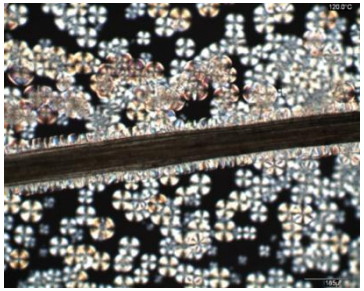

18min.

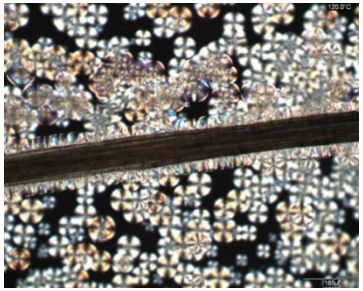

20min.

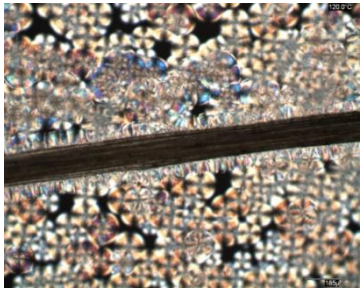

25min.

Figure A3: Isothermal transcrystalline growth. Caustic soda treated sisal fibre (6 wt%). Cooling rate 5°C/min. Isothermal temperature 120°C.

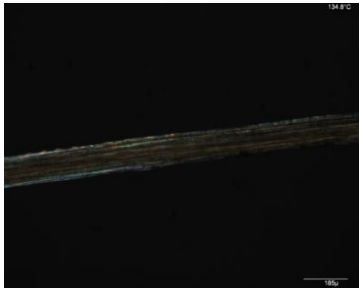

0min.

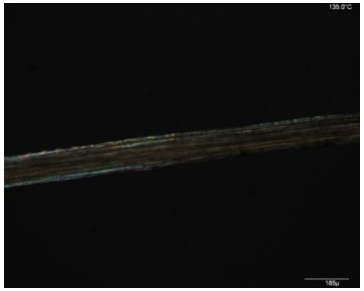

2min.

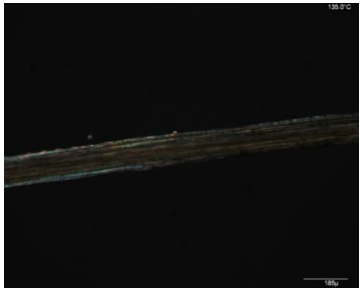

4min.

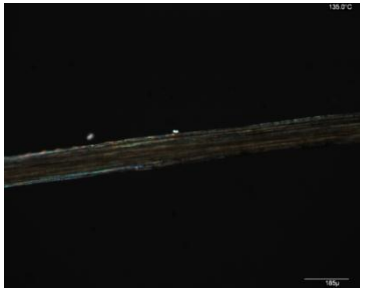

6min.

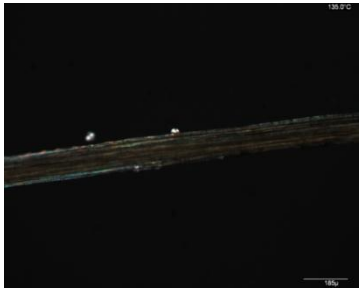

8min.

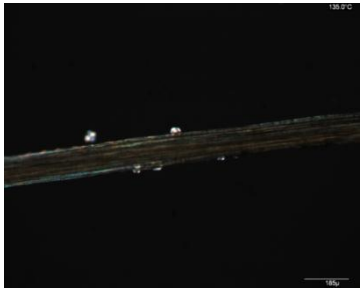

10min.

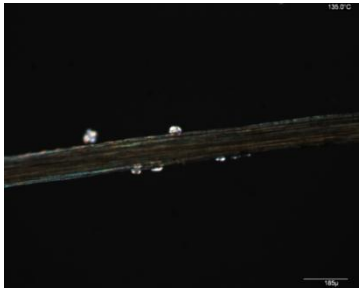

12min.

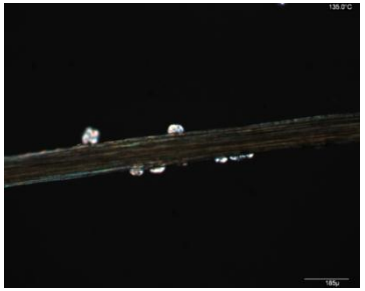

15min.

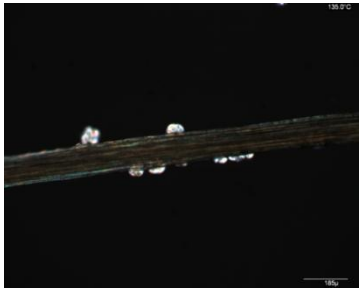

16min.

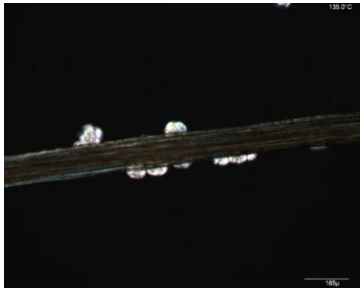

18min.

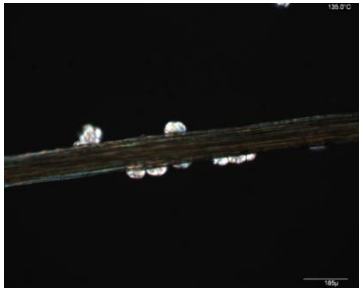

20min.

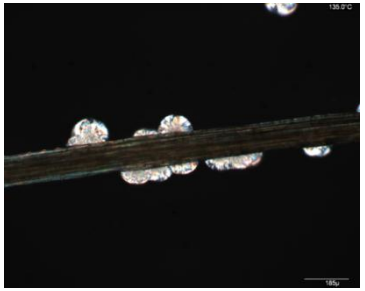

30min.

Figure A4: Isothermal spherullitic growth. Caustic soda treated sisal fibre (6 wt%). Cooling rate 5°C/min. Isothermal temperature 135°C.

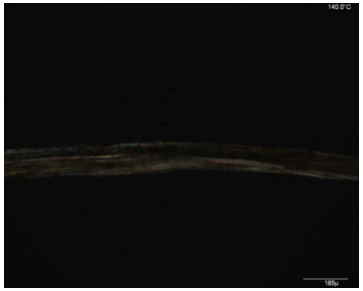

2min.

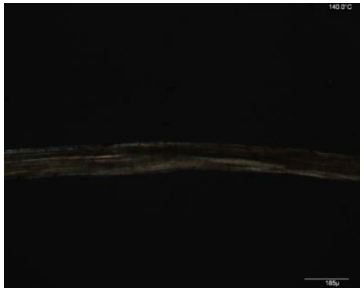

4min.

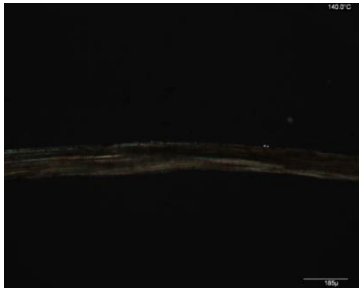

6min.

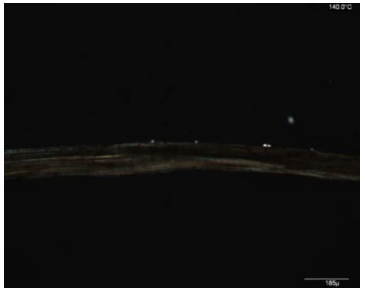

8min.

10min.

12min.

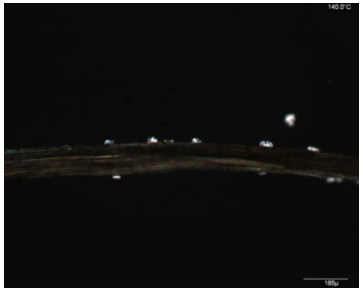

14min.

15min.

16min.

18min.

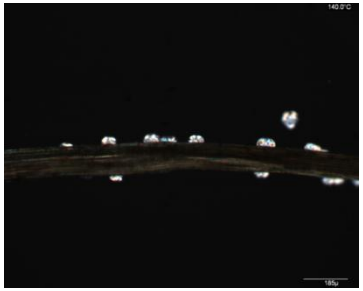

20min.

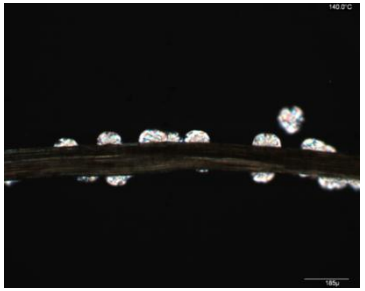

30min.

Figure A5: Isothermal spherullitic growth. Caustic soda treated sisal fibre (6 wt%). Cooling rate 5°C/min. Isothermal temperature 140°C.

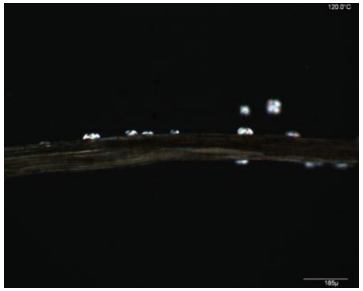

0min.

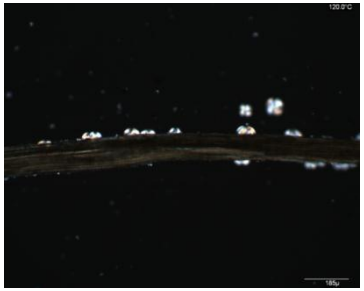

2min.

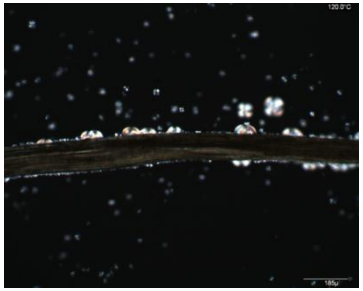

4min.

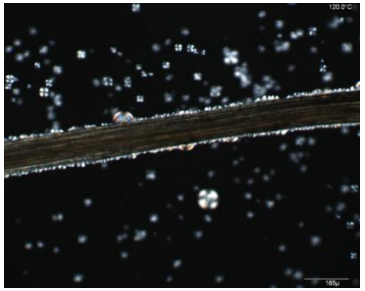

6min.

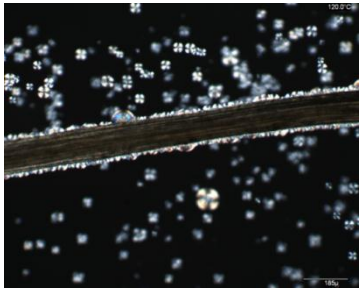

8min.

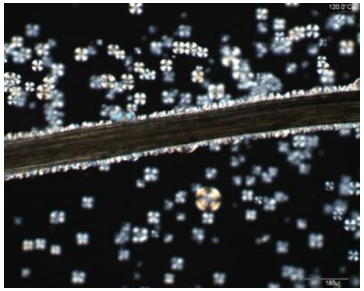

10min.

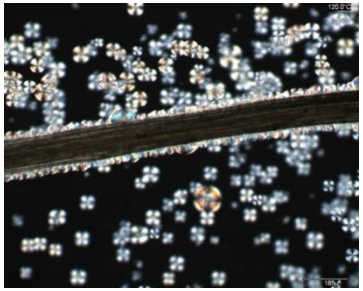

12min.

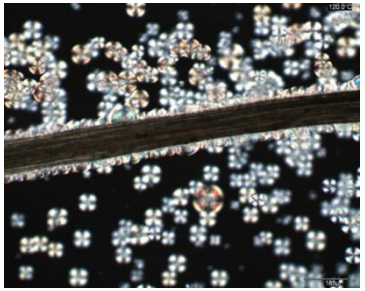

14min.

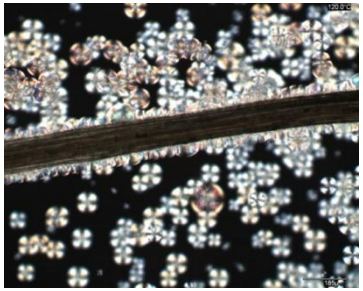

16min.

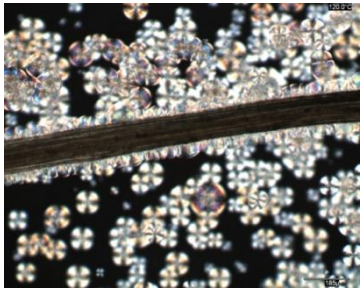

18min.

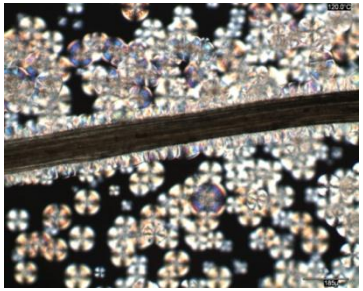

20min.

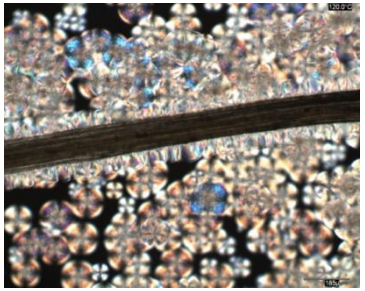

25min.

Figure A6: Isothermal transcrystalline growth. Caustic soda treated sisal fibre (6 wt%). Cooling rate 2°C/min. Isothermal temperature 120°C.

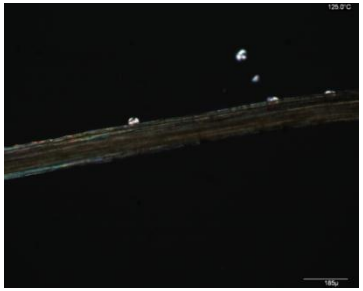

2min.

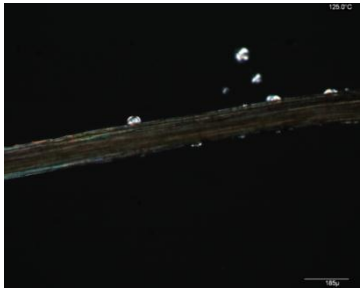

4min.

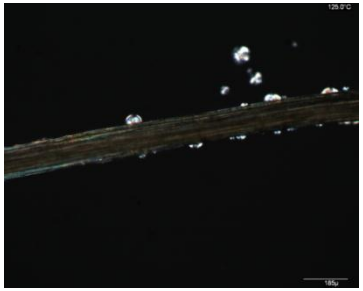

6min.

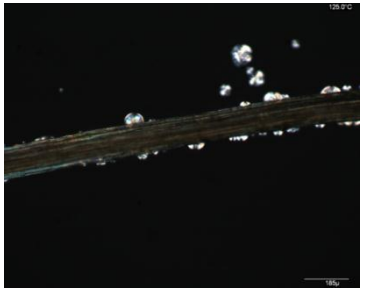

8min.

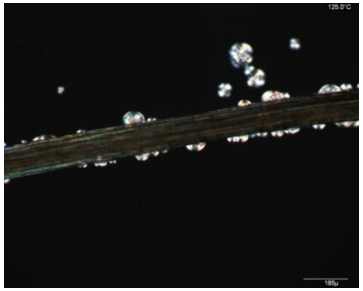

10min.

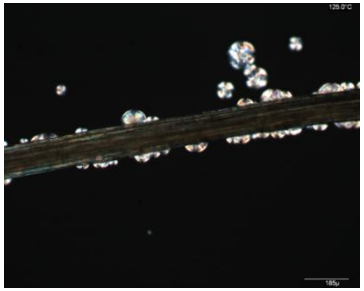

12min.

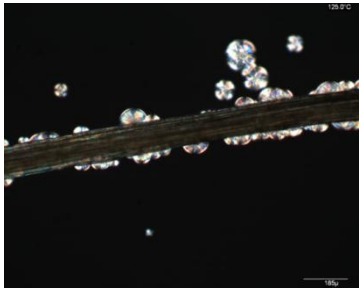

14min.

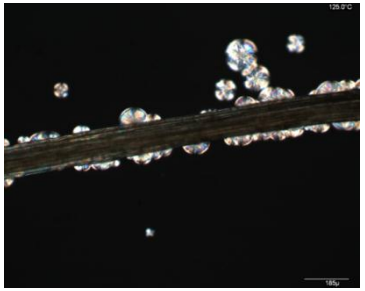

15min.

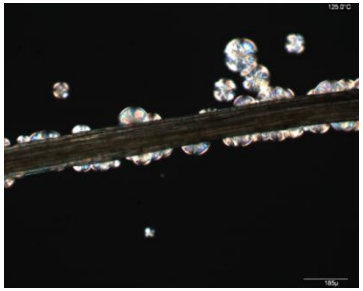

16min.

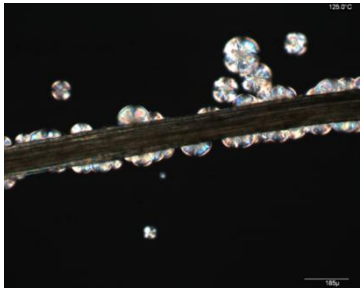

18min.

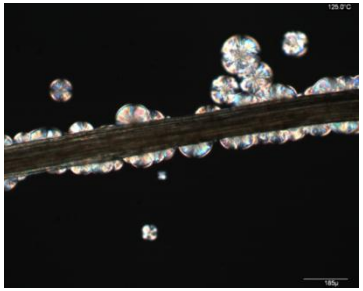

20min.

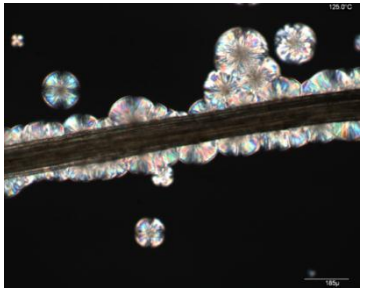

30min.

Figure A7: Isothermal spherullitic growth. Caustic soda treated sisal fibre (6 wt%). Cooling rate 2°C/min. Isothermal temperature 125°C.

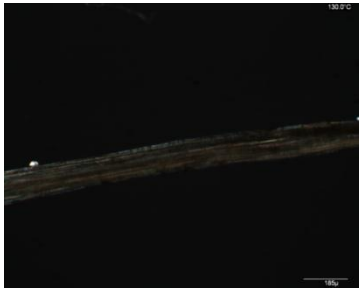

2min.

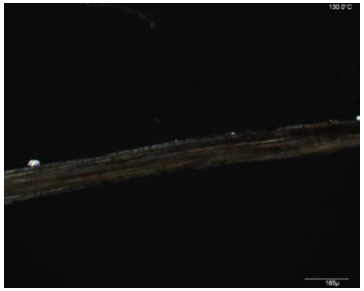

4min.

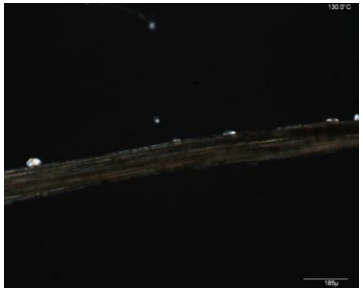

6min.

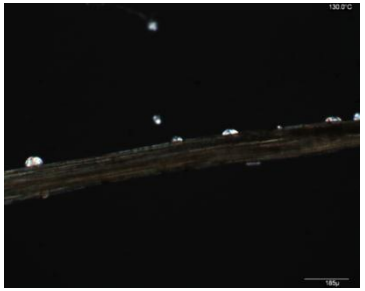

8min.

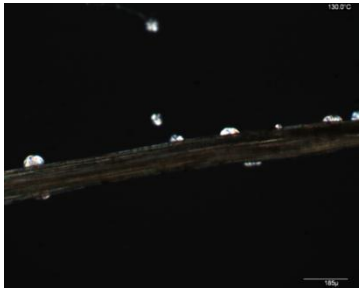

10min.

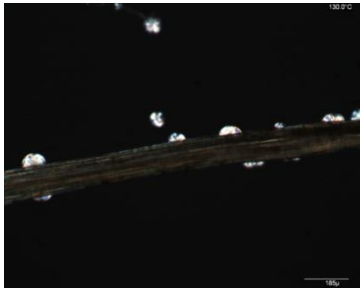

12min.

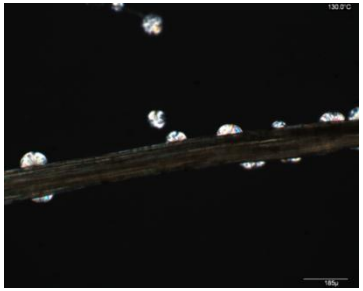

14min.

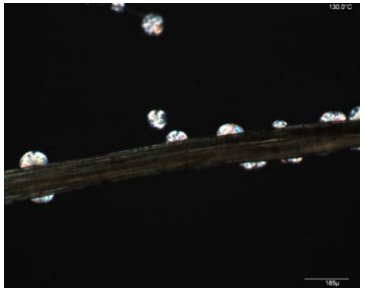

15min.

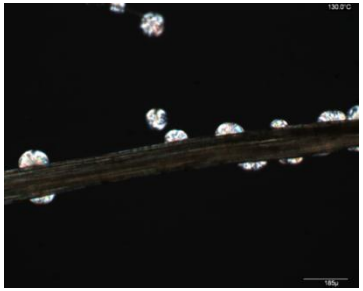

16min.

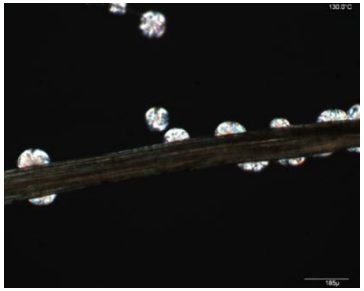

18min.

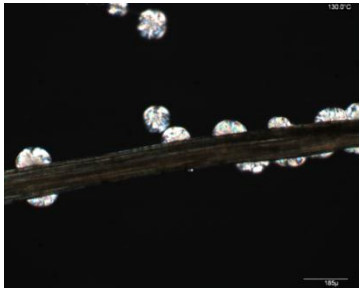

20min.

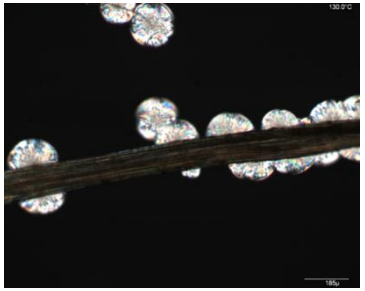

30min.

Figure A8: Isothermal spherullitic growth. Caustic soda treated sisal fibre (6 wt%). Cooling rate 2°C/min. Isothermal temperature 130°C.

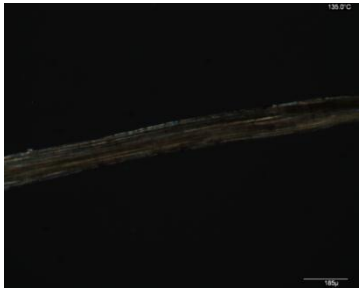

2min.

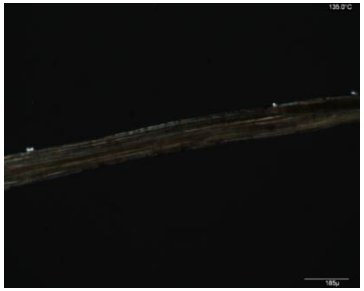

4min.

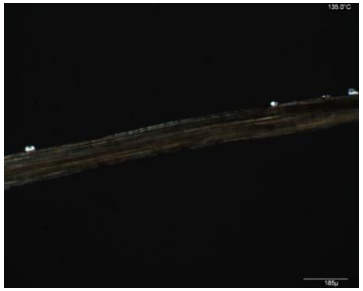

6min.

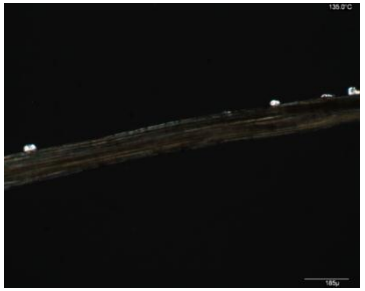

8min.

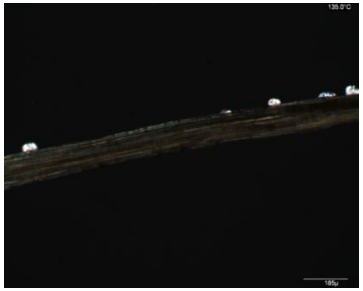

10min.

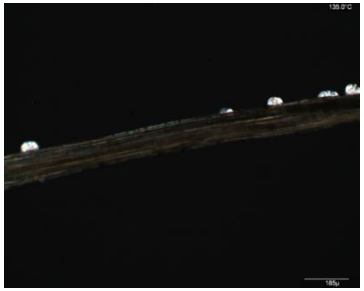

12min.

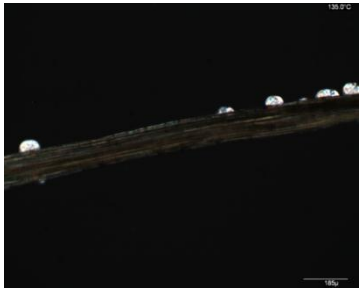

14min.

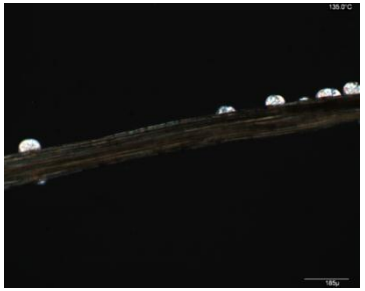

15min.

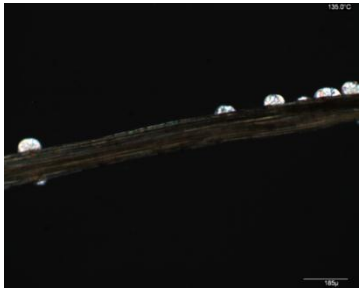

16min.

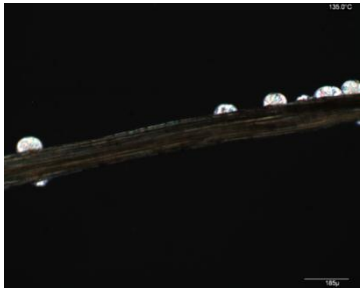

18min.

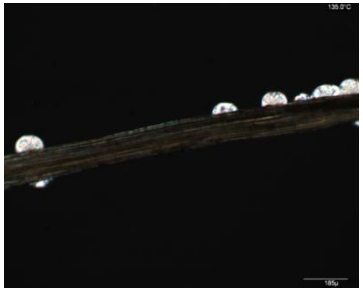

20min.

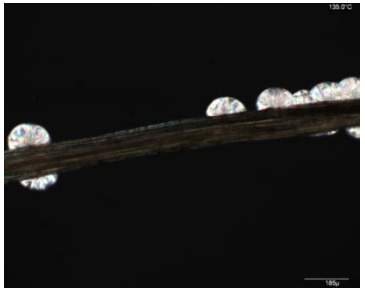

30min.

Figure A9: Isothermal spherullitic growth. Caustic soda treated sisal fibre (6 wt%). Cooling rate 2°C/min. Isothermal temperature 135°C.

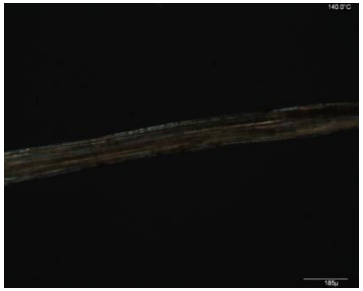

2min.

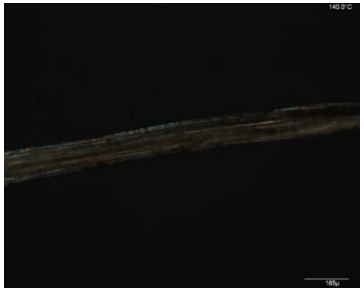

4min.

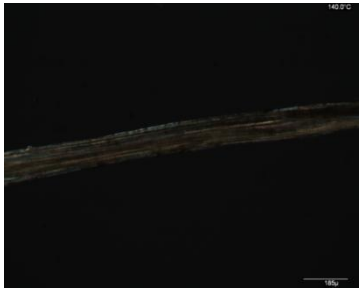

6min.

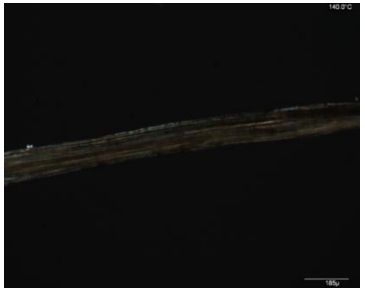

8min.

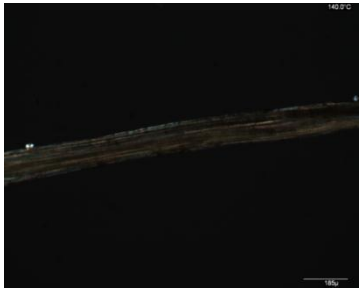

10min.

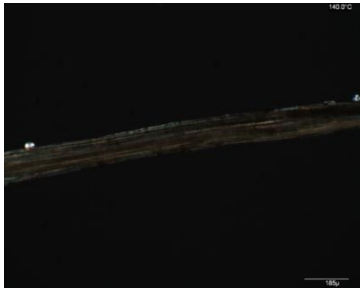

12min.

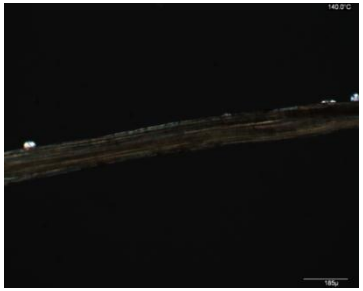

14min.

15min

16min.

18min.

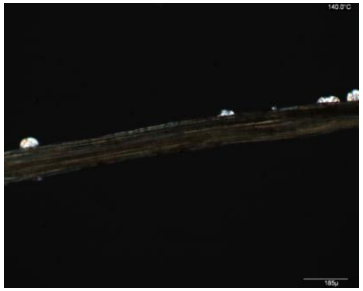

20min.

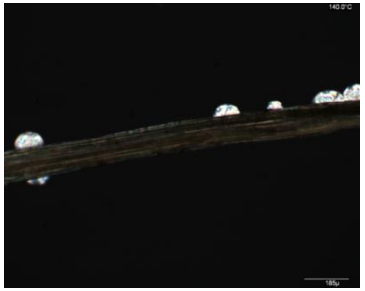

30min.

Figure A10: Isothermal spherullitic growth. Caustic soda treated sisal fibre (6 wt%). Cooling rate 2°C/min. Isothermal temperature 140°C.

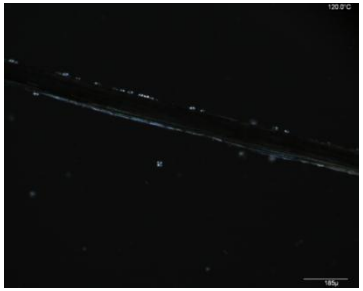

2min.

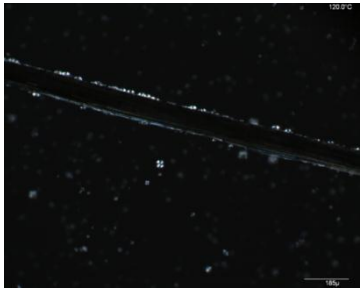

4min.

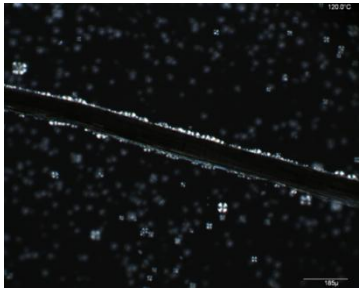

6min.

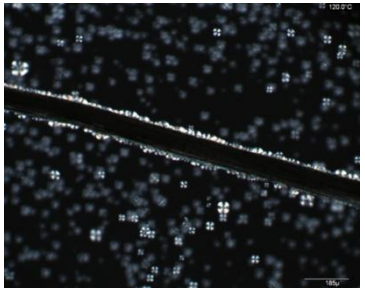

8min.

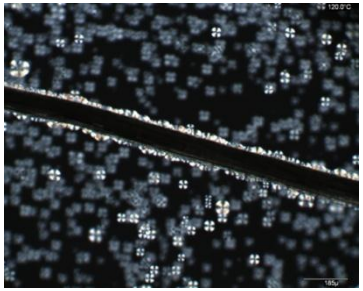

10min.

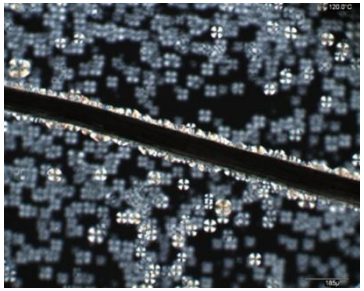

12min.

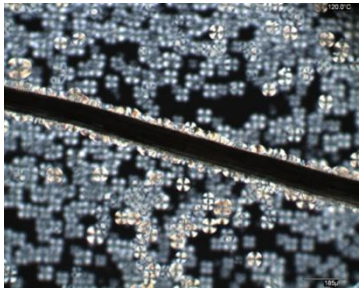

14min.

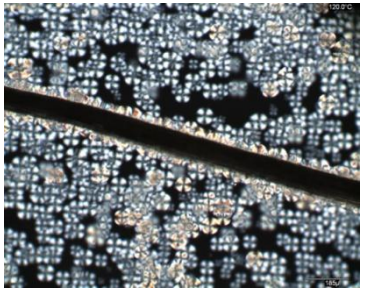

15min.

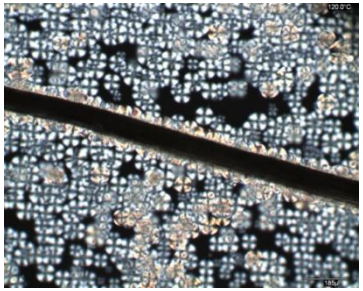

16min.

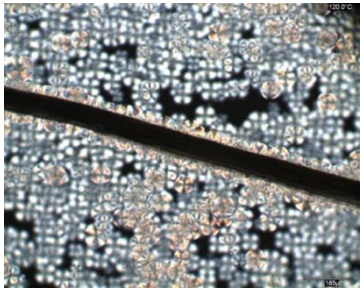

18min.

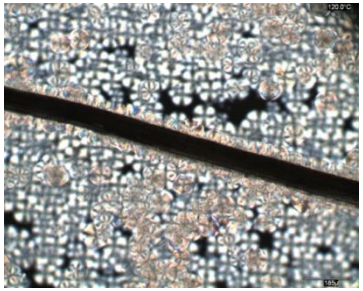

20min.

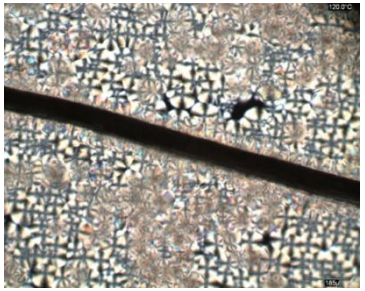

25min.

Figure A11: Isothermal spherulitic growth. Untreated sisal fibre. Cooling rate 5°C/min. Isothermal temperature 120°C.

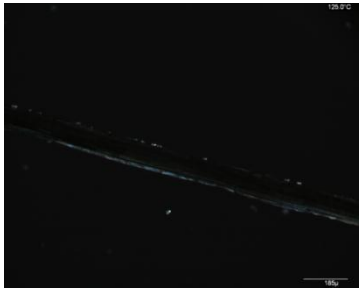

2min.

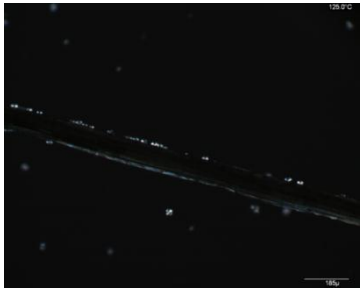

4min.

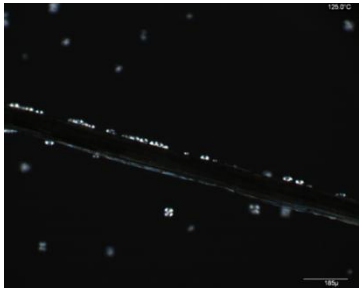

6min.

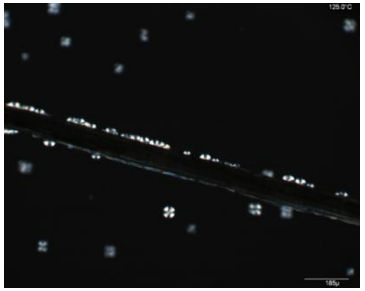

8min.

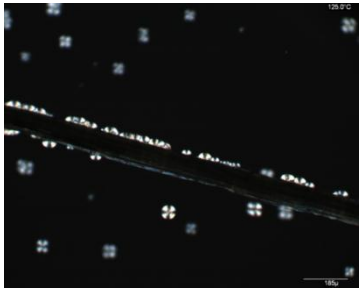

10min.

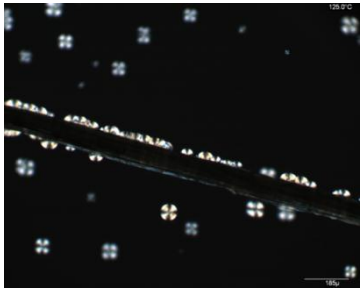

12min.

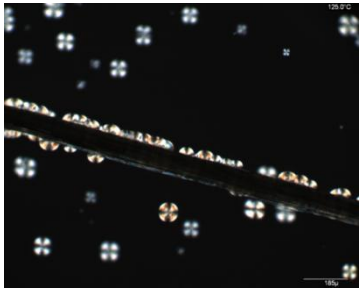

14min.

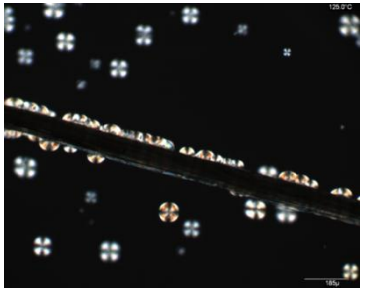

15min.

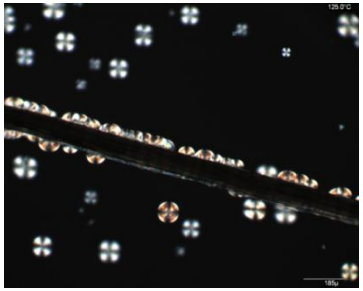

16min.

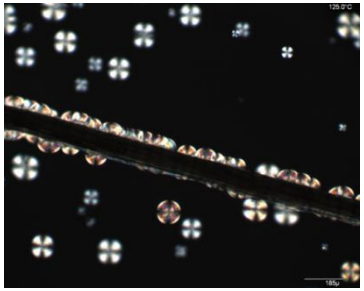

18min.

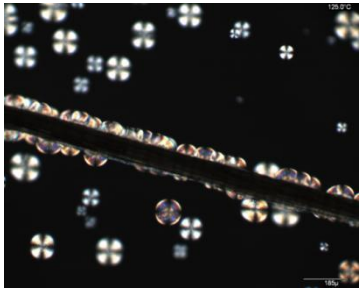

20min.

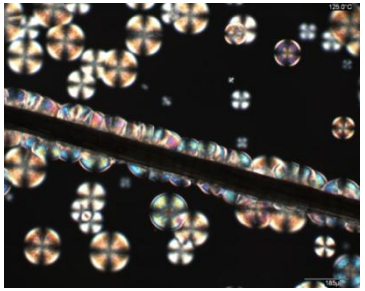

30min.

Figure A12: Isothermal spherullitic growth. Untreated sisal fibre. Cooling rate 5°C/min. Isothermal temperature 125°C.

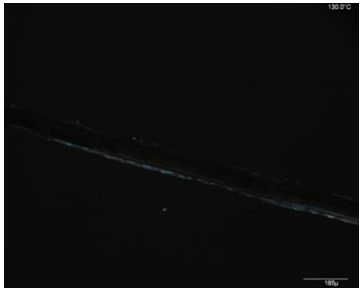

2min.

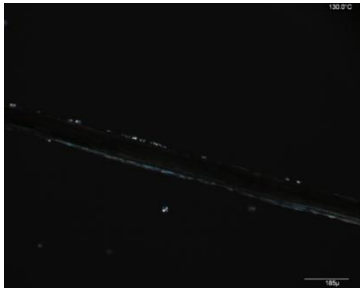

4min.

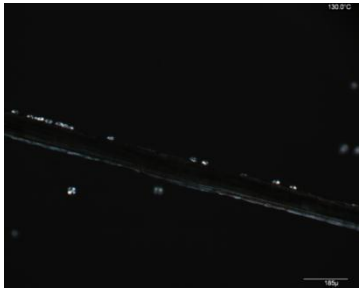

6min.

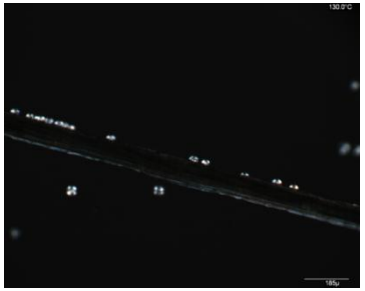

8min.

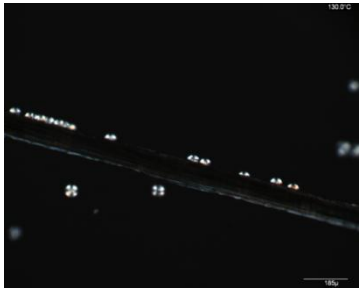

10min.

12min.

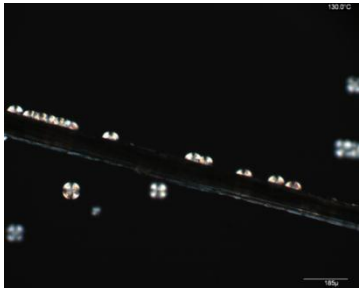

14min.

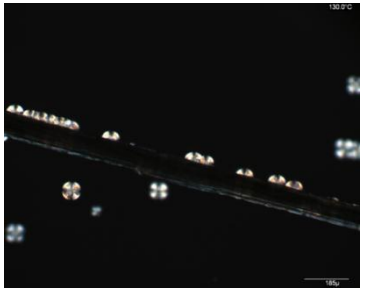

15min.

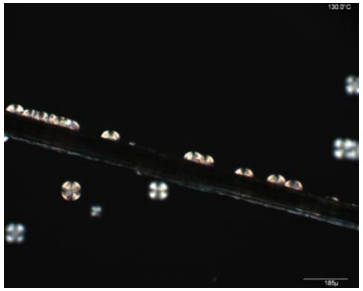

16min.

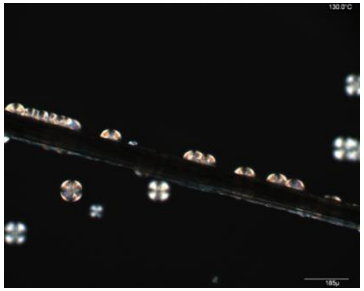

18min.

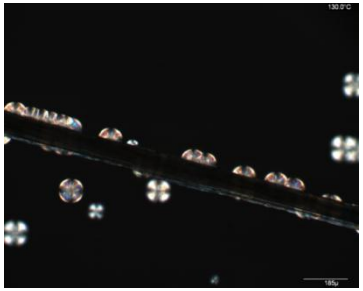

20min.

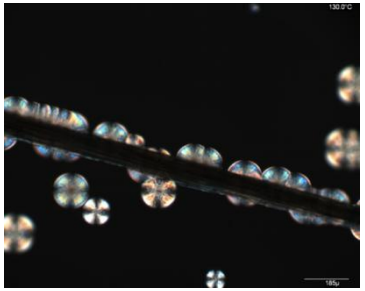

30min.

Figure A13: Isothermal spherullitic growth. Untreated sisal fibre. Cooling rate 5°C/min. Isothermal temperature 130°C.

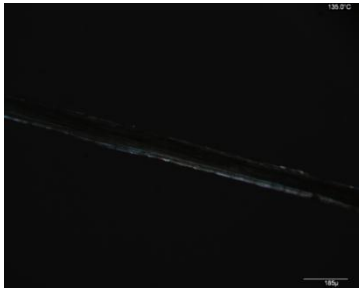

2min.

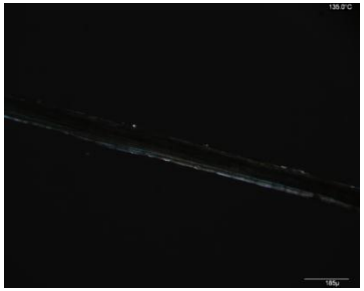

4min.

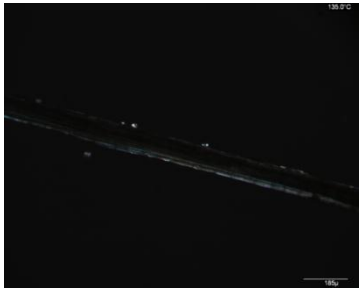

6min.

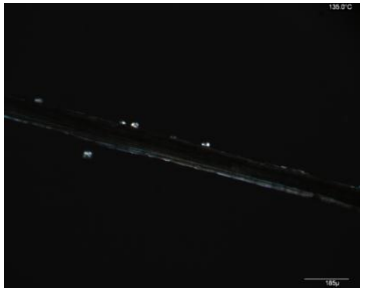

8min.

10min.

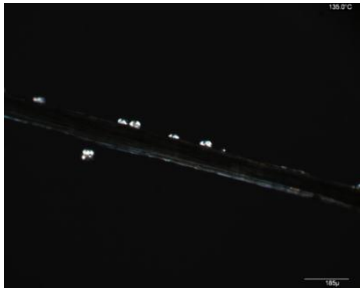

12min.

14min.

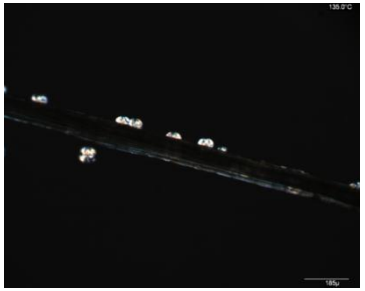

16min.

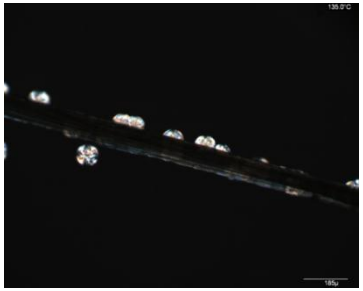

20min.

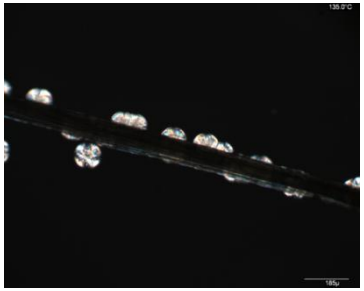

25min.

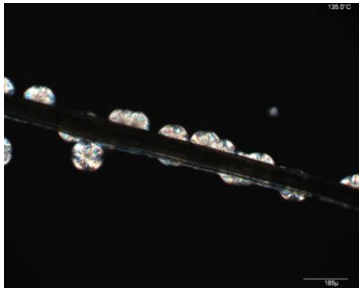

30min.

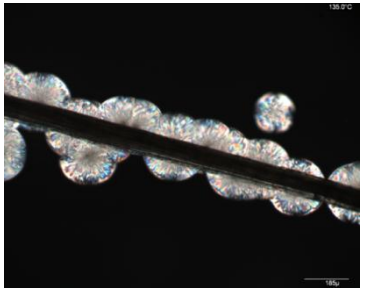

55min.

Figure A14: Isothermal spherullitic growth. Untreated sisal fibre . Cooling rate 5°C/min. Isothermal temperature 135°C.

2min.

4min.

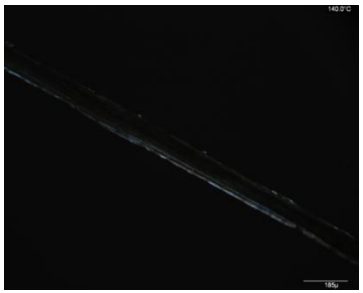

6min.

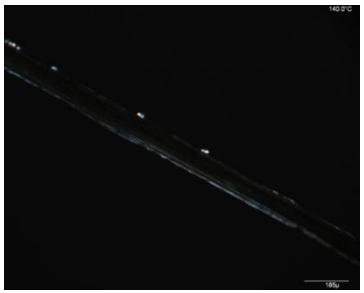

8min.

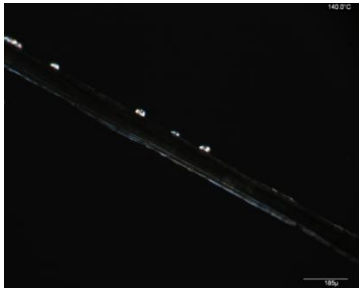

10min.

12min.

14min.

15min.

16min.

18min.

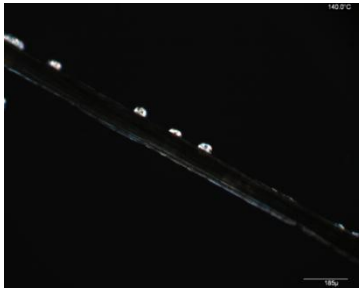

20min.

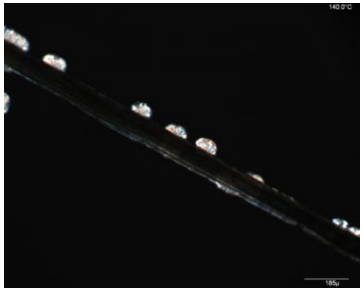

30min.

Figure A15: Isothermal spherullitic growth. Untreated sisal fibre (6 wt%). Cooling rate 5°C/min. Isothermal temperature 140°C.

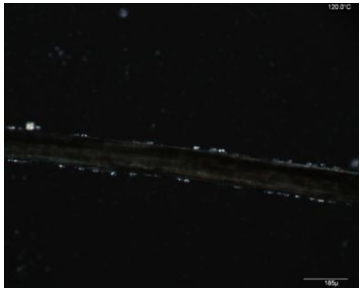

2min.

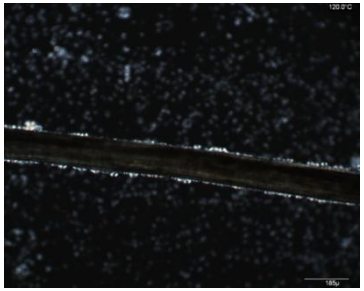

4min.

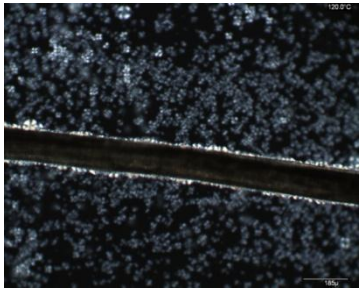

6min.

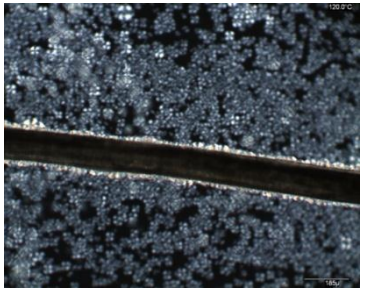

8min.

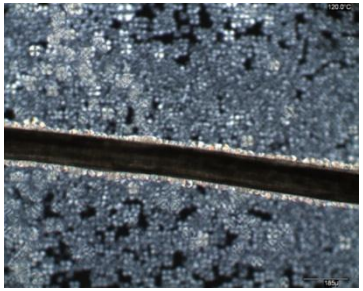

10min.

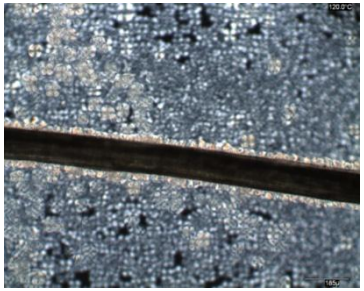

12min.

14min.

16min.

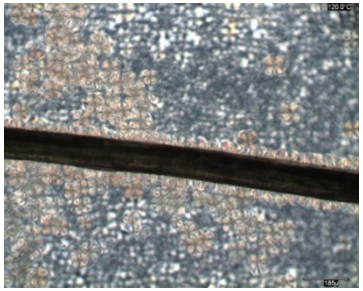

18min.

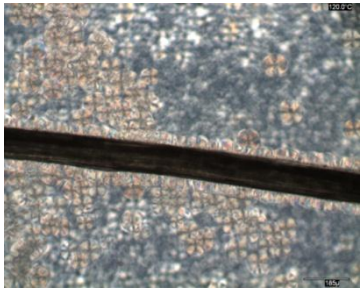

20min.

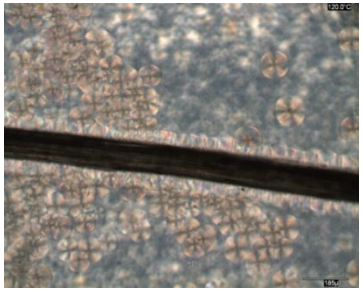

25min.

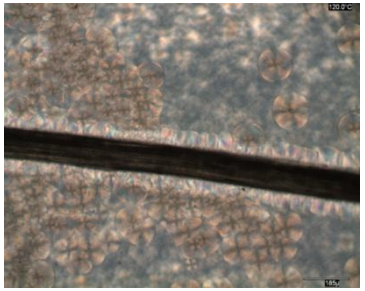

30min.

Figure A16: Isothermal transcrystalline growth. Caustic soda treated sisal fibre (2wt%). Cooling rate 5°C/min. Isothermal temperature 120°C.

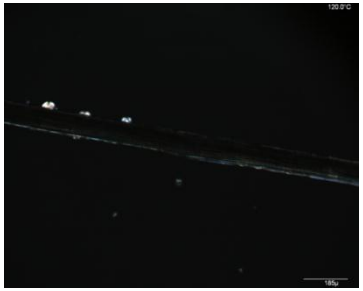

0min.

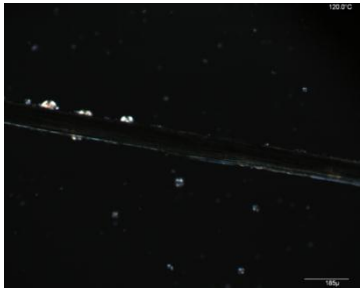

2min.

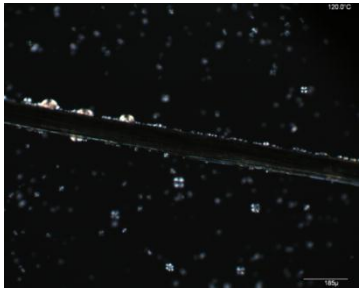

4min.

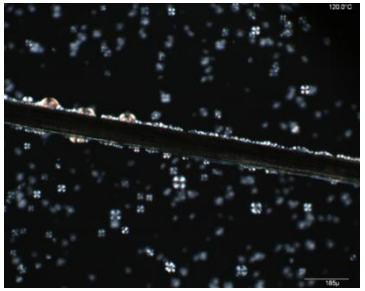

6min.

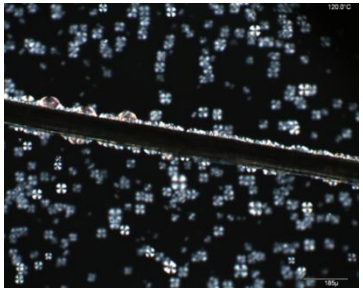

8min.

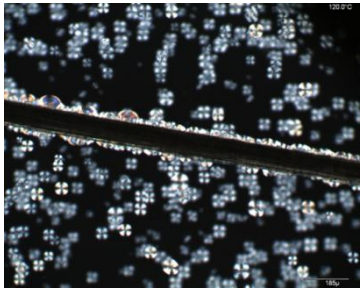

10min.

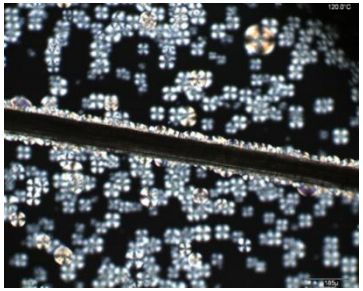

12min.

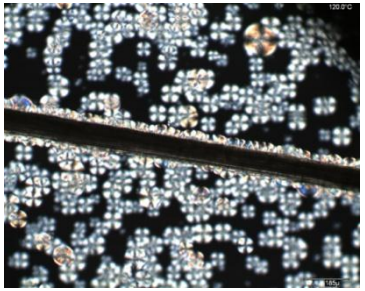

14min.

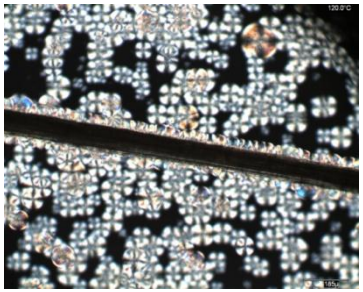

16min.

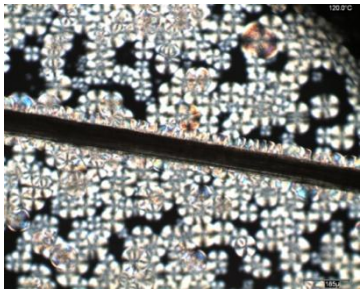

18min.

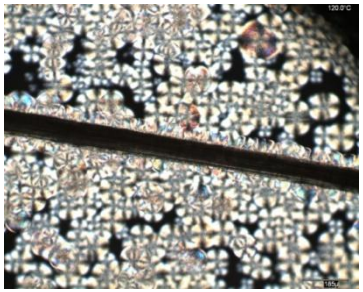

20min.

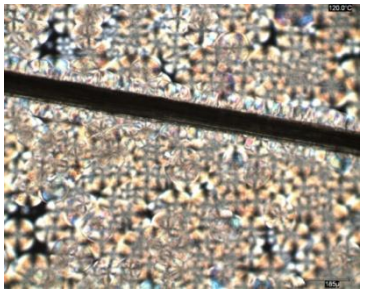

25min.

Figure A17: Isothermal spherullitic growth. Untreated sisal fibre. Cooling rate 2°C/min. Isothermal temperature 120°C.

2min.

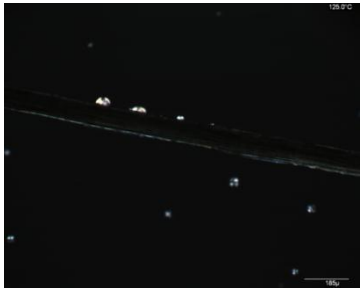

4min.

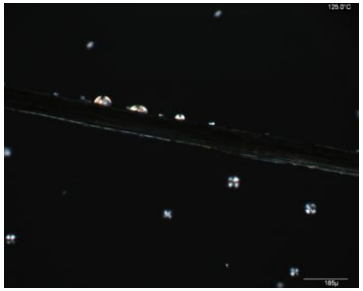

6min.

8min.

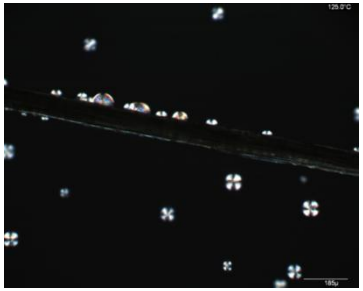

10min.

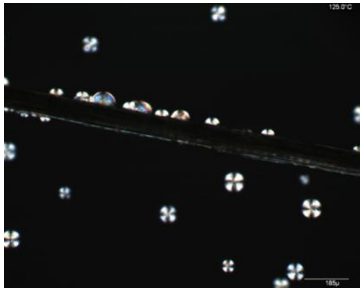

12min.

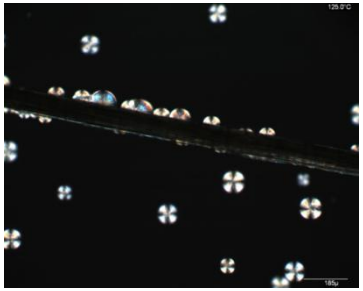

14min.

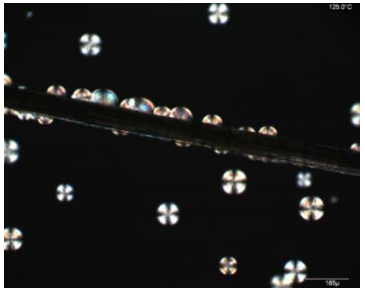

16min.

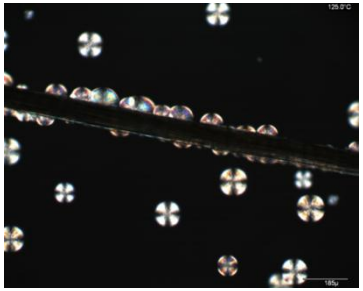

18min.

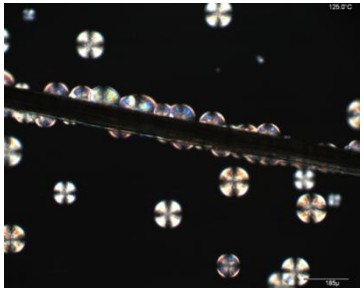

20min.

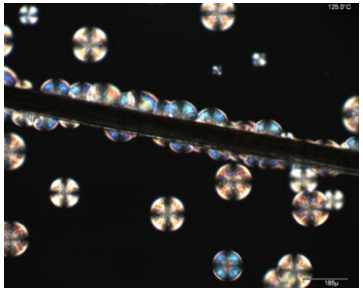

25min.

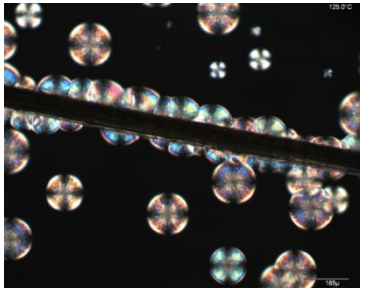

30min.

Figure A18: Isothermal spherullitic growth. Untreated sisal fibre. Cooling rate 2°C/min. Isothermal temperature 125°C.

2min.

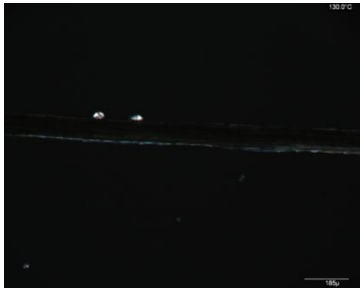

4min.

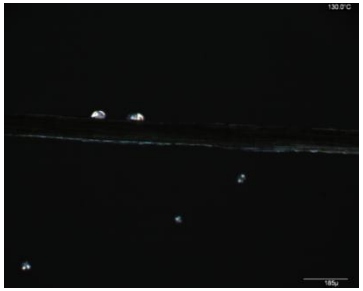

6min.

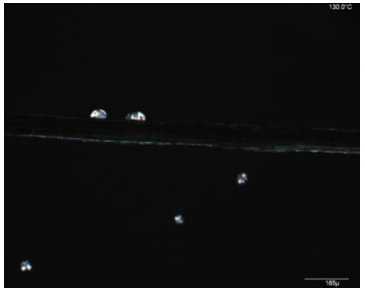

8min.

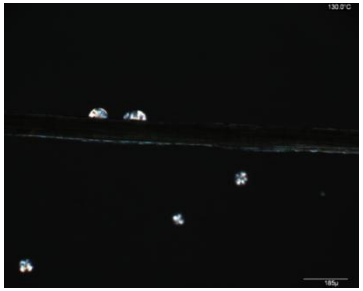

10min.

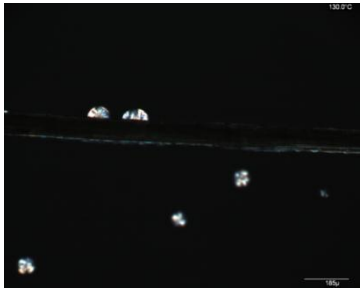

12min.

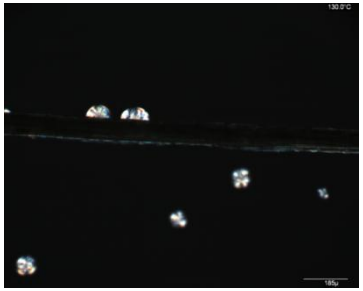

14min.

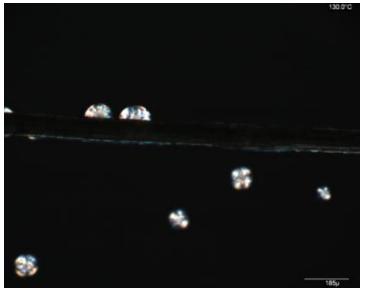

16min.

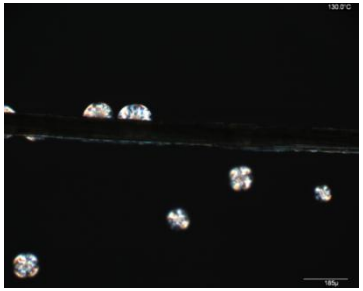

18min.

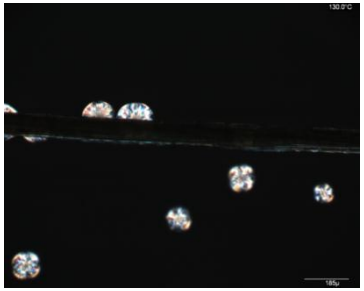

20min.

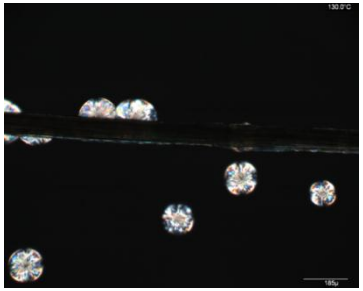

25min.

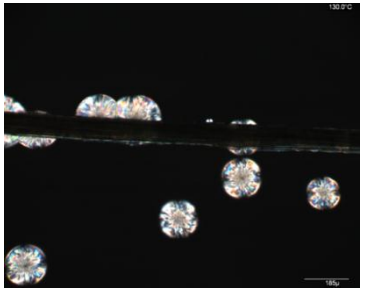

30min.

Figure A19: Isothermal spherullitic growth. Untreated sisal fibre. Cooling rate 2°C/min. Isothermal temperature 130°C.

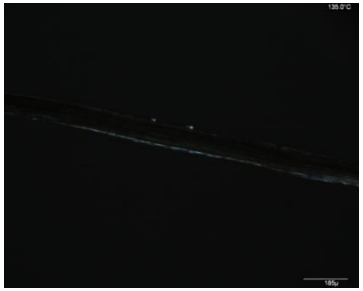

2min.

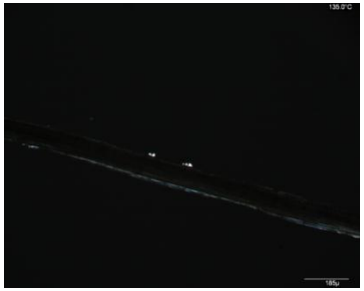

4min.

6min.

8min.

10min.

12min.

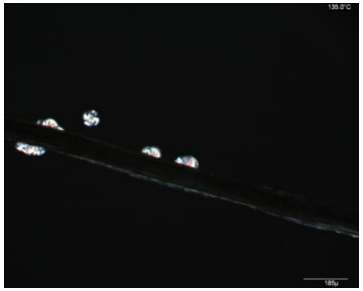

14min.

16min.

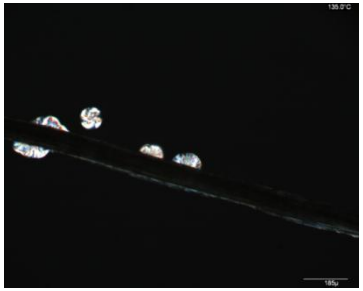

18min.

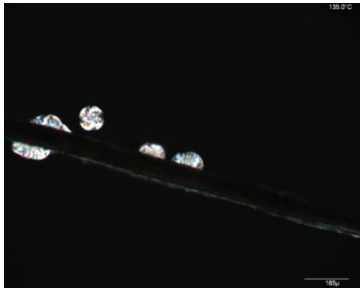

20min.

25min.

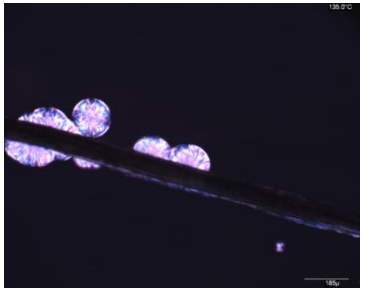

30min.

Figure A20: Isothermal spherullitic growth. Untreated sisal fibre. Cooling rate 2°C/min. Isothermal temperature 135°C.

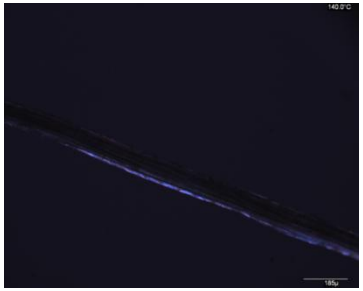

0min.

2min.

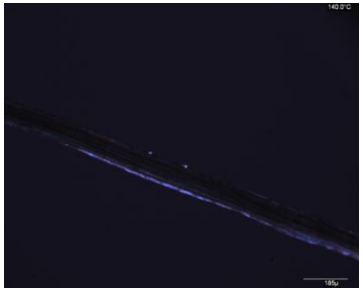

4min.

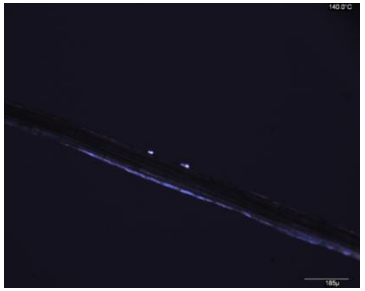

6min.

8min.

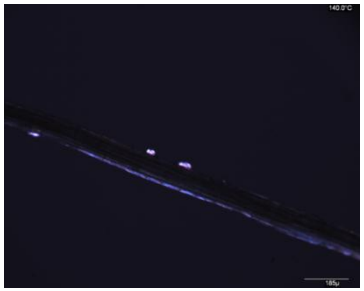

10min.

12min.

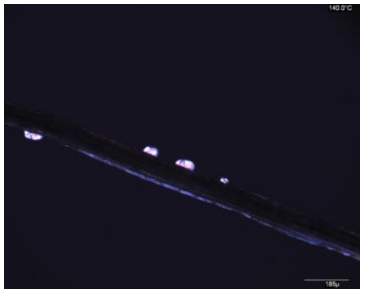

16min.

18min.

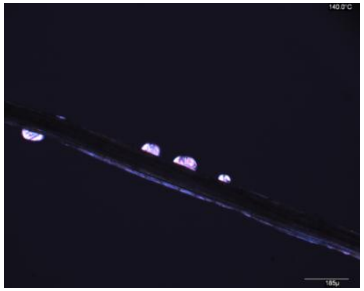

20min.

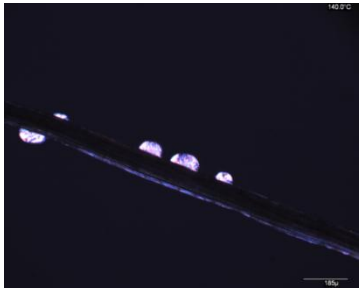

25min.

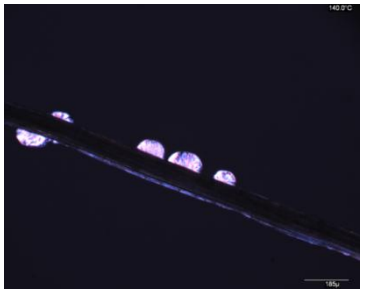

30min.

Figure A21: Isothermal spherullitic growth. Untreated sisal fibre. Cooling rate 2°C/min. Isothermal temperature 140°C.

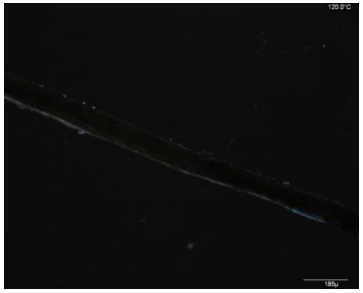

2min.

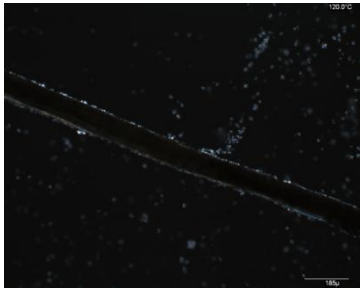

4min.

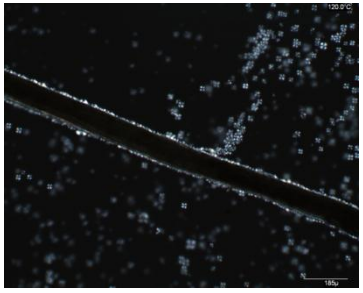

6min.

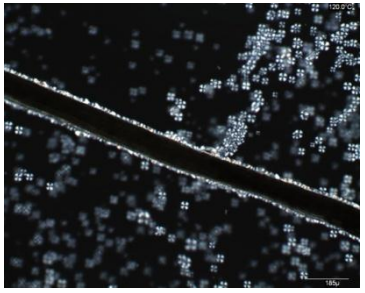

8min.

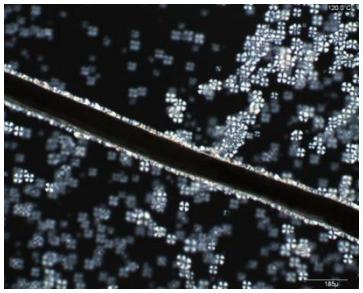

10min.

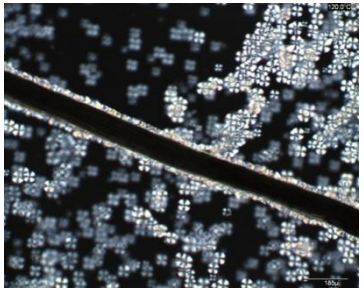

12min.

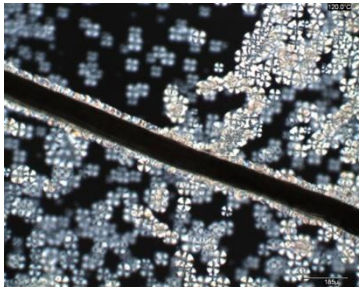

14min.

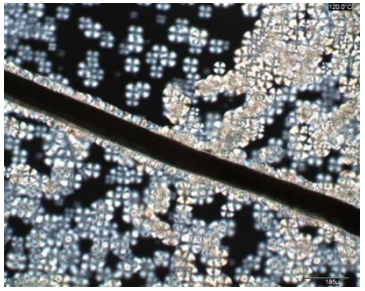

16min.

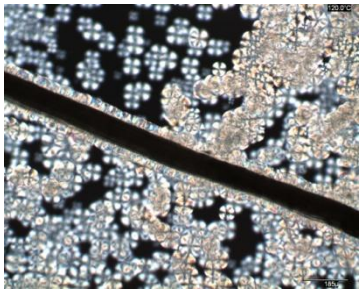

18min.

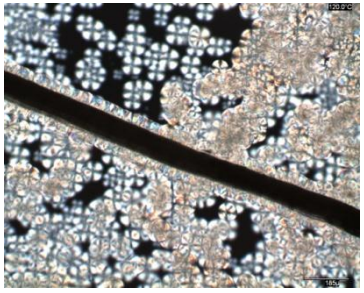

20min.

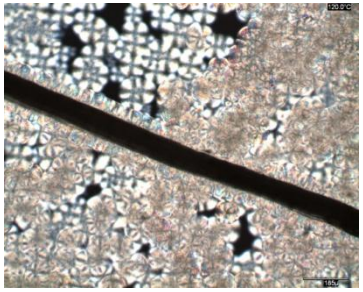

25min.

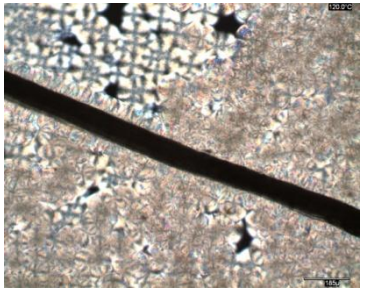

30min.

Figure A22: Isothermal transcrystalline growth. Caustic soda treated sisal fibre (0.16 wt%). Cooling rate 5°C/min. Isothermal temperature 120°C.

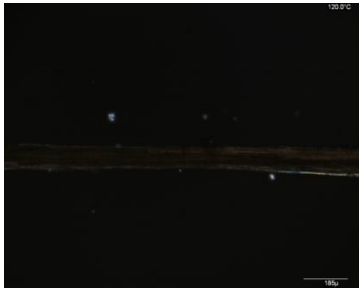

2min.

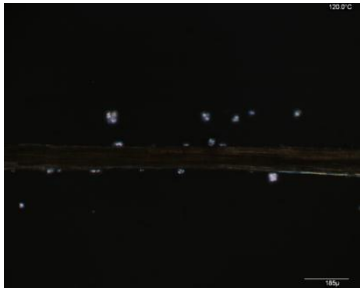

4min.

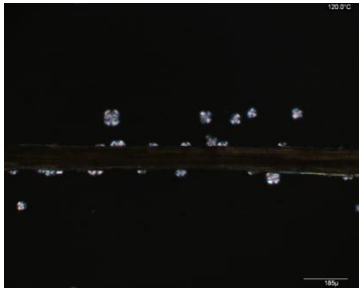

6min.

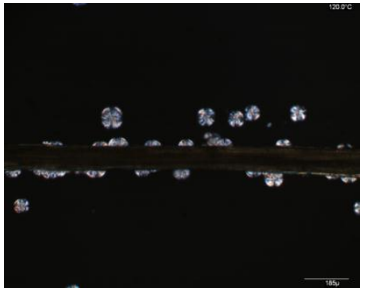

8min.

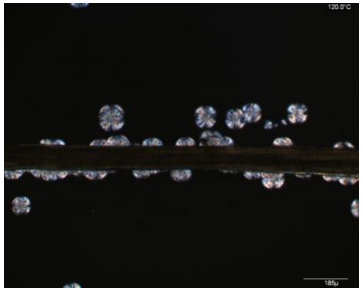

10min.

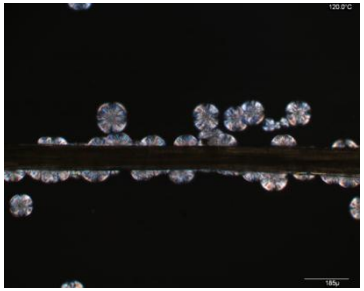

12min.

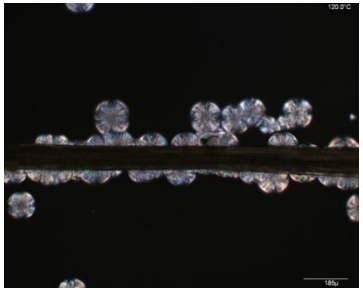

14min.

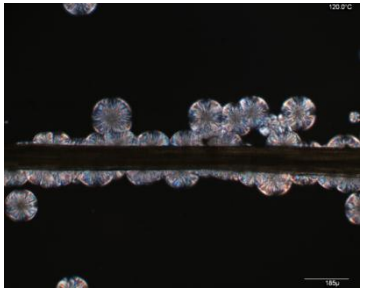

16min.

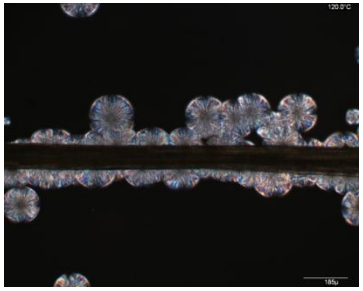

18min.

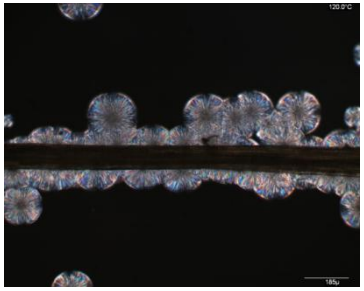

20min.

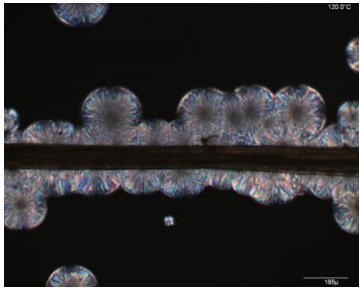

25min.

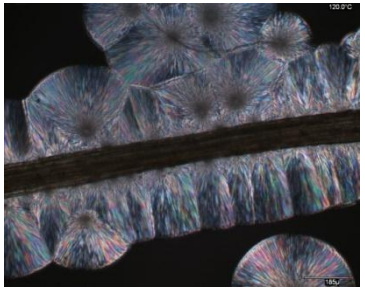

60min.

Figure: A23: Isothermal spherullitic growth. Caustic soda treated sisal fibre (6 wt%). Cooling rate 9°C/min. Isothermal temperature 120°C.

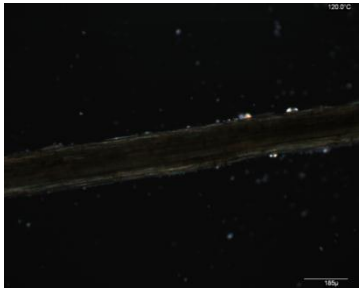

2min.

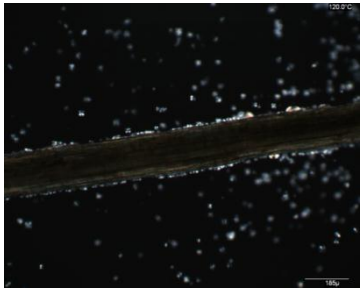

4min.

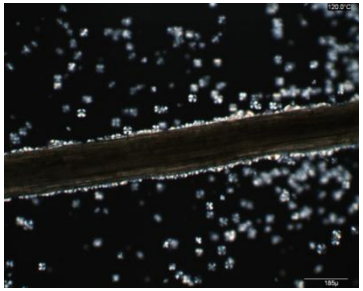

6min.

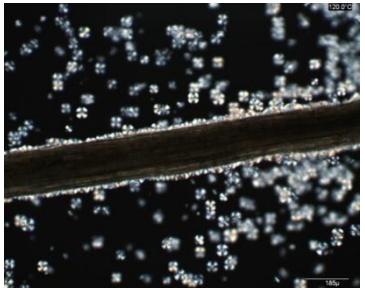

8min.

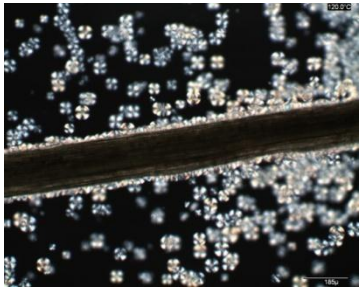

10min.

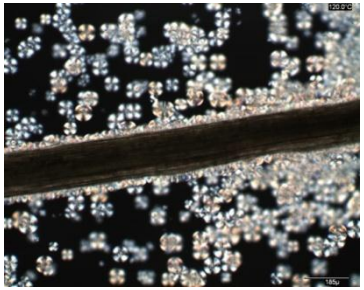

12min.

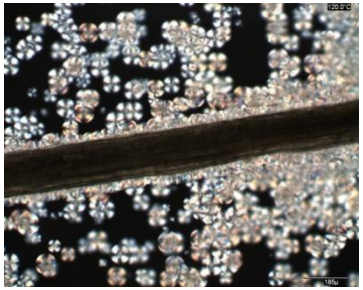

14min.

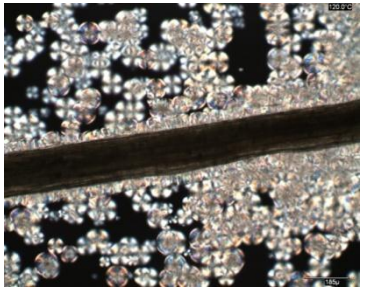

16min.

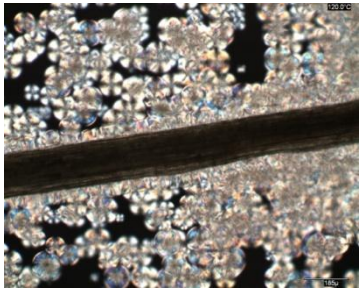

18min.

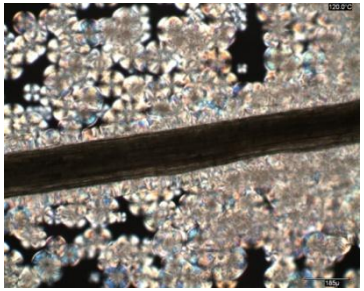

20min.

25min.

30min.

Figure A24: Isothermal transcrystalline growth. Caustic soda treated sisal fibre (6 wt%). Cooling rate 3°C/min. Isothermal temperature 120°C.

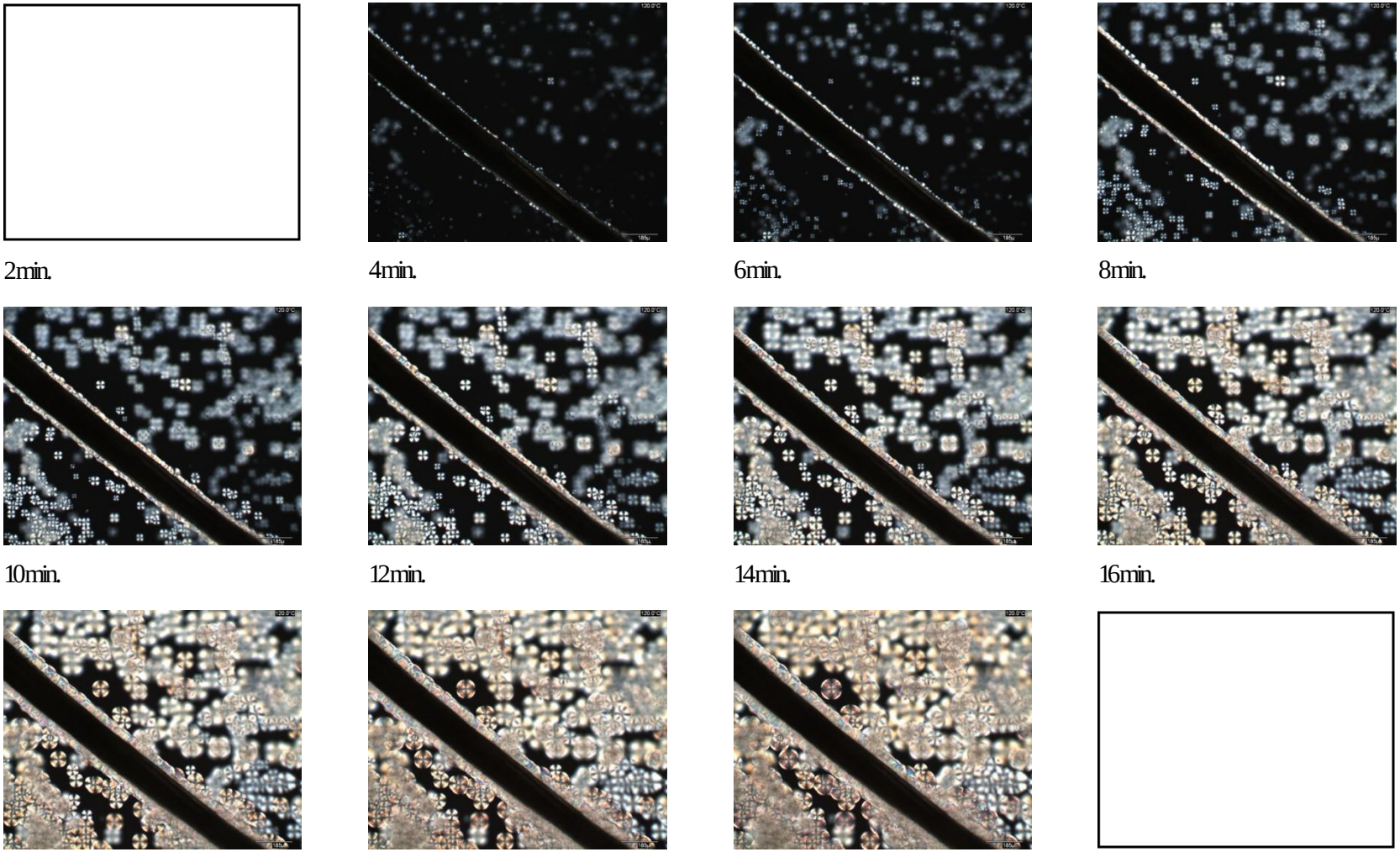

Figure A25: Isothermal transcrystalline growth. Caustic soda treated sisal fibre (4wt%). Cooling rate 5°C/min. Isothermal temperature 120°C.

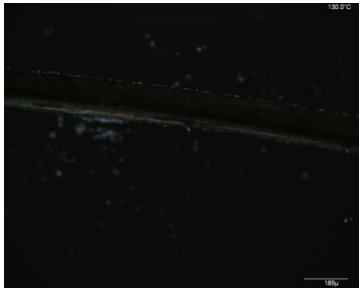

2min.

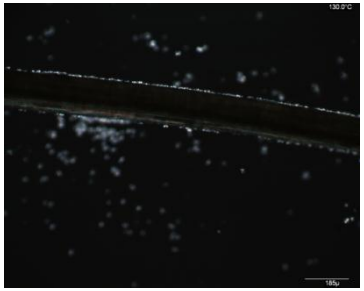

4min.

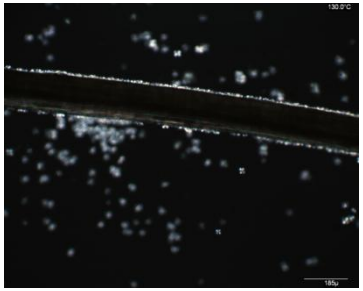

6min.

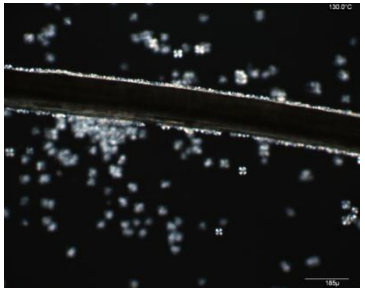

8min.

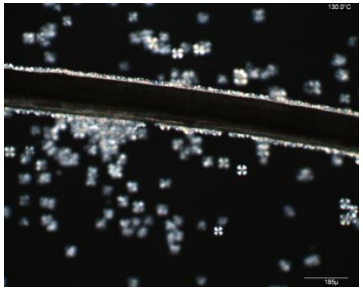

10min.

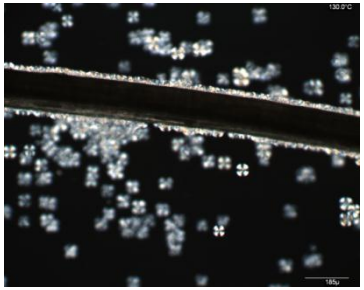

12min.

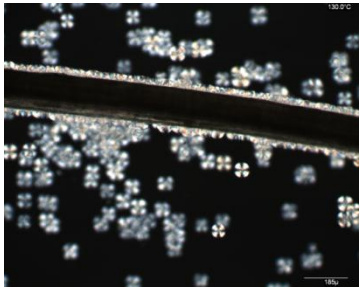

14min.

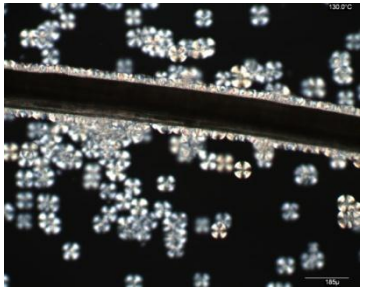

16min.

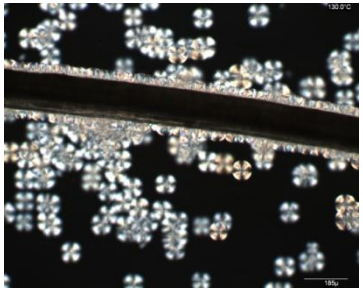

18min.

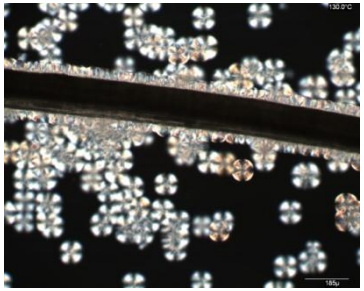

20min.

25min.

30min.

Figure A26: Isothermal transcrystalline growth. Caustic soda treated sisal fibre (8wt%). Cooling rate 7°C/min. Isothermal temperature 130°C.

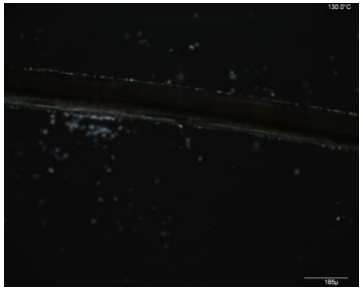

2min.

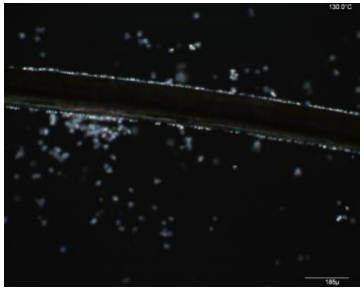

4min.

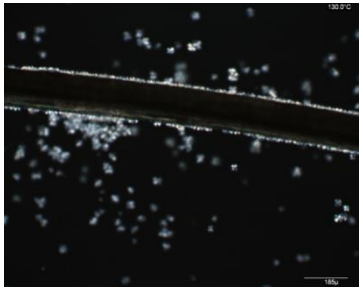

6min.

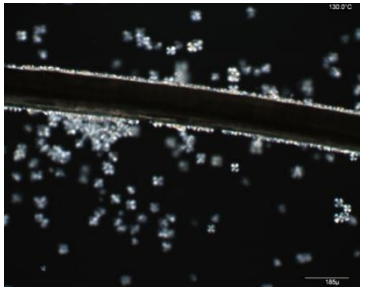

8min.

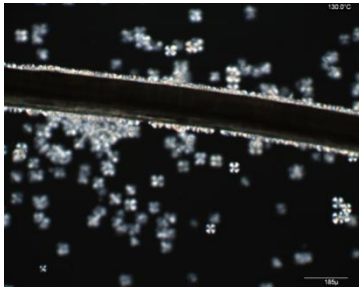

10min.

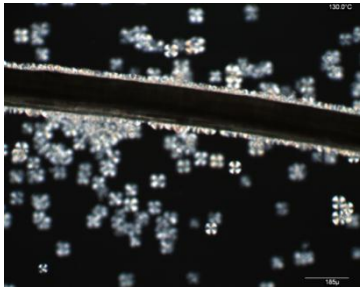

12min.

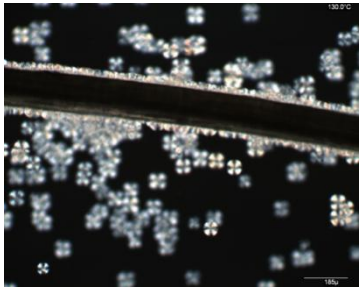

14min.

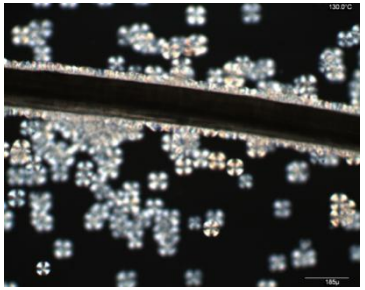

16min.

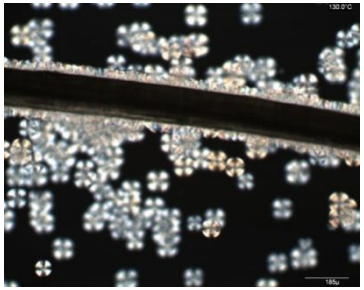

18min.

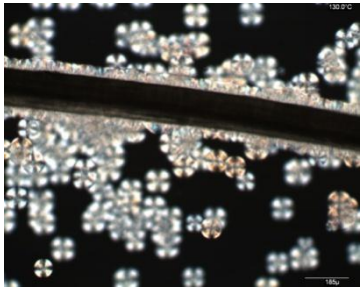

20min.

25min.

30min.

Figure A27: Isothermal transcrystalline growth. Caustic soda treated sisal fibre (8wt%). Cooling rate 5°C/min. Isothermal temperature 130°C.

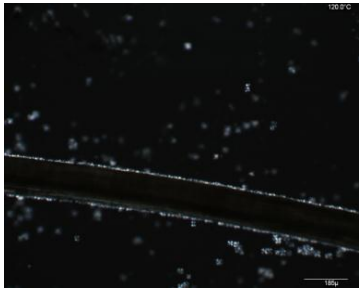

2min.

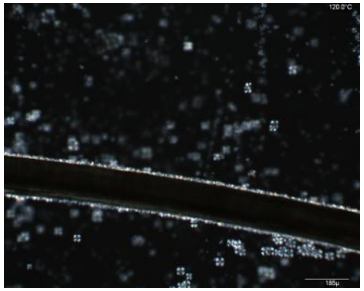

4min.

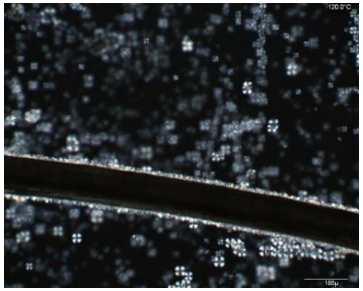

6min.

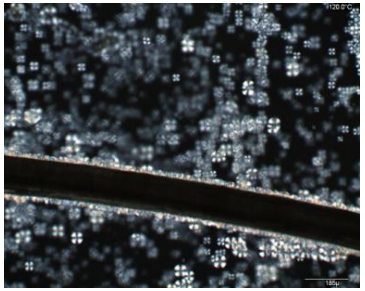

8min.

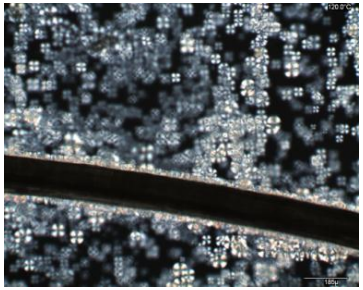

10min.

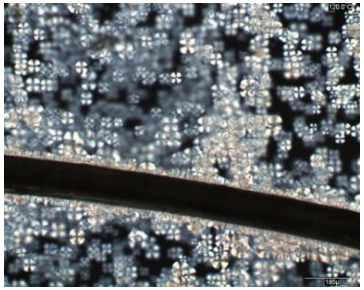

12min.

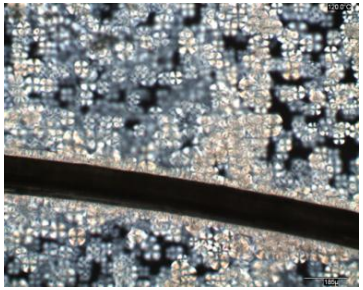

14min.

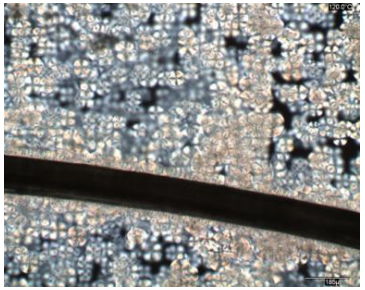

16min.

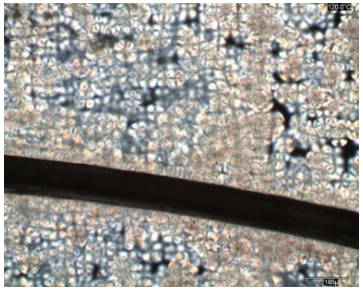

18min.

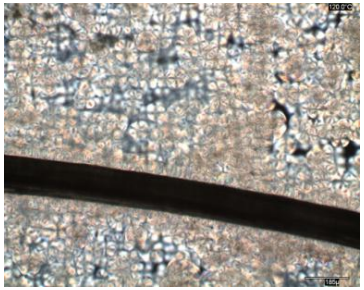

20min.

25min.

30min.

Figure A28: Isothermal transcrystalline growth. Caustic soda treated sisal fibre (8wt%). Cooling rate 5°C/min. Isothermal temperature 120°C.

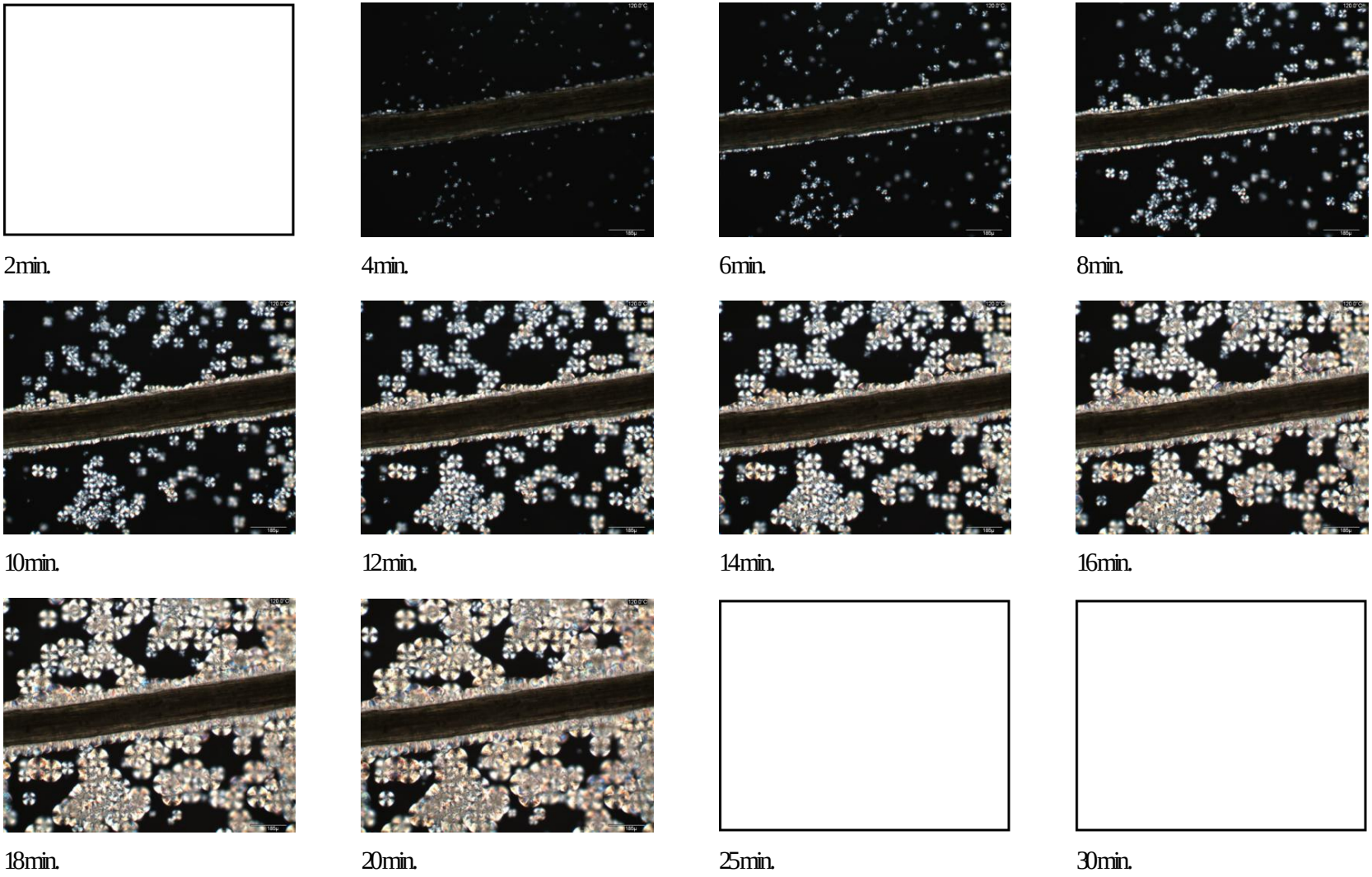

Figure A29: Isothermal transcrystalline growth. Caustic soda treated sisal fibre (6 wt%). Cooling rate 7°C/min. Isothermal temperature 120°C.

2min.

4min.

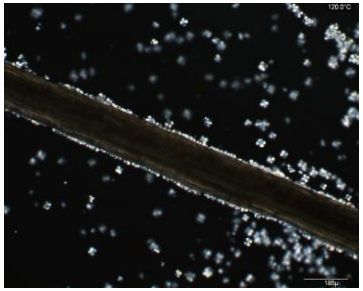

6min.

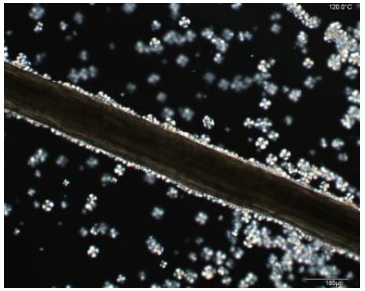

8min.

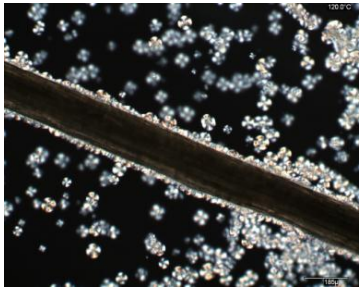

10min.

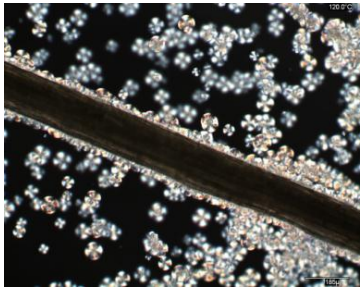

12min.

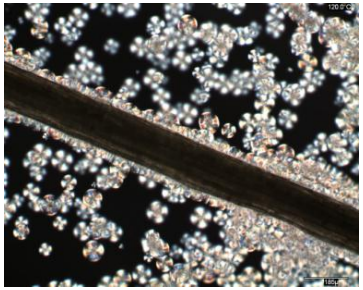

14min.

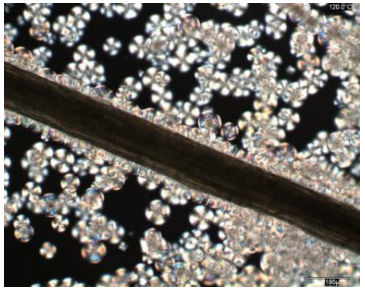

16min.

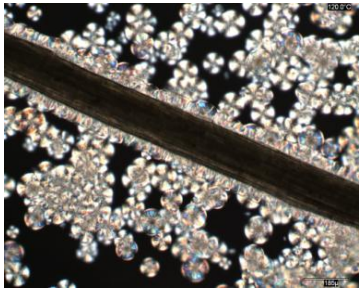

18min.

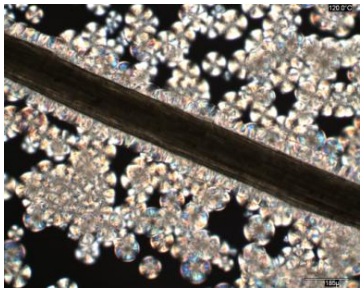

20min.

25min.

30min.

Figure A30: Isothermal transcrystalline growth. Caustic soda treated sisal fibre (6 wt%). Cooling rate 6°C/min. Isothermal temperature 120°C.

120°C

112°C

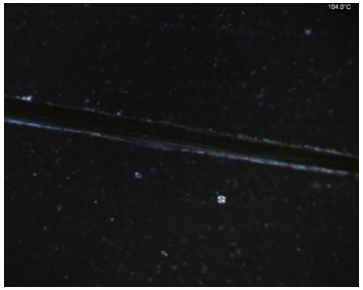

104°C

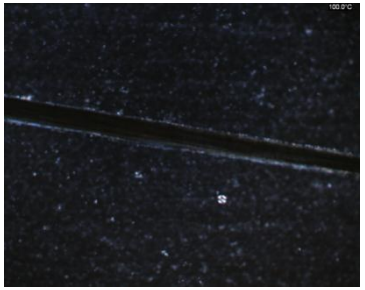

100°C

98°C

96°C

94°C

92°C

90°C

88°C

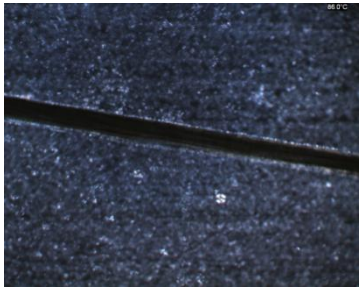

86°C

80°C

Figure A31: Non-isothermal transcrystalline growth. Caustic soda treated sisal fibre (6 wt%). Cooling rate 5°C/min.

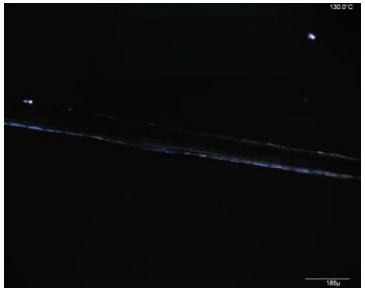

130°C

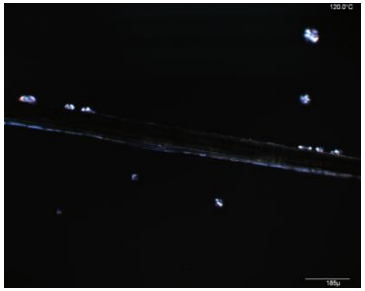

120°C

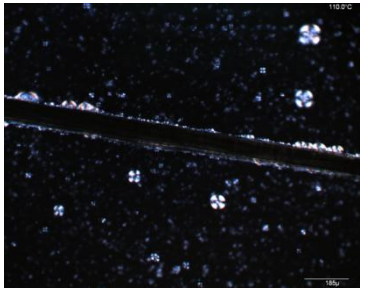

118°C

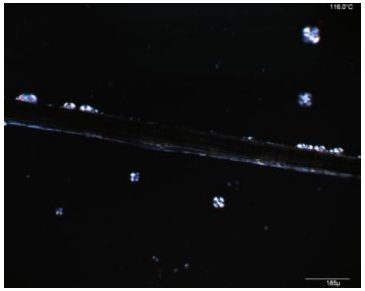

116°C

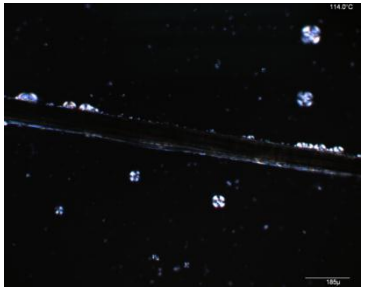

114°C

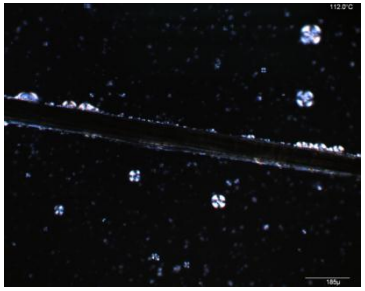

112°C

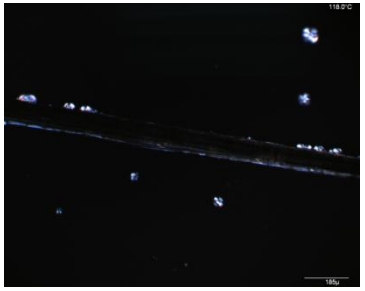

110°C

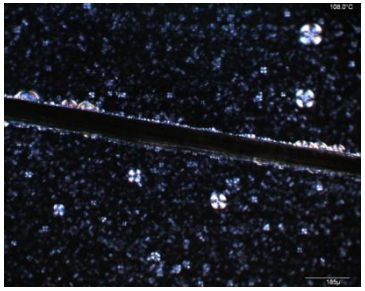

108°C

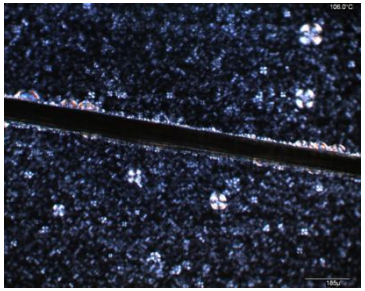

106°C

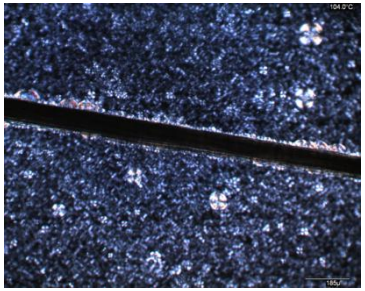

104°C

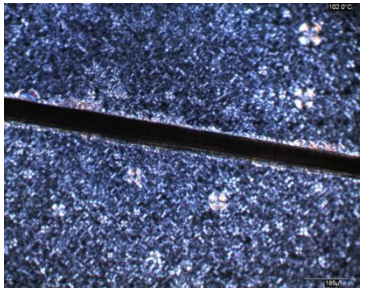

102°C

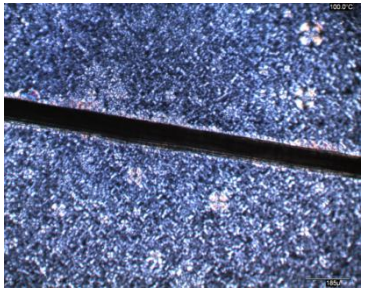

100°C

Figure A32: Non-isothermal transcrystalline growth. Caustic soda treated sisal fibre (6 wt%). Cooling rate 2°C/min.

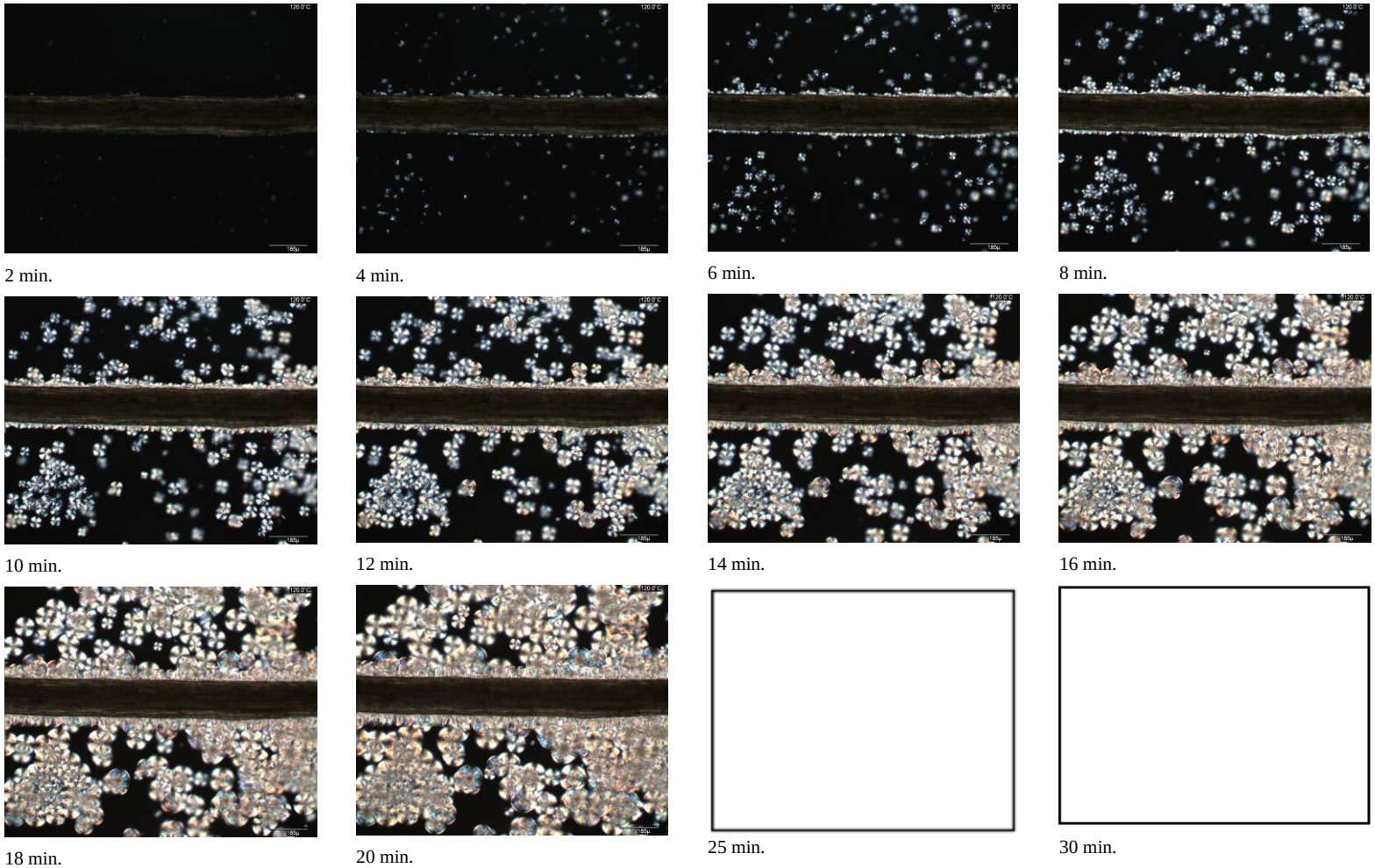

Figure A33: Isothermal transcrystalline growth. Caustic soda treated sisal fibre (6 wt%). Cooling rate 6°C/min. Isothermal temperature 120°C.

Appendix B: Sisal fibre

Table B1: General description of sisal plant/fibre (Rankilor, 2000).

Fibre names and family	Sisal
Genus and species	Agave sisalana (Leaf fibres)
Plant type – harvesting	Perennial plant, leaves 1–2 m long each containing about 1000 fibres.
Countries of cultivation	Central America, Mexico, Brazil, Philippines, India, Florida, Africa, Venezuela, Tanzania, Kenya, Madagascar, Mozambique, Angola and Ethiopia.
Environmental – climate requirements	If rainfall is erratic growth is spasmodic, thus low annual yield. Temperature between 27–32 °C (<16 °C), frost damages leaves, optimum rainfall 1200–1800mm, but can withstand droughts, when other plants would perish, requires substantial amounts of strong sunlight.
Soil type	Grows on dry, porous, rocky, not too acidic or low in nutrients free draining soils. Hardy plant can grow in minimum rainfall 250–375 mm per year. Water logging and salinity are fatal to sisal.
Components of yield	If the leaves are in the shade poor quality fibre is produced. Also cold, frost and hail can damage the leaves (fibre). There are spines at the tips of leaves. The leaves are harvested after 2–4 years of growth and then at intervals, after efflorescence plant dies, 45kg of leaves produce approximately 2 kg of long and tow fibre.
Uses	Twines, ropes, rugs, sacking, carpets, cordage and agricultural. Tow (waste product) used for upholstery.
World annual production (tones)	378 000
£ per tone	450–1100
Fibre extraction – retting	Within 48 hours if not the plant juices become gummy, thus fibre extraction is more difficult and unclean fibre is produced. Machines are used which scrape the pulpy material from the fibre, after washing, the fibre is dried and bleached in the sun, or oven-dried.
Effects from water, sea water, pests, etc.	It was once believed that sisal deteriorated rapidly in salt water; experience has shown that this is not the case. Sisal is widely used for marine ropes.
Cross-section bundles	(i) Crescent to horse-shoe often split. (ii) Few or no hemi-concentrical bundles with cavities. (iii) Round ellipt.
Ultimate fibre	Polygonal wall, thick to medium. Stiff in texture, wide central cavity (may be wider than the cell wall), marked towards the middle.
Longitudinal view	Smooth.
Fibre cell ends	Same thickness as abaca, but half as long. Rounded tips, seldom forked – pointed.
Properties compared to other fibres	Shorter, coarser and not quite as strong as abaca. Also lower breaking load and tends to break suddenly without warning. Can be spun as fine as jute. Sisal can be grown under a wider range of conditions then henequen.
General fibre detail colour, etc.	Light yellow in colour, smooth, straight, very long and strong fibre. Number of different types of cells inside a sisal plant; normal fibre cell straight, stiff, cylindrical and often striated.
General	Blooms once in its lifetime then dies. Cheap, stiff, inflexible, high strength and good luster. Sisal fibre is equivalent hand or machine stripped. Dark bluish-green leaves, having a waxy surface to reduce water loss.

Appendix D: Compression mould drawings.

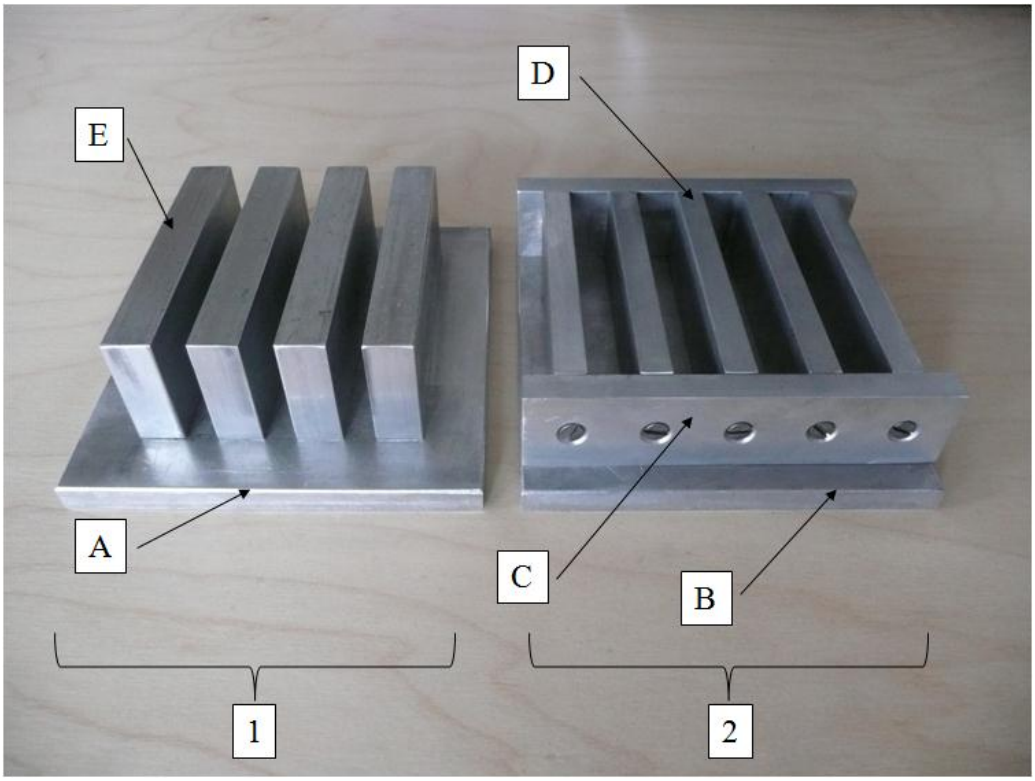

Figure D1: Open compression mould showing individual parts.

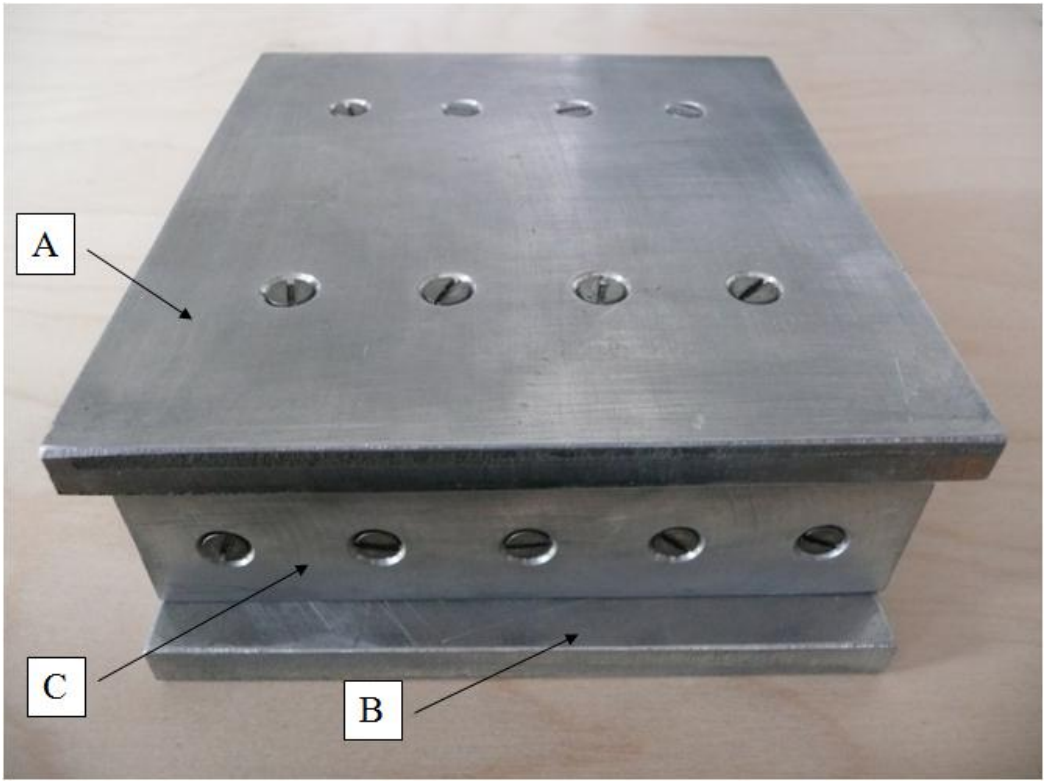

Figure D2: Closed compression mould.

Mould description:

The compression mould is made of aluminium. It consists of 13 pieces in total which are screwed together to form an upper movable part 1 (pieces A and E) and a lower fixed part 2 (pieces B, C and D). The mould can be dismantled. The individual pieces are as follows:

A Upper plate (1)

B Lower plate (1)

C Face (2)

D Lower rib (5)

E Upper rib (4)

The number in brackets stands for the quantity of a piece.

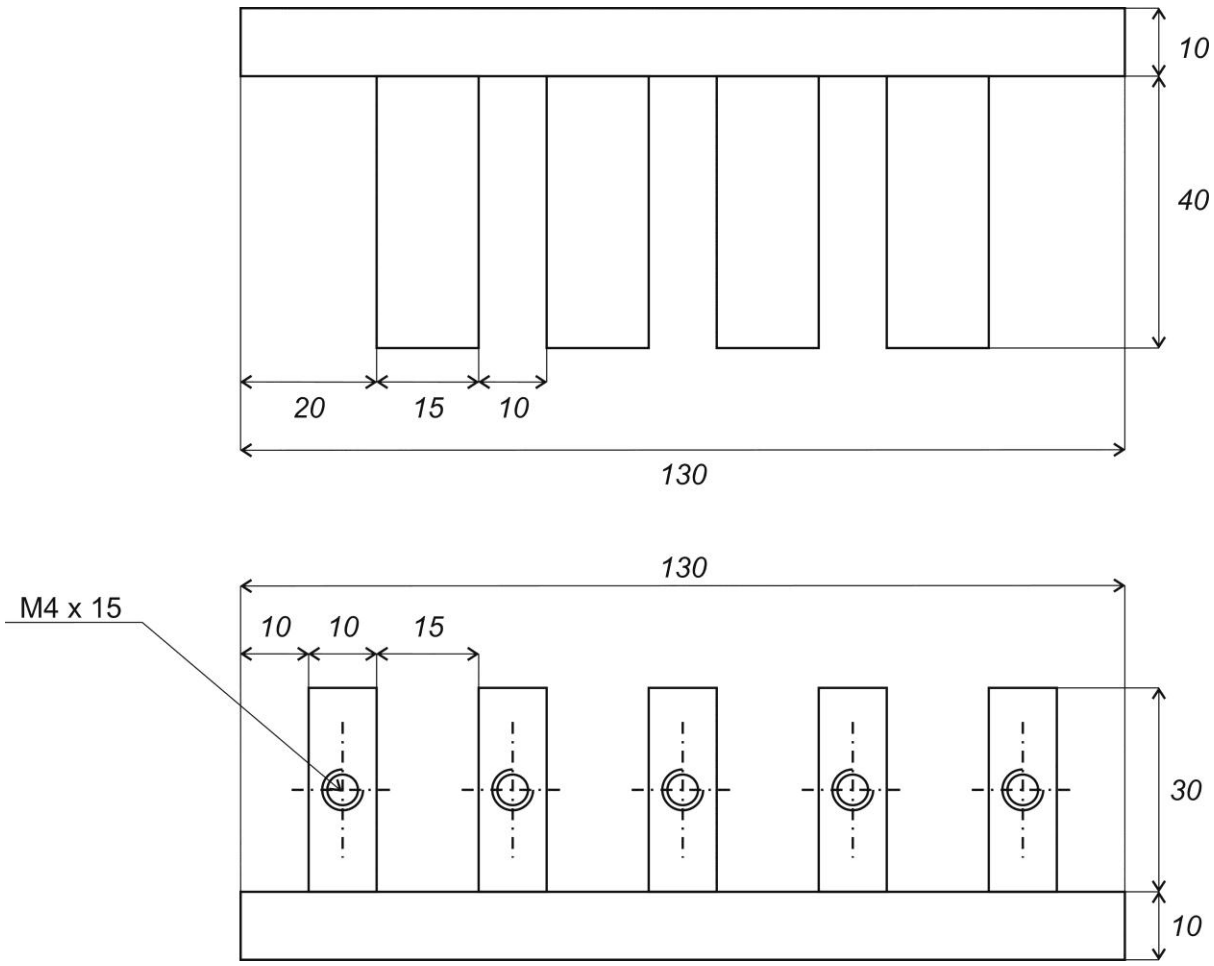

Title	Compression mould	**Part**	Section through the mould assembly	**No.**	1/6
		Material	Aluminium		
Name	Marek Prajer				

Signature		**Scale**	1:1	**Date**	06/06/2009
Company	University of Bath				

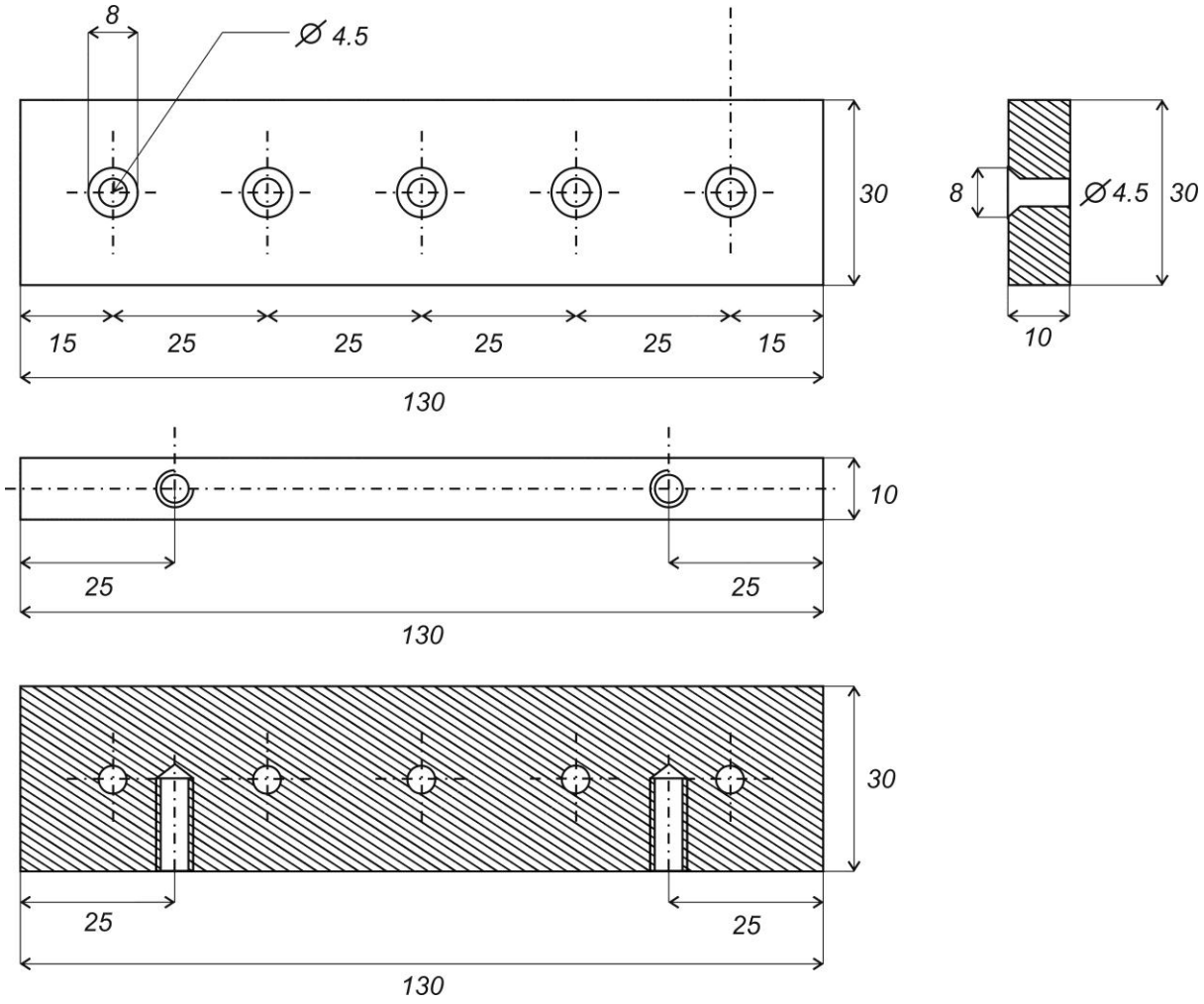

Title	Compression mould	**Part**	Face (C)	**No.**	2/6
		Material	Aluminium		
Name	Marek Prajer				
Signature		**Scale**	1:1	**Date**	06/06/2009
Company	University of Bath				

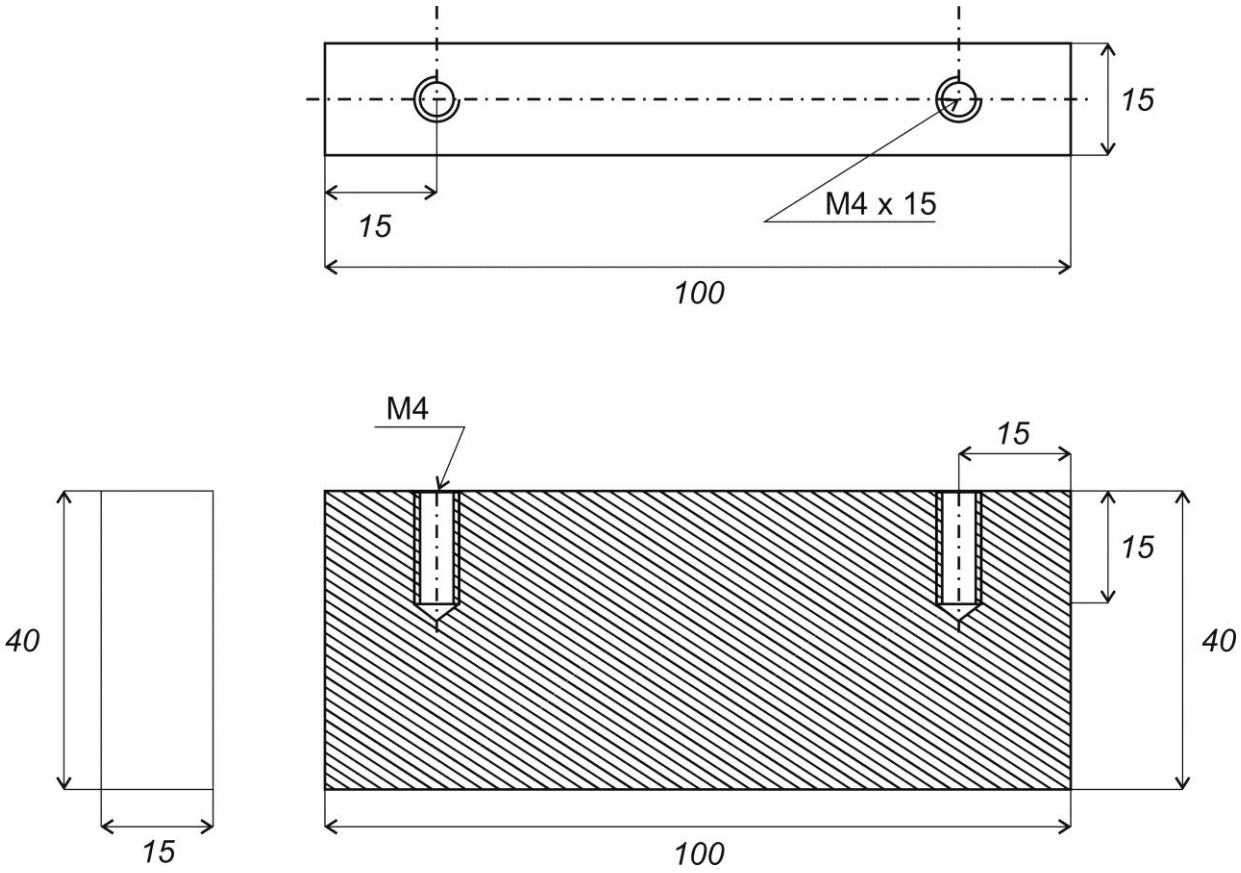

Title	Compression mould	**Part**	Rib-upper (E)	**No.**	3/6
		Material	Aluminium		
Name	Marek Prajer				
Signature		**Scale**	1:1	**Date**	06/06/2009
Company	University of Bath				

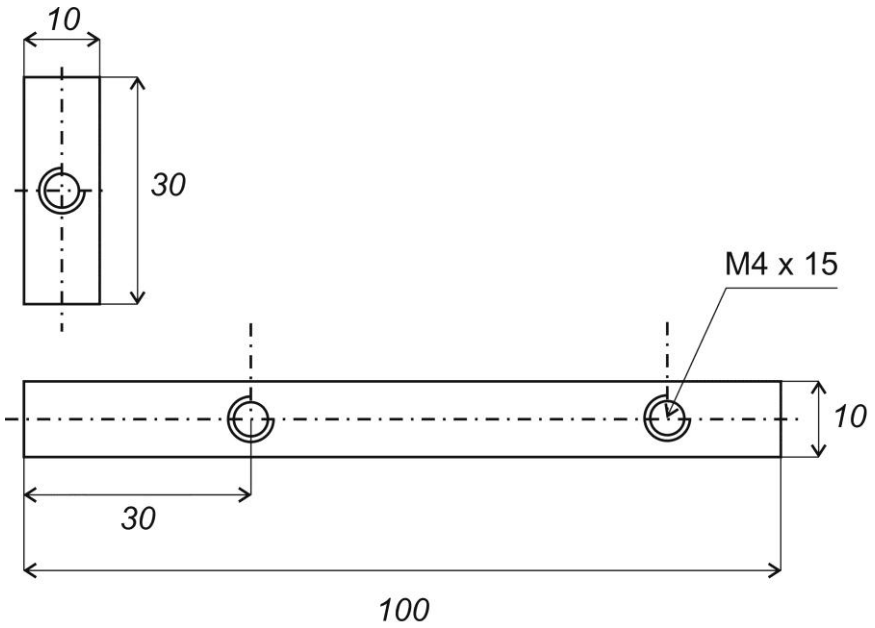

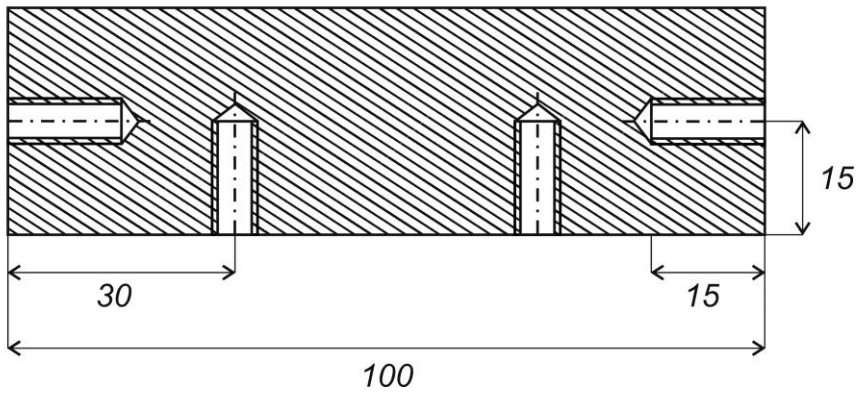

Title	Compression mould	**Part**	Rib-lower (D)	**No.**	4/6
		Material	Aluminium		
Name	Marek Prajer				
Signature		**Scale**	1:1	**Date**	06/06/2009
Company	University of Bath				

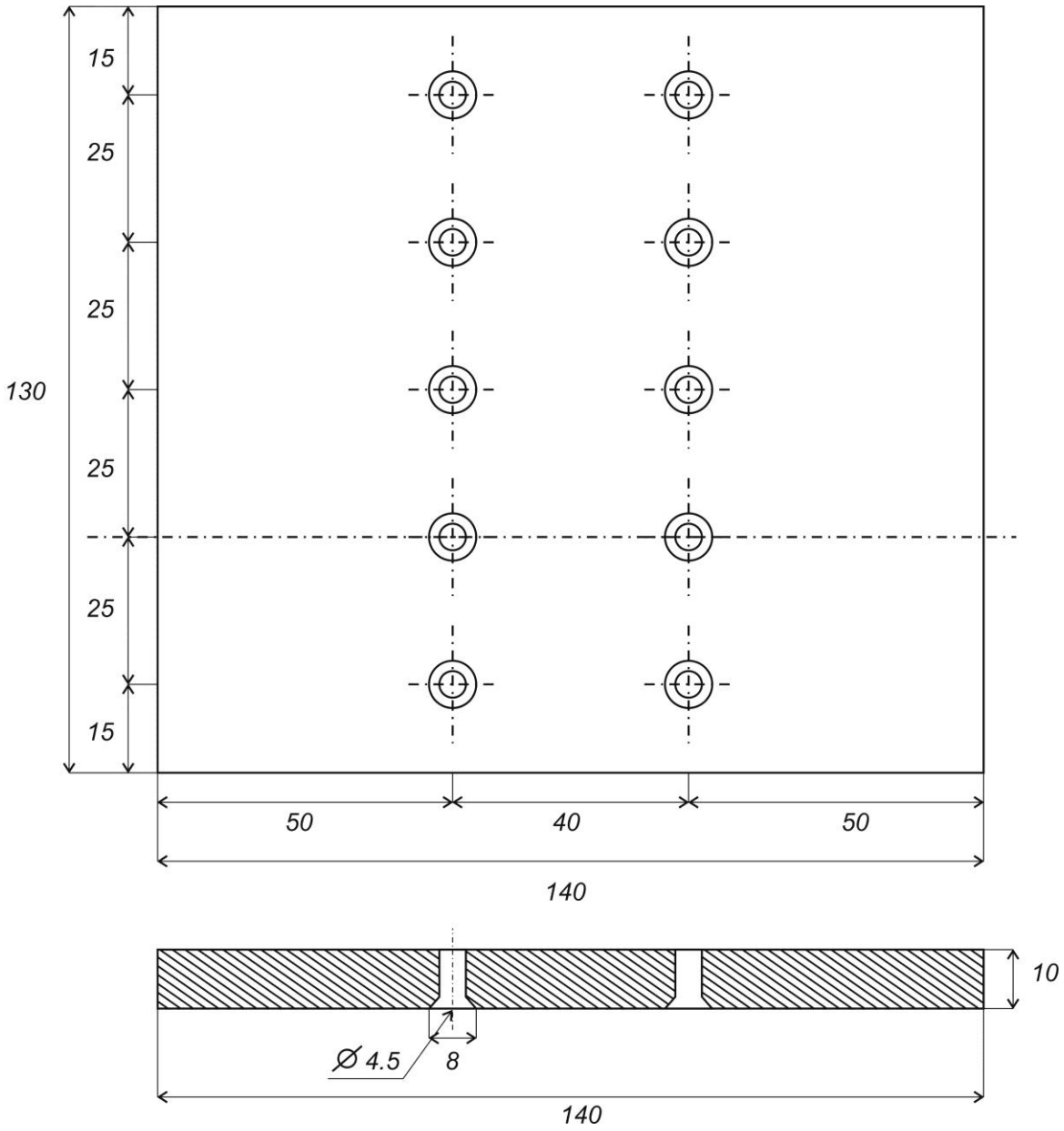

Title	Compression mould	**Part**	Plate-lower (B)	**No.**	5/6
		Material	Aluminium		
Name	Marek Prajer				
Signature		**Scale**	1:1	**Date**	06/06/2009
Company	University of Bath				

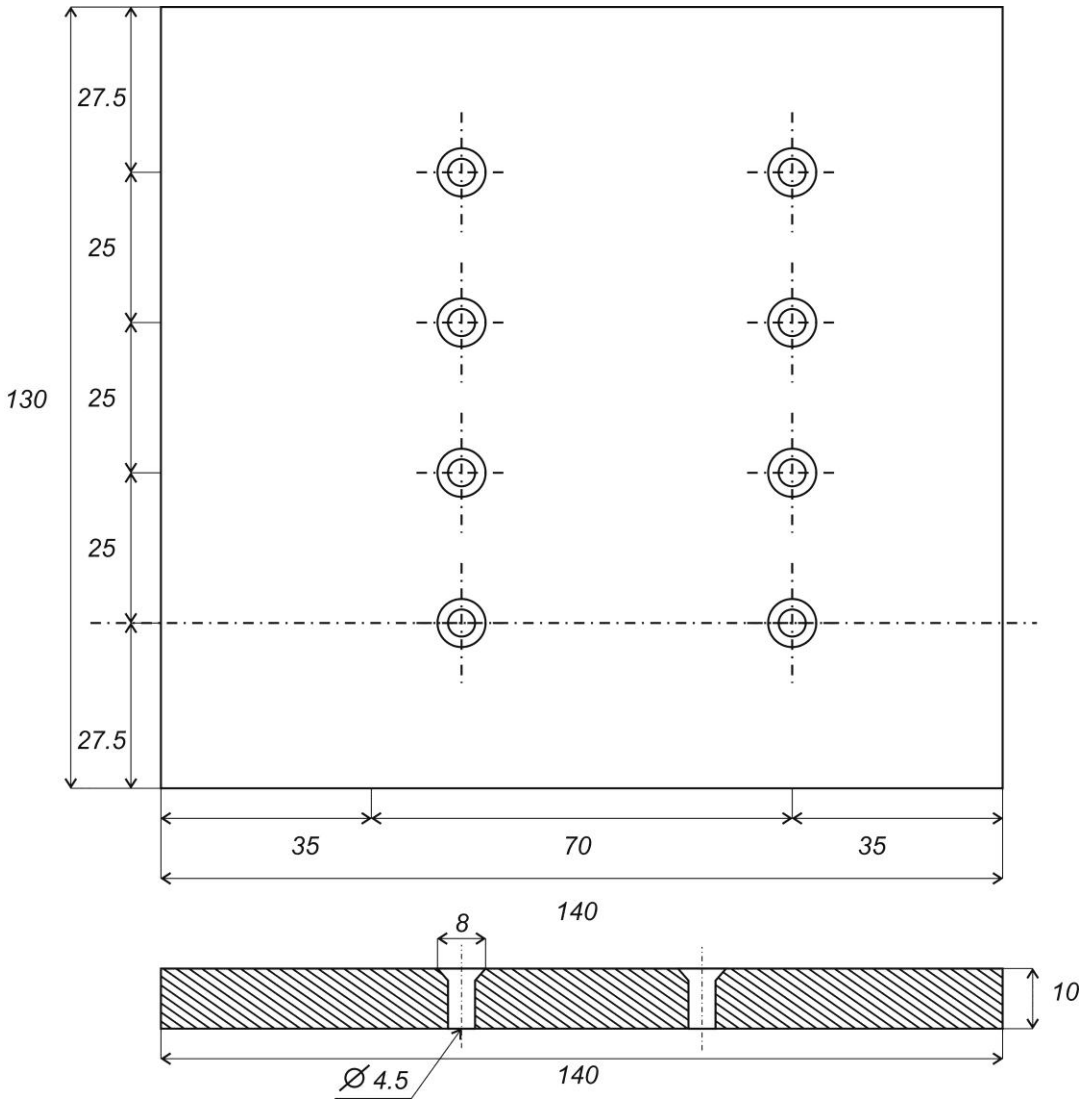

Title	Compression mould	**Part**	Plate-upper (D)	**No.**	6/6
		Material	Aluminium		
Name	Marek Prajer				
Signature		**Scale**	1:1	**Date**	06/06/2009

Company	University of Bath				

Appendix E: Measured data

Appendix E: Measured data

Table 1: Benzene density measurement.					
-	Flask with stopper and solvent	Empty flask with stopper	Flask volume	Solvent temperature	Solvent density
No. (Measurement)	m	m	V	T	ρ (benzene)
[-]	[g]	[g]	[cm^3]	[°C]	[g/cm^3]
1	27.4622	18.6337	10	23.5	0.8829
2	27.4644	18.6336	10	23.5	0.8831
3	27.4648	18.6336	10	23.5	0.8831
Average					**0.8830**
St. Dev.					0.00015
CoV					0.01650

Table 2.: Determination of density of untreated sisal fibres (0 wt%NaOH).					
No. (Measurement)	Fibre length	Pocet vlaken	m (air)	m(liquid)	ρ (fibre)
[-]	[mm]	[pieces]	[g]	[g]	[g/cm^3]
1	50	10	0.0141	0.0035	1.1746
2	50	10	0.0177	0.0054	1.1007
3	50	10	0.0176	0.0052	1.1022
4	50	10	0.0167	0.0047	1.1171
5	50	10	0.0166	0.0046	1.1189
6	50	10	0.0175	0.0049	1.1038
7	50	10	0.0164	0.0047	1.1226
8	50	10	0.0160	0.0038	1.1303
9	50	10	0.0189	0.0054	1.0837
10	50	10	0.0181	0.0048	1.0947
Average					**1.115**
St. Dev.					0.0253
CoV					2.27

Table 3.: Determination of density of caustic soda treated sisal fibres (6 wt% NaOH).					
No. (Measurement)	Fibre length	Pocet vlaken	m (air)	m(liquid)	ρ (fibre)
[-]	[mm]	[pieces]	[g]	[g]	[g/cm^3]
1	50	10	0.0144	0.0056	1.4449
2	50	10	0.0132	0.0050	1.5337
3	50	10	0.0150	0.0060	1.4091
4	50	10	0.0158	0.0062	1.3678
5	50	10	0.0158	0.0061	1.3678
6	50	10	0.0145	0.0055	1.4386
7	50	10	0.0149	0.0056	1.4147
8	50	10	0.0149	0.0061	1.4147
9	50	10	0.0128	0.0046	1.5698
10	50	10	0.0148	0.0058	1.4205
Average					**1.4382**
St. Dev.					0.0655
CoV					4.56

Strain untreated sisal fibres.			
GL = 10 mm	Length = 85 mm		
No.	Sample	Extension	Strain
[-]	[-]	[mm]	[%]
1	D1	0.37581	3.7581
2	D2	0.33181	3.3181
3	D3	0.43162	4.3162
4	D4	0.31344	3.1344
5	D5	0.53994	5.3994
6	D6	0.65075	6.5075
7	D7	0.34156	3.4156
8	D8	0.37406	3.7406
9	D9	0.48531	4.8531
10	D10	0.65581	6.5581
11	D11	0.68244	6.8244
12	D12	0.71406	7.1406
13	D13	0.64187	6.4187
14	D14	0.586	5.86
15	D15	0.57012	5.7012
16	D16	0.53481	5.3481
17	D17	0.63844	6.3844
18	D18	0.51244	5.1244
19	D19	0.60412	6.0412
20	D20	0.61756	6.1756

Strain untreated sisal fibres.			
GL = 15 mm	Length = 85 mm		
No.	Sample	Extension	Strain
[-]	[-]	[mm]	[%]
1	E1	0.63975	4.2650
2	E2	0.61075	4.0717
3	E3	0.76569	5.1046
4	E4	0.55231	3.6821
5	E5	0.53525	3.5683
6	E6	0.54581	3.6387
7	E7	0.7475	4.9833
8	E8	0.59662	3.9775
9	E9	0.57194	3.8129
10	E10	0.58331	3.8887
11	E11	0.6625	4.4167
12	E12	0.63244	4.2163
13	E13	0.51912	3.4608
14	E14	0.62669	4.1779
15	E15	0.59256	3.9504
16	E16	0.80319	5.3546
17	E17	0.63406	4.2271
18	E18	0.77919	5.1946
19	E19	0.74237	4.9491
20	E20	0.68319	4.5546

Strain untreated sisal fibres.			
GL = 20mm	Length = 85 mm		
No.	Sample	Extension	Strain
[-]	[-]	[mm]	[%]
1	F1	0.62319	3.11595
2	F2	0.94587	4.72935
3	F3	0.52925	2.64625
4	F4	0.53994	2.6997
5	F5	0.61837	3.09185
6	F6	0.68487	3.42435
7	F7	0.68494	3.4247
8	F8	0.78275	3.91375
9	F9	0.85231	4.26155
10	F10	0.77656	3.8828
11	F11	0.6985	3.4925
12	F12	1.03494	5.1747
13	F13	0.80075	4.00375
14	F14	0.62744	3.1372
15	F15	0.79419	3.97095
16	F16	0.95406	4.7703
17	F17	1.05594	5.2797
18	F18	0.84662	4.2331
19	F19	0.61837	3.09185
20	F20	0.81331	4.06655

Strain untreated sisal fibres.			
GL = 25mm	Length = 85 mm		
No.	Sample	Extension	Strain
[-]	[-]	[mm]	[%]
1	MH30	0.80675	4.03375
2	MH29	0.64425	3.22125
3	MH27	1.31981	6.59905
4	MH28	0.97344	4.8672
5	MH22	0.76069	3.80345
6	MH32	1.08919	5.44595
7	MH37	1.00006	5.0003
8	MH36	0.90187	4.50935
9	MH35	1.10431	5.52155
10	MH33	1.01231	5.06155
11	MH39	0.84081	4.20405
12	MH40	0.90737	4.53685
13	MH34	1.17519	5.87595
14	MH21	0.76581	3.82905
15	MH31	0.84737	4.23685
16	MH26	0.51737	2.58685
17	MH25	0.92762	4.6381
18	MH24	0.96912	4.8456
19	MH32	0.96475	4.82375
20	MH38	0.79737	3.98685

Strain untreated sisal fibres.			
GL = 30mm	Length = 85 mm		
No.	Sample	Extension	Strain
[-]	[-]	[mm]	[%]
1	MG1	1.25594	6.2797
2	MG18	1.25912	6.2956
3	MG19	1.10606	5.5303
4	MG20	1.09087	5.45435
5	MG15	1.01575	5.07875
6	MG17	0.92694	4.6347
7	MG8	0.87087	4.35435
8	MG10	0.71831	3.59155
9	MG7	1.10519	5.52595
10	MG11	1.2475	6.2375
11	MG12	0.99581	4.97905
12	MG16	1.15419	5.77095
13	MG9	0.86675	4.33375
14	MG13	1.13662	5.6831
15	MG14	1.10919	5.54595
16	MG2	0.8415	4.2075
17	MG3	0.9315	4.6575
18	MG4	0.8715	4.3575
19	MG6	0.70744	3.5372
20	MG5	0.88837	4.44185

Strain treated sisal fibres. (6 wt% NaOH)			
GL = 10 mm	Length = 85 mm		
No.	Sample	Extension	Strain
[-]	[-]	[mm]	[%]
1	MA50	0.25006	2.5006
2	MA35	0.40081	4.0081
3	MA33	0.425	4.25
4	MA48	0.28081	2.8081
5	MA45	0.26694	2.6694
6	MA44	0.28662	2.8662
7	MA42	0.40931	4.0931
8	MA36	0.48156	4.8156
9	MA49	0.49581	4.9581
10	MA41	0.44512	4.4512
11	MA43	0.44194	4.4194
12	MA37	0.38331	3.8331
13	MA47	0.35337	3.5337
14	MA38	0.31	3.1
15	MA39	0.23325	2.3325
16	MA40	0.40994	4.0994
17	MA51	0.46581	4.6581
18	MA32	0.37612	3.7612
19	MA34	0.51519	5.1519
20	MA46	0.40756	4.0756

Strain treated sisal fibres. (6 wt% NaOH)			
GL = 15 mm	Length = 85 mm		
No.	Sample	Extension	Strain
[-]	[-]	[mm]	[%]
1	MC49	0.55237	3.682467
2	MC10	0.44344	2.956267
3	MC11	0.46669	3.111267
4	MC7	0.36756	2.4504
5	MC8	0.32575	2.171667
6	MC4	0.41406	2.7604
7	MC9	0.50081	3.338733
8	MC50	0.54244	3.616267
9	MC51	0.711	4.74
10	MC54	0.29331	1.9554
11	MC53	0.53387	3.559133
12	MC52	0.60556	4.037067
13	MC48	0.63531	4.2354
14	MC46	0.47406	3.1604
15	MC47	0.49912	3.327467
16	MC2	0.46744	3.116267
17	MC3	0.54662	3.644133
18	MC1	0.60075	4.005
19	MC6	0.38906	2.593733
20	MC5	0.46737	3.1158
Strain treated sisal fibres. (6 wt% NaOH)			

GL = 20 mm	Length = 85 mm		
No.	Sample	Extension	Strain
[-]	[-]	[mm]	[%]
1	ME62	0.4025	2.0125
2	ME55	0.51912	2.5956
3	ME61	0.41006	2.0503
4	ME56	0.55987	2.79935
5	ME21	0.68575	3.42875
6	ME22	0.63594	3.1797
7	ME23	0.57319	2.86595
8	ME24	0.63419	3.17095
9	ME63	0.54431	2.72155
10	ME64	0.54687	2.73435
11	ME65	0.57319	2.86595
12	ME25	0.56487	2.82435
13	ME27	0.65975	3.29875
14	ME26	0.59612	2.9806
15	ME29	0.42944	2.1472
16	ME30	0.66781	3.33905
17	ME60	0.46587	2.32935
18	ME59	0.61587	3.07935
19	ME57	0.75931	3.79655
20	ME58	0.74181	3.70905

Strain treated sisal fibres. (6 wt%NaOH)			
GL = 25 mm	Length = 85 mm		
No.	Sample	Extension	Strain
[-]	[-]	[mm]	[%]
1	MB29	0.59994	2.39976
2	MB27	0.68981	2.75924
3	MB26	0.61444	2.45776
4	MB24	0.6065	2.426
5	MB25	0.61156	2.44624
6	MB12	0.63337	2.53348
7	MB22	0.55506	2.22024
8	MB13	0.73669	2.94676
9	MB15	0.88069	3.52276
10	MB23	0.64669	2.58676
11	MB28	0.56744	2.26976
12	MB14	0.47	1.88
13	MB20	0.73481	2.93924
14	MB21	0.57981	2.31924
15	MB17	0.6865	2.746
16	MB16	0.725	2.9
17	MB19	0.56675	2.267
18	MB18	0.5615	2.246
19	MB30	0.74075	2.963
20	MB31	0.84237	3.36948

Strain treated sisal fibres. (6 wt% NaOH)			
GL = 30 mm	Length = 85 mm		
No.	Sample	Extension	Strain
[-]	[-]	[mm]	[%]
1	MD20	0.89244	2.9748
2	MD18	0.57156	1.9052
3	MD19	0.54644	1.821467
4	MD6	0.85769	2.858967
5	MD5	0.77169	2.5723
6	MD4	0.70744	2.358133
7	MD3	0.80919	2.6973
8	MD17	0.84181	2.806033
9	MD2	0.86406	2.8802
10	MD16	0.60094	2.003133
11	MD10	0.88756	2.958533
12	MD11	0.7975	2.658333
13	MD1	0.5535	1.845
14	MD15	0.70912	2.363733
15	MD9	0.73606	2.453533
16	MD13	0.7515	2.505
17	MD14	0.734	2.446667
18	MD7	0.85231	2.841033
19	MD8	0.61262	2.042067
20	MD12	0.69981	2.3327

Strain untreated sisal/ 3wt% H2O2			
GL = 25 mm	Length = 85 mm		
No.	Sample	Extension	Strain
[-]	[-]	[mm]	[%]
1	MI_60	1.00819	4.03276
2	MI_54	0.80831	3.23324
3	MI_44	0.50837	2.03348
4	MI_45	0.61675	2.467
5	MI_55	0.97825	3.913
6	MI_43	0.82737	3.30948
7	MI_41	0.81919	3.27676
8	MI_47	0.54669	2.18676
9	MI_58	0.89237	3.56948
10	MI_52	1.04412	4.17648
11	MI_56	0.75912	3.03648
12	MI_53	1.03175	4.127
13	MI_46	1.0415	4.166
14	MI_48	0.86094	3.44376
15	MI_49	0.79669	3.18676
16	MI_50	0.87925	3.517
17	MI_57	0.76012	3.04048
18	MI_51	0.60406	2.41624
19	MI_42	0.78337	3.13348
20	MI_59	0.62606	2.50424

Strain treated sisal (6 wt% NaOH/3wt%H_2O_2)			
GL = 25 mm	Length = 85 mm		
No.	Sample	Extension	Strain
[-]	[-]	[mm]	[%]
1	MF49	0.95331	3.81324
2	MF48	0.63687	2.54748
3	MF47	0.6175	2.47
4	MF50	0.79325	3.173
5	MF53	0.80825	3.233
6	MF54	0.95244	3.80976
7	MF55	0.61675	2.467
8	MF51	0.74575	2.983
9	MF59	0.76337	3.05348
10	MF57	0.74819	2.99276
11	MF60	0.79062	3.16248
12	MF58	0.78481	3.13924
13	MF43	1.03406	4.13624
14	MF44	0.86675	3.467
15	MF45	0.7225	2.89
16	MF46	0.54862	2.19448
17	MF42	0.82912	3.31648
18	MF52	0.89906	3.59624
19	MF56	0.69181	2.76724
20	MF41	0.80094	3.20376

Modulus untreated sisal fibres			
GL = 10 mm	Length = 85 mm		
No.	Sample	m	Modulus
[-]	[-]	[g]	[GPa]
1	D18	0.0017	16.85
2	D7	0.0013	16.029
3	D8	0.0016	17.75
4	D9	0.002	14.741
5	D10	0.0015	12.887
6	D17	0.0015	15.383
7	D6	0.0027	14.77
8	D5	0.0024	15.131
9	D4	0.0015	15.193
10	D3	0.0013	17.201
11	D16	0.0038	13.099
12	D2	0.0014	15.311
13	D1	0.0027	11.996
14	D33	0.0016	23.981
15	D12	0.003	13.046
16	D11	0.0018	11.091
17	D13	0.0016	12.361
18	D14	0.0028	11.549
19	D19	0.0028	15.921
20	D15	0.0029	13.455
Average			**14.88725**
St. Dev.			**2.865586**

Modulus untreated sisal fibres			
GL = 15 mm	Length = 85 mm		
No.	Sample	m	Modulus
[-]	[-]	[g]	[GPa]
1	E26	0.0021	17.274
2	E3	0.002	14.914
3	E2	0.0017	20.987
4	E1	0.0017	20.961
5	E30	0.0029	17.303
6	E9	0.0026	15.5
7	E8	0.0021	17.315
8	E7	0.0026	10.3
9	E15	0.0029	17.028
10	E13	0.0023	18.115
11	E20	0.0025	16.229
12	E12	0.0026	14.86
13	E4	0.0024	15.682
14	E6	0.002	16.541
15	E5	0.0035	14.236
16	E32	0.0032	13.505
17	E11	0.003	10.992
18	E10	0.003	17.075
19	E18	0.0023	18.138
20	E17	0.0026	17.288
Average			**16.21215**
St. Dev.			**2.681607**

Modulus untreated sisal fibres			
GL = 20 mm			
No.	Sample	m	Modulus
[-]	[-]	[g]	[GPa]
1	F30	0.0008	12.714
2	F29	0.0008	19.994
3	F28	0.0026	19.004
4	F27	0.0005	22.802
5	F26	0.0038	18.091
6	F25	0.0034	18.908
7	F24	0.0016	15.589
8	F23	0.001	20.847
9	F22	0.0013	17.841
10	F21	0.0037	12.105
11	F20	0.003	19.337
12	F19	0.0018	18.589
13	F18	0.003	18.645
14	F17	0.0018	18.142
15	F16	0.0024	17.11
16	F15	0.0019	10.081
17	F14	0.0018	21.654
18	F13	0.0022	17.067
19	F12	0.0034	14.662
20	F11	0.0038	18.459
Average			**17.58205**
St. Dev.			**3.19265**

Modulus untreated sisal fibres			
GL = 25 mm			
No.	Sample	m	Modulus
[-]	[-]	[g]	[GPa]
1	MH30	0.0013	13.168
2	MH29	0.0012	21.306
3	MH27	0.0007	37.137
4	MH28	0.0016	11.769
5	MH22	0.0013	20.054
6	MH32	0.0007	32.852
7	MH37	0.0013	17.007
8	MH36	0.0014	14.685
9	MH35	0.0007	15.462
10	MH33	0.0013	18.765
11	MH39	0.0006	27.88
12	MH40	0.0006	14.917
13	MH34	0.0024	14.51
14	MH21	0.0018	16.171
15	MH31	0.0008	14.958
16	MH26	0.0018	7.567
17	MH25	0.0012	22.631
18	MH24	0.0014	14.064
19	MH32	0.0013	9.456
20	MH38	0.0006	25.724
Average			**18.50415**
St. Dev.			**7.568604**

Modulus untreated sisal fibres			
GL = 30 mm	Length = 85 mm		
No.	Sample	m	Modulus
[-]	[-]	[g]	[GPa]
1	MG1	0.0019	16.331
2	MG18	0.0009	13.266
3	MG19	0.0017	18.045
4	MG20	0.0011	14.975
5	MG15	0.0018	14.937
6	MG17	0.0018	17.641
7	MG8	0.0018	24.349
8	MG10	0.0011	23.94
9	MG7	0.0022	20.872
10	MG11	0.0006	16.23
11	MG12	0.001	13.935
12	MG16	0.0008	16.445
13	MG9	0.0004	34.075
14	MG13	0.0013	14.485
15	MG14	0.0022	15.412
16	MG2	0.0012	20.19
17	MG3	0.0013	15.656
18	MG4	0.0017	18.856
19	MG6	0.0007	28.938
20	MG5	0.0014	19.138
Average			**18.8858**
St. Dev.			**5.348392**

Modulus treated sisal (6 wt% NaOH)			
GL = 10 mm	Length = 85 mm		
No.	Sample	m	Modulus
[-]	[-]	[g]	[GPa]
1	MA50	0.001	28.906
2	MA35	0.0008	26.316
3	MA33	0.0011	32.374
4	MA48	0.0013	20.858
5	MA45	0.0006	34.9
6	MA44	0.0012	19.498
7	MA42	0.0015	20.644
8	MA36	0.0021	19.081
9	MA49	0.0023	20.451
10	MA41	0.0014	23.563
1	MA43	0.0013	30.231
2	MA37	0.0011	21.478
3	MA47	0.0011	16.033
4	MA38	0.0004	11.331
5	MA39	0.001	27.213
6	MA40	0.0015	18.066
7	MA51	0.0028	20.234
8	MA32	0.0014	20.701
9	MA34	0.002	20.184
10	MA46	0.0016	17.14
Average			**22.4601**
St. Dev.			**5.852181**

Modulus treated sisal (6 wt% NaOH)			
GL = 15 mm	Length = 85 mm		
No.	Sample	m	Modulus
[-]	[-]	[g]	[GPa]
11	MC49	0.0023	23.078
12	MC10	0.001	20.553
13	MC11	0.0017	25.764
14	MC7	0.0016	20.916
15	MC8	0.0007	33.339
16	MC4	0.0004	35.081
17	MC9	0.0009	26.462
18	MC50	0.0012	30.827
19	MC51	0.0017	15.339
20	MC54	0.0015	22.296
1	MC53	0.0016	26.581
2	MC52	0.0019	19.333
3	MC48	0.0028	22.79
4	MC46	0.0014	29.986
5	MC47	0.0019	26.853
6	MC2	0.0012	14.844
7	MC3	0.0016	24.975
8	MC1	0.003	21.812
9	MC6	0.001	24.3
10	MC5	0.0009	23.865
Average			**24.4497**
St. Dev.			**5.258869**

Modulus treated sisal (6 wt% NaOH)			
GL = 20 mm	Length = 85 mm		
No.	Sample	m	Modulus
[-]	[-]	[g]	[GPa]
1	ME62	0.0011	28.397
2	ME55	0.0016	27.024
3	ME61	0.0009	27.059
4	ME56	0.0012	20.917
5	ME21	0.0016	34.729
6	ME22	0.0014	35.216
7	ME23	0.0015	22.489
8	ME24	0.0009	15.824
9	ME63	0.001	29.755
10	ME64	0.0012	27.649
11	ME65	0.0012	27.766
12	ME25	0.0008	32.577
13	ME27	0.0016	32.649
14	ME26	0.0012	15.607
15	ME29	0.0013	18.241
16	ME30	0.0023	23.523
17	ME60	0.0012	34.031
18	ME59	0.0007	31.65
19	ME57	0.0015	32.323
20	ME58	0.0029	31.636
Average			**27.4531**
St. Dev.			**6.149246**

Modulus treated sisal (6 wt% NaOH)			
GL = 25 mm	Length = 85 mm		
No.	Sample	m	Modulus
[-]	[-]	[g]	[GPa]
1	MB29	0.0014	28.504
2	MB27	0.0015	29.705
3	MB26	0.0011	28.159
4	MB24	0.0014	18.791
5	MB25	0.0019	25.737
6	MB12	0.0018	25.0355
7	MB22	0.0017	24.247
8	MB13	0.0009	22.094
9	MB15	0.0014	20.908
10	MB23	0.0017	22.76
11	MB28	0.001	31.027
12	MB14	0.0016	30.393
13	MB20	0.0011	29.5
14	MB21	0.0008	23.909
15	MB17	0.001	24.137
16	MB16	0.0011	23.374
17	MB19	0.0007	31.816
18	MB18	0.0013	25.925
19	MB30	0.0003	25.0355
20	MB31	0.0019	39.793
Average			**26.5425**
St. Dev.			**4.718742**

Modulus treated sisal (6 wt% NaOH)			
GL = 30 mm	Length = 85 mm		
Test No.	Sample	m	Modulus
[-]	[-]	[g]	[GPa]
1	MD20	0.0018	26.565
2	MD18	0.0023	31.065
3	MD19	0.001	24.198
4	MD6	0.0013	30.74
5	MD5	0.0023	21.561
6	MD4	0.0007	30.194
7	MD3	0.0013	27.376
8	MD17	0.0011	38.895
9	MD2	0.0014	31.363
10	MD16	0.002	24.174
11	MD10	0.0014	21.149
12	MD11	0.0015	23.229
13	MD1	0.0006	30.722
14	MD15	0.0007	42.185
15	MD9	0.0011	32.457
16	MD13	0.0007	27.125
17	MD14	0.0016	28.604
18	MD7	0.0019	30.39
19	MD8	0.0016	32.072
20	MD12	0.0011	32.613
Average			**29.33385**
St. Dev.			**5.291684**

Modulus untreated sisal/ 3wt% H_2O_2			
GL = 25 mm	Length = 85 mm		
No. Test	Sample	m [g]	Modulus [GPa]
1	MI_60	0.0012	25.769
2	MI_54	0.0007	30.03
3	MI_44	0.0009	34.616
4	MI_45	0.0007	44.777
5	MI_55	0.0008	18.7
6	MI_43	0.0007	26.099
7	MI_41	0.0013	23.107
8	MI_47	0.0009	29.589
9	MI_58	0.0009	34.908
10	MI_52	0.0015	19.891
11	MI_56	0.002	22.548
12	MI_53	0.0013	27.861
13	MI_46	0.0013	25.989
14	MI_48	0.0007	28.909
15	MI_49	0.0006	29.006
16	MI_50	0.0008	26.568
17	MI_57	0.0017	23.545
18	MI_51	0.0013	22.807
19	MI_42	0.0009	30.425
20	MI_59	0.0014	28.785
Average			**27.69645**
St. Dev.			**5.864832393**

Modulus treated sisal (6 wt% NaOH/3wt%H_2O_2)			
GL = 25 mm	Length = 85 mm		
No. Test	Sample	m [g]	Modulus [GPa]
1	MF49	0.001	5.094
2	MF48	0.0009	25.574
3	MF47	0.001	21.864
4	MF50	0.0016	30.255
5	MF53	0.0018	19.696
6	MF54	0.0017	11.906
7	MF55	0.0026	20.189
8	MF51	0.002	26.618
9	MF59	0.0017	32.006
10	MF57	0.0021	26.937
11	MF60	0.0018	17.287
12	MF58	0.0012	16.252
13	MF43	0.0016	19.633
14	MF44	0.0016	20.875
15	MF45	0.0023	25.18
16	MF46	0.0017	26.097
17	MF42	0.0014	19.745
18	MF52	0.0015	15.244
19	MF56	0.0015	15.861
20	MF41	0.0013	26.475
Average			**21.1394**
St. Dev.			**6.511906467**

Modulus treated sisal (0.16 wt%NaOH)			
GL = 25 mm	Length = 85 mm		
No.	Sample	m	Modulus
[-]	[-]	[g]	[GPa]
1	X38	0.0019	17.997
2	X24	0.0021	21.858
3	X40	0.0013	16.184
4	X37	0.0012	17.054
5	X35	0.0019	18.811
6	X34	0.0018	15.45
7	X39	0.0016	16.846
8	X44	0.0018	16.436
9	X42	0.001	13.833
10	X43	0.0015	18.833
11	X36	0.0015	15.701
12	X41	0.0017	17.666
13	X33	0.0015	19.422
14	X28	0.002	18.207
15	X4	0.0013	18.711
16	X5	0.0018	17.734
17	X8	0.0017	16.521
18	X6	0.002	18.19
19	X9	0.0018	20.983
20	X11	0.0009	16.25
Average			**17.63435**
St. Dev.			**1.886535**

Modulus treated sisal (2 wt% NaOH)			
GL = 25 mm	Length = 85 mm		
No.	Sample	m	Modulus
[-]	[-]	[g]	[GPa]
1	Y13	0.0021	12.995
2	Y30	0.0023	14.056
3	Y18	0.0017	16.645
4	Y33	0.0021	16.441
5	Y29	0.0018	17.605
6	Y15	0.0013	15.797
7	Y6	0.0021	15.828
8	Y10	0.0016	20.739
9	Y22	0.0019	15.472
10	Y1	0.0016	15.368
11	Y20	0.0013	16.47
12	Y25	0.0024	9.558
13	Y38	0.0027	10.509
14	Y44	0.0014	16.228
15	Y43	0.0016	16.978
16	Y40	0.0014	14.335
17	Y37	0.0017	10.847
18	Y39	0.0025	14.192
19	Y35	0.0016	18.702
20	Y34	0.0023	13.885
Average			**15.1325**
St. Dev.			**2.728023**

Modulus treated sisal (0.16 wt%NaOH)			
GL = 25 mm	Length = 85 mm		
No.	Sample	Extension	Strain
[-]	[-]	[mm]	[%]
1	X25	0.4375	1.75
2	X2	0.44825	1.793
3	X43	0.55494	2.21976
4	X30	0.60419	2.41676
5	X20	0.61256	2.45024
6	X8	0.62069	2.48276
7	X36	0.63225	2.529
8	X12	0.6875	2.75
9	X23	0.69344	2.77376
10	X29	0.69994	2.79976
11	X38	0.72819	2.91276
12	X26	0.72994	2.91976
13	X24	0.74831	2.99324
14	X3	0.76675	3.067
15	X28	0.79906	3.19624
16	X5	0.81994	3.27976
17	X27	0.82081	3.28324
18	X10	0.83006	3.32024
19	X42	0.83156	3.32624
20	X9	0.86012	3.44048

Modulus treated sisal (2 wt%NaOH)			
GL = 25 mm	Length = 85 mm		
No.	Sample	Extension	Strain
[-]	[-]	[mm]	[%]
1	Y13	1.71206	6.84824
2	Y35	0.4875	1.95
3	Y20	0.69781	2.79124
4	Y34	0.77331	3.09324
5	Y22	0.81594	3.26376
6	Y10	0.83762	3.35048
7	Y29	0.85237	3.40948
8	Y1	0.861	3.444
9	Y18	0.89744	3.58976
10	Y33	0.92162	3.68648
11	Y40	1.01012	4.04048
12	Y6	1.04494	4.17976
13	Y43	1.051	4.204
14	Y44	1.10187	4.40748
15	Y15	1.14406	4.57624
16	Y30	1.20031	4.80124
17	Y39	1.2285	4.914
18	Y37	1.35094	5.40376
19	Y38	1.70662	6.82648
20	Y25	2.76244	7.04976

Untreated				
Sample D	GL = 10			
Rank	**Tensile stress**	**Failure probability**	**X**	**Y**
n	**σ**	**P_f**	**ln σ**	**ln(-ln(1-P_f))**
-	**[MPa]**	**P_f = (n-0.5)/N**	**-**	**-**
1	361	0.025	5.888877958	-3.676247258
2	363	0.075	5.894402834	-2.551539632
3	372	0.125	5.918893854	-2.013418678
4	389	0.175	5.963579344	-1.64832484
5	460	0.225	6.131226489	-1.366914374
6	460	0.275	6.131226489	-1.134497663
7	465	0.325	6.142037406	-0.933837306
8	465	0.375	6.142037406	-0.755014863
9	472	0.425	6.156978986	-0.591700887
10	485	0.475	6.184148891	-0.439502333
11	510	0.525	6.234410726	-0.295122383
12	519	0.575	6.251903883	-0.155875037
13	523	0.625	6.259581464	-0.019356889
14	527	0.675	6.267200549	0.116831558
15	528	0.725	6.269096284	0.255404859
16	564	0.775	6.335054251	0.399886159
17	585	0.825	6.371611847	0.555590156
18	660	0.875	6.492239835	0.732099368
19	711	0.925	6.56667243	0.951761023
20	726	0.975	6.587550015	1.305322741

Untreated				
Sample E	GL = 15			
Rank	**Tensile stress**	**Failure probability**	**X**	**Y**
n	**σ**	**P_f**	**ln σ**	**ln(-ln(1-P_f))**
-	**[MPa]**	**P_f = (n-0.5)/N**	**-**	**-**
1	316	0.025	5.755742214	-3.676247258
2	336	0.075	5.81711116	-2.551539632
3	399	0.125	5.988961417	-2.013418678
4	413	0.175	6.023447593	-1.64832484
5	446	0.225	6.100318952	-1.366914374
6	448	0.275	6.104793232	-1.134497663
7	453	0.325	6.115892125	-0.933837306
8	460	0.375	6.131226489	-0.755014863
9	470	0.425	6.152732695	-0.591700887
10	495	0.475	6.204557763	-0.439502333
11	506	0.525	6.226536669	-0.295122383
12	516	0.575	6.246106765	-0.155875037
13	542	0.625	6.295266001	-0.019356889
14	543	0.675	6.29710932	0.116831558
15	552	0.725	6.313548046	0.255404859
16	564	0.775	6.335054251	0.399886159
17	579	0.825	6.361302478	0.555590156
18	580	0.875	6.363028104	0.732099368
19	643	0.925	6.466144724	0.951761023
20	688	0.975	6.533788838	1.305322741

Untreated				
Sample F	GL = 20			
Rank	**Tensile stress**	**Failure probability**	**X**	**Y**
n	**σ**	**P_f**	**ln σ**	**ln(-ln(1-P_f))**
-	**[MPa]**	Pf = (n-0.5) / N	**-**	**-**
1	312	0.025	5.743003188	-3.676247258
2	332	0.075	5.805134969	-2.551539632
3	385	0.125	5.953243334	-2.013418678
4	386	0.175	5.955837369	-1.64832484
5	429	0.225	6.061456919	-1.366914374
6	449	0.275	6.107022888	-1.134497663
7	455	0.325	6.120297419	-0.933837306
8	457	0.375	6.124683391	-0.755014863
9	469	0.425	6.150602768	-0.591700887
10	470	0.475	6.152732695	-0.439502333
11	484	0.525	6.182084907	-0.295122383
12	498	0.575	6.210600077	-0.155875037
13	502	0.625	6.21860012	-0.019356889
14	520	0.675	6.253828812	0.116831558
15	522	0.725	6.257667588	0.255404859
16	544	0.775	6.298949247	0.399886159
17	557	0.825	6.32256524	0.555590156
18	565	0.875	6.336825731	0.732099368
19	642	0.925	6.464588304	0.951761023
20	663	0.975	6.49677499	1.305322741

Untreated				
Sample MH	GL = 25			
Rank	**Tensile stress**	**Failure probability**	**X**	**Y**
n	**σ**	**P_f**	**ln σ**	**ln(-ln(1-P_f))**
-	**[MPa]**	Pf = (n-0.5) / N	**-**	**-**
1	264	0.025	5.575949103	-3.676247258
2	322	0.075	5.774551546	-2.551539632
3	329	0.125	5.796057751	-2.013418678
4	352	0.175	5.863631176	-1.64832484
5	410	0.225	6.01615716	-1.366914374
6	412	0.275	6.021023349	-1.134497663
7	412	0.325	6.021023349	-0.933837306
8	446	0.375	6.100318952	-0.755014863
9	451	0.425	6.11146734	-0.591700887
10	453	0.475	6.115892125	-0.439502333
11	464	0.525	6.139884552	-0.295122383
12	473	0.575	6.159095388	-0.155875037
13	475	0.625	6.163314804	-0.019356889
14	515	0.675	6.244166901	0.116831558
15	520	0.725	6.253828812	0.255404859
16	549	0.775	6.308098442	0.399886159
17	577	0.825	6.357842267	0.555590156
18	635	0.875	6.453624999	0.732099368
19	660	0.925	6.492239835	0.951761023
20	667	0.975	6.502790046	1.305322741

Untreated				
Sample MG	GL = 30			
Rank	**Tensile stress**	**Failure probability**	**X**	**Y**
n	**σ**	**P_f**	**ln σ**	**ln(-ln(1-P_f))**
-	**[MPa]**	Pf = (n-0.5) / N	**-**	**-**
1	238	0.025	5.472270674	-3.676247258
2	316	0.075	5.755742214	-2.551539632
3	353	0.125	5.866468057	-2.013418678
4	368	0.175	5.908082938	-1.64832484
5	368	0.225	5.908082938	-1.366914374
6	377	0.275	5.932245187	-1.134497663
7	389	0.325	5.963579344	-0.933837306
8	418	0.375	6.035481433	-0.755014863
9	441	0.425	6.089044875	-0.591700887
10	444	0.475	6.095824562	-0.439502333
11	453	0.525	6.115892125	-0.295122383
12	458	0.575	6.126869184	-0.155875037
13	458	0.625	6.126869184	-0.019356889
14	473	0.675	6.159095388	0.116831558
15	492	0.725	6.198478716	0.255404859
16	510	0.775	6.234410726	0.399886159
17	574	0.825	6.352629396	0.555590156
18	626	0.875	6.439350371	0.732099368
19	644	0.925	6.467698726	0.951761023
20	665	0.975	6.499787041	1.305322741

Treated 6CS				
Sample MA	GL = 10			
Rank	**Tensile stress**	**Failure probability**	**X**	**Y**
n	**σ**	**P_f**	**ln σ**	**ln(-ln(1-P_f))**
-	**[MPa]**	**P_f = n / (N+1)**	**-**	**-**
1	269	0.047619048	5.59471138	-3.02022654
2	461	0.095238095	6.13339804	-2.30175086
3	503	0.142857143	6.22059017	-1.86982471
4	511	0.19047619	6.23636959	-1.55443332
5	511	0.238095238	6.23636959	-1.30219694
6	547	0.285714286	6.3044488	-1.08923964
7	555	0.333333333	6.31896811	-0.90272046
8	555	0.380952381	6.31896811	-0.73485899
9	565	0.428571429	6.33682573	-0.58050482
10	592	0.476190476	6.38350663	-0.4359854
11	620	0.523809524	6.42971948	-0.29849048
12	648	0.571428571	6.4738907	-0.16570298
13	649	0.619047619	6.47543272	-0.03554335
14	675	0.666666667	6.51471269	0.094047828
15	686	0.714285714	6.53087763	0.225351487
16	708	0.761904762	6.56244409	0.36122375
17	755	0.80952381	6.62671775	0.505749609
18	809	0.857142857	6.69579892	0.665729811
19	876	0.904761905	6.77536609	0.855000373
20	909	0.952380952	6.81234509	1.113344054

Treated 6CS				
Sample MC	GL = 15			
Rank	**Tensile stress**	**Failure probability**	**X**	**Y**
n	**σ**	**P_f**	**ln σ**	**ln(-ln(1-P_f))**
-	**[MPa]**	**P_f = n / (N+1)**	**-**	**-**
1	408	0.047619048	6.011267174	-3.02022654
2	432	0.095238095	6.068425588	-2.30175086
3	443	0.142857143	6.09356977	-1.86982471
4	499	0.19047619	6.212606096	-1.55443332
5	512	0.238095238	6.238324625	-1.30219694
6	520	0.285714286	6.253828812	-1.08923964
7	546	0.333333333	6.302618976	-0.90272046
8	548	0.380952381	6.306275287	-0.73485899
9	569	0.428571429	6.343880434	-0.58050482
10	578	0.476190476	6.359573869	-0.4359854
11	590	0.523809524	6.380122537	-0.29849048
12	616	0.571428571	6.423246964	-0.16570298
13	636	0.619047619	6.455198563	-0.03554335
14	648	0.666666667	6.473890696	0.094047828
15	651	0.714285714	6.478509642	0.225351487
16	666	0.761904762	6.501289671	0.36122375
17	669	0.80952381	6.50578406	0.505749609
18	672	0.857142857	6.510258341	0.665729811
19	694	0.904761905	6.542471961	0.855000373
20	798	0.952380952	6.682108597	1.113344054

Treated 6CS				
Sample ME	GL = 20			
Rank	**Tensile stress**	**Failure probability**	**X**	**Y**
n	**σ**	**P_f**	**ln σ**	**ln(-ln(1-P_f))**
-	**[MPa]**	**P_f = n / (N+1)**	**-**	**-**
1	214	0.047619048	5.365976015	-3.02022654
2	293	0.095238095	5.680172609	-2.30175086
3	338	0.142857143	5.823045895	-1.86982471
4	345	0.19047619	5.843544417	-1.55443332
5	477	0.238095238	6.167516491	-1.30219694
6	496	0.285714286	6.206575927	-1.08923964
7	502	0.333333333	6.21860012	-0.90272046
8	503	0.380952381	6.22059017	-0.73485899
9	515	0.428571429	6.244166901	-0.58050482
10	531	0.476190476	6.274762021	-0.4359854
11	595	0.523809524	6.388561406	-0.29849048
12	615	0.571428571	6.421622268	-0.16570298
13	630	0.619047619	6.445719819	-0.03554335
14	642	0.666666667	6.464588304	0.094047828
15	647	0.714285714	6.472346295	0.225351487
16	688	0.761904762	6.533788838	0.36122375
17	713	0.80952381	6.56948142	0.505749609
18	782	0.857142857	6.661854741	0.665729811
19	803	0.904761905	6.688354714	0.855000373
20	821	0.952380952	6.710523109	1.113344054

Treated 6CS				
Sample MB	GL = 25			
Rank	**Tensile stress**	**Failure probability**	**X**	**Y**
n	**σ**	**P_f**	**ln σ**	**ln(-ln(1-P_f))**
-	**[MPa]**	**P_f = n / (N+1)**	**-**	**-**
1	312	0.047619048	5.743003188	-3.02022654
2	388	0.095238095	5.96100534	-2.30175086
3	417	0.142857143	6.033086222	-1.86982471
4	418	0.19047619	6.035481433	-1.55443332
5	429	0.238095238	6.061456919	-1.30219694
6	429	0.285714286	6.061456919	-1.08923964
7	461	0.333333333	6.133398043	-0.90272046
8	472	0.380952381	6.156978986	-0.73485899
9	475	0.428571429	6.163314804	-0.58050482
10	498	0.476190476	6.210600077	-0.4359854
11	532	0.523809524	6.276643489	-0.29849048
12	549	0.571428571	6.308098442	-0.16570298
13	561	0.619047619	6.329720906	-0.03554335
14	566	0.666666667	6.338594078	0.094047828
15	599	0.714285714	6.395261598	0.225351487
16	660	0.761904762	6.492239835	0.36122375
17	666	0.80952381	6.501289671	0.505749609
18	688	0.857142857	6.533788838	0.665729811
19	819	0.904761905	6.708084084	0.855000373
20	862	0.952380952	6.759255271	1.113344054

Treated 6CS				
Sample MD	GL = 30			
Rank	**Tensile stress**	**Failure probability**	**X**	**Y**
n	**σ**	**P_f**	**ln σ**	**ln(-ln(1-P_f))**
-	**[MPa]**	**P_f = n / (N+1)**	**-**	**-**
1	171	0.047619048	5.141663557	-3.02022654
2	330	0.095238095	5.799092654	-2.30175086
3	373	0.142857143	5.92157842	-1.86982471
4	381	0.19047619	5.942799375	-1.55443332
5	403	0.238095238	5.998936562	-1.30219694
6	424	0.285714286	6.049733455	-1.08923964
7	449	0.333333333	6.107022888	-0.90272046
8	451	0.380952381	6.11146734	-0.73485899
9	458	0.428571429	6.126869184	-0.58050482
10	485	0.476190476	6.184148891	-0.4359854
11	487	0.523809524	6.188264123	-0.29849048
12	539	0.571428571	6.289715571	-0.16570298
13	553	0.619047619	6.315358002	-0.03554335
14	585	0.666666667	6.371611847	0.094047828
15	610	0.714285714	6.413458957	0.225351487
16	613	0.761904762	6.418364936	0.36122375
17	618	0.80952381	6.426488457	0.505749609
18	619	0.857142857	6.428105273	0.665729811
19	749	0.904761905	6.618738984	0.855000373
20	792	0.952380952	6.674561392	1.113344054

Treated 0.16 CS				
Sample X	GL = 25			
Rank	Tensile stress	Failure probability	X	Y
n	σ	Pf	ln σ	ln(-ln(1-Pf))
-	[MPa]	Pf = (n-0.5) / N	-	-
1	238	0.025	5.472270674	-3.67624726
2	255	0.075	5.541263545	-2.55153963
3	283	0.125	5.645446898	-2.01341868
4	293	0.175	5.680172609	-1.64832484
5	306	0.225	5.723585102	-1.36691437
6	320	0.275	5.768320996	-1.13449766
7	322	0.325	5.774551546	-0.93383731
8	332	0.375	5.805134969	-0.75501486
9	346	0.425	5.846438775	-0.59170089
10	367	0.475	5.905361848	-0.43950233
11	368	0.525	5.908082938	-0.29512238
12	371	0.575	5.916202063	-0.15587504
13	387	0.625	5.958424693	-0.01935689
14	391	0.675	5.96870756	0.116831558
15	395	0.725	5.978885765	0.255404859
16	402	0.775	5.996452089	0.399886159
17	412	0.825	6.021023349	0.555590156
18	437	0.875	6.079933195	0.732099368
19	446	0.925	6.100318952	0.951761023
20	471	0.975	6.154858094	1.305322741

Treated 2 CS				
Sample Y	GL = 25			
Rank	Tensile stress	Failure probability	X	Y
n	σ	Pf	ln σ	ln(-ln(1-Pf))
-	[MPa]	Pf = (n-0.5) / N	-	-
1	245	0.025	5.501258211	-3.67624726
2	257	0.075	5.549076085	-2.55153963
3	276	0.125	5.620400866	-2.01341868
4	296	0.175	5.690359454	-1.64832484
5	304	0.225	5.717027701	-1.36691437
6	309	0.275	5.733341277	-1.13449766
7	318	0.325	5.762051383	-0.93383731
8	329	0.375	5.796057751	-0.75501486
9	351	0.425	5.860786223	-0.59170089
10	357	0.475	5.877735782	-0.43950233
11	366	0.525	5.902633333	-0.29512238
12	371	0.575	5.916202063	-0.15587504
13	387	0.625	5.958424693	-0.01935689
14	396	0.675	5.981414211	0.116831558
15	407	0.725	6.008813185	0.255404859
16	418	0.775	6.035481433	0.399886159
17	427	0.825	6.056784013	0.555590156
18	445	0.875	6.098074282	0.732099368

19	449	0.925	6.107022888	0.951761023
20	502	0.975	6.21860012	1.305322741

Sample	MI	GL = 25[mm]	UN/H2O2	
No.	**m**	**hmotnost [g]**	**load [N]**	stress [Pa]
51	15	0.0015	5.58	352563000
55	8	0.0008	3.51	415825312.5
56	20	0.0020	9.09	430752375
59	14	0.0014	6.40	433257142.9
57	17	0.0017	7.84	437080000
47	9	0.0009	4.26	448601666.7
52	15	0.0015	7.55	477034166.7
44	9	0.0009	4.57	481246388.9
43	7	0.0007	3.64	492830000
50	8	0.0008	4.17	494014687.5
41	13	0.0013	7.35	535843269.2
46	13	0.0013	7.65	557714423.1
60	12	0.0012	7.09	559962291.7
58	9	0.0009	5.39	567596944.4
42	9	0.0009	5.50	579180555.6
48	7	0.0007	4.30	582189285.7
49	6	0.0006	3.82	603400833.3
53	13	0.0013	8.44	615308461.5
45	7	0.0007	4.79	648531785.7
54	7	0.0007	4.91	664778928.6

Sample	MF	GL = 25[mm]	6CS/H2O2	
No.	**m**	**hmotnost [g]**	**load [N]**	**Tensile stress [Pa]**
55	26	0.0026	6.71	315491296.2
47	10	0.001	2.92	356961240
49	10	0.001	2.97	363073590
60	18	0.0018	5.97	405452550
42	14	0.0014	5.05	440962392.9
46	17	0.0017	6.28	451594800
54	17	0.0017	6.37	458066700
45	23	0.0023	9.22	490051017.4
56	15	0.0015	6.06	493877880
51	20	0.002	8.53	521383455
53	18	0.0018	7.68	521587200
57	21	0.0021	8.97	522169328.6
43	16	0.0016	6.89	526426143.8
44	16	0.0016	6.92	528718275
48	9	0.0009	4.02	546036600
52	15	0.0015	6.7	546036600
41	13	0.0013	6.49	610294638.5
58	12	0.0012	6.1	621422250
59	17	0.0017	9.04	650066400
50	16	0.0016	9.02	689167462.5

Pull out test; 6 CS treated sisal; PLA transcrystalline morphology					
Specimen label	Max. Load	OM diameter	Lem		IFSS
[-]	[N]	[μm]	[μm]	rank	[MPa]
8A	0.64	109	231	1	8.10
5A	3.15	142	354	2	19.98
7B	2.66	135	415	3	15.10
11A	5.68	178	536	4	18.97
10B	4.45	114	542	5	22.96
6B	2.18	136	550	6	9.28
1A	1.93	98	576	7	10.89
3A	4.05	234	640	8	8.62
3B	6.75	229	654	9	14.36
10A	2.92	130	706	10	10.13
6A	3.61	190	754	11	8.03
2A	4.37	162	773	12	11.12
8B	3.05	97	891	13	11.24
9A	2.56	55	955	14	15.53
2B	3.97	162	1216	15	6.42

Pull out test; 6 CS treated sisal; PLA transcrystalline morphology				
rank	τ	P_f	ln τ	ln(-ln(1-P_f))
n		$P_f = n / (N+1)$		
	[MPa]			
1	6.42	0.0625	1.86	-2.74
2	8.03	0.1250	2.08	-2.01
3	8.10	0.1875	2.09	-1.57
4	8.62	0.2500	2.15	-1.25
5	9.28	0.3125	2.23	-0.98
6	10.13	0.3750	2.32	-0.76
7	10.89	0.4375	2.39	-0.55
8	11.12	0.5000	2.41	-0.37
9	11.24	0.5625	2.42	-0.19
10	14.36	0.6250	2.66	-0.02
11	15.10	0.6875	2.71	0.15
12	15.53	0.7500	2.74	0.33
13	18.97	0.8125	2.94	0.52
14	19.98	0.8750	2.99	0.73
15	22.96	0.9375	3.13	1.02

Pull-out test; untreated sisal fibre in PLA				
Test results				Embedded
	Specimen	Max. load	Diameter	length
		(N)	[mm]	[mm]
1	A1	4.28	0.172	0.9438
2	A2	2.31	0.203	0.4672
3	A3	3.8	0.194	0.5544
4	A4	5	0.163	0.9868
5	A5	3.36	0.227	0.3094
6	A6	8.94	0.184	0.9284
7	A7	2.42	0.177	0.3043
8	A8	1.15	0.167	0.2074
9	A9	5.59	0.156	0.7428
10	A10	0.74	0.059	0.6600
11	A15	4.21	0.15	0.8145
12	A16	3.65	0.14	1.2053
13	A17	2.74	0.163	0.8230
14	A18	5.55	0.154	0.9730
15	A19	2.76	0.209	1.0590
16	A20	9.12	0.355	0.6413
17	A21	6.36	0.207	1.2148
18	A22	2.79	0.146	1.0930
19	A23	9.29	0.185	0.8607
20	A24	5.37	0.171	0.6338
21	A26	7.63	0.297	0.7204
22	A27	6.14	0.163	0.8112
23	A28	7.07	0.233	0.9687
24	A29	6.63	0.211	1.1187
25	A30	8.1	0.29	0.6835
26	A31	2.56	0.227	0.6587
27	A32	4.61	0.383	0.6088
28	A33	2.91	0.278	0.4790
29	A34	1.85	0.137	0.5743
30	A35	3.92	0.275	0.9623
31	A37	4.61	0.217	0.6432
32	A38	6.81	0.205	0.7193
33	A39	4.85	0.323	0.5160
34	A40	4.39	0.226	0.6318

Pull out test, 6 CS treated sisal fibre in PLA				
Test results				Embedded
	Specimen	Max. load	Diameter	length
				l_m
		(N)	[mm]	[mm]
26	B26	0.12	0.201	0.097
25	B25	1.2	0.17	0.181
18	B18	1.27	0.156	0.177
15	B15	1.57	0.16	0.176
29	B29	1.84	0.212	0.236
30	B30	2.23	0.171	0.429
9	B9	2.34	0.19	0.781
3	B3	2.51	0.104	0.461
23	B23	2.6	0.239	0.289
19	B19	3.57	0.312	0.297
16	B16	3.61	0.176	0.412
6	B6	3.82	0.289	0.444
24	B24	4	0.187	0.400
22	B22	4.01	0.281	0.653
28	B28	4.14	0.166	0.338
8	B8	4.19	0.191	0.680
5	B5	4.39	0.227	0.405
12	B12	4.44	0.159	0.523
27	B27	4.57	0.227	0.288
13	B13	4.59	0.174	0.616
17	B17	5.15	0.212	0.414
7	B7	5.54	0.168	0.476
10	B10	5.88	0.243	0.665
4	B4	5.97	0.16	0.686
11	B11	6.53	0.196	0.340

Tensile test; 6 CS treated sisal/PLA composites					
Sample	h	w	Load	Tensile strength	Modulus
	[mm]	[mm]	[N]	[MPa]	[GPa]
1	1.28	15.53	4217	212.1	14.48
2	1.04	15.77	3045	185.7	10.95
3	1.03	15.57	2997	186.9	13.04
4	1.24	15.58	4428	229.2	12.47
5	1.13	15.52	3667	209.1	10.86
6	1.13	15.75	3626	203.7	11.67
			AVG	204.5	12.2
			STDEV	16.5	1.39

Tensile test; untreated sisal/PLA composites					
Sample	h	w	Load	Tensile strength	Modulus
	[mm]	[mm]	[N]	[MPa]	[GPa]
1	1.29	15.37	3674	185.3	9.72
2	1.18	15.56	2486	135.4	8.81
3	1.11	15.45	2435	142.0	9.62
4	1.31	15.15	3796	191.3	11.03
5	1.19	15.4	3056	166.8	10.67
6	1.24	15.62	3114	160.8	6.93
			AVG	163.6	9.5
			STDEV	22.4	1.47

PLA/40 % UN sisal; 3PB flexure					
	h	w	Load	Flexural strength	Flexural modulus
	[mm]	[mm]	[N]	[MPa]	[GPa]
1	1.28	7.19	104	211.88	
2	1.08	7.27	96	271.71	
3	1.14	7.27	98	248.94	
4	1.18	7.12	112	271.13	
5	1.19	7.51	104	234.70	
6	1.36	7.34	102	180.32	
			AVG	236.45	
			STDEV	35.66	

PLA/40 % 6CS sisal; 3PB flexure					
	h	w	Load	Flexural strength	Flexural modulus
	[mm]	[mm]	[N]	[MPa]	[GPa]
1	1.18	7.15	104	250.71	
2	1.14	7.21	96	245.89	
3	1.16	7.18	98	243.44	
4	1.18	7.24	97	230.93	
5	1.19	7.14	95	225.50	
6	1.21	7.14	105	241.06	
			AVG	239.59	
			STDEV	9.53	

PLA/60 % UN sisal; 3PB flexure					
	h	w	Load	Flexural strength	Flexural modulus
	[mm]	[mm]	[N]	[MPa]	[GPa]
1	1.25	15.13	281	285.27	
2	1.3	15.11	255	239.66	
3	1.27	15.07	267	263.63	
4	1.22	14.88	293	317.51	
5	1.19	14.92	296	336.23	
6	1.41	15.08	287	229.75	
			AVG	278.68	
			STDEV	42.44	

PLA/60 % 6CS sisal; 3PB flexure					
	h	w	Load	Flexural strength	Flexural modulus
	[mm]	[mm]	[N]	[MPa]	[GPa]
1	1.16	14.69	234	284.11	
2	1.19	14.57	228	265.21	
3	1.16	14.54	230	282.14	
4	1.21	14.34	242	276.63	
5	1.19	14.41	248	291.68	
6	1.09	14.59	229	317.06	
			AVG	286.14	
			STDEV	17.52	

Test method	Three-point bending			
	Flexural modulus [GPa] of composites			
Matrix	PLA	PLA	PLA	PLA
Fibre	sisal	sisal	sisal	sisal
Treatment	UN	UN	6CS	6CS
Fibre volume fraction	$V_f = 0.4$	$V_f = 0.6$	$V_f = 0.4$	$V_f = 0.6$
1	9.81	20.54	10.84	22.69
2	8.36	19.72	12.28	21.92
3	10.78	20.85	11.47	22.56
4	8.97	17.37	10.71	19.57
5	10.36	19.48	10.33	21.47
6	10.48	18.12	10.95	22.54
AVG	9.79	19.35	11.10	21.79
STDEV	0.95	1.36	0.69	1.18

PLA/UN sisal; ILSS				
	h	w	Load	ILSS
	[mm]	[mm]	[N]	[MPa]
1	2.48	14.45	372	7.79
2	2.49	13.04	436	10.07
3	2.49	13.4	326	7.33
4	2.59	13.56	381	8.14
5	2.48	13.56	376	8.39
6	2.48	13.69	434	9.59
7	2.63	13.23	298	6.42
8	2.35	13.93	406	9.30
			AVG	8.38
			STDEV	1.23

PLA/6 CS sisal; ILSS				
	h	w	Load	ILSS
	[mm]	[mm]	[N]	[MPa]
1	2.05	12.92	482	13.65
2	2.04	13.07	638	17.95
3	1.88	13.23	378	11.40
4	2.18	13.43	562	14.40
5	1.98	13.53	467	13.07
6	2.14	13.95	578	14.52
7	2.18	14.27	768	18.52
			AVG	14.79
			STDEV	2.58